UNIVERSIDADE DE LISBOA

FACULDADE DE CIÊNCIAS

DEPARTAMENTO DE GEOLOGIA

TECTONICS OF THE GULF OF CADIZ: THE ROLE OF THE GIBRALTAR ARC IN THE REACTIVATION OF THE SW IBERIA MARGIN

João Daniel Casal Duarte

DOUTORAMENTO EM GEOLOGIA

(GEODINÂMICA INTERNA)

2011

UNIVERSIDADE DE LISBOA

FACULDADE DE CIÊNCIAS

DEPARTAMENTO DE GEOLOGIA

TECTONICS OF THE GULF OF CADIZ: THE ROLE OF THE GIBRALTAR ARC IN THE REACTIVATION OF THE SW IBERIA MARGIN

João Daniel Casal Duarte

DOUTORAMENTO EM GEOLOGIA

(GEODINÂMICA INTERNA)

Tese orientada pelos Profs. Drs. Pedro Terrinha e Filipe Rosas

2011

ABSTRACT

The process of spontaneous subduction initiation at passive margins plays a central role in the plate tectonics theory, in particular in the Wilson Cycle paradigmatic concept, which states that oceans form, evolve and finally close. The Wilson Cycle requires that after a certain time of oceanic drifting passive margins are reactivated and subduction initiates. However, the process of transformation of passive continental margins into active continental margins with subduction zones is still far from understood, and spontaneous transition examples between these two types of margins are not known. In addition, recent works based on theoretical calculations and physical modeling showed that it is mechanically unfeasible to form a new subduction system in isolation from an already existing one, i.e. spontaneous subduction initiation. One way to solve this problem is to consider that subduction initiation may generally be induced by the proximity of another subduction zone or by stress transference from a nearby collision belt, i.e. induced subduction initiation. Therefore, passive margins in the proximity of pre-existing subduction zones would represent preferential sites for the formation of new subduction zones. In this work, the Gibraltar Arc and the Southwest Iberia Margin are used as case studies to investigate the role that the orogenic arcs may have in the formation of new subduction systems at passive margins.

The Atlantic margins are generally described as the typical case of passive margins, often termed Atlantic type margins. However, there are at least two regions where the Atlantic oceanic lithosphere is being consumed in subduction zones: in the Scotia and in the Lesser Antilles arcs (in the Southwestern and central West Atlantic, respectively). These subduction zones seem to have been transferred from the Eastern Pacific ocean to the Atlantic domain and potentially represent precursors to a system of convergent zones that might ultimately result in the closure of the Atlantic Ocean. However, in these two systems the oceanic lithosphere has been subducted since at least the Early Cenozoic, without lateral propagation of the subduction zones along the adjacent Atlantic passive margins. The Gulf of Cadiz, i.e. the foreland of the Gibraltar orogenic arc, has been proposed as a potential locus for a subduction zone to propagate into the open Atlantic. On the other hand, the proximity of the Gibraltar collision belt to the Southwest Iberia Margin, together with the existing overall convergence between

Africa and Iberia, induces compressive stresses that, in association with the existence of more than 100 km long active thrusts (e.g. Horseshoe Fault and Gorringe Bank), make this margin a strong candidate for the nucleation of a new subduction zone.

In order to better evaluate the post-Miocene tectonics and the main tectonic driving mechanism operating in the Gulf of Cadiz an up-to-date tectonic map of this area was produced. This map was based on the coupled analysis of a multi-survey MCS dataset and the recently compiled high resolution bathymetry dataset (the SWIM bathymetry). The mapping revealed the existence of three main systems of tectonic structures: i) the subduction-related Gulf of Cadiz Accretionary Wedge (CGAW); ii) a set of WNW-ESE striking dextral strike-slip faults (the SWIM fault system); and iii) a group of NE-SW striking northwest-directed thrusts located in the Southwest Iberia Margin (the NE-SW thrust system).

The subduction-related accretionary wedge (GCAW) is materialized on the seafloor by a west dipping U-shaped surface and consists in an eastward thickening pile of westwards thrusted sediments. There are evidences that this thrust wedge is active and propagating westward.

The SWIM fault system is a group of WNW-ESE striking subvertical strike-slip faults extending from the eastern part of the Gulf of Cadiz, i.e. the northwest Moroccan shelf, to the Horseshoe Abyssal Plain. These faults were interpreted in this work as the Present day dextral reactivation of the old Mesozoic Tethyan plate boundary.

The NE-SW striking thrust system is a group northwest directed thrusts located along the Southwest Iberia Margin, comprising the Horseshoe fault, the Marquês de Pombal fault, the Tagus Abyssal Plain fault and the Gorringe northern thrust. This NE-SW thrust system seems to be the result of the migration of the deformation, in the Pliocene-Quaternary, from the realm of the Gibraltar wedge to the west (onto the Horseshoe fault region) and to the north along the West Portuguese Margin. These structures may be the expression of a new compressive deformation front.

Besides these three tectonic systems, other important structures were also promptly recognized such as the ENE-WSW to E-W striking system of thrusts (e.g. the Portimão pop-up and the Coral Patch Ridge), related with the overall Cenozoic Nubia-

Iberia N-S convergence, and NE-SW striking Cadiz fault, a dextral strike-slip fault that probably accommodates part the westward movement of the Gibraltar Arc.

The analysis of the multibeam bathymetry data from the northwestern part of the Gulf of Cadiz also revealed the existence of several intriguing kilometric crescentic depressions lying at depths between -4300 m and -4700 m, never before reported to occur at such great depths in the scientific literature. These features are located in the Horseshoe Valley between two major tectonic structures: the GCAW and the Horseshoe fault. Morphological parameterization of these features, coupled with detailed analysis of multi-channel and middle resolution seismic profiles, showed that these crescent-shaped features were formed due to the existence of specific interaction between: a) regional active thrusts on top of which most crescentic depressions are carved; and b) tectonically induced scouring comprising localized erosion and simultaneous progradational sedimentation, produced by downslope turbiditic currents. The obtained results also suggest a possible contribution of fluid migration and extrusion processes, such as mud volcanism and associated pockmark formation, besides gravity driven landslides and slumping, in the development of the studied crescentic depressions. The active (mainly blind) thrusts in which the crescentic depressions are carved root in the GCAW décollement layer, to the west of the GCAW deformation front. Therefore, the crescentic depressions are interpreted as the morphological expression of the westward propagation of the deformation related with the GCAW, into the Horseshoe Valley domain.

Besides the new produced cartography of the Gulf of Cadiz, the present work also benefited from the instrumental use of analog modeling experiments. Three main different modes of tectonic interference between the SWIM strike-slip fault system (related with the overall Nubia-Iberia convergence) and the GCAW (related with the Gibraltar subduction) were tested through analog sand-box modeling, namely: a) An active accretionary wedge on top of a pre-existent inactive basement fault; b) An active strike-slip fault cutting a previously formed, inactive, accretionary wedge; and c) Simultaneous activity of both the accretionary wedge and the strike-slip fault. The results obtained and the comparison with the natural deformation pattern favor a tectonic evolution comprising two main steps: i) the development of the Gulf of Cadiz Accretionary Wedge on top of inactive, Tethyan-related, basement faults (Middle Miocene to ~1.8 Ma); ii) subsequent reactivation of these basement faults with dextral

strike-slip motion (~1.8 Ma to Present) simultaneously with continued tectonic accretion in the GCAW. These results exclude the possibility of ongoing active SWIM wrench system cross-cutting an inactive GCAW structure. The results also support a new interpretation of the SWIM wrench system as fundamentally resulting from strike-slip reactivation of an old (Tethyan-related) plate boundary.

Detail mapping in the Horseshoe Abyssal Plain also revealed the existence of a new morphotectonic pattern near the intersection (corner zone) of the SWIM 1 fault and the Horseshoe fault. Based on combined analog and numerical experiments this pattern was interpreted as resulting from the (wrench-thrust) tectonic interference between two of the main tectonic systems recognized in the Gulf of Cadiz area: the SWIM faults and the NE-SW thrusts.

Finally, the results presented in this work favor a hypothetic scenario in which the Gibraltar subduction is active, but decreasing in activity since the Miocene, at the same time that an incipient subduction zone may be nucleating in the Southwest Iberia Margin. The Gulf of Cadiz may be thus seen as a place where the proximity of a pre-existent subduction system could be inducing the formation of a new subduction zone in the Atlantic.

Keywords: Subduction initiation; Gulf of Cadiz; Tectonic Map; Crescent-shaped Depressions; Thrust-Wrench Interference.

RESUMO

O processo de iniciação espontânea de novas zonas de subducção ao longo de margens passivas tem um papel central na teoria da tectónica de placas, em particular no conceito paradigmático de Ciclo de Wilson, que afirma que os oceanos formam-se, evoluem e finalmente acabam por fechar. O Ciclo de Wilson requer que após um determinado tempo de evolução de um oceano as suas margens passivas sejam reactivadas e que uma nova zona de subducção se inicie. No entanto, o processo de transformação de margens continentais passivas em margens continentais activas com zonas de subducção é praticamente desconhecido, sendo que não se encontra documentado nenhum caso de transição espontânea entre estes dois tipos de margens. Acresce ainda que, trabalhos recentes de modelação numérica e cálculos teóricos mostraram que é fisicamente implausível a formação de novos sistemas de zonas de subducção isolados de zonas de subducção pré-existentes, isto é subducção espontânea. Uma forma de ultrapassar esta inconsistência é considerar que a iniciação de novas zonas de subducção é em geral induzida pela proximidade de outras zonas de subducção ou por compressão induzida a partir de um orógeno próximo, isto é, subducção induzida. Deste modo, as margens passivas próximas de zonas de subducção pré-existentes podem ser vistas como os locais preferenciais para a formação de novas zonas de subducção. No presente trabalho, usa-se o Arco de Gibraltar e a Margem Sudoeste Ibérica como casos de estudo na tentativa de abordar a temática do papel que os arcos orogénicos podem ter na formação de novas zonas de subducção ao longo de margens passivas.

As margens Atlânticas são geralmente descritas como o caso típico de margens passivas, pelo que estas são comummente denominadas de margens do tipo Atlântico. No entanto, há pelo menos dois locais na Terra onde litosfera oceânica Atlântica é consumida em zonas de subducção: no arco Scotia e no arco das Pequenas Antilhas (no Sudoeste Atlântico e no Atlântico Oeste central, respectivamente). Estes dois casos de zonas de subducção parecem ter sido transferidas do Oceano Pacífico oriental para o domínio Atlântico e podem ser vistos como os precursores do desenvolvimento de um novo limite de placas convergente que poderá em última instancia levar ao fecho do Oceano Atlântico. Porém, a litosfera oceânica tem vindo a ser subductada nestes dois

sistemas desde pelo menos o Cenozóico inferior, sem ter ocorrido a propagação da subducção ao longo das margens passivas atlânticas adjacentes. O Golfo de Cádis, isto é, a bacia de ante-país do arco orogénico de Gibraltar, tem sido descrito como o terceiro local na Terra onde existe o potencial para uma zona de subducção pré-existente propagar-se para domínio Atlântico. Por outro lado, a proximidade do Arco de Gibraltar em relação à Margem Sudoeste Ibérica, em conjunto com a existência de convergência generalizada entre as placas tectónicas África e Ibéria, induz tensões compressivas nesta margem o que, em associação com a existência de cavalgamentos activos de largura superior a 100 km (por exemplo a Falha da Ferradura e o Banco Gorringe), a tornam numa forte candidata ao processo de nucleação de uma nova zona de subducção.

Com o objectivo de melhorar a compreensão da tectónica pós-miocénica e dos principais mecanismos tectónicos forçadores a actuar no Golfo de Cádis foi elaborado um mapa tectónico actualizado à escala do golfo. Este mapa foi preparado com base na análise conjunta de dados de diversas campanhas de sísmica de reflexão multi-canal e de dados de batimetria multi-feixe de alta resolução recentemente compilados (batimetria SWIM). A cartografia mostrou a existência de três sistemas de estruturas tectónicas principais: i) o Prisma Acrecionário do Golfo de Cádis (PAGC); ii) um grupo de falhas de desligamento direito com a direcção WNW-ESE (sistema de falhas SWIM) e; iii) um grupo de cavalgamentos com a direcção NE-SW, vergentes para noroeste, localizados ao longo da Margem Sudoeste Ibérica (sistema de cavalgamentos NE-SW).

O prisma acrecionário (PAGC) destaca-se no fundo do mar pela presença de um relevo morfológico positivo em forma de U que consiste na expressão superficial do empilhamento de sedimentos cavalgados para oeste. Este prisma gerou-se como resultado da existência da referida zona de subducção mergulhante para Este sob o Arco de Gibraltar. Existem evidências de que este prisma acrecionário ainda está activo e a propagar-se para oeste.

O sistema de falhas SWIM constitui um grupo de falhas de desligamento direito, sub-verticais, que se estendem desde a área mais oriental do Golfo de Cádis, na plataforma continental do noroeste de Marrocos, até à Planície Abissal da Ferradura. Estas falhas foram interpretadas neste trabalho como tendo resultado da reactivação direita da fronteira de placas Mesozóica do Tétis.

O sistema de cavalgamentos NE-SW é constituído por um grupo de cavalgamentos com direcção NE-SW, vergentes para noroeste localizados ao longo da Margem Sudoeste Ibérica que compreende a falha da Ferradura, a falha do Marquês de Pombal, a falha da Planície Abissal do Tejo e o cavalgamento norte do Gorringe. A deformação pliocénica-quaternária deste sistema é interpretada como a expressão da migração da deformação da frente de deformação do PAGC para oeste (até à zona da falha da Ferradura) e para norte ao longo da Margem Oeste Portuguesa. Estas estruturas parecem corresponder a uma nova frente de deformação compressiva, afastada do Arco de Gibraltar, que eventualmente poderá resultar na nucleação de uma nova zona de subducção na margem Sudoeste da Ibéria.

Para além destes três sistemas tectónicos, foram reconhecidas outras estruturas importantes como é o caso dos cavalgamentos com direcção ENE-WSW a E-W (e.g. Banco de Portimão e Crista Coral Patch), relacionados com a convergência N-S generalizada entre as placas Núbia e Ibéria no Cenozóico, e a falha de Cádis que corresponde a um desligamento direito de direcção NE-SW e que acomoda parte do movimento para oeste do Arco de Gibraltar e da deformação limítrofe da margem sul portuguesa.

Os dados de batimetria multi-feixe da área noroeste do Golfo de Cádis revelaram ainda a existência de um conjunto de intrigantes depressões em forma de crescente com dimensões quilométricas, localizadas entre os -4300 m e os -4700 m de profundidade. Objectos morfológicos com estas características nunca haviam sido identificados a tão grandes profundidades. Estas depressões estão localizadas no Vale da Ferradura entre duas estruturas tectónicas importantes: o PAGC e a falha da Ferradura. A análise morfológica destas formas, em conjunto com a análise detalhada de perfis de reflexão sísmica multi-canal e de média resolução, revelou que estas estruturas em crescente se formaram como resultado da interacção entre: a) actividade de falhas de cavalgamento que geram degraus tectónicos no topo dos quais os crescentes estão encaixados e b) erosão e re-deposição simultânea de sedimentos produzidos pela acção de correntes de fundo, provavelmente de origem turbidítica, que interagem com estes degraus tectónicos. Os resultados obtidos sugerem também uma contribuição de processos de migração e extrusão de fluidos, como vulcanismo de lama e formação de *pockmarks*, para além de movimentos de massa, no desenvolvimento das depressões em forma de crescente estudadas. Os cavalgamentos (essencialmente cegos) no topo dos quais os

crescentes estão encaixados enraízam ao nível do descolamento basal do PAGC, a oeste da sua frente de deformação morfológica. Deste modo, estas depressões em forma de crescente são também interpretadas como a expressão da migração da deformação relacionada com o PAGC para oeste, em direcção à área do Vale da Ferradura.

Para além da nova cartografia tectónica do Golfo de Cádis, sustentada na interpretação de dados de sísmica multi-canal e batimetria multifeixe, este trabalho beneficiou ainda do uso instrumental de modelação análoga. Três modos de interferência tectónica entre o sistema de desligamentos SWIM (relacionado com a convergência generalizada entre a Núbia e a Ibéria) e o PAGC (relacionado com a zona de subducção do Arco de Gibraltar) foram testados através de modelação análoga, usando ”caixas de areia”, compreendendo: a) a formação de um prisma acrecionário sobre uma falha basal inactiva pré-existente; b) a actividade de uma falha de desligamento afectando um prisma acrecionário inactivo previamente formado; e c) a actividade simultânea de um prisma acrecionário e de uma falha de desligamento. Os resultados obtidos e a comparação com o padrão de deformação natural observado favorecem um cenário de evolução tectónica que compreende duas etapas principais: i) o desenvolvimento do PAGC sobre falhas basais inactivas, relacionadas com a abertura do Tétis (entre o Miocénico Médio e os 1,8 Ma); ii) subsequente reactivação destas falhas com movimento de desligamento direito (~1,8 Ma até ao presente) ao mesmo tempo que o PAGC se continuava a desenvolver. Os resultados excluem a possibilidade de existência de um sistema de desligamentos (SWIM) a cortar um prisma acrecionário inactivo (PAGC). Estes resultados suportam ainda uma nova interpretação do sistema SWIM, na qual estes desligamentos resultam fundamentalmente da reactivação direita da antiga fronteira de placas do extremo ocidental do oceano Tétis Alpino.

A cartografia detalhada realizada na região da Planície Abissal da Ferradura permitiu também reconhecer um novo padrão morfo-tectónico existente na zona de intersecção (zona de canto) da falha SWIM 1 com a falha da Ferradura. Com base no uso conjunto de modelação análoga e numérica este padrão foi interpretado como tendo resultado da interferência tectónica (desligamento-cavalgamento) entre dois dos principais sistemas tectónicos activos no Golfo de Cádis: as falhas SWIM e os cavalgamentos NE-SW.

Por último, os resultados apresentados neste trabalho favorecem um cenário tectónico hipotético no qual a actividade da zona de subducção presente sob o Arco de Gibraltar tem vindo a decrescer desde o Miocénico, ao mesmo tempo que uma zona de subducção incipiente poderá estar a desenvolver-se na Margem Sudoeste Ibérica. O Golfo de Cádis pode assim ser visto como um local onde a proximidade de uma zona de subducção pré-existente poderá estar a induzir a formação de uma nova zona de subducção no Atlântico.

Palavras-chave: Iniciação de subducção; Golfo de Cádis; Mapa Tectónico; Depressões em forma de Crescente; Interferência Cavalgamento-Desligamento.

ACKNOWLEDGEMENTS

This research project would not have been possible without the support of many people. It is a pleasure to convey my gratitude to them all in my humble acknowledgment.

I firstly would like to express my deep gratitude to my supervisors, Pedro Terrinha and Filipe Rosas, for their support and guidance. Thank you for the numerous suggestions, edits and encouragement which helped to bring this project to completion.

Financially, this work was supported by a scholarship from the Fundação para a Ciência e Tecnologia (FCT; Ref: SFRH/BD/31188/2006).

This work also benefited from the support provided by the following projects: NEAREST (European Commission); ALMOND (FCT); TOPOEUROPE/0001/2007-TOPOMED (ESF/EUROMARGINS); SWITNAME (FCT); SWIMGLO (FCT); MVSEIS (ESF/EUROMARGINS); and SWIM (ESF/EUROMARGINS).

The support by Landmark Graphics Corporation via the Landmark University Grant Program, ARCGIS-ESRI, IVS-3D Fledermaus and NASA WorldWind are also acknowledged.

I would like to thank my institutions: University of Lisbon, in the particular the Department of Geology; LNEG (Laboratório Nacional de Energia e Geologia); and IDL (Instituto Dom Luíz) for providing me crucial support, equipment and workspace.

I would like to thank Eulàlia Grácia the access to the SWIM-2006 MCS profiles and for inviting me for several cruises in the Gulf of Cadiz and Alboran Sea. I also thank Nevio Zitellini for the access to MCS profiles from the Scotia Arc. Thank you also for kindly receiving me in the ISMAR Bologna.

Vasco Valadares deserves a specially thanks for being always available whenever I needed. Thank you for all your amazing pictures, helpful advices and friendship.

I am also very grateful to my colleagues and friends from the Marine Geology Unit (LNEG): Cristina Roque, Henrique Duarte, Sónia Silva, José Vicente, Tiago

Cunha, Luís Batista, João Noiva, Rui Quartau, Gabriela Carrara, Rubén Borges, Ana Fernandes and Fátima Cardoso.

Ana Costa, Sónia Silva, André Blanco, Ruth Kepler and Liliana D'Almeida are acknowledged for their help in the analog modeling lab.

Luís Matias, Satanu Bose and António Ribeiro are thanked for insightful discussions on the Gulf of Cadiz tectonics and subduction initiation.

A special thanks goes to Marc-André Gutscher for insightful discussions on the Gulf of Cadiz tectonics, and also suggestions and help in the analog modeling work.

I also thank Jacques Malavieille, Sandy Cruden, Christoph Schrank, David Boutelier, Stéphane Dominguez and Santanu Bose for insightful discussions and suggestions on analog modeling.

Jean-Pierre Henriet, Rui Taborda, Susana Lebreiro, David Piper and Hernández-Molina are thanked for insightful discussions on deep sea sedimentary processes.

A very special thanks goes to Luis Pinheiro and Vitor Magalhães, with who I shared countless days in the waters of the Gulf of Cadiz.

I also have to thank my geologist friends Rui Miranda, Ricardo Ressurreição, Ícaro Fróis, David Gamboa, Pedro Almeida, André Pinto, João Marques, Marco Ferraz, Ana Costa, Carlos Pinto, Paula Figueiredo and Carlos Nogueira for their friendship and support during these years.

I am also grateful to my non geologist friends André Trindade, David Negrão, Diogo Morgado, Manuel Caiano, João Paulo, António and Ricardo Fernandes.

To my best friend, Noémie Wouters, I thank all the love and support during these years. I would not have done it without your courage and strength.

Finally, I would also like to thank my family (in particular my mother Maria de Lurdes, my father Joaquim and my sister Helena). Thank you for the support you provided me through my entire life.

I dedicate this thesis to my dear nephews, Pedro and Diogo, whose pictures (with two big smiles) were always on my desk.

TABLE OF CONTENTS

Abstract I

Resumo V

Acknowledgments XI

Table of contents XIII

Chapter 1 – Introduction 1

1.1. Motivation 1

1.2. The Gulf of Cadiz 3

1.3. Aim of the work 7

Chapter 2 - Main acknowledged concepts 9

2.1. Subduction zones 9

2.1.1. When did subduction begin? 10

2.1.2. Subduction initiation at passive margins 12

2.2. On the closure of the Atlantic Ocean 17

2.2.1. The Scotia and Lesser Antilles arcs 18

2.2.2. The Gibraltar Arc and West Portuguese Margin 20

2.2.3. Was the 1755 Great Lisbon Earthquake triggered in a subduction zone? 21

2.3. The Gulf of Cadiz geodynamic evolution 24

Chapter 3 - Methods and data 29

3.1. Bathymetric data 30

3.2. Seismic reflection data 32

3.3. Analogue Modeling 33

Chapter 4 - The Gulf of Cadiz main tectonic features **35**

4.1. The Gulf of Cadiz Accretionary Wedge 38

4.2. The SWIM fault system 40

4.3. The NE-SW thrusts 47

4.3.1. The Horseshoe Fault 48

4.3.2. The Marquês de Pombal Fault 50

4.3.3. The Tagus Abyssal Plain Fault 51

4.3.4. The Gorringe Northern Thrust 52

4.4. Other important tectonic structures 55

4.4.1. The ENE-WSW to E-W thrust system 55

4.4.2. The Cadiz Fault 59

Chapter 5 - Paper 1 (Duarte et al., 2010; published in Marine Geology): "Crescent-shaped morphotectonic features in the Gulf of Cadiz (offshore SW Iberia)" **63**

Abstract 64

5.1. Introduction 65

5.1.1. Previous work 65

5.1.2. General tectonic setting and geomorphology 66

5.2. Methodology and data 70

5.2.1. Multibeam swath bathymetry data 70

5.2.2. Seismic reflection data 71

5.3. Morphotectonic characterization of the crescentic depressions 71

5.3.1. Morphotectonic setting: the Horseshoe Valley 71

5.3.2. Geometry of the Horseshoe Valley crescentic depressions 74

5.3.2.1. Height and slope of the crescentic depression scarps 75

5.3.2.2. Crescentic depression axial ratio – a 77

5.3.3. Sedimentary and tectonic structure of the crescentic depressions 78

5.3.3.1. Multi-channel seismic profile IAM4e 78

5.3.3.2. Middle resolution seismic profiles (PSAT-246 and PSAT-244) 81

5.4. Discussion 84

5.4.1. Active tectonics 84

5.4.2. Hypothetic hydrodynamic models 85

5.4.2.1. Bottom currents 85

5.4.2.2. Turbidity currents 86

5.4.3. Interplay between active tectonics and turbidity currents 88

5.4.4. The possible role of fluid escape processes 91

Chapter 6 - Paper 2 (Duarte et al., submitted): "Thrust - wrench interference tectonics in the Gulf of Cadiz (Africa - Iberia plate boundary in the North-East Atlantic): insights from analog models" **93**

Abstract 94

6.1. Introduction 95

6.2. Morphotectonic characterization of the study area 99

6.2.1. The SWIM-GCAW interference area 102

6.3. Analog Modeling 104

6.3.1. Experimental method 104

6.3.1.1. Material properties and scaling 104

6.3.1.2. Apparatus and initial stage 105

6.3.1.3. Procedure 106

6.3.2. Experimental results 107

6.3.2.1. Experiment 1: active thrust wedge and inactive basement fault 107

6.3.2.2. Experiment 2: active basement fault and inactive thrust wedge 108

6.3.2.3. Experiment 3: active basement fault and active thrust wedge 110

6.4. Discussion 112

6.4.1. Tectonic implications 113

6.5. Conclusions 116

Chapter appendix 6.A. – Scaling 117

Chapter 7 - Paper 3/Discussion (Duarte, in prep.): "The Gibraltar arc and the SW Iberia passive margin: a case of subduction propagation or induced subduction initiation?" **119**

Abstract 120

7.1. Introduction 121

7.2. The problem of subduction initiation at passive margins 124

7.2.1. The peri-Atlantic arcs and the "infection" of the Atlantic 125

7.3. The case study of the Gulf of Cadiz 126

7.3.1. Main tectonic features 126

7.3.1.1. The Subduction-related Accretionary Wedge 127

7.3.1.2. The NE-SW striking thrust system 129

7.3.1.3. The SWIM fault system 130

7.3.1.4. Thrust-wrench tectonic interference in the study area 130

7.3.2. Was the 1755 Great Lisbon Earthquake a subduction-related event? 131

7.4. An evolution model for the Gulf of Cadiz region 132

7.4.1. The formation of the Gibraltar Arc 132

7.4.2. The present-day tectonic driving mechanisms 135

7.4.3. The future of the NE Atlantic Gulf of Cadiz region: subduction propagation or induced subduction initiation? 136

7.5. Conclusions 139

Chapter 8 - Synthesis and conclusions 141

Suggestions for future work 146

References 147

Appendixes: 171

In Appendix:

Duarte et al. (2009): Anatomy and tectonic significance of WNW-ESE and NE-SW lineaments at a transpressive plate boundary (Nubia-Iberia).

Terrinha et al. (2009): Morphotectonics and Strain Partitioning at the Iberia–Africa plate boundary from multibeam and seismic reflection data.

Rosas et al. (2009): Morphotectonic characterization of major bathymetric lineaments in NW Gulf of Cadiz (Africa-Iberia plate boundary): insights from analogue modelling experiments.

Rosas et al. (submitted): Thrust-wrench interference between major active faults in the Gulf of Cadiz (Africa-Eurasia plate boundary, offshore SW Iberia): tectonic implications from analogue and numerical modeling.

Chapter 1
Introduction

1.1. Motivation

Earth is a singular planet and plate tectonics is one of its most distinctive features. Missions to other planets and moons revealed that the Earth is the only body in the solar system with subduction zones and an active plate tectonic regime (Stern et al., 2004; Stevenson, 2003). One of the most paradigmatic concepts in the plate tectonics theory is the Wilson Cycle which states that oceans form, evolve and close (Wilson, 1966). This dynamic process is based on the fact that the Earth's lithosphere is composed of several plates separated by three types of boundaries: divergent, transform and convergent (Isacks et al., 1968; Vine and Hess, 1970). Subduction zones are the convergent boundaries where oceanic lithosphere is recycled in the mantle, allowing the differentiation of continents and heat transfer from the Earth's interior (Stern, 2002). The Wilson Cycle requires that after a certain time of an ocean evolution, passive margins are reactivated and subduction initiates. However, the process by which a passive margin converts into an active margin is still controversial and fundamentally unknown (e.g. Mueller and Philips, 1991; Stern, 2002 and 2004; Gurnis et al., 2004; Nikolaeva, et al., 2010). Despite the abundance of both passive and active continental margins on Earth, no obvious cases of transition between these two types of margins have been identified so far (Nikolaeva, et al., 2010). One way to overcome this apparent paradox is to consider that subduction initiation may generally be induced by the proximity of another subduction zone or by stress transference from a near collision belt. Therefore, passive margins in the proximity of a mature subduction complex would represent preferential sites for trench formation (Mueller and Philips, 1991).

The Atlantic margins are generally described as the typical case of passive margins (Gibbs, 1984). However, there are at least two regions where Atlantic oceanic lithosphere is being consumed in subduction zones: in the Scotia and in the Lesser

Antilles arcs (Deuser, 1970; Schellart and Lister, 2004; Fig. 1.1). These subduction zones seem to have been transferred from the Eastern Pacific ocean to the Atlantic domain (Mueller and Phillips, 1991; Royden, 1993; Goren et al., 2008). These arcs potentially represent precursors to a system of convergent zones that might ultimately result in the destruction of the Atlantic Ocean (Mueller and Phillips, 1991). The Gulf of Cadiz, i.e. the foreland of the Gibraltar Arc (Figs. 1.1 and 1.2), is the third place that was described as a potential locus for subduction to propagate to open Atlantic (Royden, 1993). On the other hand, the proximity of the Gibraltar collision belt to the Southwest Iberia Margin (see Fig. 1.2), together with the existing overall convergence between Africa and Iberia, induces compressive stresses that make this margin a strong candidate for the nucleation of a new subduction zone.

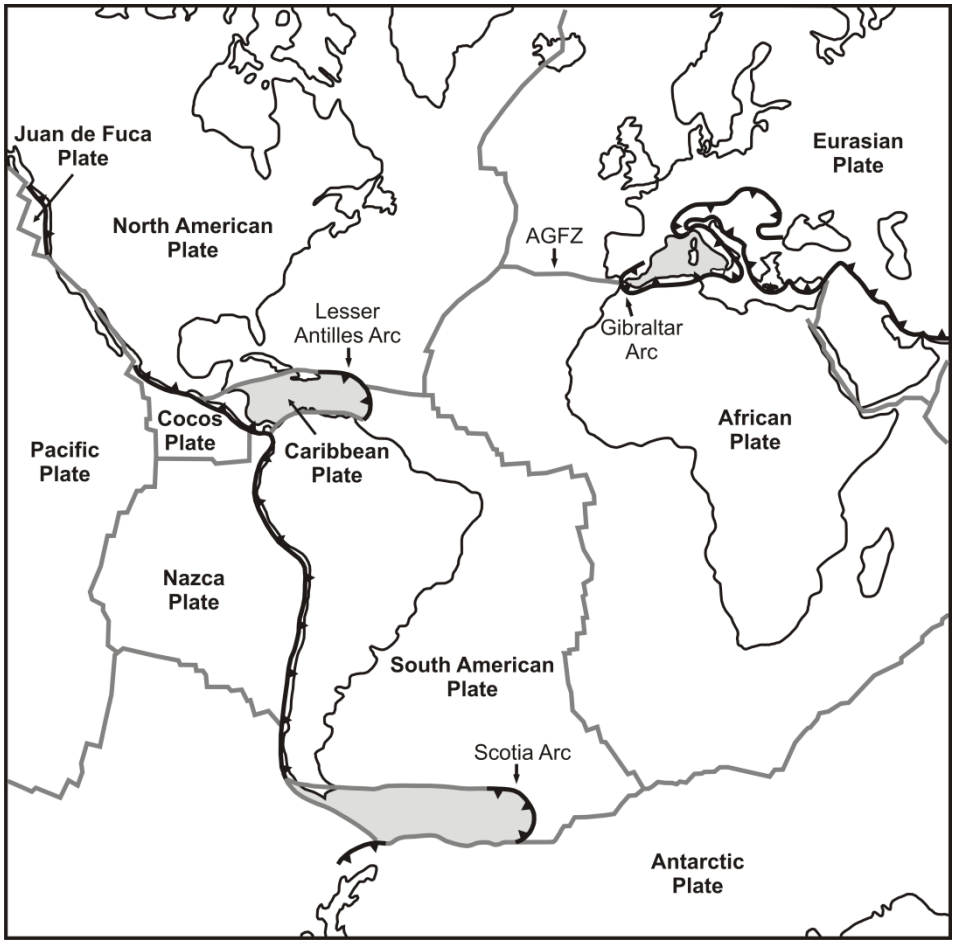


Figure 1.1 – Simplified tectonic map of the Atlantic and surrounding regions with the location of the Atlantic arcs (Scotia, Lesser Antilles and Gibraltar). Thick black lines indicate convergent plate boundaries; thick gray lines indicate divergent or transform plate boundaries (Adapted from Schellart and Lister, 2004); grey areas roughly correspond to back-arc basins.

1.2. The Gulf of Cadiz

The Gulf of Cadiz is situated in the North Atlantic Ocean, west of the Gibraltar Straits, offshore SW Iberia and NW Morocco (Fig. 1.2). It corresponds to the transition zone between the Mediterranean Alpine Collision Belt and the Atlantic Azores – Gibraltar Fracture Zone (AGFZ), encompassing a puzzling segment of the Africa-Eurasia plate boundary. Although in this region the nature of the boundary is not yet entirely understood and it is subject of a debate, geological and geophysical data point to the existence of a non-discrete lithospheric limit. In accordance, some authors described this region as a diffuse plate boundary (e.g. Sartori et al., 1994; Morel and Meghraoui, 1996; Medialdea et al., 2004; Terrinha et al., 2009; Zitellini et al., 2009), in which several differently oriented tectonic structures, mainly Northwestwards directed thrusts and W-E to WNW-ESE wrench faults, are responsible for the dissipation of the compressive stress associated to a WNW-ESE Present day convergence between Eurasia (Iberia sub-plate) and Africa (Nubia sub-plate) at a rate of ca. 4 mm/yr (Argus et al., 1989; DeMets et al., 1994; Sella et al., 2002; Calais et al., 2003; Fernandes et al., 2003; Fernandes, 2004; Nocquet and Calais, 2004; Fernandes et al., 2007).

The Gulf of Cadiz area has been proposed as the locus of the 1755 Great Lisbon Earthquake (estimated magnitude of 8.5 to 8.9; Abe et al, 1979; Johnston, 1996; Batista et al., 1998; Martinez-Solares and Arroyo, 2004) that originated a devastating tsunami and destroyed the Portuguese capital (Baptista et al., 1998; Zitellini et al., 2001; Martinez-Solares and Arroyo, 2004). The precise location of its source is subject of ongoing debate (e.g. Baptista et al., 1998; Buforn et al., 1998; Zitellini et al., 2001; Gutscher et al., 2002; Gutscher, 2004; Gracia et al., 2003b; Terrinha et al., 2003; Gutscher, 2004; Terrinha et al., 2009). Major efforts were made to map the main tectonic structures that historical and instrumental seismic events have shown to be potentially capable of generating moderate to high magnitude earthquakes (e.g. Ms=7.9 and Mw=6.0, 28/02/1969 and 12/02/2007 earthquakes respectively; Fukao, 1973 and Stich et al., 2006, 2007). New findings emerged from the interpretation of a great variety of recently acquired data (e.g. multibeam swath bathymetry, reflection and refraction seismics, geodetic), which allowed a better understanding of the Gulf of Cadiz tectonic evolution (e.g. Johnston, 1996, Gonzalez et al., 1996; Zitellini et al.,

2001; Gutscher et al., 2002, 2009a,b; Baptista et al., 2003; Gracia et al., 2003a,b; Mulder et al., 2003; Zitellini et al., 2004; Rosas et al., 2009; Terrinha et al., 2009; Zitellini et al., 2009).

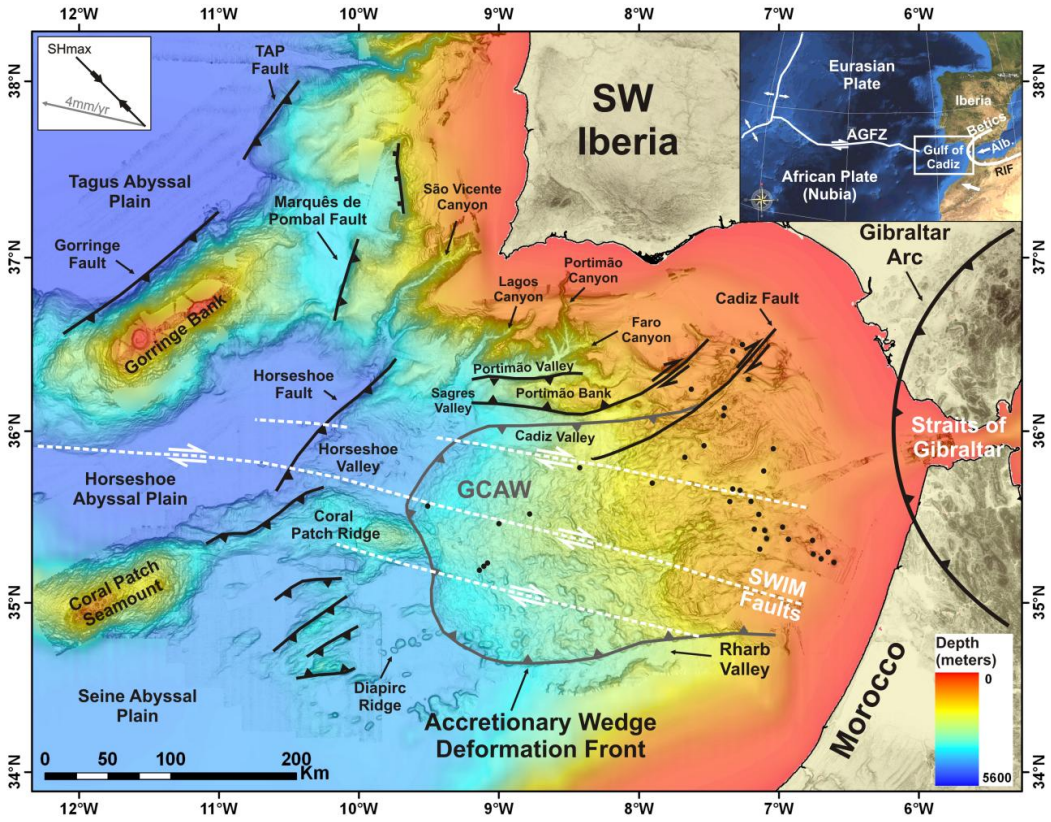


Figure 1.2 – Simplified tectonic map of the Gulf of Cadiz area (Adapted from Duarte et al., 2010; TAP Fault from Cunha et al., 2010; bathymetry and altimetry from the SWIM compilation published in Zitellini et al., 2009). GCAW - Gulf of Cadiz Accretionary Wedge; SWIM faults - dashed white lines. Black dots - mud volcanoes (Hensen et al., 2007; Duarte et al., 2010). Inset in the upper left showing (in black) average direction of the Maximum Horizontal Stresses—SHmax, and (in grey) the direction of the 4 mm/yr convergence rate between Nubia and Iberia (Nocquet and Calais, 2004; Stich et al., 2006; Fernandes et al., 2007). Inset in the upper right showing the location of the Gulf of Cadiz area in the general tectonic setting of the western Nubia - Eurasia plate boundary.

Gutscher et al. (2002), building on previously ideas put forward by other authors (e.g. Royden, 1993; Lonergan and White, 1997), considered the tectonic evolution of this area as being dominated by active retreating subduction along an E-W oceanic corridor, caused by the roll-back of an east-dipping lithospheric slab, presently positioned underneath the Gibraltar Arc (Figs. 1.3 and 1.4A). This hypothesis is compatible with the geodetic data that show a portion of the Gibraltar Arc moving

southwestwards relatively to a stable Iberia at a rate of ca. 3.5 mm/yr, and obliquely to Africa (Fig 1.4B; Stich et al., 2006; Fernandes et al., 2007; Tahayt et al., 2008). On the other hand, the West Iberia Margin also shows evidences of tectonic reactivation (see Fig. 1.4A and C), possibly as the consequence of the westward movement of the Gibraltar Arc and of the present WNW-ESE trajectory of Nubia in relation to Iberia (Terrinha et al., 2009). In this context, two end members of working hypothesis/models can be envisaged: (1) The Gulf of Cadiz subduction zone is active and retreating towards open Atlantic (Gutscher et al., 2002), comparable to what happened in the Scotia and Lesser Antilles arcs; (2) The subduction is blocked/inactive and the Southwest Portuguese Margin is being reactivated and possibly constitutes an example of an incipient subduction (Ribeiro et al., 1996). Recently, another significant tectonic feature was indentified in the Gulf of Cadiz: the SWIM faults system (Duarte et al., 2009; Terrinha et al., 2009; Zitellini et al., 2009). These faults were proposed to be the expression a newly formed plate boundary, corresponding to a broad transpressive deformation band, connecting the Gibraltar Arc to the compressive structures in the Southwest Iberia Margin (Zitellini et al., 2009; see Figs. 1.2 and 1.4C).

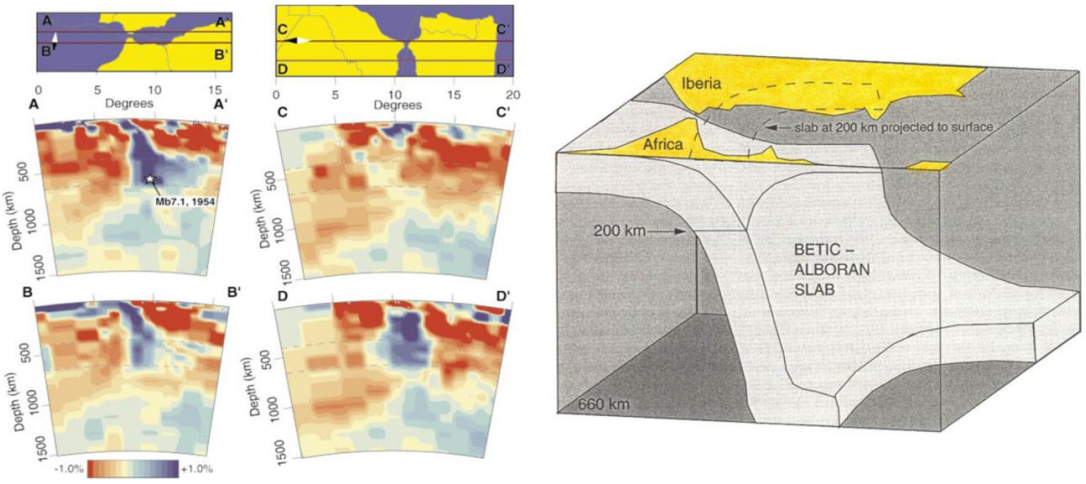


Figure 1.3 – Sections from nonlinear inversion of global earthquake traveltime data (Bijwaard and Spakman, 2000; Gutsher et al., 2002). A-A' and B-B': East-west sections showing a continuous high-velocity P-wave anomaly descending from Atlantic domain in Gulf of Cadiz to merge with region of deep-focus earthquakes below 600 km depth beneath Granada (see Fig. 1.4A). This anomaly was interpreted as a slab of Mesozoic oceanic lithosphere (see scheme on the right; Spakman and Wortel, 2004). C-C' and D-D9' North-south cross sections show a narrow "slab" (<200 km width) at shallow depth (40–150 km) beneath Gibraltar and deeper to east.

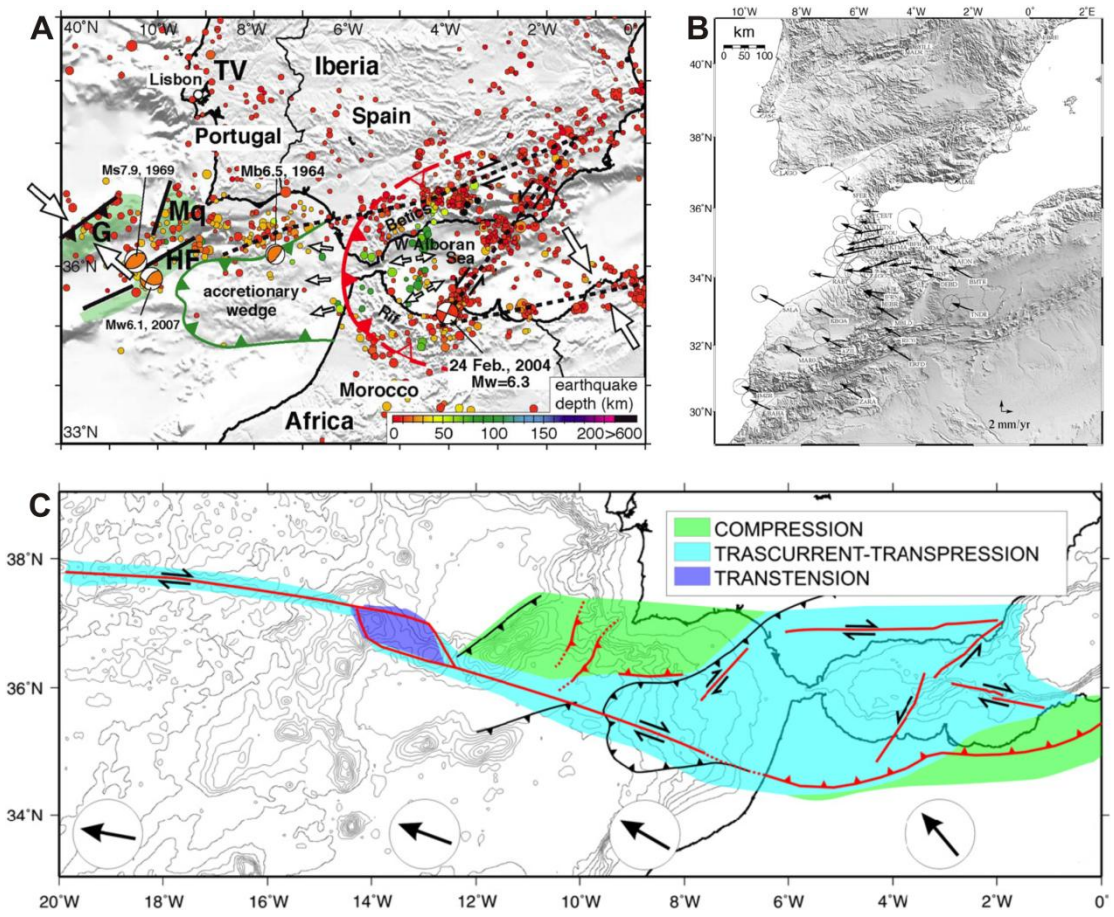


Figure 1.4 – (A) Active subduction model proposed by Gutscher et al. (2002; 2004; 2009). Red thrust teeth symbols indicate Gibraltar Arc; green thrust teeth symbols indicate the GCAW. Seismicity from Engdahl et al. (1998; M ≥ 3); (B) GPS velocity field with respect to the Eurasia plate. Ellipses delimit the region of 95% confidence (Tahayt et al., 2008); (C) Model proposed by Zitellini et al. (2009); red lines: main active faults, black lines: inactive faults, arrows: relative motion of Africa with respect to Eurasia.

1.3. Aim of the work

The initial motivation of this work was to investigate the role that orogenic arcs may have in the reactivation of passive margins, using the Gulf of Cadiz (foreland of the Gibraltar arc) and the Southwest Iberia (passive) Margin as a case study. In this context, this Ph.D. thesis specifically aims at: a) unraveling the main tectonic structures in the Gulf of Cadiz, producing a new up-dated tectonic map of the region, based on the interpretation of recently acquired bathymetric and seismic data; b) unravel the present day tectonics of this key segment of the Iberia-Nubia plate boundary, based on the interpretation of the mapped structures, seeking to know what are dominant tectonic driven mechanisms: the overall convergence between Africa and Eurasia, the westward movement of the Gibraltar Arc, or both; and c) test previous models, and newly proposed assumptions, through analogue (physical) modeling experiments.

The body of the manuscript is structured in eight Chapters. The first three Chapters correspond to the introduction of the problematic at stake and the used methods; the fourth chapter corresponds to the up-dated tectonic map of the Gulf of Cadiz region; and the following three chapters are structured as research papers (including Duarte et al., 2010; Duarte et al., submitted; and Duarte, in prep.). A final chapter of conclusions is also included in the body of the manuscript. Three research papers in which the author of the thesis is co-author and were also part of the work involved in this PhD project are incorporated as appendixes (Terrinha et al., 2009; Rosas et al., 2009; Rosas et al., submitted), together with another paper published by the author (Duarte et al., 2009)

Chapter 2
Main acknowledged concepts

2.1. Subduction zones

Planet Earth has a cool strong external layer named lithosphere. This layer is fragmented in several tectonic plates moving in relation to each other with convergent, divergent or transform kinematics above the less viscous and weaker asthenosphere. Subduction is the process that takes place at convergent boundaries by which one tectonic plate, typically more dense, sinks under another into the mantle (Fig. 2.1). The oceanic lithosphere becomes denser than the underlying asthenosphere within 20-50 Ma after it forms (Oxburgh & Parmentier, 1977; Davis, 1992). At this stage the lithosphere becomes unstable and subduction initiation is the Earth's way to maintain its thermodynamic equilibrium (Stern, 2004). In this context, subduction zones are the three-dimensional manifestation of the Earth convective downwelling, and arc-trench complexes are the crustal manifestations of a subduction zone operating beneath it (Stern, 2002). Subduction zones are defined by the inclined array of earthquakes known as the Wadati-Benioff Zone (red stars in Fig. 2.1).

One paradigmatic idea of the early Plate Tectonic Theory was that mantle thermal convection moves the lithosphere, dragging the plates as it moves (Holmes, 1929; Mckenzie, 1969). This idea is deeply rooted in the scientific and pedagogic community and it is generally spread among tectonics introductory books (Stern, 2004). However, it is now widely accepted that Earth's mantle convects mostly because cold lithosphere sinks at subduction zones (Elsasser, 1967; Hager & O'Connell, 1981; Davis & Richards, 1992; Hamilton, 2003; Stern, 2004). The base of the continents may be locally dragged by the circulating mantle but is the slab pull (and slab suction), resulting from the negative buoyancy of the cooler and denser lithosphere at subduction zones, that drives the tectonic plates (see Fig. 2.1; Elsasser, 1971; Forsyth and Uyeda, 1975;

Bott and Kusznier, 1984; Davis, 1992; Anderson, 2002; Conrad & Lithgow-Bertelloni, 2002; Hamilton, 2003). Elder (1976), based on laboratory models, also concluded that there is no direct link between asthenospheric flow and plate motion, and thus plates cannot be driven by "mantle drag" (Park, 1988). According with Lithgow-Bertelloni and Richards (1995) 90% of the force needed to move the plates is caused by the sinking of lithospheric slabs in subduction zones (slab pull), as the other 10% is originated in the rift zones, consequence of oceanic spreading (ridge push; Stern, 2004).

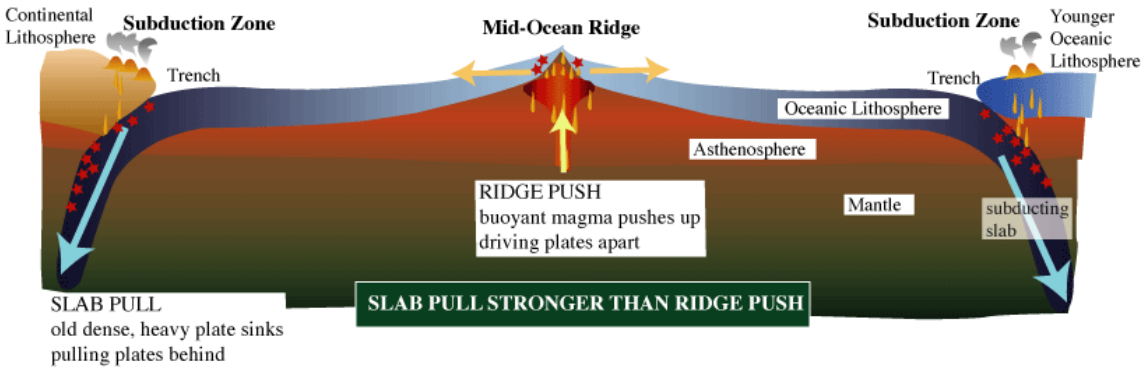


Figure 2.1 – Sketch illustrative of the two main forces driving plate tectonics: slab pull and ridge push (Extracted from UCSD-SIO15: Natural Disasters Course).

2.1.1. When did subduction begin?

One of the major challenges in modern geology is to understand how and where subduction initiates. To address this problem it is important to try to recognize when the Present plate tectonic regime was established on Earth and when did subduction become a dominant process. Given the present state of knowledge on planetary evolution, it is not reasonable to assume that the Earth had the same tectonic regime for the last 4.4 Ga. It is known that Earth was hotter in the past and consequently both crustal and mantle processes, including subduction, changed throughout the planet cooling process (Hamilton, 2003). For instance, if subduction is strongly dependent on the density increase of the oceanic crust, and this increase is the result of its cooling, it is possible to

assume that in the past, due to the higher planet's temperature, the crust probably did cool slowly and thus would take more time to become unstable and start to subduct. Also, the high heat flux probably caused high crustal melting and thickening. Given that the crust is much less denser than the asthenosphere, a thicker crust would inhibit lithosphere to sink (Stern, 2004). With this reasoning becomes clear that plate tectonics requires a planet to be in delicate thermal equilibrium (Sleep, 2000). Plate tectonics can always be shut down either by rift lock, if the mantle is too cold to allow adiabatic melting, or by trench lock, if the mantle is to hot that oceanic crust becomes too thick to subduct (Stern, 2004).

Recent studies indicate that the Earth did not have a conventional tectonic plate regime for a major part of its history. It is generally accepted that before 1.0 to 2.0 Ga the Earth's surface was not cold enough to sustain plate tectonic and subduction zones (Kontinen, 1987; Scott et al., 1992; Davis, 1992; Davis and Richards, 1992; Kuski, 2001; Hamilton, 2003; Stern, 2004). According to Hamilton (2003) the crust and upper mantle have formed a mostly closed system throughout geologic time, and their temporal changes are responses to cooling. The changing processes define a Punctuated Gradualism rather than the classical Uniformitarianism (Hamilton, 2003). Major stages in Earth evolution are (Hamilton, 2003):

(1) 4.567–ca. 4.4 Ga. Hot accretion and major irreversible mantle fractionation;

(2) 4.4–3.5 Ga. Era of nearly global felsic crust, too hot and mobile to stand as continents;

(3) 3.5–2.0 Ga. Granite-and-greenstone era. Permanent hydrosphere. Old crust cooled to density permitting mafic melts to reach surface. Diapiric batholiths mobilized from underlying old crust;

(4) 2.0 Ga–continuing. Plate tectonic era. Distinct continents and oceans. Top-down cooling of oceanic lithosphere enables subduction that drives plates and forces spreading.

Also new planetary geological data, resulting from the studies of silicate planets and moons in the Solar System, allowed the recognition of three general states of planetary evolution based on different mantle convection modes: 1) magma ocean, 2) plate tectonics and 3) stagnant lid (Sleep, 2000). Mercury, Venus and Mars, despite the

existence of some mantle convection, are presently recognized to be in the stagnant lid state. Actually, Venus may be in the transition stage from plate tectonic to stagnant lid (Stevenson, 2003). The understanding of the geodynamical past and present of the other planets and moons is one of the most promising investigation lines in the planetary geology discipline, which may help to comprehend Earth's evolution and its past geodynamical regimes. Specifically, it is crucial to understand if the Earth's plate tectonic regime with subduction zones is exclusive from our planet or if it might exist or have existed in other rocky bodies.

2.1.2. Subduction initiation at passive margins

Despite the widespread occurrence of subduction zones in our planet, the process by which a passive margin converts into an active margin is still highly controversial and fundamentally unknown (Stern, 2002; 2004; Gurnis et al., 2004; Nikolaeva et al., 2010). It is traditionally assumed that spontaneous subduction initiation at passive margins occurs when the gravitational unstable oceanic lithosphere collapses into the asthenosphere, consequence of density excess resulting from lithosphere aging. This process is a corollary of the Wilson Cycle and has been for long the most widely accepted model for trench formation (e.g. Vlaar and Wortel, 1976; Davies, 1999). However, several works showed that the strength of the oceanic lithosphere also increases with age and thus its aging by itself does not make it more susceptible to spontaneously collapse in the asthenosphere (Fig. 2.2; McKenzie, 1977; Cloetingh et al., 1984; Mueller and Phillips, 1991). This conclusion is supported by the existence of 170 Ma old oceanic crust adjacent to the NW Africa and NE America passive margins. In addition, according to Mueller and Phillips (1991), the geological record does not reveal a single example of an Atlantic-type margin evolving into an Andean-type without the intervening of an arc-continent collision. One way to explain subduction initiation is to consider that it may be induced by the proximity of another subduction zone or by stress transference from a near collision belt. Therefore, fractured passive margins and transform faults in the proximity of a mature subduction complex would represent preferential sites for trench formation (Mueller and Phillips, 1991).

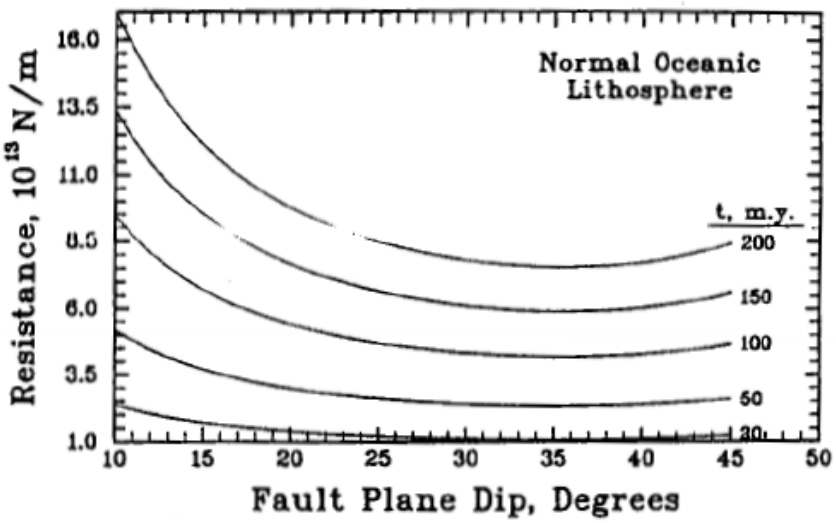


Figure 2.2 – Minimum force (per unit of distance) required to promote incipient lithospheric convergence within normal oceanic lithosphere as function of fault plane angle. Lithosphere of all ages (t) is capable of withstanding compressional stresses associated with ridge push (that are of the order of 10^{12} N/m). This is why seafloor does not spontaneously founder upon achieving negative buoyancy (Extracted from Mueller and Phillips, 1991). Note that slab pull forces may exceed 10^{14} N/m and typically are about 5 x 10^{13} N/m (Mueller and Phillips, 1991).

Stern (2004), in its seminal paper, argues that in principle subduction zones can form by two distinct ways: induced or spontaneous. In its simpler form induced subduction results from the continued plate convergence after a subduction fails due to continental collision, leading to the formation of a new subduction out of the collision zone. Note that in the case of induced subduction initiation the plates are already converging before the new subduction forms. In Figure 2.3 it is shown how this continued convergence can trigger the formation of a new subduction zone. Two sub-cases are distinguished: transference and polarity reversal. Induced initiation by transference occurs when a less dense buoyant continental bloc or submarine plateau approaches (or even enters) the subduction zone and causes it to fail. As consequence, a new subduction forms outboard of the collision zone (see fig. 2.3). Induced subduction by polarity reversal also occurs when a buoyant block approaches the trench. However, contrary to the transference case, the subduction nucleates in the original overriding plate (Stern, 2004).

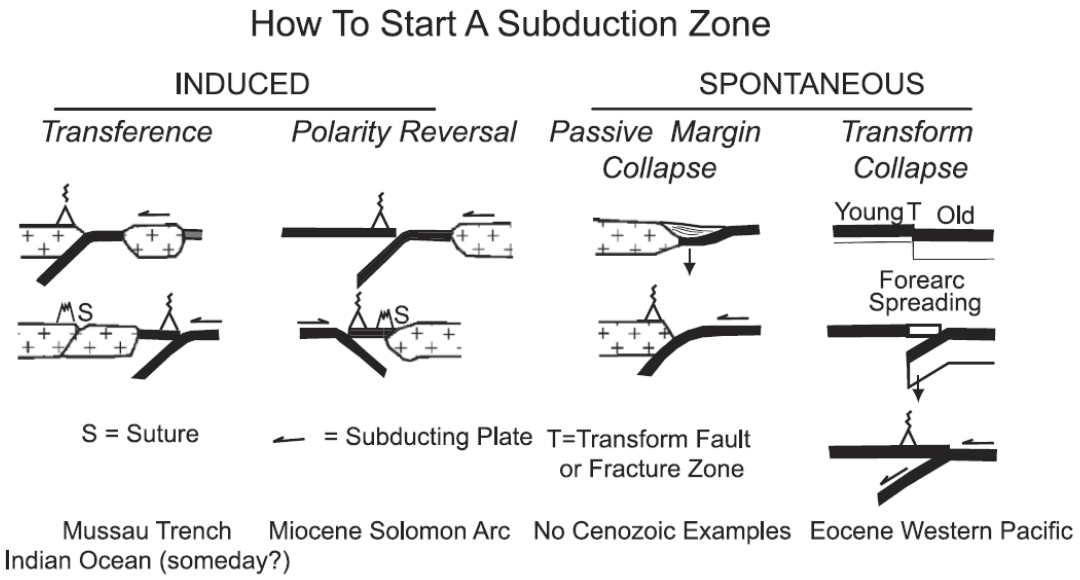


Figure 2.3 – General classes, subclasses and examples of how subduction zones form (Extracted from Stern, 2004).

In Figure 2.3 are also shown two possible ways for a subduction to initiate spontaneously: passive margin collapse and transform collapse. The first corresponds to the model of passive margin collapse due to density excess and sedimentary loading traditionally required for the closing phase of the Wilson cycle. In this examples convergence only start after the subduction, corresponding to a newly formed plate boundary, is completely developed. However, as mentioned above, it is known that lithosphere becomes more rigid with aging and thus this process requires some kind of weakening mechanism like serpentinization or the existence of a pre-fractured extensional zone, since lithosphere easily fails when subjected to traction forces (Clothing et al., 1989; Stern, 2004). Furthermore, Stern (2004) shows that there is no known example of spontaneous subduction nucleation in the Cenozoic, and that Pre-Cenozoic examples should be avoided because the evidences are ambiguous and reconstructions more conjectural. Also, Mueller and Philips (1991) demonstrate that simple models of passive margin collapse cannot be quantitatively substantiated and are not evident in the geological record. Nevertheless, if plate tectonics started sometime in the Precambrian and plates are driven by slab pull at subduction zones, then spontaneous nucleation of at least one subduction zone is required to first set the plates in motion (Stern, 2004), unless there was a progressive transition mode, from the “pre-

plate-tectonics" regime to the present-day plate tectonics regime, in which segments of the lithosphere were already sinking in the asthenosphere.

Figure 2.3 also shows another possible way for a spontaneous initiation of subduction: along a transform boundary or a fracture zone. This may occur when one of two juxtaposed plates collapse as consequence of density differences. However, recent geodynamical modeling carried out by Hall et al. (2003) demonstrate that this process requires a previous plate convergence of about 2 cm/yr to overcome plate strength (Stern, 2004).

Nikolaeva et al. (2010) synthesized several previously proposed forces/mechanisms/processes besides slab pull and ridge push that could account for subduction initiation (Table 2.1), however, the ongoing debate on this topic in the scientific community is still far from a consensus. Some authors even proposed that subduction initiated on the Earth by exogenic processes such as meteorite impacts (Hansen, 2007). There is not even agreement on whether old passive margins constitute likely sites for subduction initiation, as required by the traditional closing phase of the Wilson cycle. Thus, the identification of an incipient subduction at a passive margin is one of the major challenges in the modern plate tectonics. A natural case study would permit to constrain the previously vast amount of proposed models and allow a better understanding of one of the most enigmatic processes on Earth: the formation of a subduction zone. In the present work, we explore the possibility of the Gulf of Cadiz tectonic setting as being one natural case of subduction initiation.

Table 2.1 – Several proposed hypothesis for subduction initiation (Adapted from Nikolaeva et al., 2010)

Forces/Processes/Mechanisms	Examples in literature
Plate rupture within an oceanic plate or at a passive margin.	McKenzie, 1977; Dickinson and Seely, 1979; Mitchell, 1984; Mueller and Phillips, 1991
Reversal of the polarity of an existing subduction zone.	Mitchell, 1984
Change of transform faults into trenches.	Uyeda and Ben-Avraham, 1972; Hilde et al., 1977; Karson and Dewey, 1978; Casey and Dewey, 1984
Sediment or other topographic loading at passive margins.	Dewey, 1969; Fyfe and Leonardos, 1977; Karig, 1982; Cloetingh et al., 1982; Erickson, 1993; Pascal and Cloetingh, 2009
Forced convergence at oceanic fracture zones.	Mueller and Phillips, 1991; Toth and Gurnis, 1998; Doin and Henry, 2001; Hall et al., 2003; Gurnis et al., 2004
Tensile decoupling of the continental and oceanic lithosphere due to rifting.	Kemp and Stevenson, 1996
Rayleigh-Taylor instability due to a lateral buoyancy contrast within the lithosphere.	Niu et al., 2003
Addition of water into the lithosphere.	Regenauer-Lieb et al., 2001; Van der Lee et al., 2008
Spontaneous thrusting of the buoyant continental crust over the oceanic plate due chemical density contrast.	Mart et al., 2005
Small-scale convection in the sublithospheric mantle.	Solomatov, 2004
Interaction of thermal-chemical plumes with the lithosphere.	Ueda et al., 2008

2.2. On the closure of the Atlantic Ocean

The absence on Earth of oceanic crust older than 200 Ma, with the exception of a small portion of Tethyan crust in the eastern Mediterranean (Fig. 2.4), suggests that new subduction systems should initiate repeatedly (Goren et al., 2008). Passive margins are the reasonable place for trench formation since most of the existing subduction zones are located along continental margins (Goren et al., 2008; Nikolaeva et al., 2010). Also, the current state of relatively young oceanic lithosphere is best achieved by subducting the oldest oceanic lithosphere, which occurs at passive margins, before younger oceanic lithosphere (Goren et al., 2008; Nikolaeva et al., 2010).

The oldest oceanic lithosphere in the Atlantic basin is about 170 Ma, preferably located near the passive margins that almost entirely bound this ocean (see Fig. 2.4). According to some authors, the Atlantic has already entered in its closing phase (e.g. Mueller and Philips, 1991; Ribeiro et al., 2006). In fact, there are already two places where Atlantic oceanic crust is being consumed in subduction zones: in the Scotia arc and in the Lesser Antilles arc (Deuser, 1970; Goren et al., 2008; see Figs. 1.1 and 2.4). These arcs may be the precursors of a system of convergence zones that might ultimately result in the closing of the Atlantic Ocean (Mueller and Philips, 1991).

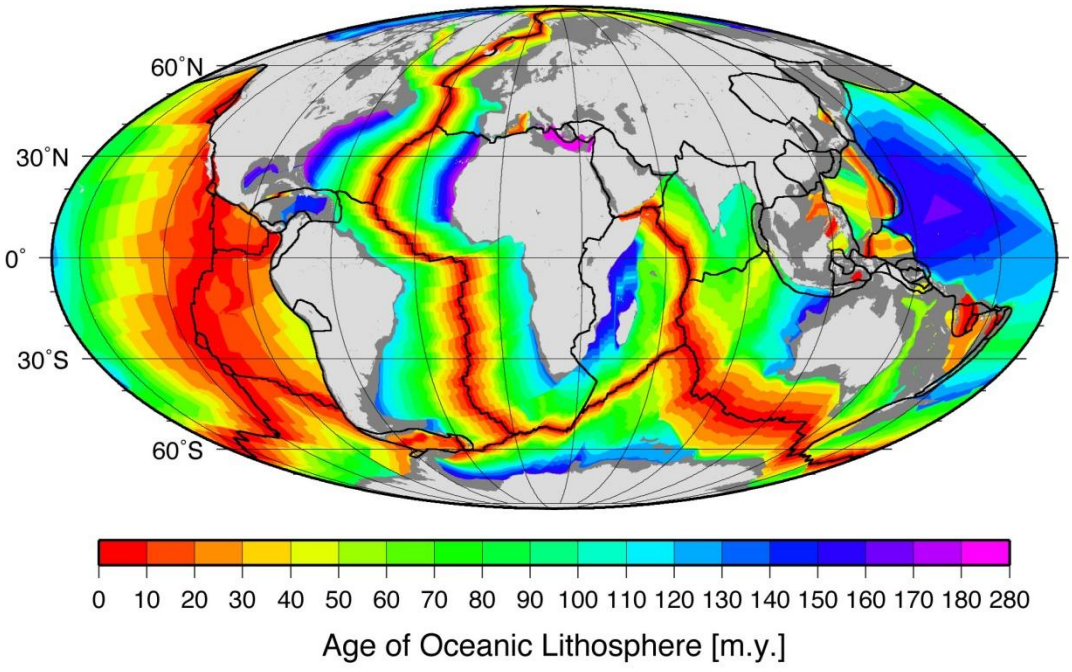


Figure 2.4 – Worldwide map of the oceanic lithosphere age (Extracted from Muller et al., 2008).

2.2.1. The Scotia and Lesser Antilles arcs

The Scotia and the Lesser Antilles arcs (see Fig. 1.1) seem to correspond to two cases of induced subduction initiation. Some authors proposed that once existed a continuous east deeping subduction system extending from NW American margin to the Antarctica (e.g. Goren et al., 2008; Fig. 2.5A). The two narrow continental landmasses existing between the Pacific and the Atlantic (marked with ellipses in Fig. 2.5) may have allowed the transmission of stress between basins, inducing the nucleation of two subduction zones in Atlantic domain (Fig. 2.5B). According with Mueller and Phillips (1991), in the Caribbean region the Pacific and Atlantic crust may even had been in direct contact by a corridor of oceanic crust generated during a rifting phase between North and South America. Goren et al. (2008) speculated that the nucleation of the Atlantic subductions was facilitated by the addition of water and melts into the upper continental plates, weakening it and reducing its viscosity (see Fig. 2.5C). Both the Scotia and the Lesser Antilles arcs then retreated around 2000 km to their present position. The subduction of Atlantic seafloor occurred simultaneously with seafloor spreading in the back-arcs. Having reached the open ocean, the advance across oceanic lithosphere is essentially unhampered because an almost limitless supply of negatively buoyant lithosphere is available to drive subduction (Royden, 1993).

Mueller and Phillips (1991) used an interesting and, in accordance with the authors, particularly imaginative analogy. They consider that the introduction of subduction zones into a previously pristine oceanic basin (i.e. without subduction zones) might be viewed, figuratively, as a contagious process in which an “infected” ocean (i.e. with subduction zones) infects an uninfected basin. Once that the first subduction zone has invaded the pristine ocean the potential to multiply and eradicate the entire basin clearly exists. The exact form by which this process may occur is still unclear and in some extent speculative. Nevertheless, two additional important characteristics of the Scotia and Lesser Antilles arcs are conspicuous. Firstly, both these arcs are retreating bounded by transform faults and trenches that do not seem to be propagating laterally (see Fig. 1.1.). Secondly, both the Scotia and Lesser Antilles arcs are propagating along two transform plate boundaries that connect the arcs to the Mid-Atlantic Ridge (see Figs. 1.1 and 2.4). There is a striking similarity between these two arcs and the Gibraltar Arc (see Fig. 1.1), which is also connected to the Mid-Atlantic Ridge by the Azores-

Gibraltar Fracture Zone, a transform plate limit extending from the Azores triple junction to the Gulf of Cadiz, the foreland of the Gibraltar Arc (see Figs. 1.1 and 1.2). This work investigates the possibility of this area to correspond to the third place where an initial stage of the subduction "infection" process might be occurring at present, in accordance with some ideas addressed by Mueller and Phillips (1991) and Royden, (1993).

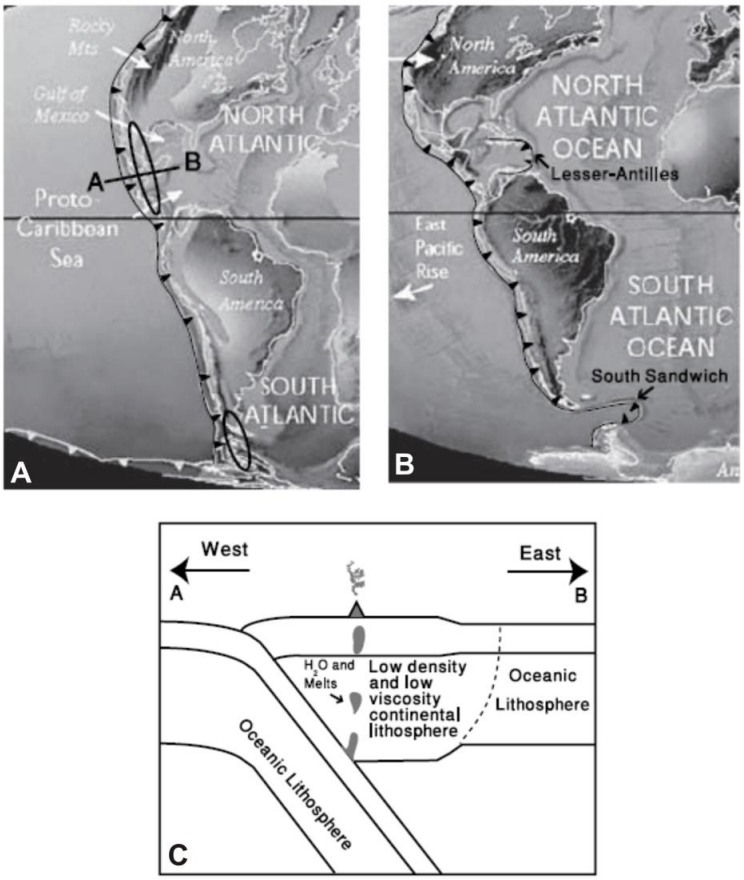


Figure 2.5 – (a) Paleo-tectonic configuration of the Americas during the Late Cretaceous, showing a continuous subduction system to the west of the continents (marked by black triangles), and narrow continental masses (black ellipses). (b) Paleo-tectonic configuration of the Americas during middle Miocene, showing two new segments of subduction, the Lesser Antilles and South Sandwich (Scotia) arcs, to the east of the continents, correlated with the locations of the narrow continental strips. (c) Schematic model (proposed by Goren et al., 2008) of the lithosphere-asthenosphere structure along section AB as appears in plate a. Subduction beneath a narrow continental lithosphere is favorable for the development of lateral density contrast that may lead to low-angle subduction. Subduction system with east dipping slab is active to the west of a narrow strip of continental lithosphere. Water and melts induced by the active subduction infiltrate into the upper continental plate, weaken it and reduce its density and viscosity. As a result, a density contrast develops between the narrow continental lithosphere and the oceanic lithosphere to its east. Then, low-angle subduction to the east of the continent with a west dipping slab may develop (Extracted and adapted from Goren et al., 2008).

2.2.2. The Gibraltar Arc and West Portuguese Margin

The subduction zone now present beneath the Gibraltar Arc developed within the Mediterranean Alpine Collision Belt and is a remnant of the subduction system that consumed most of the Western Mediterranean Tethyan Ocean (see bellow section 2.3). Royden et al. (1993) suggested that this subduction is still retreating westwards toward Atlantic domain (see Fig., 1.1). This idea was at the time somehow speculative and lacking the support of geophysical data. Also, further works presented by Lonergan and White (1997) and Maldonado et al. (1999) suggested that the subduction was inactive since Miocene times. The idea of a present day active slab roll back was re-introduced by Gutscher et al. (2002) who related the existence of an east dipping slab below the Gibraltar Arc (Bijwaard and Spakman, 2000) to the presence of a west verging accretionary wedge (GCAW) in the Atlantic domain (see Figs. 1.2, 1.3 and 1.4). The authors proposed that the slab is retreating along an East-West corridor of oceanic lithosphere that once connected the Tethyan and the Atlantic oceanic basins (Fig. 2.6; see section 2.3). Several authors still argue that the Gibraltar subduction system is no longer active (e.g. Zitellini et al., 2009) or that it had diminished dramatically its activity since latest Miocene times (Terrinha et al., 2009). According to Terrinha et al. (2009), the present stress regime caused the migration of the deformation from the realm of the GCAW to the west (onto the Horseshoe fault region; Fig. 2.7) and to the north along the West Portuguese Margin. The 300 km long NE–SW trending fault system (Horseshoe, Marquês do Pombal, Gorringe and Tagus Abyssal Plain faults; see Figs. 2.7 and 1.2) is considered by the authors as the expression of the propagation of a new compressive deformation front, which will eventually lead to the nucleation of a West Iberian subduction zone, as proposed by Ribeiro et al. (1996; Fig. 2.8). In addition, the tomography data presented in Gutscher et al. (2002) suggests that the Horseshoe Fault may penetrate at least till 100 km in the lithosphere. On the other hand, Masson et al. (1994) also speculated that subduction may be nucleating further north in the Iberian Abyssal Plain ocean-continent transition (see Fig. 2.8). Here a thinned rifted crust is overlying a body of serpentinized peridotite. Serpentinization can provide an efficient weakening mechanism that may facilitate lithospheric rupture and subduction initiation (Cloetingh et al., 1984; Masson et al., 1994)

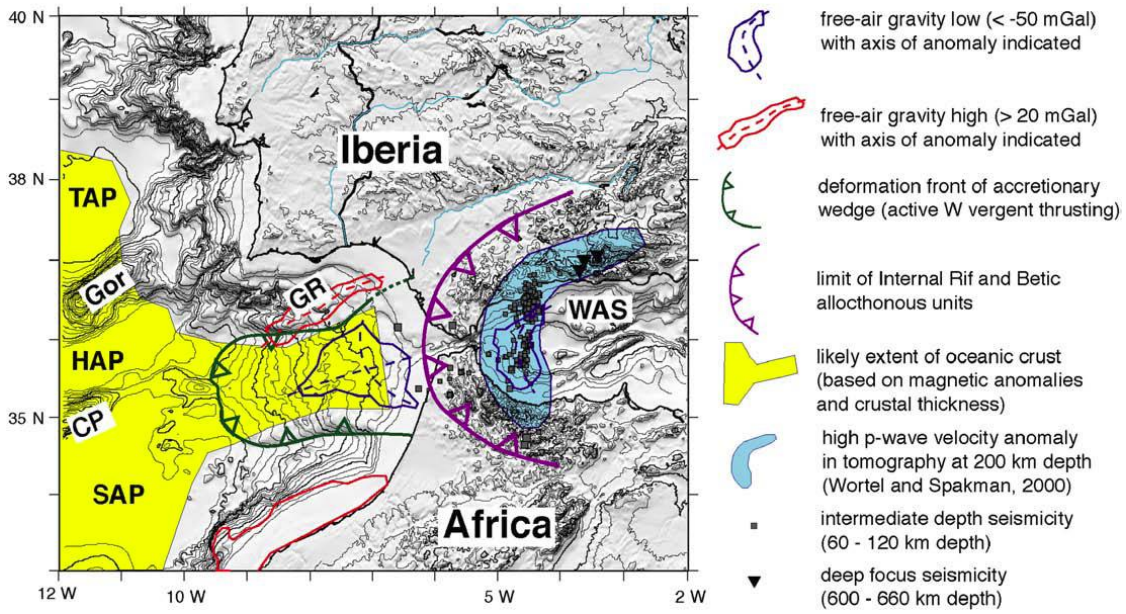


Figure 2.6 - Relief map of Southern Iberia region with location of arcuate structures, along the trend of the straits of Gibraltar, shown in map view (see explanation in figure). Regions likely floored by oceanic crust are shown in yellow. Note the narrow E-W oceanic corridor between South Portugal and NW Morocco. TAP - Tagus Abyssal Plain, HAP - Horseshoe Abyssal Plain, SAP - Seine Abyssal Plain, Gor - Gorringe Bank, CP - Coral Patch seamount, GR - Guadalquivir Ridge; WAS - West Alboran Sea. (Extracted from Gutscher et al., 2009).

2.2.3. Was the 1755 Great Lisbon Earthquake triggered in a subduction zone?

The 1755 Great Lisbon Earthquake had an estimated magnitude of 8.5 to 8.9 and is one of the highest magnitude earthquakes in the history of Europe (Johnston, 1996; Batista et al., 1998). Several structures were proposed to be the source of this earthquake: e.g. the Gorringe Bank (Johnston, 1996), the Marquês de Pombal fault (Zitellini et al., 2001) and the Tagus Valley fault (Vilanova et al., 2003). However, the empirical relationships proposed by Wells and Coppersmith (1994) indicate that such release of elastic energy requires a rupture area of approximately 27,000 km^2 and a fault length of around 370 km (Gutscher et al., 2009a). Since the above structures are not long enough to produce such energy (see Figs. 2.7 and 1.2), they were progressively abandoned as possible sources. To overcome this difficulty, other models proposed the

existence of two faults acting simultaneously to generate the 1755 event by adding up their rupture areas: e.g. the Marquês de Pombal fault and the Horseshoe fault (Terrinha et al., 2003; Gràcia et al., 2003a,b; see Fig. 2.7) and the Marquês de Pombal Fault and the Guadalquivir Bank Fault (Baptista et al., 2003). Also, Zitellini et al. (2009) proposed a possible link between the Horseshoe and the SWIM faults that together can comprise in total more than 400 km of connected fault segments (see Fig. 1.2). This last hypothesis was investigated in detail by Rosas et al (submitted) and is also part of the work involved in this PhD project (see appendix).

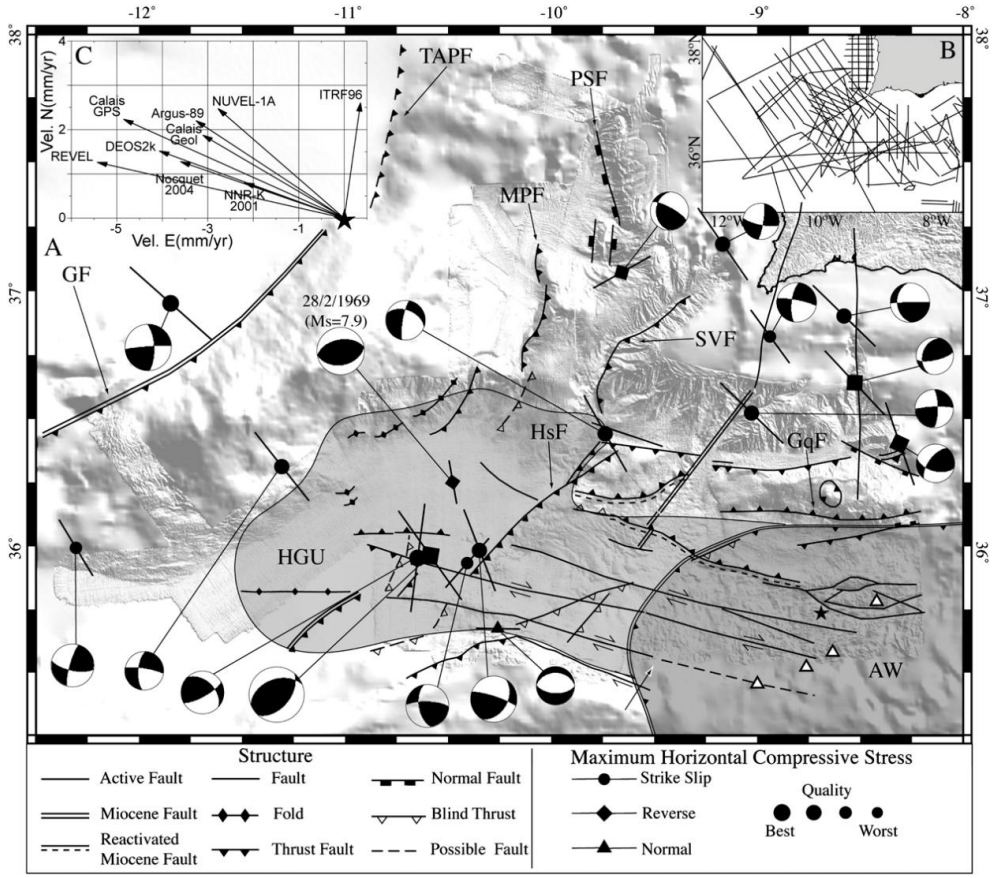


Figure 2.7 - A) Structural map of the Southwest Portuguese Margin with a compilation of stress indicators and focal mechanisms. Stress indicators computed from earthquake focal mechanisms and faults from interpretation of MCS profiles dataset shown in inset B). Mud volcanoes - white triangles; AW – Accretionary Wedge; GbF — Portimão/Guadalquivir fault; GF – Gorringe fault; HGU – Horseshoe Gravitational Unit; HsF – Horseshoe fault; MPF – Marquês de Pombal fault; PSF – Pereira de Sousa fault; SVF — S. Vicente fault; TAPF — Tagus Abyssal Plain fault. C) Plate kinematic data taken from various indicated sources. Black star shows position of computed movements of Nubia with respect to Iberia (Extracted from Terrinha et al., 2009, in appendix).

Alternatively, Gutscher et al. (2002) and Gutscher (2004) proposed that the 1755 Great Lisbon Earthquake was generated in the Gibraltar subduction fault plane. Their argument was mostly based on extensive geological and geophysical data, but also in the fact that most of the large magnitude earthquakes (M≥8.5) are generated in subduction zones. Accordingly, 11 of the 12 greatest earthquakes (M≥8.5) of the past 100 years occurred along subduction fault planes (the exception was a magnitude 8.6 earthquake in the Himalaya collision belt). However, the Gulf of Cadiz subduction fault plane shows negligible instrumental high magnitude seismic events. Gutscher et al. (2006) offers three possible explanation for such an absence: (1) the subduction is inactive and has ceased; (2) the subduction is active, but aseismic; (3) the subduction is active and a locked seimogenic zone exists, gradually accumulating stress until it releases the next great earthquake, a similar behavior as the Nankai (SW Japan), Cascadia (NW USA), and Northern Sumatra (Indonesia) subduction zones. Based on recently acquired seafloor and GPS data the authors favor the last hypothesis.

Ribeiro et al. (2006) agree that the source mechanism of such a large earthquake requires generation at a subduction zone. However, they proposed that the source was not the Gibraltar subduction, but an incipient subduction zone that is presently developing in the West Iberia Margin (Fig. 2.8). Also Terrinha et al. (2009) proposed that the Horseshoe, Marquês de Pombal and Tagus Abyssal Plain compressive structures (the crustal expression of this hypothetical incipient subduction zone; see Fig. 2.7) may be linked at depth and thus providing a possible and reliable source mechanism for the generation of the 1755 Great Lisbon Earthquake.

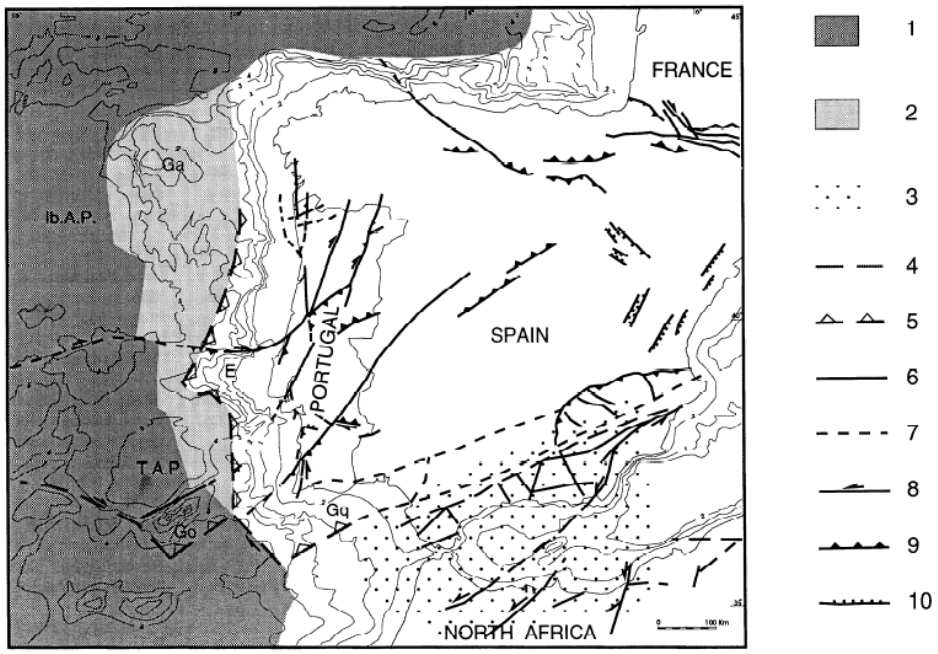


Figure 2.8 – Regional geodynamical framework of Iberia and the incipient subduction at the West Iberia Margin as proposed by Ribeiro et al. (1996). Numbers indicate: 1 - oceanic crust; 2 - thinned continental crust; 3 - diffuse plate boundary; 4 - plate boundary (approximate location); 5 - subduction south of Gorringe and Guadalquivir banks and along the base of the western continental slope; 6 - active fault; 7 - probable active fault; 8 - active fault with significant strike-slip movement; 9 - reverse fault; 10 - normal active fault. Abbreviations are: Ga - Galiza bank; Ib.A.P - Iberia Abyssal Plain; E - Estremadura high; T.A.P. - Tagus Abyssal Plain; Go - Gorringe bank; Gq - Guadalquivir bank.

2.3. The Gulf of Cadiz geodynamic evolution

The tectonic features present in the Gulf of Cadiz (see Fig. 1.2) are the result of a complex tectonic evolution including rifting, compression and strike-slip motion between Africa and Eurasia since the Triassic (Wilson et al., 1989; Dewey et al., 1989; Maldonado et al., 1999; Terrinha et al., 2009). During the Mesozoic, this area was part of the more occidental Alpine-Tethys rift system (see Fig. 2.9) that comprised an oceanic domain separating two newly formed passive margins. (Dercourt et al., 1986; Sanz de Galdeano, 1990; Srivastava et al, 1990a; 1990b; Maldonado et al., 1999; Stampli et al., 2002). This domain included several spreading axes and transform faults that formed as result of the extensional reactivation of Variscan structures (Terrinha, 1998).

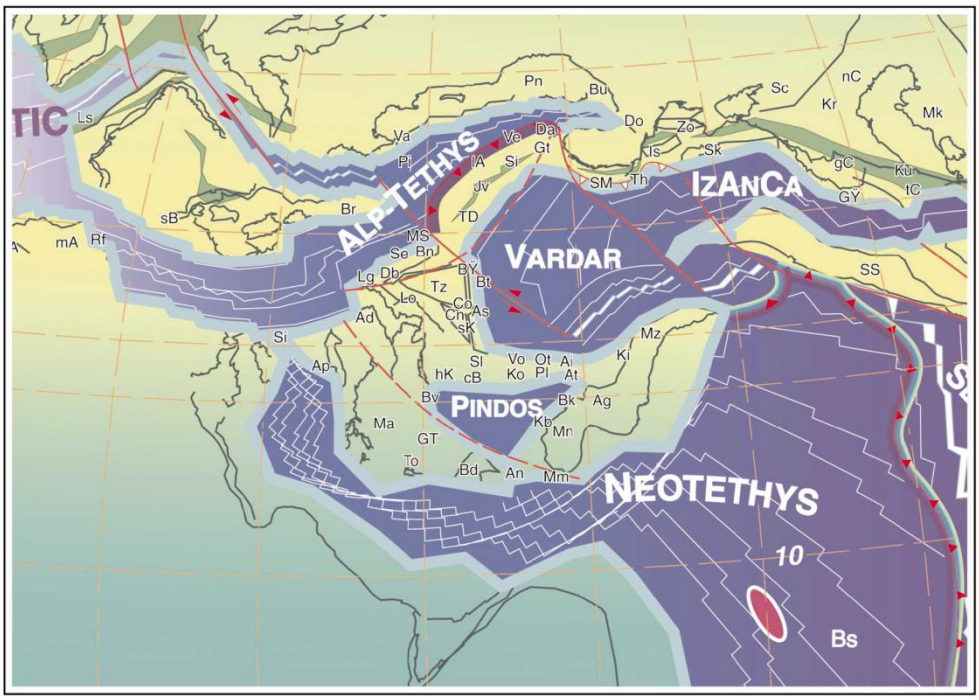


Figure 2.9 – Reconstructions of the Western Tethyan realm in the Aptian, Lower Cretaceous (~120 Ma.). Note the position of the Iberian Peninsula at the left top, before initiating its Cretaceous 35º counterclockwise rotation (Stampli et al., 2002).

In the Eocene-Oligocene most of the Gulf of Cadiz (and SW Iberia) Mesozoic rifting faults were tectonically inverted as the result of the convergence between Africa and Eurasia that started in the Upper Cretaceous (Terrinha et al., 2009). This convergence was accommodated by northwards dipping subduction of the Alpine-Tethys oceanic lithosphere that extended from the SE Iberia to the Alps (see Fig. 2.10; Rehault et al., 1985; Malinverno and Ryan, 1986; Dewey et al., 1989; Rosenbaum et al., 2002; Jolivet et al., 2006). Since the Oligocene, the continental collision in the Alps absorbed the bulk compression of the Africa-Eurasia convergence, as consequence, the northwards Alpine-Tethys subduction along Europe's meridional margin slowed down and became primarily driven by the density collapse of the subducting oceanic slab (op.cit). This, triggered slab roll-back, which led to the formation of the West Mediterranean back-arc basins and associated continental terranes, among which the Betic-Rif (Figs. 2.10 and 2.11; Rosenbaum et al., 2002, 2004). Concomitantly, the convergence direction between Africa and Eurasia in the western Mediterranean region rotated progressively from the N-S to WNW-ESE (Maldonado et al., 1999; Fernandes et al., 2003; Fernandes, 2004).

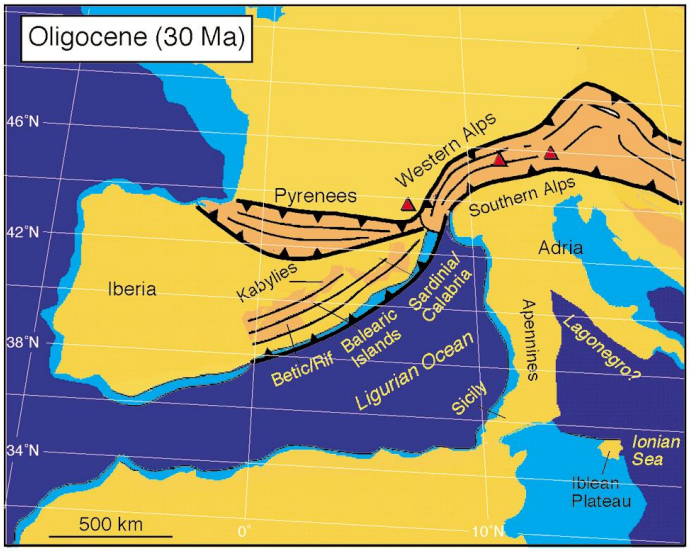


Figure 2.10 – Reconstructions of the Western Mediterranean region in the Oligocene (~30 Ma.; Rosenbaum et al., 2002). Note the existence of an oceanic corridor connecting the Tethyan Liguarian Ocean to the Atlantic and the position of the northwest dipping subduction before it started to retreat.

In the Middle Miocene, the continuation of the southwestwards drifting of the Alboran terrane (see Fig. 2.11) led to its collision with the SE Iberia and NW Africa forming the Gibraltar Arc (see Fig. 2.11; also known as Betic-Rif Arc). In the Tortonian, the westward overthrusting of the Gibraltar Arc into Atlantic domain led to the emplacement of an accretionary wedge in the Gulf of Cadiz (GCAW; see Figs. 1.2, 2.6 and 2.11; Lonergan and White, 1997; Gutscher et al., 2002). It was recently confirmed by geodetic data that the Gibraltar Arc region is moving westward at a rate of ca. 3.5 mm/yr relatively to Iberia (Fadil et al., 2006; Stich et al., 2006; Tahayt et al., 2008). According to Gutscher et al. (2002; 2009a) this movement is a consequence of the active roll back of the east dipping oceanic slab that still exists between the Iberia and Africa plates as imaged by teleseismic tomography (Gutscher et al., 2002; Spakman and Wortel, Transmed Atlas, 2004). The existence of Tethyan oceanic lithosphere in the Gulf of Cadiz beneath the accretionary wedge was recently confirmed using seismic refraction data (Sallarès et al., 2011). This oceanic corridor can provide a path for the subduction hinge retreat further west.

Presently, the Gulf of Cadiz region experiences a large scale NW to WNW directed convergence between Nubia and Iberia, at a rate of ca. 4 mm/yr (Argus et al., 1989; DeMets et al., 1994; Sella et al., 2002; Calais et al., 2003; Fernandes et al., 2003;

Fernandes, 2004; Nocquet and Calais, 2004; Fernandes et al., 2007). A general strain partitioning scenario (Terrinha et al., 2009) considers this convergence to be accommodated both along the WNW-ESE dextral strike-slip faults (including the SWIM faults), and along NE-SW westwards thrust faults, such as the Horseshoe, Marquês de Pombal and Tagus Abyssal Plain faults and the Gorringe Bank northern thrust (see Figs.1.2 and 2.7).

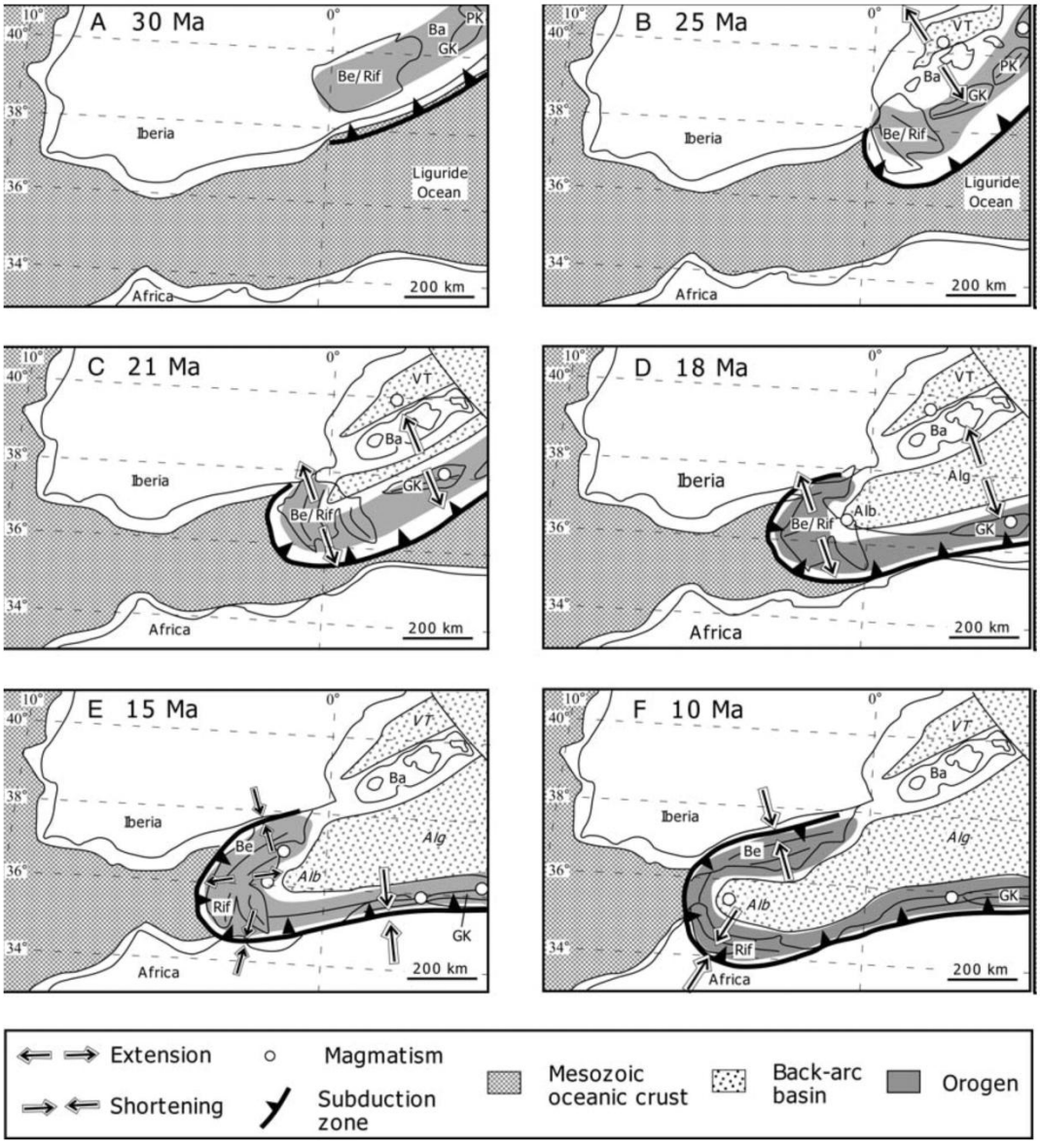


Figure 2.11 – Schematic evolution of the Gibraltar Arc/Betic-Rif arc (Rosenbaum et al., 2004). Alb - Alboran Sea; Alg - Algerian Basin; Ba - Balearic Islands; Be - Betic; GK - Grand Kabylie; PK - Petite Kabylie; VT - Valencia Trough.

Chapter 3
Methods and data

Due to the oceanic water column, direct access to the sea floor and underlying crust is very difficult. Therefore nearly all tectonic studies in marine environment require the use of geophysical methods. The present work was done based on the combined analysis and interpretation of ca. 180,000 km^2 of high-resolution multibeam swath bathymetry and more than 20,700 km of multi-channel seismic reflection profiles. The combination of bathymetric data and interpretation of the main tectonic structures in the seismic lines was the basis for a thorough morphotectonic characterization of the main structural features of the Gulf of Cadiz, which resulted in the production of a new tectonic map of the region (see next chapter). Based on this new map several geotectonic models regarding the interpretation of the tectonic evolution of the Gulf of Cadiz were proposed. Different assumptions of these interpretations were tested using sandbox analogue modeling experiments. The obtained results provided new insights regarding several problems at stake, and, I hope, progress in the understanding of the tectonics of this key segment of the Iberia-Nubia plate boundary.

3.1. Bathymetric data

The used high-resolution bathymetric dataset was produced under the European Science Foundation EuroMargins SWIM project (acronym for "earthquake and tsunami hazards of active faults at the South West Iberian Margin: deep structure, high-resolution imaging and paleoseismic signature"; Fig. 3.1). This project promoted a collaborative research agreement to coordinate marine cruises with the goal of acquiring new bathymetric data and making all existent data of the Gulf of Cadiz region available to the whole scientific community. It resulted from the compilation of 19 surveys over 200 days ship time, performed between 2000 and 2006 by teams belonging to 14 research institutions from 7 European countries (Table 3.1). Each institution provided data files and Digital Terrain Models (DTM) at a 100 m grid spacing in order to produce the SWIM multibeam compilation published and available online in Zitellini et al. (2009). Interpretation was made using terrain analysis techniques and image analysis of the bathymetry using commercial software, ArcGIS and Fledermaus.

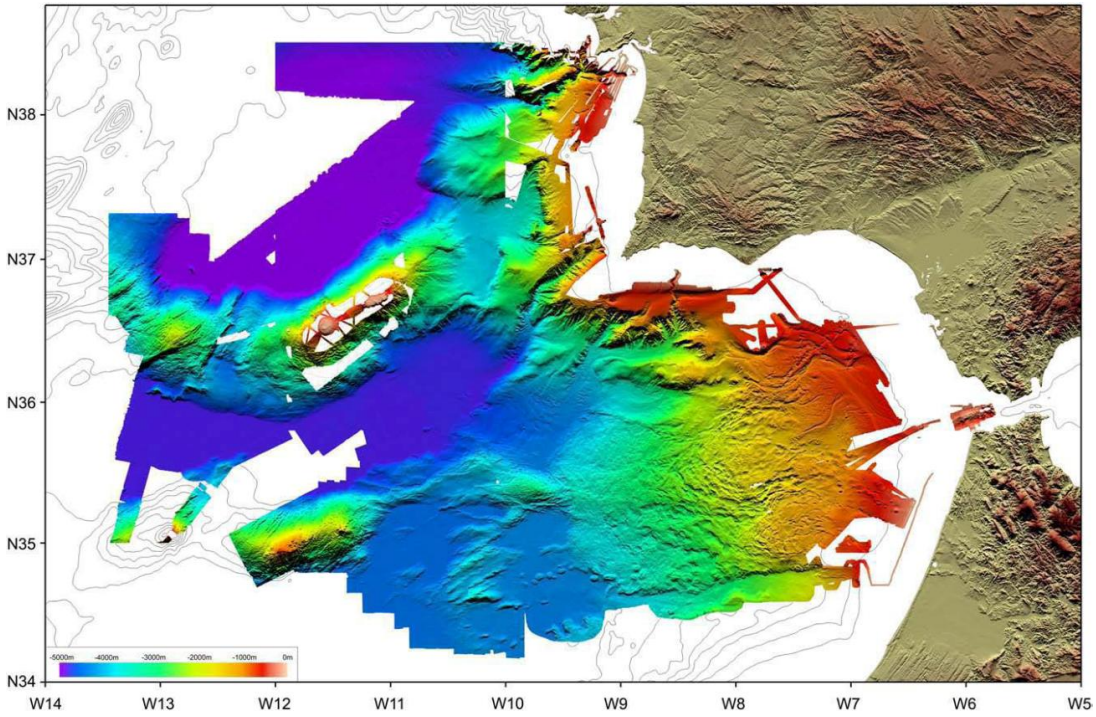


Figure 3.1 – The SWIM multibeam compilation (Zitellini et al., 2009). Swath bathymetry map compiled on behalf of the SWIM collaborative research agreement; see Table 3.1 for complete list of contributors. Color scale in meters. Background bathymetric contour lines from GEBCO digital atlas. Isobaths spacing: 200 meters. Topography from STRM 3'' (Shuttle Radar Topography Mission 3 arc-second grid), NASA.

Table 3.1 – Multibeam SWIM bathymetry data sources (Adapted from Zitellini et al., 2009)

Cruise	Year	Research Vessel	System	Institution
ESPICHEL	1991	L'Atalante	Simrad EM12D	Ifremer (France)
TASYO	2000	Hespérides	Simrad EM12S	GM-IGME (Spain)
PARSIFAL	2000	Hespérides	Simrad EM12S	UTM-CSIC, CMIMA (Spain)
CADISAR-1	2001	Le Suroît	Simrad EM300	DGO, Uni. Bordeaux (France)
HITS	2001	Hespérides	Simrad EM12S	UTM-CSIC, CMIMA (Spain)
CADIPOR	2002	Belgica	Simrad 1002	RCMG Ghent University (Belgium)
GORRINGE	2003	Urania	Reason Seabat 8101	IAMC-CNR (Italy)
TV-GIB	2003	Le Suroît	Simrad EM 300	IUEM/UBO (France)
PICABIA	2003	Marione Dufresne	Thomson Sea Falcon 11	UTM-CSIC, CMIMA (Spain)
GAP	2003	Sonne	Simrad EM 120	Uni. Bremen (Germany)
MATESPRO	2004	D. Carlos I	Simrad EM 120	CGUL (Portugal)
CADISAR-2	2004	Le Suroît	Simrad EM 300	DGO, Uni. Bordeaux (France)
DELILA	2004	D. Carlos I	Simrad EM 120	IUEM/UBO (France)
DELSIS	2005	D. Carlos I	Simrad EM 120	IUEM/UBO (France)
SWIM-2	2005	OGS Explora	Reason Seabat 8150	ISM, ISMAR (Italy)
HERMES	2006	Charles Darwin	Simrad EM 12S	NOC, Southampton (UK)
SWIM	2006	Hespérides	Simrad EM 120	UTM-CSIC, CMIMA (Spain)
Digital Terrain Model from EMEPC (Portugal) Data from R/V D. Carlos, Simrad 120				
Several R/V L'Atalante and R/V J. Charcot transit data provided by SISMER database				

3.2. Seismic reflection data

The multi-channel seismic reflection (MCS) database used in this work was compiled under the NEAREST project (acronym for "Integrated observations from NEAR shore sourcES of Tsunamis: towards an early warning system"), co-founded by the European Commission. The MCS profiles were acquired in the Gulf of Cadiz and Western Iberia Margin, from 1992 through 2006, during the geophysical missions: ARRIFANO, IAM, BIGSETS, VOLTAIRE, SISMAR and SWIM 2006 (Fig. 3.2). They were later imported into a data management and interpretation software suite from Landmark Corporation (OpenWorks, SeisWorks and ZMap-plus) at the laboratory of seismic data of the Unit of Marine Geology of the National Laboratory of Energy and Geology (LNEG – Portuguese acronym). Information on acquisition parameters and geometry of these profiles is summarized in Table 3.2. All the MCS profiles were analyzed and interpreted in order to produce the new tectonic map presented in the next chapter. Two single channel seismic profiles (PSAT 244 and 246) and a 24 channel DELSIS profile were also used in Chapter 5 (Duarte et al., 2010) and in Chapter 6 (Duarte et al., submitted), respectively.

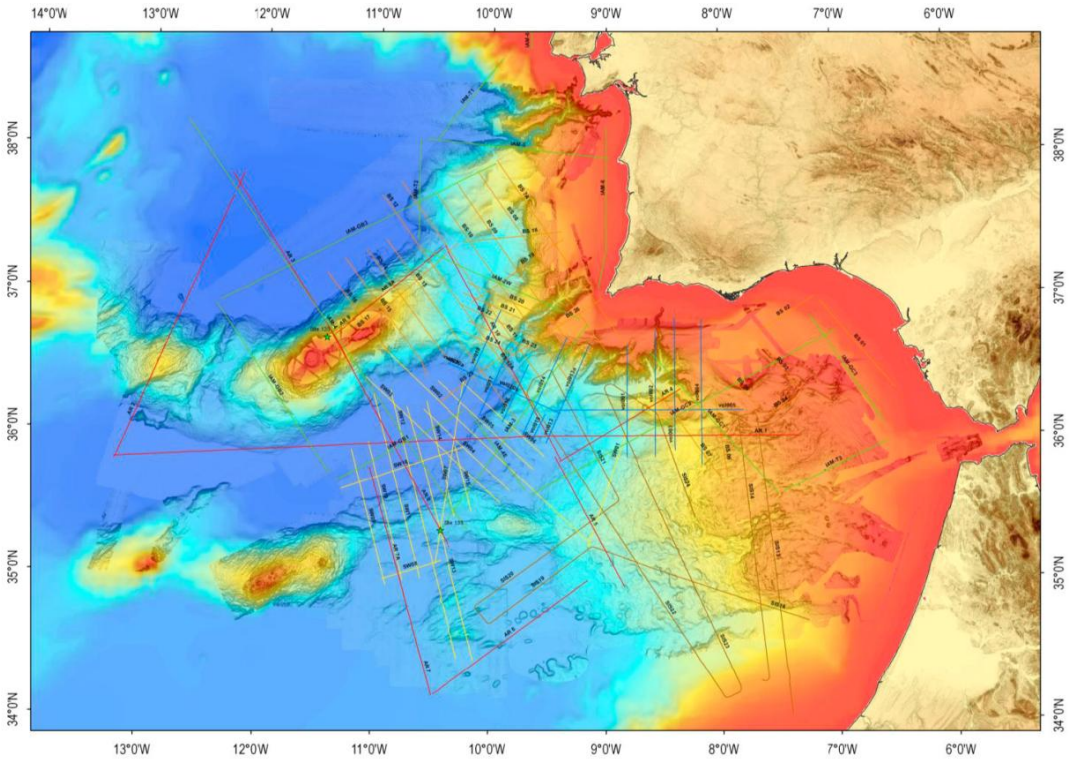


Figure 3.2 – Location of the used MCS profiles (see Table 3.2).

Table 3.2 – Parameters of the MSC profiles used in this work.

	ARIFANO	IAM	BIGSETS	SISMAR	VOLTAIRE	SWIM 2006
Year	1992	1993	1998	2001	2002	2006
Vessel	R/V Explora	Geco Sigma	R/V Urania	R/V Nadir	R/V Urania	R/Hesperides
Reference	Sartori et al. (1994)	Banda et al. (1995)	Zitellini et al. (2004)	Thiebot and Gutscher (2006)	Zitellini et al. (2002)	Martinez-Loriente et al. (2008)
Seismic source	32 aiguns	30 airguns	1 GI gun	-	2 GI guns	8 aiguns
Shooting interval	50 m	74 m	25 m	75-150 m	50 m	25 m
Sample interval	1 ms	4 ms	4 ms	4 ms	1 ms	2 ms
Nº of channels	120	192	48	360	48	96
Resampling	4 ms	8 ms	4 ms	4 ms	2 ms	-
Resolution	20 m	20 m	-	-	15 m	-

3.3. Analogue Modeling

Physical (analogue) modeling is the study of natural tectonic processes by means of simplified scaled models in laboratory. Physical modeling makes use of different materials, mostly granular and viscous with known properties, as analogues of natural rocks. The materials are chosen in order to fulfill the "similarity criteria", i.e. their physical parameters and properties are chosen to mimic geometric, kinematic and dynamic natural conditions (Hubbert, 1937; Ramberg, 1967). The similarity criteria is achieved by scaling the model through an dimensional analysis assuring that the dimension, velocities and forces in the model are proportional to those in the prototype. The purpose of analogue modeling is not simply to reproduce the natural prototype

(nature observations), but to test by controlled experiments hypotheses as to the driving mechanism of the tectonic processes (Ranalli, 2001).

In the study of nature it is only possible to access the final stage of a tectonic process, and attempt to reconstruct the possible chronological sequence of events that led to that final stage (Eulerian approach). The major advantage of analogue modeling is that it allows to simulate and test different possibilities of evolution of the original prototype, i.e. to reproduce in laboratory sequences of chronological events that may have led to that specific final stage (Lagrangian approach), at a suitable geometric scale and time ratio (Ramberg, 1967). This is of special importance because different sequence of events may lead to the same final stage. Also, the fact of laboratory models being three dimensional make it a powerful tool in the gain of a qualitative mechanical intuition of the processes at stake and the thorough identification of patterns of repeatability. Ideally, analogue modeling should be complemented with numerical modeling, which allows a more efficient thermo-mechanical and analytical approach.

In this work analogue modeling experiments were produced to better understand the deformation patterns resulting from thrust-wrench fault interference in the study area. These experiments revealed to be crucial in the understanding of the driven mechanism that account for the observed structures present in the Gulf of Cadiz. The experiments were designed according to fallowing steps:

1. Identification of a key problem;
2. Determination of the materials that satisfy the similarity criteria (scaling);
3. Building of the apparatus given the chosen scale;
4. Running the experiments;
5. Verification of the repeatability patterns of salient observables;
6. Interpretation of the obtained results;
7. Elaboration of a generalized explanatory theory or conceptual model integrating the experimental results in coherent framework;
8. Finally, integrate the modeling outcomes into the broader geodynamical evolution model of the studied area.

Since this work is partially organized in research papers and in order to avoid repetitions, all the experimental problematic, scaling, materials and used apparatus is provided in the respective analogue modeling chapters and papers.

Chapter 4
The Gulf of Cadiz main tectonic features

In the last two decades several efforts were made to produce a tectonic map of the Gulf of Cadiz active structures (e.g. Tortella et al., 1997; Medialdea et al., 2004; Iribarren et al., 2007; Zitellini et al., 2009; Fig. 4.1). Most of these maps were done using one recently acquired MCS dataset or in other cases using datasets that covered the study area in a non systematic manner. Usually the MCS surveys were obtained for thematic studies and not for the overall mapping of the Gulf of Cadiz. The novelty of the map presented in this work (Fig. 4.2) is that it was made by a thorough review of a multi-survey dataset (six MCS surveys) coupled with the analysis of the recently compiled high resolution bathymetry, which provided detailed morpho-tectonic information at the scale of the whole study area (see previous chapter). This map benefited from the existence of a stratigraphic model by Roque (2007) which correlated the different areas around SW Iberia.

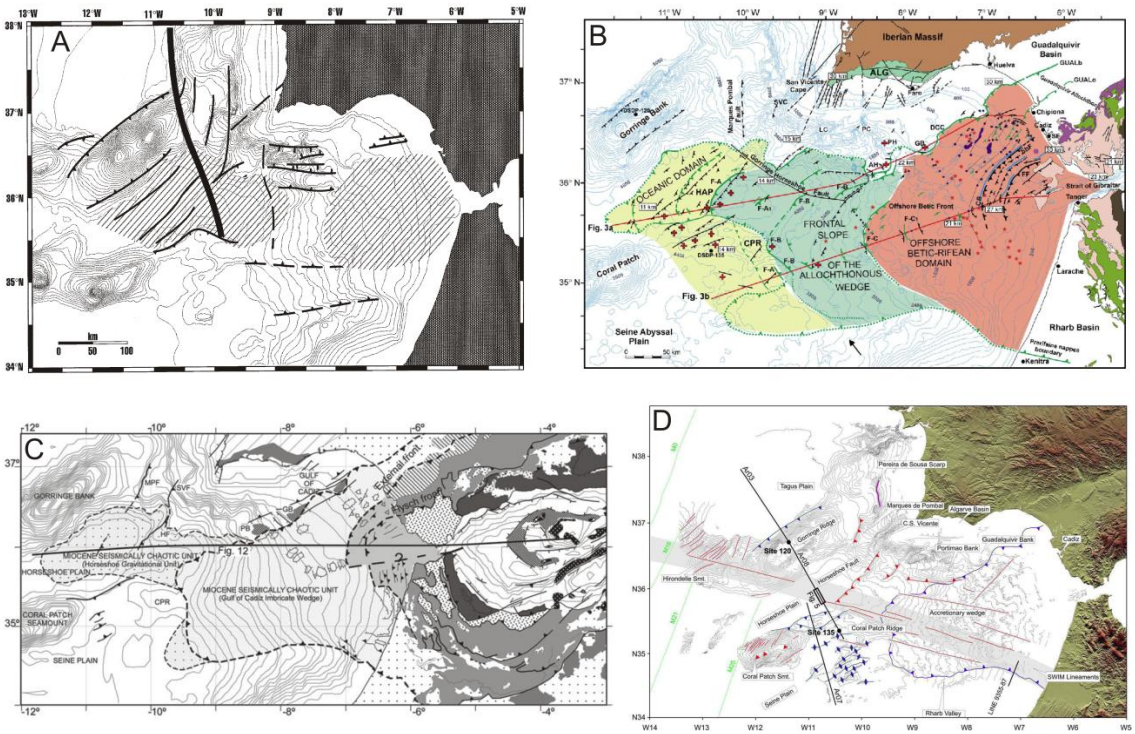


Figure 4.1 – Four different tectonic maps of the Gulf of Cadiz region proposed in the last two decades: A) Tortella et al. (1997), B) Medialdea et al. (2004), C) Iribarren et al. (2007), D) Zitellini et al. (2009).

The map shown in Fig. 4.2 depicts the Gulf of Cadiz - SW Iberia main active tectonic structures. Three main systems of structures are promptly recognized: i) the subduction-related Gulf of Cadiz Accretionary Wedge (CGAW; marked in grey in Fig. 4.2); ii) a set of WNW-ESE striking dextral strike-slip faults (the SWIM fault system; marked in white); and a group of NE-SW striking northwest-directed thrusts located in the Southwest Iberia Margin (marked in yellow). These three systems are described in separated sections below. Other noteworthy structures depicted in the map of Fig. 4.2, such as the more ENE-WSW thrusts and the Cadiz fault, will also be briefly described in a fourth section.

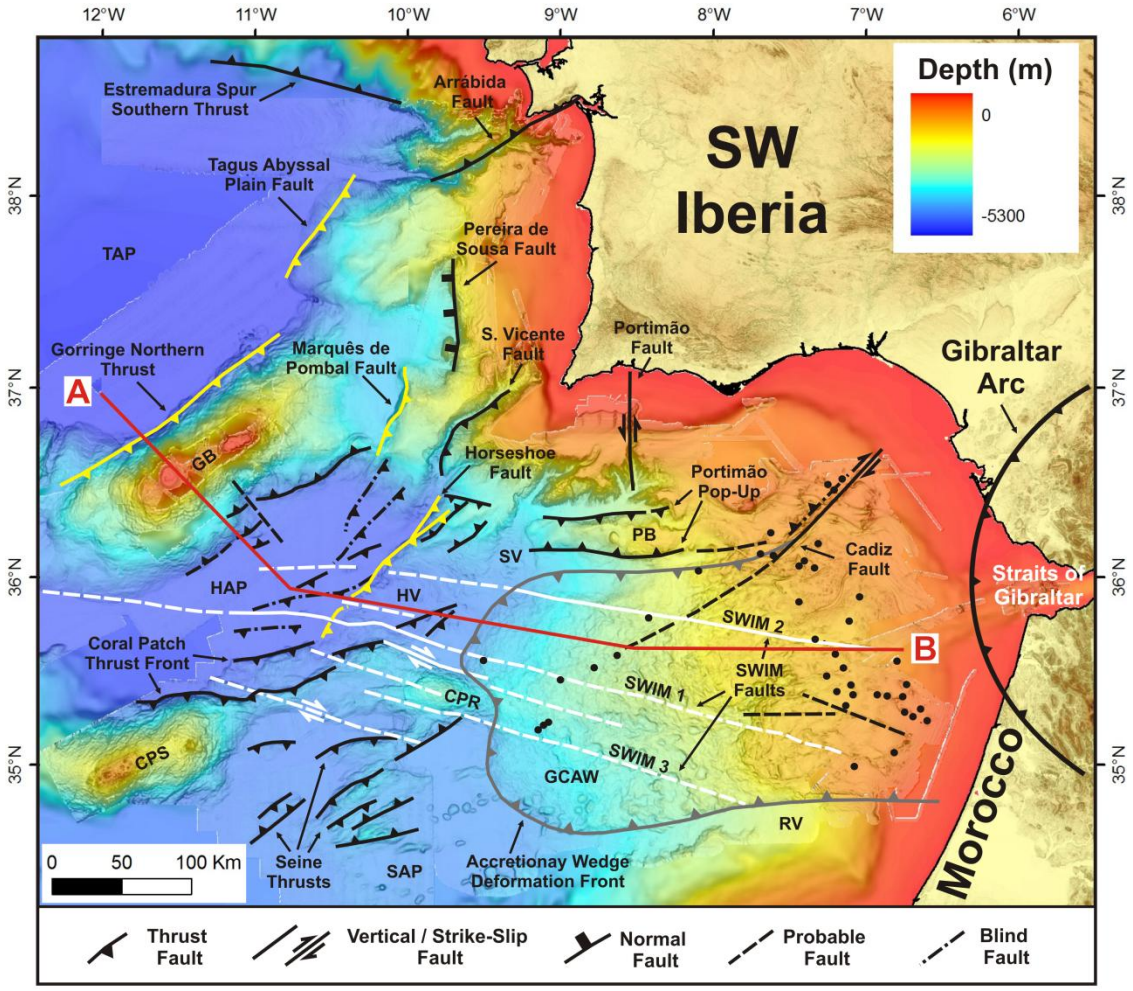


Figure 4.2 – The tectonic map of the Gulf of Cadiz region and SW Iberia. The Gulf of Cadiz Accretionary Wedge (GCAW) is shown in grey, the SWIM faults are shown in white and the SW Iberia NE-SW thrusts are shown in yellow. The Tagus Abyssal Plain fault was taken from Cunha et al. (2010); the Estremadura Spur Southern Thrust and the Arrábida fault were taken from Terrinha et al. (in prep.). CPR – Coral Patch Ridge; CPS – Coral Patch Seamount; GB – Gorringe Bank; HAP – Horseshoe Abyssal Plain; HV – Horseshoe Valley; PB – Portimão Bank; RV – Rharb Valley; SAP – Seine Abyssal Plain; SA – Sagres Valley. Profile A-B is presented in Figure 4.3.

The tectonic map was made using an extensive dataset of stratigraphically calibrated seismic reflection profiles (see Fig. 3.2). However, the seismic sections presented in this Chapter aim only to illustrate the main studied features and not to be an exhaustive characterization of all the structures present in the Gulf of Cadiz. Specially, because a significant part of these structures were previously characterized with some detail in previous works (e.g. Gutscher et al., 2002; 2009a,b; Gracia et al., 2003a,b; Terrinha et al., 2003; Zitelini et al., 2004; Cunha et al., 2010) some of which included in other chapters and appendixes of this thesis (Terrinha et al., 2009; Duarte et al., 2009; Rosas et al., 2009; Duarte et al., 2010; Duarte et al., submitted; Rosas et al., submitted). The adopted simplified stratigraphy is shown in Figure 4.3 (after Torelli et al., 1997; Tortella et al., 1997; and Roque, 2007). In general, it is possible to identify three basic variations (A, B and C in Fig. 4.3) of a stratigraphic column constituted by three main tectono-stratigraphic mega-sequences: i) a succession of mostly Mesozoic sediments, occasionally with some units extending through the Eocene-Oligocene, overlying a basement of oceanic nature, with exception of the Gorringe Bank, a region where sediments lay directly on top of serpentinized mantle; ii) Miocene sediments often exhibiting a chaotic acoustic facies, including the Chaotic Body (which may locally incorporate sediments of Eocene-Oligocene age) and the GCAW; iii) an overlying succession of mostly Pliocene-Quaternary sediments. Some degree of stratigraphic lateral variations may occur between profiles or even within the same profile.

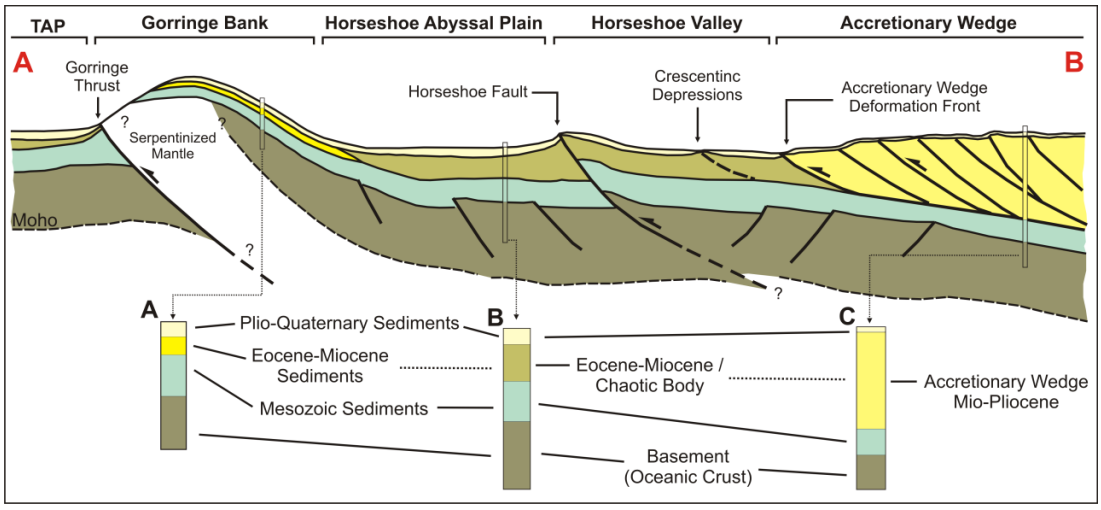


Figure 4.3 – Schematic W-E profile of the Gulf of Cadiz region (see Fig. 4.2 for location; not to scale) showing the main representative tectono-stratigraphic mega-sequences, and three variations of a simplified stratigraphic column (A, B and C), used in the interpretation of the seismic profiles presented in this work (after: Sartori et al., 2004; Torelli et al., 1997; Terrinha, 1998; Roque, 2007).

4.1. The Gulf of Cadiz Accretionary Wedge

The Gulf of Cadiz Accretionary Wedge (GCAW) is one of the most prominent morphological features depicted in the high-resolution bathymetry, occupying a significant area of the Gulf of Cadiz (see Figs. 4.2 and 4.4). It is materialized on the seafloor by a west dipping U-shaped surface that extends for more than 250 km from about longitude 7º to 9º30', with depths ranging from 200 to 4300 meters. It narrows slightly to the west with a width varying from 160 to 140 km. Its northeastern limit is marked by the Cadiz fault (see Fig. 4.2 and 4.4; Duarte et al., 2009) and the Iberian continental shelf. The northwestern part is limited by the uplifted continental slope of the Portuguese margin, an area dominated by the presence of plateaus incised by canyons and submarine valleys (see Fig. 4.2 and 4.4). The southern limit of the GCAW is well marked by the Rharb Valley that extends from the Moroccan continental shelf to the Seine Abyssal Plain. To the west, the rim of the wedge corresponds to the eastern limit of the Horseshoe Valley and the Seine Abyssal Plain. In this region, it is possible to observe that the wedge deformation front is asymmetrically indented by the Coral Patch Ridge (see Fig. 4.4; see Gutscher et al., 2009a).

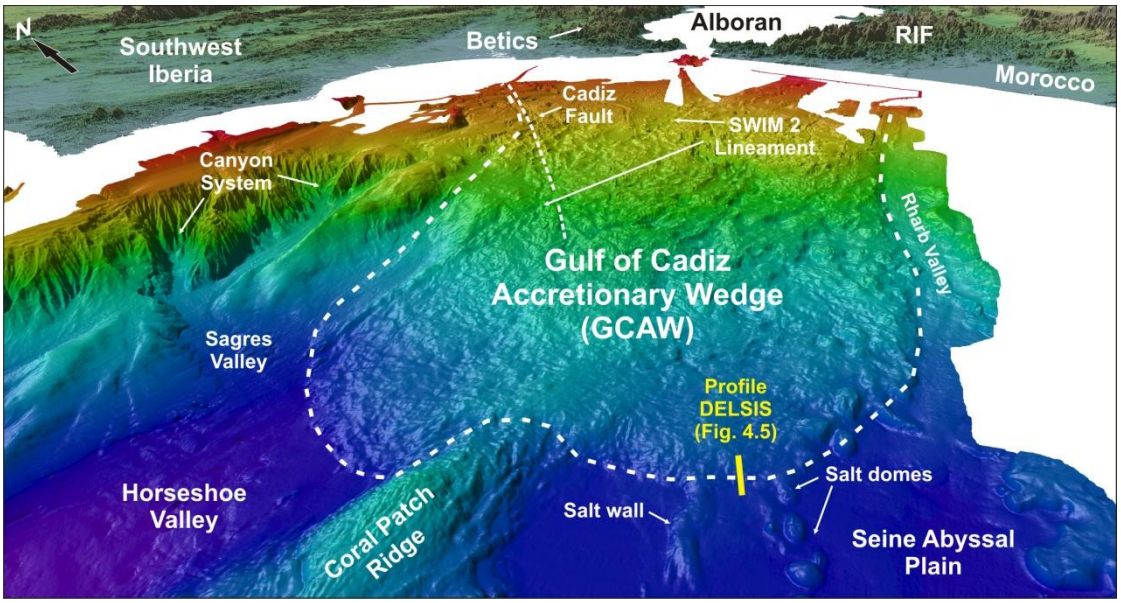


Figure 4.4 – Perspective view (from southwest) of the Gulf of Cadiz Accretionary Wedge (GCAW) surface and adjacent areas (Adapted from Duarte et al., submitted)

The present morphology of the GCAW is the result of the activity of a wide variety of tectonic, gravitational and fluid escape processes. The particular wrinkled appearance of its surface comprises thrust-related slope breaks and associated folds, "raft-tectonics" type features, abundant sub-circular collapse depressions and several mud volcanoes and salt domes (Torelli et al., 1997; Mulder et al., 2003; Pinheiro et al., 2003; Gutscher et al., 2009b; Terrinha et al., 2009; Zitellini et al., 2009). From a structural point of view, the GCAW corresponds to an eastward thickening pile of westwards thrusted sediments (Fig. 4.5), reaching a maximum thickness of ca. 15 km near the Gibraltar Straits (Thiebot and Gutscher, 2006; Gutscher et al., 2009a). The thrusts are rooted in a common sub-horizontal to gently east dipping décollement layer, exhibiting an overall geometry interpreted as compatible with on-going eastwards subduction beneath the Gibraltar Arc (Gutscher et al., 2002). During the last 5 Ma the E-W convergence rate implied in such a subduction is thought to have diminished from ca. 2 cm/yr to 0.5 cm/yr (Gutscher et al., 2009a), with a consequent decrease in the activity of the wedge thrusts during this time span. Accordingly, the same authors argue that the Present day internal deformation is more likely to be accommodated by small increments of local reactivation of inherited blind thrusts, being more homogeneously distributed over the entire wedge rather than concentrated on newly formed major frontal thrusts disrupting the seafloor. However, a detailed study of the Horseshoe Valley region (see Fig. 4.2), presented in the next chapter (Duarte et al., 2010), suggests that the accretionary is still propagating to the west.

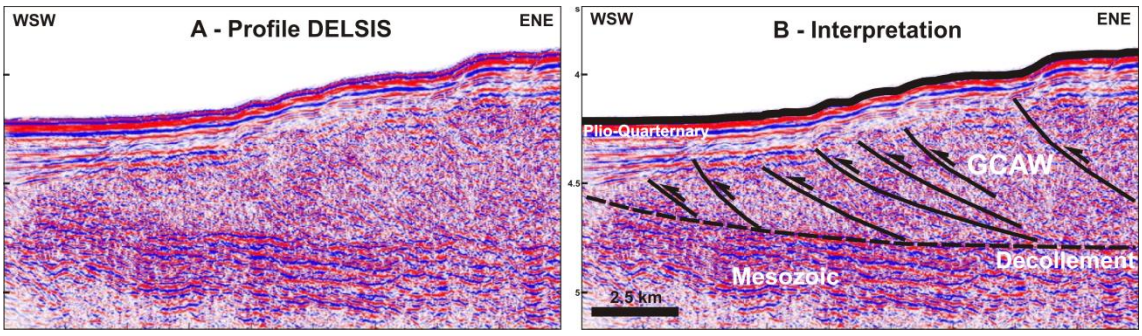


Figure 4.5 – Multi-channel seismic Delsis profile (A) and respective interpretation (B) across the GCAW deformation front; see stratigraphic column C in Fig. 4.3 for correlation of the observed seismic units (see Fig. 4.4 for location; Adapted from Duarte et al., submitted).

4.2. The SWIM fault system

The SWIM fault system is a group of WNW-ESE striking subvertical faults extending along 600 km from the eastern part of the Gulf of Cadiz to the southern limit of the Gorringe Bank (see Fig. 4.2). These tectonic features seemingly interfere with several different morphotectonic domains such as the GCAW, the Horseshoe Valley and the Horseshoe Abyssal Plain (see Fig. 4.6). The morphologic expression of the SWIM faults corresponds to a more or less continuous alignment of seafloor crests and troughs with wavelengths of the order of tens of kilometers, sometimes exhibiting an en echelon geometrical disposition (Fig. 4.6), and commonly punctuated by active mud volcanoes within the domain of the accretionary wedge (see Fig. 4.2) and possibly just outboard to the west. The linear morphologic expression of the SWIM faults is more prominent both close to the northern part of the accretionary wedge deformation front and in the Horseshoe Valley (Fig. 4.7 and 4.8), where the lineament corresponding to the morphological expression of the SWIM 1 fault can be followed almost continuously for about 200 kilometers and the width of the affected area is of a few hundred metres. In some segments of this lineaments is possible to identify undulations, striking E-W, with maximum lengths of about 8 km. These features also show an “en echelon” pattern that was interpreted to correspond to NE-SW oriented folds of the Recent sedimentary cover (see Fig. 4.8; Rosas et al., 2009, in appendix). Despite the fact that the lineaments can sometimes exhibit some continuity reaching more than 200 km, this does not mean that the underlying faults are strictly continuous and connected. Quite on the contrary, the lineaments seem to be controlled by a discontinuous alignment of deep rooted faults probably resulting from a complex tectonic evolution (see text below and Chapter 6 for a more detailed discussion). Also note that in this work there are noteworthy discrepancies in the interpretations of these structures. This results from the fact that the earliest interpretations of the SWIM strike-slip faults were done using limited bathymetry datasets, which did not allow an accurate cartography and sometimes led to misleading or alternative interpretations. With the increasing availability of new bathymetry data (and MCS profiles), the interpretations were progressively upgraded. In addition, other authors proposed different interpretations for the SWIM fault system (e.g. Zitellini et al., 2009). The upgraded tectonic map presented in Fig. 4.2 intends to include the more recent interpretation of these features, though with some degree of

simplification due to the scale adopted. The different sections of this manuscript and associated papers may present alternative or simplified interpretations of these same (SWIM) features.

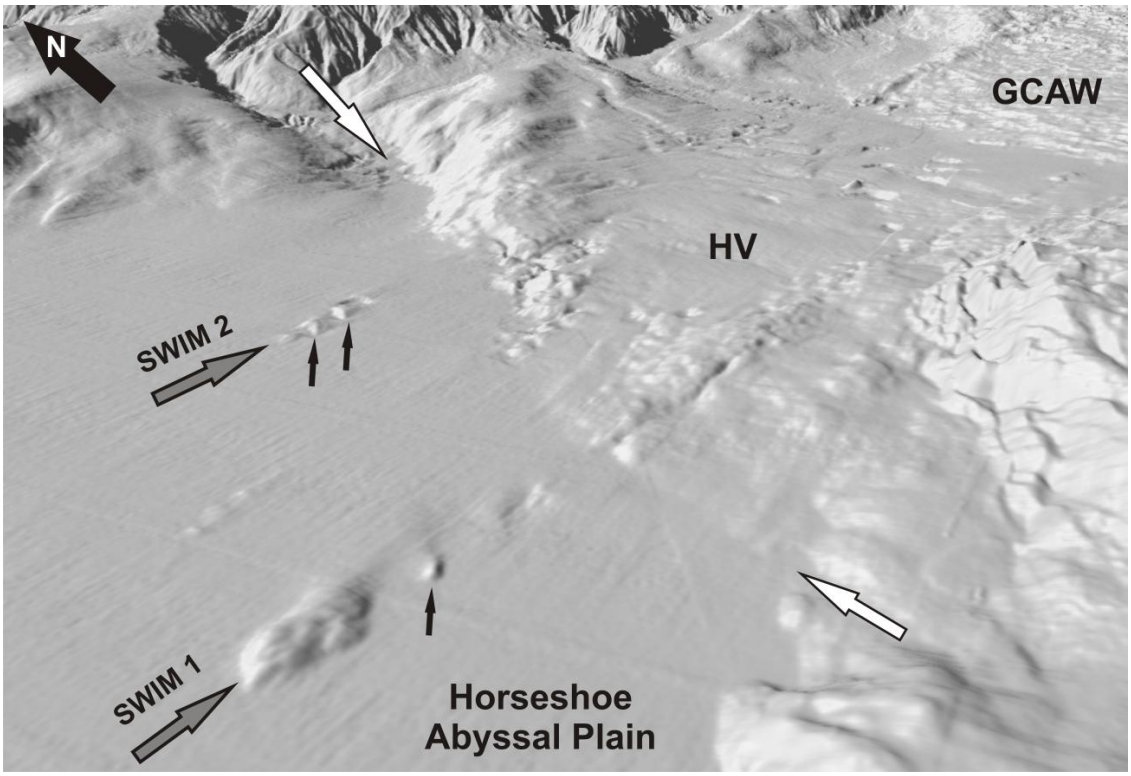


Figure 4.6 – Shaded relief image of the Horseshoe Abyssal Plain and continental rise to the NE; view from SW, showing the morphological expression of the SWIM faults 1 and 2, indicated by grey arrows. The small black arrows show seafloor deformation probably corresponding to NE-SW oriented "en echelon" folds. White arrows indicate the slope break that corresponds to the morphological expression of the Horseshoe fault. HV - Horseshoe Valley; GCAW - Gulf of Cadiz Accretionary Wedge (Extracted from Duarte et al., 2009, in appendix).

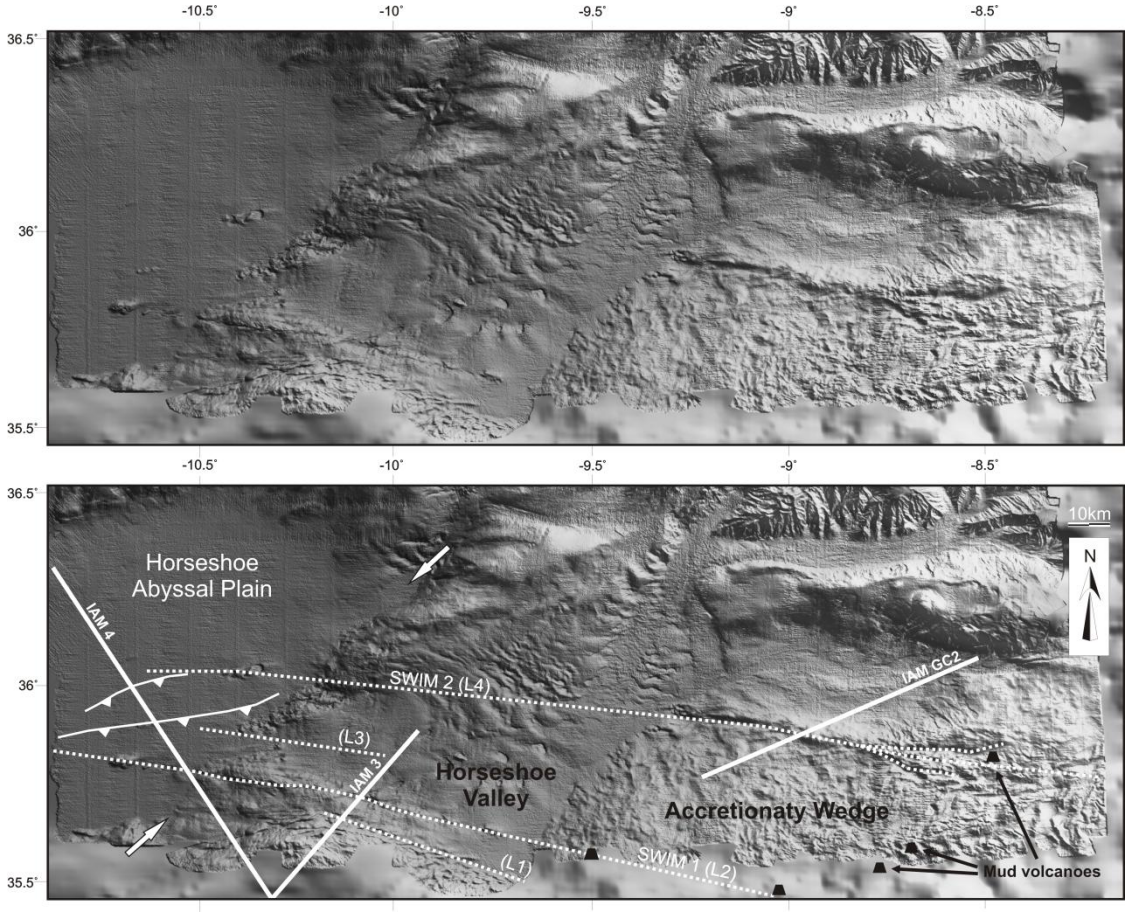


Figure 4.7 – Bathymetry of NW Gulf of Cadiz showing the approximately linear morphologic expression of the SWIM 1 and 2 (corresponding to the lineaments L2 and L4 from Rosas et al., 2009) and L1 and L3, close to the northern part of the accretionary wedge deformation front and the Horseshoe Valley. Location of the IAM multi-channel seismic reflection profiles intersecting the SWIM 1 and 2, interpreted in Figs 4.9 and 4.10. White arrows indicate the slope break that corresponds to the morphological expression of the Horseshoe fault (Adapted from Rosas et al., 2009, in appendix). Thrusts marked in white correspond to the "corner faults" formed as the result of the interference between the Horseshoe fault and the SWIM 1 fault shown in Fig. 4.9 (see Rosas et al., submitted, in appendix, for a detailed discussion on the origin of these structures).

The coupled inspection of the bathymetric dataset and seismic profiles allowed the mapping of the overall extent of the SWIM structures (Terrinha et al., 2009; Rosas et al., 2009; Duarte et al., 2009; Duarte et al., 2010). The seismic data showed that the lineaments correspond to the morphological expression of more or less aligned arrays of deep-rooted faults, often breaching out through Present day seafloor sediments (Fig. 4.9; Rosas et al., 2009; Terrinha et al., 2009; Duarte et al., submitted; Rosas et al, submitted).

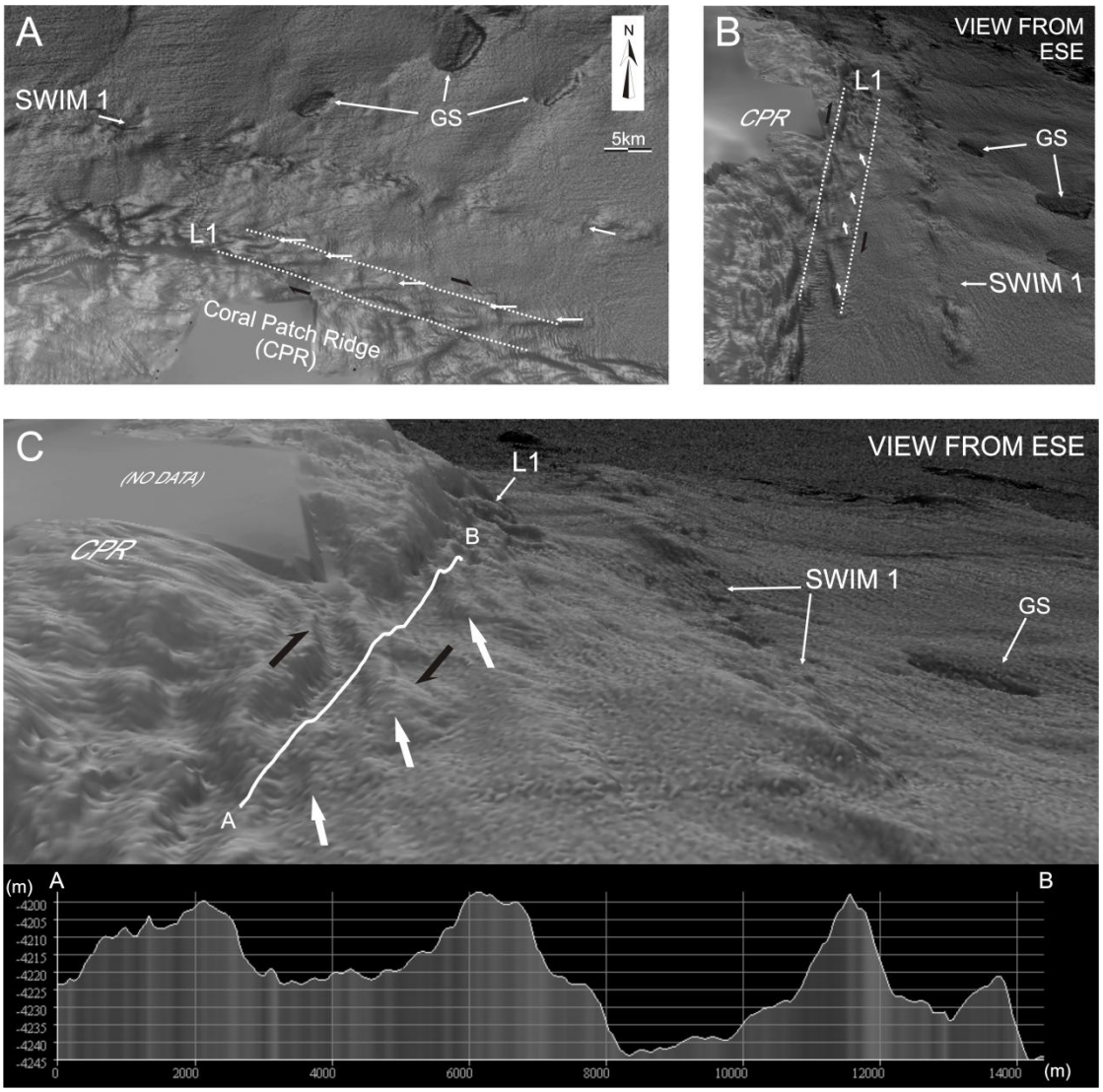


Figure 4.8 – (A and B) Different views of the L1 and SWIM 1 lineaments and associated morphologic features. (C) View of L1 from ESE. AB bathymetric profile just north of L1. White arrows point the en echelon morphologic crests and troughs; CPR - Coral Patch Ridge; GS - Crescent Giant Scours (see Duarte et al. 2010, next chapter). Black arrows indicate the interpreted sense of shear (Adapted from Rosas et al., 2009, in appendix).

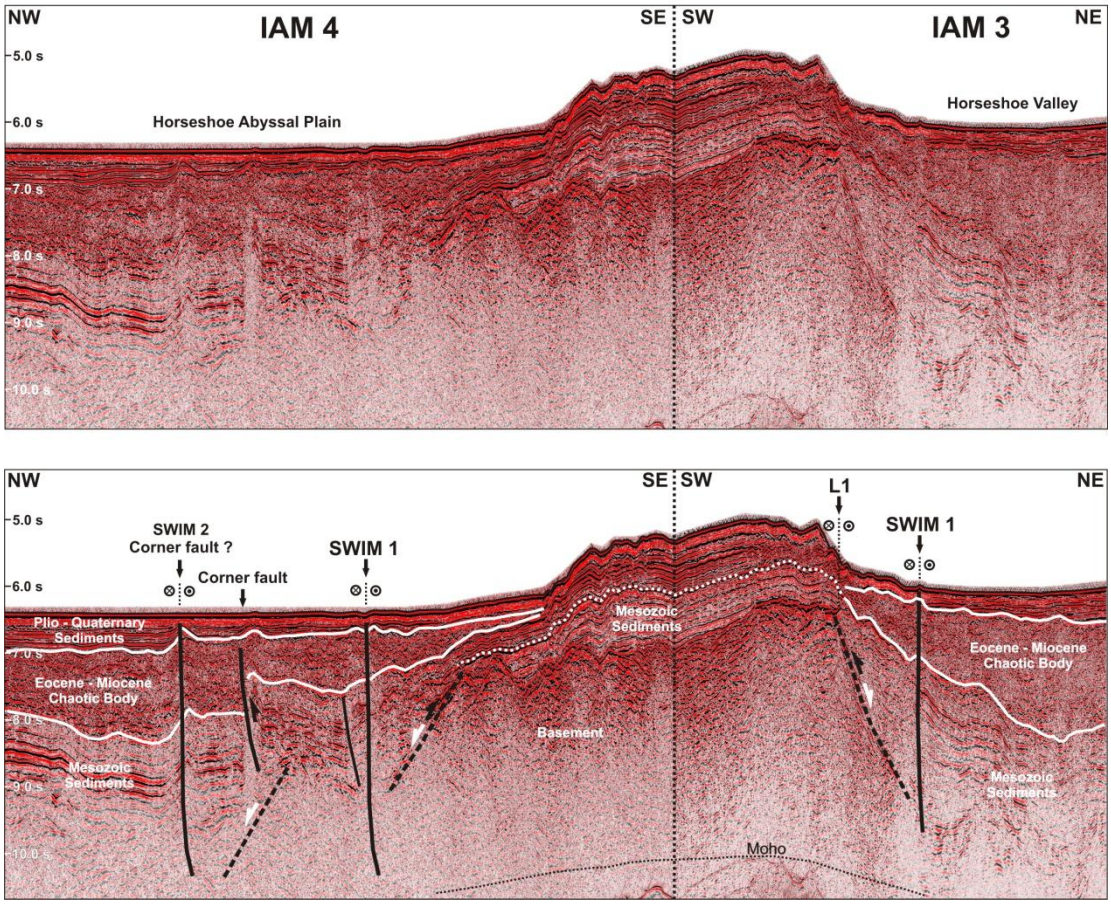


Figure 4.9 – Multi-channel seismic profiles IAM-4 and IAM-3 (A) and respective interpretation (B; location in Fig. 4.7: Adapted from Duarte et al., submitted), crosscutting the SWIM faults 1 and 2. Rosas et al. (submitted) presented an alternative interpretation for the structure corresponding to the SWIM 2, according to these authors it may correspond to a corner thrust formed as the result of the interference between the Horseshoe fault and the SWIM 1 fault (note in Fig. 4.7 that the two structures seem to merge in this area). Stratigraphy corresponding approximately to the column B in Fig. 4.3. Black dashed lines – normal faults affecting Mesozoic sediments, inverted during Cenozoic events (black arrows). Approximately position of the Moho in all figures taken from Sartori et al. (1994), Tortella et al. (1997) and Roque (2007).

From the inspection of the IAM 3 and 4 seismic profiles in Fig. 4.9 it is evident that the SWIM faults are aligned along basement normal faults controlling the geometry of the Mesozoic sediments. These faults are interpreted as being formed during the Mesozoic rifting events. This interpretation is supported by the presence of a growth wedge contemporaneous of a normal movement (Fig. 4.10 - Unit B). In this figure it also possible to observe that the SWIM 2 structure was reactivated, after the extensional event, with southwards reverse movement given that the growth wedge is over-thrust

towards the southwest. The thrusting seems to be contemporaneous of the emplacement of the accretionary wedge (Unit D and D') since this clearly tapers towards the northeast. From the inspection of the seismic profiles it is possible to observe that the SWIM 2 fault deforms the Pliocene-Quaternary units, breaching through the seafloor. It is also noticeable that the more recent cover sediments are strongly deformed mostly to the south of the SWIM 2 (see Unit E in Fig. 4.10), suggesting that this sub-vertical fault corresponds to the present deformation limit of the accretionary wedge in this area.

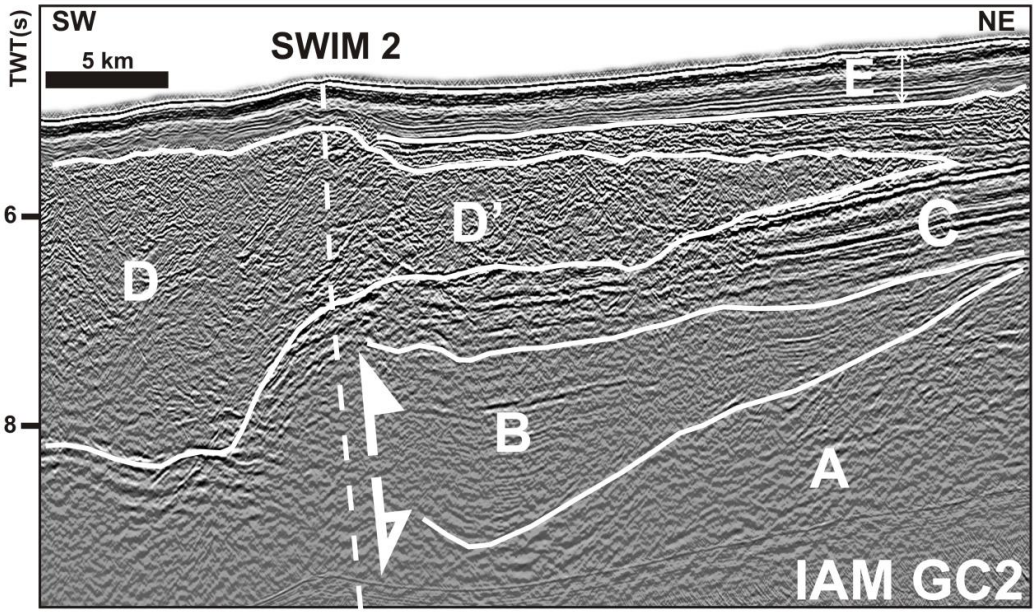


Figure 4.10 – Multi-channel seismic reflection profile IAM GC2 (see Fig. 4.7 for location). The white dashed line mark the SWIM 2 fault zone. The profile shows two previous movements along this structure (normal and reverse, white open and closed arrows, respectively). A - Basement; B - Growing wedge (Mesozoic age); C - Post-rift unit (Meso-Cenozoic age); D and D' - Accretionary Wedge unit (Miocene age to Pliocene-Quaternary); E - Cover unit (Pliocene-Quaternary age). D' corresponds to the unit emplaced during late Miocene, while the deposition of unit D continued to more recent times (Adapted from Duarte et al., 2009, in appendix).

Rosas et al. (2009; in appendix), based on the age of the sedimentary units and in the en echelon folding geometry (see Fig. 4.8), estimated that the SWIM faults dextral strike-slip reactivation in the Horseshoe Abyssal Plain and Horseshoe Valley may had initiated at ca. 1.8 Ma ago. This is in agreement with the recent kinematic models derived from geodetic observations, indicating that the ca. 4 mm/yr Present day convergence between Nubia and Iberia is subparallel to these faults. In fact the present convergence direction is the most reliable (indirect) observation supporting the

interpretation of the SWIM faults as dextral strike-slip faults. Although, dextral offsets of other structures along the SWIM faults are sparse. For instance, the Horseshoe Fault has two segments that seem to be offset by one structure with the same direction of the SWIM faults (see Fig. 4.2 and 4.11). However, both the SWIM faults and the Horseshoe fault are presently active and thus complex thrust-wrench interference patterns are expected to occur, which appear to be the case in this region, as reported by Rosas et al. (submitted, in appendix). Also, in the region of the Coral Patch Thrust Front (see Fig. 4.2 and 4.11) some of the active thrusts appear to be delimited and displaced along the SWIM faults. However, this displacement is most probably false, since it completely vanishes onto the Coral Patch Ridge. Here, the thrusts are most likely using the SWIM anisotropies as lateral ramps, since they clearly bound major thrusts without an obvious offset. Another important observation is that the SWIM faults do not displace the front of the accretionary wedge (see Fig. 4.11), which should be expected if the front of the wedge was nearly inactive since the Miocene as suggested by Zitellini et al. (2009). This is a major paradox in this area and will be investigated in detail in Chapter 6 (Duarte et al., submitted).

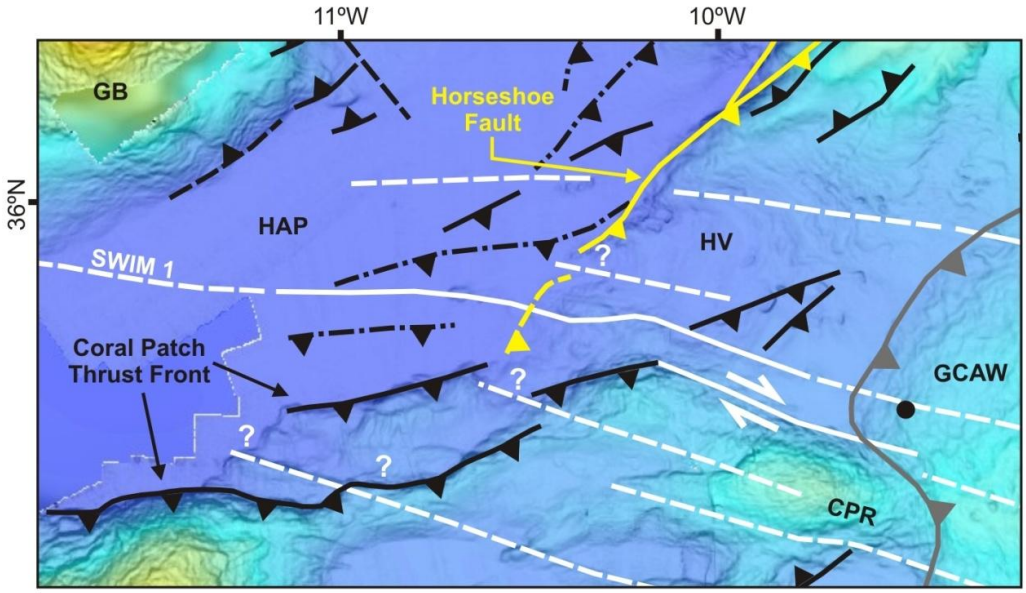


Figure 4.11 – Detailed bathymetry and structural setting of the Horseshoe Abyssal Plain (HAP) region. Note the possible dextral offsets of thrusted structures and morphologies along the SWIM faults (interrogation points). CPR - Coral Patch Ridge; GB - Gorringe Bank; GCAW - Gulf of Cadiz Accretionary Wedge; HAP - Horseshoe Abyssal Plain; HV - Horseshoe Valley.

4.3. The NE-SW thrusts

The approximately NE-SW striking thrust system comprises the Horseshoe fault, the Marquês de Pombal fault, the Tagus Abyssal Plain fault and the Gorringe northern thrust (Fig. 4.12; see e.g. Zitellini et al., 1999; Gràcia et al., 2003a,b; Terrinha et al., 2003; Rovere et al., 2004; Zitellini et al., 2004; Terrinha et al., 2009; Cunha et al., 2010). This system extends for approximately 300 km from near the contact with the Coral Patch Ridge (35.5ºN), towards the north, along the West Portuguese Margin until a latitude of ~38ºN. These compressive structures correspond in general to deep rooted basement faults with prominent escarpments, possible cutting the lithosphere at different levels, as attested by seismic imagery and deep instrumental seismicity (see e.g. Fig. 1.4A; Stich et al., 2007; Terrinha et al., 2009; Cunha et al., 2010; Silva et al., 2010).

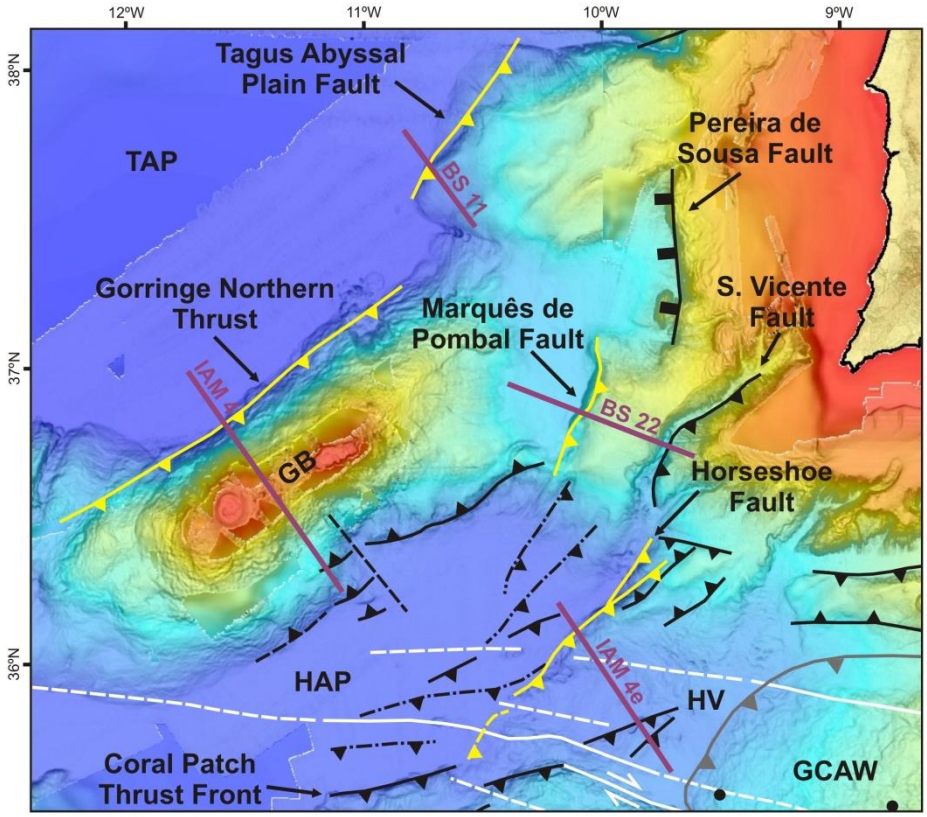


Figure 4.12 – Detailed bathymetry and structural setting of the NE-SW thrusts area (marked in yellow). Seismic profiles tracks are shown in purple (see below). GB - Gorringe Bank; GCAW - Gulf of Cadiz Accretionary Wedge; HAP - Horseshoe Abyssal Plain; HV - Horseshoe Valley.

4.3.1. The Horseshoe Fault

The Horseshoe fault extends for about 100 km, bounding to the East the Horseshoe Abyssal Plain (see Fig. 4.12). The fault scarp is only well developed on its nothern segment, where it reaches a height of about 1000 meters. The southern segment of the Horseshoe scarp is being eroded by the South Portuguese canyons drainage system and widsepred mass transport processes (Terrinha et al., 2009, in appendix; Duarte et al., 2010, next chapter). Close to the intersection with the SWIM structures the trace of the fault becomes less evident and appears to interfere with the SWIM faults (see also Figs. 4.6, 4.7 and 4.11 and Rosas et al., submitted, in appendix). To the south, the Horseshoe fault probably connects with the Coral Patch thrusts. To the north, the fault split in several branches, where a couple of associated back-thrust are also recognized. Here, the fault seems to terminate against a small WNW-ESE thrust. Nevertheless, a relatively minor fault (the S. Vicente fault) can be traced northwards along the S. Vicente canyon. The IAM-4e seismic profile (Fig. 4.13) crosscuts the Horseshoe fault around shot point 1000. The fault is clearly imaged as a SE dipping, deep seated fault, rooting well into the basement (possible through Moho), prolonging upwards across the overlying units, and breaching out at the seafloor, where a resulting prominent deformation is marked by an offset of ca. ~0.6s TWT. The NW directed thrusting kinematics is clearly shown by the geometry of the folds affecting the Mesozoic, and by the unambiguous offset of the surface marking the top of the Mesozoic unit (see Fig. 4.13). To the SE of the Horseshoe fault, other relatively minor thrusts affecting the basal Mesozoic unit were previously described (e.g. Terrinha et al., 2009, in appendix; Duarte et al., 2010, next chapter), although these only affect the base of the overlying chaotic body, lacking any kind of bathymetric expression (see Fig. 4.13). The same authors also report some degree of tectonic imbrication within the Miocene chaotic body further to SE, perturbing the seafloor morphology and controlling the formation of a group of "crescentic" depressions (see Duarte et al., 2010 - Chapter 5 for a detailed discussion on the origin of these features).

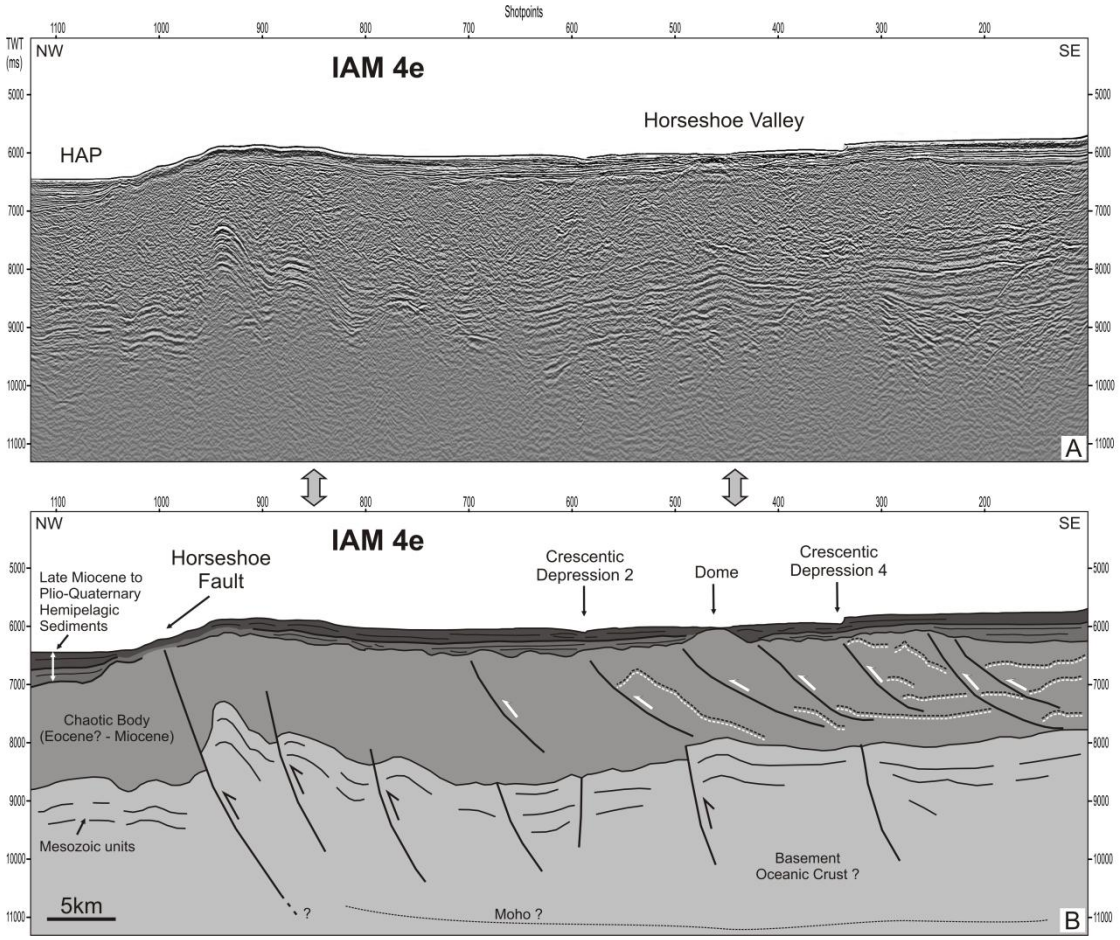


Figure 4.13 – (A) Seismic section of the profile IAM-4e intercepting the Horseshoe thrust fault (see Fig. 4.12 for location) and the Horseshoe Valley, where a group of crescentic depressions can be observed (see Duarte et al., 2010 - Chapter 5 for a detailed discussion on the origin of these features); (B) Tectonic interpretation (seismo-stratigraphy approximately corresponding to the column B in Fig. 4.3). Double-dashed black and white lines — intra-chaotic body reflections interpreted as décollement horizons and folded layered sediments. Note that crescentic depressions 2 and 4 are located on top of blind thrusts rooted in the sole of the chaotic body, probably at the same structural level as the accretionary wedge décollement.

4.3.2. The Marquês de Pombal Fault

The Marquês de Pombal fault strikes close to N-S, parallel to the Portuguese coast line, extending for about 60 km (see Fig. 4.12). It has a prominent scarp reaching a maximum height of about 1800 meters, limiting a submarine plateau. The BS-22 seismic section (Fig. 4.14) shows that the Marquês de Pombal fault also roots deep in the basement, probably throughout the Moho. It is also possible to observe that the fault breaches out at the seafloor, offsetting the entire sedimentary cover by ~1.5 seconds. The NW directed thrusting kinematics is clearly shown by the geometry of the folds affecting the Meso-Cenozoic sedimentary sequence (see Fig. 4.14).

To the south of the Marquês de Pombal structure two blind northwest-directed thrusts were also identified (see Fig. 4.12), presenting an en echelon disposition in relation both to the Marquês de Pombal and Horseshoe faults. It is not clear if all these faults are connected in depth to a common décollement level or if they are linked by lateral ramps, and thus forming a single complex structure.

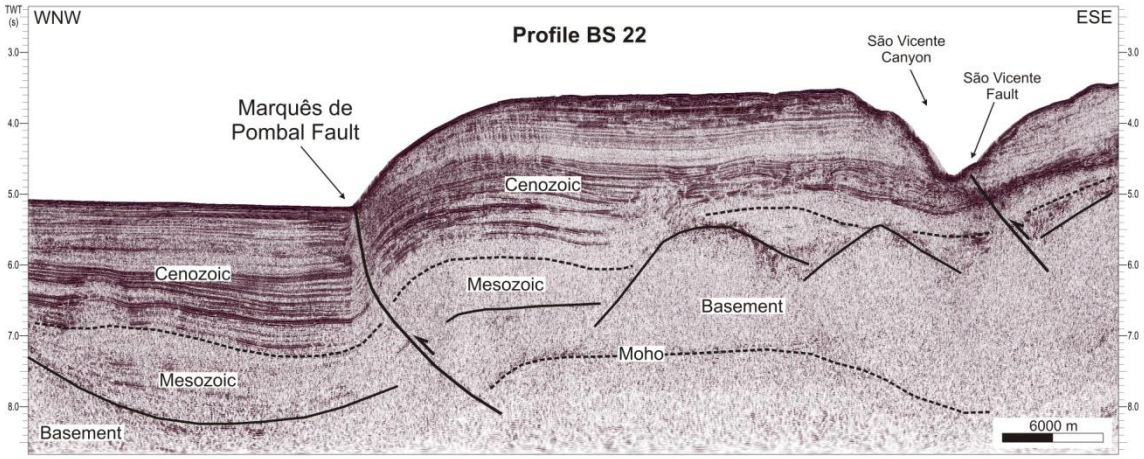


Figure 4.14 – Seismic section of the profile BS-22 intercepting the Marquês de Pombal thrust fault (see Fig. 4.12 for location). Seismo-stratigraphy approximately corresponding to column A in Fig. 4.3. Note that the sequence of Meso-Cenozoic sediments is overlaying a thinned crustal continental basement (Cunha et al., 2010).

4.3.3. The Tagus Abyssal Plain Fault

The Tagus Abyssal Plain fault extends for about 70 km with a prominent but rather irregular scarp (see Fig. 4.12), reaching a maximum height of about 1500 meters. The scarp is steeper close to its southern tip and smoothing progressively towards the north, where manifestations of mass transport processes are observed. The BS-11 seismic section (Fig. 4.15) shows that the fault zone corresponds to a basement rooted east deeping thrust, offsetting the seafloor and the cover units by ca. 1 second. In the imaged segment of the profile, associated with the Tagus Abyssal Plain fault, it is also possible to observe two west dipping back-thrusts limiting a slightly asymmetric anticline. Toward the southern part of the profile minor anticlines controlled by faults affecting the Meso-Cenozoic units are also observed. Among the four reported NE-SW thrust structures, the Tagus Abyssal Plain fault is the one with less instrumental seismicity (see Fig. 1.4 and Fig 4.17 below). Also, the inspection of available seismic profile shows recent sediments (darker top reflectors in Fig. 4.15) onlapping the fault scarp, which suggests that the peak activity of this segment of the Tagus Abyssal Plain Fault was in the Upper Pliocene. Present day deformation seems to be preferentially accommodated in the back-thrusts that cut through the seafloor

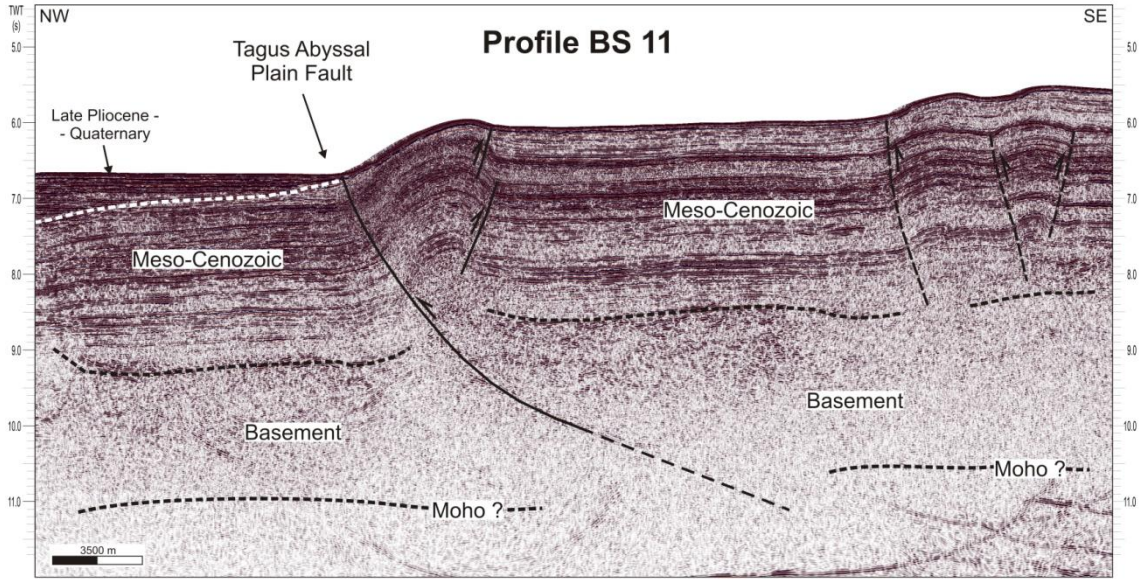


Figure 4.15 – Seismic section of the profile BS-11 intercepting the Tagus Abyssal Plain thrust fault (see Fig. 4.12 for location). Seismo-stratigraphy approximately corresponding to column A in Fig. 4.3.

4.3.4. The Gorringe Northern Thrust

The Gorringe Bank is the most impressive feature present in the SW Portuguese Margin (see Fig. 4.12), believed to be constituted by exhumed highly serpentinized mantle peridotites (Girardeau et al., 1998). The northern flank of the Gorringe Bank is limited by a major thrust (the Gorringe northern thrust), that extends for about 130 km, upthrusting the seafloor from −5000 m to −24 m. The fault scarp is highly sharp and steep (~10º). A major mass transport scar and correspondent deposit is observed in the northern segment of the fault attesting for its recent activity. The IAM-4 seismic section (Fig. 4.16) shows that the Gorringe northern thrust bounds a short flank of a major northwest vergent asymmetric anticline, comprising the entire Gorringe Bank structure. This fault probably roots very deep in the basement since it offsets the seafloor in about 6 seconds, in an area of oceanic domain. Despite the general westward vergence of the Gorringe, some eastwards vergent back-thrust-related folds can be detected, particularly in the base of its southern flank. In the northern segment of the profile a wedge of an acoustic chaotic unit is clearly observed, progressively thickening towards the north flank of the Gorringe Bank. This wedge corresponds to a gravity unit believed to have formed in a period of paroxysmal tectonic activity during the late Oligocene-Miocene age (Sartori et al., 1994; Tortella et al., 1997; Terrinha et al., 2009; Jimenez-Munt et al., 2010). Since then, the Gorringe has undergone a minimum shortening of 20 to 50 km (Hayward et al., 1999; Jimenez-Munt et al., 2010). The present activity of the Gorringe Northern Thrust is attested by a cluster of instrumental seismicity (see Fig. 4.17).

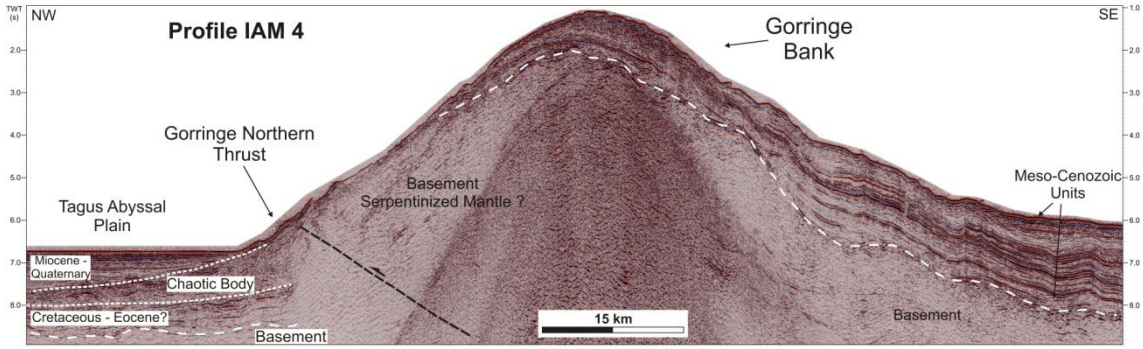


Figure 4.16 – Seismic section of the profile IAM-4 intercepting the Gorringe Bank and the Gorringe Northern thrust (see Fig. 4.12 for location). Simplified seismo-stratigraphy corresponding to column B in Fig. 4.3. Note the presence of a wedge (Chaotic Body) progressively thickening towards the north flank of the Gorringe Bank. (Sartori et al., 1994; Tortella et al., 1997; Jimenez-Munt et al., 2010).

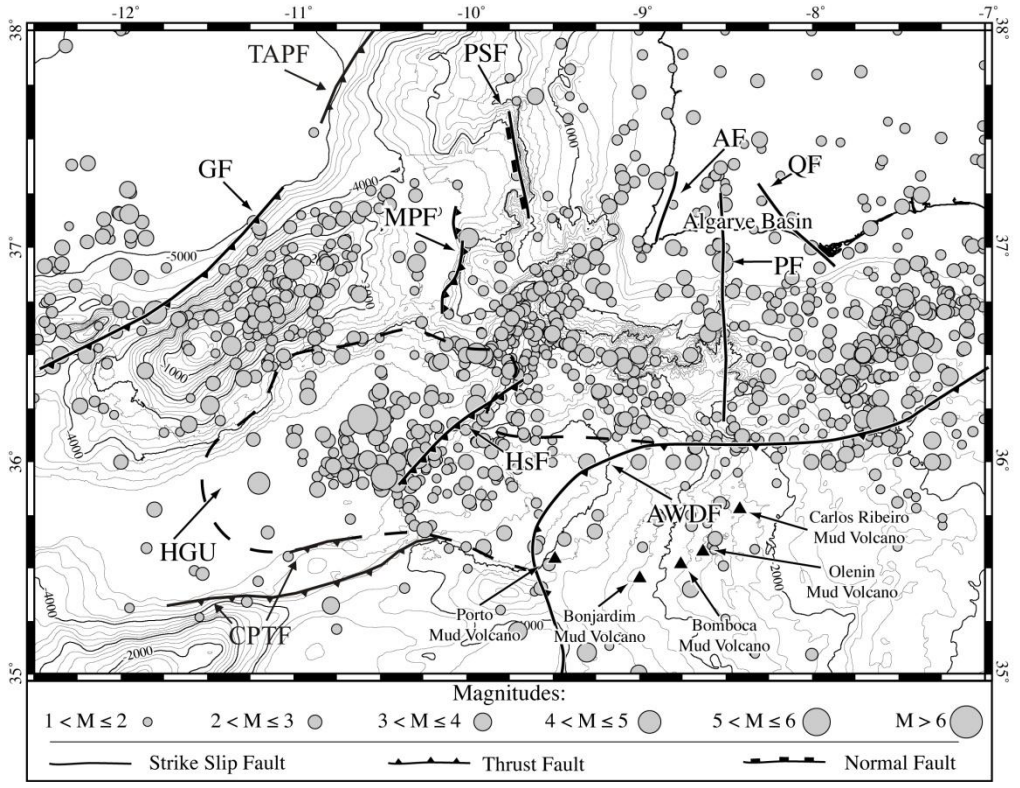


Figure 4.17 – Instrumental seismicity of the SW Iberia Margin (Adapted from Terrinha et al., 2009, in appendix), most faults and boundaries of the accretionary wedge of the Gulf of Cadiz and Horseshoe Gravitational Unit as mapped in previous works (Sartori et al., 1994; Torelli et al., 1997; Gutscher et al., 2002; Gràcia et al., 2003a; Terrinha et al., 2003; Iribarren et al., 2007; Cunha et al., 2010). AF - Aljezur fault; AWDF - Accretionary Wedge Deformation Front; CPTF - Coral Patch Thrust Front; GF - Gorringe (Northern Thrust) fault; HGU - Horseshoe Gravitational Unit (Chaotic Body); HsF - Horseshoe fault; MPF - Marquês de Pombal fault; PF - Portimão fault; PSF - Pereira de Sousa fault; QF - Quarteira fault; TAPF – Tagus Abyssal Plain fault; black triangles show the locations of mud volcanoes.

It is not clear if the Gorringe northern thrust is connected to the Tagus Abyssal Plain fault (see Fig. 4.12) or if these structures are separated by lateral ramps, which could also be linked to the Marquês de Pombal - Horseshoe system (Fig. 4.18). This possibility is congruent with the conspicuous presence of WNW-ESE morphological scarps in this area (noticeably the same direction of the SWIM faults), suggesting that such lateral ramps exist, connecting the NE-SW thrusts. Also, a cluster of instrumental seismicity between the Horseshoe and the Marquês de Pombal faults and a few events between the north tips of the Horseshoe fault and the Gorringe northern thrust suggests the existence of such structures (see Figs. 4.17; see also Fig. 2.7). These lateral ramps may be accommodating the strike-slip component of WNW-ESE convergence between Nubia and Iberia in a scenario of strain partition as suggested by Terrinha et al. (2009, in appendix). If this is the case, it bears major implications for the seismogenic potential of this area, and for the understanding of the margin reactivation process. Accordingly, further work needs to be made to test this hypothesis.

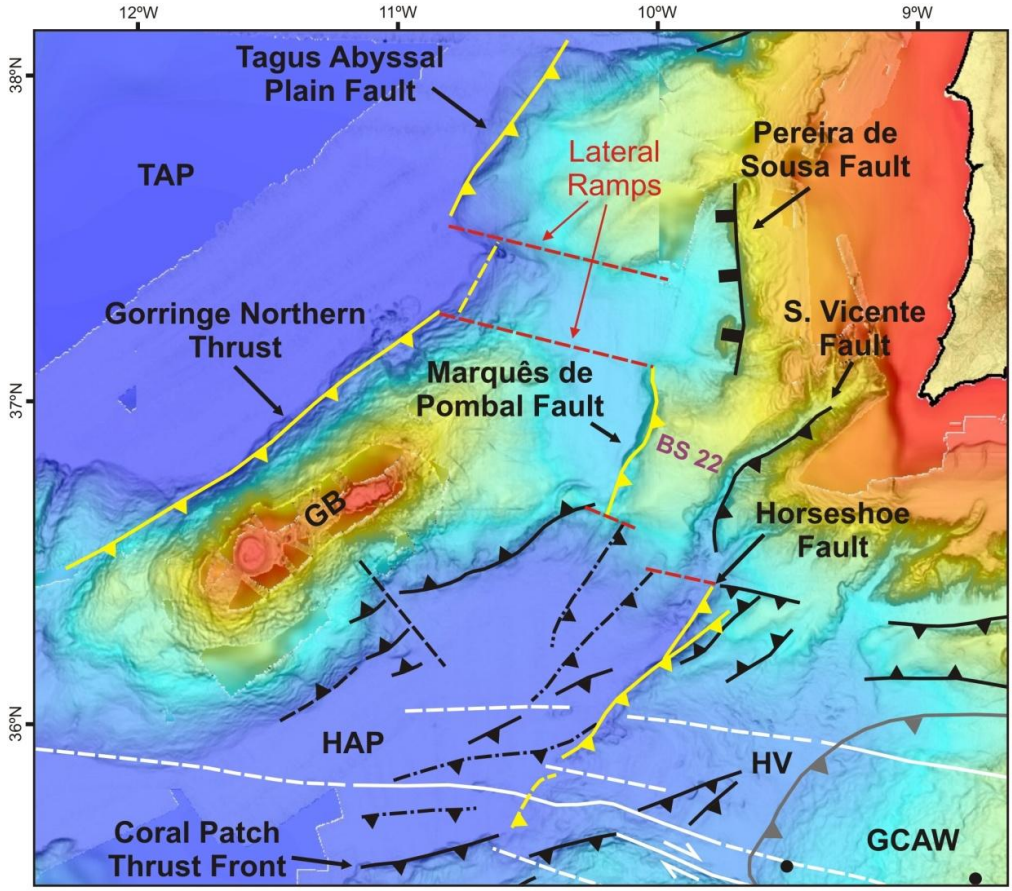


Figure 4.18 – Re-interpretation of the area shown in Fig. 4.12 showing the hypothetical structures (lateral ramps - dashed red lines) connecting the NE-SW thrust system.

4.4. Other important tectonic structures

Besides the three previously described groups of structures, which included the Gulf of Cadiz Accretionary Wedge, the SWIM faults system and the SW Iberia NE-SW thrusts, other important structures were also recognized in study area, such as the ENE-WSW to E-W striking system of thrusts and the NE-SW striking Cadiz fault (see Fig. 4.2). The Seine thrusts and the Coral Patch thrust front that are predominantly northwestwards directed thrusts show a larger variation in fault strikes with respect to the ones located further north. These thrusts may also have a different geological history, related to the evolution of the Moroccan margin, which was not studied in detailed in this work. Nevertheless, they will be described below with some detail since they may be important for the understanding of the overall picture of the Gulf of Cadiz geotectonic evolution.

4.4.1. The ENE-WSW to E-W thrust system

The ENE-WSW to E-W striking thrust system comprise the Coral Patch thrust front, the Seine thrusts and the Portimão pop-up (see Fig. 4.2; and also Figs. 4.17 and 4.22 below). The Coral Patch thrust front and the Seine thrusts are a system of faults striking approximately ENE-WSW located off to the west of SW part of Gulf of Cadiz region (Fig. 4.19), extending from the southern Horseshoe Abyssal Plain (~36ºN) to the inner part of the Seine Abyssal Plain (~34ºN). This fault system consists of scattered to more or less continuous sub-parallel thrusts, often exhibiting a few hundred meters high linear scarps, with the exception of the Coral Patch Ridge and the Coral Patch Seamount that rise 1000 and 3500 meters, respectively, above the surrounding seafloor. The Coral Patch thrust front is interpreted as a low angle thrust that carries the Seine Abyssal Plain over the Horseshoe Abyssal Plain (Figs 4.20 and 4.21). The NE-SW striking Seine thrusts are isolated in the middle of the Seine Abyssal Plain with hanging-wall anticlines that correspond to linear hills with a maximum elevation of 800 meters above the seafloor. From the inspection of the seismic section shown in Figure 4.21 it is possible to observe that the Coral Patch thrust front and the Seine thrust form an active

thick-skinned North-vergent fold-and-thrust belt, offsetting the sedimentary cover around 1 second. The major thrusts root deep in the basement (at around 11 seconds), possible at the base of the oceanic crust, (or even deeper in the mantle). In addition, the presence of a blind thrust in the southern part of the Horseshoe Abyssal Plain (see Fig. 4.19, detected in the northern segment of the MCS profile (see Fig.4.21), strongly suggests that these thrusts are propagating northwards, to an area where major instrumental earthquakes occur (see Figs. 1.4 and 4.17). This thrust system is likely to have originated as result of the Africa-Iberia convergence that started in the Upper Cretaceous. Despite de fact that some of these structures seem to be active, their activity has probably diminished since the Miocene as the result of the change to a more oblique convergence direction (WNW-ESE), as attested by the almost lack of seismicity on most of the thrusts (see Figs. 1.4 and 4.17).

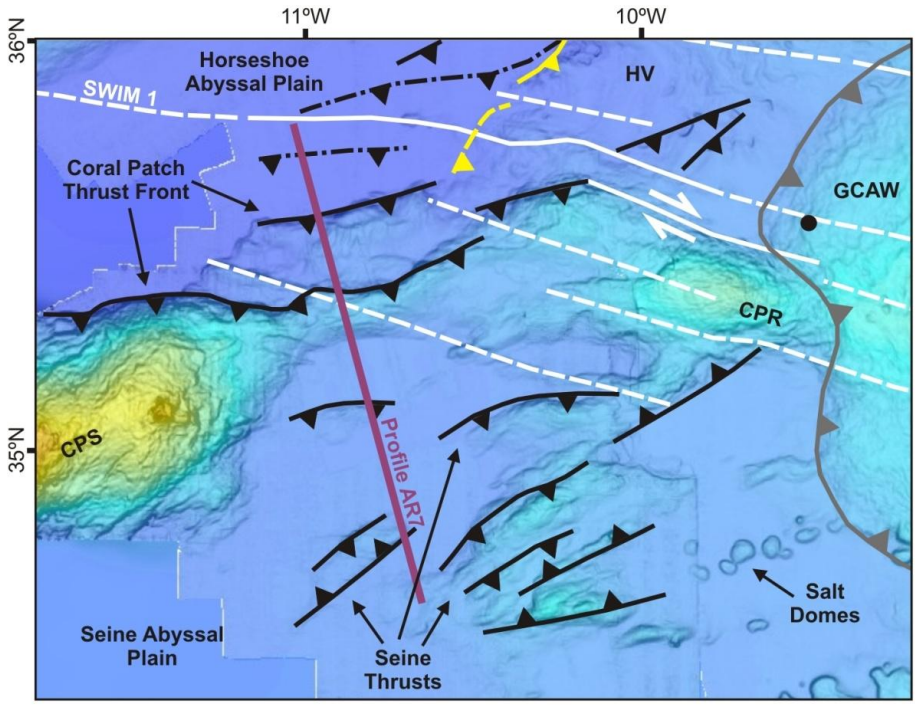


Figure 4.19 – Detailed bathymetry and structure of the Coral Patch thrust front and Seine thrusts region (see Fig. 4.2). The AR-7 seismic profile track and bathymentric profile are coincident and shown in purple (see Figs. 4.22 and 4.21, respectively).

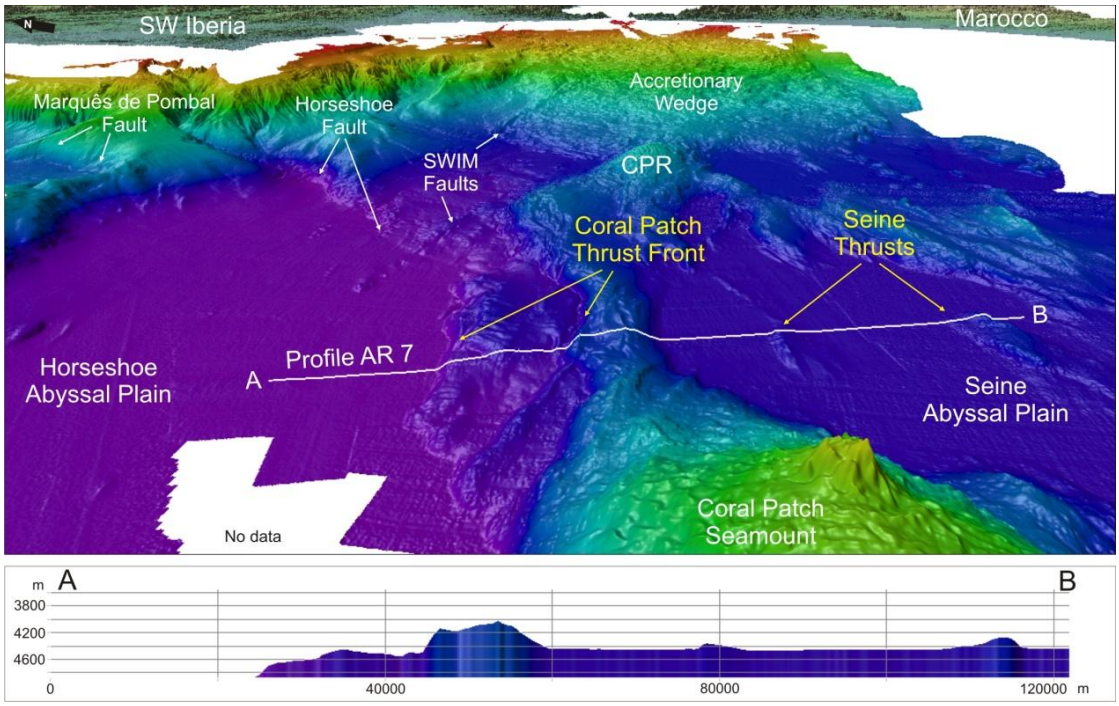


Figure 4.20 – Perspective view from WSW of the area shown in Fig. 4.19 and a bathymetric profile along the seismic line track. Note the relative elevation of the Seine Abyssal Plain in relation to the Horseshoe Abyssal Plain.

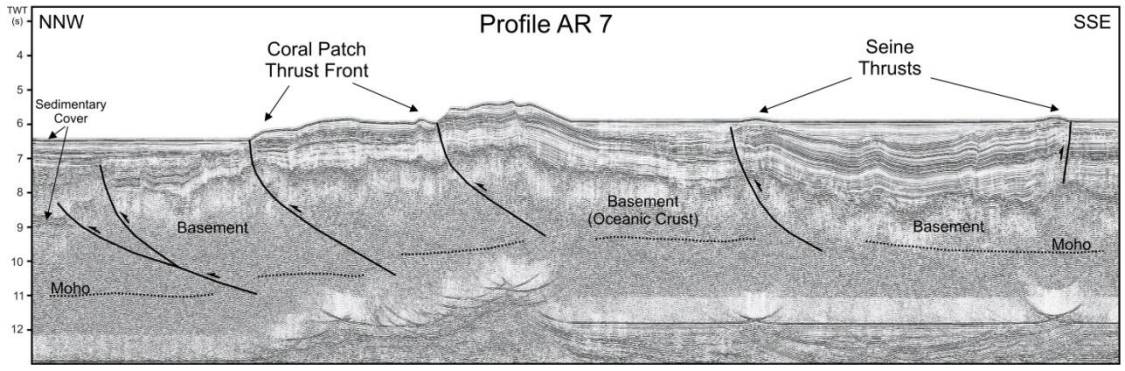


Figure 4.21 – Seismic section of the profile AR-7 intercepting the Coral Patch thrust front and the Seine thrusts (see Fig. 4.19 for location). Seismo-stratigraphy approximately corresponding to column A in Fig. 4.3.

The Portimão pop-up structure comprises two E-W antithetic thrusts bounding the Portimão Bank morphological high (Fig. 4.22). The E-W scarps are more prominent in the eastern part of the bank, where widespread landslide scars are observed, attesting for the activity of this structure (see Terrinha et al., 2009, in appendix). To the East the Portimão Bank is connected to the shelf by a relatively gentle slope. The southern thrust probably extends further east connecting with another thrust sub-parallel to the Cadiz fault (see Fig. 4.22 and text below). From the inspection of the seismic section presented in Fig. 4.23 it is possible to observe that the Portimão pop-up forms a slightly north-vergent anticline bounded by two thrusts that breach out through the seafloor, offsetting the cover sediments in more than 1 second. The southern thrust appears to have a wrenching component as attested by the presence of other minor faults, defining a flower-like structure (see Fig. 4.23). The Portimão pop-up also seems to have formed during the early Cenozoic in a phase of more North-directed convergence (see Terrinha et al., 2009, in appendix). Presently, this structure is probably accommodating some of the shortening component associated to the more oblique Nubia-Iberia convergence.

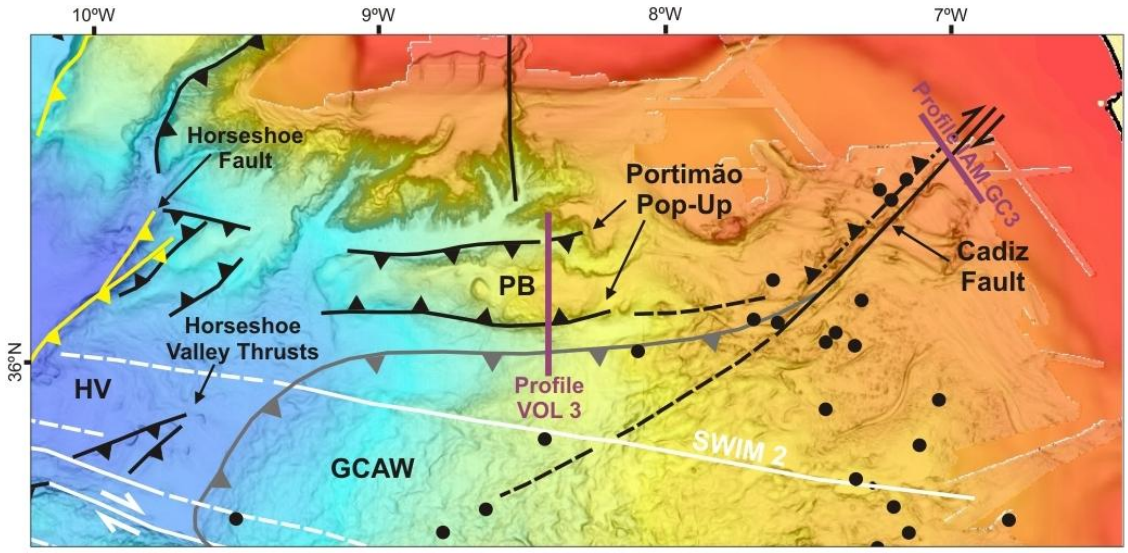


Figure 4.22 – Detailed bathymetry and structure of the Portimão pop-up and Cadiz fault region (see Fig. 4.2). The VOL-3 and IAM-GC3 seismic profile tracks (Figs. 4.23 and 4.25) are shown in purple. Black dots stand for mud volcanoes.

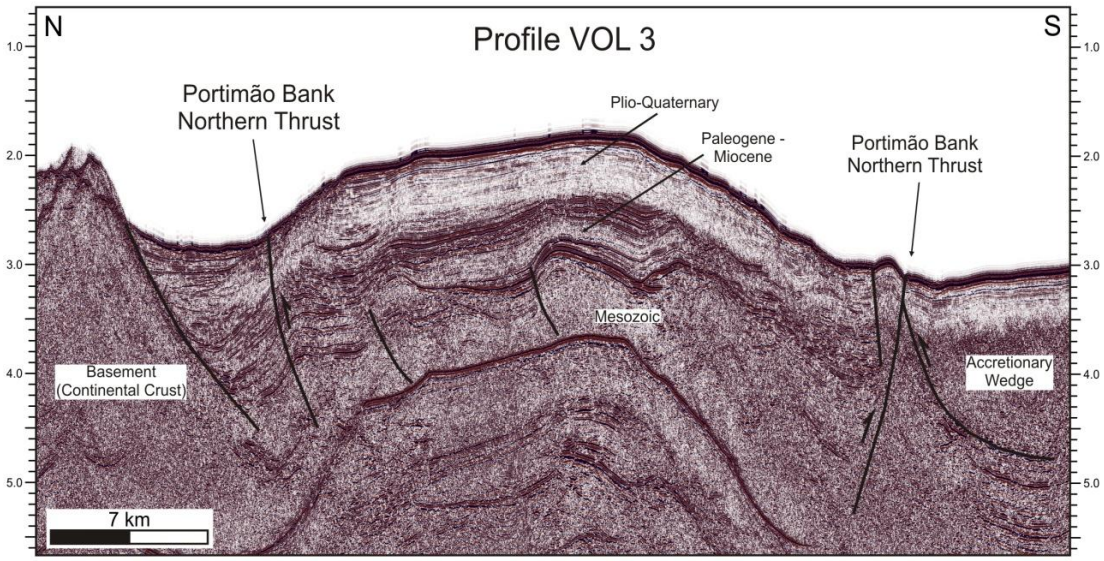


Figure 4.23 – Seismic section of the profile VOL-3 intercepting the Portimão pop-up structure (see Fig. 4.22 for location). Seismo-stratigraphy approximately corresponding to columns A and C in Fig. 4.3 (profile reinterpreted and simplified after Roque, 2007 and Terrinha et al., 2009, in appendix).

4.4.2. The Cadiz Fault

The Cadiz fault strikes approximately NE-SW and extends for about 200 km from the northeastern Gulf of Cadiz continental shelf to the inner part of the accretionary wedge (Fig. 4.22: see also Figs. 4.2 and 4.4). The fault probably extends towards the NE into the Guadalquivir river basin, in the Betics foreland. The fault is slightly curved towards the west in its southern segment where it intersects the SWIM 2 fault (see Fig. 4.22). Its seafloor morphology is complex (Fig. 4.24), defined by a relatively diffuse broad area with widths varying from several hundreds of meters to a few kilometers, materialized on the seafloor by the alignment of several different features such as crests, scarps, channels and diapiric ridges (see Figs. 4.22 and 4.24). The Cadiz fault morphological expression is more prominent in its northeastern segment and loses most of its expression progressively towards the South, vanishing in the surroundings of the SWIM 2 (see Figs. 4.2 and 4.22). However, several mud volcanoes are traceable southwards along the direction of the Cadiz fault suggesting that it may extend further south. The seismic section crossing the Cadiz fault (Fig. 4.25) shows that it is sub-parallel to a basement southeastwards-directed blind thrust, probably

contemporaneous of the Late Mesozoic - Early Cenozoic N-S convergence. The thrust movement is supported by the gentle folding of the reflectors of the basement. In the seismic profile is also possible to observe a thin-skinned fault accommodating the over-thrusting of the accretionary wedge Miocene deformation front towards NE, over the basement. Near the surface the more continuous Pliocene-Quaternary cover sediments are clearly folded; though, they do not show evidences of major vertical faulting and displacement, attesting for wrenching movement of the Cadiz fault, discussed in Duarte et al. (2009, in appendix). No kinematic indicators could clearly be detected, probably due to the high rate of recent sedimentation associated with the proximal parts of the Mediterranean Outflow Water and as well as to the extrusion of fluidized material along mud volcanoes. The same authors, based on data published by Stich et al. (2006), which reported a 3.5 mm.a-1 of westward motion of the Gibraltar arc relative to intra-plate Iberia, proposed that the Cadiz lineament is a major dextral strike-slip fault zone accommodating the westward expulsion of the Gibraltar Arc relative to Iberia (see Fig. 4.2). Also, a NE-SW elongated cluster of low to intermediate seismicity exists in this area attesting for the activity of this structure (see Fig. 4.17; and also Fig. 1.4).

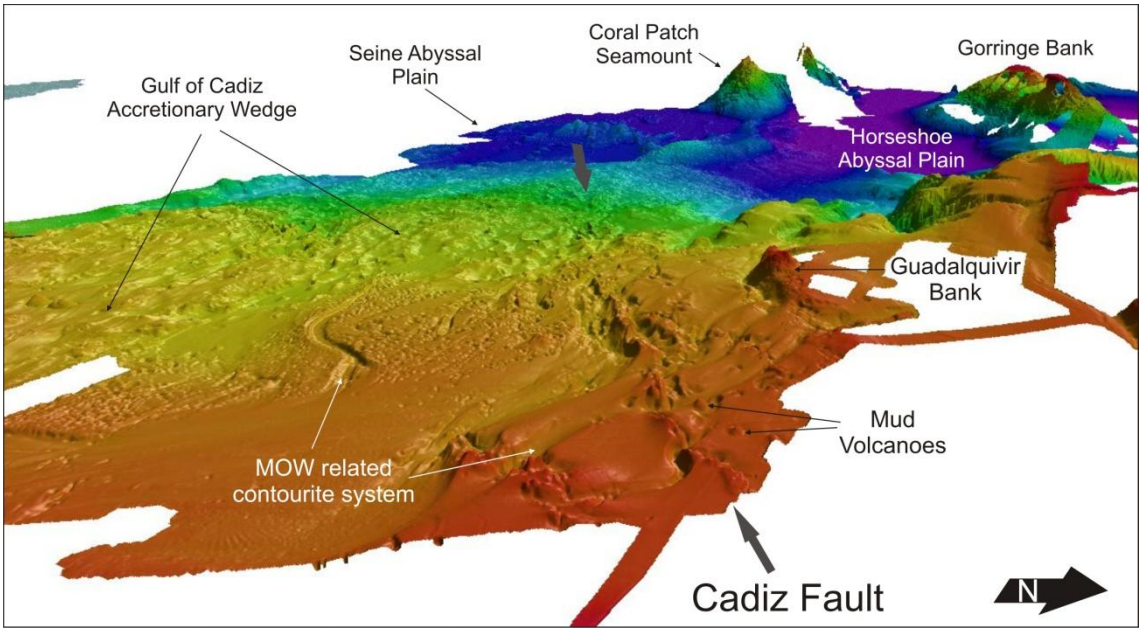


Figure 4.24 – Perspective view form NE of the Gulf of Cadiz. Note the morphological expression of the Cadiz fault (indicated by the two grey arrows) corresponding to a continuous alignment of crests and troughs, extending from the continental shelf to the accretionary wedge.

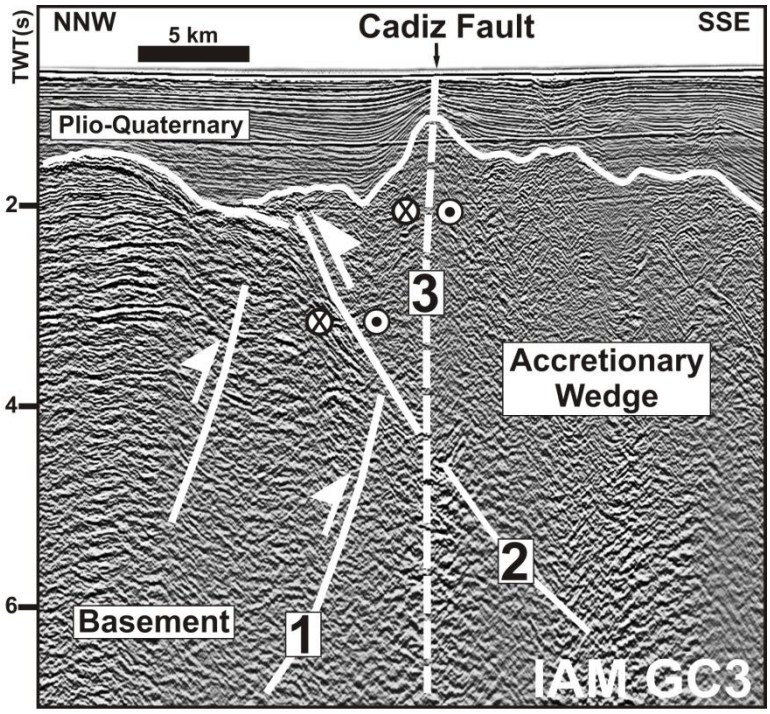


Figure 4.25 – Seismic section of the profile IAM-GC3 intercepting the Cadiz fault (see Fig. 4.22 for location). Seismo-stratigraphy approximately corresponding to column C in Fig. 4.3 (Modified from Duarte et al., 2009, in appendix). 1 – Southeastwards directed thick-skinned thrust possibly of Late Mesozoic- Early Cenozoic age; 2 – Northwestwards thin-skinned up-thrusting of the accretionary wedge Miocene deformation front; 3 - Present day strike-slip movement along the Cadiz fault.

Chapter 5
Crescent-shaped morphotectonic features in the Gulf of Cadiz (offshore SW Iberia)

J.C. Duarte, P. Terrinha, F.M. Rosas, V. Valadares, L.M. Pinheiro, L. Matias, V. Magalhães, C. Roque.

(This chapter is presented in a paper format, as published in Marine Geology; Duarte et al., 2010).

The subject of this chapter is a group of intriguing kilometric crescent-shaped depressions lying in the Horseshoe Valley, between the GCAW and Horseshoe fault (see area in Fig. 4.2). A detailed morphotectonic analysis of the Horseshoe Valley contributed for the unraveling of the processes that originated these crescentic depressions. The present work showed that these features formed as the result of the interaction between downslope currents and tectonically-originated slope breaks. The crescentic depressions are controlled by active (blind) thrust faults that root at the GCAW décollement layer, to the west of the GCAW deformation front. Therefore, the crescentic depressions seem to correspond to the morphological expression of the westward propagation of the deformation from the realm of the accretionary wedge (GCAW), into the Horseshoe Valley domain.

Abstract

Multibeam swath bathymetry data from the Northwestern part of the Gulf of Cadiz revealed the existence of several intriguing kilometric crescentic depressions lying between -4300 m and -4700 m, never before reported to occur at such great depths. Morphological parameterization of these features, coupled with detailed analysis of multi-channel and middle resolution seismic profiles, showed that these crescent-shaped features were formed due to the existence of specific time-recurrent interaction between: a) regional active thrusts, which portray the overall tectonic scenario in the area, and on top of which most crescentic depressions are carved; and b) tectonically induced scouring comprising localized erosion and simultaneous progradational sedimentation, produced by downslope currents of probable turbiditic origin. The obtained results also suggest a possible contribution of fluid migration and extrusion processes, such as mud volcanism and associated pockmark formation, besides gravity driven landslides and slumping, in the development of the studied crescentic depressions.

Keywords: Gulf of Cadiz morphotectonics; deep sea crescent-shaped features; deep-water sedimentary processes; deep sea scouring.

5.1. Introduction

5.1.1. Previous work

Crescent-shaped morphologies in association with escarpments are common in submarine and sub-aerial slope surfaces (e.g. sand dunes). They are frequently associated with gravitational mass transport (e.g. landslides and slumps), fluid escape and erosive processes. Landslides are typically bounded by arcuate, concave-downhill head scarps and concave uphill toes (Locat and Lee, 2000; McAdoo et al., 2000; Wilson et al., 2004; Martel, 2004). Features caused by collapse processes associated with fluid escape and mud volcanism can also exhibit crescent-shaped morphologies (Dimitrov and Woodside, 2003; Somoza et al., 2003; León et al., 2006), as in the case of asymmetrical pockmarks when occurring on slopes (Hovland and Judd, 1988). Submarine crescent-shaped morphologies related to erosional processes, such as scouring, are also documented in various geological settings, and usually associated with turbidity, downslope and bottom currents: Faugères et al. (1997) reported the existence of erosion scours in the termination of the Barbados Prism, at depths of about 3000 m; Bulat and Long (2001) described a group of crescent-shaped scours in the Faroe-Shetland Channel with escarpments up to 200 m high, lying at depths of 200 m; Bonnel et al. (2005) described features in the Gulf of Lions formed by erosion-deposition processes associated with turbidity currents; Verdichio and Trincardi (2006) reported a set of crescent-shaped features at depths of about 600 m with escarpments up to 50 m in the Southwest Adriactic Margin, formed by bottom currents; Fildani et al. (2006) recognized a group of crescent-shaped giant scours with escarpments up to 100 m height at depths of about 3500 m near Monterey East Channel.

In the North-eastern part of the Gulf of Cadiz, sub-circular seafloor features interpreted as asymmetrical pockmarks, slide scars and erosion scours, associated with mud volcanism, hydrocarbon seepage, mass wasting processes and bottom currents activity have also been described (e.g. Somoza et al., 2003; Léon et al., 2006; Hernández-Molina et al., 2006; Mulder et al., 2006; Hanquiez et al., 2007). However, unlike the ones discussed in this work, most of these features are located at relatively shallow depths, ranging from the outer continental shelf to the middle continental slope.

In the present paper we report the existence of submarine kilometric crescentic depressions at depths of more than 4000 m (between -4300 m and -4700 m). Based on recently acquired multibeam swath bathymetry data (Zitellini et al., 2009; Terrinha et al., 2009), coupled with the analysis of available multi-channel seismics (MCS) and middle resolution seismic profiles, we supply a detailed morphological description of these features, their internal sedimentary structure and their structural setting and discuss different processes that could have led to their formation.

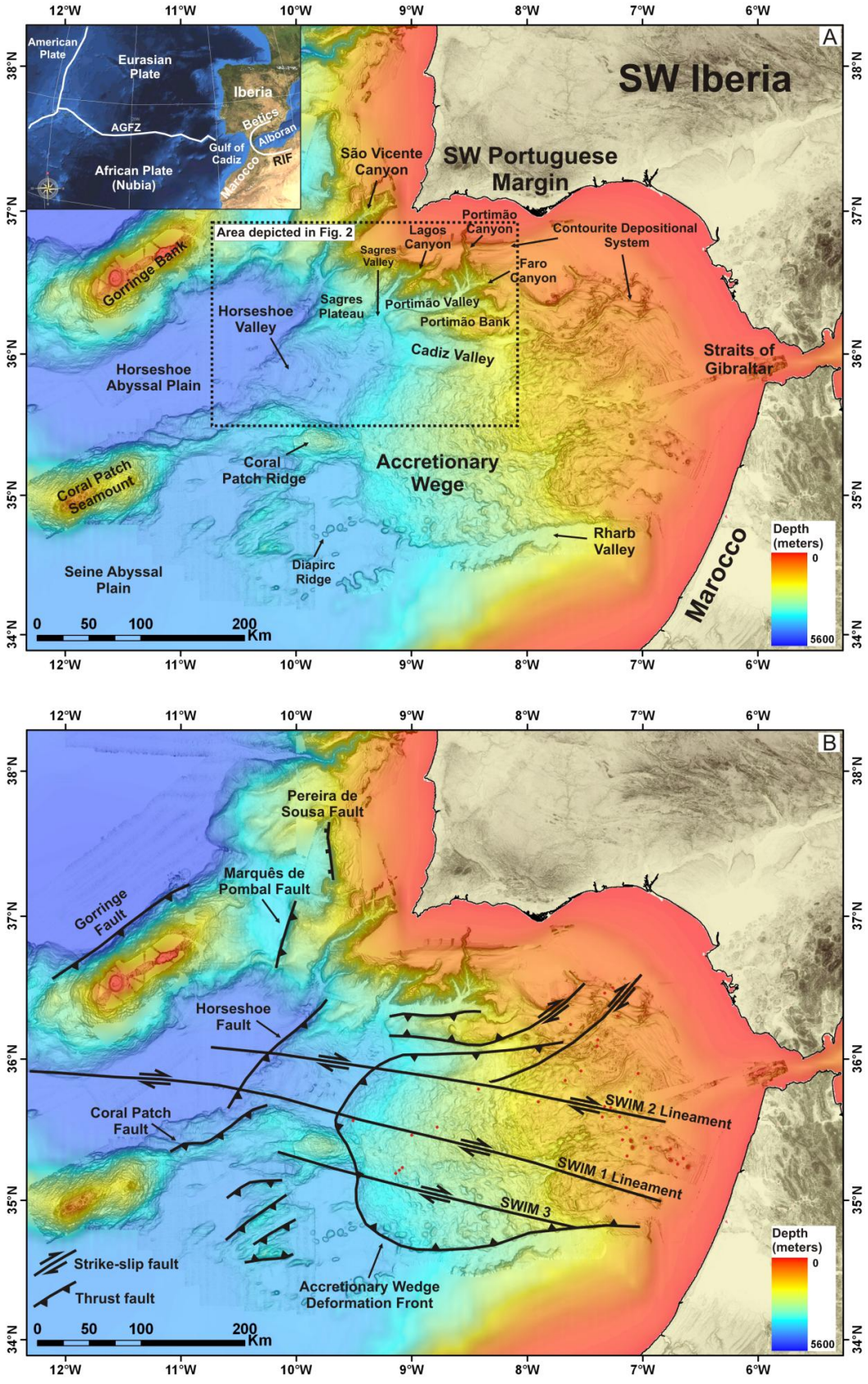
5.1.2. General tectonic setting and geomorphology

The Gulf of Cadiz is located in the Atlantic Ocean offshore SW Iberia and NW Morocco (Fig. 5.1A and inset), comprising the easternmost segment of the Azores-Gibraltar Fracture Zone, which is interpreted as the Atlantic Africa-Eurasia main plate boundary (e.g. Purdy, 1975; Zitellini et al., 2009). The most important tectonic features presently observed in the Gulf of Cadiz (Fig. 5.1B) result from the Early Cenozoic to Late Miocene Alpine orogenesis overprinted onto preexistent extensional basins of Triassic-Cretaceous age (Terrinha, 1998). This evolution is associated with the collision between Iberia and northwest Africa (Nubia) tectonic plates, which ultimately led to the formation of the Betic-Rif orogenic arc in Miocene times and the submarine accretionary wedge of the Gulf of Cadiz (e.g. Srivastava et al., 1990; Lonergan and White, 1997; Maldonado et al., 1999; Rosenbaum et al., 2002a,b, Gutscher et al., 2002; Iribarren et al., 2007). Late Miocene to present tectonics is mainly determined by: a) oblique convergence between Nubia and Eurasia (Iberia) plates (Calais et al., 2003); and b) Eastward dipping subduction of an oceanic slab with development of the Gulf of Cadiz accretionary prism (Gutscher et al., 2002).

The overall morphological shaping of the Gulf of Cadiz results from the interaction between regional active tectonics, sedimentation and erosional processes, fluid migration and escape and oceanographic dynamics (Gutscher et al., 2002; Gutscher et al., 2009; Pinheiro et al., 2003; Somoza et al., 2003; Hernández-Molina et al., 2006; Terrinha et al., 2009). The form and geographic location of this region,

enclosing in its easternmost domain the gateway to the Mediterranean Sea across the Straits of Gibraltar (Fig. 5.1), locally determines the behaviour of various major water masses, such as the North Atlantic Deep Water and particularly the Mediterranean Outflow Water - MOW (e.g. Ambar and Howe, 1979a,b; Llave et al., 2001; Johnson et al., 2002; Llave et al., 2006; Mulder et al., 2006; Hernández-Molina et al., 2006, 2008). A more detailed characterization of the Gulf of Cadiz allowed the recognition of the several main geomorphologic features depicted in Fig. 5.1A. The kilometric crescentic depressions targeted in this work are located in the so called Horseshoe Valley, offshore the SW Iberian margin (see Fig. 5.1A, 5.2, 5.3). This area displays a network of well developed submarine, canyons, gulleys and wide valleys, which are related to the channelling of downslope and turbidity currents, driving the sediments from the continental shelf and slope to the abyssal plain (Fig. 5.2B). Here, the impact of downslope processes on the shaping of the seafloor is clearly dominant. Moreover, this area is subjected to tectonic uplift (Terrinha et al., 2003, Gràcia et al., 2003), related to general north-westward thrusting in the Gulf of Cadiz, which favours erosion by valley inception as a response to higher slope and more abrupt morphology building (Zitellini et al., 2004, Terrinha et al., 2009).

Figure 5.1 (next page) – (A) Gulf of Cadiz main geomorphologic features. Inset: Location of the Gulf of Cadiz area in the general tectonic setting of the Eurasia (Iberia) - Africa (Nubia) plate boundary (AGFZ - Azores-Gibraltar Fracture Zone); (B) Simplified tectonic map of the Gulf of Cadiz area. Offshore bathymetry from SWIM Compilation (Zitellini et al., 2009) completed with GEBCO (2003). SWIM lineaments correspond to aligned arrays of deep seated, sub-vertical, dextral strike-slip faults (op. cit.). Red dots correspond to mud volcanoes (Hensen et al., 2007).


A
SW Iberia
SW Portuguese Margin
São Vicente Canyon
Portimão Canyon
Contourite Depositional System
Lagos Canyon
Sagres Valley
Faro Canyon
Area depicted in Fig. 2
Gorringe Bank
Horseshoe Valley
Sagres Plateau
Portimão Valley
Portimão Bank
Cadiz Valley
Straits of Gibraltar
Horseshoe Abyssal Plain
Coral Patch Ridge
Accretionary Wege
Coral Patch Seamount
Rharb Valley
Diapirc Ridge
Seine Abyssal Plain
Marocco
Depth (meters)
0
5600
0 50 100 200 Km
American Plate
Eurasian Plate
Iberia
Betics
Alboran
AGFZ
Gulf of Cadiz
RIF
African Plate (Nubia)
Marocco
B
Pereira de Sousa Fault
Marquês de Pombal Fault
Gorringe Fault
Horseshoe Fault
Coral Patch Fault
SWIM 2 Lineament
SWIM 1 Lineament
SWIM 3
Strike-slip fault
Thrust fault
Accretionary Wedge Deformation Front
Depth (meters)
0
5600
0 50 100 200 Km
12°W
11°W
10°W
9°W
8°W
7°W
6°W
38°N
37°N
36°N
35°N
34°N

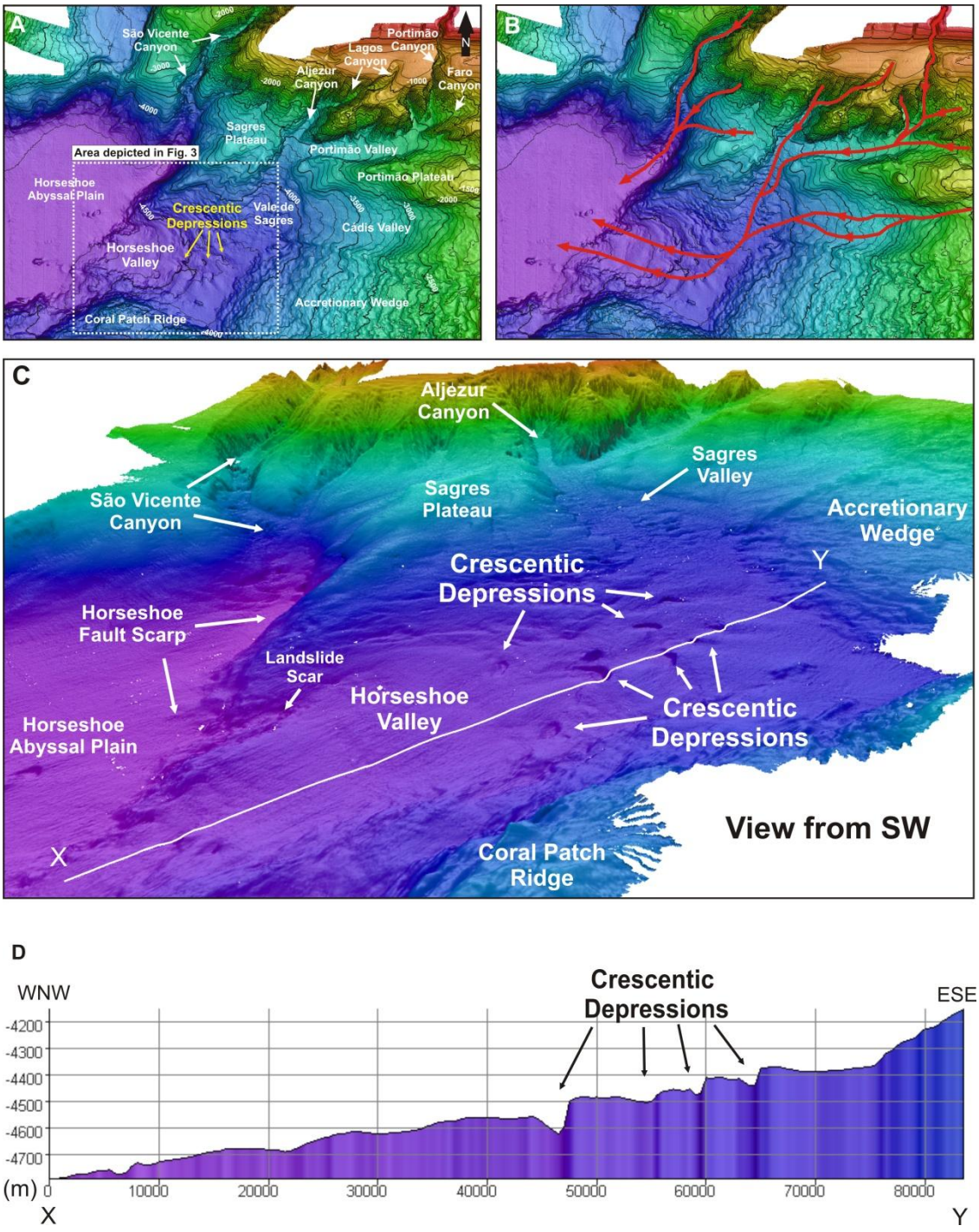


Figure 5.2 – (A) Location of the studied crescentic depressions offshore SW Iberian Margin (3D digital bathymetry model from MATESPRO dataset, Terrinha et al., 2009); (B) General drainage system of the local continental shelf and slope (after Duarte, 2007); (C) Perspective view (from SW) of the Horseshoe Valley and surrounding main morphotectonic features; (D) WNW-ESE bathymetric profile along the Horseshoe Valley intersecting the crescentic depressions (vertical exaggeration factor of 8).

5.2. Methodology and data

The discovery of the seafloor crescentic depressions described in this paper resulted from the analysis of two main sets of data: multibeam swath bathymetry and seismic reflection. The bathymetry data were used to characterize the geomorphology of the area where the crescentic depressions are situated and also to accomplish a detailed morphological parameterization of these features. The seismic reflection dataset comprises multi-channel and middle resolution seismics. The multi-channel seismics were used to unravel the general deep structure of the area where the crescentic depressions are located, whereas the analysis of higher resolution profiles aimed at a detailed characterization of the shallow structure and sedimentary architecture of these features.

5.2.1. Multibeam swath bathymetry data

The multibeam swath bathymetry dataset was acquired during the MATESPRO (Major TEctonic and Sedimentary PROcesses in the Portuguese Margins – see Figs. 5.2, 5.4) cruise, onboard the Portuguese vessel NRP D. Carlos I in June/July 2004 (Terrinha et al., 2009). The cruise covered a total area of approximately 38 000 km^2 in the northwestern part of the Gulf of Cadiz region. The bathymetric data were acquired using a hull-mounted Simrad EM120 multibeam echosounder, fulfilling the rules established by the International Hydrographic Organization for an order 3 hydrographic survey (see Terrinha et al., 2009). Interpretation was made using terrain analysis techniques and image analysis of the bathymetry using commercial software, ArcGIS and Fledermaus.

5.2.2. Seismic reflection data

Multi-channel seismic profiles of the Iberian Atlantic Margin campaign (Banda et al., 1995; Tortella et al., 1997) were used for the inspection of the deep structure. Two single-channel seismic profiles were acquired (PSAT-244 and 246) during the 14th Training-Through-Research cruise of UNESCO –IOC, Leg 1, onboard of the Russian vessel RV Professor Logachev in July/August 2004 (Fig. 5.3; Kenyon et al., 2006), in the scope of the MVSEIS Euromargins Project. The MCS has a vertical resolution between 20 and 50 m and the single channel have a vertical resolution of about 2 to 5 m.

5.3. Morphotectonic characterization of the crescentic depressions

5.3.1. Morphotectonic setting: the Horseshoe Valley

The Horseshoe Valley, together with the S. Vincent canyon, is one of the two collectors of the shelf and slope erosive system of southwest Iberia that converge into the Horseshoe Abyssal Plain. The studied crescentic depressions are located in the Horseshoe Valley (HV) (Figs. 5.2, 5.3) that collects the Aljezur, Portimão, Lagos and Faro Canyons, the Portimão and the Cadiz Valley. The HV has a trapezoidal shape with depths varying between -4200 m to -4800 m and a mean slope of 0.5º to the west.

The HV is delimited by the Sagres Plateau in the North, by the Coral Patch Ridge in the South, and by the deformation front of the Gulf of Cadiz accretionary wedge in the East (Figs. 5.2A, C, 5.3). To the West, the HV is bounded by the NE-SW trending Horseshoe Fault, which corresponds to a westward directed active thrust (Gràcia et al., 2003, Zitellini et al., 2004), whose morphologic expression is marked by a hundred meter high scarp separating this domain from the westward adjacent Horseshoe Abyssal Plain (see Figs. 5.1B, 5.2C). The drainage system finds its way

across the Horseshoe Fault scarp along narrows gullies that are the loci of retreating erosion showing evidences of landslide occurrence (Fig. 5.2).

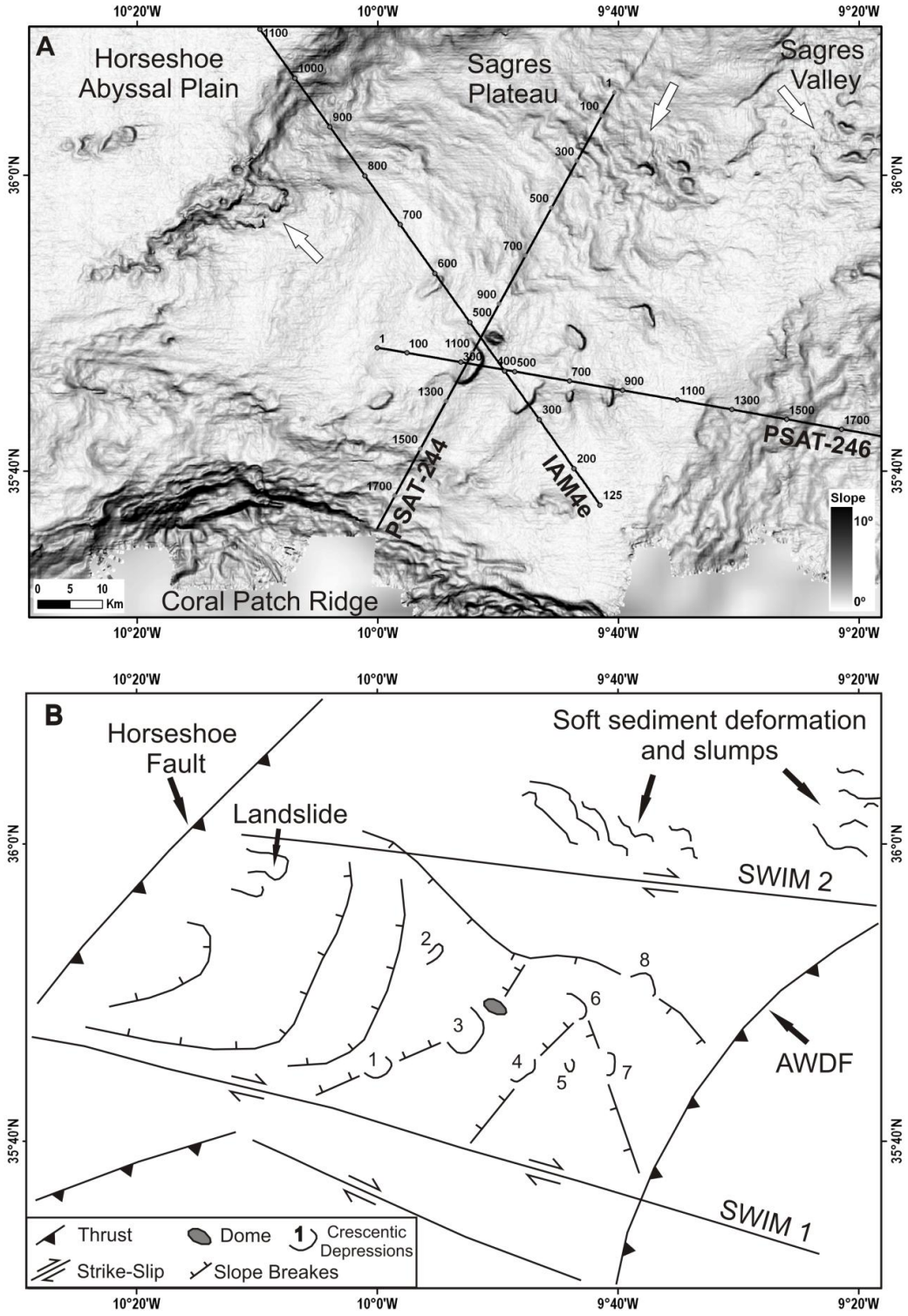


Figure 5.3 – (A) Bathymetry and slope map of the Horseshoe Valley. Location of the seismic profiles IAM-4e, PSAT-244 and PSAT-246; White arrows refer to the location of undulated seafloor features, e.g. slumps and landslides. (B) Line drawing depicting the interpretation of the main morphotectonic features observed and the numbering of the study crescentic depressions.

The flat area of the Horseshoe Valley is thus interpreted as being uplifted on the hanging wall of the deep seated Horseshoe Fault (e.g. Tortella et al., 1997; Zitellini et al., 2004; Terrinha et al., 2009). This area is also affected by several major WNW-ESE trending lineaments, the SWIM lineaments (Figs. 5.1B, 5.3B), which were recently interpreted as aligned arrays of also deep seated, sub-vertical, dextral strike-slip faults (Terrinha et al., 2009; Rosas et al., 2009; Zitellini et al., 2009). The transitional area from the Sagres Valley to the Horseshoe Valley displays an undulated seafloor surface comprising waves varying from hundreds of meters to more than 10 km in length, and up to 5 km across (white arrows in Fig. 5.3). These features are generally straight to slightly sinuous, and their undulated surfaces have also been previously interpreted as the bathymetric expression of mass transport processes and soft sediment deformation, including gravity driven folds, small scale slumps and turbiditic erosional/deposition features (Terrinha et al., 2009).

Despite the shallow dip of the Horseshoe Valley, a thorough analysis of its bathymetry allowed the identification of slope breaks, separating a staircase-like series of flats, descending in the direction of the Horseshoe Abyssal Plain (Fig. 5.3). Some of these scarps correspond to NE-SW trending folds sitting on top of westwards directed blind thrusts as described elsewhere in this work. The crescentic depressions reported in this work are located on these slope breaks (Figs. 5.3, 5.4).

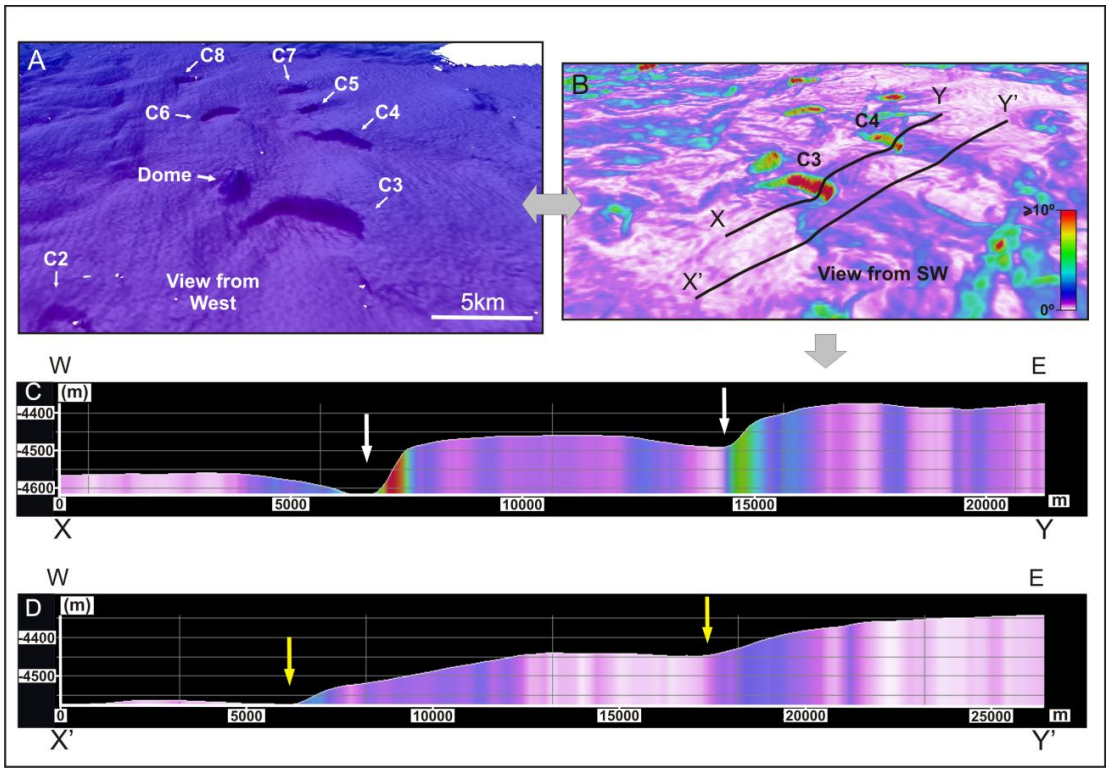


Figure 5.4 –3D imaging of the Horseshoe Valley domain comprising the study crescentic depressions (digital bathymetry model from MATESPRO dataset, vertical exaggeration factor of 8): (A) General view from West of crescentic depressions C2 to C8; (B) Depiction of slope value distribution in the study area (SW view); (C) Bathymetric profile X-Y intersecting two slope breaks corresponding to the depressions 3 and 4 (white arrows), illustrating the striking contrast between the smooth dip of the Horseshoe Valley seafloor and the abruptness of the crescentic escarpments; (D) Parallel bathymetric profile X'-Y' that does not cut across the crescentic depressions, depicting the existence of smoother slope breaks in the Horseshoe Valley seafloor (yellow arrows).

5.3.2. Geometry of the Horseshoe Valley crescentic depressions

The study objects of this work are the crescentic depressions that are located strictly within the HV only. This is because, *firstly*, they bear no obvious association with gravity or mass transport processes as others in the Gulf of Cadiz, like the ones located further north on the slope of the Sagres plateau (see Fig. 5.3), *secondly*, they cluster within the shallow dipping channel (HV mean dip is 0.5º and the maximum local dip is 3º) that collects the drainage system already mentioned, *thirdly*, they are located between two main tectonic structures, the Horseshoe Fault and the accretionary wedge

and, *fourthly*, they are probably the deepest crescent shapes described in the scientific literature, between -4300m and -4700m.

The crescentic depressions exhibit a morphology consisting of downslope concave crescent-shaped escarpments surrounding an internal depression with kilometric lengths (Figs. 5.4, 5.5A). Morphological parameters were used to describe eight crescentic depressions in the HV, as depicted in Fig. 5.5B and in Table 5.1.

5.3.2.1. Height and slope of the crescentic depression scarps

The height and slope of the crescent-shaped escarpments can be seen as expressing the degree of abruptness (or steepness) of these features. The measured data (Table 5.1) show a mean slope value of approximately 0.2 (~11º dip), with the exception of crescentic depression 5 in which the escarpment exhibits a higher slope of 0.51 (~27º dip). The escarpment heights vary mostly between 80 m and 120 m, with the exceptions of depressions 1 and 2, which show heights of 50 m and 30 m respectively. Based on these data (slope and height) no consistent relationship can be drawn between the variation of the abruptness of the individual crescentic depressions and their location in the HV. In fact, the data shows that some constancy exists in the steepness of the escarpment crescents regardless of their different locations, shapes and sizes. The roughly linear relationship between height and width suggests that the steepness might depend on material properties, such as cohesion or plastic yield point, for the cases of loose materials like sand or clays, respectively.

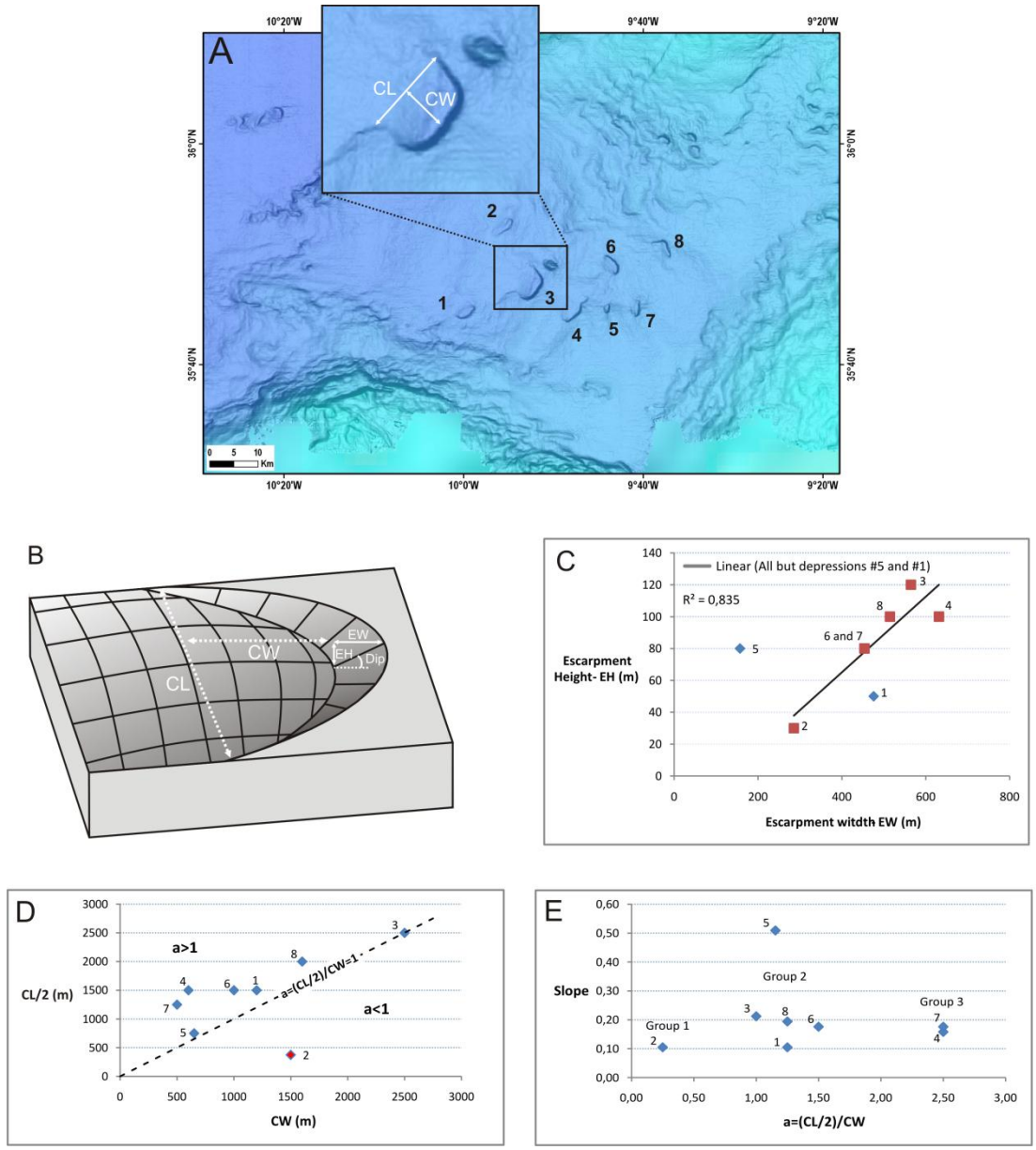


Figure 5.5 – Morphological parameterization of the studied crescentic depressions. (A) Location of the crescentic depressions in the Horseshoe Valley (1 to 8), and zoom of depressions 3; (B) - 3D sketch of a crescentic depressions illustrating the used morphological parameters: CL - Crescentic depression Length; CW - Crescentic depression Width; EW - Escarpment Width; EH - Escarpment Height; (C) Graphic display of measured values of EH versus EW (escarpment slope) for all the studied features; (D) Graphic display of CL/2 versus CW (parameter a) for the studied features (dashed line corresponds to CL/2=CW); (E) Graphic display of obtained values of slope versus a parameter for all crescentic depressions. See further explanation in the text. R2 - squared linear correlation coefficient.

5.3.2.2. Crescentic depression axial ratio - a

The internal depressions of the studied features exhibit widths and lengths (parameters CW and CL as defined in Figs. 5.5A – inset, and B) that vary from 500 m to 2500 m, and between 750 and 5000 m, respectively (Table 5.1). The axial ratio of the crescentic depressions is here defined as:

$$a = \frac{CL/2}{CW}$$

Parameter *a* equals 1 when the general overall shape of the depression approximates a semi-circumference. If depressions show semi-elliptical shapes, *a* is either >1, when CL/2> CW as is generally the case, or *a* <1, when CL/2<CW.

Similarly to what was referred above for height and slope, no coherent/linear relationship exists between *a* and the individual location of the crescentic depressions in the Horseshoe Valley. Moreover, it is also clear from the graphic in Fig. 5.5D that with the exception of feature 2, all samples plot at values of $a \geq 1$, meaning that crescentic depressions tend to develop similar shapes in spite of their different locations.

In Fig. 5.5E, the relationship between the slope and the axial ratio is graphically illustrated. Because the slope values are constant (between ~0.1 and ~0.25, see Fig. 5.5C), all samples but feature 5 cluster under constant slope of ~0.25 and it is clear that the crescentic depressions cluster in three groups as a function of their different values of *a*. The first group (Group 1 in Fig. 5.5E) consists of feature 2 only, which exhibits a singular low *a* value, implying an extreme concavity, and a highly elongated geometry parallel to the direction of its longest CW axis (see Figs. 5.3B, 5.4, 5.5A). Group 2 includes 5 of the 8 crescentic depressions with *a* values comprised between 1.0 and 1.5 (mean *a* value of ~1.23). Finally, the third group comprises crescentic depressions 4 and 7 with relatively high *a* values of 2.5, implying highly elongated semi-elliptical shapes.

It should be noted that with the exception of crescentic depressions 2 and 5, which show anomalous values of axial ratio and slope, all the crescentic escarpments are oriented parallel to the direction of the large scale slope breaks that disrupt the Horseshoe Valley seafloor (see Figs. 5.3, 5.4).

Table 5.1 – Measured morphological parameters.

Crescentic Depressions (see Fig. 5.5)	Escarpment Height - EH (m)	Escarpment Width - EW (m)	Dip (°)	Slope	Crescentic Depressions Length - CL (m)	CL/2 (m)	Crescentic Depressions Width - CW (m)	Axial ratio a=(CL/2)/CW
1	50	476	6	0.11	3000	1500	1200	1.25
2	30	285	6	0.11	750	375	1500	0.25
3	120	565	12	0.21	5000	2500	2500	1.00
4	100	631	9	0.16	3000	1500	600	2.50
5	80	157	27	0.51	1500	750	650	1.15
6	80	454	10	0.18	3000	1500	1000	1.50
7	80	454	10	0.18	2500	1250	500	2.50
8	100	514	11	0.19	4000	2000	1600	1.25
Mean values	80	442	11.38	0.20	2843.75	1421.88	1193.75	1.43

5.3.3. Sedimentary and tectonic structure of the crescentic depressions

The description of the detailed structural architecture of the crescentic depressions was based on the interpretation of multi-channel (IAM4e, Fig. 5.6) and middle resolution seismic profiles (PSAT246 and PSAT 244, Figs. 5.7, 5.8).

5.3.3.1. Multi-channel seismic profile IAM4e

The IAM4e profile strikes NW-SE along the Horseshoe Valley intersecting crescentic depressions 2 and 4 and passing close to number 3 (see Fig. 5.6; 5.3 for the location of the profile). It comprises the following seismostratigraphic units and sub-units:

a) A basal unit (A) of coherent high amplitude, continuous and parallel reflections, with a thickness of about 2 s (twt), corresponding to Mesozoic through Eocene rocks (Tortella et al., 1997). This unit is cut by several reverse faults that also affect the overlying units, but do not breach out at the seafloor surface. The exception to this is the Horseshoe Fault, which cuts through all the cover units offsetting them by approximately 1 s (twt).

b) Unit B is approximately ~1.5 s (twt) thick, has a semi-chaotic seismic signature, characterized by high amplitude shallow dipping discontinuous seismic reflections with continuous eastwards dipping reflections. The latter can be continuously followed for more than 10km and have been interpreted by various authors as thrust imbricate of middle Miocene age, and olistostromes deposits (Torelli et al., 1997; Tortella et al., 1997), that detach at the sole of Unit B (Fig. 5.6). Some of these thrusts were reactivated as blind thrusts in Pliocene-Quaternary times because they deform the sediments of this age that are included in Unit C. The deformation caused by the blind thrusts is accommodated by the top Unit C by folds that account for the stepped morphology of the HV. The majority of the crescentic depressions are located along these folds, carved in their slope breaks that disrupt the Horseshoe Valley seafloor (see Fig. 5.3, 5.4, 5.6).

c) A top Unit C of ~ 0.5 s (twt) of thickness, generally characterized by very well imaged parallel reflections, corresponding to a hemi-pelagic sedimentary cover that accordingly with Tortella et al. (1997) comprises two seismostratigraphic sub-units of different age (SU1 and SU2 in Fig. 5.6):

- A Late Miocene sub-unit (SU1) that exhibits a thickness varying between 0.1 s to 0.3 s (twt), consisting of high amplitude, high frequency, coherent reflections with onlap and downlap terminations on top of a folded and faulted basal discontinuity, which separates SU1 from the underlying lower to middle Miocene unit;

- A Pliocene-Quaternary sub-unit (SU2) with a fairly constant thickness of about 0.2 s (twt), consisting of a sequence of high amplitude reflections, although less coherent than those of SU1, showing a parallel to prograding geometry, with downlap and onlap terminations.

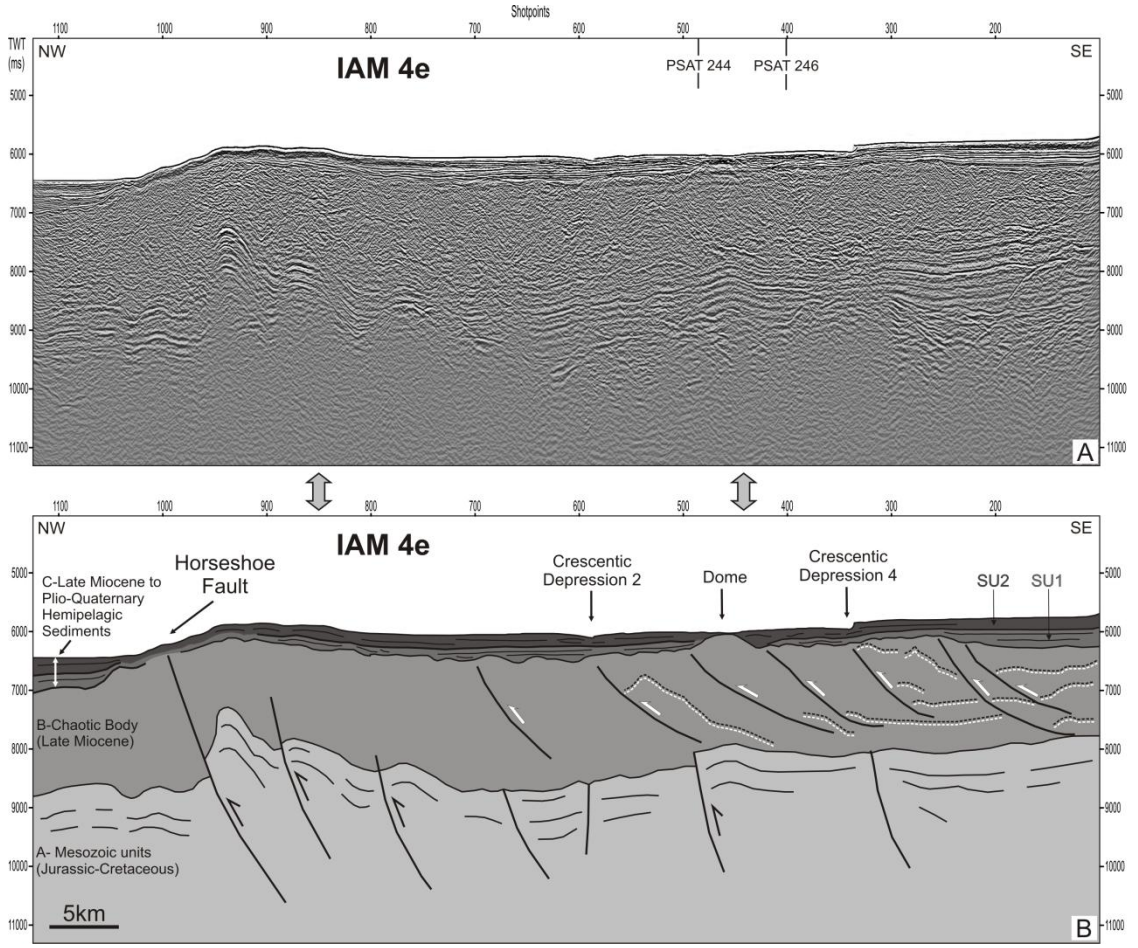


Figure 5.6 – (A) Multi-channel seismic profile IAM-4e intersecting crescentic depressions 2 and 4 (see Fig. 5.3 for location); (B) Correspondent seismostratigraphic and tectonic interpretation. Thin black lines - seismic reflectors interpreted as stratigraphic horizons; Double-dashed black and white lines - intra-chaotic body reflections interpreted as décollement horizons and folded layered sediments. Note that crescentic depressions 2 and 4 are located on top of blindthrusts rooted in the sole of the chaotic body. SU1 and SU2 – Late Miocene to Plio-Quaternary sub-units.

In the IAM4e profile a dome-like structure at the top of Unit B can be seen around shot point 460 (Fig. 5.6). This dome is seemingly impinging the uppermost cover unit, reaching the seafloor surface and producing a bathymetric ellipsoidal ridge in the vicinity of crescentic depression 3, clearly seen in the bathymetry (see Figs. 5.3, 5.4). This dome shows a WNW-ESE elongation and a maximum high of 100 m.

Crescentic depressions 2 and 4 incise the subunit SU2 as imaged at shot points 587 and 340 in the IAM4e profile (Fig. 5.6). These crescentic depressions are located on top of hanging wall anticlines of upward propagating blind thrusts that are well

recognized in Unit B. Despite the low resolution of this multi-channel seismic reflection profile it is clear that the escarpment of depression 4 corresponds to an erosional surface, since it truncates the uppermost seismic horizons. An upward convex geometry of the internal part of the depression is also detectable at this resolution and is imaged at a higher resolution in Fig. 5.7.

5.3.3.2. Middle resolution seismic profiles (PSAT-246 and PSAT-244)

The detailed structure of the crescentic depression could only be comprehensively addressed through the examination of the higher resolution seismic profiles PSAT-246 and PSAT-244 specifically acquired for this purpose. The attenuation of acoustic energy by the water column of 4 km and sediments did not allow imaging below stratigraphic Unit C, to a maximum of circa 0.5 s (twt). The base of Unit C was cross checked with IAM4e seismic profile.

The WNW-ESE oriented PSAT-246 profile cuts across crescentic depressions 3 and 7 (Fig. 5.7, 5.3 for location). In its eastern part, between the Accretionary Wedge Deformation Front (AWDF) and depression 7, the lower SU1 sub-unit shows a succession of coherent reflectors with parallel, gently folded configuration (Fig. 5.7). The continuation of this unit to the West of depression 7 is not clear, and it was only interpretatively assumed by correlation with the slightly oblique (NW-SE) IAM4e profile (see Fig. 5.3). The sub-unit SU2 is recognizable along the whole of the WNW-ESE profile length. Between the AWDF and crescentic depression 7, the reflectors in this sub-unit also exhibit a slightly folded configuration, but this is attenuated towards the surface, where the reflections are almost horizontal (Fig. 5.7). Close to crescentic depressions 7 and 3, to the West of each of their escarpments, sub-unit SU2 consists of several individual uphill progradation bodies. This, together with the truncation of sub-unit SU2 horizons behind the crescent-shaped scarps suggests uphill progradation of the sedimentary infill simultaneous with escarpment retreat (Fig. 5.7B). In the internal part of depression 3 several progadation bodies are buried (SU2a, SU2b and SU2c - Fig.

5.7C), separated by planar discontinuities (d2, d3 and d4, respectively) matching erosive truncations, against which the reflectors often exhibit onlap and downlap terminations.

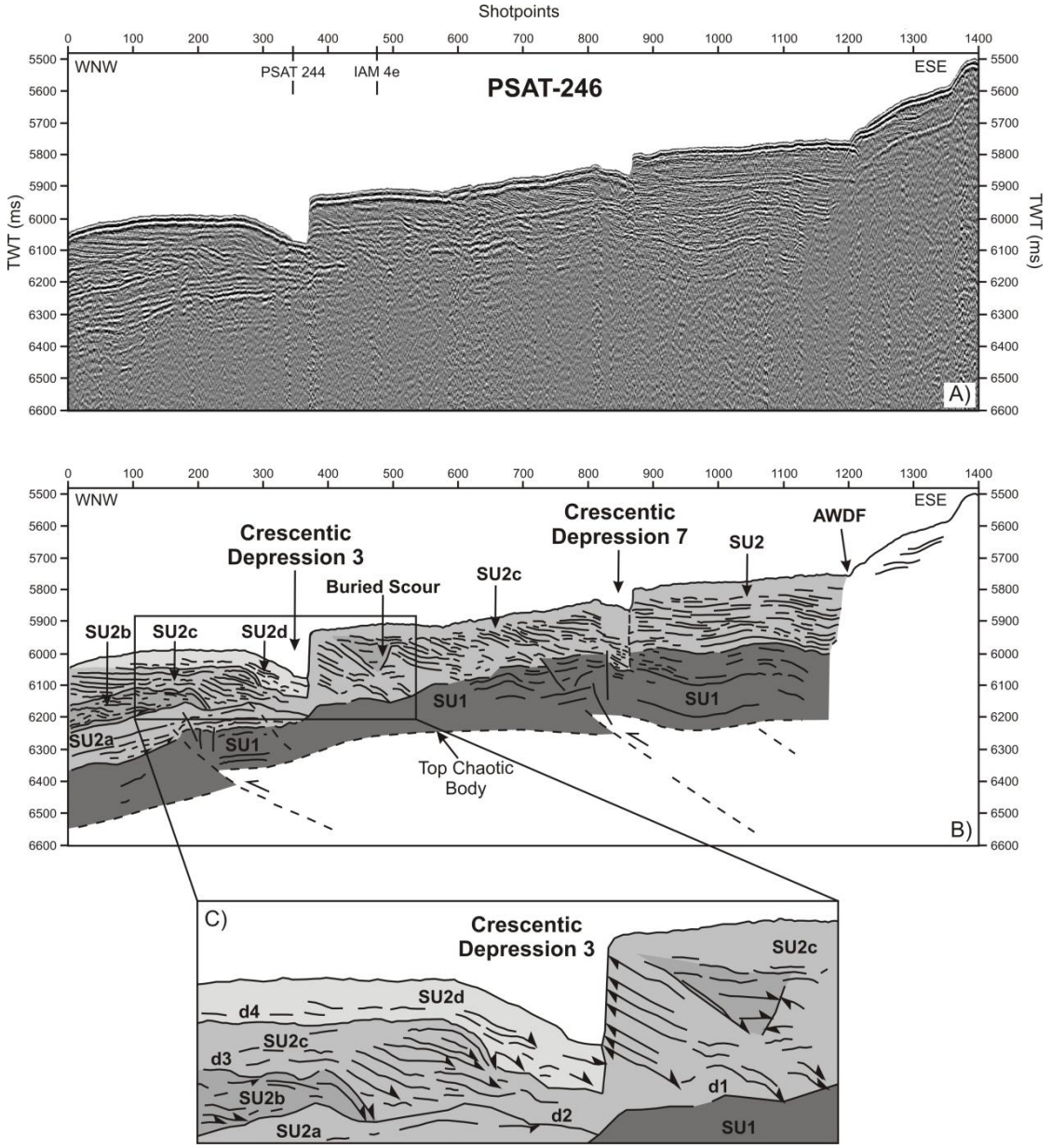


Figure 5.7 – (A) PSAT-246 seismic profile, intersecting the Accretionary Wedge Deformation Front (AWDF), and crescentic depressions 3 and 7 (see Fig. 5.3 for location); (B) Simplified seismostratigraphic/structural interpretation. SU1 and SU2 – Late Miocene to Plio-Quaternary sub-units; SU2a-d – Progradational bodies (lobes); d1-4 –Stratigraphic discontinuities.

The NE-SW oriented PSAT-244 profile intersects the internal part of crescentic depression 3, thus providing a strike-section of the prograding internal bodies and sections across the tip points of the depressions scarp (Figs. 5.3, 5.8). It is also possible to observe the dome-like structure (shot points 1026 in PSAT-244 and 460 in IAM4e, Figs. 5.6, 5.8, respectively) underlain by a seismically transparent zone, the origin of which is unknown. Considering the widespread existence of mud volcanoes and salt diapirs with morphological expression on the seafloor in the Gulf of Cadiz, it is hypothesized that this dome could correspond to a fluid escape structure as well.

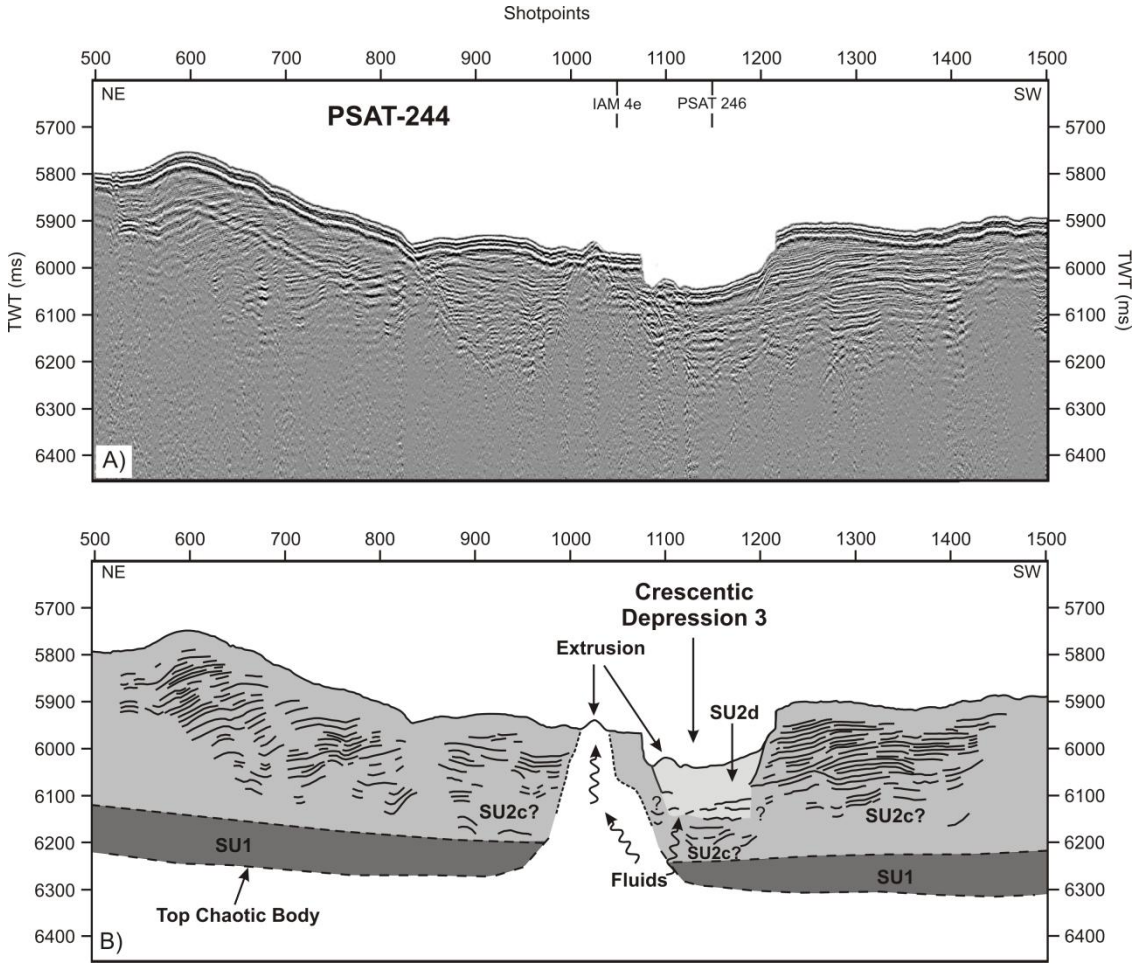


Figure 5.8 – (A) PSAT-244 seismic profile intersecting crescentic depression 3 (see Fig. 5.3 for location); (B) Simplified seismostratigraphic interpretation. Note the dome-like structure related with fluid migration and extrusion processes in the vicinity of the crescentic depression.

5.4. Discussion

The morphologic parameters of the studied crescentic depressions determined above (section 5.3.2), specifically slope and axial ratio (*a*), show that both their general shape and the steepness of their escarpments are independent of their location along the westwards smoothly dipping Horseshoe Valley, whose general morphology is most probably essentially related with the collection and transport of sediments from the shallower northern and northeastern domains of the Gulf of Cadiz (continental shelf and slope, see Figs. 5.1A, 5.2B). This suggests a similar fundamental origin for these features, associated with natural processes other than only, or predominantly, the varying smooth slope of the Horseshoe Valley as a whole.

5.4.1. Active tectonics

The studied features consist of crescent-shaped erosional depressions carved in seafloor slope breaks (see Fig. 5.3, 5.4) that correspond to the morphologic expression of blind thrusts, as shown in Fig. 5.6. The interpretation of the middle resolution seismic profiles (Fig. 5.7) also showed that the sedimentary units deposited within the crescentic depressions, and the external ones eroded by the retreating scarp (SU2 in Fig. 5.7C), are of the same age at the considered timescale. This scenario is compellingly indicative of the control exerted by present day active thrusting in the formation and localization of the crescentic depressions.

5.4.2. Hypothetic hydrodynamic models

In the present situation, hydrodynamic models can only be discussed hypothetically, given the fact that the detailed deep-water circulation in the Gulf of Cadiz, and particular in the Horseshoe Valley, is still fundamentally unknown. The progradational architecture of the sedimentary lobes (section 5.3.3.2) is indicative of upslope deposition towards the internal part of the crescentic depressions, coeval with upslope erosion of their scarps. This requires the existence of deep water currents, which would be responsible for simultaneous localized erosion and sedimentation. Such specific dynamics of interaction between a flow current and a pre-existent morphology has previously been described worldwide by several authors, although at shallower depths (Stow et al., 2002a,b; Verdicchio and Trincardi, 2006; Bulat and Long, 2001; Fildani et al., 2006; Normark et al., 2009).

5.4.2.1. Bottom currents

In this case, the observed erosional scarps and upslope progradational bodies could hypothetically be both generated by the lateral movement of a bottom current, such as the North Atlantic Deep Water, parallel to the tectonically originated slope breaks. However, this interaction would preferably cause the formation of more linear erosive and depositional features, similarly to mounded, elongated and separated drifts (Faugères et al., 1999; Rebesco and Stow, 2001; Gràcia et al., 2009), rather than confined crescentic depressions.

Alternatively, the crescentic depressions could also be generated by the action of vertical eddies associated to this same type of current, at least by two different mechanisms (e.g. Hernández-Molina et al., 2008): i) the influence of energetic Meddies in the base of the Mediterranean Outflow Water, which could propagate to the seafloor; and ii) due to the local interaction of different water masses with similar densities. Accordingly, vertical eddy movement could generate erosional/depositional seafloor features, characterized by less linear, i.e. more equidimensional, morphologies

(Hernández-Molina et al., 2008). An objection to this, is the fact that even the more equidimensional features generated by vertical eddies would probably tend to display a random localization in the HV and have a sub-circular (or semi-circular) geometry, rather than corresponding to sets of crescentic depressions with scarps systematically orientated downslope located on morphologic steps of the seafloor, as observed in the present case. In addition, this mechanism also does not provide a clear explanation for the formation of the observed upslope sedimentary bodies.

Another possibility corresponds to admit that the crescentic scarps could represent the scars of major landslides triggered by tectonic events, which would later be reworked and filled in with sediments by the action of bottom currents, in a similar manner to the formation of the "infill drifts" (Rebesco and Stow, 2001).

5.4.2.2. Turbidity currents

The existence of erosive crescentic scarps consistently oriented downslope along the Horseshoe Valley main drainage axis (see Fig. 5.2B), strongly suggests the contribution of downslope turbity currents to the formation of these features. Such currents have previously been reported to interact with seafloor localized morphologies causing simultaneous erosion (scouring) and (re)deposition (Fildani et al., 2006; Alexander, 2008; Lamb et al., 2008; Heinio and Davies, 2009; Normark et al., 2009).

In the Monterey East system Fildani et al. (2006) studied several features that originated in a field of sandwaves, geometrically similar to the ones described here. Following previous theoretical (Parker and Izumi, 2000; Sun and Parker, 2005) and laboratory (Koyama and Ikeda, 1998; Taki and Parker, 2005) work, the cited authors modelled the formation of linear sets of crescentic giant scours based on the idea of cyclic steps. The formation of cyclic steps (Fig. 5.9A) is determined by the occurrence of hydraulic jumps (Fig. 5.9B), in which a flow makes a rapid change from thin, rapid supercritical flow (Froude number>1) to thick, tranquil sub-critical flow (Froude number<1, Fildani et al., 2006; Normark et al., 2009). According to these ideas, in the Horseshoe Valley, the flow of an overriding turbidity current could be forced to

accelerate to supercritical velocities (i.e. with a Froude number>1) as a consequence of straightening caused by the seafloor uplift on the hanging wall of the blind thrusts underlying the studied crescentic depressions (see Fig. 5.9). When passing one of these obstacles the flow would be abruptly slowed, increasing in height and dissipating some of its own kinematic energy through turbulence (hydraulic jump; see Fig. 5.9B). Upstream of the hydraulic jump the occurrence of high bed shear stress would locally favour erosion, while downstream of the jump, very rapid deposition would be favoured (see Fig. 5.9B). These two areas would move in tandem upstream, forcing the hydraulic jump in the same direction (see Fig. 5.9A, Fildani et al., 2006; Alexander, 2008; Lamb et al., 2008; Heinio and Davies, 2009; Normark et al., 2009).

It should be noted that unlike the features studied by Fildani et al. (2006), the crescentic depressions described in the present paper are not aligned in one single linear train, but rather scattered along a broad area (see Fig. 5.3). These different spatial configurations are probably due to the broad and curved geometry of the thalweg in the upper part of the Horseshoe Valley (see Fig. 5.2B), which forces the flow to spread and sub-divide. On the other hand, some degree of lateral alignment (Fig. 5.3B) concurs with the tectonic control determined by the existent underlying blind thrusts (see above section 5.4.1.).

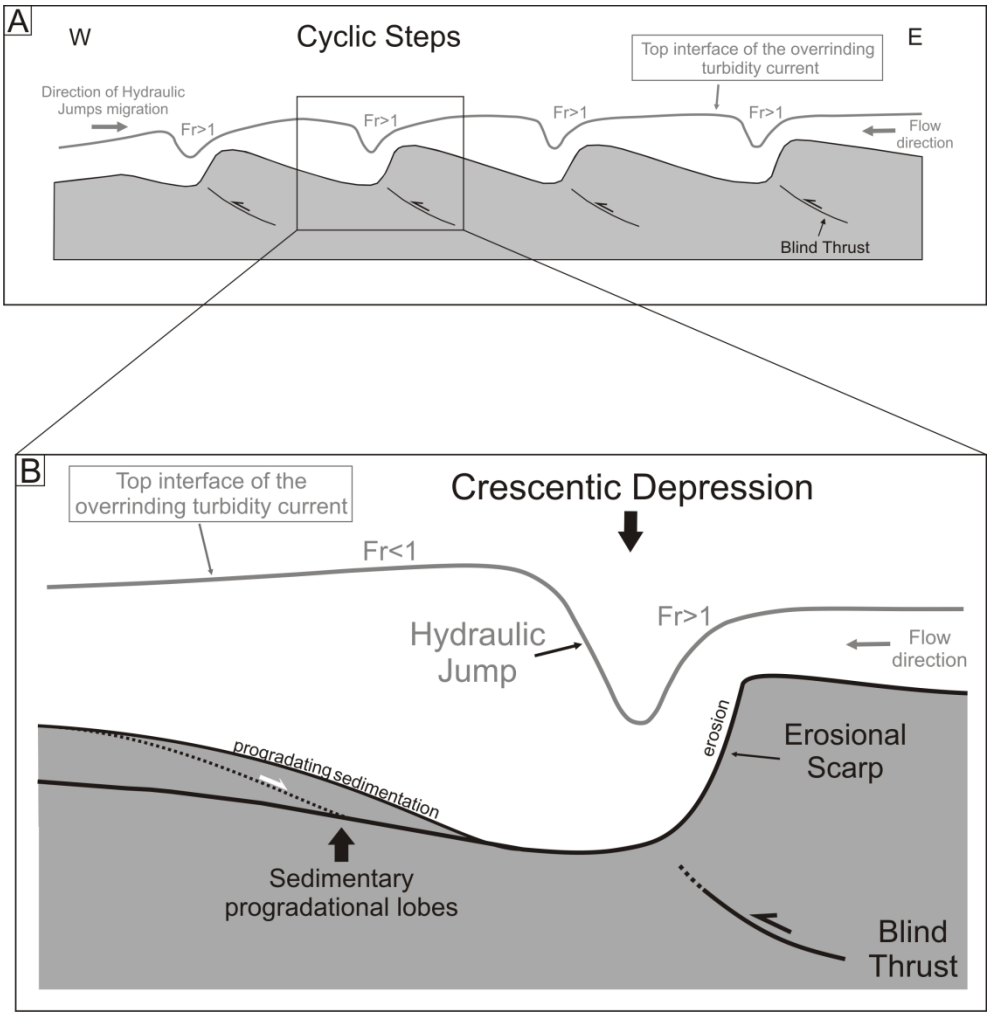


Figure 5.9 - Hypothetical adaptation of the conceptual model of cyclic steps (as proposed by Fildani et al., 2006) to the studied crescentic depressions in the Horseshoe Valley. (A) Schematic illustration of the formation of cyclic steps by a net-erosional turbidity current (adapted from op. cit.). Fr - Froude number; (B) Zoomed individual crescentic depression: sketch illustration of a hydraulic jump depicting progradational sedimentation downstream (Fr<1) and simultaneous erosion upstream (Fr>1).

5.4.3. Interplay between active tectonics and turbidity currents

The above discussion of the possible hydrodynamic models, shows that the contribution of bottom currents for the formation of the study crescentic features should not be discarded, namely in view of previously reported interpretations for similar features in somewhat different contexts (e.g. Bulat and Long, 2001; Stow et al., 2002a,b; Verdicchio and Trincardi, 2006; Hernández-Molina et al., 2008). However, in

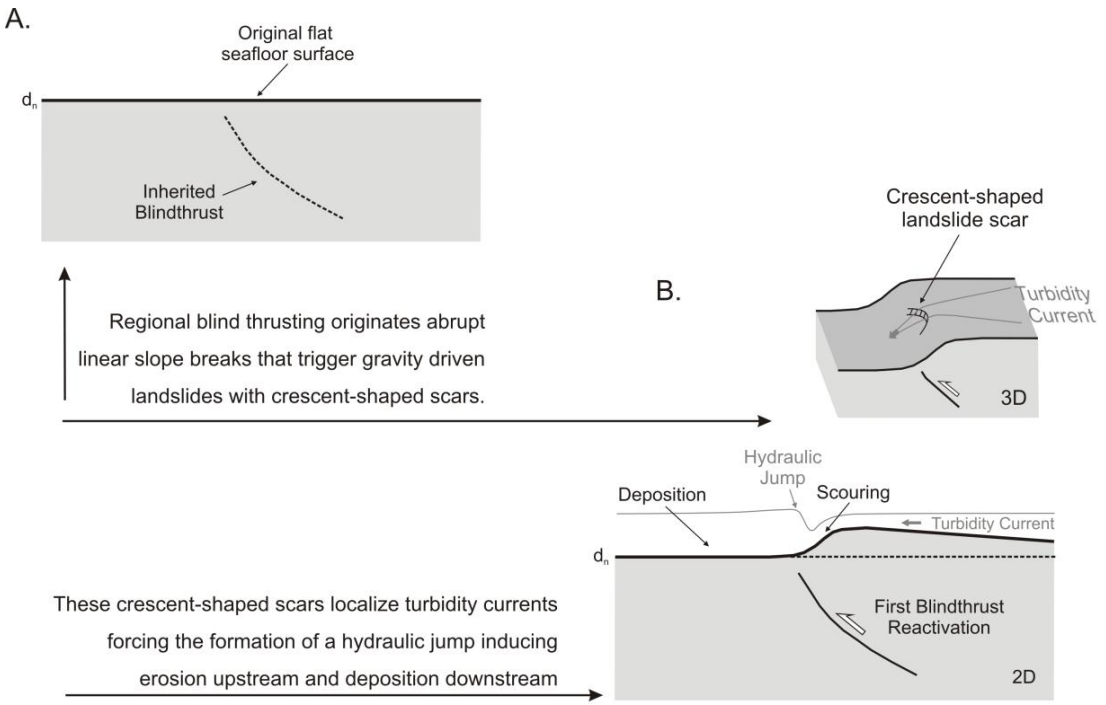
the present case, the observed crescentic shape of the studied depressions, as well as their particular architecture resulting from simultaneous erosion and deposition, are still difficult to explain exclusively as the result of these processes. Because of this, the contribution of downslope turbidity currents should also be considered, and in the face of the presently available dataset, the formation and upstream migration of a tectonically controlled hydraulic jump seemingly provides a simpler explanation for the particular crescentic shape of the observed erosional scarps and associated upslope sedimentary bodies. In accordance, the following events must be considered to explain the origin of the crescentic depressions (Fig. 5.10):

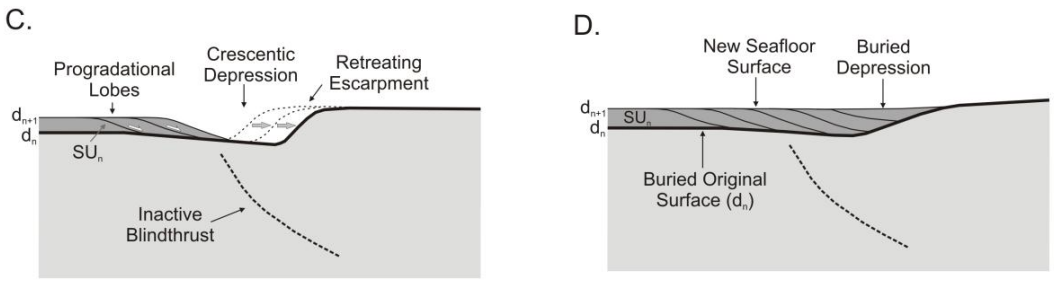
a) Active blind thrusting was responsible for the formation of several morphological steps in the smooth seafloor of the Horseshoe Valley (Fig. 5.10A-B).

b) These abrupt linear slope breaks can originate gravity instabilities that exhibit crescent-shaped scarps. These scarps localize the downslope turbidity currents (Fig. 5.10B, inset), triggering the formation of a hydraulic jump, inducing scouring upstream of the jump and simultaneous prograding sedimentation of the eroded material downstream (Fig. 5.10B-C).

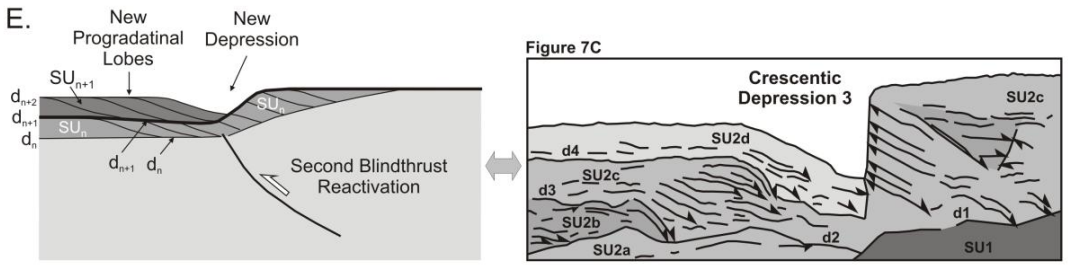
c) The fact that some of the progradational sedimentary lobes are buried and incised by shallower ones, strongly suggests a tectonic reactivation of the main blind thrusts, thus resetting the whole process, steepening the eroded retreated escarpments, or forming new ones, retriggering scouring and prograding sedimentation (Fig. 5.10D-E).

Figure 5.10 – Schematic representation of the main succeeding events envisaged as leading to the formation of the crescentic depressions in the Horseshoe Valley seafloor. (A) Initial stage representing an original smooth surface in the Horseshoe Valley and an underlying inactive (inherited) blindthrust; (B) First blindthrust reactivation event creates an abrupt slope break and triggers coeval scouring and sedimentation associated to an hydraulic jump; Inset: crescent-shaped landslide scar could be responsible for channelling and localization of turbidity currents; (C) Evolution of a retreating escarpment and simultaneous sedimentation with the formation of the progradational body SUn; (D) Eventual complete smoothing of the surface stepping morphology, as a consequence of simultaneous sedimentation and erosion. Note preservation of a buried (paleo) slope break marked by surface dn, underlying SUn; (E) Second blind thrust reactivation and resetting of the cycle, with retriggering of scouring implying erosion of the previously formed SUn subunit, and simultaneous aggradation leading to Sun+1 formation. Comparison with the geometric configuration deduced from the PSAT246 seismic profile.





Simultaneous erosion of the newly formed ecarpments and progadating sedimentation of the eroded material towards these same escarpments, ultimately leading to the eventually complete smoothing of the stepping morphology



Resetting of the whole process by tectonic reactivation of the main (blind)thrusts, and consequent retriggering of scouring and progradating sedimentation. Comparison with the overall geometric configuration deduce from the PSAT246 sesmic profile (Fig. 7C)

5.4.4. The possible role of fluid escape processes

Besides tectonics and scouring associated with the downslope currents, the middle resolution seismic data also reveals the possible importance of fluid escape processes, in the formation of the crescentic depressions as discussed elsewhere in the text and shown in Figs. 5.6, 5.8 and in the bathymetry (see Figs. 5.3, 5.4). The assumption that the dome localized close to crescentic depression 3 can be related to fluid escape processes is based not only on the transparent character of a shallow stratigraphic unit, but also by the fact that in the Gulf of Cadiz, particularly in the shallow sediments of the accretionary wedge domain, several tectonically controlled mud volcanoes and pockmarks of similar dimensions (Fig. 5.1A) have also been reported by other authors (e.g. Pinheiro et al., 2003; Somoza et al., 2003). These are described to be associated with widespread occurrence of fluid flow, and more recently were also reported to exist at greater depths, close to the Accretionary Wedge Deformation Front (e.g. Hensen et al., 2007). Moreover, some asymmetrical pockmarks also exhibit ground collapse geometries remarkably similar to the presently studied crescentic depressions (Schroot et al., 2003; Somoza et al., 2003; Dimitrov et al., 2003). However, because there is only one of these structures nearby one of the studied features, this mechanism alone could not account for the generalized origin of these features, and should preferably be seen as one possible contribution amid the dominant cause related to the tectonic/turbidity currents interplay.

Chapter 6
Thrust - wrench interference tectonics in the Gulf of Cadiz (Africa - Iberia plate boundary in the North-East Atlantic): insights from analog models

J. C. Duarte, F. M. Rosas, P. Terrinha, M-A. Gutscher, J. Malavieille, S. Silva, L. Matias

(This chapter is presented in a paper format, as submitted to Marine Geology.)

The SWIM faults seem to be active dextral strike-slip lithospheric faults. The subduction-related GCAW, which is crosscut by the SWIM faults, is also considered active. If this is the case then some kind of tectonic interference patterns between these structures should be expected to occur. Conversely, if one of these structures is not presently active then some cross-cutting relationships should be apparent in the available dataset, and it is not. Moreover, both the SWIM system and the GCAW appear to be associated with different tectonic driving mechanisms: the SWIM faults are associated to the Nubia-Iberia convergence and the GCAW is related to the Gibraltar Arc retreating subduction. Thus, the interplay in space and time between these major structures can provide fruitful insights on how those driving mechanisms operated in past, as well as on the recent geodynamic evolution of the Gulf of Cadiz. With this objective, three different modes of tectonic interference between an accretionary wedge and strike-slip faults were tested using analog sand-box modeling. Another paper (Rosas et al., submitted), concerning the tectonic interference between the SWIM 1 strike-slip fault and the Horseshoe fault (part of the NE-SW Thrust System), is also presented in appendix.

Abstract

In the Gulf of Cadiz, a segment of the Africa-Iberia plate boundary in the North-East Atlantic ocean, three main different modes of tectonic interference between a recently identified wrench system (SWIM) and the Gulf of Cadiz accretionary wedge (GCAW) were tested through analog sand-box modeling: a) An active accretionary wedge on top of a pre-existent inactive basement fault; b) An active strike-slip fault cutting a previously formed, inactive, accretionary wedge; and c) Simultaneous activity of both the accretionary wedge and the strike-slip fault. The results we obtained and the comparison with the natural deformation pattern favor a tectonic evolution comprising two main steps: i) the formation of the Gulf of Cadiz Accretionary Wedge on top of inactive, Tethyan-related, basement faults (Middle Miocene to ~1.8 Ma); ii) subsequent reactivation of these basement faults with dextral strike-slip motion (~1.8 Ma to Present) simultaneously with continued tectonic accretion in the GCAW. These results exclude the possibility of ongoing active SWIM wrench system cross-cutting an inactive GCAW structure. Our results also support a new interpretation of the SWIM wrench system as fundamentally resulting from strike-slip reactivation of an old (Tethyan-related) plate boundary**.**

Keywords: SWIM wrench system; Gulf of Cadiz Accretionary Wedge (GCAW); Thrust - wrench interference; Analog modeling; Tethyan-related plate boundary

6.1. Introduction

The Gulf of Cadiz is situated in the North-East Atlantic Ocean, west of the Gibraltar Straights, offshore SW Iberia and NW Morocco (Fig. 6.1). This zone marks the transition between the Mediterranean Alpine Collision Belt and the Atlantic Azores – Gibraltar Fracture Zone (AGFZ; see Fig. 6.1) and corresponds to a segment of the Africa-Eurasia plate boundary previously described as tectonically diffuse (e.g. Sartori et al., 1994; Medialdea et al., 2004). Accordingly, a variety of tectonic structures with different orientations, corresponding mostly to W-NW directed thrusts and WNW-ESE dextral strike-slip faults (Fig. 6.1B), are thought to accommodate a WNW-ESE Present day convergence between Eurasia (Iberia sub-plate) and Africa (Nubia sub-plate) at a rate of ca. 4-5 mm/yr (Argus et al., 1989; DeMets et al., 1994; Sella et al., 2002; Calais et al., 2003; Fernandes et al., 2003; Fernandes, 2004; Nocquet and Calais, 2004; Fernandes et al., 2007).

The seismicity of this domain has been characterized as moderate, although several high magnitude historical and instrumental earthquakes are known (e.g. Ms=7.9 28/02/1969 and and Mw=6.0,12/02/2007 earthquakes, respectively; Fukao, 1973 and Stich et al., 2006, 2007). Among these, the 1755 Great Lisbon Earthquake (estimated magnitude of 8.5 to 8.7; Abe et al, 1979; Johnston, 1996; Martinez-Solares and Arroyo, 2004) that triggered a devastating tsunami and destroyed the Portuguese capital (Baptista et al., 1998; Zitellini et al., 2001; Martinez-Solares and Arroyo, 2004). Despite recent mapping updates of the main tectonic structures of this region based on the interpretation of a great variety of newly acquired data (e.g. multi-beam swath bathymetry, reflection and refraction seismics, geodetic; Johnston, 1996, Gonzalez et al., 1996; Zitellini et al., 2001; Gutscher et al., 2002, 2009a,b; Baptista et al., 2003; Gracia et al., 2003a,b; Mulder et al., 2003; Zitellini et al., 2004; Rosas et al., 2009; Terrinha et al., 2009; Zitellini et al., 2009), the precise location of the seismogenic/tsunamigenic source of 1755 major event is still the subject of ongoing debate (e.g. Baptista et al., 1998; Buforn et al., 1988; Zitellini et al., 2001; Gracia et al., 2003a,b; Terrinha et al., 2003; Gutscher, 2004; Gutscher et al., 2006; Terrinha et al., 2009).

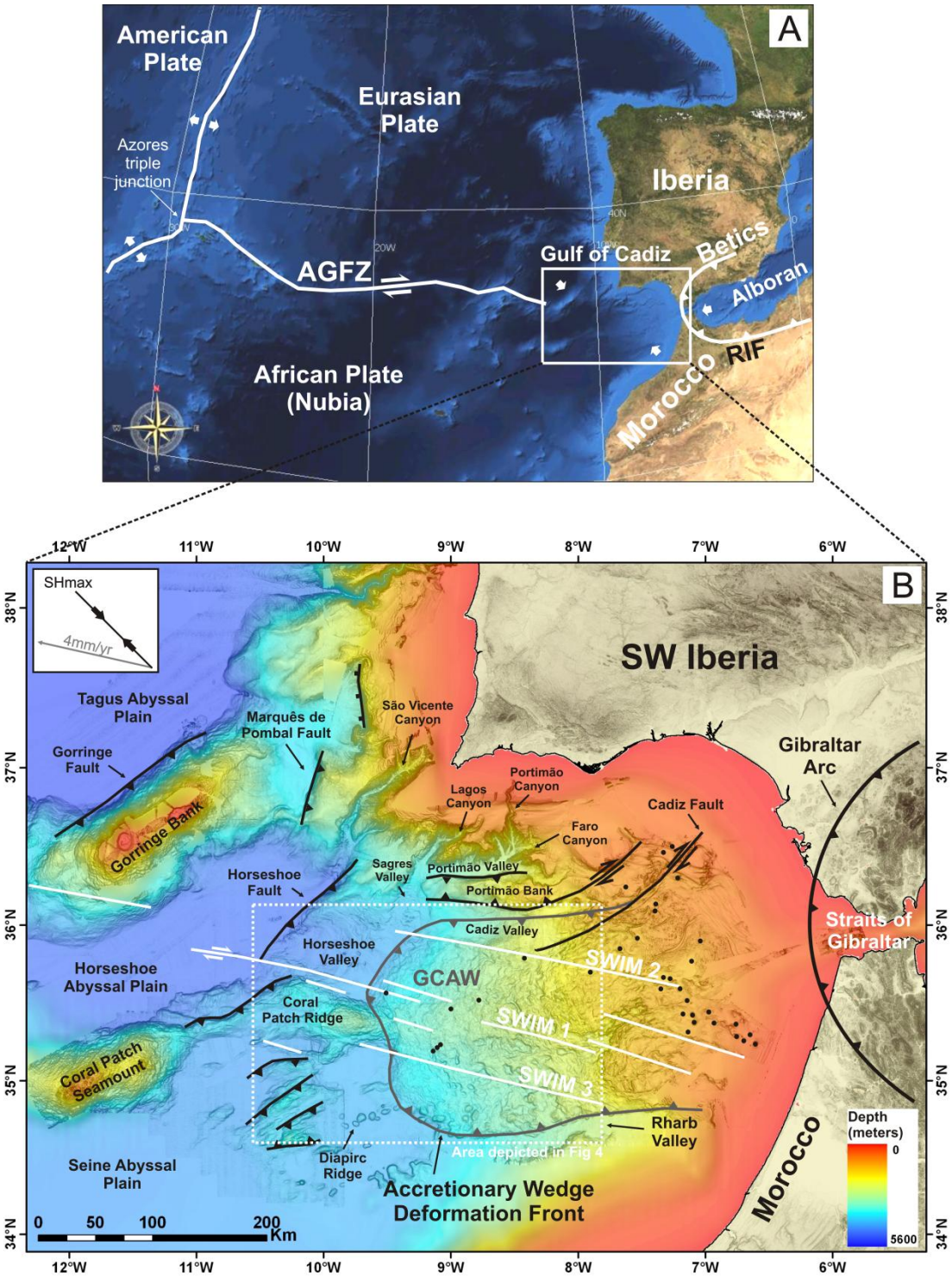


Figure 6.1 - (A) Location of the Gulf of Cadiz area in the general tectonic setting of the Eurasia - Africa plate boundary. AGFZ - Azores-Gibraltar Fracture Zone; (B) Simplified tectonic map of the Gulf of Cadiz area (adapted from Duarte et al., 2009, Terrinha et al., 2009, Zitellini et al., 2009 and Duarte et al., 2010; bathymetry from the SWIM compilation; Zitellini et al., 2009). Gulf of Cadiz Accretionary Wedge (GCAW) - dark grey outline; SWIM wrench system according to Zitellini et al. (2009) - white lines. Black dots correspond to the location of known mud volcanoes (e.g. Hensen et al., 2007).

In the tectonic map of Fig. 6.1B three main sets of structures are promptly recognized: a) several NE-SW striking, westwards directed thrust faults (e.g. Gorringe, Horseshoe and Marquês de Pombal faults); b) major WNW-ESE striking dextral strike-slip faults (the SWIM faults) and c) a major thrust bounding the so called Gulf of Cadiz Accretionary Wedge (GCAW frontal thrust). Structures of the first set have previously been described as active and, individually (e.g Gorringe fault), or together (Marques de Pombal and Horseshoe faults), successively considered and dismissed as possible seismogenic/tsunamigenic sources of the 1755 Great Lisbon Earhquake (e.g. Baptista et al., 1998; Buforn et al., 1988; Zitellini et al., 2001; Terrinha et al., 2009). The other two sets of tectonic structures support the following two fundamental ideas for the interpretation of the Gulf of Cadiz tectonic framework (Gutscher et al., 2002; Zitellini et al., 2009):

- Gutscher et al. (2002), building on previously reported similar ideas (e.g. Royden, 1993 and Lonergan and White, 1997), consider the tectonic evolution of this plate boundary as being dominated by active (roll back) subduction of a retreating east-dipping lithospheric slab, presently positioned beneath the Gibraltar Arc (Fig. 6.1B). Accordingly, associated synthetic accretion of sediments is also reported to occur, represented by the Gulf of Cadiz Accretionary Wedge (GCAW, Fig. 6.1B), in which several imbricated west-directed active thrusts accommodate on-going shortening.

- Zitellini et al. (2009) argue for the existence of a broad transpressive deformation band, comprising a set of WNW-ESE striking, subvertical, dextral strike-slip faults (SWIM faults in Fig. 6.1B), which as a whole extend for more than 600 km, from the eastern part of the Gulf of Cadiz to the southern limit of the Gorringe bank. These faults are interpreted by the cited authors as lithospheric faults, and in view of that the SWIM fault system was proposed to mark a newly formed plate boundary connecting the AGFZ to the Rif Mountain belt in northern Morocco.

It should be noted that Zitellini et al. (2009) considered the dextral transcurrent SWIM faults in the Gulf of Cadiz as presently active, and cutting the GCAW thrusts, whose activity is considered to be negligible since late Miocene times. Conversely, Gutscher et al. (2002) consider the GCAW thrusts as still active, and as referred above related with Present day on-going subduction beneath the Gibraltar Arc.

In the present work, we test the above assumptions using analog modeling sand-box experiments to model the interference between the two major tectonic systems in the Gulf of Cadiz, i.e. SWIM dextral wrenching and GCAW thrusting, assuming three main different possibilities:

1) The GCAW is presently active and the SWIM faults are thought to correspond to inactive basement faults, inherited from a previous tectonic evolution;

2) The SWIM faults are thought to correspond to major, presently active, dextral strike-slips, cutting a previously formed inactive GCAW;

3) Both tectonic systems are presently active.

Thorough comparison of the obtained results with the observed natural morphotectonic pattern is carried out for each of the above cases. Accordingly, resulting tectonic implications for the local and whole scale evolution of this segment of the Eurasia-Africa plate boundary are carefully evaluated and explored.

6.2. Morphotectonic characterization of the study area

The morphology of the Gulf of Cadiz is largely controlled by the main tectonic processes in the area: the thrusting accommodating the GCAW accretion and the wrenching associated to the SWIM fault system. The high-resolution bathymetry of the GCAW shows a west dipping U-shaped body (Figs. 6.1B and 6.2A) that extends for more than 250 km from about longitude 7ºW to 9º30'W, with depths ranging from 200 to 4300 meters. It narrows slightly to the west with a width varying from 160 to 140 km (see Fig. 6.1B and 6.2A). Its wrinkled surface morphology is shaped not only by thrust-related slope breaks and associated folds, which define a large scale stepping morphology, but is also the result of the different combined manifestations of gravitational and fluid escape processes (e.g. "raft-tectonics" type features, sub-circular collapse depressions, mud volcanoes, salt diapirs; Mulder et al., 2003; Pinheiro et al., 2003; Gutscher et al., 2009b; Zitellini et al., 2009; Terrinha et al., 2009). From a structural point of view, the accretionary wedge corresponds to an eastward thickening pile of westwards thrust sediments (Fig. 6.2B and C), reaching a maximum thickness of ca. 15 km near the Gibraltar Straits (Thiebot and Gutscher, 2006; Gutscher et al., 2009a). The thrusts root in a common sub-horizontal to gently east dipping décollement layer, exhibiting an overall geometry complying with on-going eastwards subduction beneath the Gibraltar Arc (Gutscher et al., 2002). During the last 5 Ma the E-W convergence rate implied in such a subduction is thought to have diminished from ca. 2 cm/yr to 0.5 cm/yr (Gutscher et al., 2009a), with a consequent decrease in the activity of the wedge thrusts during this time span. Accordingly, the same authors argue that the Present day internal deformation is preferably accommodated by small increments of local reactivation of inherited blind thrusts, being more homogeneously distributed over the entire wedge, rather than concentrated on newly formed major frontal thrusts.

The morphologic expression of the SWIM faults corresponds to a continuous alignment of seafloor crests and troughs, sometimes exhibiting an en echelon geometrical disposition, and commonly punctuated by active mud volcanoes within the domain of the accretionary wedge (see Fig. 6.1B; Duarte et al., 2009; Terrinha et al., 2009; Zitellini et al., 2009). This overall linear morphology is more prominent both

close to the northern part of the GCAW front and in the Horseshoe Valley, where lineaments can be followed almost continuously for more than 200 kilometers (e.g. SWIM 1 in Fig. 6.1B and 6.3A).

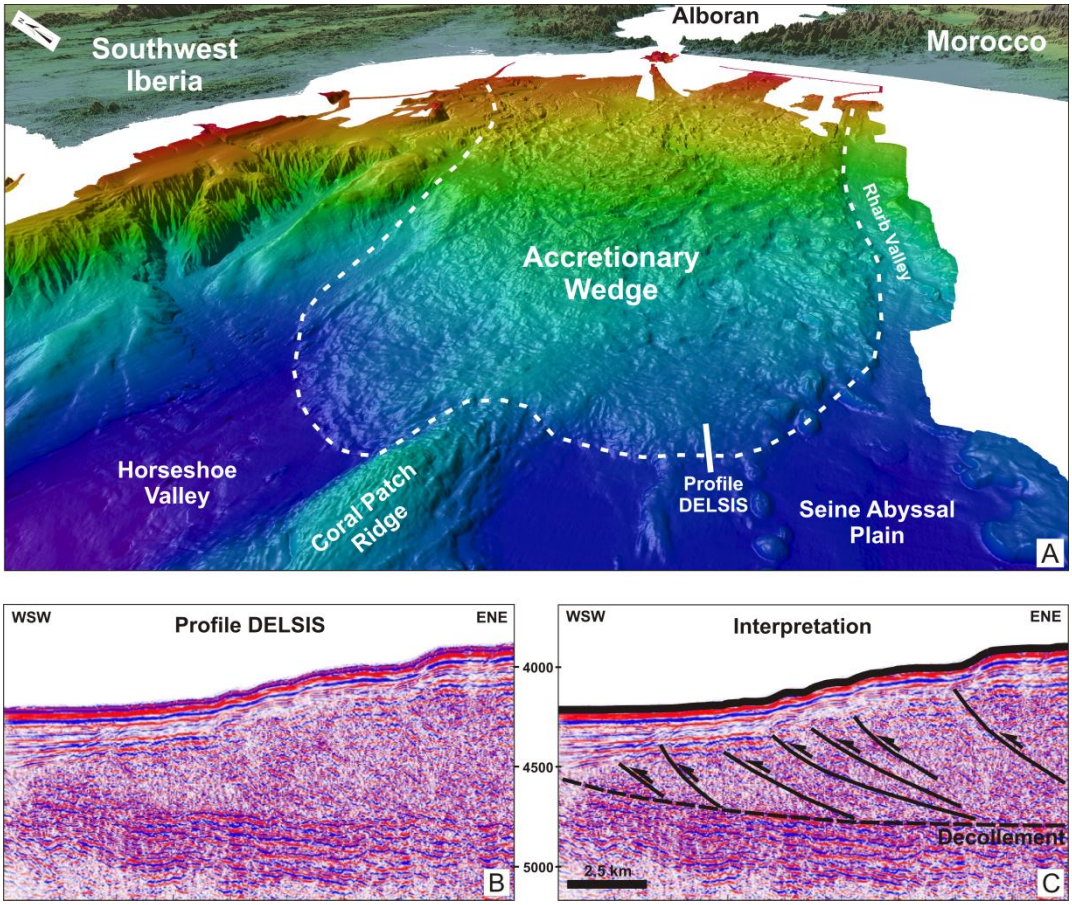


Figure 6.2 - (A) Perspective view (from southwest) of the Gulf of Cadiz Accretionary Wedge surface and adjacent areas; (B) Delsis Multichannel seismic profile across the accretionary wedge deformation front (see Fig. 6.2A for location) and (C) respective interpretation.

The available reflection seismic dataset in the study area shows that the SWIM faults correspond to aligned arrays of deep-rooted faults, often breaching out through Present day seafloor sediments and showing extensive evidence for associated fluid migration (e.g. seismic blanking along fluid extrusion paths in Fig. 6.3B and C; Rosas et al., 2009; Terrinha et al., 2009). From the inspection of the IAM 4 and 3 seismic profiles in Fig. 6.3, it is apparent that the SWIM faults are aligned along basement pre-existent (Mesozoic) faults (dashed black lines in Fig. 6.3; see also Duarte et al., 2009 and Terrinha et al., 2009). Analog modeling of sets of en echelon folds formed in soft-cover sediments overlying some of the SWIM basement dextral strike-slips (Rosas et al., 2009) yielded an age for their activeness of ca. 1.8 Ma.

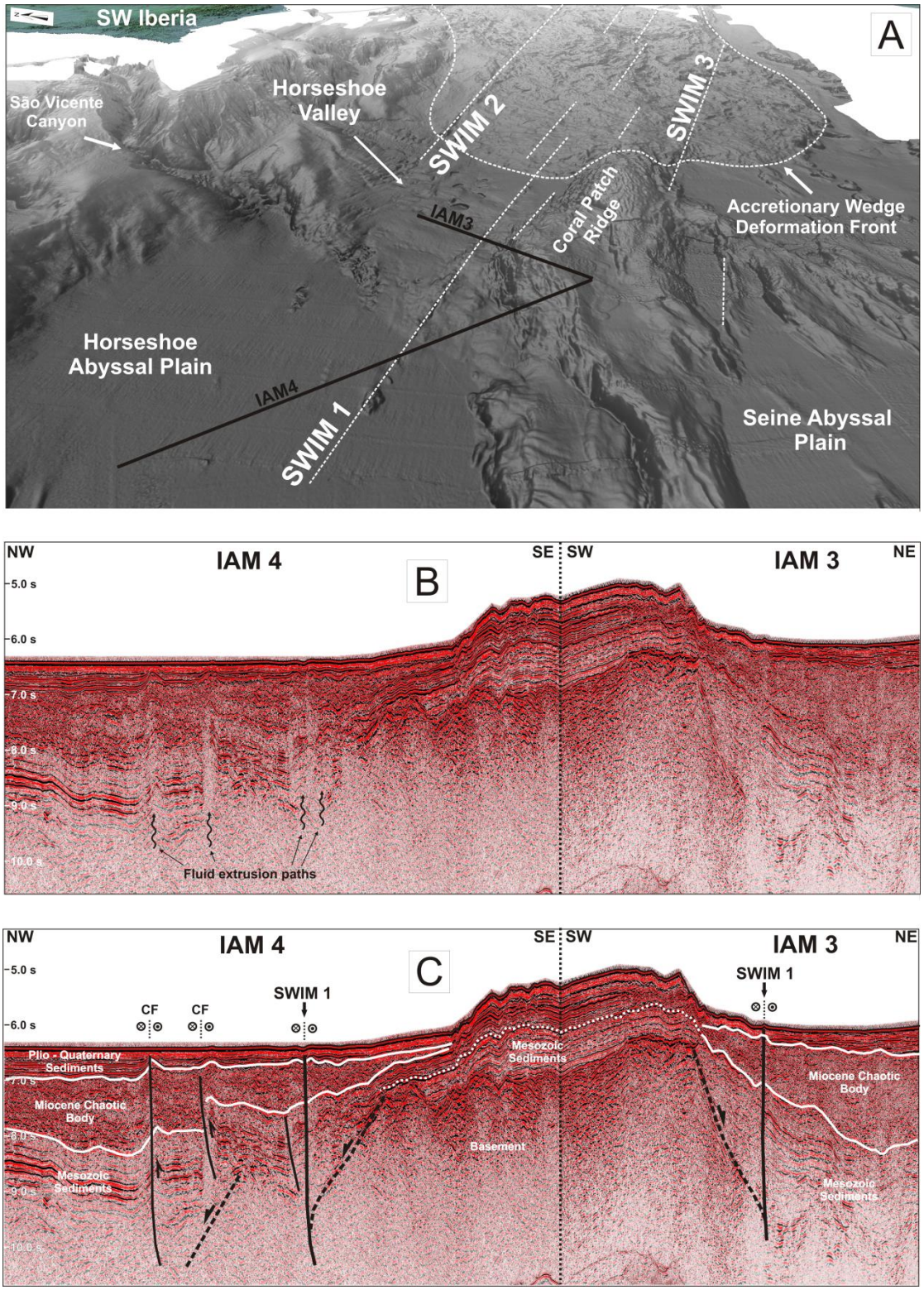


Figure 6.3 - (A) Perspective view (from southwest) of the SWIM lineaments; (B) Multichannel seismic profiles IAM-4 and IAM-3 crosscutting SWIM fault 1 and (C), and respective interpretation; note the Mesozoic rift-related faults (black dashed lines). CF – Oblique dextral-reverse faults (Corner Faults of Rosas et al., submitted). See location in Fig. 6.3A.

6.2.1. The SWIM-GCAW interference area

The critical area to understand the interference between the SWIM strike-slips and the GCAW is close to its deformation front (Fig. 6.4A). Along this front, from North to South, three interference sub-areas were thoroughly analyzed (B to D in Fig. 6.4). The SWIM 2 fault intersects a northern segment of the GCAW front (Fig. 6.4B) in the vicinity of the Sagres Valley, at an angle of about 40º. Within the thrust wedge to the East, the morphological expression of the SWIM 2 is well marked by a slightly arched trough that splays in the same direction. Conversely, in the Sagres Valley it is almost indiscernible due to the widespread presence of scours and slumps, and it is only detectable by the presence of a gentle slope break. In this area no offset of the wedge deformation front is observed, instead only a small wrinkled WNW-ESE elongate bulge can be detected in the bathymetry of the frontal GCAW (see Fig. 6.4B). The SWIM 1 fault exhibits a clear morphological expression in the Horseshoe Valley, intersecting the wedge deformation front just to the north of the Coral Patch Ridge, at an angle of about 70º (Fig. 6.4C). Its continuation to the East is less visible, although punctuated by mud volcanoes. Similarly to what was described for the SWIM 2 fault, there is no bathymetric evidence for the offset of the wedge front by the SWIM 1 fault. The SWIM 3 fault cuts along the southern flank of the Coral Patch Ridge with a strong morphological imprint (Fig. 6.4D), corresponding to a lineament marked by several elongated WNW-ESE ridges, troughs and slope breaks. To the East, this lineament crosses a small portion of the Seine Abyssal Plain and intersects the accretionary wedge deformation front, at an angle of about 80º. In this location the wedge front is marked by a slight embayment. On the wedge surface to the north of the fault and parallel to it, an elongated protuberance is also unmistakably observed, limited by two descending slope breaks and vanishing progressively towards the East. As in the two cases described above, the observed morphology does not account for any kind of fault offset overprint relationships.

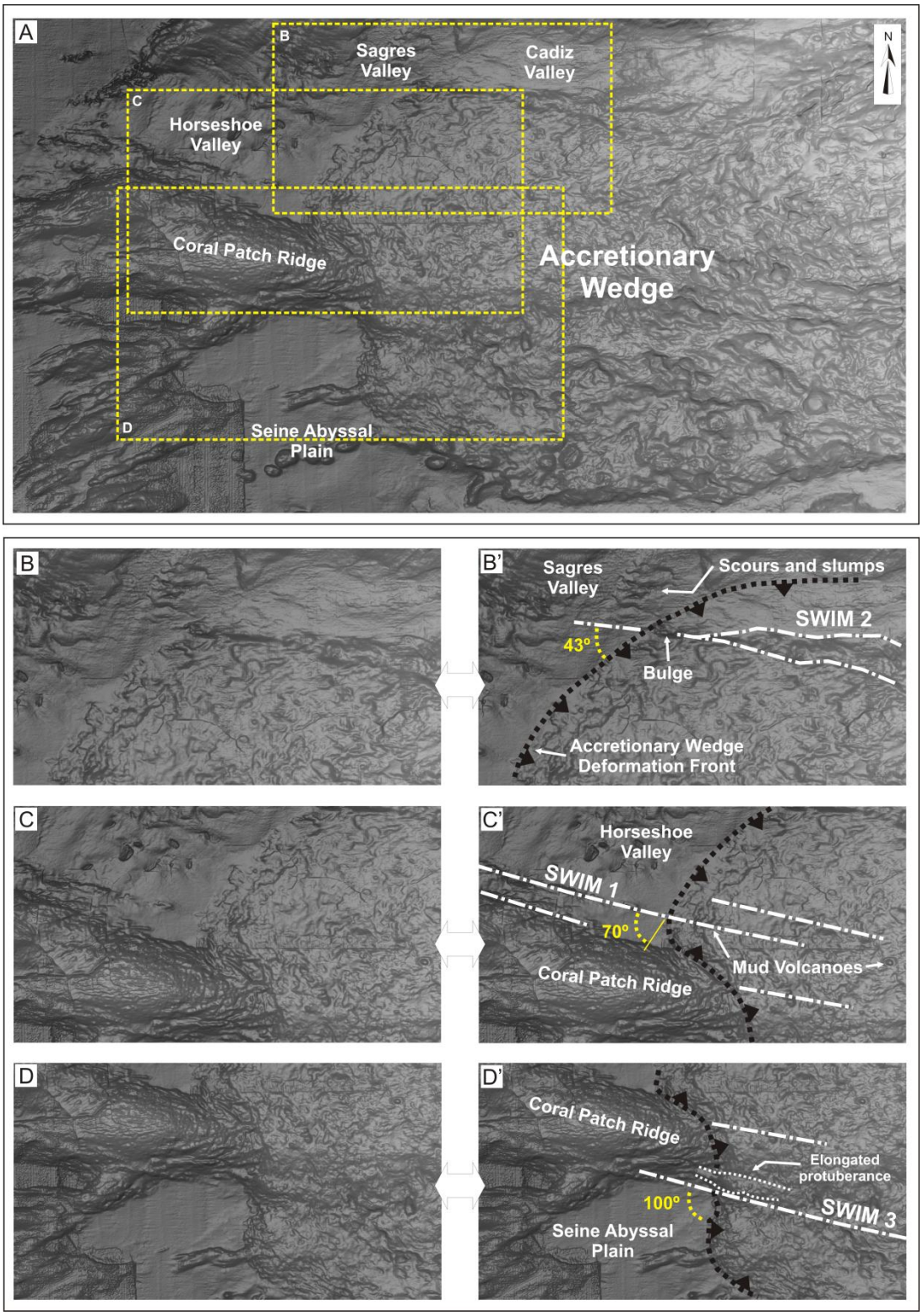


Figure 6.4 - General (A) and detailed (B, C and D) bathymetric imaging and respective morphotectonic interpretation (B', C', and D') of the interference area between the accretionary wedge deformation front and the SWIM 1, 2 and 3 strike-slip faults. Note the absence of offset overprint relationships

6.3. Analog Modeling

Our objective is to test several simple chronological possibilities of mechanical interference between a strike-slip fault and a thrust wedge front, under model conditions comparable to the ones governing the SWIM-GCAW tectonic interference. Three main experiments were carried out to investigate the different deformation patterns resulting from: a) A thrust wedge developed on top of an inactive basement (strike-slip) fault; b) An active dextral strike-slip fault affecting an inactive thrust wedge; c) The simultaneous alternate activity of a thrust wedge front and a dextral strike-slip fault. Experiments were performed to respect the general, simplified, geometry, kinematics and rheology ascribed to the natural strike-slip (SWIM) system, and to the (GCAW) thrust wedge. However, analog modeling with dry granular materials cannot reproduce all the complex processes (e.g. fluid overpressure and expulsion, sedimentary deposition, and local gravitational instabilities) which occur in submarine environments. Nevertheless, the regional kinematic and relative timing caused by the local tectonic driving forces and the ensuing structural evolution can be well investigated.

6.3.1. Experimental method

6.3.1.1. Material properties and scaling

The material used as an analog of the GCAW sedimentary rocks was dry quartz sand, whose properties are summarized in Table 6.1. Sand is considered a Coulomb material deforming in a brittle way according to the Coulomb fracture criterion (e.g. Hubbert, 1937, 1951; Davis et al., 1983, Appendix 6.A), and it has been extensively used in scaled model experiments simulating similar brittle deformation in the upper crust (e.g. Mandl et al., 1977; Davis et al., 1983; Malavieille, 1984; Mulugeta, 1988; Malavieille et al., 1991; Liu et al., 1992; Gutscher et al., 1998a,b; Casas et al., 2001; Marques and Cobbold, 2002; Le Guerroue and Cobbold, 2006; Rosas et al., 2009; Gutscher et al., 2009a; Malavieille, 2010). The present models were properly scaled

according to the scale model theory of Hubbert (1937). The assumed model - prototype ratios are presented in Table 6.1, and the detailed procedure of scaling is specified in Appendix 6.A

Table 6.1 - Parameters and material properties

Parameters and material properties	**Quartz sand (model)**	**Natural prototype**	**Ratio: Model/Nature**
Composition (%)	99.7 % quartz	-	-
Grain shape	well-rounded	-	-
Grain size (mm)	< 0.30	-	-
Density (kgm^{-3})	1300	2600	$\delta = 0.5$
Internal friction angle, ϕ (^{o})	~30	-	-
Coefficient of internal friction, μ_c	~0.6	0.6-0.85	-
Cohesion, c_0 (Pa)	negligible	$40x10^6$	-
Gravity accelaration, g (ms^{-2})	9.81	9.81	$\gamma_g = 1$
Length, L (m)	0.01	5000	$\mathbf{\lambda = 2\times10^{-6}}$
Mass, M (Kg)	-	-	$\mathbf{\mu = 4x10^{-18}}$

Note:
- Scaled fundamental units are in **bold**

- A mean cohesion of $\mathbf{C_o}$**=40 MPa** was assumed from the natural prototype (e.g. Hoshino et al., 1972; Weijermars et al., 1993)

6.3.1.2. Apparatus and initial stage

Experiments were done using a rectangular 100cm × 60cm Perspex deformation rig, comprising two laterally juxtaposed basal plates and a moving backstop (Fig. 6.5A). In the initial stage of the experiments, 1cm thick layered sand cake was built on top of the basal rigid plates by pouring batches of differently colored sand from a moving elongated funnel, guarantying the leveling of its top surface. The basal plates in the model move laterally relatively to each other, and account for the natural basement beneath the thrust wedge décollement (see Fig. 6.2C). The vertical contact plane between these plates complies with the dominant WNW-ESE orientation of the SWIM 1 fault system (see Fig. 6.1 and 6.4). The model sand cake corresponds to the overlying cover sediments, in which accretion is simulated by pushing against it a backstop that

slides on top of both basal plates. The backstop lacks any kind of correspondence with any natural feature, and was exclusively used to produce a classical model thrust wedge. Likewise the (~0.2 cm thick) layering in the sand cake has also no correspondence with any natural structures, and was used merely as a 3D passive strain marker. In all experiments the dimensions of the deformation rig were sufficiently large to guarantee that the bulk of the model was not affected by boundary conditions. The experiments were repeated several times to ensure the reproducibility of the obtained results. Top view photographs were taken at regular time intervals. The final stage of the model was humidified and serially sectioned for three-dimensional analysis.

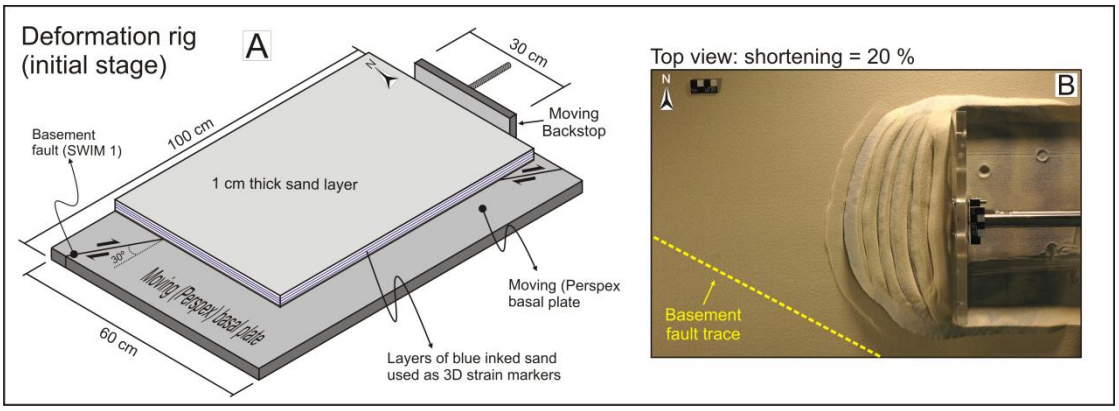


Figure 6.5 - (A) – Sketch of experimental apparatus and model set-up at initial stage. (B) Model top view after 20 % of shortening.

6.3.1.3. Procedure

Three main experiments were carried out two study three basic possibilities of mechanical interference between a strike-slip basement fault and a thrust wedge:

1) Active thrust wedge and inactive basement fault: the backstop was initially pushed against the sand-cake, on top of the two immobile basal plates.

2) Active basement fault and inactive thrust wedge: after a thrust wedge was previously formed in the sand, the basal plates were dextrally moved relatively to each other.

3) Active basement fault and active thrust wedge: the reactivation of a previously formed thrust wedge was successively alternated with the right-lateral movement between the basal plates.

6.3.2. Experimental results

6.3.2.1. Experiment 1: active thrust wedge and inactive basement fault

Up until ~30% of shortening a thrust wedge was classically obtained, through the forward propagation of regularly spaced thrusts, as a result of moving the backstop to the left (see Fig. 6.5B and Fig. 6.6A). For a shortening of 31 % (Fig. 6.6A) the front of the accretionary wedge developed an embayment coinciding with the direction of the inactive basement fault (yellow dashed line in Fig. 6.6A). For a shortening of 38 % a new thrust (n+1 in Fig. 6.6B) was formed exclusively to the north of that basement discontinuity. Only when the shortening reached 39 %, did the equivalent new thrust form to the south, resulting in a misleading left-lateral offset geometry (yellow arrows in Fig. 6.6C), in spite of the total absence of relative movement between the two basal rigid plates. For a shortening of 48 % this false offset in front of the newer thrust disappeared (Fig. 6.6D). In the wedge lower area a linear southeastward splaying, slightly anastomosing, deformation pattern (white lines in Fig. 6.6D) was progressively developed as shortening accumulated and new outward thrusts successively formed.

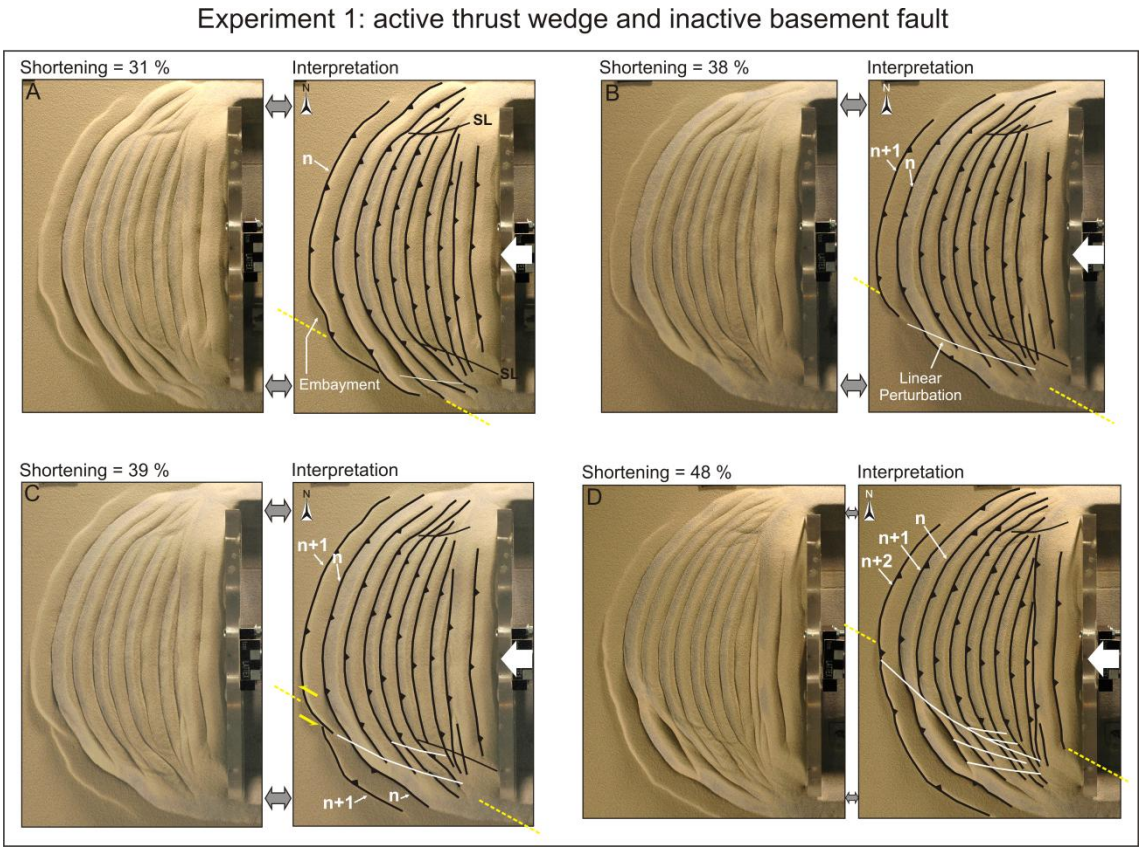


Figure 6.6 - Results of Experiment 1: active thrust wedge and inactive basement fault. A, B, C and D - Model top view after 31, 38, 39 and 48 % of shortening, respectively. Yellow dashed line - direction of basement (inactive) fault; White arrow – direction of shortening; Yellow half arrows - apparent left-lateral offset; White lines mark the inner splaying geometry of the wedge surface perturbation; n, n+1, …n+n refer to the relative chronology of thrust propagation in B, C and D. SL (thin black lines) - slip lines (Note that the slip lines are a byproduct of boundary conditions due to backstop finite length).

6.3.2.2. Experiment 2: active basement fault and inactive thrust wedge

After 48% of shortening the basement strike-slip fault was activated with dextral movement (Fig. 6.7). When the horizontal displacement between the basal plates reached only 0.2 cm, a thin elongated bulge formed coinciding with the basement strike-slip direction (Fig. 6.7A). At this stage no offset of the thrust wedge was observed. A further right-lateral displacement of 0.6 cm between the basal plates clearly offset the thrust wedge, preferably affecting its frontal outer thrust (Fig. 6.7B). For a displacement of 1.3 cm the strike-slip fault seemingly propagated inwards, but only across the

following three thrusts (Fig. 6.7C-D). The resultant model deformation pattern always showed the preferential offset of the frontal thin part of the accretionary wedge, relative to its innermost domains that remained unaffected.

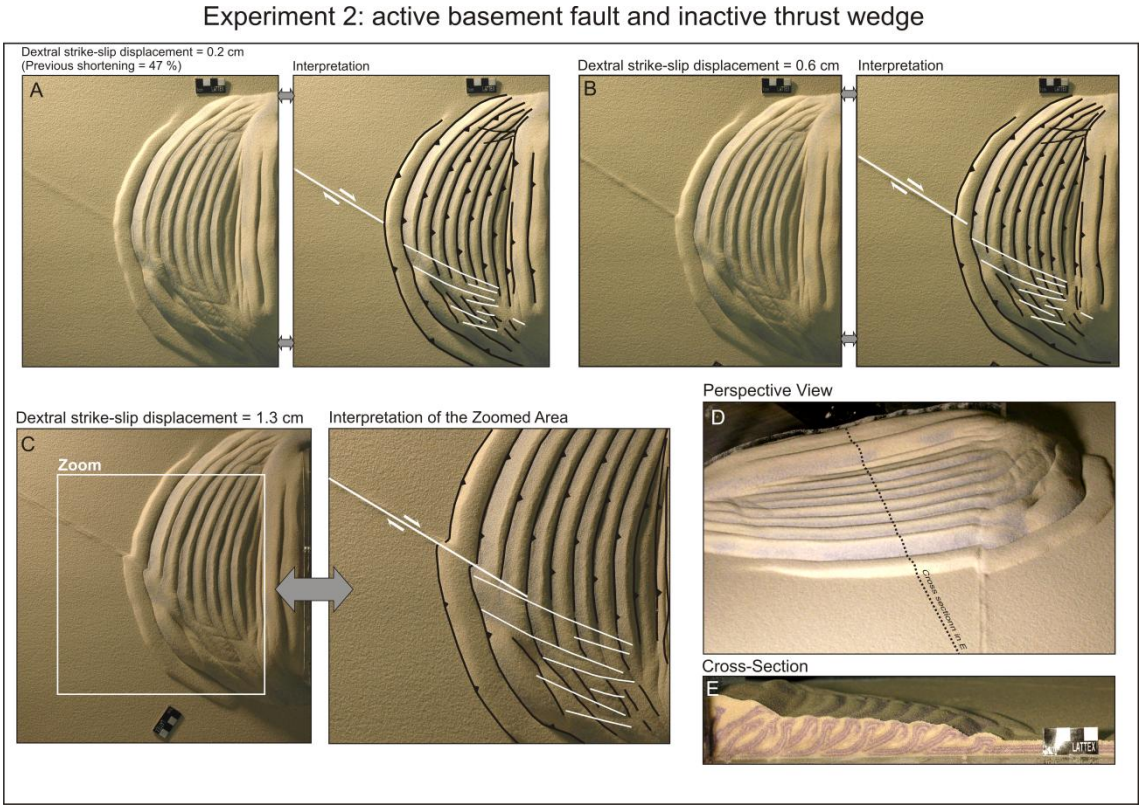


Figure 6.7 - Results of Experiment 2: active basement fault and inactive thrust wedge. A, B and C - Model top view after 0.2, 0.6 and 1.3 cm of right-lateral strike-slip displacement, respectively. D - Perspective view of the deformation stage illustrated in C. E - Orthogonal cross section of the thrusted wedge (see location in D). White half arrows indicate right-lateral offset.

6.3.2.3. Experiment 3: active basement fault and active thrust wedge

After the formation of a thrust wedge due to 47% of shortening, a right-lateral displacement of 1cm was applied to the basal plates (Fig. 6.8A). As a result, a linear bulge formed in the sand foreland, along the strike-slip direction, cutting across the thrust wedge and offsetting its front. Similarly to experiment 2, the amount of right-lateral displacement diminished towards the thicker inner part of the wedge. Subsequently, another 0.4% of incremental shortening was applied to the model (Fig. 6.8B). As a result, a new frontal thrust formed, but only to the north of the strike-slip fault. The resultant geometry mimics a false left-lateral offset of the outer frontal thrust (apparently n+1 in Fig. 6.8B), although careful consideration of the propagation chronology of the thrusts revealed a true dextral offset (affecting thrust n in Fig. 6.8B), complying with the underlying basement fault kinematics. Further 1% of applied shortening (Fig. 6.8C) produced the new thrust (n+1) also to the south of the strike-slip fault, erasing the previously formed false offset. Another 3.5 cm of dextral strike-slip displacement was additionally applied to the basal plates (Fig. 6.8D), and as a consequence, the wedge front was once more kinematically truly dextrally offset. Riedel faults formed on the wedge surface displaying a clear en echelon spatial disposition, and interfering with the preexistent stepping morphology associated with the thrust stacking. Finally, after another 2.6% of shortening (Fig. 6.9), reaching a total accumulated amount of 51%, the frontal wedge offset was once again almost completely attenuated, although the total accumulated basal strike-slip displacement was of 4.5 cm (corresponding to 22.5 km). It should be noted that the previously formed linear en echelon pattern was preserved in the wedge surface, including in its innermost domain.

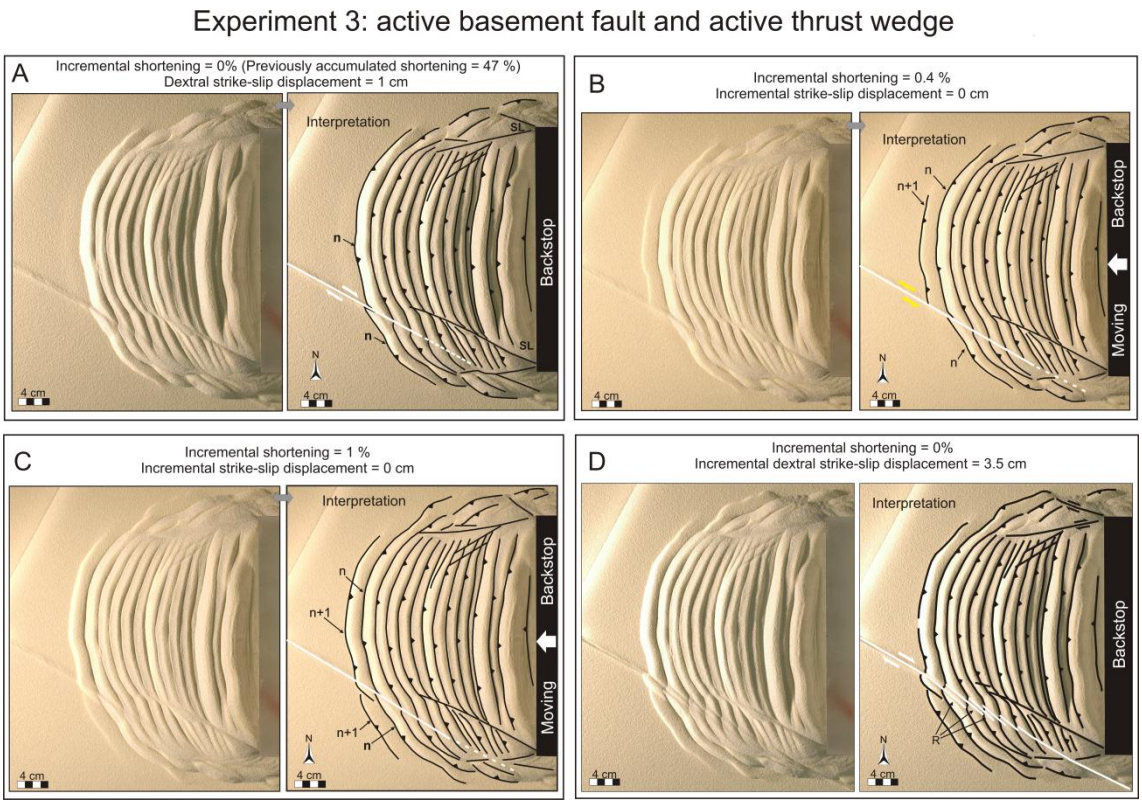


Figure 6.8 - Results of Experiment 3: active basement fault and active thrust wedge. A, B, C and D - Model top view after different increments of shortening and dextral strike-slip displacements; n, n+1, …n+n refer to the relative chronology of thrust propagation; White line - dextral strike-slip fault trace (R – en echelon Riedels). White half arrows - dextral offset; Yellow half arrows - false left-lateral offset of the frontal wedge thrust.

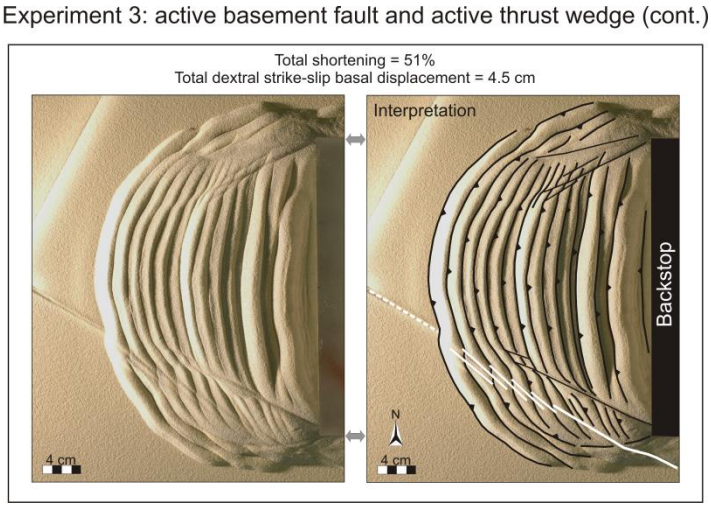


Figure 6.9 - Final stage of Experiment 3: active basement fault and active thrust wedge (continuation). Model top view after 51 % of shortening and 4.5 cm of dextral strike-slip displacement. Note the practical absence of corresponding offset in the frontal thrust wedge.

6.4. Discussion

Experiment 1 shows that an active thrust wedge forming in cover sediments above an inactive basement fault records the resultant mechanical interference in the form of a linear, inner splaying, perturbation of the wedge morphological surface (white lines in Fig. 6.6C-D). This formed as the result of the successive thrust propagation across the basement anisotropy, which behaved as a mechanical obstacle for the lateral propagation of the frontal thrust. Since this basement anisotropy remains stationary relatively to an external reference frame, and the thrust front propagates forward (to the left), the resultant interference area between both these features migrates from the lower periphery of the thrust front to its central domain (compare the position of the linear perturbation pattern in Figs. 6.6A to D). Comparison with the natural example shows that the observed inner splaying lineaments in the GCAW (see SWIM 1 in Fig. 6.1B and SWIM 2 in Fig. 6.4B), could have originated simply as a consequence of preexisting inactive basement faults. This agrees with the fact that these lineaments are observed in the inner thicker part of the natural thrust wedge, in the complete absence of offset of its thinner frontal part.

Experiment 2 shows that an active basement strike-slip fault affecting an overlying preexistent thrust-wedge, must produce a clear offset of its thinner front, even for minor increments of strike-slip basal displacement (1.3 cm corresponding to 6.5 Km). This offset vanishes rapidly towards the inner thicker parts of the wedge, affecting almost exclusively the outer frontal thrusts. Comparison with the natural example shows that if the GCAW is presently inactive, and cut by active dextral strike-slip (SWIM) faults, then unambiguous offset of the GCAW front has to exist, which is clearly not the case (see Figs. 6.1B, 6.2 and 6.4).

Experiment 3 shows that if both the basal strike-slip fault and the thrust wedge are active, with alternating incremental fault slips, then the resultant interference deformation pattern can be the cyclic repetition of the following three possibilities: a) true right-lateral offset of the thrust wedge front (see Fig. 6.8A and D); b) false left-lateral offset of the thrust wedge front (see Fig. 6.8B, similar to experiment 1 see Fig. 6.6C); c) no offset of the thrust wedge front (see Fig. 6.8C and 6.9). It should be noted that the absence of thrust wedge offset does not imply an absence of basement strike-

slip displacement, which quite on the contrary is continually increasing. However, the alternation with the incremental shortening that drives the successive forward thrust propagation cyclically erases the offset of the frontal thrust wedge. Differently, the resultant linear en echelon interference pattern tends to be increasingly well marked, including in the innermost domains of the thrust wedge (compare the lineament in the Figs. 6.8A and 6.9). Similarly to experiment 1, the intermediate experimental stage in which a false left-lateral offset originates (see Fig. 6.8B), is here interpreted as the result of a delayed propagation of the newer outer thrust across the strike-slip fault, which in accordance seemingly behaves as a mechanical obstacle to such propagation.

In view of these results, and considering the fact that in the natural example the GCAW front is not offset across any of the mapped SWIM faults, one of the two following tectonic scenarios is possible: a) either the GCAW is active, and forming over a basement anisotropy (inactive SWIM fault?); or b) Both the GCAW and the SWIM faults are active. The possibility of an inactive GCAW being cut by active dextral strike-slip SWIM faults is clearly ruled out by the present experimental results.

6.4.1. Tectonic implications

The west Mediterranean tectonic evolution comprised the Mesozoic opening of the Tethys Ocean (Fig. 6.10A; e.g. Maldonado et al., 1999; Gutscher et al., 2002; Gràcia et al., 2003a; Stampli et al., 2002; Jiménez-Munt et al., 2010). This would account for a basement tectonic anisotropy, hypothetically, either consisting in previous transform faults, or in rift-related normal faults (Fig. 6.10A and B). In view of the presented experimental results, the accretionary wedge (GCAW) is here interpreted to have formed on top of such basement faults (present day SWIM faults) as a consequence of roll-back subduction beneath Gibraltar. During this period (Middle Miocene to ~1.8Ma?, Figs. 6.10C to E) these faults were probably inactive, although capable of originating a linear-like perturbation in the GCAW surface morphology (experiment 1). At same time, the main regional convergence direction between Iberia and Nubia gradually suffered a counterclockwise rotation, shifting from N-S (Fig. 6.10 B) to near

WNW-ESE (Fig. 6.10E). Such reorientation is interpreted to have triggered (since at least ~1.8Ma) a dextral strike-slip reactivation of the basement (SWIM) faults (Fig. 6.10F), during a period in which the subduction driving the GCAW growth was still active (experiment 3), although slowing down (Gutscher, 2009a). It should be noted that this rotation of the main convergence direction also agrees with the general strain partitioning tectonic scenario previously proposed by Terrinha et al. (2009), according to which besides dextral strike slip faulting along near E-W orientated faults, northwest directed thrusts also occur along NE-SW orientated tectonic structures (e.g. Horseshoe, Marquês de Pombal and Gorringe faults in Fig. 6.1B).

Other indirect evidence supporting Present day SWIM and GCAW simultaneous activity include the fact that, not only all known mud volcanoes in the Gulf of Cadiz are located on top of the accretionary wedge, but also the circumstance that most of the deep mud volcanoes are symptomatically aligned and coincident with the SWIM faults (Fig. 6.1A). This suggests that the fluid migration and escape may be simultaneously controlled by the activity of both structures. If that is in fact the case, then the mud volcanoes could be preferentially located in the intersection between the SWIM strike-slip and the GCAW thrust faults, with such loci providing good pathways for the fluid to ascend (Pinheiro et al., 2003, 2005; Duarte et al., 2005; Rosas et al., 2009; Zitellini et al., 2009; Terrinha et al., 2009).

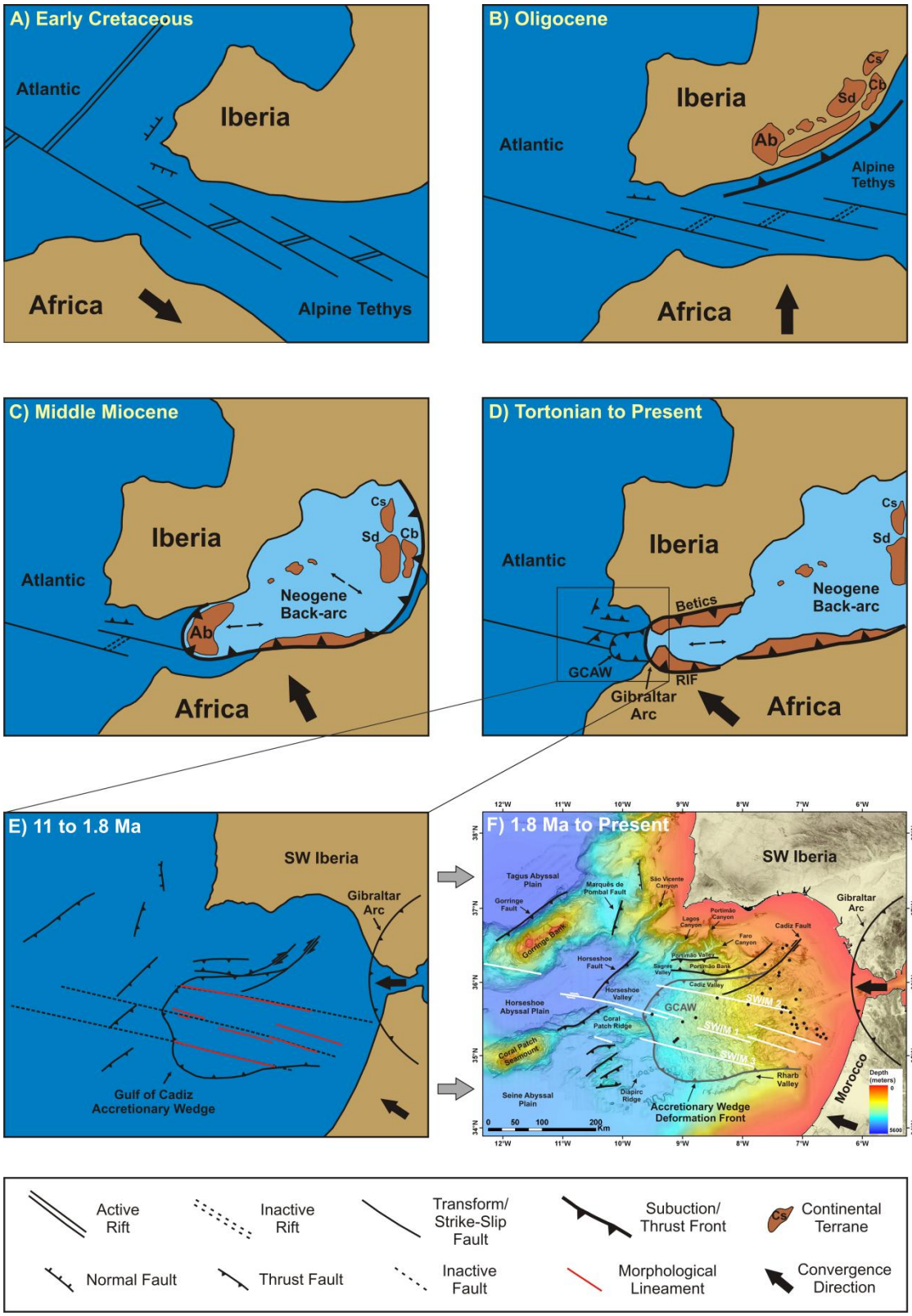


Figure 6.10 - Tectonic model: summarized, schematic representation of the main chronologic events leading to the formation of the Present day main tectonic features in the Gulf of Cadiz (stages A to D are modified from Rosenbaum et al., 2002 and 2004; and complemented with Maldonado et al., 1999; Michard et al., 2002; Gràcia et al., 2003a and Terrinha et al., 2009). Ab – Alboran; Cb - Calabria; Cs - Corsica; Sd - Sardinia. See detailed explanation in the text.

6.5. Conclusions

1. In view of the presented experimental results, the observed morphotectonic pattern of the frontal GCAW area is compatible with:

   i) The development of the GCAW on top of inactive, previously formed, basement faults (present day SWIM fault system).

   ii) The simultaneously (alternating) activity of the GCAW thrusting with the activity of the SWIM-related dextral strike-slip faults.

Conversely, the comparison of the same experimental results with the natural example unambiguously excludes the possibility of active strike-slip faulting (SWIM system) affecting an inactive preexistent GCAW, implying that if the SWIM fault system is active then the GCAW must also be presently active.

2. The main tectonic implications of the above conclusions comprise an initial (Middle Miocene to ~1.8 Ma) accretion of the GCAW sediments on top of preexistent Tethyan rift-related faults, preceding strike-slip reactivation of these faults (SWIM system), simultaneously with decreasing GCAW activity (~1.8 Ma to Present), as a function of counterclockwise rotation of the main Iberia-Nubia convergence direction.

3. The modeling and morphological observations favor the interpretation of the SWIM fault system as the strike-slip reactivation of pre-existent basement faults. This suggests that the SWIM plate boundary proposed by Zitellini et al. (2009) may in fact correspond to the local reactivation of the older Tethyan plate boundary.

Chapter appendix 6.A. - Scaling

The material used as an analog of the upper crust sedimentary rocks was dry quartz sand, which is considered a Coulomb material deforming in a brittle way according to the Coulomb fracture criterion (e.g. Hubbert, 1937, 1951; Davis et al., 1983):

$$\tau_{ss} = \mu_c \sigma_n + c_0 \ (1)$$

where τ_{ss} is the shear stress, μ_c is the coefficient of internal friction ($\mu_c = \tan\phi$, and $\phi =$ internal friction angle), σ_n is the normal stress, and c_0 is the cohesion of the material. According to the scale model theory (Hubbert, 1937), proper scaling is achieved when the ratios between model and natural prototype are independently established for the three fundamental units of length (λ), time (τ) and mass (μ):

$$\lambda = \frac{L_{(m)}}{L_{(p)}};\ \tau = \frac{T_{(m)}}{T_{(p)}};\ \mu = \frac{M_{(m)}}{M_{(p)}} \ (2)$$

where L = length, T = time and M = mass, and (m) stands for model and (p) for natural prototype. The Coulomb fracture criterion governs time independent deformation of brittle materials like sedimentary upper crustal rocks, since yield stress is insensitive to the rate of deformation provided that the inertial forces are negligible, as in the present case. This means that τ ratio is not needed for scaling in this situation. Length ratio (λ) was chosen given the maximum dimensions of the deformation apparatus used in the experiments (see section 3), and was conveniently established as $\lambda = 2 \times 10^{-6}$. In the present case, of the two relevant material properties, coefficient of internal friction (μ_c) and cohesion (c_0), the first is dimensionless, and approximately the same in both model and prototype, whereas the second has dimension of stress and thus must be scaled accordingly (Hubbert, 1937):

$$\Sigma = \frac{c_{0(m)}}{c_{0(p)}} = \frac{\mu\gamma}{\lambda^2} \quad (3)$$

where Σ and γ are the model/prototype ratio for stress and for acceleration respectively. Since inertial forces are negligible when compared with gravity,

$$\gamma = \gamma_g = \frac{g_{(m)}}{g_{(p)}} = \frac{\lambda}{\tau^2} = 1 \quad (4)$$

where γ_g is the model/prototype gravity acceleration ratio. Thus, substituting $\gamma = 1$ in equation (3) allows the following simplification:

$$\Sigma = \frac{c_{0(m)}}{c_{0(p)}} = \frac{\mu}{\lambda^2} = \frac{\mu\lambda}{\lambda^3} = \delta\lambda \quad (5)$$

where δ corresponds to the model/prototype density ratio. Substituting δ and λ in equation (5) by the respective values in Table 6.1, immediately allows the determination of the implied mass ratio $= 4 \times 10^{-18}$. It should also be noted that since δ is generally close to one (between 0.5 and 0.7, e.g. Withjack et al., 2007) the strength of the materials expressed by Σ is scaled with the lengh (λ). Given the fact that in the present case $\lambda = 2 \times 10^{-6}$ and since cohesion for upper crustal rocks is clearly typically less than 50 MPa, it becomes immediately evident the utility of model materials with very low cohesion (<100Pa), such as dry quartz sand, as analogs of upper crustal rocks.

Chapter 7
Discussion: The Gibraltar Arc and the SW Iberia (passive) Margin: a case of subduction propagation or induced subduction initiation?

J. C. Duarte

(This chapter is presented in a paper format since it is being prepared to be submitted to a science journal)

In this chapter, a discussion of the main ideas previously addressed in this Thesis is attempted, through a comprehensive integration of the diverse data and information presented herein (previous chapters, papers that are part of the thesis and papers in appendix).

Abstract

The process of spontaneous subduction initiation at passive margins played a central role in the original Wilson Cycle concept. However, recent works showed that it is not feasible to form a new subduction zone in isolation from a previous existing one. The unraveled tectonic framework of the Gibraltar Arc and the Southwest Iberia Margin (presented and discussed in the previous chapters) is here used as a case study to address the role that orogenic arcs may have in the nucleation of new subduction zones at passive margins. An updated tectonic map of the Gulf of Cadiz (the foreland of the Gibraltar Arc) is presented and analyzed in the view of the more recent published works, and the possible tectonic reactivation of the Southwest Iberia Margin is evaluated within the context of the two main driving mechanisms accounting for the recognized tectonic structures in the area: the westward over-thrusting of the Gibraltar Arc and the Present day WNW-ESE dextral oblique convergence between Nubia and Iberia. The role of orogenic arcs in the formation of new subduction systems is hypothetically proposed as of significant importance in plate tectonics.

7.1. Introduction

The Wilson Cycle is one of the most paradigmatic ideas in the plate tectonic theory, stating that oceans form, evolve and finally close (Wilson, 1966). This process requires that after a certain time of the evolution of an ocean, the passive margins collapse and new subduction systems initiate. However, the process by which a passive margin converts into an active margin is still controversial and fundamentally unknown (Nikolaeva, et al., 2010; Stern, 2002; Stern, 2004; Gurnis et al., 2004). There are even substantial doubts whether if it is possible to initiate a new subduction system in isolation from a previous existing one (e.g. Guarnis et al., 2004; Stern, 2004). Also, despite the abundance of both passive and active continental margins on Earth, no cases of transition between these two types of margins has been identified (Nikolaeva et al., 2010). The quest for the identification of an incipient subduction zone at a "passive margin" is a challenge in modern plate tectonics. A natural case study would permit to constrain the previously amount of proposed models on subduction initiation (see a list in Nikolaeva et al., 2010; and Table 2.1 in Chapter 2) and allow a better understanding on the forces driving and resisting plate tectonics (Guarnis et al., 2004).

The margins of the Atlantic Ocean are generally described as the typical case of passive margins, often termed Atlantic type margins (Gibbs, 1984). However, there are two regions where Atlantic oceanic lithosphere is already being consumed in subduction zones: in the Scotia and in the Lesser Antilles arcs (Fig. 7.1, Deuser, 1970; Schellart and Lister, 2004; Goren et al., 2008). These subduction zones are thought to have been transferred from the Eastern Pacific Ocean to the Atlantic domain (Mueller and Phillips, 1991; Royden, 1993; Goren et al., 2008), and have been described as potential precursors to a system of convergent zones that might ultimately result in the closing of the Atlantic Ocean (Mueller and Phillips, 1991).

The Gulf of Cadiz, i.e. the foreland of the Gibraltar Arc (or Betic-Rif Arc; Fig. 7.1 and 7.2), is the third place that has been described as potential locus for a subduction to propagate into the open Atlantic (Royden, 1993), as the result of active roll-back of a narrow oceanic corridor that once connected the Tethyan basin and the Atlantic (Gutscher et al., 2002). On the other hand, the proximity of the westward migrating Gibraltar Arc to the Southwest Iberia Margin (see Fig. 7.2), together with the Present

day WNW-ESE convergence between Nubia and Iberia, induces compressive stresses that make this margin a strong candidate for the nucleation of a new subduction zone, in accordance to what was previously proposed by Ribeiro et al. (1996). The anomalous high magnitude seismicity in this area, such as the magnitude >8.5 Great Lisbon Earthquake of 1755 and the 28/02/1969 earthquake (M~8; Fukao, 1973), complies with such a scenario (Gutscher, 2004 and 2006; Ribeiro et al., 2006).

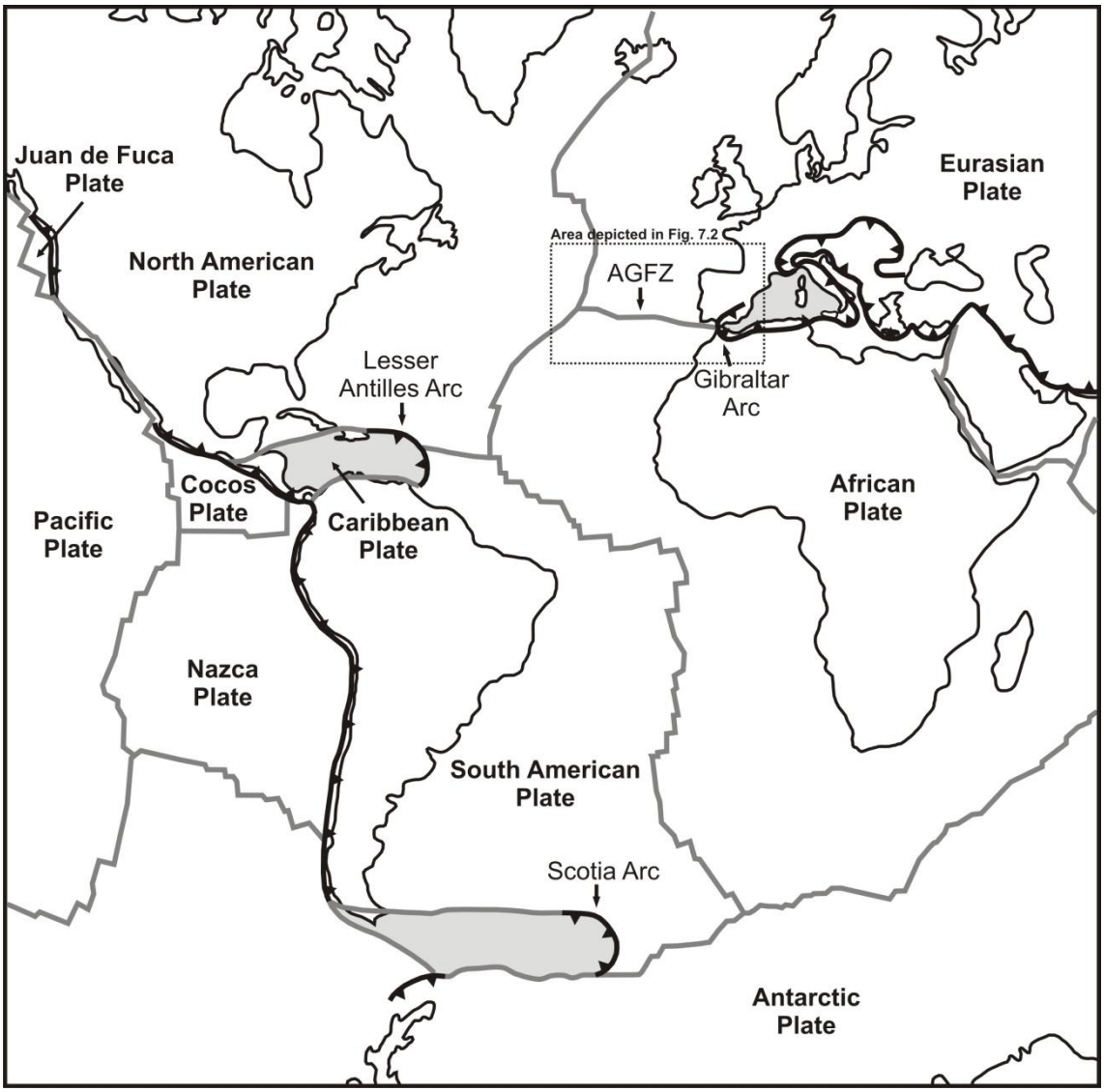


Figure 7.1 – Simplified tectonic map of the Atlantic and surrounding regions with the location of the Atlantic arcs (Scotia, Lesser Antilles and Gibraltar). Thick black lines indicate convergent plate boundaries; thick gray lines indicate divergent or transform plate boundaries (Adapted from Schellart and Lister, 2004); grey areas roughly correspond to back-arc basins.

Using the Gibraltar Arc and Southwest Iberia Margin as case studies, the present work aims at providing insights on the role that preexistent orogenic arcs may have in the reactivation of passive margins and subduction initiation. The discussion is based on an updated tectonic map of this region, based on which the prevailing tectonic driving mechanisms that account for the observed structures were recently interpreted (see Chapter 4; Duarte et al., 2009; Terrinha et al., 2009; Rosas et al., 2009, in appendix Duarte et al., submitted, Chapter 6). The key question concerning whether the Gibraltar subduction zone is active and propagating into the open Atlantic domain, or practically inactive at its present location but a new subduction zone is nucleating westwards along the West Iberia Margin (see Fig. 7.2) is also addressed and tentatively answered.

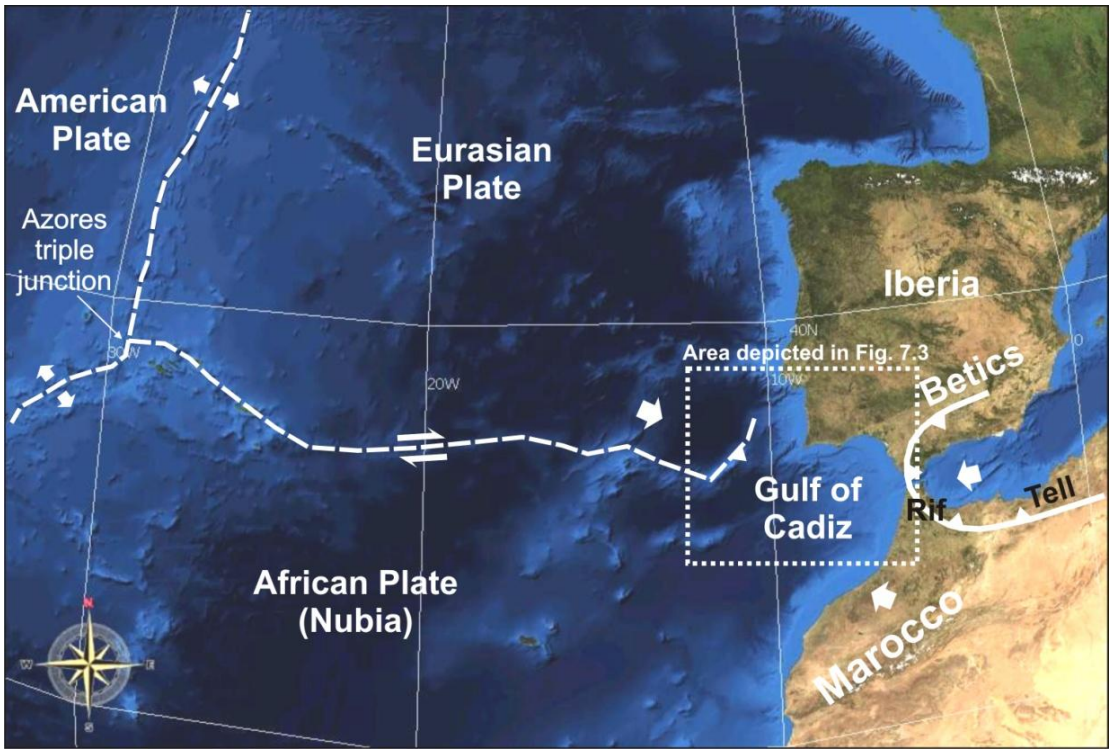


Figure 7.2 – Location of the Gulf of Cadiz area in the general tectonic setting of the western Eurasia (Iberia) - Africa (Nubia) plate boundary.

7.2. The problem of subduction initiation at passive margins

Assuming that various Wilson Cycles occurred in the last 1 to 2 Ga, the almost complete absence of oceanic crust older than 200 Ma suggests that new subduction systems have to initiate repeatedly at passive margins in order to close the oceans that were once formed (Goren et al., 2008). In addition, passive margins have long been considered the more logical place for subduction to initiate, for two main reasons: i) most of the existing subduction zones are located along continental margins and ii) the Present day state of relatively young oceanic lithosphere is only achieved if the oldest oceanic lithosphere, which occurs at passive margins, is subducted before younger lithosphere (Goren et al., 2008; Nikolaeva et al., 2010). It is traditionally assumed that spontaneous subduction initiation at passive margins occurs when the cold gravitationally unstable oceanic lithosphere collapses into the asthenosphere, as consequence of density excess due to its aging. However, several works showed that the strength of the oceanic lithosphere also increases with aging and consequently does not make it more susceptible to spontaneously collapse into the asthenosphere (see Fig. 2.2 in Chapter 2; Mueller and Phillips, 1991; see also McKenzie, 1977 and Cloetingh et al., 1984;). This conclusion is supported by the existence of 170 Ma old oceanic lithosphere adjacent to the Northwest of Africa and the Northeastern American passive margins. On the other hand, the geological record does not seem to reveal one single example of an Atlantic-type margin evolving spontaneously into an Andean-type margin (Mueller and Phillips, 1991). One way to overcome this apparent contradiction is to consider that subduction initiation at passive margins may generally be induced by the proximity of another subduction zone or by stress transference from a nearby subduction zone or collision belt. Therefore, passive margins in the proximity of a mature subduction complex would represent preferential sites for trench formation (Muller and Philips, 1991).

7.2.1. The peri-Atlantic arcs and the "infection" of the Atlantic

The Atlantic is almost entirely bounded by passive margins (see Fig. 7.1). However, according to some authors, the Atlantic has already entered in its closing phase (e.g. Mueller and Philips, 1991; Ribeiro et al., 2006). In fact, there are two regions where Atlantic oceanic lithosphere is by now being consumed in subduction zones: in the Scotia and in the Lesser Antilles arcs (Deuser, 1970; Goren et al., 2008; see Fig. 7.1). These arcs seem to correspond to cases where the initiation of the subduction was induced by the proximity of another subduction system. It was proposed that these two systems formed due to stress transmission across narrow continental landmasses that once existed between the Pacific and the Atlantic (see Fig. 2.5 in Chapter 2; Mueller and Philips, 1991; Goren et al., 2008). Mueller and Philips (1991) used an interesting and particularly creative analogy to describe this phenomenon. They consider that subduction zones may be introduced into a pristine oceanic basin (i.e. without subduction zones), in a way that might be viewed, figuratively, as a process in which an infected ocean (i.e. with subduction zones) comes in contact with, and infects, an uninfected basin. It should be noted that both the Scotia and Lesser Antilles arcs are propagating along two transform plate boundaries that connect these arcs to the Mid-Atlantic Ridge (see Fig. 7.1). The third limit of this type in the Atlantic is the Azores-Gibraltar Fracture Zone, which extends from the Azores triple junction (in the Mid-Atlantic Ridge) to the foreland of the Gibraltar Arc (see Fig. 7.1). This area was proposed to be the third place where an initial stage of this "infection" process could be occurring at the present (Mueller and Philips, 1991; Royden, 1993). However, both the Scotia and the Lesser Antilles arcs have retreated around 2000 km and their trenches do not seem to have propagated laterally, along the adjacent passive margins (see Fig. 7.1), contrary to the foreland of the Gibraltar Arc, where the deformation is propagating northeastwards along the Southwest Iberia Margin (see Chapter 4; Terrinha et al., 2009 in appendix; and further in this chapter). We hypothesize that this difference may be related to the fact that the plates bounding the Gibraltar Arc, Nubia and Eurasia (Fig. 7.2), are converging, which is not the case with the plates bounding the Scotia and the Lesser Antilles arcs. This convergence may constrain the arc laterally inducing the migration of the deformation away from it into the Atlantic.

7.3. The case study of the Gulf of Cadiz

7.3.1. Main tectonic features

In the Gulf of Cadiz tectonic map shown in Fig. 7.3 it is possible to identify three main tectonic systems: i) the subduction-related Accretionary Wedge (marked in grey); ii) a set of WNW-ESE striking dextral strike-slip faults (the SWIM fault system; marked in white); and iii) a group of NE-SW striking northwest-directed thrusts concentrated in the Southwest Iberia Margin (marked in yellow).

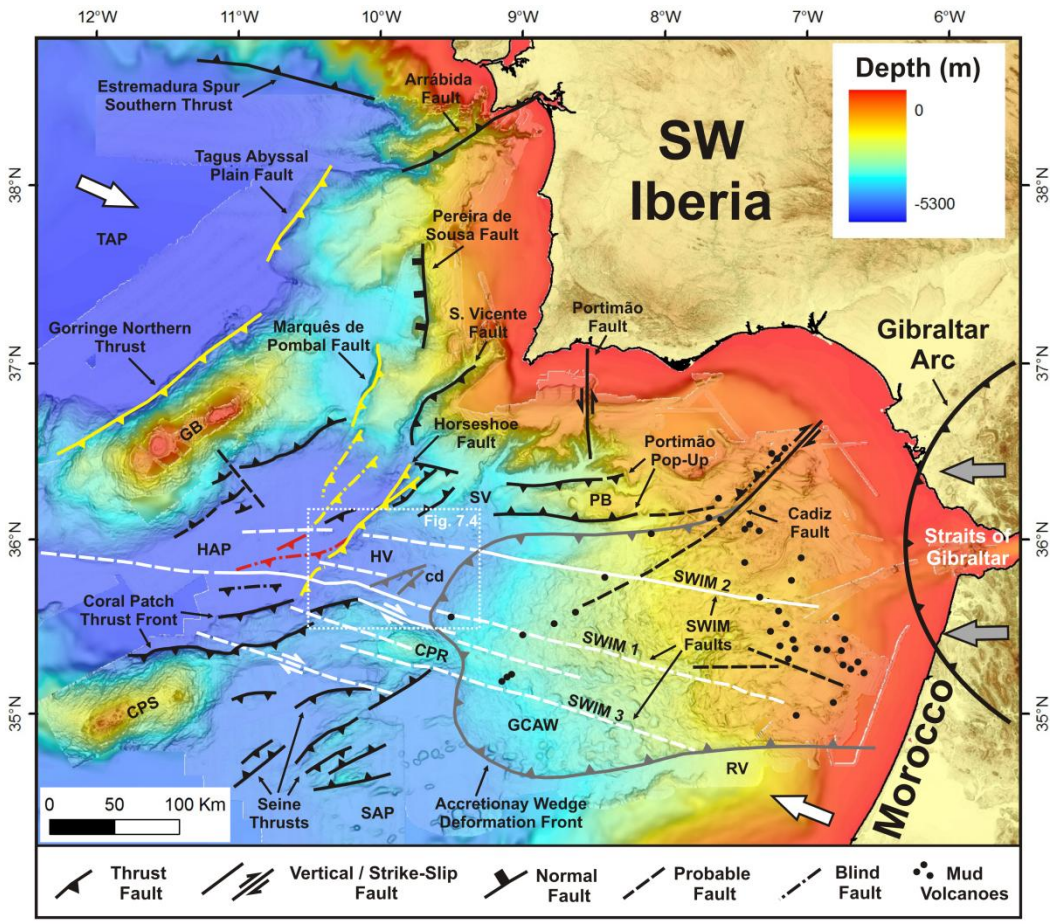


Figure 7.3 – Tectonic map of the Gulf of Cadiz and SW Iberia. The GCAW front is shown in grey, the SWIM faults in white; the SW Iberia NE-SW thrusts in yellow and the "corner faults" in red. The Tagus Abyssal Plain fault from Cunha et al. (2010); Estremadura Spur Southern Thrust and the Arrábida fault from Terrinha et al. (in prep.). CPR - Coral Patch Ridge; CPS - Coral Patch Seamount; GB - Gorringe Bank; HAP - Horseshoe Abyssal Plain; HV - Horseshoe Valley; PB - Portimão Bank; RV - Rharb Valley; SAP - Seine Abyssal Plain; SA - Sagres Valley, cd - crescentic depressions. Grey arrows - Gibraltar Arc westward movement; Whithe arrows - Nubia-Iberia WNW-ESE convergence (Gutscher et al., 2002; Nocquet and Calais, 2004; Stich et al., 2006; Fernandes et al., 2007; Tahayt et al., 2008).

7.3.1.1. The Subduction-related Accretionary Wedge

The accretionary wedge occupies a broad area of the Gulf of Cadiz (see Fig. 7.3) and its influence on the seafloor is materialized by a west dipping U-shaped surface that extends for more than 250 km from about longitude 7º to 9º30'. From the structural point of view, this feature consists in an eastward thickening pile of westwards thrusted sediments that may exceed 10 km of thickness (Thiebot and Gutscher, 2006; Gutscher et al., 2009a; Duarte et al., submitted). The thrusts root in a gently east dipping décollement layer, exhibiting an overall geometry compatible with on-going eastwards subduction beneath the Gibraltar Arc (Gutscher et al., 2002 and 2009a,b). The existence of a subduction zone in this area is supported by seismic tomography data, which shows an east dipping slab below the Gibraltar Arc prolonging 670 km deep into the mantle. This subduction zone is believed to have developed within the Mediterranean Alpine Collision Belt and is a remnant of the subduction system that consumed most of the Western Mediterranean Tethyan Ocean during the Cenozoic (Lonergan and White, 1997; Rosenbaum et al., 2002). Gutscher et al. (2002) proposed that the subduction is still active and retreating westwards along an East-West trending corridor of remnant (Jurassic) oceanic lithosphere. The presence of such an oceanic corridor was recently confirmed by seismic refraction data (Sallarès et al., 2011). Also, recent detailed structural mapping of the Horseshoe Valley area revealed the existence of an intriguing set of kilometric crescentic depressions lying at depths between -4300 and -4700 m (Fig. 7.4A; see location in Fig. 7.3; see also Chapter 5 for a detailed study on the origin of these features - Duarte et al., 2010). The thorough analysis of seismic reflection profiles from this area revealed that: i) the crescentic depressions are carved on the edge of morphological slope breaks (see Fig. 7.4A); ii) the morphology of the depressions is shaped by the interaction of downslope currents with this slope breaks; and iii) the slope breaks are tectonically controlled by blind thrusts that root at the level of the accretionary wedge décollement (see Fig. 7.4B). These blind thrusts are located to the west and in front of the outermost limit of the accretionary wedge (thrusts marked in grey in Fig. 7.3). These features are thus interpreted as the morphological (i.e. bathymetric) expression of Present day westward propagation of the accretionary wedge.

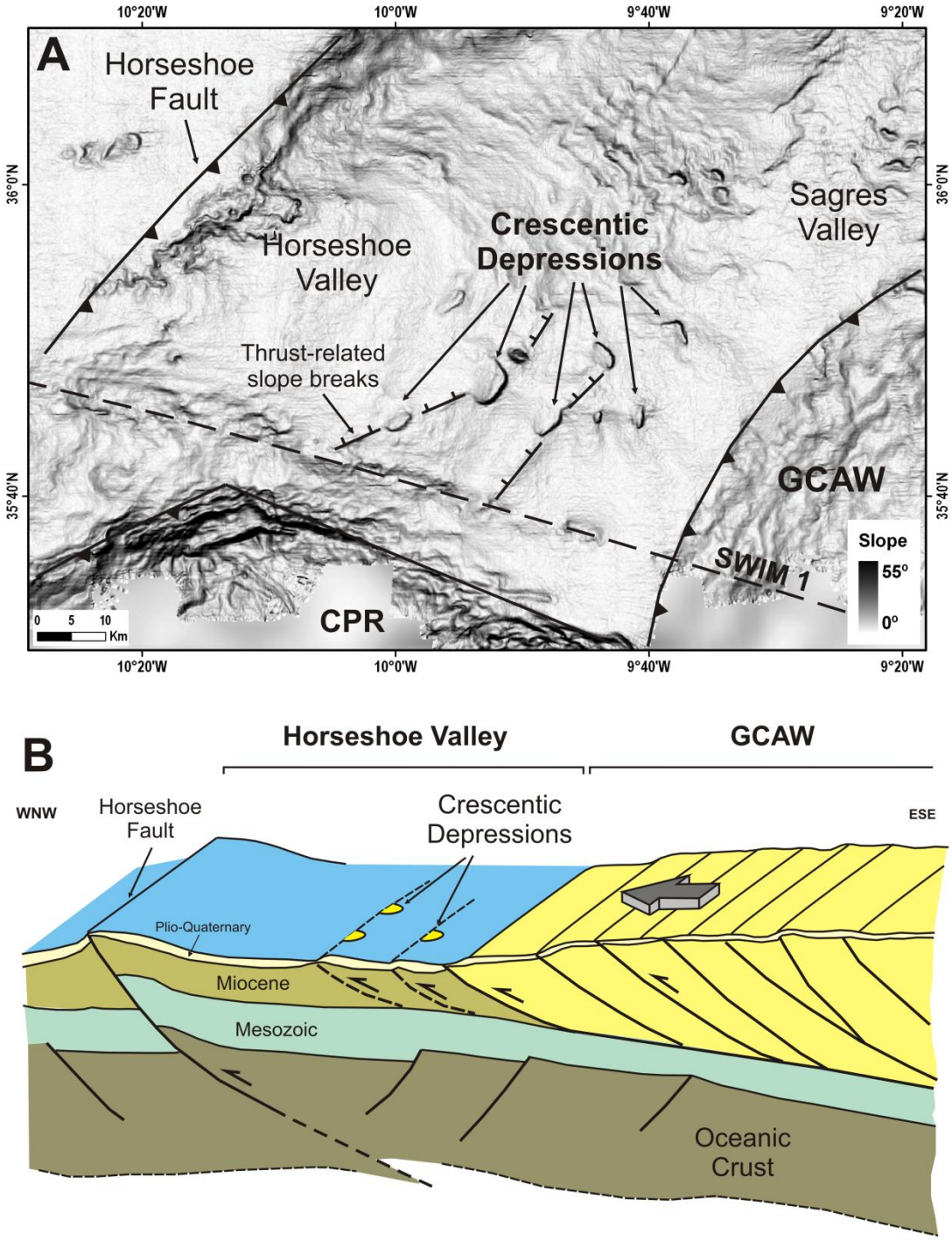


Figure 7.4 – A) Slope map of the Horseshoe Valley comprising the Crescentic Depressions studied in Duarte et al. (2010) – Chapter 5. The Horseshoe Valley is delimited to the east by the Gulf of Cadiz Accretionary Wedge (GCAW) and to the west by the scarp of the Horseshoe fault; B) Schematic representation of the Horseshoe Valley and surrounding regions (not to scale). Note in Fig. 7.4A that most of the Crescentic Depressions are coincident with slope breaks, corresponding to the morphological expression of blind-thrusts that root at the GCAW décollement level (see 7.4B and Duarte et al., 2010). Grey arrow – sense of propagation of the deformation. CPR – Coral Patch Ridge.

7.3.1.2. The NE-SW striking thrust system

The generally NE-SW striking thrust system comprises mainly the Horseshoe fault, the Marquês de Pombal fault, the Tagus Abyssal Plain fault and the Gorringe northern thrust (Fig. 7.3; Zitellini et al., 1999; Gràcia et al., 2003a,b; Terrinha et al., 2003; Rovere et al., 2004; Zitellini et al., 2004; Terrinha et al., 2009; Cunha et al., 2010). This thrust system extends for approximately 300 km from the Coral Patch Ridge area (35.5ºN), towards the north, along the West Portuguese Margin until a latitude of 38ºN, with an apparent en echelon spatial disposition (see thrusts marked in yellow in Fig. 7.3). The thrust structures have prominent escarpments reaching up to 2000 meters in height and seem to root deep into the basement, possibly cutting into the mantle, as suggested by seismic imagery and deep instrumental seismicity (Stich et al., 2007; Terrinha et al., 2009; Cunha et al., 2010; Silva et al., 2010). According to Terrinha et al. (2009), this NE-SW striking thrust system is the result of the migration of the deformation from the realm of the Gibraltar wedge to the west (onto the Horseshoe fault region) and to the north along the West Portuguese Margin. This migration is believed to have been caused in part by the rotation of the convergence direction between Nubia and Iberia since the Miocene (Terrinha et al., 2009). The same authors considered that these structures may be the expression of a new compressive deformation front, away from the Gibraltar Arc and along the West Iberia Margin, corresponding to the onset of its tectonic inversion, which could eventually lead to the nucleation of a subduction zone (Ribeiro et al., 1996). Note that in this region, the Gorringe Bank (see Fig. 7.3) was shown to be mostly constituted by highly serpentinized mantle peridotites (Girardeau et al., 1998; Jimenez-Munt et al., 2010). Serpentinization, in addition to induced compression, can provide an efficient weakening mechanism that may facilitate lithospheric rupture and subduction initiation (Cloetingh et al., 1984; Masson et al., 1994).

7.3.1.3. The SWIM fault system

The SWIM fault system is a group of WNW-ESE striking subvertical structures, interpreted as dextral strike-slip faults (Terrinha et al., 2009; Rosas et al., 2009), extending from the eastern part of the Gulf of Cadiz across the Horseshoe Abyssal Plain (see Fig. 7.3; Duarte et al., 2009; Terrinha et al., 2009; Zitellini et al., 2009). The SWIM faults were interpreted by Zitellini et al. (2009) as corresponding to a newly formed dextral transcurrent plate boundary connecting the Azores-Gibraltar Fracture Zone (see Fig. 7.1) to the Rif Mountain belt in northern Morocco. The morphologic expression of the SWIM faults corresponds to a more or less continuous alignment of seafloor crests and troughs locally punctuated by active mud volcanoes within the domain of the accretionary wedge (Hensen et al., 2007). Terrinha et al. (2009) and Duarte et al. (2009) showed that these WNW-ESE structures seem to correspond to the dextral reactivation of basement normal faults probably formed during Mesozoic extensional events. Furthermore, the morphotectonic interpretation of strike-slip associated en echelon folds, based on analogue modeling experiments, suggested that the dextral movement initiated at least 1.8 Ma ago (Rosas et al., 2009). The SWIM fault system may be presently acting as a transfer zone connecting the two main compressive systems (the Gibraltar Arc/GCAW and the Southwest Iberia NE-SW thrusts).

7.3.1.4. Thrust-wrench tectonic interference in the study area

Assuming that the SWIM dextral strike-slip faults are active (Zitellini et al., 2009) and cutting other (also active) structures, such as the Horseshoe thrust fault and the accretionary wedge (Terrinha et al., 2009; Gutscher et al., 2002, Fig. 7.3), some kind of tectonic interference is expected to occur between these major tectonic features, eventually expressed by complying cross-cutting relationships, or corresponding interference structural patterns. Confirming this, Rosas et al. (submitted) reported, characterized and modeled the tectonic interference pattern between the SWIM 1 fault and the Horseshoe thrust fault, mostly consisting in secondary “corner” faults connecting the two tectonic systems as a result of ongoing thrust-wrench interference in

this specific area (see "corner faults" shown in red in Fig. 7.3 and Rosas et al., submitted, in appendix). Likewise, based on analog modeling experiments, Duarte et al. (submitted; see Chapter 6) showed that the observed morphotectonic interference pattern between the SWIM faults and the accretionary wedge thrust front is not compatible with the possibility previously put forward by Zitellini et al. (2009), according to which the accretionary wedge is presently inactive and cut by active translithospheric (SWIM) dextral strike-slip faults. These same authors showed that if this was the case, an important dextral offset (at least c.a. 7 km) of the accretionary wedge deformation front should occur, and be plainly observed, which is simply not observed in the surveyed bathymetry (Figs. 7.3 and 7.4; see Duarte et al., submitted). Instead, the same reported modeling results suggest that the easiest way to explain the observed absence of cross-cutting relationships is by considering both the SWIM and accretionary wedge active (Duarte et al., submitted – Chapter 6). Also, based on the same results these authors interpreted the SWIM system as the strike-slip reactivation of pre-existent rift-related basement faults, originally formed during the opening of the Alpine-Tethys, rather than corresponding to the expression of the onset of a new plate boundary as previously proposed (by Zitellini et al, 2009).

7.3.2. Was the 1755 Great Lisbon Earthquake a subduction-related event?

One major issue that should be taken into account when trying to understand significance of the main tectonic structures in the Gulf of Cadiz (and Southwest Iberia Margin) is the 1755 Great Lisbon Earthquake that had an estimated magnitude between 8.5 and 8.9 (Johnston, 1996; Batista et al., 1998). The location of the source of this historical earthquake still remains one of the major unsolved questions regarding the tectonics of this area (e.g. Gutscher et al., 2002; Terrinha et al., 2009 and Zitellini et al., 2009). Gutscher et al. (2002; 2004) argued that the 1755 earthquake requires a rupture area only compatible with a subduction zone plane and proposed the Gibraltar Arc subduction as the most reliable source. Their argument was not only based on the geological and geophysical data, but also in the fact that most of the large magnitude earthquakes ($M \geq 8.5$) are generated in subduction zones. Accordingly, 11 of the 12

greatest earthquakes (M≥8.5) of the past 100 years occurred along subduction fault planes (the exception was a magnitude 8.6 earthquake in the Himalaya collision belt). However, the Gulf of Cadiz subduction fault plane shows negligible instrumental high magnitude seismicity. Gutscher et al. (2006) offers three possible explanations for such an absence: (1) subduction is inactive and has ceased; (2) subduction is active, but aseismic; (3) subduction is active and a locked seimogenic zone exists, gradually accumulating stress until it releases the next great earthquake. Based on recently acquired seafloor and GPS data the authors favor the last hypothesis. Ribeiro et al. (2006) agree that the source mechanism of such a large earthquake requires generation at a subduction zone. However, they proposed that the source of the 1755 event was not the Gibraltar Arc subduction, but an incipient subduction zone that would be presently developing in the West Iberia Margin. Terrinha et al. (2009) proposed that the Horseshoe, Marquês de Pombal, Tagus Abyssal Plain and Gorringe compressive structures are the crustal expression of this hypothetical incipient subduction zone (see Fig. 7.2 and 7.3). Some of these structures may be linked at depth and/or connected by lateral ramps, providing a possible and reliable source mechanism for the generation of a seismic event such as the 1755 Great Lisbon Earthquake.

7.4. An evolution model for the Gulf of Cadiz region

7.4.1. The formation of the Gibraltar Arc

The area that presently corresponds to the Gulf of Cadiz (the foreland of the Gibraltar Arc) was initially formed during the Mesozoic as part of the more occidental Alpine-Tethys rift system (Fig. 7.5A), which comprised an oceanic domain separating two newly formed passive margins. (Dercourt et al., 1986; Sanz de Galdeano, 1990; Srivastava et al, 1990a,b; Maldonado et al., 1999; Rosenbaum et al., 2002; Stampli et al., 2002). At this stage, a continuous corridor of oceanic lithosphere probably existed connecting the Alpine-Tethys to the Atlantic Ocean.

In the Eocene-Oligocene, Africa and Eurasia were already converging (Fig. 7.5B). This convergence started in the Upper Cretaceous and led to the reactivation of most of the Gulf of Cadiz Mesozoic extensional structures (e.g. previous transform and rifted-related normal faults; Duarte et al., 2009; Terrinha et al., 2009). The North-South convergence was accommodated by the northwards subduction of the Alpine-Tethys oceanic lithosphere that extended from the SE Iberia to the western Alps (see Fig. 7.5B; Rehault et al., 1985; Malinverno and Ryan, 1986; Dewey et al., 1989; Rosenbaum et al., 2002; Jolivet et al., 2006). Since the Oligocene, the continental collision in the Alps absorbed the bulk compression implied in the convergence of both plates and, as consequence, the northwards Apline-Tethys subduction along Europe's meridional margin slowed down and became primarily driven by the density collapse of the subducting oceanic slab (op.cit). This, triggered slab roll-back, which led to the formation of the West Mediterranean back-arc basins and associated continental terranes, among which Sardinia, Corsica, Calabria and Alboran (Fig. 7.5C; Rosenbaum et al., 2002; 2004). In the Middle Miocene, the Alboran terrane was migrating almost unimpeded in direction of the Atlantic Ocean. Note that if Africa and Iberia were not converging the Gibraltar Arc could have "invaded" the Atlantic Ocean, propagating in a similar manner to what is presently occurring in the Scotia and Lesser Antilles arcs. However, the continued convergence between Africa and Eurasia caused the narrowing of the East-West oceanic corridor existing between Africa and Iberia (see Fig. 7.5C) and led to the collision of the Alboran terrane with the SE Iberia and NW Africa forming the Gibraltar (or Betic-Rif) Arc.

In the Tortonian, the Gibraltar Arc was still migrating westwards, at the same time as the accretionary wedge was forming synthetically with the associated eastwards subduction of the Tethyan slab beneath Gibraltar (Fig. 7.5D; Lonergan and White, 1997; Gutscher et al., 2002). At the Present day the Alboran block is nearly trapped between Nubia and Iberia, and the subducted slab could have been partially delaminated. It is however debatable if there is in the Gulf of Cadiz enough oceanic lithosphere, attached to the slab, available to be subducted by roll-back (driven by slab-pull). On the other hand, even though the subduction may be nearly locked, the N-S component of convergence between Africa and Eurasia may also contribute to some degree of lateral expulsion of the Alboran block (and the Gibraltar Arc). This could be also contributing to the outward propagation of the accretionary wedge to the west even

in the absence of major activity along the subduction plane. Such lateral expulsion, together with the counter-clockwise rotation of the Nubia-Iberia convergence direction since the Miocene (see Fig. 7.5), may be causing the concentration of stress in the Southwest Iberia Margin triggering the activity of the structures present there, since the cratonic Iberia would behave essentially as an undeformable rigid block (see Fig. 7.5D).

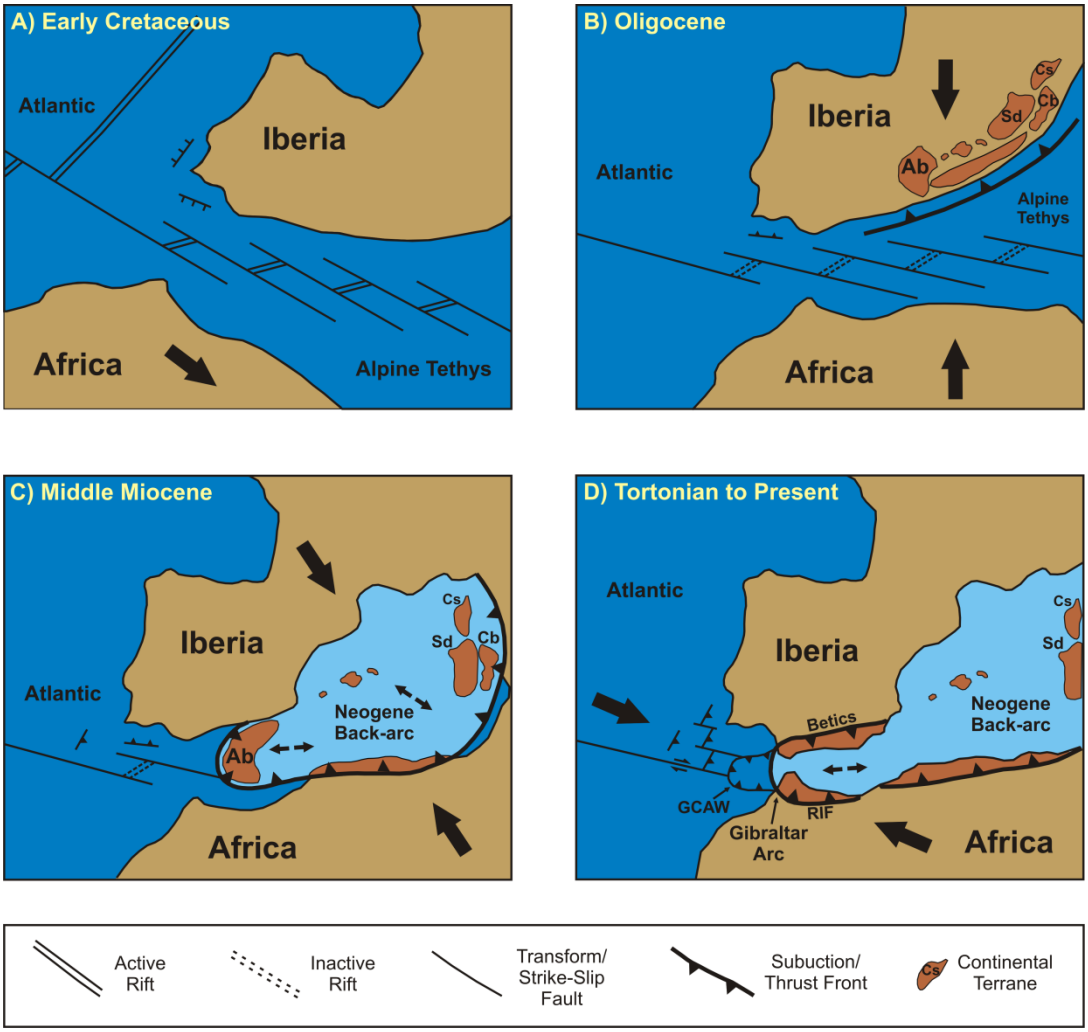


Figure 7.5 – Schematic reconstruction of the tectonic evolution of the Southwest Iberia Margin and the Western Mediterranean region from the Mesozoic to Present (modified from Maldonado et al., 1999; Rosenbaum et al., 2002; Michard et al., 2002; Terrinha et al., 2009). Ab - Alboran; Cb - Calabria; Cs - Corsica; Sd - Sardinia.

7.4.2. The present-day tectonic driving mechanisms

Two main tectonic driving mechanisms can be envisaged as accounting for the present-day active structures in the Gulf of Cadiz: i) the WNW-ESE convergence between Nubia and Iberia (see Figs. 7.3 and 7.5A; Nocquet and Calais, 2004; Stich et al., 2006; Fernandes et al., 2007; Tahayt et al., 2008; Duarte et al., submitted) and ii) the westward movement of the Gibraltar Arc (Gutscher et al., 2002; Tahayt et al., 2008; Duarte et al., submitted).

The first driving mechanism is a consequence of the overall convergence between Africa and Eurasia. In the Gulf of Cadiz this convergence is almost perpendicular to the NE-SW striking thrust system and sub-parallel to the WNW-ESE striking SWIM system (see Fig. 7.5D). These two tectonic systems are thought to accommodate this convergence within a general overall scenario of strain partitioning, in which the NE-SW striking structures accommodate the thrusting/shortening component and the more WNW-ESE striking structures (including the SWIM faults) accommodate the dextral strike-slip movement (Terrinha et al., 2009).

The second driving mechanism has its origin in the westward roll-back implied by the eastward Gibraltar subducting slab that has led to the emplacement of the accretionary wedge in the Gulf of Cadiz since the Miocene. Evidence of blind-thrusting to the West of the accretionary wedge front (see Fig. 7.4; Duarte et al., 2010), suggests that this system westwards propagation is still presently ongoing.

This interpretation, according to which both driving mechanisms are active, is supported by GPS data that show, not only a WNW-ESE ~4 $mm.yr^{-1}$ convergence between Nubia and Iberia, but also 3.5 $mm.yr^{-1}$ of oblique westward movement of the Gibraltar Arc in relation to Iberia (Stich et al., 2006; Tahayt et al., 2008). One major question remaining is whether the seismogenic zone of the Gibraltar subduction system is locked, even if the Gibraltar Arc is still moving westwards. If this is the case, to what extent is this movement being accommodated to the west of the accretionary wedge forcing the activation of the Southwest Iberia Margin thrust system? Is the Gibraltar subduction “trapped” and slowing down, while the stress is transmitted to the West Iberia Margin thus eventually favoring the formation of a new subduction zone?

7.4.3. The future of the NE Atlantic Gulf of Cadiz region: subduction propagation or induced subduction initiation?

At the present state of the knowledge it is difficult to quantify the specific contribution of each of the two main driving mechanisms (WNW-ESE convergence between Iberia and Núbia, and westward migration of the Gibraltar Arc) that best comply with the evolving active tectonic framework in the study area. Further numerical modeling could provide significant insight on this matter. Nevertheless, it is possible to speculate on the evolution scenarios that can be tested in the future, both through modeling and enhanced new observations provided by new geophysical surveys. Two plausible evolution scenarios that can be foreseen as two competing end members are proposed and discuss:

i) Subduction propagation - The first scenario considers the westward roll-back of the Gibraltar subduction as the main tectonic driving mechanism acting in the Gulf of Cadiz region (see Fig. 7.6A). Accordingly, the subduction could hypothetically continue to retreat and propagate westwards to Atlantic domain (see Fig. 7.6B-Alternative I). However, even though there apparent evidences of the westward propagation of the GCAW, the rate of migration of the Alboran Block/Gibraltar Arc seems to be decreasing. It is possible that such a decrease is being primarily caused by the N-S constriction imposed by the Africa-Iberia convergence, which may also be causing the delamination of the subducting slab. Other mechanisms such as the approximation of highly buoyant serpentinized basements highs (Gorringe Bank and Coral Patch Seamount; see Fig. 7.3) could also inhibit the bending of the lithosphere that together with the entrance of ridges (such as the Coral Patch Ridge; see location Fig. 7.3) in the subduction plane could contribute to the decrease in the subduction rate or even cause its total blocking. In this scenario, even if the subduction succeeds to propagate further west into the Horseshoe Abyssal Plain domain, it will be hardly feasible to subduct the more than 4 km high Gorringe Bank and Coral Patch Seamount.

ii) Induced subduction initiation - The second scenario considers the Gibraltar Arc subduction system decreasing in activity (until it becomes completely inactive) and the Southwest Portuguese Margin as being reactivated, leading to the formation of a new incipient subduction zone (see Fig. 7.5B-Alternative II). If this was the case it

would be important to clarify, and if possible to quantify, what is the main mechanism driving the reactivation of the margin: the westward movement of the Gibraltar Arc? The WNW-ESE convergence between Nubia and Eurasia? Or both? It would be also crucial to quantify the magnitude of the forces involved in this process, with the objective of trying to understand if they are sufficiently high to overcome lithospheric strength and to produce large scale bending of the lithosphere, which is required for subduction initiation.

Even though there are uncertainties on the role of the driving mechanisms operating in this region, it seems clear that a new convergent system is developing in the Gulf of Cadiz. The formation of this system seems to have been induced by the proximity of the Mediterranean orogenic arcs (see Fig. 7.1). This hypothesis is in agreement with the Muller and Philips (1991) ideas that passive margins in the proximity of mature subduction systems are favorable sites for trench formation. This type of passive margin induced reactivation (by stress transference) may be seen as a way to initiate a new subduction zone in a passive margin. Thus, the connection between pristine oceans to "infected" oceans with active subduction zones, or the existence of narrow landmasses in between, may have a crucial role in plate tectonic. In particular, in the beginning of the closing phase of the Wilson Cycle.

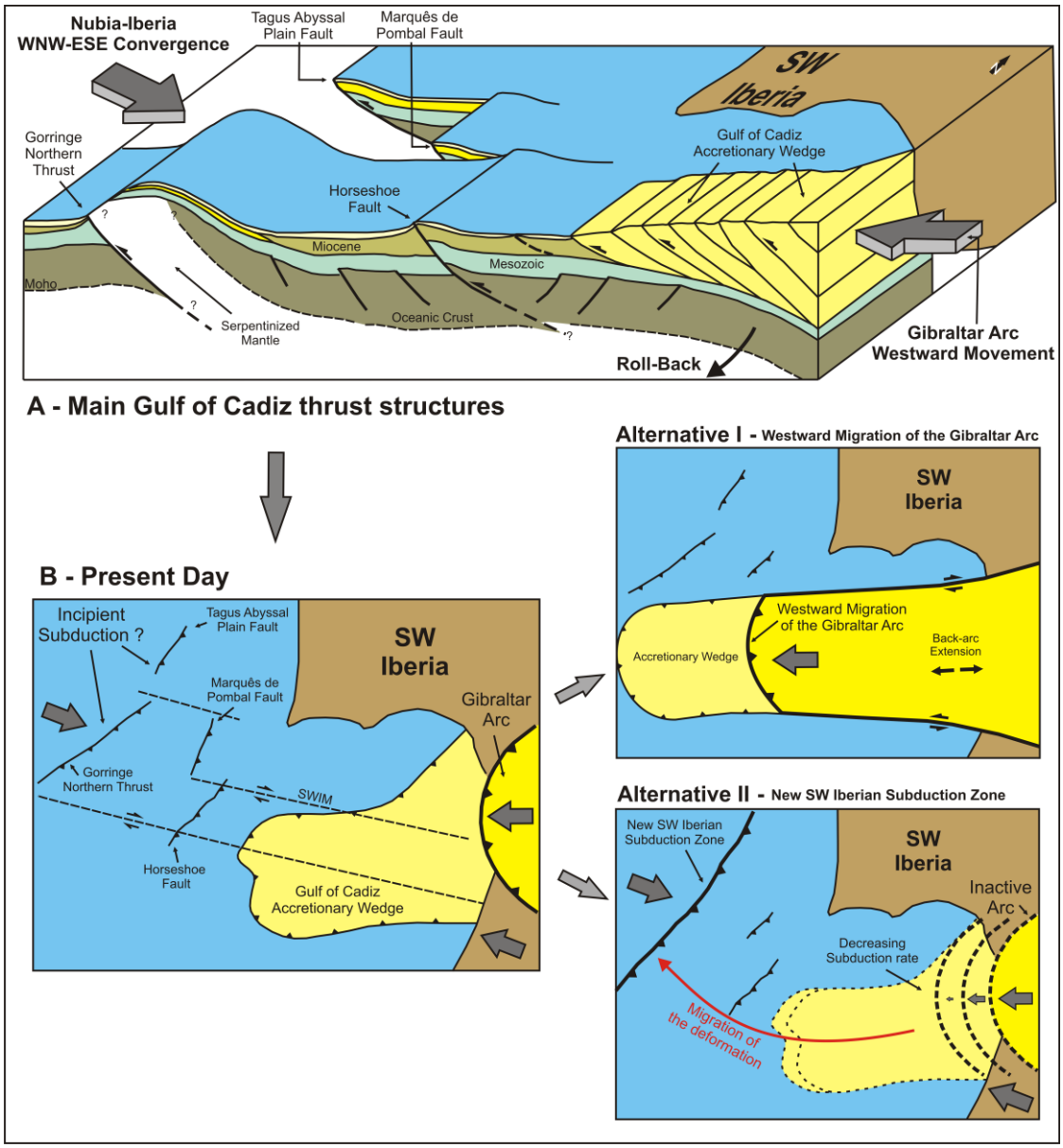


Figure 7.6 – (A) Schematic representation of the main thrust structures present in the Gulf of Cadiz and SW Iberian Margin (see Fig. 7.3); big grey arrows represent the two main tectonic driving mechanisms – the westward movement of the Gibraltar Arc and the Nubia-Iberia convergence; (B) Present day schematic setting of the main thrust structures and two hypothetical evolution scenarios: Alternative I - the Gibraltar subduction migrates to the Atlantic domain; Alternative II - a new subduction system forms in the SW Iberia Margin while the Gibraltar subduction progressively becomes inactive.

7.5. Conclusions

In this work it was tentatively addressed the problematic of the role of orogenic arcs in the initiation of subduction at passive margins, using the Gibraltar Arc and the Southwest Iberia Margin as case studies. To do so, it was analyzed an updated tectonic map of the Gulf of Cadiz area (the foreland of the Gibraltar Arc). Our analysis showed that at the Present day there are two tectonic driving mechanisms operating in the Gulf of Cadiz region: the westwards migration of the Gibraltar Arc and the local WNW-ESE convergence between Nubia and Iberia. The Gibraltar Arc and the GCAW are part of a subduction system that originated in the Western Mediterranean and seems to be propagating to Atlantic domain, however at a significant lower rate than in the Miocene. On the other hand, the westward movement of the Gibraltar Arc, together with the Present day Nubia-Iberia convergence, seems to be forcing/inducing the reactivation of the Southwest Iberia Margin and the formation of a new incipient subduction zone. According to this scenario, the Gulf of Cadiz may be seen as a place where a pre-existent subduction system is "infecting" the Atlantic. Together with the Scotia and the Lesser Antilles arcs, the Gibraltar Arc foreland may represent part of the nucleation locus of a new subduction system that might ultimately lead to the closing of the Atlantic Ocean.

Chapter 8
Synthesis and conclusions

In this chapter, the major out puts of the several subjects studied in this thesis are presented, outlining the main attained conclusions. Suggestions for further work are also presented in the end of the chapter.

The Gulf of Cadiz tectonic structures

- A new tectonic map of the Gulf of Cadiz was produced using the coupled analysis of a multi-survey MCS dataset and the recently compiled high resolution SWIM bathymetry. The map depicts three main tectonic systems: i) the subduction-related Gulf of Cadiz Accretionary Wedge (CGAW), materialized on the seafloor by a west dipping U-shaped surface, which is the morphological expression of an eastward thickening pile of westwards thrusted sediments; ii) a set of WNW-ESE striking dextral strike-slip faults (the SWIM fault system), extending from the eastern part of the Gulf of Cadiz to the Horseshoe Abyssal Plain; iii) and a group of NE-SW striking northwest-directed thrusts located in the Southwest Iberia Margin (the NE-SW thrust system), comprising mainly the Horseshoe fault, the Marquês de Pombal fault, the Tagus Abyssal Plain fault and the Gorringe northern thrust. Despite these main systems, other new structures were recognized, such as the "corner faults" connecting the SWIM wrench system to the Horseshoe thrust fault, the thrusts located in the Horseshoe Valley region to which the crescentic depression are associated, and the NE-SW striking Cadiz fault, a major dextral strike-slip fault located in the northeastern part of the Gulf of Cadiz.

The crescentic depressions and the GCAW propagation

- The morphotectonic mapping of the Gulf of Cadiz revealed a group of kilometric crescentic depressions lying at depths between -4300 m and -4700 m. The detailed morphotectonic analysis of these features showed that they were formed due to the existence of specific time-recurrent interaction between: a) regional active thrusting on top of which most crescentic depressions are carved; and b) tectonically induced scouring comprising localized erosion and simultaneous progradational sedimentation, produced by downslope currents of probable turbiditic origin. The thrusts on top which the crescentic depressions are carved are active (mainly blind) thrust faults that root in the GCAW décollement layer to the west of its morphological deformation front. The crescentic depressions are interpreted to correspond to the morphological expression of the westward propagation of the deformation from the realm of the accretionary wedge (GCAW).

Thrust-wrench tectonic interference

1. SWIM-1 vs. Horseshoe Fault

- Detail mapping in the Horseshoe Abyssal Plain revealed the existence of a new morphotectonic pattern near the intersection (corner zone) of the SWIM-1 fault and the Horseshoe fault. Based on combined analog and numerical experiments this pattern was interpreted as resulting from the (thrust-wrench) tectonic interference between two of the main tectonic systems recognized in the Gulf of Cadiz area: the SWIM faults and the NE-SW thrusts.

2. SWIM faults vs. GCAW frontal thrusts

- Detailed morphotectonic analysis showed that there are no apparent crosscutting relationships between the SWIM faults and the GCAW. Physical modeling on the interference between an accretionary wedge and a strike-slip fault showed that the observed morphotectonic pattern of the frontal GCAW area is compatible with:

    i) The development of the GCAW on top of inactive, previously formed, basement faults (Present day SWIM fault system).

    ii) The simultaneously (alternating) activity of the GCAW thrusting with the activity of the SWIM-related dextral strike-slip faults.

- The comparison of the obtained experimental results with the natural example unambiguously excludes the possibility of active strike-slip faulting (SWIM system) affecting an inactive preexistent GCAW, implying that if the SWIM fault system is active then the GCAW must also be presently active.

- Tectonic implications of the experiments on the tectonic interference between the GCAW and the SWIM faults comprise:

    i) The formation of the GCAW on top of preexistent Tethyan rift-related faults (from Middle Miocene to ~1.8 Ma);

    ii) Strike-slip reactivation of these faults (SWIM system) simultaneously with decreasing GCAW activity (~1.8 Ma to Present), as a function of counterclockwise rotation of the Iberia-Nubia convergence direction.

- The analog modeling experiments together with the geological observations favor the interpretation of the SWIM faults as corresponding to the strike-slip reactivation of pre-existent basement normal faults.

- The SWIM fault system is interpreted to correspond to the local reactivation of the old Tethyan plate boundary, instead of the expression of the onset of a new transcurrent plate boundary as argued by Zitellini et al. (2009).

The Gulf of Cadiz tectonic driving mechanisms

- There are at the Present two driving mechanisms operating in the Gulf of Cadiz region:

    i) The local WNW-ESE oblique convergence between Nubia and Iberia;

    ii) The westward overthrusting of the Gibraltar Arc.

- The convergence of Nubia with respect to Iberia generates strain partitioning by means of dextral wrenching on the WNW–ESE striking steep faults (including the SWIM faults) and thrusting on the NE–SW striking thrust faults.

- The westward directed thrusting seems to be propagating from the realm of the Gibraltar Arc to the west (Horseshoe fault) and to the north along the Portuguese margin (Marquês de Pombal fault, Gorringe northern thrust and Tagus Abyssal Plain fault).

Westward Gibraltar subduction propagation or induced subduction initiation at the Southwest Iberia Margin?

- The Gibraltar Arc and the GCAW are part of a subduction system that originated in the Western Mediterranean. The detailed study on the crescentic depressions revealed that the deformation related with the GCAW is still propagating westwards, however at a slower rate than in Miocene, in agreement to what was suggested by Gutscher et al. (2009a). It is speculated that this deceleration is primarily caused by the constraining of the Alboran block between the converging Iberia and Nubia.

- The westward movement of the Gibraltar Arc and the GCAW, together with the Present day WNW-ESE local Nubia-Iberia convergence, may be forcing/inducing the reactivation (in compression) of the Southwest Iberia Margin. This reactivation is materialized by the presence of a set of NE-SW striking major thrust faults (Horseshoe fault, Marquês de Pombal fault, Gorringe northern thrust and Tagus Abyssal Plain fault). The SWIM strike-slip faults may be acting as transfer zones connecting the two main compressive systems (the Gibraltar Arc/GCAW and the Southwest Iberia NE-SW thrusts).

- A scenario in which the Gibraltar Arc subduction and GCAW is decreasing in activity, at the same time that an incipient subduction zone is nucleating in the Southwest Iberia Margin, is favored, in agreement to what was previously proposed by Ribeiro et al. (1996). The Gulf of Cadiz may be thus seen as a place where the proximity of a pre-existent subduction system is "infecting" the Atlantic, in a comparable manner to what happen in the Scotia and in the Lesser Antilles arcs, however in an earlier stage of the process. Contrary to these two arcs, in the Gulf of Cadiz the new potential subduction system seems to be propagating laterally along the adjacent Portuguese Margin.

- Finally, this work supports the speculation that the Gulf of Cadiz (Ribeiro et al., 1996), together with Scotia and the Lesser Antilles arcs (Mueller and Phillips, 1991), may correspond to the precursors of a subduction system that will ultimately lead to the closing of the Atlantic Ocean.

Suggestions for future work

- Perform a systematic MCS and high resolution seismic reflection survey (and subsequent detailed tectonic cartography) in the area where the NE-SW thrusts are located. It would be important to understand if these structures are connected by lateral ramps or if they root in a common structural level. This possibility could also be tested using sand-box analog modeling and numerical modeling.

- Carry out a systematic seismic refraction survey at the scale of the whole Gulf of Cadiz, collecting several orthogonal profiles. This would be important to obtain a good 3D rheological structure of the lithosphere. In particular, it would allow recognizing the nature and limits of the existing types of oceanic lithosphere, such as the Tethyan and the Atlantic (both Nubian and Iberian).

- Test the Gulf of Cadiz tectonic evolution models using 3D numerical modeling with the main objective of quantifying the contribution of each driving mechanisms acting in the Gulf of Cadiz to the observed deformation pattern.

- Finally, collect cores and obtain a good coverage of high resolution seismic profiles in the area where the crescentic depressions are located. A more detailed study would allow a better understanding of the processes that lead to the formation of these features. Also, if the crescentic depressions are controlled by tectonic activity, a detailed tectono-stratigraphic study of the existing buried features could provide constrains in the timing of recent tectonic events.

References

Abe, K., 1979. Size of Great Earthquakes of 1837-1974 inferred from Tsunami Data. Journal of Geophysical Research, 84 (NB4), 1561-1568.

Alexander, J., 2008. Bedforms in Froude-supercritical flow. Marine and River Dune Dynamics Proceedings, April 2008. Leeds, U.K.

Ambar, I., Howe, M. R., 1979a. Observations of the Mediterranean outflow-I. Mixing in the Mediterranean Outflow. Deep-Sea Res. 26A, 555–568.

Ambar, I., Howe, M. R., 1979b. Observations of the Mediterranean outflow-II. The deep circulation in the vicinity of the Gulf of Cadiz. Deep-Sea Res. 26A, 555–568.

Anderson, D.L., 2001. Plate tectonics as a far-from-equilibrium self-organized system, in: S. Stein, J.T. Freymueller (Eds.), Plate Boundary Zones, vol. 30, American Geophysical Union, Washington DC, 411– 425.

Argus, D.F., Gordon, R.G., DeMets, C., Stein, S., 1989. Closure of the Africa-Eurasia-North America plate motion circuit and tectonics of the Gloria Fault. J. Geophys. Res. B, Solid Earth and Planets 24, 5585–5602. doi:10.1016/j.marpetgeo.2007.11.008.

Banda, E., Torné, M., IAM group, 1995. IAM group investigates deep structure of ocean margins: EOS (transaction of Am. Gephys. Union) 76, 25–29.

Baptista, M.A., Heitor, S., Miranda, J.M., Miranda, P.M.A., Mendes Victor, L., 1998. The 1755 Lisbon tsunami; evaluation of the tsunami parameters. J. Geodyn. 25 (1–2), 143–157.

Baptista, M.A., Miranda, J.M., Chierici, F., Zitellini, N., 2003. New study of the 1755 earthquake source based on multi-channel seismic survey data and tsunami modeling. Natural Hazards and Earth System Sciences 3, 333–340.

Bijwaard, H., and Spakman, W., 2000. Non-linear global P-wave tomography by iterated linearized inversion. Geophysical Journal International 141, 71–82.

Bonnel, C., Dennielou, B., Droz, L., Mulder, T., Berné, S., 2005. Architecture and depositional pattern of the Rhône Neofan and recent gravity activity in the Gulf of Lions (western Mediterranean). Marine and Petroleum Geology 22, 827–843

Bott, M.P. and Kusznir, N.J., 1984. Origins of tectonic stress in the lithosphere. Tectonophysics 105, 1-14.

Buforn, E., Udias, A., Colombas, M.A., 1988. Seismicity, source mechanisms and tectonics of the Azores–Gibraltar plate boundary. Tectonophysics 152 (1–2), 89–118.

Bulat J. and Long D., 2001. Images of the seabed in the Faroe-Shetland Channel from commercial 3D seismic data. Marine Geophysical Researches 22**,** 345–367.

Calais, E., DeMets, C., Nocquet J.-M., 2003. Evidence for a post-3.16-Ma change in Nubia-Eurasia-North America plate motions? Earth and Planetary Science Letters 216, 81-92.

Casas, A.M., Gapais, D., Nalpas, T., Besnard, K., Román-Berdiel, K., 2001. Analogue models of transpressive systems. Journal of Structural Geology. 23, 733–743.

Casey, J.F. and Dewey, J.F., 1984. Initiation of subduction zones along transforms and accreting plate boundaries, triple junction evolution, and forearc spreading centers: Implications for ophiolitic geology and obduction. In Ophiolites and Oceanic Lithosphere. Edited by I. G. Gass, S. J. Lippard, and A. W. Shelton, Geological Society Special Publication 13, 269–290.

Cloetingh, S.A.P.L., Wortel, M.J.R. and Vlaar, N.J., 1982. Evolution of passive continental margins and initiation of subduction zones. Nature 297, 139–142. doi:10.1038/297139a0.

Cloetingh, S.A.P.L., Wortel, M.J.R. and Vlaar, N.J., 1984. Passive margin evolution, initiation of subduction and the Wilson cycle. Tectonophysics 109, 147–163. doi:10.1016/0040-1951(84)90175-6.

Cloetingh, S., Wortel, R. and Vlaar, N.J. 1989. On the initiation of subduction zones. Pure and Applied Geophysics 129, 7 – 25.

Conrad, C.P. and Lithgow-Bertelloni, C., 2002. How mantle slabs drive plate tectonics, Science 298 (5591), 207– 209.

Cunha, T.A., Watts, A.B., Pinheiro, L.M., Myklebust, R., 2010. Seismic and gravity anomaly evidence of large-scale compressional deformation off SW Portugal. Earth Planetary Science Letters 293, 171-179. doi:10.1016/j.epsl.2010.01.047

Davis, D., Suppe, J., Dahlen, F.A., 1983. Mechanics of fold and thrust belts and accretionary wedges. Journal of Geophysical Research 88, 1153–1172.

Davies, G.F., 1992. On the emergence of plate tectonics, Geology 20, 963– 966.

Davies, G.F. and Richards, M.A., 1992. Mantle convection. Journal of Geology 100, 151– 206.

Davies, G. F. 1999. Dynamic Earth Plates, Plumes and Mantle Convection. New York: Cambridge University Press, 458 pp.

Dercourt, J., Zonenshain, L.P., Ricou, L.E., Zazmin, V.G., Le Pichon, X., Knipper, A.L., Grandjacquet, C., Shotshickov, I.M., Geyssant, J., Lepvrier, C., Perchersky, D.H., Boulin, J., Sibuet, J.C., Savostin, L.A., Sorokthin, O., Westphal, M., Bazhenov, M.L., Lauer, J.P., Biju Duval, B., 1986. Geological evolution of the Tethys belt from the Atlantic to the Pamirs since the Lias. Tectonophysics 123, 265–283.

DeMets, C., Gordon, R.G., Argus, D.F., Stein, S., 1994. Effect of recent revisions to the geomagnetic reversal time scale on estimates of current plate motions. Geophysical Research Letters 21 (5), 2191–2194.

Deuser, W.G., 1970. Hypothesis of the formation of the Scotia and Caribbean seas. Tectonophysics 10, 391-401.

Dewey, J.F., 1969. Continental margins: A model for conversion of Atlantic type to Andean type. Earth Planetary Science Letters 6, 189–197. doi:10.1016/0012-821X(69)90089-2.

Dewey, J.F., Helman, M.L., Turco, E., Hutton, D.H., Knott, S.D., 1989. Kinematics of the Western Mediterranean. In: Coward, M.P., Dietrich, D.,Park, R.G (eds), Alpine Tectonics, Geological Society Special Publication 45, 265-283.

Dickinson, W.R. and Seely, D.R., 1979. Structure and stratigraphy of fore-arc regions. American Association of Petroleum Geologists Bulletin 63, 2–31.

Dimitrov, L. and Woodside, J., 2003. Deep sea pockmark environments in the eastern Mediterranean. Marine Geology 195, 263-276.

Doin, M.-P. and Henry, P., 2001. Subduction initiation and continental crust recycling: The roles of rheology and eclogitization. Tectonophysics 342, 163–191. doi:10.1016/S0040-1951(01)00161-5.

Duarte, J.C., Rosas, F., Pinheiro, L.M., Matias, L.M., Carvalho, A.M., Terrinha, P., Ivanov, M., 2005. Interpretation of recent sedimentary and tectonic structures off SW Iberia from multibeam bathymetry, seismic reflection and experimental modelling. in: Geophysical Research Abstracts, vol. 7, 07867. European Geosciences Union 2005.

Duarte, J.C., 2007. Morfoestruturas quilométricas em forma de crescente nas águas profundas do Golfo de Cádis, MSc thesis, 118pp., Univ. Évora, Évora, Portugal.

Duarte, J.C., Valadares, V., Terrinha, P., Rosas, F., Zitellini, N., Gràcia, E., 2009. Anatomy and tectonic significance of WNW-ESE and NE-SW lineaments at a transpressive plate boundary (Nubia-Iberia). Trabajos de Geología 29, 237-241.

Duarte, J.C., Terrinha, P., Rosas, F.M., Valadares, V., Pinheiro, L.M., Matias, L., Magalhães, V., Roque, C., 2010. Crescent-shaped morphotectonic features in the Gulf of Cadiz (offshore SW Iberia). Marine Geology 271, 236–249.

Duarte, J.C, Rosas, F.M., Terrinha, P., Gutscher, M-A., Malavieille, J., Silva, S., Matias, L., Submitted to Marine Geology. Thrust - wrench interference tectonics in the Gulf of Cadiz (Africa - Iberia plate boundary in the North-East Atlantic): insights from analog models.

Elder, J., 1976. The Bowels of the Earth. Oxford, 222 pp.

Elsasser, W.M., 1967. Convection and stress propagation in the upper mantle. In Runcorn, S.K. (ed.), The Application of Modern Physics to the Earth and Planetary Interiors, Wiley Interscience, London, 223-246.

Elsasser, W.M., 1971. Sea floor spreading as thermal convection. Journal of Geophysical Research 76, 1101-1112.

Engdahl, E.R., van der Hilst, R.D., and Buland, R., 1998. Global teleseismic earthquake relocation with improved travel times and procedures for depth relocation: Seismological Society of America Bulletin 88, 722–743.

Erickson, S.G., 1993. Sedimentary loading, lithospheric flexure, and subduction initiation at passive margins. Geology 21, 125–128. doi:10.1130/0091 7613(1993)021<0125:SLLFAS>2.3.CO;2.

Fadil, A., Vernant, P.,McClusky, S., Reilinger, R., Gomez, F., Ben Sari, D.,Mourabit, T., Feigl, K., Barazangi, M., 2006. Active tectonics of the western Mediterranean: evidence for rollback of a delaminated subcontinental lithospheric slab beneath the Rif Mountains Morocco. Geology 34, 529–532.

Faugères J.C, Gonthier È., Bobier C., Griboulard R., 1997. Tectonic control on sedimentary processes in the southern termination of the Barbados Prism. Marine Geology 140, 117-140.

Faugères, J.C., Stow, D.A.V., Imbert, P., Viana, A., 1999. Seismic features diagnostic of contourite drifts. Marine Geology, 162, 1-38.

Fernandes, R.M.S., Ambrosius, B.A.C., Noomen, R., Bastos, L.,Wortel, M.J.R., Spakman,W., Govers, R., 2003. The relative motion between Africa and Eurasia as derived from ITRF 2000 and GPS data. Geophysical Research Letters 30 (16), 1828.

Fernandes, R.M.S, 2004. Present-day kinematics at the Azores-Gibraltar plate boundary as derived from GPS observations. Delft University Press, The Netherlands.

Fernandes, R.M.S, J.M. Miranda, R.M.L. Meijninger, M.S. Bos, R. Noomen, L. Bastos,B.A.C. Ambrosius and R.E.M. Riva, 2007. Surface velocity field of the IberoMaghrebian segment of the Eurasia–Nubia plate boundary, Geophysical Journal International 169, 315–324.

Fildani, A., Normark, W.R., Kostic, S., Parker, G., 2006. Channel formation by flow stripping: large-scale scour features along the Monterey East Channel and their relation to sediment waves. Sedimentology 53, 1265–1287.

Forsyth, D. and Uyeda, S., 1975. On the relative importance of the driving forces of plate motions. Geophysical Journal of the Royal Astronomical Society 43, 163– 200.

Fukao, Y., 1973. Thrust faulting at a lithospheric plate boundary, The Portugal earthquake of 1969. Earth and Planetary Science Letters 18: 205-216.

Fyfe, W.S. and Leonardos, O.H., 1977. Speculations on causes of crustal rifting and subduction, with applications to the Atlantic margin of Brazil. Tectonophysics 42, 29–36. doi:10.1016/0040-1951(77)90015-4.

García, M., Hernández-Molina, F.J., Llave, E., Stow, D.A.V., León, R., Fernández-Puga, M.C., Díaz del Río, V., Somoza, L., 2009, Contourite erosive features caused by the Mediterranean Outflow Water in the Gulf of Cadiz: Quaternary tectonic and oceanographic implications. Marine Geology 257, 24-40.

Gebco, 2003. GEBCO Digital Atlas, British Oceanographic Data Centre on behalf of IOC and IHO.

Gonzalez, A., et al., 1996. Crustal thinning in the southwestern Iberia margin. Geophys. Res. Lett. 23 (18), 2477–2480.

Gràcia, E., Danobeitia, J., Verges, J., Bartolome, R., 2003a. Crustal architecture and tectonic evolution of the Gulf of Cadiz, SW Iberia, at the convergence of the Eurasian and African plates. Tectonics 22 (4), 1033.

Gràcia, E., Danobeitia, J., Vergés, J., Cordoba, D., PARSIFAL Team, 2003b. Mapping active faults offshore Portugal (36 degrees N–38 degrees N); implications for seismic hazard assessment along the Southwest Iberian margin. Geology (Boulder) 31 (1), 83–86.

Gibbs, A.D., 1984. Structural evolution of extensional basin margins. Journal of the Geological Society of London 141, 609-620.

Girardeau, J., G. Cornen, M.O. Beslier, B. Le Gall, C. Monnier, P. Agrinier, G. Dubuisson, L. Pinheiro, A. Ribeiro, and H. Whitechurch (1998), Extensional tectonics in the Gorringe Bank rocks, eastern Atlantic ocean: Evidence of an oceanic ultra-slow mantellic accreting centre, Terra Nova, 10, 330–336.

Goren, L., Aharonov, E., Mulugeta, G., Koyi, H.A., Mart, Y., 2008. Ductile deformation of passive margins: A new mechanism for subduction initiation, J. Geophys. Res., 113, B08411, doi:10.1029/2005JB004179.

Gurnis, M., Hall, C., and Lavier, L., 2004. Evolving force balance during incipient subduction. Geochemistry, Geophysics, Geosystems (G^3) 5, Q07001. doi:10.1029/2003GC000681.

Gutscher, M.A., Kukowski, N., Malavieille, J., Lallemand, S., 1998a. Episodic imbricate thrusting and underthrusting: analog experiments and mechanical analysis

applied to the Alaskan accretionary wedge. Journal of Geophysical Research 103, 10161–10176.

Gutscher, M.A., Kukowski, N., Malavieille, J., Lallemand, S., 1998b. Material transfer in accretionary wedges from analysis of a systematic series of analog experiments. Journal of Structural Geology 20, 407–416.

Gutscher, M.-A., Malod, J., Rehault, J.-P., Contrucci, I., Klingelhoefer, F., Spakman, W., Mendes-Victor, L., 2002. Evidence for active subduction beneath Gibraltar. Geology 30 (12), 1071–1074.

Gutscher, M-A., 2004. What caused the Great Lisbon earthquake? Science 305, 1247–1248.

Gutscher, M-A, 2006. The great Lisbon earthquake and tsunami of 1755: lessons from the recent Sumatra earthquakes and possible link to Plato's Atlantis. European Review 14, Issue 2, 181-191.

Gutscher, M-A., Dominguez, S., Westbrook, G.K., Leroy, P., 2009a. Deep structure, recent deformation and analog modeling of the Gulf of Cadiz accretionary wedge: Implications for the 1755 Lisbon earthquake. Tectonophysics 475, 85–97.

Gutscher, M-A., Dominguez, S., Westbrook, G.K., Gente, P., Babonneau, N., Mulder, T., Gonthier, E., Bartolome, R., Luis, J., Rosas, F., Pedro T., and the Delila and DelSis Scientific Teams, 2009b. Tectonic shortening and gravitational spreading in the Gulf of Cadiz accretionary wedge: observations from multi-beam bathymetry and seismic profiling. Marine and Petroleum Geology 26, 647-659.

Hager, B.H. and O'Connell, R.J., 1981. A simple global model of plate dynamics and mantle convection. Journal of Geophysical Research 86, 4843-4867.

Hall, C.E., Gurnis, M., Sdrolias, M., Lavier, L.L., Muellar, R.D., 2003. Catastrophic initiation of subduction following forced convergence across fracture zones. Earth and Planetary Science Letters 212, 15–30.

Hamilton, W., 2003. An alternative earth. GSA Today 13 (11), 4– 12.

Hanquiez, V., Mulder, T., Lecroat, P., Gonthier, E., Marchès, E., Voisset, M., 2007. High resolution seafloor images in the Gulf of Cadiz, Iberian Margin. Marine Geology 246, 42-59.

Hansen, V.L., 2007. Subduction origin on early Earth: A hypothesis. Geology 35; 1059-1061. doi:10.1130/G24202A.1

Hayward, N., Watts, A.B., Westbrook, G.K., Collier, J.S., 1999. A seismic reflection and GLORIA study of compressional deformation in the Gorringe Bank region, eastern North Atlantic. Geophysical Journal International 138, 831–850.

Heinio, P., and Davies, R.J., 2009, Trails of depressions and sediment waves along submarine channels on the continental margin of Espirito Santo Basin, Brazil, GSA Bulletin 121, 698-711.

Hensen, C., Nuzzo, M., Hornibrook, E., Pinheiro, L.M., Bock, B.,Magalhaes, V.H., Bruckmann, W., 2007. Sources of mud volcano fluids in the Gulf of Cadiz — indications for hydrothermally alteres fluids. Geochim. Cosmochim. Acta 71, 1232–1248.

Hernández-Molina, F.J., Llave, E., Stow, D.A.V., García, M., Somoza, L., Vázquez, J.T., Lobo, F.J., Maestro, A., Díaz del Río, V., León, R. Medialdea, T., Gardner, J., 2006. The contourite depositional system of the Gulf of Cádiz: A sedimentary model related to the bottom current activity of the Mediterranean outflow water and its interaction with the continental margin. Deep-Sea Research II 53, 1420–1463.

Hernández-Molina, F. J., Maldonado, A., Stow, D.A.V. 2008. Abyssal Plain contourites. In: Contourites, Rebesco, M. & Camerlenghi, A. (Eds.). Elsevier, Developments in Sedimentology 60, 347-377.

Hilde, T.W.C., Uyeda, S. and Kroenke, L., 1977. Evolution of the western Pacific and its margin, Tectonophysics, 38, 145–165, doi:10.1016/0040- 1951(77)90205-0.

Holmes, A., 1929. Radioactivity and earth movements. Transactions of the Geological Society of Glasgow 18, 559-606.

Hovland, M. and Judd, A.G., 1988. Seabed Pockmarks and Seepages. Impact on Geology, Biology and the Marine Environment. Graham and Trotman Inc., Norwell, USA, 302 p.

Hubbert, M.K., 1937. Theory of scale models as applied to the study of geologic structures. Geological Society of America Bulletin, 48, 1459-1520.

Hubbert, M.K., 1951. Mechanical basis for certain familiar geologic structures. Geological Society of America Bulletin 62, 355– 372.

Iribarren, L., Vergés, J., Camurri, F., Fullea, J., Fernàndez, M., 2007. The structure of the Atlantic–Mediterranean transition zone from the Alboran Sea to the Horseshoe Abyssal Plain (Iberia–Africa plate boundary). Marine Geology 243, 97–119.

Isacks, B., Oliver, J., Sykes, L.R., 1968. Seismology and the new global tectonics. Journal of Geophysical Research 73, 5855-5899.

Jiménez-Munt I., Fernàndez, M. Vergés, J., Afonso, J.C., Garcia-Castellanos, D., Fullea, J., 2010, The lithospheric structure of the Gorringe Bank: insights into its origin and tectonic evolution, Tectonics, 29, TC5019, doi:10.1029/2009TC002458.

Johnson, I., Ambar, I., Serra, N., Stevens, I., 2002. Comparative studies of the spreading of Mediterranean water through the Gulf of Cadiz. Deep-Sea Research II 49, 4179–4193.

Johnston, A., 1996. Seismic moment assessment of earthquakes in stable continental regions: III. New Madrid, 1811–1812, Charleston 1886 and Lisbon 1755. Geophysical Journal International 126, 314–344.

Jolivet, L., Augier, R., Robin, C., Suc, J-P., Rouchy, J.M., 2006. Lithospheric-scale geodynamic context of the Messinian salinity crisis. Sedimentary Geology 188-189, 9-33.

Karig, D.E., 1982. Initiation of subduction zones: Implications for arc evolution and ophiolite development. Geological Society Special Publication 10, 563– 576. doi:10.1144/GSL.SP.1982.010.01.37.

Karson, J. and Dewey, J.F., 1978. Coastal Complex, western Newfoundland: An early Ordovician oceanic fracture zone. Geological Society American Bulletin 89, 1037–1049. doi:10.1130/0016-7606(1978)89<1037:CCWNAE>2.0.CO;2.

Kemp, D.V. and Stevenson, D.J., 1996. A tensile, flexural model for the initiation of subduction. Geophysical Journal International 125, 73–94. doi:10.1111/j.1365-246X.1996.tb06535.x.

Kenyon, N.H.; Ivanov, M.K.; Akhmetzhanov, A.M.; Kozlova, E.V., 2006. Interdisciplinary geoscience studies of the Gulf of Cadiz and Western Mediterraneanbasins: preliminary results of investigations during the TTR-14 cruise of RV Professor Logachev, July-September, 2004, IOC. Technical series; 70

Kontinen, A., 1987. An early Proterozoic ophiolite: the Jormua mafic–ultramafic complex, northeastern Finland, Precambrian Research 35, 313– 341.

Koyama, T. and Ikeda, H. (1998) Effect of riverbed gradient on bedrock channel configuration: a flume experiment. Proceedings of the Environmental Research Center, Tsukuba University, Japan, 23, 25–34.

Kusky, T.M., Li, J.H., Tucker, R.T., 2001. The Dongwanzi Ophiolite: complete Archean ophiolite with extensive sheeted dike complex, North China craton, Science 292, 1142–1145.

Lamb, M.P., Parsons, J.D., Mullenbach, B.L., Finlayson, D.P., Orange, D.L., Nittrouer, C.A., 2008. Evidence for superelevation, channel incision, and formation of cyclic steps by turbidity currents in Eel Canyon, California. GSA Bulletin120, 463-475.

Le Guerroue, E. and Cobbold, P.R., 2006. Influence of erosion and sedimentation on strike-slip fault systems: insights from analogue models. Journal of Structural Geology, 28(3): 421-430.

León, R., Somoza. L., Medialdea T., Maestro A., Díaz-del-Río V., Fernández-Puga M.C., 2006. Classification of sea-floor features associated with methane seeps along the Gulf of Cádiz continental margin. Deep-sea Research Part II 53, 1464-1481.

Lithgow-Bertelloni, C. and Richards, M.A., 1995. Cenozoic plate driving forces. Geophysical Research Letters 22, 1317– 1320.

Liu, H., McClay, K.R., Powell, D., 1992. Physical models of thrust wedges. In: McClay, K.R. (Ed.), Thrust Tectonics. Chapman & Hall, London, pp. 71– 82.

Llave, E., Schonfeld, J., Hernández-Molina, F.J., Mulder, T., Somoza, L., Díaz del Río, V., Sánchez-Almazo, I., 2006. High-resolution stratigraphy of the Mediterranean outflow contourite system in the Gulf of Cadiz during the late Pleistocene: The impact of Heinrich events. Marine Geology 227, 241– 262.

Llave, E., Hernández-Molina, F. J., Somoza, L., Díaz-del-Río, V., Stow, D. A. V., Maestro, A., Alveirinho Dias J. M., 2001. Seismic stacking pattern of the Faro-Albufeira contourite system (Gulf of Cadiz): a Quaternary record of paleoceanographic and tectonic influences. Marine Geophysical Researches 22, 487–508

Lonergan, L., and White, N., 1997. Origin of the Betic-Rif mountain belt: Tectonics, v. 16, 504–522.

Malavieille, J., 1984, Modélisation expérimentale des chevauchements imbriqués: application aux chaînes de montagnes : Bulletin de la Société Géologique de France, v. 26, p. 129-138.

Malavieille, J., Calassou, S., Larroque, C., Lallemand, S. and Stephan, J. -F., 1991. Modelisation analogique des prismes d'accrétion océaniques: Montage d'animation vidéo de 27', Serie Cours M037, Formation exploration, Elf SNEAP.

Malavieille, J., 2010. Impact of erosion, sedimentation and structural heritage on the structure and kinematics of orogenic wedges: analog models and case studies. Geological Society of America, account *GSA Today*, v. 20, no. 1, doi: 10.1130/GSATG48A.1

Maldonado, A., Somoza, L., Pallares, L., 1999. The Betic orogen and the Iberian-African boundary in the Gulf of Cadiz: geological evolution (central North Atlantic). Marine Geology 155,(1-2), 9-43.

Malinverno, A. and Ryan, W.B.F., 1986. Extension in the Tyrrhenian Sea and shortening in the Apennines as a result of arc migration driven by sinking of the lithosphere. Tectonics 5, 227-243.

Mandl, G., L.N.J. de Jong, and A. Maltha, 1977. Shear zones in granular material; an experimental study of their structure and mechanical genesis, Rock Mechanics, 9, 95-144.

Marques, F.O., Cobbold, P.R., 2002. Topography as a major factor in the development of arcuate thrust belts: insights from sandbox experiments. Tectonophysics 348, 247–268.

Mart, Y., Aharonov, E., Mulugeta, G., Ryan, W., Tentler, T., Goren, L., 2005. Analogue modelling of the initiation of subduction. Geophysical Journal International 160, 1081–1091. doi:10.1111/j.1365-246X.2005.02544.x.

Martel, S.J., 2004. Mechanics of landslide initiation as a shear fracture phenomenon. Marine Geology 203, 319-339

Martinez-Loriente, S., Gràcia, E., Bartolomé, R., Sallarès, V., Dañobeitia, J.J., And Swim-06 Cruise Party (2008). Pre-stack depth migration seismic imaging of the Coral

Patch Ridge and adjacent Horseshoe and Seine Abyssal Plains (Gulf of Cadiz): Tectonic implications. Trabajos de Geología, 30, 49-54.

Martinez-Solares, J.M., López Arroyo, A., 2004. The great historical 1755 earthquake: effects and damage in Spain. J. Seismol. 8, 275–294.

Martinez-Solares, J.M., López Arroyo, A., 2004. The great historical 1755 earthquake: effects and damage in Spain. J. Seismol. 8, 275–294.

Masson, D.G., Cartwright, J.A., Pinheiro, L.M., Whitmarsh, R.B., Beslier, M.-O., Roeser, H.A., 1994. Compressional deformation at the ocean–continent transition in the NE Atlantic. Journal of the Geological Society 151, issue.4, 607-613.

McAdoo, B.G., Pratson, L.F., Orange, D.L., 2000. Submarine landslide geomorphology, US continental slope. Marine Geology 169, 103–136.

McKenzie, D.P., 1969. Speculations on the consequences and causes of plate motion. Geophysical Journal of the Royal Astronomical Society 18, 1-32.

McKenzie, D.P., 1977. The initiation of trenches: A finite amplitude instability. In Island Arcs, Deep Sea Trenches, and Back-Arc Basins. Maurice Ewing Ser., vol. 1, edited by M. Talwani and W. C. Pitma III, pp. 57–61, AGU, Washington, D. C.

Medialdea, T., Vegas, R., Somoza, L., Vázquez, J.T., Maldonado, A., Díaz-del-Río, V., Maestro, A., Córdoba, D., Fernández-Puga, M.C., 2004. Structure and evolution of the ‘‘Olistostrome'' complex of the Gibraltar Arc in the Gulf of Cádiz (eastern Central Atlantic): evidence from two long seismic cross-sections. Mar. Geol 209, 173–198.

Michard, A., Chalouan, A., Feinberg, H., Goffé, B., Montigny, R., 2002. How does the Alpine belt end between Spain and Moroco?. *Bull. Soc. Geol. Fr.*, 173 (1), p. 3-15.

Mitchell, A.H.G., 1984. Initiation of subduction of post-collision foreland thrusting and back-thrusting. Journal of Geodynamics 1, 103–120. doi:10.1016/0264-3707(84)900231.

Morel., J.L., Megrhraoui, M., 1996. Gorringe-Alboran-Tell tectonic zone: A transpressive system along the Africa-Eurasia plate boundary. Geology, 24, (8), 755-758.

Mulder, T., Voisset, M., Lecroart, P., Le Drezen, E., Gonthier, E., the Cadisar Shipboard Party, 2003. The Gulf of Cadiz: an unstable giant contouritic levee. Geo-Marine letters 23, 7–18.

Mulder, T., Voisset, M., Lecroart, P., Le Drezen, E., Gonthier, E., et l'equipe embarqué e Cadisar 2, 2006. The western part Gulf of Cádiz: interaction between contour and turbidity currents. Geo-Marine Letters 26, 31–41.

Muller, S. & Phillips, R.J., 1991. On the Initiation of Subduction. Journal of Geophysical Research 96, 651-665.

Muller, R.D., Sdrolias, M.C., Gaina, C., Roest, W.R., 2008. Age, spreading rates and spreading symmetry of the world's ocean crust, Geochemistry, Geophysics, Geosystems (G^3) 9, Q04006, doi:10.1029/2007GC001743.

Mulugeta, G., 1988. Modelling the geometry of Coulomb thrust wedges. Journal of Structural Geology 10, 847–859.

Nikolaeva, K., Gerya, T.V., Marques, F.O., 2010. Subduction initiation at passive margins: Numerical modeling. Journal of Geophysical Research 115, B03406, doi:10.1029/2009JB006549.

Niu, Y., O'Hara, M.J. and Pearce, J.A., 2003. Initiation of subduction zones as a consequence of lateral compositional buoyancy contrast within the lithosphere: A petrological perspective. Journal of Petrology 44(5), 851–866. doi:10.1093/petrology/44.5.851.

Nocquet, J.M., Calais, E., 2004. Geodetic measurements of crustal deformation in the western Mediterranean and Europe. Pure Appl. Geophys. 161 (3), 661–681.

Normark, W.R.; Paull, C.K.; Caress, D.W.; Ussler, W.III.; Sliter, R., 2009. Fine-scale relief related to Late Holocene channel shifting within the floor of the upper Redondo Fan, offshore Southern California. Sedimentology 56, 1690–1704.

Oxburgh, E.R. and Parmentier, E.M., 1977. Compositional and density stratification in oceanic lithosphere—causes and consequences. Journal of the Geological Society (London) 133, 343– 355.

Park, R.G., 1988. Geological Structures and Moving Plates. 337pp. Glasgow, London: Blackie; New York: Chapman and Hall.

Parker, G. & Izumi, N. 2000. Purely erosional cyclic and solitary steps created by flow over a cohesive bed. Journal of Fluid Mechanics 419, 203–238.

Pascal, C. and Cloetingh, S.A.P.L., 2009. Gravitational potential stresses and stress field of passive continental margins: Insights from the south-Norway shelf. Earth and Planetary Science Letters 277, 464–473. doi:10.1016/j.epsl.2008.11.014.

Pinheiro, L., Ivanov, M.K., Sautkin, A., Akhmanov, G., Magalhães, V., Volkonskaya, A., Monteiro, J.H., Somoza, L., Gardner, J., Hamouni, N., Cunha, M.R., 2003. Mud volcanism in the Gulf of Cadiz: results from the TTR-10 cruise. Marine Geology 195, 131–151.

Purdy, G.M., 1975. The eastern end of the Azores–Gibraltar plate boundary. Geophys. J. R. Astr. Soc., 43, 973–1000.

Ramberg, H., 1967. Gravity, deformation and the Earth's Crust, as studied by centrifugal models. Academic Press Inc., London and New York, second edition 1981, 452 pp.

Rannali, G., 2001. Experimental tectonics: from Sir James Hall to the present. Journal of Geodynamics 32, 65–76.

Rebesco, M., Stow, D., 2001. Seismic expression of contourites and related deposits: a preface. Marine Geophysical Researches 22, 303-308.

Regenauer-Lieb, K., Yuen, D.A. and Branlund, J., 2001. The initiation of subduction: Critically by addition of water? Science, 294, 578–580. doi:10.1126/science.1063891.

Rehault, J.-P., Boillot, G., and Mauffret, A., 1985. The western Mediterranean Basin, *in* Stanley, D.J., and Wezel, F.C., eds., Geological evolution of the Mediterranean Basin: Berlin, Springer, 101–129.

Ribeiro, A., Cabral, J., Baptista, R., Matias, L., 1996. Stress pattern in Portugal mainland and the adjacent Atlantic region, West Iberia. Tectonophysics 15 (2), 641–659.

Ribeiro, A., Mendes-Victor, L., Cabral, J., Matias, L., Terrinha, P., 2006. The 1755 Lisbon earthquake and the beginning of closure of the Atlantic. European Review 14, Issue 2, 193-205.

Roque, C., 2007. Tectonostratigrafia do Cenozóico das margens continentais Sul e Sudoeste Portuguesas: um modelo de correlação sismostratigráfica. Universidade de Lisboa. Departamento de Geologia.

Rosas, F.M., Duarte, J.C., Terrinha, P., Valadares, V., Matias, L., 2009. Morphotectonic characterization of major bathymetric lineaments in NW Gulf of Cadiz (Africa-Iberia plate boundary): insights from analogue modelling experiments. Marine Geology 261, 33–47.

Rosas, F.M., Duarte, J.C., Neves, M.C., Terrinha, P., Silva, S., Matias, L., Submitted. Thrust-wrench interference between major active faults in the Gulf of Cadiz (Africa-Eurasia plate boundary, offshore SW Iberia): tectonic implications from analogue and numerical modeling.

Rosenbaum, G., Lister G.S., Duboz C., 2002a. Relative motions of Africa, Iberia and Europe during Alpine orogeny. Tectonophysics 359, 117-129.

Rosenbaum G., Lister G.S., Duboz C., 2002b. Reconstruction of the tectonic evolution of the western Mediterranean since the Oligocene. In: Rosenbaum G. and Lister G.S. (2002) - Reconstruction of the evolution of the Alpine-Himalayan Orogen. Journal of the Virtual Explorer 8, 107-126.

Rosenbaum, G., and Lister, G.S., 2004. Formation of arcuate orogenic belts in the western Mediterranean region, *in* Sussman, A.J., and Weil, A.B., eds., Orogenic curvature: Integrating paleomagnetic and structural analyses: Boulder, Colorado, Geological Society of America Special Paper 383, 41–56.

Rovere, M., Ranero, C.R., Sartori, R., Torelli, L., Zitellini, N., 2004. Seismic images and magnetic signature of the Late Jurassic to Early Cretaceous Africa–Eurasia plate boundary off SW Iberia. Geophysical Journal International 158 (2), 554–568.

Royden, L.H., 1993. Evolution of retreating subduction boundaries formed during continental collision. Tectonics 12, 629–638.

Sallarès, V., Gailler, A., Gutscher, M-A., Bartolomé, R., Díaz, J., Gràcia, E., Graindorge, D., 2011. Seismic evidence for the presence of Jurassic oceanic crust in the Gulf of Cádiz (SW Iberia). Geophysical Research Abstracts, Vol. 13, EGU2011-3274-1.

Sanz de Galdeano, C. and Vera, J.A., 1999. Stratigraphic record and palaeogeographic context of Neogene basins in the Betic Cordillera, Spain. Basin Research 4, 21–36.

Sartori, R., Torelli, L., Zitellini, N., Peis, D., Lodolo, E., 1994. Eastern segment of the Azores–Gibraltar line (central-eastern Atlantic): an oceanic plate boundary with diffuse compressional deformation. Geology 22, 555–558.

Schellart, W.P., and Lister, G.S., 2004. Tectonic models for the formation of arc-shaped convergent zones and backarc basins, *in* Sussman, A.J., and Weil, A.B., eds., Orogenic

Curvature: Integrating Paleomagnetic and Structural Analyses: Geological Society of America Special Paper 383, 237–258.

Schroot, B.M. and Schfittenhelm R.T.E., 2003. Shallow gas and gas seepage: expressions on seismic and other acoustic data from the Netherlands North Sea. Journal of Geochemical Exploration 78-79, 305 – 309.

Scott, D.J., Helmstaedt, H., Bickle, M.J., 1992. Purtuniq Ophiolite, Cape Smith Belt, northern Quebec, Canada: a reconstructed section of early Proterozoic oceanic crust, Geology 20, 173–176.

Sella, G.F., Dixon, T.H., Mao, A., 2002. REVEL; a model for recent plate velocities from space geodesy. Jounal of Geophysical Research 107 (B4), 17.

Silva, S., Matias, L., Romsdorf, M., Geissler, W., Terrinha, P., Nearest working group, 2010. Instrumental seismicity in the Gulf of Cadiz: Results from the NEAREST Project acquisition campaign. e –Terra 10, 6.

Sleep, N.L., 2000. Evolution of the mode of convection within terrestrial planets. Journal of Geophysical Research 105 (E7), 17563– 17578.

Solomatov, V.S., 2004. Initiation of subduction by small-scale convection. Journal of Geophysical Research 109, B05408. doi:10.1029/2004JB003143.

Somoza, L., Díaz-del-Río, V., León, R., Ivanov, M., Fernandez-Puga, M.C., Gardner, J.M., Hernández-Molina, F.J., Pinheiro, L.M., Rodero, J., Lobato, A., Maestro, A., Vázquez, J.T., Medialdea, T., Fernández-Salas, L.M., 2003. Seabed morphology and hydrocarbon seepage in the Gulf of Cádiz mud volcano area: Acoustic imagery, multibeam and ultra-high resolution seismic data. Marine Geology 195, 153-176.

Spakman, W. and R. Wortel, 2004. A tomographic view on Western Mediterranean Geodynamics, in: The TRANSMED Atlas, The Mediterranean Region from Crust to Mantle, Edited by: Cavazza W, Roure F, Spakman W., Stampfli GM, Ziegler P., 31 52.

Srivastava, S.P., Roest, W.R., Kovacs, L.C., Oakey, G., Lévesque, S., Verhoef, J., Macnab, R. 1990a. Motion of Iberia since the Late Jurassic: results from detailed aeromagnetic measurements in the Newfoundland Basin. Tectonophysics 184, 229–260.

Srivastava, S.P., Schouten, H., Roest, W.R., Klitgord, K.D., Kovacs, L.C., Verhoef, J., Macnab, R., 1990b. Iberian plate kinematics: a jumping plate boundary between Eurasia and Africa. Nature 344, 756–759.

Stampfli, G. M., Borel, G. D., Marchant, R., Mosar, J. 2002. Western Alps geological constraints on western Tethyan reconstructions. In: Rosenbaum, G. and Lister, G. S. 2002. Reconstruction of the evolution of the Alpine-Himalayan Orogen. Journal of the Virtual Explorer 8, 77 - 106.

Stern, R.J., 2002. Subduction Zones, Reviews of Geophysics, 2002,

Stern, R.J., 2004. Subduction initiation: spontaneous and induced. Earth and Planetary Science Letters 226, 275- 292.

Stevenson, D.J., 2003. Styles of mantle convection and their influence on planetary evolution. Comptes rendus Gèoscience 335, 99-111.

Stich, D., Serpelloni, E., Mancilla, F.-L., Morales, J., 2006. Kinematics of the Iberia–Maghreb plate contact from seismic moment tensors and GPS observations. Tectonophysics 426, 295-317.

Stich, D., Mancilla, F. de L., Pondrelli, S., Morales, J., 2007. Source analysis of the February 12th 2007, M_w 6.0 Horseshoe earthquake: Implications for the 1755 Lisbon earthquake. Geophysical Research Letters 34, 12.

Stow, D.A.V., Pudsey, C.J., Howe, J.A., Faugères, J.C., Viana, A.R., 2002a. Deep water Contourite Systems: Modern Drifts and Ancient Series, Seismic and Sedimentary Characteristics, Memoirs, vol. 22. Geological Society of London, London, 464pp.

Stow, D.A.V., Faugères, J.C., Howe, J.A., Pudsey, C.J., Viana, A.R., 2002b. Bottom currents, contourites and deep-sea sediment drifts: current state-of-the-art. In: Stow, D.A.V., Pudsey, C.J., Howe, J.A., Faugères, J.C., Viana, A.R. (Eds.), Deep-water Contourite Systems: Modern Drifts and Ancient Series, Seismic and Sedimentary Characteristics. Geological Society of London, Memoirs 22, pp. 7–20.

Sun, T. & Parker, G. 2005. Transportational cyclic steps created by flow over an erodible bed. Part 2. Theory and numerical simulation. Journal of Hydraulic Research 43, 502–514.

Tahayt, A., Mourabit, T., Rigo, A., Feigl, K. L., Fadil, A., McClusky, S., Reilinger, R., Serroukh, M., Ouazzani-Touhami, A., Sari, D. B., & Vernant, P., 2008. Present-day movements of tectonic blocks in the betic-rif arc from GPS measurements 1999-2005; mouvements actuels des blocs tectoniques dans l'arc betico-rifain a partir des measures GPS entre 1999 et 2005. Comptes Rendus - Geoscience, 340(6), 400-413.

Taki, K. & Parker, G. 2005. Transportational cyclic steps created by flow over an erodible bed. Part 1. Experiments. Journal of Hydraulic Research 43, 488–501.

Terrinha, P., 1998. Structural Geology and Tectonic Evolution of the Algarve Basin, South Portugal. Department of Geology. London, University of London.

Terrinha, P., Pinheiro, L.M., Henriet, J.-P., Matias, L., Ivanov, M.K., Monteiro, J.H., Akhmetzhanov, A., Volkonskaya, A., Cunha, T., Shaskin, P., Rovere, M., 2003. Tsunamigenic–seismogenic structures, neotectonics, sedimentary processes and slope instability on the southwest Portuguese Margin. Marine Geology 195 (1–4), 55–73.

Terrinha, P., Matias, L., Vicente, J.C., Duarte, J., Luís, J., Pinheiro, L., Lourenço, N., Diez, S., Rosas, F.M., Magalhães, V., Valadares, V., Zitellini, N., Mendes-Víctor, L., MATESPRO Team, 2009. Morphotectonics and Strain Partitioning at the Iberia–Africa plate boundary from multibeam and seismic reflection data. Marine Geology 267, 156-174.

Terrinha, P., Matias, L., Valadares, V., Roque, C., Duarte, J., Rosas, F., Iribarren, L., Silva, S., Cunha, T., Batista, L., Duarte, D., Neves, M.C., Carrara, G., Zitellini, N., Gràcia, E., Gutscher, M-A., Lourenço, N., Pinto de Abreu, M., submitted. A Margem Sul Portuguesa Profunda, *in* Geologia de Portugal no contexto da Ibéria.

Thiebot, E., Gutscher, M.A., 2006. The Gibraltar Arc seismogenic zone (part1): constraints on a shallow east dipping fault plane source for the 1755 Lisbon earthquake provided by seismic data, gravity and thermal modeling. Tectonophysic 427, 135–152. doi:10.1016/j.tecto.2006.02.024 (Special Volume "Natural laboratories on seismogenic faults").

Torelli, L., R. Sartori and N. Zitellini, 1997. The giant chaotic body in the Atlantic Ocean off Gibraltar: new results from a deep seismic reflection survey. Marine and Petroleum Geology 14(2): 125-134.

Tortella, D., Torné, M., Pérez-Estáun, A., 1997. Geodynamic Evolution of the Eastern Segment of the Azores-Gibraltar Zone: The Gorringe Bank and the Gulf of Cadiz Region.Marine Geophysical Researches 19(3): 211-230.

Toth, J. and Gurnis, M., 1998. Dynamics of subduction initiation at preexisting fault zones. Journal of Geophysical Research 103, 18,053–18,067. doi:10.1029/98JB01076.

UCSD-SIO15: Natural Disasters Course.
http://quakeinfo.ucsd.edu/~gabi/sio15/Lecture04.html. Consulted in December, 2010.

Ueda, K., Gerya, T. and Sobolev, S.V., 2008. Subduction initiation by thermal-chemical plumes: Numerical studies. Physics of the Earth and Planetary Interiors 171, 296–312. doi:10.1016/j.pepi.2008.06.032.

Uyeda, S. and Ben-Avraham, Z., 1972. Origin and development of the Philippine Sea. Nature 240, 176–178.

Van der Lee, S., Regenauer-Lieb, K. and Yuen, D.A., 2008. The role of water in connecting past and future episodes of subduction. Earth Planetary Science Letters 273, 15–27. doi:10.1016/j.epsl.2008.04.041.

Verdicchio G. and Trincardi F., 2006. Short-distance variability in slope bed-forms along the Southwestern Adriatic Margin (Central Mediterranean). Marine Geology 234, 271-292.

Vilanova, S.P., Nunes, C.F. and Fonseca, J.F.B.D., 2003. Lisbon 1755: A Case of Triggered Onshore Rupture? Bulletin of the Seismological Society of America 93 (5), 2056-2068. doi: 10.1785/0120020245

Vine, F.J. and Hess, H.H., 1970. Sea-floor spreading. In Maxwell, A.E., Bullard, E.C., Goldberg, E., Worzal, J.L. (eds), The sea, vol. 4, Wiley Interscience, New York.

Vlaar, N.J. and Wortel, M.J.R., 1976. Lithospheric aging, instability and subduction. Tectonophysics 32, 331.

Wells, D.L., Coppersmith, K.J., 1994. New empirical relationships among magnitude, rupture length, rupture width, rupture area, and surface displacement. Bulletin of the Seismological Society of America 84 (4), 974–1002.

Wilson, C. K., Long, D., Bulat, J., 2004. The morphology, setting and processes of the Afen Slide. Marine Geology, 213, 149–167.

Wilson, J.T., 1966. Did the Atlantic close and then reopen? Nature (London) 211, 676.

Wilson, R.C., Hiscott, R.N., Willis, M.G., Gradstein, F.M., 1989. The Lusitanian basin of West-central Portugal: Mesozoic and Tertiary tectonic, stratigraphic, and subsidence history. In: Extensional Tectonics and Stratigraphy of the North Atlantic Margins, Tankard, A.J. and Balkwill, H.R., Editors, AAPG Mem. 46 (1989), 341–361.

Withjack, M.O., Schlische, R.W., Henza, A.A., 2007. Scaled Experimental Models of Extension: Dry Sand vs.Wet Clay. Houston Geological Society Bulletin, 49 (8): 31-49.

Zitellini, N., Chierici, F., Sartori, R., Torelli, L., 1999. The tectonic source ofthe 1755 Lisbon earthquake and tsunami. Ann. Geofis. 42, 49-55.

Zitellini, N., Mendes, L. A., Cordoba, D., Danobeitia, J., Nicolich, R., Pellis, G., Ribeiro, A., Sartori, R., Torelli, L., Bartolomé, R., Bortoluzzi, G., Calafato, A., Carrilho, F., Casoni, L., Chierici, F., Corela, C., Correggiari, A., Della Vedova, B., Gràcia, E., Jornet, P., Landuzzi, M., Ligi, M., Magagnoli, A., Marozzi, G., Matias, L., Penitenti, D., Rodriguez, P., Rovere, M., Terrinha, P., Vigliotti, L., Zahinos Ruiz, A., 2001. Source of 1755 Lisbon Earthquake and Tsunami Investigated. Eos Trans. AGU, 82, (26), 285, 290–291.

Zitellini, N., Rovere,M., Terrinha, P., Chierici, F.,Matias, L., Team, B., 2004. Neogene through quaternary tectonic reactivation of SW iberian passive margin. Pure and Applied Geophysics 161, 565–587.

Zitellini, N., Gracia, E., Matias, L., Terrinha, P., Abreu, M.A., DeAlteriis, G., Henriet, J.P., Dañobeitia, J.J., Masson, D.G., Mulder, T., Ramella, R., Somoza, L., Diez, S., 2009. The quest for the Africa-Eurasia plate boundary west of the Strait of Gibraltar. Earth and Planetary Science Letters, 280, 1-4, pp: 13-50.

Appendixes

Duarte, J.C., Valadares, V., Terrinha, P., Rosas, F., Zitellini, N., Gràcia, E., 2009. Anatomy and tectonic significance of WNW-ESE and NE-SW lineaments at a transpressive plate boundary (Nubia-Iberia). Trabajos de Geología 29, 237-241.

Terrinha, P., Matias, L., Vicente, J.C., **Duarte, J.**, Luís, J., Pinheiro, L., Lourenço, N., Diez, S., Rosas, F.M., Magalhães, V., Valadares, V., Zitellini, N., Mendes-Víctor, L., MATESPRO Team, 2009. Morphotectonics and Strain Partitioning at the Iberia–Africa plate boundary from multibeam and seismic reflection data. Marine Geology 267, 156-174.

Rosas, F.M., **Duarte, J.C.**, Terrinha, P., Valadares, V., Matias, L., 2009. Morphotectonic characterization of major bathymetric lineaments in NW Gulf of Cadiz (Africa-Iberia plate boundary): insights from analogue modelling experiments. Marine Geology 261, 33–47.

Rosas, F.M., **Duarte, J.C.**, Neves, M.C., Terrinha, P., Silva, S., Matias, L., Submitted. Thrust-wrench interference between major active faults in the Gulf of Cadiz (Africa-Eurasia plate boundary, offshore SW Iberia): tectonic implications from analogue and numerical modeling.

Trabajos de Geología, Universidad de Oviedo, 29 : 237-241 (2009)



Anatomy and tectonic significance of WNW-ESE and NE-SW lineaments at a transpressive plate boundary (Nubia-Iberia)

J. C. DUARTE[1, 2*], V. VALADARES[1, 2], P. TERRINHA[1, 2], F. ROSAS[1], N. ZITELLINI[3] AND E. GRÀCIA[4]

[1]LATTEX, IDL, UL, Faculdade de Ciências da Universidade de Lisboa, Edificio C6, Piso 3, Campo Grande, 1749-016 Lisboa, Portugal.

[2]UGM-LNEG, Estrada da Portela Zambujal, Alfragide, Apartado 7586, 2720-866 Amadora, Portugal.

[3]Istituto di Scienze Marine, (ISMAR, Área della ricerca di Bologna, Via Pierro Gobetti,101-40129, Bologna, Italy.

[4]Unidad de Tecnología Marina, CSIC, Passeig Maritim de la Barceloneta, 37-49, 08003 Barcelona, Spain.

[*]e-mail: joao.duarte@lneg.pt

Abstract: Recent mapping of the Gulf of Cadiz seafloor permitted to identify major tectonic lineaments: the SWIM lineaments (Zitellini *et al.*, 2009) and Cadiz lineament, striking WNW-ESE and NE-SW, respectively. Multibeam swath bathymetry and interpretation of multi-channel seismic data indicate that these features can be interpreted to correspond to the seafloor morphological expression of active dextral strike-slip faults. Based on the interpreted data and recently published GPS plate kinematic velocity vectors of Nubia with respect to Iberia and the Alboran block (e.g. Fernandes *et al.*; 2003 Stich *et al.*, 2006) we propose that the SWIM Faults are related to the general NW-SE convergence of Nubia with respect to Iberia, and the Cadiz fault is related to the westward movement of the Gibraltar orogenic arc.

Keywords: Gulf of Cadiz, seafloor mapping, SWIM lineaments, Cadiz lineament, active tectonics, Alboran block, Gibraltar orogenic arc.

The Gulf of Cadiz is located in a complex tectonic area, encompassing the controversial SW Eurasia-NW Africa plate boundary (see figure 1). Some authors believe that this is a diffuse plate boundary (Sartori *et al.*, 1994; Medialdea *et al.*, 2004), other describe an active subduction with roll-back of a subducted slab (Gutscher *et al.*, 2002), while others postulate a prolongation of a transpressive deformation belt from the Rif-Tell (Morel and Meghraouie, 1996; Zitellini *et al.*, 2009). This region experiences a general NW-SE to WNW-ESE convergence between Nubia and Eurasia at a rate of 5-6 mm a^{-1} (Calais *et al.*, 2003). Stich *et al.* (2006) proposed that the SW Iberian Margin is also accommodating a 3.5 mm a^{-1} of westward motion of the Gibraltar arc relative to intraplate Iberia. Seismicity is distributed over a more than 400 km wide zone between the Gibraltar arc and the Horseshoe fault (Fig. 1) and earthquakes are characterized by magnitudes usually smaller than 5.5. In the western part of the Gulf of Cadiz, in the area that encompasses the Horseshoe fault until the eastern part of the Gloria fault, seismicity is distributed over a narrower area and instrumental seismicity is higher, with recent events of M=6

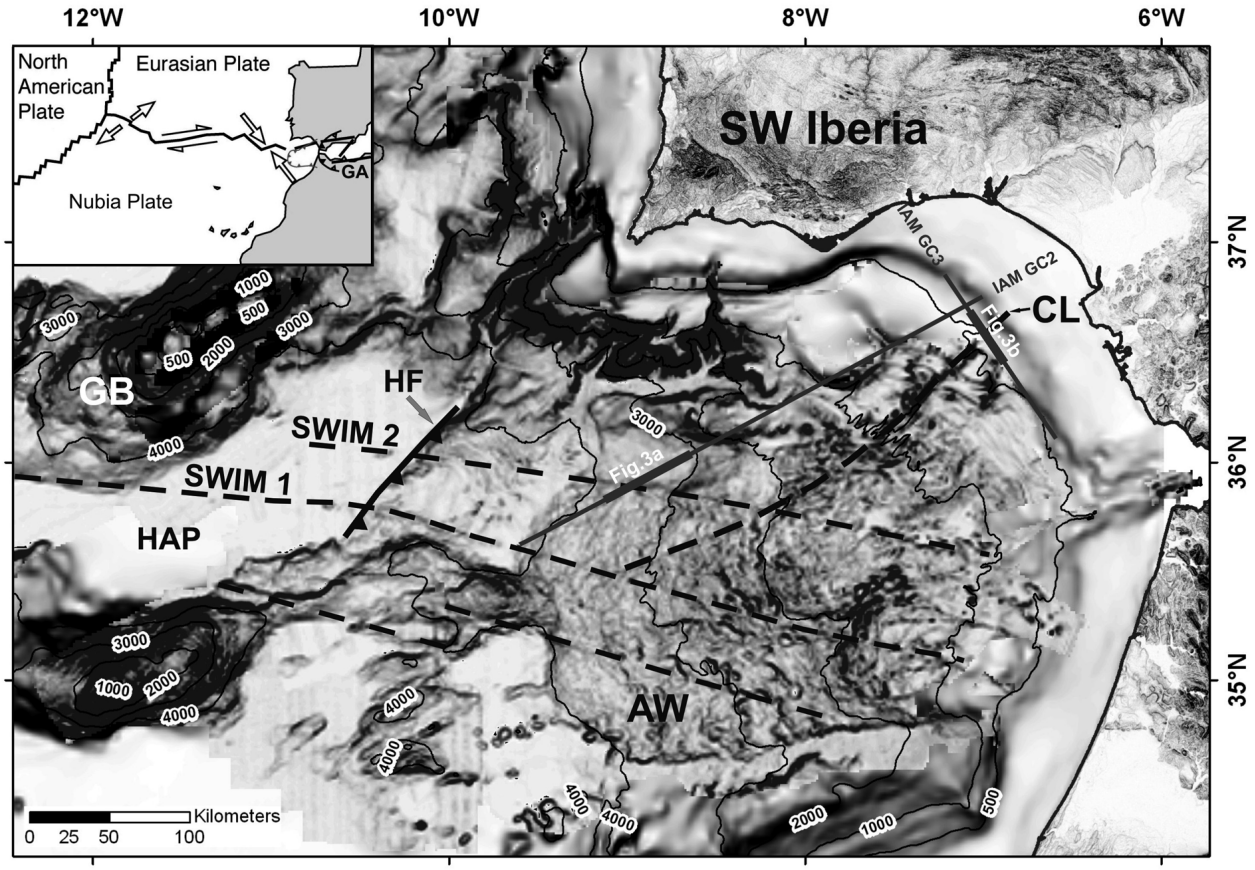


Figure 1. Bathymetric map of the Gulf of Cadiz (low resolution multibeam compilation of the SWIM dataset and GEBCO bathymetry). Topography of onshore area is also shown as shaded relief. Dashed lines represent the main tectonic lineaments studied in this work. The inset shows the tectonic context of the area (adapted from Gutscher *et al.*, 2002). The location of two seismic profiles, IAM GC2 and IAM GC3, are also shown. AW: Accretionary Wedge; CL: Cadiz Lineament; GA: Gibraltar Arc; GB: Gorringe Bank; HF: Horseshoe Fault; HAP: Horseshoe Abyssal Plain.

and the 1969 event of M=7.9 (Fukao, 1973; Stich *et al.*, 2006). Zitellini *et al.* (2004) described a number of active structures scattered along the Gulf of Cadiz and SW Portugal showing that tectonic strain is presently accommodated between 35.5º N and 38º N (approximately 250 km), which suggests a diffuse strain distribution of the plate convergence.

Over the last two decades a large amount of geological and geophysical data have been collected aiming at identifying the main tectonic features present in the Gulf of Cadiz and to clarify how deformation has been accommodated during Alpine to present times (Zitellini *et al.*, 2009). In this work we describe the morphology and structure of WNW-ESE and one NE-SW trending lineaments recently mapped in the Gulf of Cadiz region and discuss their tectonic significance.

This work is extracted from a much larger study based on the analysis and interpretation of 180,000 km^2 of multibeam swath bathymetry and reflectivity (backscatter) data of the Gulf of Cadiz area and more than 20,700 km multi-channel seismic profiles. This dataset was collected throughout several surveys carried out by international teams of several countries and compiled for the ESF Eurocores EuroMargins SWIM project (Earthquake and Tsunami hazards of active faults at the South-West Iberian Margin: deep structure, high-resolution imaging and paleo-seismic signature, REN2002-11234-EMAR, 01-LEC-EMA09 F) (http://www.swim.ul.pt/index_topo.htm) and NEAREST project (Integrated observations from NEAR shore sourcES of Tsunamis: towards an early warning system, GOCE Contract n. 037119) (http://nearest.bo.ismar.cnr.it/).

The SWIM lineaments

Morphology

The SWIM lineaments are linear features that strike approximately WNW-ESE and extend from the east-

ernmost part of the Gulf of Cadiz accretionary wedge until the Horseshoe abyssal plain, south of the Gorringe submarine mountain (Fig. 1). They cut across various morphological domains, contain various active mud volcanoes along their path and offset the NE-SW Horseshoe fault scarp (Fig.2), an active reverse fault (Gràcia *et al.*, 2003; Zitellini *et al.*, 2004). These linear features correspond to the alignment of elongated crests and troughs on the sea floor with wavelengths of the order of tens of kilometers. According to Zitellini *et al.* (2009), the longest of the SWIM lineaments, SWIM 1, exceeds 600 km, and it can be followed from the Gorringe bank southern flank to the Morocco shelf and corresponds to a strike-slip fault. In some segments of this lineament it is possible to identify E-W-striking undulations with maximum lengths of about 8 km (Fig. 2). These features show an en echelon pattern that corresponds to oriented folds of the recent sedimentary cover, allowing us to establish a dextral strike-slip movement. The width of each individual SWIM lineament is only of a few hundreds of meters.

ment because the wedge (Unit B) is over-thrusted towards the SW. This reactivation probably occurred during Paleogene to Miocene times (Rosas *et al.*, *in press*; Terrinha *et al.*, 2009). This movement seems to be coeval with the installation of the Accretionary wedge (Unit D) since it clearly tapers towards the eastern part of the profile. The SWIM fault also deforms and folds the Plio-Quaternary unit (Unit E) and cuts through the seafloor.

The Cadiz lineament

Morphology

The morphology of the Cadiz lineament is more complex than that of the SWIM 2 lineament. It is relatively diffuse and occupies a broader area, with widths varying from several hundreds of meters to a few kilometers. It strikes approximately NE-SW and extends for about 200 km from the northeastern Gulf of Cadiz continental shelf to the westernmost

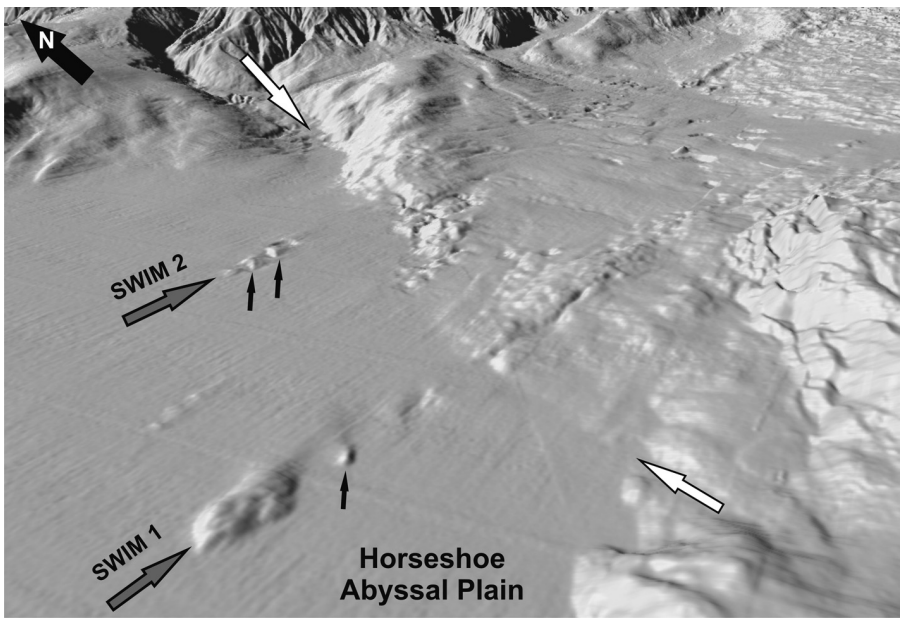


Figure 2. Shaded relief 3D image of the Horseshoe Abyssal Plain and continental rise to the east; view from SW, showing the SWIM tectonic lineaments 1 and 2, indicated by grey arrows; MATESPRO bathymetric data Terrinha *et al.* (2009) and Rosas *et al.* (2009). The small black arrows show seafloor deformation corresponding to NE-SW-oriented en echelon folds. The white arrows indicate the slope break that corresponds to the morphological expression of the Horseshoe Fault.

Structure

The interpretation of a segment of a profile across SWIM 2 lineament (Fig. 3a) shows that it corresponds to a fault that cuts through Mesozoic sediments (Unit A) (Tortella *et al.*, 1997). This fault formed during the Mesozoic rifting as a normal fault. This assumption is corroborated by the presence of a syn-rift growth wedge (Unit B). The SWIM 2 fault was later reactivated with a southwards reverse move-

part of the accretionary wedge (Fig.1). The lineament is slightly curved towards the west at the south-western part where it meets the SWIM 1 fault (Fig. 1). It is materialized on the seafloor by the alignment of several different features such as crests, scarps, channels and diapiric ridges (Somoza *et al.*, 2003). The Cadiz lineament is more prominent in its northeastern segment, where it is adjacent to the Guadalquivir bank (a basement high with active seismicity) and it loses morphological expression progressively towards

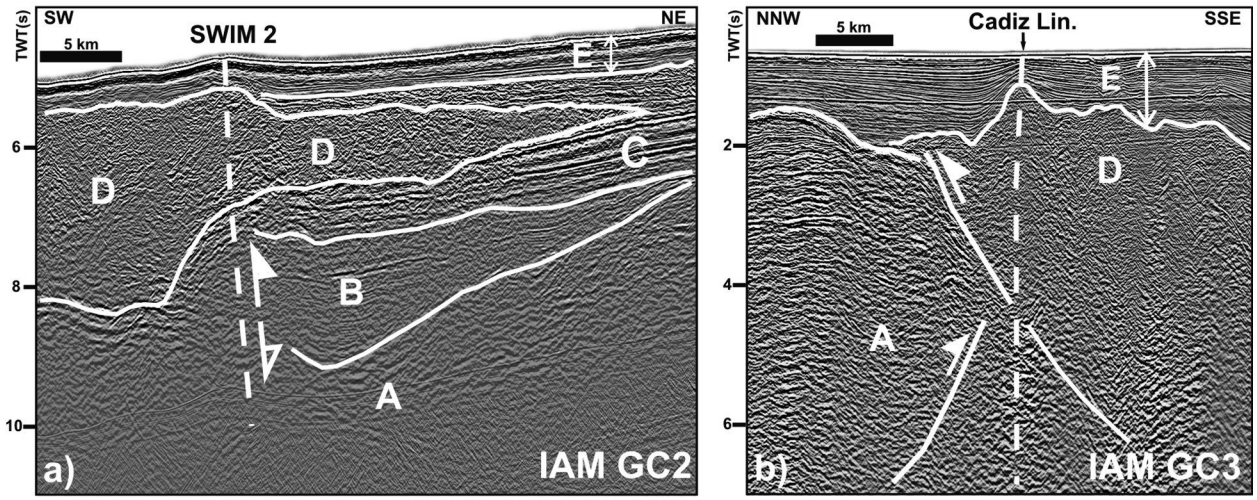


Figure 3. (a) Multi-channel seismic reflection profiles IAM GC2, and (b) IAM GC3. The white dashed lines mark the fault zones corresponding to the lineaments (SWIM 2 on the left and the Cadiz Lineament on the right). The profile a) shows two previous vertical movements of the SWIM fault (white arrows). On profile b) the following features are pointed out, reverse fault of the Guadalquivir basement to the SSE; and a thin-skinned fault of accommodating the over-thrusting movement of the Accretionary wedge over the Guadalquivir basement. A: Basement; B: Sin-rift wedge (Mesozoic age); C: Post-rift unit; D: Accretionary Wedge unit (Miocene age); E: Cover unit (Plio-Quaternary age).

the SW, where it intercepts the SWIM 2 lineament and is almost untraceable in the surroundings of the SWIM 1 lineament.

Structure

A segment of IAM GC3 seismic profile (Fig. 3b) across the Cadiz lineament shows that it seats on top of a fault zone. This fault is parallel to the deep blind thrust of the Guadalquivir bank towards the SE, as interpreted in figure 3 (Unit A). This movement is corroborated by the gentle folding of the reflectors of Unit A. It is also possible to observe a thin-skinned fault accommodating the over-thrusting of the accretionary wedge described by Gutscher *et al.* (2002) towards NE over the Guadalquivir basement (Unit D). This unit corresponds to imbrications of NNW-verging thrusts, as shown by the planar fabric of the acoustic facies. Near the surface the more continuous cover sediments are clearly folded; however, they do not show evidences of major vertical displacement (Unit E).

Discussion

Based on bathymetric and structural observations we interpret the SWIM lineaments as the morphological expression of dextral WNW-ESE trending strike-slip faults rooted in the Mesozoic rift basin. This interpretation is derived from both observed coherent en echelon folding pattern on the seafloor associated with the faults and the minor vertical displacement of the post-Miocene cover. This assumption is in agreement with recent work by Zitellini *et al.* (2009) and Terrinha *et al.* (2009) that describes in detail the kinematic indicators and the age of these faults. Rosas *et al.* (2009), using analogue models and the en echelon folds has markers for a quantitative strain analysis, suggested that the SWIM lineaments initiated their strike-slip movement 1.8 Ma ago, at least. This interpretation is also in agreement with the general NW-SE to WNW-ESE convergence between Africa and Eurasia at a rate of 5-6 mm a^{-1} and the fact that the SWIM faults offset the Late Miocene movement of the Horseshoe Fault. In this way, the SWIM lineaments can be accommodating a strike-slip component of this convergence, while the main shortening is being accommodated in the northwestwards directed thrusts of the SW Iberian Margin, for example the Horseshoe fault.

The Cadiz lineament has a strong morphological expression, mainly in its northeastern part where salt diapirs have extruded (Somoza *et al.*, 2003). However, no kinematic indicators could clearly be detected in our analysis. It corresponds to an almost vertical fault that deforms the sedimentary cover with no major vertical displacement. Based on recent data published by Stich *et al.* (2006), that reported a 3.5 mm a^{-1} of westward motion of the Gibraltar arc relative to intra-plate Iberia, we propose that the Cadiz lineament is a major dextral strike-slip fault zone that is accommodating this

relative motion in the Gulf of Cadiz area. The lack of good strike-slip kinematic indicators in this part of the study area is probably due to the higher rate of recent sedimentation associated with the proximal parts of the Mediterranean Outflow Water and discharge of the Guadalquivir river as well as the extrusion of fluidized material along diapiric ridges (Somoza *et al.* 2003), as well as to the pure shortening at the front of the Guadalquivir bank thrust, as argued in this work.

Conclusions

In this work we studied various major tectonic lineaments localized in the Gulf of Cadiz area. We showed that they correspond to major transpressive dextral strike-slip faults with two different orientations: the WNW-ESE SWIM faults and the NE-SW Cadiz fault. Both faults are active and are probably related with two different driving mechanisms. The SWIM faults are related to the general WNW-ESE convergence between Nubia and Eurasia and the Cadiz fault is related to the westward expulsion of the Gibraltar Arc relative to Iberia, possibly associated with the convergence between the two lithospheric plates.

Acknowledgements

It is acknowledged the FCT PhD grant provided to support the work of J. Duarte (SFRH/BD/31188/2006) and V. Valadares (SFRH/BD/17603/2004). We acknowledge the support by Landmark Graphics Corporation via the Landmark University Grant Program.

References

Calais, E., DeMets, C. and Nocquet, J. M. (2003): Evidence for a post-3.16 Ma change in Nubia-Eurasia-North America plate motions? *Earth Planet. Sc. Lett.*, 216: 81-92.

Fernandes, R. M. S., Ambrosius, B. A. C., Noomen, R., Bastos, L., Wortel, M. J. R., Spakman, W. and Govers, R. (2003): The relative motion between Africa and Eurasia as derived from ITRF2000 and GPS data. *Geophys. Res. Lett.*, 30, 16.

Fukao, Y. (1973): Thrust faulting at a lithospheric plate boundary Portugal earthquake of 1969. *Earth Planet. Sc. Lett.*, 18: 205-216.

Gràcia, E., Dañobeitia, J., Vergés, J. and R. Bartolomé, R. (2003a): Crustal architecture and tectonic evolution of the Gulf of Cadiz (SW Iberian margin) at the convergence of the Eurasian and African plates. *Tectonics*, 22, 4: 1-19

Gutscher, M. A., Malod, J., Rehault, J. P., Contrucci, I., Klingelhoefer, F., Mendes-Victor, L. and Spakmanc, W. (2002): Evidence for active subduction beneath Gibraltar. *Geology*, 30, 12: 1071-1074.

Medialdea, T., Vegas, R., Somoza, L., Vazquez, J. T., Maldonado, A., Diaz-del Rio, V., Maestro, A., Cordoba, D. and Fernandes-Puga, M. C. (2004): Structure and evolution of the "Olistostrome" complex of the Gibraltar Arc in the Gulf of Cadiz (eastern Central Atlantic): evidence from two long seismic cross-sections. *Mar. Geol.*, 209, 1-4: 173-198.

Morel, J. L. and Megrhraoui, M. (1996): Gorringe-Alboran-Tell tectonic zone: A transpressiva system along the Africa-Eurasia plate boundary. *Geology*, 24, 8: 755-758.

Rosas, F., Duarte, J., Terrinha, P., Valadares, V., Matias, L. and Gutscher, M. A. (2009): Major bathymetric lineaments and soft sediment deformation in NW Gulf of Cadiz (Africa-Iberia plate boundary): new insights from high resolution multibeam bathymetry data and analogue modelling experiments. *Mar. Geol.,* 261: 33-47.

Sartori, R., Torelli, L., Zitellini, N., Peis, D. and Lodolo, E. (1994): Eastern segment of the Azores-Gibraltar line (central-eastern Atlantic): an oceanic plate boundary with diffuse compressional deformation. *Geology*, 22: 555-558.

Somoza, L., Díaz-del-Río, V., León, R., Ivanov, M. K., Fernández-Puga, M. C., Gardner, J. M., Hernández-Molina, F. J., Pinheiro, L. M., Rodero, J., Lobato, A., Maestro, A., Vázquez, J. T., Medialdea, T. and Fernández-Salas, L. M. (2003): Seabed morphology and hydrocarbon seepage in the Gulf of Cadiz mud volcano area: Acoustic imagery, multibeam and ultra-high resolution seismic data. *Mar. Geol.*, 195: 153-156.

Stich, D., Serpelloni, E., Mancilla, F. and Morales, J. (2006): Kinematics of the Iberia-Maghreb plate contact from seismic moment tensors and GPS observations. *Tectonophysics*, 426: 295-317.

Terrinha, P., Matias, L., Vicente, J. C., Duarte, J., Luís, J., Pinheiro, L., Lourenço, N., Diez, S., Rosas, F. M., Magalhães, V., Valadares, V., Zitellini, N., Mendes-Víctor, L., and MATESPRO Team (2009): Morphotectonics and Strain Partitioning at the Iberia-Africa plate boundary from multibeam and seismic reflection data. *Mar. Geol.,* 267: 156-174.

Tortella, D., Torne, M., and Pérez-Estaún, A. (1997): Geodynamic Evolution of the Eastern Segment of the Azores-Gibraltar Zone: The Gorringe Bank and the Gulf of Cadiz Region. *Mar. Geophys. Res.*, 19: 211–230.

Zitellini, N., Rovere, M., Terrinha, P., Chierici, F. and Matias, L. (2004): Neogene through quaternary tectonic reactivation of SW Iberian passive margin. *Pure Appl. Geophys.*, 161: 565-587.

Zitellini, N., Gràcia, E., Gutscher, M. A., Matias, L., Masson, D., Mulder, T., Terrinha, P., Somoza, L., de Alteriis, G., Henriet, J. P., Dañobeitia, J. J., Ramella, R., Pinto de Abreu, M. A. and Diez, S. (2009): The quest for the Iberia-Africa Plate boundary west of Gibraltar. *Earth Planet Sc. Lett.*, 280, 1-4: 13-50.

Marine Geology 267 (2009) 156–174

Contents lists available at ScienceDirect

Marine Geology

journal homepage: www.elsevier.com/locate/margeo

Morphotectonics and strain partitioning at the Iberia–Africa plate boundary from multibeam and seismic reflection data

P. Terrinha [a,d,*], L. Matias [b], J. Vicente [c], J. Duarte [a,d], J. Luís [e], L. Pinheiro [f], N. Lourenço [e,g], S. Diez [h], F. Rosas [d], V. Magalhães [f], V. Valadares [a,d], N. Zitellini [i], C. Roque [a,g], L. Mendes Víctor [b], MATESPRO Team [1]

[a] *Laboratório Nacional de Energia e Geologia (LNEG), Unidade de Geologia Marinha, Portugal*
[b] *Fac. Science Univ. Lisbon (CGUL, IDL), Portugal*
[c] *Câmara Municipal de Lisboa, Portugal*
[d] *Fac. Science Univ. Lisbon (LATTEX, IDL), Portugal*
[e] *Univ. Algarve, CIMA, Portugal*
[f] *Universidade de Aveiro, CESAM, Portugal*
[g] *EMEPC, Portugal*
[h] *Unidad de Tecnología Marina (UTM-CSIC), Barcelona, Spain*
[i] *Istituto di Scienze Marine, (ISMAR), Bologna, Italy*

ARTICLE INFO

Article history:
Received 2 March 2009
Received in revised form 23 September 2009
Accepted 29 September 2009
Available online 13 October 2009

Communicated by D.J.W. Piper

Keywords:
Gulf of Cadiz
Southwest Iberia Margin
multibeam bathymetry
morphotectonics
seismotectonics
wrench tectonics
strain partitioning
migration of deformation

ABSTRACT

The Gulf of Cadiz, off SW Iberia and the NW Moroccan margin, straddles the cryptic plate boundary between Africa and Eurasia, a region where the orogenic Alpine compressive deformation in the continental collision zone passes laterally to the west to strike-slip deformation. A set of new multibeam bathymetry, multi-channel and single-channel seismic data presented here image the main morphological features of tectonic origin of a significant part of the Gulf of Cadiz from the continental shelf to the abyssal plain. These morphotectonic features are shown to result from the reactivation of deeply rooted faults that changed their kinematics from the early Mesozoic rifting, through the Late Cretaceous–Paleogene collision, to the Pliocene–Quaternary thrusting and wrenching. The old faults control deep incised, more than 100 km long canyons and valleys. Several effects of neotectonics on deep water seabed are shown. These include: i) the complex morphology caused by wrenching on the 230 km long WNW–ESE faults that produced en echelon folds on the sediments; ii) the formation of up to 5 km wide crescent shaped scours at roughly 4 km water depth by reactivation of thrusts; iii) 10 km long creep folds on the continental slope; and iv) the formation of landslides on active fault escarpments. The present day deformation is partitioned on NE–SW thrusts and WNW–ESE to W–E strike-slip faults and is propagating northwards on N–S trending thrusts along the West Iberia Margin from 35.5°N to 38°N, which should be considered for seismic hazard.

© 2009 Elsevier B.V. All rights reserved.

1. Introduction

1.1. Scope and objectives

In recent years the Gulf of Cadiz (Fig. 1) has been recognized as a key site to understand a broad spectrum of geological issues, such as: i) the tectonic evolution of the Africa–Iberia plate boundary, the formation of the Gibraltar orogenic arc, the earthquake and tsunamigenic structures, the origin of the catastrophic 1755 Lisbon earthquake and tsunami (Argus et al., 1989; DeMets et al., 1994; Sillard et al., 1998; Maldonado et al., 1999; Kreemer and Holt, 2001; Zitellini et al., 2001; Gutscher et al., 2002; Sella et al., 2002; Calais et al., 2002; Calais et al., 2003; Terrinha et al., 2003; Fernandes et al., 2003; Gràcia et al., 2003a; Gràcia et al., 2003a,b; Nocquet and Calais, 2004; Medialdea et al., 2004; Stich et al., 2006), ii) the Mediterranean Outflow Water (MOW) and its relation to sedimentation and climate changes (Ambar et al., 2002; Somoza et al., 2003; Mulder et al., 2003; Hernandez-Molina et al., 2003; Voelker et al., 2006), iii) fluid escape and mud volcanism (Somoza et al., 2003; Pinheiro et al., 2003; Van Rensbergen et al., 2005; Pinheiro et al., 2006), and iv) chemosynthetic ecosystems associated to cold seeps (Niemann et al., 2006).

Behind this diversity of processes affecting the geosphere, the biosphere and the hydrosphere, is a complex geological evolution of the area throughout the Neogene. It is now well established, after various studies based on seismic reflection profiles, sidescan sonar and ground truthing, that the whole area is under compressive deformation. A number of active tectonic structures with high tsunamigenic potential were mapped (Terrinha et al., 2003; Gràcia et al., 2003a,b; Zitellini et al., 2004) and various multilayered complexes of

* Corresponding author. Marine Geology Unit, LNEG, Estrada da Portela, 2721-866 Amadora, Portugal. Tel.: +351 21 470 55 41; fax: +351 214 719 018.
E-mail address: pedro.terrinha@ineti.pt (P. Terrinha).
[1] MATESPRO Team: Teresa Medialdea, Marzia Rovere, Caterina Basile, Toni Bermudez.

0025-3227/$ – see front matter © 2009 Elsevier B.V. All rights reserved.
doi:10.1016/j.margeo.2009.09.012

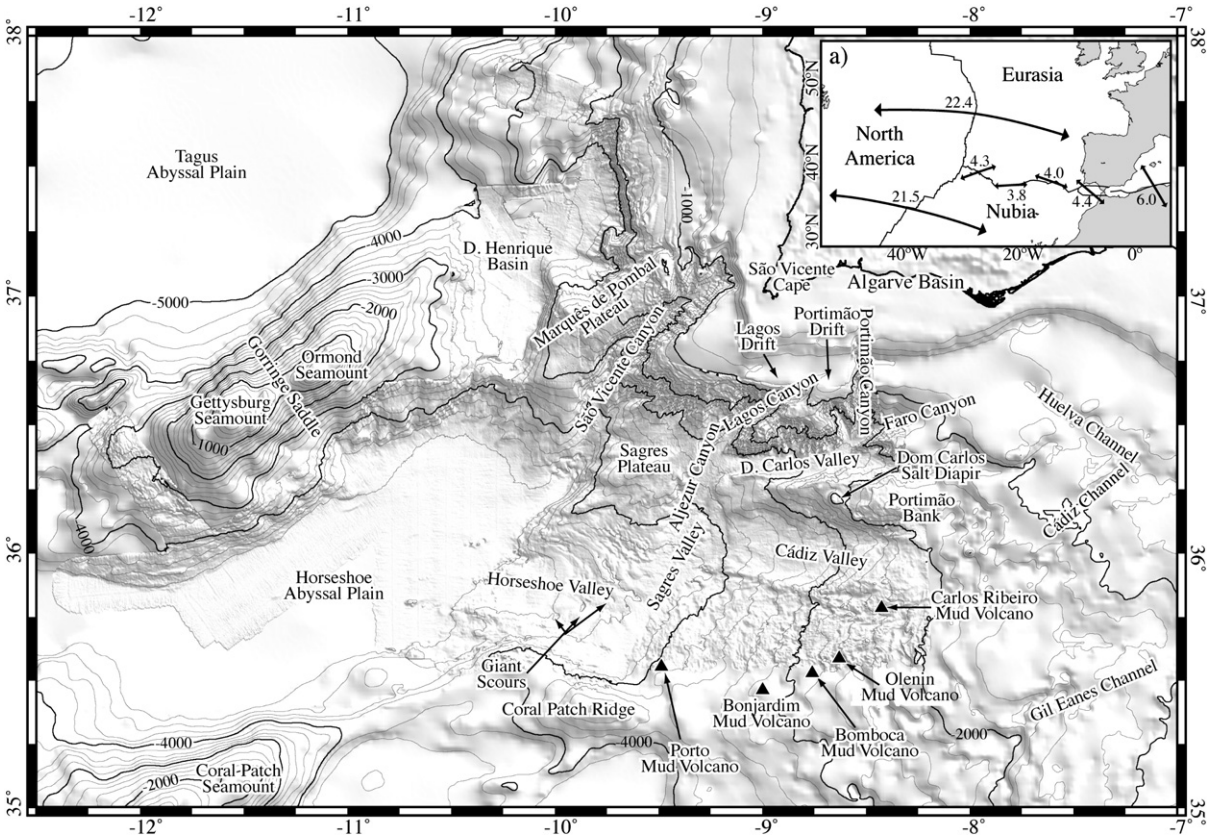


Fig. 1. Location and main morphological features of the study area. Inset shows the geotectonic location of the area and the relative motions of the Eurasia, Nubia and North America lithospheric plates in mm/yr. Triangles show the locations of mud volcanoes.

hemipelagic-mass wasting deposits of Holocene and Pleistocene age were imaged and dated (Vizcaino et al., 2006).

The morphology of the northeastern part of the Gulf of Cadiz was described by Hernandez-Molina et al. (2003), Mulder et al. (2003) and Somoza et al. (2003). The morphology of the southern part of this sector is clearly influenced by the tectonomorphic processes associated with the deformation of the Gulf of Cadiz accretionary wedge (Maldonado et al., 1999; Gutscher et al., 2002), as well as gravitational processes (Gutscher et al., 2008), while in the northern part the shaping processes are sedimentary, erosive and tectonic, associated with the MOW and to diapiric ridges.

The objective of this work is to describe the morphology of the northwestern part of the Gulf of Cadiz and discuss the morphogenetic processes in relation to the tectonic deformation of the Alpine collision front and the Gloria transform fault. This is done based on the interpretation of an original multibeam bathymetry data and seismic reflection profiles.

1.2. Geological setting

During Triassic through Early Cretaceous times the southern and western Iberian margins underwent tectonic rifting, which led to oceanic break-up of the West Iberian Margin from Barremian to Aptian times (Pinheiro et al., 1996). Although the existence of oceanic lithosphere in the Gulf of Cadiz is still a matter of debate (Srivastava et al., 1990; Gràcia et al., 2003a,b; Rovere et al., 2004), some authors postulated the existence of a south Iberia subduction zone that accommodated the Africa–Iberia convergence, from Late Cretaceous–Paleogene through Miocene times (e.g. Srivastava et al., 1990). Accordingly, this process led to the formation of back arc basins and associated tectonic terranes in the western Mediterranean, the formation of the Betic orogen, as well as to the tectonic inversion of the rifted autochthonous south Portuguese and south Spanish margins (e.g. Terrinha, 1998; Maldonado et al., 1999; Rosenbaum et al., 2002; Lopes et al., 2006). Westward directed thrusting of the Internal Betics domains and orogenic collapse, possibly associated with roll back of the Africa subducted slab, formed the Gibraltar orogenic arc, the Gulf of Cadiz accretionary wedge and lithospheric thinning in the Alboran Sea (Rosenbaum et al., 2002; Faccenna et al., 2004). These tectonic processes led to the formation of an accretionary wedge westward of the Gibraltar arc (Gutscher et al., 2002) or imbricate wedge with a westward directed tectonic transport, and an associated distal olistostrome complex (e.g., Horseshoe Gravitational Unit in Iribarren et al., 2007; Giant Chaotic Body in Torelli et al., 1997) that extends across the Horseshoe Abyssal Plain (Fig. 2). The MCS lines reveal a basal decollement horizon of the stacked thrusts of the accretionary wedge near the top of the Cretaceous. Both the accretionary prism and the olistostrome are sealed by sediments of Late Miocene to Lower Pliocene age (Tortella et al., 1997; Torelli et al., 1997; Roque, 2007). The segment of the Azores–Gibraltar Fracture Zone to the east of the Gloria Fault (inset in Fig. 1) was described by Sartori et al. (1994) as a diffuse plate tectonic boundary and various plate kinematic models indicate a 4 mm/yr rate of NW–SE to WNW–ESE convergence between Nubia and Iberia along this fault (insets in Figs. 1 and 8), (Argus et al., 1989; DeMets et al., 1994; Sillard et al., 1998; Kreemer and Holt, 2001; Sella et al., 2002; Calais et al., 2002; Calais et al., 2003; Fernandes et al., 2003; Nocquet and Calais, 2004; Stich et al., 2006). Ribeiro et al. (1996) postulated the formation of an incipient West Iberia subduction zone during Pliocene–Quaternary times, based on the computed NW–SE present day main compression direction.

N–S to NE–SW faults formed in the Permian during the late Variscan fracturing event (Arthaud and Matte, 1977; Ribeiro, 2002) and they were subsequently reactivated during the Mesozoic rifting, the Mesozoic transient compressive episodes (Terrinha et al., 2002)

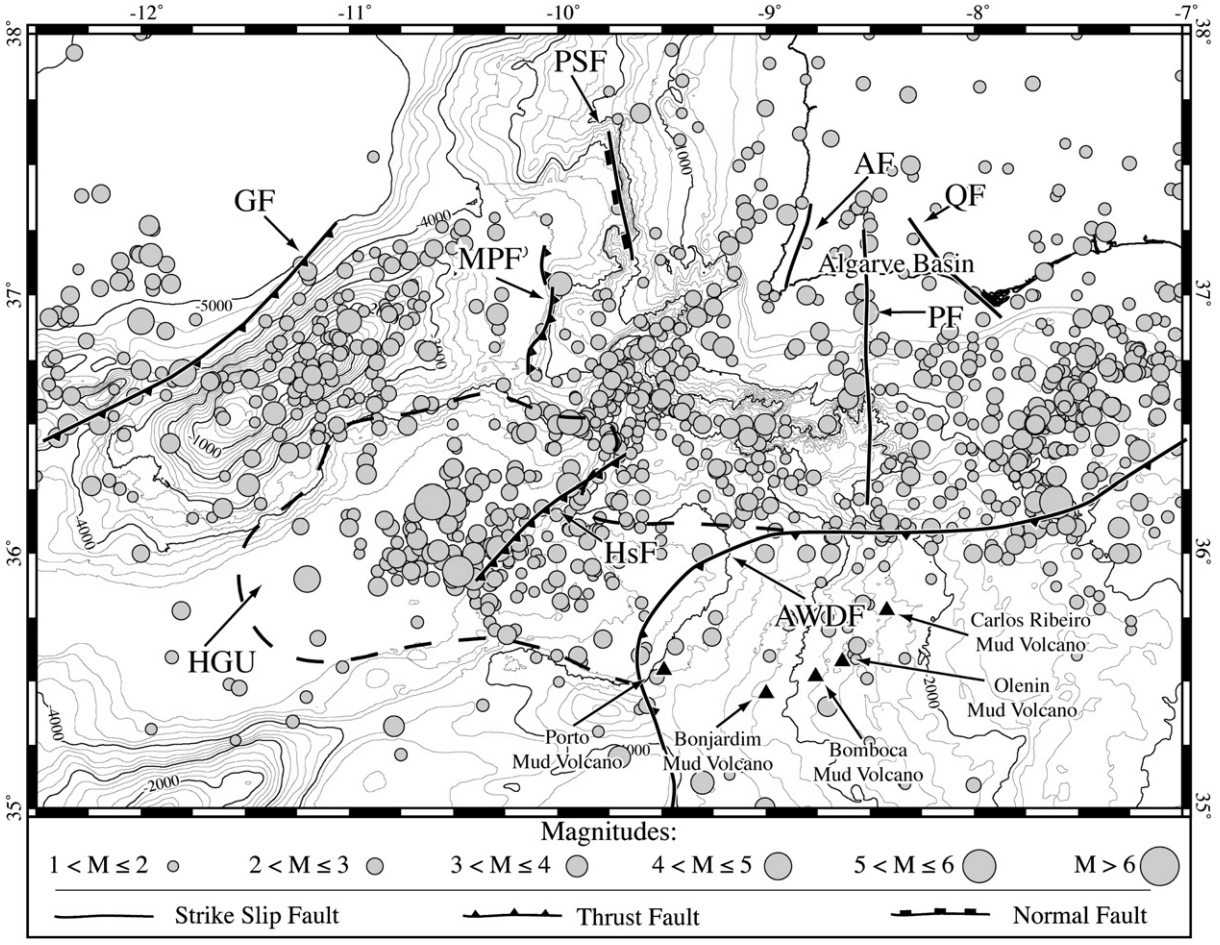


Fig. 2. Seismicity of the study area, the main faults and boundaries of the Accretionary Wedge of the Gulf of Cadiz and Horseshoe Gravitational Unit as mapped in previous works (Sartori et al., 1994; Torelli et al., 1997; Gutscher et al., 2002; Gràcia et al., 2003a; Terrinha et al., 2003; Iribarren et al., 2007). AF — Aljezur Fault; AWDF — Accretionary Wedge Deformation Front; GF — Gorringe Fault; HGU — Horseshoe Gravitational Unit; HsF — Horseshoe Fault; MPF — Marquês de Pombal Fault; PF — Portimão Fault; PSF — Pereira de Sousa Fault; QF — Quarteira Fault; triangles show the locations of mud volcanoes.

and the Cenozoic through Present compression (Fig. 2, Dias, 2001; Carrilho et al., 2004).

Offshore, the N–S trending Marquês de Pombal and Pereira de Sousa faults lie on the north to south trending southernmost segment of the West Iberian Margin. These faults were described as active in the Quaternary by Zitellini et al. (1999), Zitellini et al. (2001), Gràcia et al. (2003a,b) and Terrinha et al. (2003). The uneven surface of the Marquês de Pombal fault scarp is due to widespread slumping and landslides with mass transport distances that exceed 20 km. The Pereira de Sousa fault scarp is also heavily incised and the D. Henrique basin shows a series of radial ridges that consist of turbidite levees transported downslope from the highs that surround it (Terrinha et al., 2003; Gràcia et al., 2003a,b).

WSW–ENE to W–E trending Mesozoic rifting faults were inverted during the latest Cretaceous through early Miocene times (Terrinha, 1998; Lopes et al., 2006).

Duarte et al. (2005) showed the existence of presently active WNW–ESE trending faults in the Gulf of Cadiz and Medialdea (2007) proposed that these faults acted as transfer faults between the Gorringe Bank and the Marquês de Pombal fault across the Horseshoe fault. Onshore southwest Portugal, WNW–ESE trending Lower Jurassic extensional faults were described by Ribeiro and Terrinha (2007). Zitellini et al. (2009) proposed the existence of a Nubia–Eurasia plate boundary based on a set of 600 km long WNW–ESE trending set of strike-slip faults that cut across the Horseshoe Abyssal Plain and Gulf of Cadiz connecting the Gloria Fault and the Tell tectonic zone onshore north-west Morocco.

Earthquake frequency and epicentre location (Fig. 2) show that SW Iberia is an area of moderate seismicity which accommodates the brittle deformation associated with the Nubia–Iberia collision west of Gibraltar, by means of thrusting and strike-slip events of shallow and intermediate depth. However, the existence of historical and instrumental high magnitude earthquakes such as the 1/11/1755 Lisbon earthquake ($M = 8.5$ to 8.9) and the 28/2/1969 ($Ms = 7.9$) event require clarification of the present tectonic setting of the SW Iberia–NW Africa region, and identification of the structures that generate large magnitude earthquakes and tsunami in this area. The Gorringe Bank Fault is a north westwards directed thrust that sits at the northern base of this morphologic feature. This thrust uplifted the seafloor from approximately −5000 m to −24 m, it reached its paroxysmal activity in Miocene times and has accommodated negligible shortening since then (Sartori et al., 1994; Tortella et al., 1997). Although the Gorringe Bank is by far the most conspicuous morphotectonic structure in the study area (Fig. 1), the distribution of seismicity (Fig. 2), numerical models for tsunami wave propagation (Baptista et al., 1998) and the interpretation of MCS lines (Sartori et al., 1994), led various researchers to abandon it as the source of the 1755 Lisbon earthquake.

Recent models proposed the existence of two faults, the Marquês de Pombal Fault and the Horseshoe fault (Terrinha et al., 2003; Gràcia et al., 2003a,b) (Fig. 2) or the Marquês de Pombal Fault and the Guadalquivir Bank fault (Baptista et al., 2003), acting together simultaneously to generate the 1755 event by adding up their rupture areas (Terrinha et al., 2003; Baptista et al., 2003; Gràcia et al., 2003a,b). Alternatively, Gutscher et al. (2002) proposed that the 1755 Lisbon

earthquake was generated in the Gibraltar subduction zone imaged on seismic tomography, arguing that this was also the source of the deep 1954 Granada earthquake.

1.3. Data and methods

38,000 km^2 of multibeam swath bathymetry data were acquired in the MATESPRO Survey with a hull-mounted Simrad EM 120 echosounder aboard the research vessel *NRP D. Carlos I* in 3 legs from 14 June to 7 July 2004 (Figs. 3 and 4). The survey was carried out in order to comply with a level 3 hydrographic survey as established by the International Hydrographic Organization. The EM 120 operates at a main frequency of 12 kHz (from 11.25 to 12.6 kHz) with 191 beams covering a 150° fan with a width of 1°. In order to increase data quality the angular value was reduced to 120° and the ping width was of 2°. One sound velocity profile (SVP) was performed every 24 h and at locations chosen to spatially cover the entire area in order to compensate the effect of the Mediterranean Outflow Water on the sound velocity in the water column regionally. SVP data were acquired down to 2000 m of water depth. From −2000 to −4000 m sound velocity was taken from climatologic profiles provided by the Instituto Hidrográfico of Portugal in this area. Quality control lines were also performed totalizing about 10% of the area; the depth errors found were below 0.3% of the water depth. Bathymetric data filtering and processing was carried using CARIS HIPS software and a 100 m grid was generated.

The positioning of the vessel was done with both GPS and DGPS mounted on different parts of the vessel in order to better determinate the position and make the yaw corrections; the errors associated with the navigation positioning were around 5 m.

The seismic data presented here are of two types: multi-channel seismic (MCS) profiles from three previous surveys, ARRIFANO (acronym of Arco Rifano; Sartori et al., 1994), IAM (acronym of Iberian Atlantic Margin; Banda et al., 1995) and VOLTAIRE (acronym of Valuation Of Large Tsunamis And Iberian Risk for Earthquakes) and one single-channel profile acquired during the TTR-14 survey (Training Through Research; Kenyon et al., 2006).

The IAM and ARRIFANO deep MCS have a similar central peak frequency of approximately 30 Hz and the VOLTAIRE MCS has a central peak frequency of approximately 50 Hz. As a result, the vertical resolution in the sedimentary section is of around 20 m for the IAM and ARRIFANO profiles and of about 15 m for the VOLTAIRE data, assuming a mean seismic velocity of 2500 ms^{-1} in the sedimentary section (data from bore-holes in Fig. 3 and González et al., 1998). The central peak frequency of the single-channel TTR profile is around 100 Hz with a corresponding vertical resolution of about 6 m. Information on acquisition and processing of these profiles is summarized in Table 1.

The presented seismostratigraphic interpretation was based on the stratigraphy of five industry wells offshore the Algarve Basin (stars in Fig. 1, Lopes et al., 2006), as well as published data from the offshore Guadalquivir Basin (Maldonado et al., 1999).

2. Morphology of the NW part of the Gulf of Cadiz

The MATESPRO multibeam dataset (Fig. 4) shows a variety of seafloor major morphological features within which smaller scale features indicative of genetic processes discussed elsewhere in this paper are found.

2.1. The submarine sediment drainage system

The drainage system of the study area is subdivided in two groups: a northern one that drains the Portuguese continental margin from north to south, and a southern one that drains the western continental shelf of Spain.

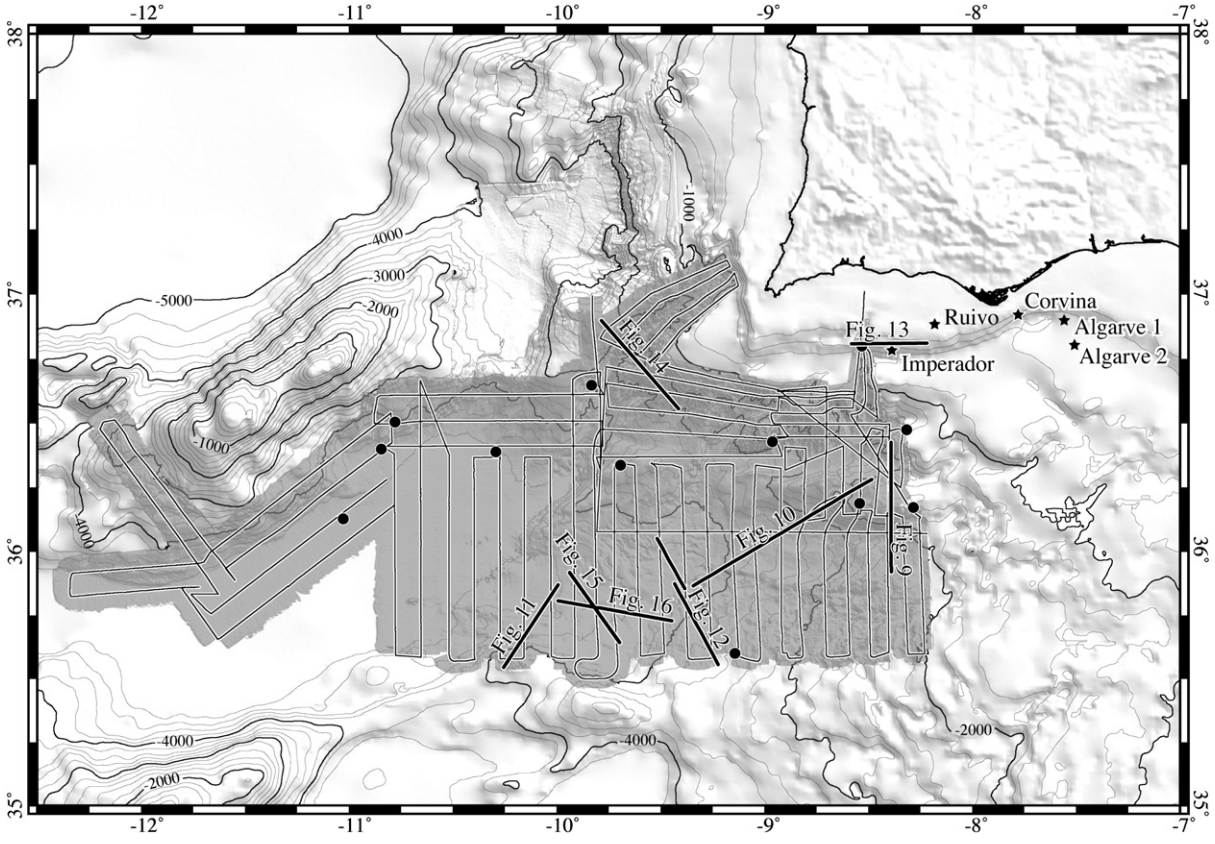


Fig. 3. Map showing the acquisition track lines of the MATESPRO multibeam bathymetry and the position of the seismic reflection lines shown in this work. Circles indicate locations of the sound velocity profiles performed. Location of oil prospection wells (stars) is also shown. Altimetry data derived from SRTM (USGS, 2004).

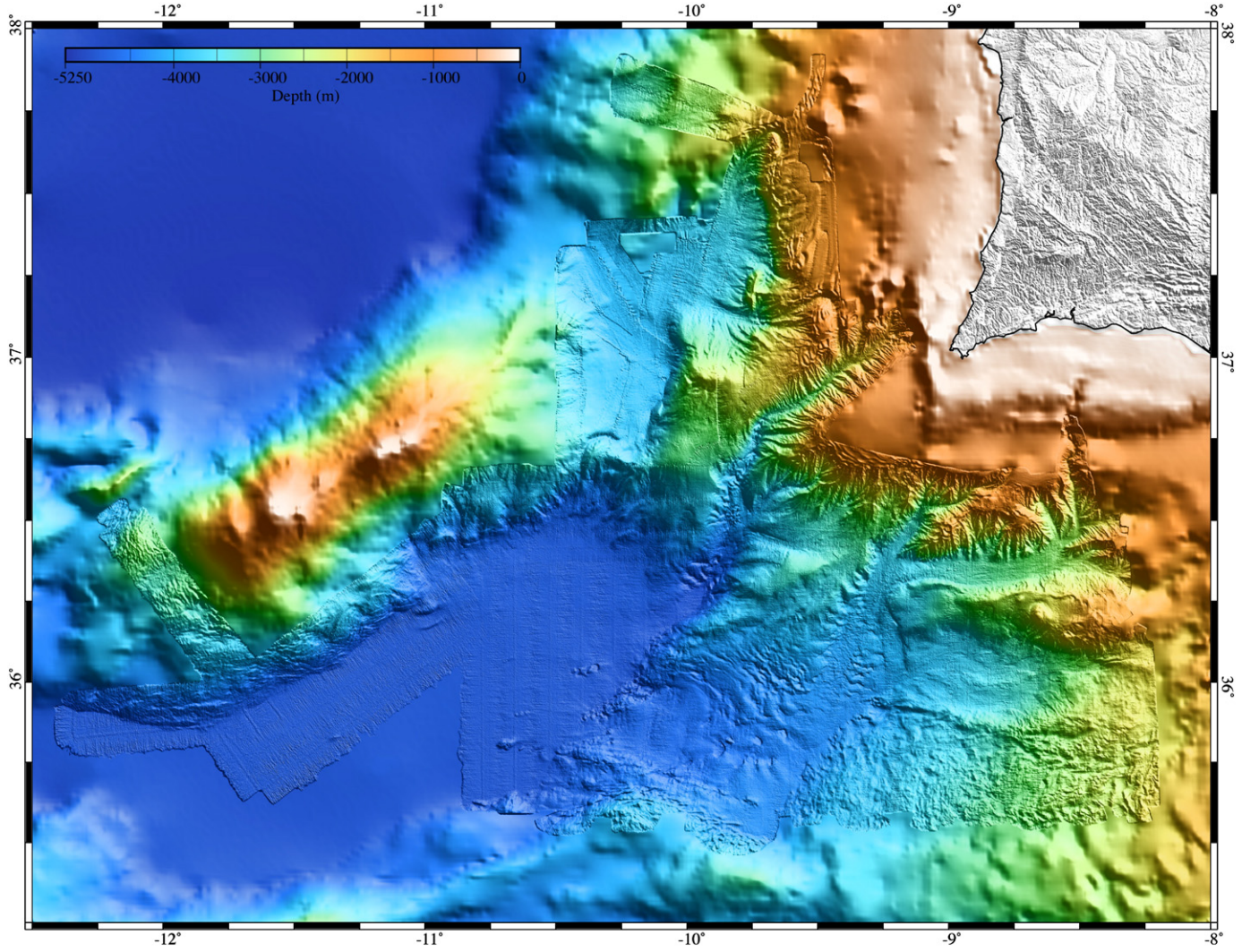


Fig. 4. Multibeam bathymetry map of the MATESPRO study area, offshore SW Iberia. Topography of onshore area also shown as shaded relief with a maximum of 902 m. Mercator projection, datum WGS84. PARSIFAL bathymetry of the Marquês de Pombal area and Pereira de Sousa escarpment published by Gràcia et al. (2003a,b). Bathymetry for other offshore areas and onshore altimetry is taken from Gebco (data from IOC et al., 2003).

2.1.1. The north to south sediment drainage system

The north to south oriented drainage system consists of a poorly organized network of gullies and canyons. The deeply incised 120 km long São Vicente canyon (Fig. 1) has its head scarp at 70 m below sea level (mbsl), cuts across the shelf and slope and ends in the Horseshoe Abyssal Plain. The maximum incision into the sedimentary substratum

Table 1
Aquisition parameters, geometry and processing for the seismic reflection profiles shown in this work.

	ARRIFANO	IAM	VOLTAIRE	TTR-14
Year	1992	1993	2002	2004
Vessel	*R/V OGS Explora*	*Geco Sigma*	*R/V Urania*	*R/V Prof Logachev*
Reference	Sartori et al. (1994)	Banda et al. (1995)	Zitellini et al. (2002)	Kenyon et al. (2006)
Seismic source	32 airguns (80 l max.)	30 airguns (125 l max.)	2 GI guns	1 airgun (120 bar)
Shooting interval	50 m	74 m	50 m	10 s (aprox. 30 m)
Sample interval recorded	1 ms	4 ms	1 ms	1 ms
Number of channels	120	192	48	1
Resampling	4 ms	8 ms	2 ms	1 ms (no resampling)
Signal processing			Trace editing	
			Shot delay removal	
	Spiking deconvolution	NMO correction	Amplitude recovery	Static correction
	Spherical divergence correction	Kirchoff migration	Predictive deconvolution	Spiking deconvolution
	NMO correction	(constant velocity 1700 m/s)	Velocity analysis every 200 CMPs	Spherical divergence correction
	Finite-difference wave-equation migration	AGC, 500 ms time gate	NMO correction	Butterworth bandpass filtering (20–60–180–240 Hz)
	Time variant bandpass frequency filter		Stack	
			Bandpass-frequency filtering	
			Time migration using stacking velocities	

on the continental slope is of 2 km. This canyon is made up of two segments oriented NE–SW and N–S that collect the sediment from the gullies that incise the shelf and slope (Figs. 4 and 5). Also note that the flanks of the NE–SW trending segment and the eastern flank of the N–S trending segment display higher degree of incision, while the western flank of the N–S trending segment and both flanks of the deepest part of the canyon are smoother. The close up in Fig. 6A shows a submarine landslide near the termination of the canyon. The lack of the mass transport deposit within the canyon is an indication of the activity of the canyon in terms of sediment erosion and transport.

The 70 km long Portimão canyon also has its head scarp in the shelf at roughly 70 mbsl. The canyon cuts across the shelf and slope sedimentary sequence with a maximum incision of 1 km. The canyon terminates abruptly at the meeting point with the Faro canyon and D. Carlos valley that drain east to west. These features have a different physiography, with a flat and broad bottom capable of accommodating larger sediment influx. The Portimão canyon is fairly rectilinear and sits along the Portimão Fault (Terrinha et al., 1999).

The Aljezur and Lagos canyons only incise the continental slope. The NNE–SSW trending Aljezur canyon is short, rectilinear and drains into the Sagres valley. The western flank of the Aljezur canyon displays a series of anastomosed submarine slide scars at approximately 1300 mbsl, at a main morphologic break of the continental slope near the base of the Lagos contourite drift (Fig. 6B).

The Sagres valley collects the east to west draining D. Carlos and Cadiz valleys and the Aljezur and Lagos canyons. The Aljezur canyon and Sagres valley lie on the southern prolongation of an important slope break that can be observed in the low resolution bathymetry (see Figs. 2, 4 and 5) and also on the southern continuation of the Aljezur Fault that cuts across the Meso–Cenozoic Algarve Basin and Paleozoic basement (Fig. 2).

The Lagos canyon has its head scarp roughly at 800 mbsl, where it incises the Pliocene through Holocene Lagos contourite drift.

2.1.2. East to west oriented sediment drainage system

The seafloor of the inner part of the Gulf of Cadiz dips to the west towards the Atlantic Ocean. The seafloor is shaped by a variety of morphological features of various scales, many of which have been described by Mulder et al. (2003), Somoza et al. (2003), Hernandez-Molina et al. (2006), and Gutscher et al. (2008).

The most important E–W trending valleys of the study area lie in the prolongation of the sinuous and broader E–W channels that initiate on the Gibraltar Arc owing to erosion and sedimentation by the MOW and to downslope gravity processes (Hernandez-Molina et al., 2003). In the study area these valleys are broad, with flat gently dipping bottom. The Faro canyon and D. Carlos valley collect the sediment transport from the South Portuguese margins, a large number of gullies, valleys and the Portimão canyon. The D. Carlos valley changes from narrow channel to broad valley downslope from the merge of the Portimão Canyon.

The Cadiz valley lies between the Portimão Bank and the wrinkled surface of the Gulf of Cadiz accretionary wedge. The Sagres valley that lies in the prolongation of the Aljezur canyon establishes the connection between the drainage system located to the east of the Horseshoe Fault scarp and the Horseshoe Abyssal Plain. The Sagres valley displays a corrugate bottom north of the confluence with the Cadiz valley; from this point to the south it has a smooth surface and less dip. The flanks of the Sagres valley display various evidences of gravity slumping (Fig. 6B).

The Horseshoe valley is a roughly rectangular area, 80 km × 50 km, dipping to the west (mean dip of ~0.5°), connecting the Gulf of Cadiz seafloor and the Horseshoe Abyssal Plain across the Horseshoe Fault scarp (Fig. 1). The valley is limited by the Sagres plateau in the north, the Coral Patch Ridge in the south and the Gulf of Cadiz accretionary wedge in the east. It is cross cut by WNW–ESE trending morphological lineaments

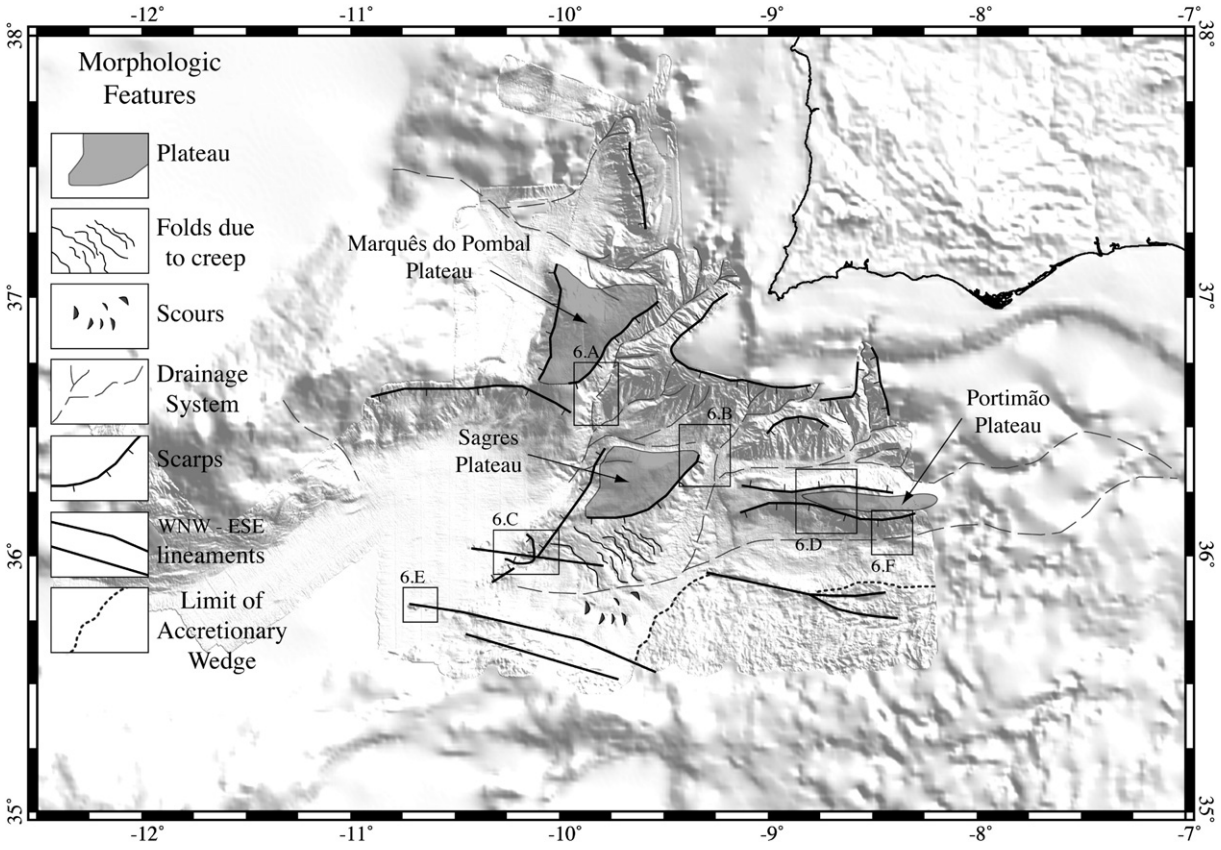


Fig. 5. Interpretative sketch of the morphology of the study area. 6.A to 6.F, locations of the features imaged in 3D in Fig. 6.

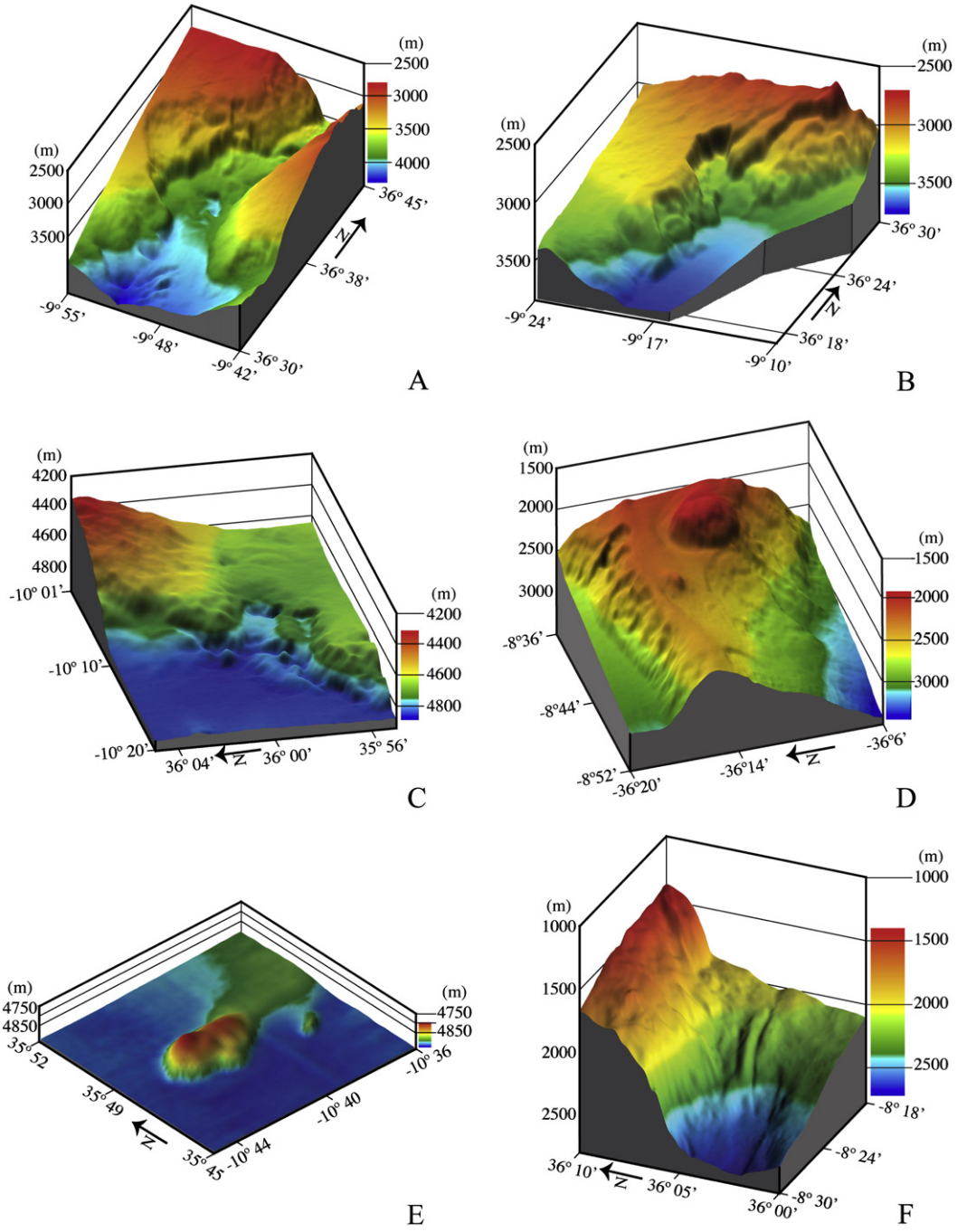


Fig. 6. 3D block diagrams of selected morphologic features of the study area. Images made from MATESPRO multibeam data presented in this work. A) Slide scar on the western flank of the S. Vicente canyon. B) Slide scar on the western flank of the Sagres valley. C) Slide scar on the Horseshoe fault scarp at the intersection with the WNW–ESE trending lineaments. D) D. Carlos salt diapir protruding through the top of the Portimão Bank (cf. with Fig. 10 for internal structure). Note the incisions on both flanks of the plateau, mainly on the northern side. E) E–W oriented hill in the Horseshoe Abyssal Plain sitting on top of one of the WNW–ESE trending lineaments. F) E–W trending channel at the foot of the Portimão Bank, whose structure in depth is imaged in MCS profile in Fig. 9. See text for detailed description.

described elsewhere in this paper. This wide valley collects the mouths of well developed canyons and valleys that drain the sediments from the north and eastern shelves. The drainage to the Horseshoe Abyssal Plain is poorly developed (Fig. 5) and the Horseshoe fault scarp is being eroded in various segments showing evidences of landsliding (Fig. 6C). These different styles and degrees of maturation of the sediment drainage pattern suggest that this area acts simultaneously as a by-pass and receptacle region for the sediments that are carried from the continental shelves to the Horseshoe Abyssal Plain.

Despite the general low slope of this area, there are NE–SW trending scarps with a maximum height of approximately 150 m (Fig. 7). The flat areas have maximum dips of 3° and slope breaks in which formed convex upwards crescent shaped escarpments. The crescent shaped three-dimensional features measure up to 5 km across, are shown in detail in Fig. 7 to occur between 3900 and 4700 mbsl, have an internal escarpment up to ~100 m high with an internal slope varying from 6° to 27°.

2.2. Plateaus and escarpments

The plateaus in the study area are the Marquês de Pombal, Sagres and Portimão plateaus (Figs. 1, 4 and 5). The Marquês de Pombal

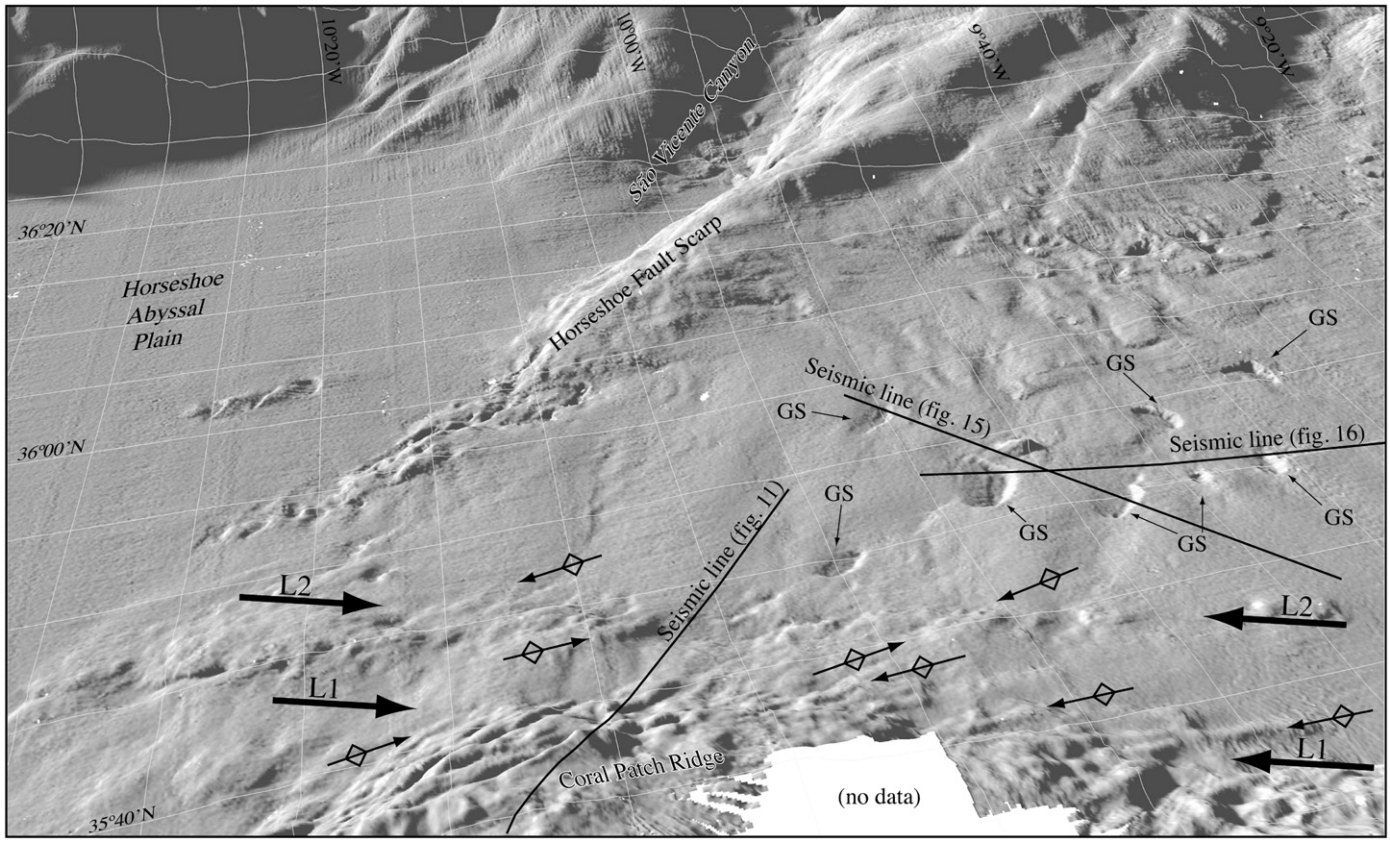


Fig. 7. Shaded relief image (perspective view) of the Giant Scours (GS), L1 and L2 WNW–ESE trending lineaments (interpreted as strike-slip faults, max. total length 250 km, see Fig. 11) and associated en echelon folds on sea floor recent sediments indicating dextral strike-slip movement component on the faults. Approximate depth 4000 m, confer with Figs. 1 and 4. Position of seismic lines in Figs. 11, 15 and 16 is also shown. Detail of the en echelon folds on L1 in the Horseshoe Abyssal Plain is shown in Fig. 6E.

plateau is a roughly rectangular surface bound by the NNE–SSW trending Marquês de Pombal reverse fault scarp in the west and by the São Vicente canyon in the east, as described by Gràcia et al. (2003a,b).

The Sagres plateau has an approximately rectangular shape divided by a diagonal NE–SW trending crest. To the west, the Sagres plateau is bound by the Horseshoe reverse fault scarp and the São Vicente canyon and by the Aljezur canyon and the Sagres Valley in the east. In the north this plateau is separated from the mid and upper continental slope and shelf by a rectilinear E–W trending valley that lies in the prolongation of the D. Carlos valley.

The Horseshoe fault scarp is only well developed on its northern segment. The southern part is being eroded (Fig. 6C) by the sediment drainage system described previously.

The southern part of the Sagres plateau dips gently towards the Horseshoe valley. This surface dips approximately 1.5°, is very uneven, and has a wavy appearance comprising undulations that vary from hundreds of meters to more than 10 km in length, and 0.5 km to 5 km across (Figs. 4 and 5).

The Portimão plateau is an E–W elongated surface limited by the two prominent escarpments which constitute flanks of the D. Carlos and Cadiz valleys. The northern escarpment is sinuous, while the southern one, is fairly rectilinear, trending WNW–ESE, draped by recent sediments carried by the local drainage. The top of this plateau shows circular positive reliefs, the larger one of which has been labeled here as the D. Carlos salt diapir (Figs. 1, 4 and 6D), whose origin is discussed elsewhere in this paper.

2.3. The Horseshoe Abyssal Plain

The extremely flat HAP has general slopes of less than 0.1° sharply contrasting with the slopes of the foot of its boundaries, between 5° and 10° in general.

The foot of the slope of the Gorringe Bank presents a remarkable offset of about 14 km at roughly 11°W (Fig. 4). This offset lies at the end of a valley that originates at the Gorringe saddle (see Fig. 1 for location). It is also clear that the southern flanks of the Gettysburg and Ormonde seamounts display fairly different topographic roughness. The Ormonde southern flank smooth topography resembles the morphological types of the continental slope or of the Sagres plateau, while the edges of the Gettysburg and Coral Patch Ridge display a similar wrinkled surface. It is possible that this offset and valley coincide with the ocean–continent boundary proposed by Rovere et al. (2004) at the Gorringe Bank.

The interior of the HAP is only locally perturbed by four elongated groups of hills that rise between 40 m and 200 m above seafloor (Fig. 4 and 6E). The largest of these groups is 16 km in length and the largest individual hill is 6 km long. The hills in each group are aligned along approximately E–W directions and each one of the hills has their crest parallel to NE–SW, approximately. These hills are aligned along the WNW–ESE oriented tectonic morphological lineaments described and discussed elsewhere in this paper.

2.4. Lineaments

Long WNW–ESE trending discrete lineaments of tectonic origin were for the first time revealed in the Gulf of Cadiz sea floor by the MATESPRO multibeam survey (Duarte et al., 2005 and Rosas et al., 2009). These lineaments consist of an aligned series of elongate WNW–ESE trending crests and troughs, more or less continuous, with a typical width of a few hundreds of meters (Figs. 4 and 7). Pervasive sets of E–W linear undulations, up to 8 km long, accompany these lineaments (Fig. 7). To the east of the Horseshoe escarpment these lineaments present uninterrupted segments as large as 100 km of length, approximately, while in the Horseshoe Abyssal Plain these

lineaments are discontinuous. Altogether, from the Gorringe Bank flank across the Horseshoe Abyssal Plain and lower continental slope of the Gulf of Cadiz, lineaments of 250 km can be identified, from approximately 4870 to 2000 mbsl (Fig. 4). It is worthwhile to note that various mud volcanoes sit on top of the lineaments (Figs. 2 and 4).

3. Structure of the NW part of the Gulf of Cadiz

A structural map of the study area based on the interpretation of the MATESPRO bathymetry and available MCS profiles is presented in Fig. 8. The main faults are here described based on MCS profiles that are quoted from published works or presented here. Fig. 8 also shows a compilation of focal mechanisms and main horizontal compression taken from Ribeiro et al. (1996).

3.1. WNW–ESE to E–W Faults

One of the most prominent features in the north-western part of the Gulf of Cadiz is the above described WNW–ESE to E–W trending set of valleys, escarpments and lineaments (Figs. 4 and 7). The seismic lines that are shown in Figs. 9–11 and hereafter described show that all these features are associated with faults, whose geometry and kinematic history are different.

The D. Carlos and Cadiz valleys that bound the Portimão plateau sit on top on two faults, as shown in Fig. 9. According to this the Portimão plateau can be interpreted as a pop-up structure. The D. Carlos valley lies at the south-western edge of the Guadalquivir acoustic basement high that, at the precise location of this seismic profile, bears a WNW–ESE strike as can be seen on the bathymetry (Fig. 4). The drag evident in the sediments of the uppermost sequence and the superficial gravity extensional faults indicate that the northernmost valley flank fault is undergoing extensional deformation at Present. The folds in the Mesozoic through Miocene–Lower Pliocene of the central and northern parts of the Portimão pop-up depict an asymmetry that indicates northwards tectonic transport on top of the acoustic basement fault.

Since it has been known for long that the Guadalquivir Bank is made up of Variscan basement metamorphosed flysch of Carboniferous age (e.g. Ribeiro et al., 1979; Gràcia et al., 2003a,b) the stratigraphy across the northern fault of the Faro valley implies that it played an extensional role during the Mesozoic followed by northwards directed thrusting during the Paleogene through Miocene and resumed extensional movement during Pliocene–Quaternary times.

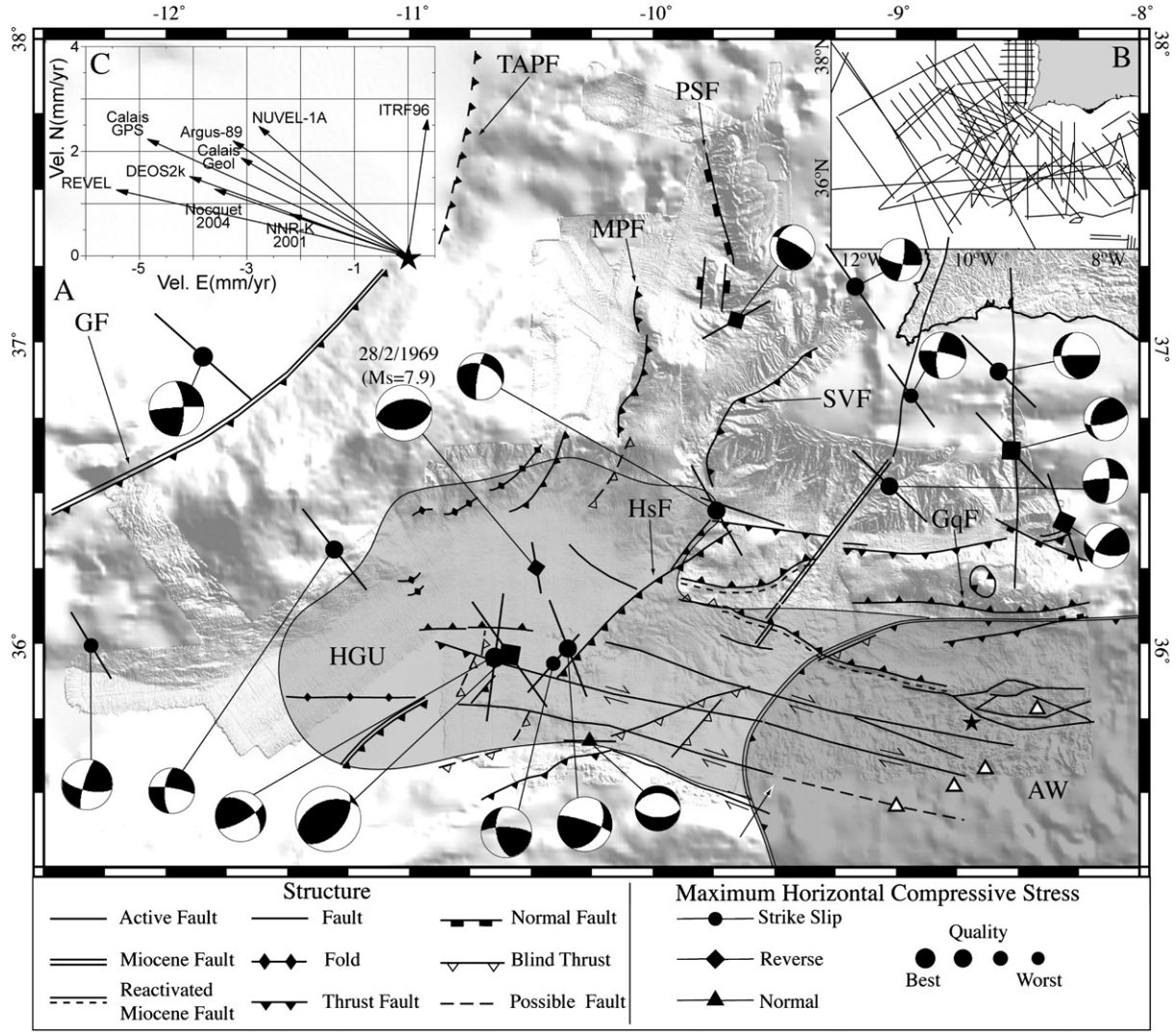


Fig. 8. A) Structural map of the study area with a compilation of stress indicators and focal mechanisms. Stress indicators computed from earthquake focal mechanisms and faults from interpretation of MCS profiles dataset shown in inset B). The size of the stress indicators is proportional to their quality. Note that the positions of mud volcanoes (white triangles) are in close spatial association with interpreted WNW–ESE dextral strike-slip faults. Fault names from published work as in Fig. 2. PbF — Portimão Bank fault; SVF — S. Vicente Fault; TAPF — Tagus Abyssal Plain Fault. B) Location of the MCS profiles used in this work. C) Plate kinematic data taken from various indicated sources indicated in the text. Black star shows position of computed movements of Nubia with respect to Iberia.

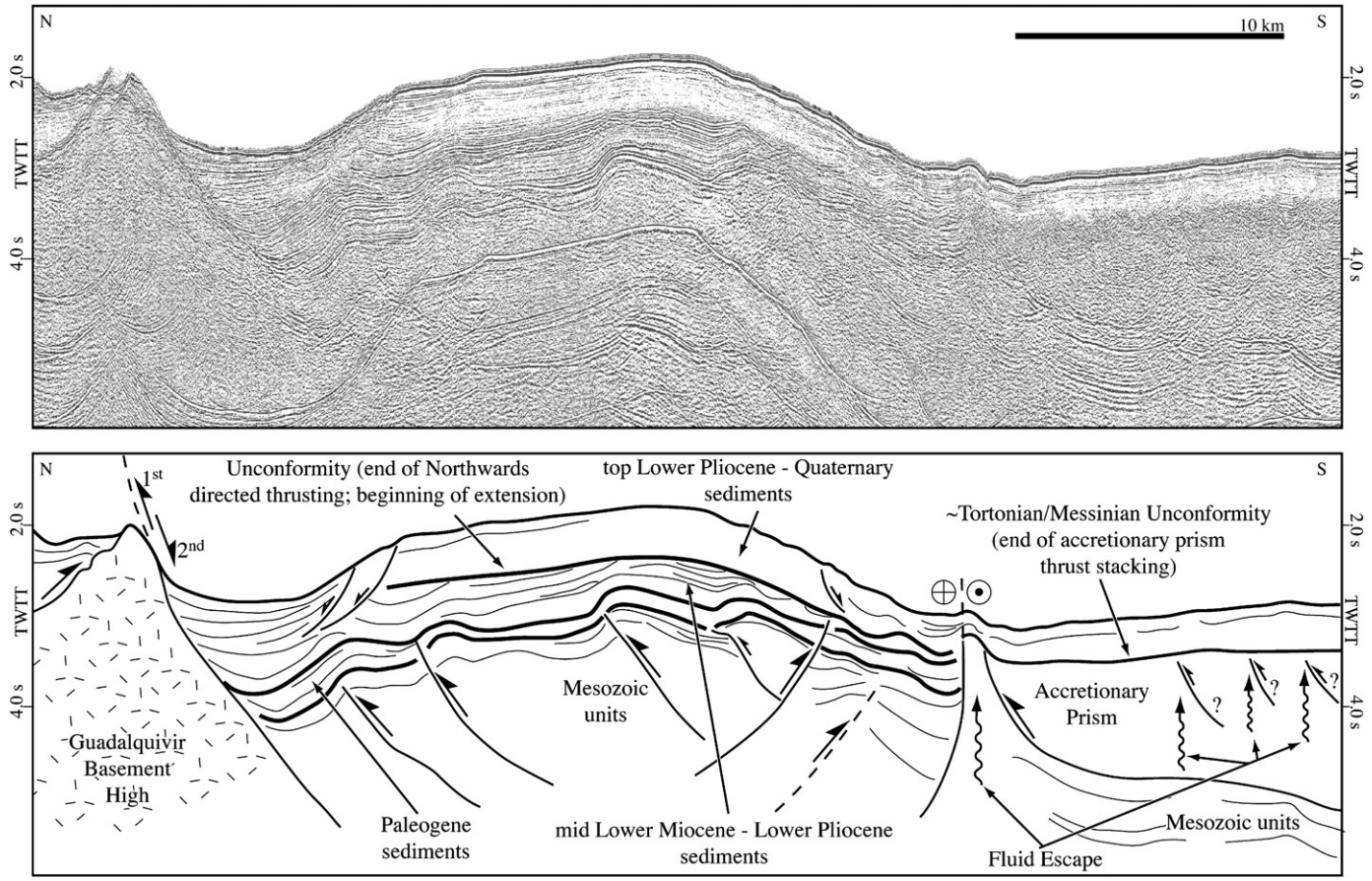


Fig. 9. Multi-channel seismic line VOLTAIRE 3 and line drawing interpretation. The Guadalquivir basement high of Carboniferous age is bound by a NW–SE trending Mesozoic extensional fault, reactivated as a reverse fault (1st movement) that resumed its extensional movement in late Miocene through Present times (see text for discussion, for location of line see Fig. 1). The topographic bulge on top of the strike-slip fault is imaged in 3D in Fig. 6F.

The southern boundary of the Portimão pop-up block shows both the topography and the Mesozoic through Quaternary sedimentary packages dipping to the south (Fig. 9). The following features are also evident in the seismic line across the southern part of Portimão plateau (Fig. 9), as follows: i) tectonic deformation affects the topmost sediments (Fig. 6F), ii) the pre-Pliocene folds asymmetry is southwards verging, iii) there is no correspondence on the seismic stratigraphy between the pre-Pliocene sediments of the Portimão pop-up and the southern counterpart and iv) the Mesozoic units show a wedge geometry. From these observations it is inferred that, firstly, this boundary of the Portimão plateau is an old fault with opposite dip with respect to the north boundary of the plateau, secondly, this was a northerly dipping extensional fault during the Mesozoic, thirdly, it was inverted with a southwards directed tectonic transport during the Paleogene through Miocene times and, fourthly it is going tectonic deformation at Present.

The southernmost segment of the seismic profile in Fig. 9 cuts across the Cadiz valley and up slope the gently dipping north western part of the Gulf of Cadiz accretionary wedge. The profile shows a sub-horizontal, mildly deformed sequence of sediments covering the chaotic seismic facies of the accretionary wedge or imbricate thrust wedge, as described by Gutscher et al. (2002) and Iribarren et al. (2007), respectively. The base of the chaotic seismic facies unit is made up by coherent high amplitude reflectors here interpreted as Jurassic through Cretaceous syn-rift sediments on top of which detached the thrust wedge. It is worthwhile to note that these sediments are disrupted by vertical discontinuities, with small vertical displacement, that can be followed up into the chaotic body and overlying topmost sequence.

The sub-vertical discontinuity that separates the Portimão plateau from the southern plain is neither compatible with thrusting nor with extensional tectonics (Fig. 9). Alternatively, it is interpreted as a transpressive E–W trending strike-slip fault at Present based on the fact that it displays evidence of shortening structures, folds and north wards and south wards directed thrusts on both sides of the fault. These observations imply that the main compression direction rotated from high angle to low angle with respect to the E–W strike of the faults, which is compatible with the counter-clockwise rotation of the movement of Africa with respect to Iberia in the Cenozoic, from approximately south to north in the Paleogene, to south east to north west in the Miocene to ESE to WNW in the Present (Dewey et al., 1989).

The circular dome protruding the top of the Portimão plateau depicted in the bathymetry is interpreted as D. Carlos salt diapir (Figs. 1, 4 and 10). The salt does not outcrop at the surface but is popping-up underneath the sedimentary cover. The two reverse faults that bound this structure were interpreted as smaller scale structures accommodating internal shortening across the Guadalquivir Bank by Zitellini et al. (2004). This is a clear example where the map view image clarifies specific not fully understood superficial structures in reflection seismics.

The deep structure of the WNW–ESE trending lineaments (Fig. 8) is imaged in the seismic profiles shown in Figs. 9, 10 and 11 in the work of Rosas et al. (2009). It can be seen in these seismic profiles that the rectilinear morphologic lineaments overlie vertical discontinuities that are rooted far below the accretionary wedge detachment, i.e. into the Jurassic sediments. These discontinuities cut the Mesozoic into blocks of 3–5 km of width, with small vertical offset and stratigraphic mismatch. The symmetry of the upward drag of the seismic horizons with respect to these discontinuities from the deepest stratigraphic levels across the chaotic facies, the disturbance observed in the cover

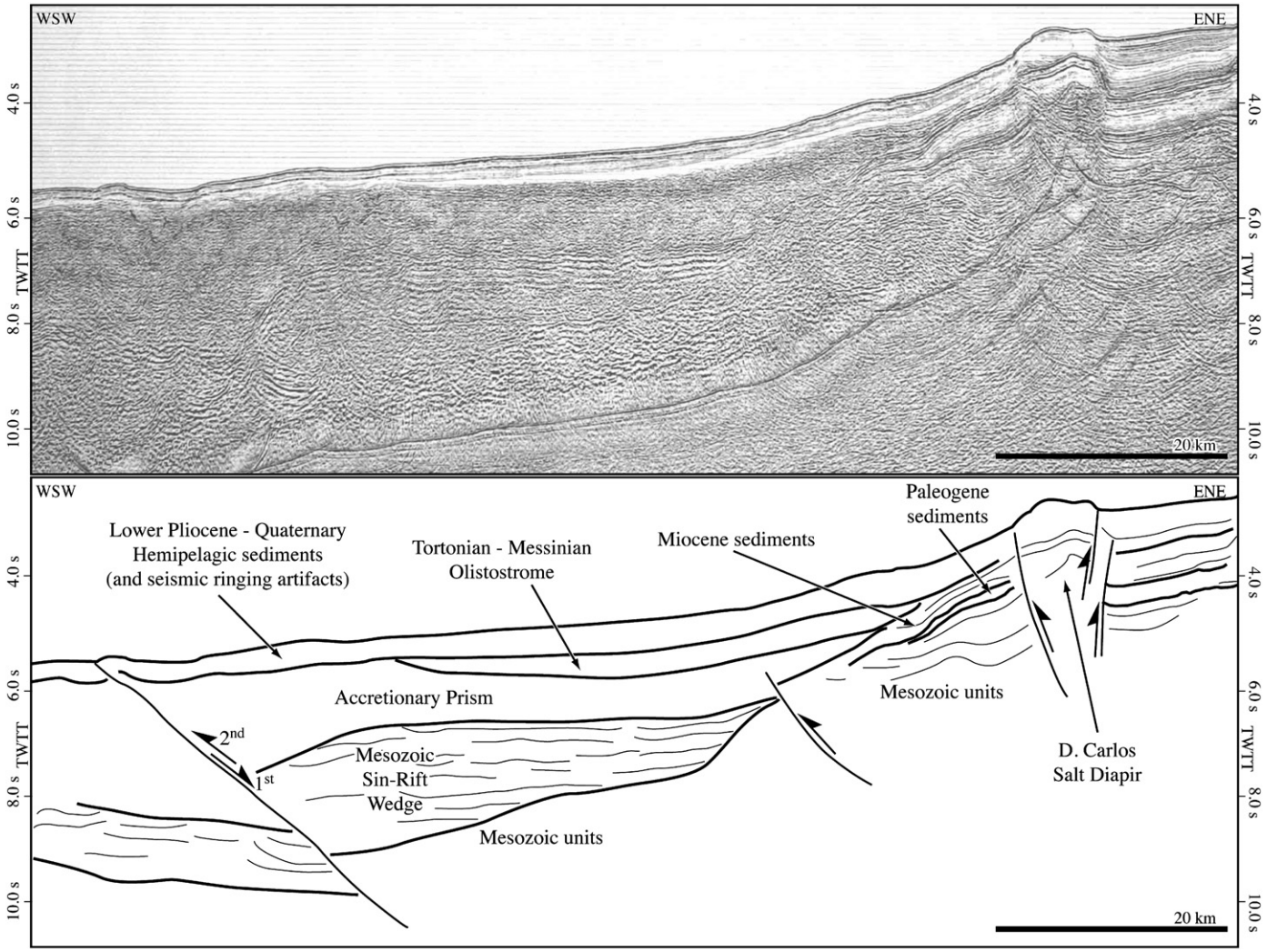


Fig. 10. Segment of multi-channel seismic line ARRIFANO 92-04 and line drawing interpretation. 1st and 2nd movements on main faults are of Jurassic–Cretaceous age and latest Miocene through Present, respectively. For location of seismic line see Fig. 3. The D. Carlos salt diapir 3D topography is shown in Fig. 6D.

sediments and the existence of mud volcanoes sitting on top of these lineaments (Figs. 8 and 12), strongly argues in favour of upward injection of fluids along these faults (cf. with Figs. 9 and 11). These characteristics strongly suggest that these discontinuities can correspond to tensile fractures with a strike-slip movement component.

The pervasive set of E–W trending undulations that accompany the E–W to WNW–ESE trending faults are en echelon folds (Figs. 7 and 11), i.e. kinematic indicators that show a dextral strike-slip lateral movement on these faults.

The growth wedge of Mesozoic sediments clearly associated to some of these WNW–ESE trending faults (Fig. 10) is another indication for the deep root of these faults.

3.2. N–S to NE–SW faults

The Aljezur canyon–Sagres valley and the Portimão canyon sit on top of the offshore prolongation of the Aljezur and Portimão faults, respectively (Figs. 2 and 8). Inspection of the seismic profiles confirms the Pliocene–Quaternary activity of these faults that show an important decrease in tectonic deformation after Miocene times (Figs. 12 and 13). The offshore mapping of these faults shows they have continuous segments larger than 100 km in length that, when added together with the onshore segments, they constitute discontinuous steep faults of approximately 200 km long, as happens with the left-lateral strike-slip late Variscan faults in the central and northern parts of the Iberian peninsula (Arthaud and Matte, 1977; Ribeiro, 2002), which are also active in the Quaternary (Cabral, 1989).

The Tagus Abyssal Plain Fault is proposed on the basis of the N–S trending sharp morphological scarp that lies to the north of the Gorringe Bank thrust. However, recent unpublished work by Cunha (2008) confirms the existence of this reverse fault that cross cuts Pliocene–Quaternary sediments.

The São Vicente Fault strikes NE–SW (Fig. 14) outcrops along the southeast flank of the São Vicente canyon. It is a southeastwards dipping steep fault, possibly part of the Odemira–Ávila fault (also known as the Messejana dyke), an approximately 600 km long vertical left-lateral late Variscan fault intruded by a basic dyke of Early Jurassic age (Dunn et al., 1998). Pliocene–Quaternary vertical displacement along this fault onshore was described by Cabral (1995).

The NE–SW trending Horseshoe fault was described as an active fault in the Present by Gràcia et al. (2003a,b) and Zitellini et al. (2004), and has a cluster of seismicity associated to it (Figs. 1 and 2). Its fault scarp is very well depicted in the MATESPRO bathymetry, from the Coral Patch Ridge well into the South Portuguese continental slope bordering the Sagres plateau. It can be seen that the height of the scarp increases northwards and it is intercepted by WNW–ESE trending faults. At these interceptions the Horseshoe fault scarp is either deflected or offset across the WNW–ESE dextral strike-slip faults and landslides formed (Figs. 4, 5, 6C and 8).

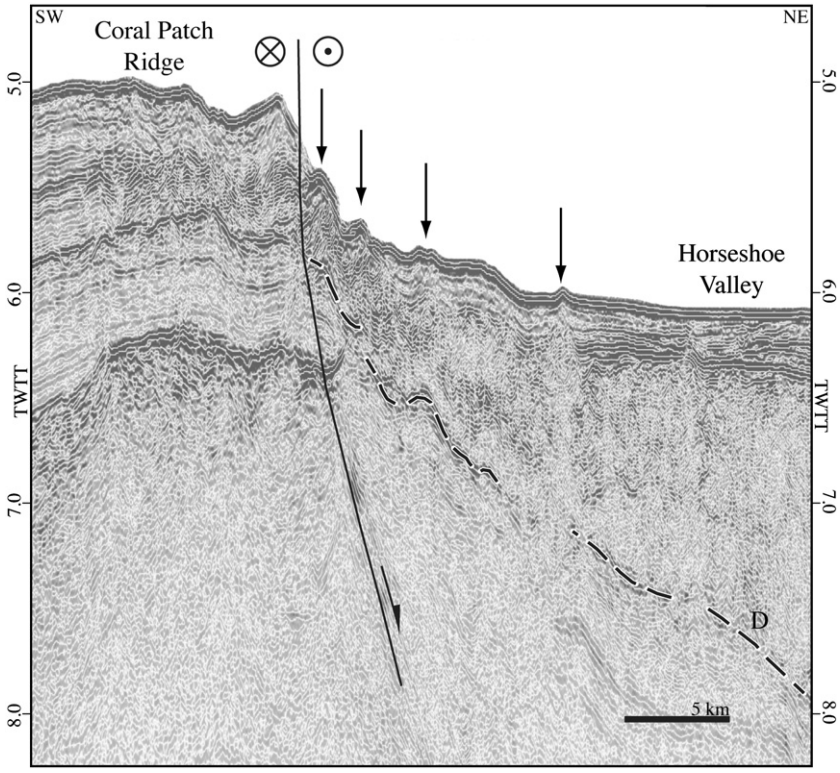


Fig. 11. Segment of multi-channel seismic profile IAM-3 at the contact between the Coral Patch Ridge (CPR) and the Horseshoe valley. Arrows point to folds in recent sediments on the seafloor as imaged on the MATESPRO bathymetry (see Figs. 3 and 7). Note that these faults cut across seismic discontinuity D that outlines the decollement of the seismic chaotic facies.

The NE–SW escarpments at the back of the Horseshoe fault host some of the crescent shaped Giant Scours described elsewhere in this work. These scarps sit on top of blind thrusts, as shown in Fig. 15 that appear to be recent reactivation of individual faults from within the Gulf of Cadiz Accretionary Wedge or Gulf of Cadiz Imbricate Unit, after Gutscher et al. (2002) or Iribarren et al. (2007), respectively. Single-channel seismic line across two of the Giant Scours show that the internal parts of the crescents consist of depressions filled in with upslope prograding sedimentary units. These units develop towards the Giant Scour crescent shaped scarp, which sharply truncates sediments behind it (Fig. 16).

3.3. Chaotic seismic units

The MATESPRO bathymetry clearly shows the divide between the wrinkled topography that overlies the Gulf of Cadiz Accretionary Wedge, after Gutscher et al. (2002) and the surrounding smoother areas (Figs. 2 and 4). The MCS profiles shown in Figs. 12 and 15 show the existence of a complex of stacked thrusts underneath the wrinkled surface of the so-called accretionary wedge and also under the smoother topography of the Sagres and Cadiz valleys.

In all seismic profiles it is evident that the complex of stacked thrusts is overlain by a package of sediments that is not involved in

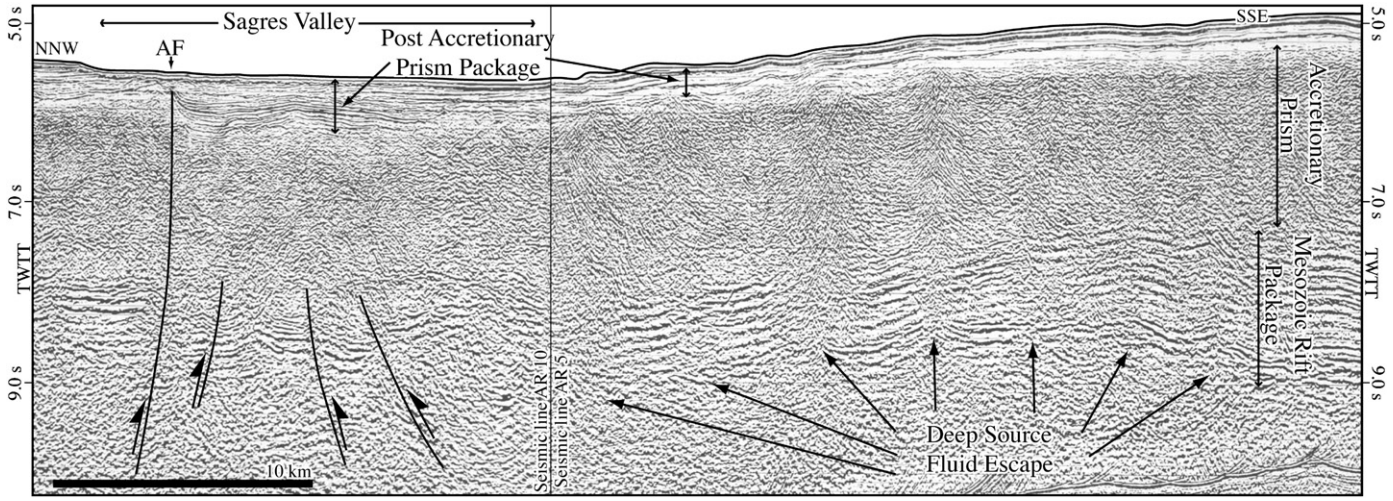


Fig. 12. Segment of multi-channel seismic line ARRIFANO 92-10 showing the deep origin of fluidized sediments breaching through the Mesozoic rift units and accretionary prism. Also note that the most recent unit is not involved in the thrust stacking tectonics of the accretionary wedge (see text for discussion, for location of line see Fig. 3). The steeply dipping north westernmost fault is the Aljezur fault bounding the deposits of the Sagres valley. Note that the chaotic body under the Sagres valley also has imbricated horizons but has no influence on the seafloor morphology (see text for discussion).

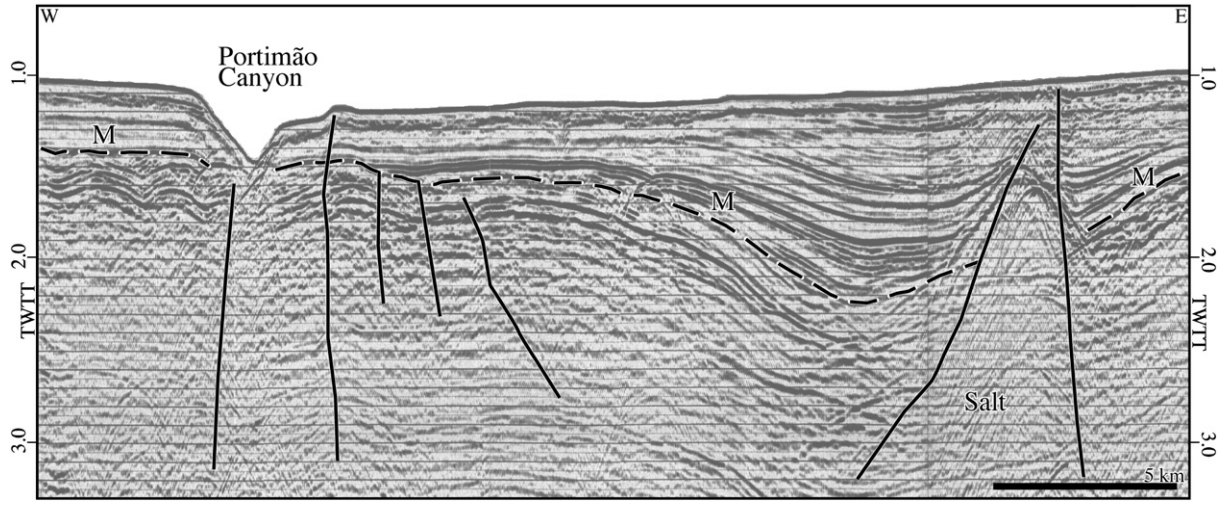


Fig. 13. Segment of multi-channel seismic line perpendicular to the Portimão canyon. Note that the Lower Miocene unconformity (M) truncates the folds that resulted from tectonic inversion on both sides of the Portimão canyon fault. However, mild deformation associated with this fault is visible on the eastern side of the fault and canyon. The salt-wall shown in the east of the profile also affects the recent sediments.

the thrust stacking. The thickness of this sedimentary cover is generally around 0.3–05 sec. TWT and the earliest age of these sediments is Early Pliocene after Roque (2007). However, this sedimentary cover is deformed by the E–W to WNW–ESE dextral strike-slip faults and by discrete reactivation of individual thrusts of the stacked thrusts units, as described elsewhere in this work, as well as, by widespread extrusion of mud volcanism, gravitational faulting described by various authors as mentioned before.

A unit of chaotic facies that has neither coherent internal layering nor imbricate fabrics, probably an olistostrome, is shown in Fig. 10. This unit is not involved in the thrust stacking of the accretionary wedge and is overlain by the well layered Pliocene–Quaternary sediments. This olistostrome lies between the Portimão Bank and the wrinkled surface of the Gulf of Cadiz Accretionary Wedge, in the Cadiz valley. It is worthwhile to note that the olistostrome pinches out on top of the Portimão Bank, suggesting that it could have been fed from the uplifted area of the Portimão Bank during the Tortonian phase of compression, i.e. the pop-up of the bank.

4. Discussion

4.1. Morphology and tectonics

4.1.1. The escarpments and seamounts

It was shown in this paper that the E–W trending Portimão Bank formed initially as a graben during Mesozoic times, was subsequently inverted during the Paleogene and Miocene compression and is now, probably since Early Pliocene times, undergoing dextral transpressive strike-slip deformation along its southern boundary, while the northern boundary experiences local extension due to a releasing bend formed by the basement fault. Seismicity and focal mechanisms (Fig. 2) attest for the compression at the southern edge of this seamount, preferentially concentrated to the east of the study area where the fault becomes NE–SW trending, i.e. at a higher angle to the main NW–SE oriented compression direction.

The Sagres plateau is bound by the NE–SW trending Horseshoe thrust of Miocene age in the west (Gràcia et al., 2003a,b, Zitellini et al., 2004) and the steeply dipping Aljezur fault in the east. The height of

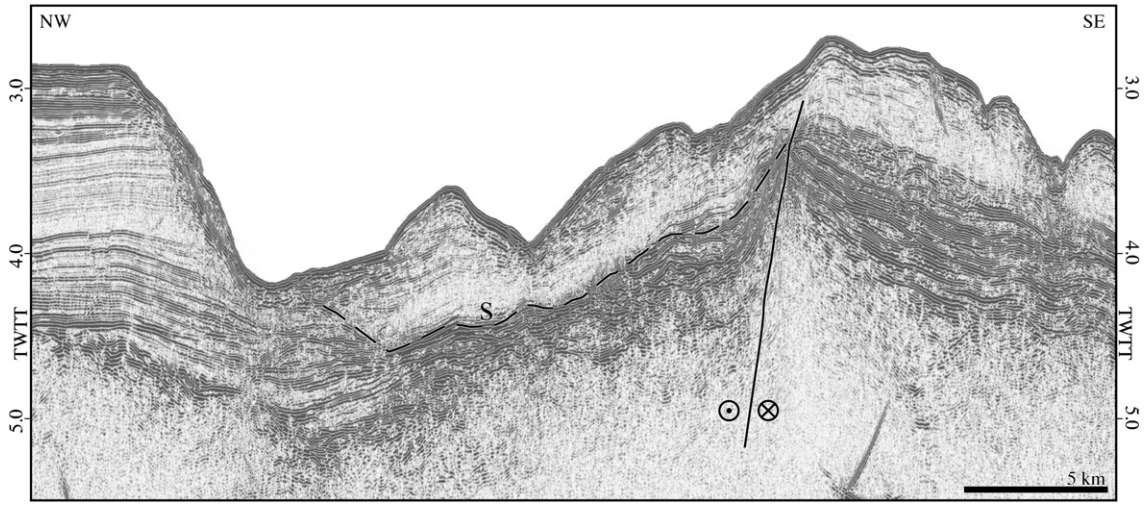


Fig. 14. Segment of multi-channel seismic line perpendicular to the S. Vicente canyon. Note the main fault controlling the position of the eastern flank of the canyon. This is a steep fault, possibly en echelon with the Messejana dyke fault (see text for description). Sediments on both sides of the fault are tilted and deformed including seismic reflector S, which is interpreted as a paleo-canyon bottom.

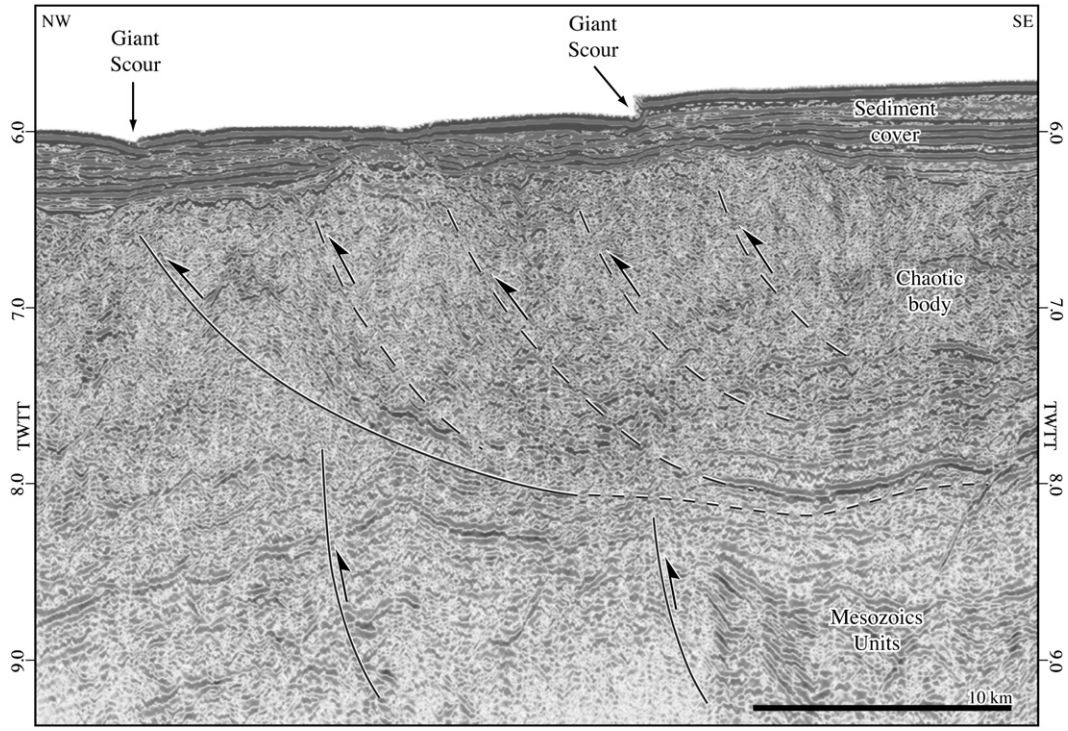


Fig. 15. Multi-channel seismic reflection profile across the Giant Scours. For location of the lines see Figs. 3 and 7. Seismic line IAM-4E shows the existence of stacked blind thrusts with present activity underneath the Giant Scours in the Sagres valley.

the plateau diminishes towards the south and its morphological expression disappears at the contact with one of the WNW–ESE strike-slip faults. The cluster of instrumental seismicity in Fig. 2 attests for its present day activity (Stich et al., 2007).

The Marquês de Pombal plateau also resulted from tectonic inversion of an N–S trending continent-wards directed extensional fault. The Pereira de Sousa fault is a N–S trending steep Mesozoic rift fault still in activity at Present (Terrinha et al., 2003; Gràcia et al., 2003a,b).

The north westwards directed Gorringe Bank thrust with a paroxysmal activity in the Tortonian (after Tortella et al., 1997; Sartori et al., 1994) is still an active structure as attested by the instrumental seismicity cluster (Fig. 2).

It can be concluded that the escarpments, seamounts and uplifted plateaus of the study area, all formed in association with compressive tectonic events and resulted from polyphase tectonics. The Pereira de Sousa fault escarpment is the only one that owes its morphology mostly to the Mesozoic rifting.

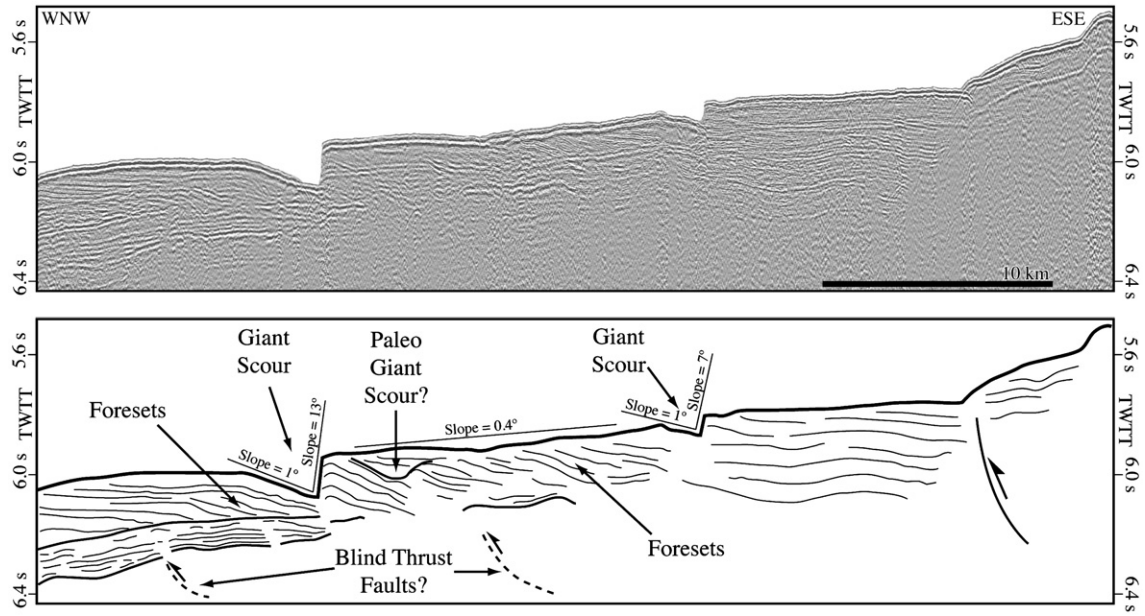


Fig. 16. Single-channel seismic line PSAT246 across two scours and line drawing interpretation. Note the erosive character of the escarpments and the sediments prograding towards the escarpment. For location see Figs. 3 and 7.

The tectonic shaping processes are still active in the Present, as shown by the on-going formation of very recent features that are indicative of uplift and tectonic instability, such as the popping-up of the D. Carlos salt diapir (Fig. 10), the mass wasting processes, such as submarine slides and various manifestations of soft sediment deformation and mass wasting processes in the Sagres plateau–Aljezur canyon, the São Vicente canyon and the Portimão plateau, Horseshoe Faul scarp, as well as, on the Marquês de Pombal, Gorringe and Pereira de Sousa escarpments as described by Gràcia et al. (2003a,b), Terrinha et al. (2003) and Vizcaino et al. (2006).

4.1.2. The Giant Scours

The Giant Scours are crescent shaped depressions with scarps that can reach more than 100 m high and slopes up to 27° located in a relative flat area of the Horseshoe Valley that collects the sediments from the Northern and North-eastern parts of the Gulf of Cadiz (Figs. 4, 5 and 7). The scours sit on the edge of folds draping Pliocene to Quaternary thrusting and the frontal depressions are filed up with upslope progradational bodies (Figs. 15 and 16). These bodies can be interpreted as been fed by material withdrawn from the retreating scarps (Fig. 17; Duarte et al., 2007). This scenario requires the existence of continuous scouring and sedimentation at unusual depths by means of bottom currents, possibly of turbidite origin as documented offshore the Shetland Islands and Monterrey East Channel (Kenyon et al., 2000; Kenyon et al., 2006; Fildani et al., 2006). The interaction of bottom and turbidity currents with seafloor morphological features formed by Recent tectonic activity can lead to flux separation and formation of vortexes that cause seafloor erosion and the formation of scours. These processes were proposed for the formation of similar structures in other places and different geological settings between 600 m and 3500 m water depth (Faugères et al., 1997; Bulat and Long, 2001; Verdicchio and Trincardi, 2006; Fildani et al., 2006). This process could account simultaneously for the formation of the scarp of the scour, the progradational bodies and the maintenance of the scarp, at least as long as the bottom current lasted and the retreating escarpment does not meet an obstacle.

An alternative model is that the Giant Scours could form due to the interaction of along slope bottom currents with the sea floor, such as the North Atlantic Deep Water. This interaction could lead to the formation of giant eddies that could locally erode and amplify pre-existing tectonic escarpments. However, the existence of along slope currents at these depths has not been documented in this area.

Evidences for alternative mechanisms for the formation of these features, such as slide–slump processes caused by slope instabilities or collapse processes associated with fluid escape along major tectonic structures (similar to those of pockmark formation), were not observed on the present dataset despite the evidences for mass wasting processes, and the existence of widespread mud volcanism and fluid migration activity in other areas of the Gulf of Cadiz.

4.1.3. The canyons

The São Vicente and Portimão canyons are by far the deepest incisions on the northern margin of the Gulf of Cadiz and they are underlain and controlled by important steep faults. The Aljezur canyon–Sagres valley system is also controlled by a steep fault. These offshore faults connect with others that were inherited from the late Variscan fracturing, subsequently reactivated during the Mesozoic rifting and Cenozoic tectonic inversion (see Fig. 2).

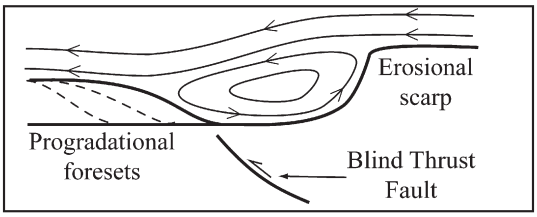


Fig. 17. Sketch of the effect of bottom currents on the retreat of the scarp and simultaneous progressive sedimentation of the progradation foresets. Scarp initially formed by uplift of hanging-wall on top of a blind thrust (see text for discussion).

The MCS profiles shown in this work attest for the Quaternary activity of these faults but also show that the deformation after Miocene times has severely diminished in the case of the Portimão and Aljezur faults.

Gràcia et al. (2003a,b) and Zitellini et al. (2004) showed the important activity of the northern segment of the Horseshoe fault that constitutes the eastern flank of the terminal part of the São Vicente canyon.

The São Vicente and Portimão canyons show important gravity slides on their western flanks. This can be interpreted as caused by the increase of the tilting associated with the west wards directed thrusting of the Marquês de Pombal and Horseshoe faults. Alternatively, in the Sagres valley the sliding can be caused by excavation at the meeting point of this valley with the Cadiz valley.

The minor present day tectonic deformation on the faults that control the localization of the canyons together with the important incision and land sliding close to the active Marquês de Pombal and Horseshoe thrusts can be interpreted as an indication of passive uplift of the continental slope carried on top of these thrusts.

4.1.4. The chaotic bodies

Three bodies of chaotic facies were distinguished in this work, all covered by unit hemipelagic sediments usually of 0.3–0.5 sec TWT. One is referred to as the Gulf of Cadiz Accretionary Wedge (GCAW) by Gutscher et al. (2002) or alternatively as the Gulf of Cadiz Imbricate Wedge by Iribarren et al. (2007). This body has a strong morphologic imprint on the seafloor morphology (Fig. 12).

A second one, that extends across the Horseshoe Abyssal Plain and Horseshoe Valley, has been considered as a gravitational unit, an olistostrome (e.g. Torelli et al., 1997; Iribarren et al., 2007). It is shown in this paper that this unit (Figs. 12 and 15) has imbricate seismic reflections that are interpreted as stacked thrusts, some of which have been recently reactivated forming blind thrusts morphologic scarps where the Giant Scours nucleated. These recent scarps are, however, the only morphologic manifestation on the seafloor surface of this body.

A third body with internal non-organized chaotic facies overlies the first described one, as shown in Fig. 10.

It is shown in this work that the two first described bodies consist of complexes of stacked thrusts and that the GCAW overthrusts the second one to the west (Fig. 10). Considering that these are tectono-stratigraphic units we speculate that only one accretionary wedge (or imbricate wedge) formed during the latest Cretaceous and Paleogene (perhaps through the Early Miocene). This event occurred before the Gibraltar arc formed (when the Internal Betic terranes were still a long way farther east, Fig. 18B). Then, from Early Miocene to earliest Pliocene (or Messinian?) times, when the Gibraltar orogenic arc formed, a part of this accretionary wedge was tectonically reworked forming the present day GCAW and its wrinkled topography (Fig. 18C). From the Pliocene to Present the thrust stacking within the GCAW severely diminished and the WNW–ESE dextral strike-slip faults formed (Fig. 18 D).

From a genetic point of view we consider the first two chaotic bodies as tectonic melanges made up of tectonised olistostromes and tectonosomes (see Camerlenghi and Pini, 2009 for discussion). The third chaotic body is a non tectonised olistostrome.

4.1.5. The WNW–ESE lineaments, strike-slip faults and recent folding

The WNW–ESE lineaments shown by the MATESPRO bathymetry in this paper (Fig. 7) display a series of en echelon folds materialized on the most recent seafloor soft sediments that indicate strain accumulation by means of dextral strike-slip (Figs. 3 and 6). Rosas et al. (2009) using quantitative strain analysis, analogue modelling and MCS data

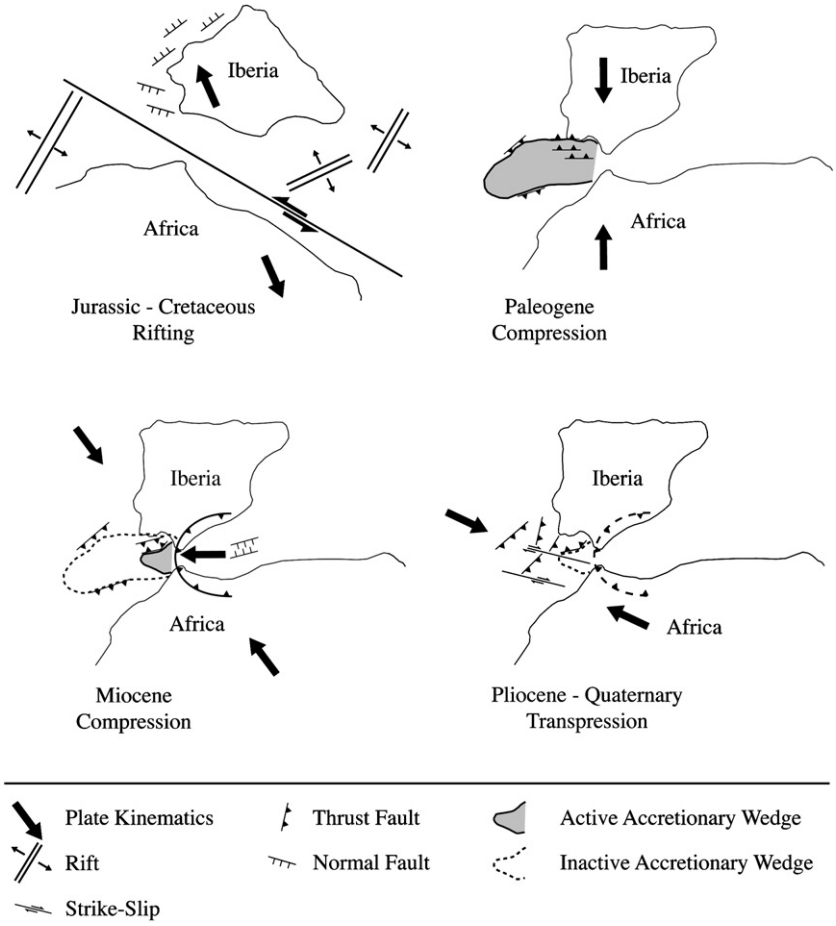


Fig. 18. Schematic tectonic evolution of the structure of the Gulf of Cadiz. In this simplified interpretation it is proposed the formation of an accretionary wedge (or thrust belt) that extended from Gibraltar across the Horseshoe Abyssal Plain during the latest Cretaceous–Paleogene compression. A second accretionary wedge formed (after Gutscher et al., 2002, or imbricate unit after Iribarren et al., 2007) during the Gibraltar orogenic arc westward overthrusting in Miocene times. In Pliocene–Quaternary times this accretionary wedge severely diminished its activity, the WNW–ESE dextral strike-slip faults formed and westward directed thrust increased along faults on the southern part of the West Portuguese Margin. See text for detailed discussion.

showed that these en echelon folds result from Quaternary reactivation of basement faults.

Inspection of MCS profiles in this paper show that these WNW–ESE faults are deeply rooted into the Jurassic–Cretaceous rift sequences, which is compatible to observations made onshore in the Algarve Basin at the Lower Jurassic of the S. Vicente cape (Ribeiro and Terrinha, 2007).

These faults also serve as conduits for the exhalation of fluidized sediments that form some of the Gulf of Cadiz mud volcanoes (Fig. 2), which is another evidence of the recent activity of the faults and also that they cut through the Gulf of Cadiz accretionary prism. Moreover, as shown on the MCS profile in Figs. 11 and 12, these strike-slip faults allow the escape of fluids from within deep in the Mesozoic sequences, probably at the Hettangian stratigraphic level that hosts the salt in south Portugal and northwest Morocco (Terrinha, 1998).

The strike-slip faults and folding are also active in the Horseshoe Abyssal Plain. However, the scarce morphotectonic features associated to these faults in the Horseshoe Abyssal Plain when compared to the continental slope to the east, suggests a westwards propagation of the recent deformation on the WNW–ESE faults, away from the Gibraltar Arc.

Because i) these faults have only recently been reactivated as strike-slip faults, ii) they strike at only a small angle to the present day trajectory of Africa with respect to Iberia, according to recently reported geodetic models (Fig. 8), iii) their minimum length exceeds 230 km as shown in the presented bathymetry and iv) they cut across the Horseshoe Abyssal Plain and the Gulf of Cadiz accretionary wedge; it is here suggested that they will play an important tectonic role in the new tectonic framework that is presently under development between Iberia and Nubia. As a matter of fact, some of the WNW–ESE faults described here are located within a 600 km × 40 km shear zone proposed by Zitellini et al. (2009) as a segment of the Eurasia–Nubia plate boundary that spans from the eastern tip of the Gloria Fault to the Rif–Tell plate boundary in north-western Morocco (Morel and Megrhraoui, 1996).

4.2. Strain partitioning, deformation migration and seismicity

The studied dataset shows that the E–W trending faults were inherited from the Jurassic–Lower Cretaceous rifting and subsequently inverted as reverse faults during the Cenozoic (Fig. 8); the same applies to the NE–SW to N–S trending faults as shown in previous works (Terrinha, 1998; Terrinha et al., 2002; Terrinha et al., 2003; Gràcia et al., 2003a; Rovere et al., 2004; Ribeiro and Terrinha, 2007). It was also shown that the Gulf of Cadiz accretionary wedge has diminished significantly its activity since latest Miocene times, possibly Early Pliocene, although disperse thrusts that still remain blind underneath the Messinian–Recent sediments are presently reactivated (Figs. 12 and 15).

Based on the presented dataset, we propose that the present day WNW–ESE convergent movement of Africa with respect to Iberia generates deformation in the study area, which is accommodated through partitioning on two approximately orthogonal fault sets, as follows. An N–S to NE–SW striking set of faults that accommodate shortening mainly by thrusting and an E–W to WNW–ESE striking, generally sub-vertical, set of faults that accommodate dextral strike-slip faulting.

The first set comprehends the main thrust faults of the area, Horseshoe Fault, Marquês de Pombal fault and Tagus Abyssal Plain

fault (see map of Fig. 2) that extend the Present east to west shortening for approximately 300 km from the South, near the contact with the Coral Patch Ridge (35.5°N), towards the north, along the West Portuguese Margin until a latitude of 38°N, as recently shown by Neves et al. (2009).

The second fault set is deeply rooted in Jurassic through Cretaceous rifting faults and were reactivated mainly in the Pliocene–Quaternary as dextral strike-slip faults, which is compatible with the present day movement of Nubia with respect to Iberia. These faults show considerably higher degree of deformation in the east than in the west, which argues in favour of propagation of deformation from east to west.

The thrusting on the N–S Marquês de Pombal fault is recent, as well as, on the Gorringe Bank fault (that had a quiescence period after the Tortonian), on the Tagus Abyssal Plain Fault (Cunha, 2008) and at the N–S trending faults at 38°N (Neves et al., 2009). Altogether, these observations lead us to argue that the deformation is migrating from the realm of Gibraltar to the west and along the Portuguese West Margin to the north.

Considering the sub-parallel strike of the N–S to NE–SW faults, their common origin in the Permian and reactivation during the Mesozoic rifting and Cenozoic inversion, it is here suggested that this 300 km en echelon fault zone can have a common detachment, underneath SW Iberia. Since the tomography data presented in Gutscher et al. (2002) suggest that the Horseshoe may penetrate at least till 100 km in the lithosphere, the 300 km long N–S trending fault system should be considered as *firstly,* a possible source candidate for the Lisbon 1/11/1755 earthquake and *secondly,* the propagation of a new front of compressive deformation towards the north along the West Portuguese Margin, which will eventually lead to the nucleation of a West Iberia incipient subduction zone, as proposed by Ribeiro et al. (1996).

Alternatively, even if these faults do not have a common detachment, a complex rupture scenario can be envisaged to explain the large energy released during the 1755 event. Complex seismic ruptures have been documented in other locations, such as, for instance the 1958 Gobi-Altay event which produced 260 km of surface rupture from the segmented main fault with a strike-slip movement and simultaneous rupture of nearby thrust faults (Kurushin et al., 1997), or the Tangshan earthquake of 1976, which was a combination of several ruptures, strike-slip and thrust faults, following each other only a few tens of seconds (Butler et al., 1979). The hypothesis of complex ruptures involving triggering or "domino-effect" is consistent with the majority of the historical documents that report a very long vibration (up to 20–30 min) and various sub-events for the 1st November 1755 earthquake (e.g. Martinez-Solares, 2001).

We also speculate that the location of recent epicentres in front of the Horseshoe fault in the Horseshoe Abyssal Plain, such as the 1969 event (Ms = 7.9) (Fukao, 1973), as well as the Mw = 6.0 12/02/2007 and the ML = 4.5 21/06/2006 events (Stich et al., 2007), all with a major dip-slip component can be interpreted as an indication of nucleation of new thrusts to the west of the main Horseshoe fault.

The NW–SE S_{Hmax} direction calculated from earthquake focal mechanism is in very good agreement with the Eurasia–Africa convergence direction estimated by the NUVEL-1 model (DeMets et al., 1994). However, recent estimates of this velocity using space geodetic techniques, and considering the Africa plate split into Nubia and Somalia, give for the Nubia–Eurasia collision a WNW–ESE direction, in the middle of the Gulf of Cadiz (Fig. 8). This discrepancy is interpreted as the coupled result of strain partitioning on E–W and NNE–SSW trending faults and aseismic deformation along the plate boundary.

5. Conclusions

The following conclusions are drawn.

1. The escarpments, seamounts and uplifted plateaus of the study area, all formed in association with polyphase compressive tectonic events from the late Cretaceous through Present, with the exception of the Pereira de Sousa fault escarpment that owes most of its morphology to the Mesozoic rifting. The Quaternary uplift has generated mass transport deposits (also reported by Gràcia et al. (2003a,b), Terrinha et al. (2003) and Vizcaino et al. (2006)), kilometric scale soft sediment unstable folds on the continental slope and incision of the canyons.
2. The Giant Scours display erosive and depositional structures that result from vortexes of high-density bottom currents at the edge of scarps formed at the crest of blind thrusts anticlines of Recent age.
3. The chaotic bodies buried under uppermost Miocene–lower Pliocene sediments in the Horseshoe Abyssal Plain and Horseshoe Valley together with the GCAW formed as stacked thrusts (possibly an accretionary wedge) in the Late Cretaceous–Earliest Miocene times before the emplacement of the Gibraltar orogenic Arc. Miocene reactivation of the eastern part of this body originated the GCAW and thrusting of this tectono-stratigraphic unit to the west. The third chaotic body corresponds to a non tectonised olistostrome that seals the most important thrust stacking in early Pliocene times.
4. The WNW–ESE trending lineaments are the superficial expression of steep faults deeply rooted in the Mesozoic substratum and underlying acoustic basement or Paleozoic basement onshore. Segments of these faults acted as rift faults during the Mesozoic and were reactivated in Quaternary times as strike-slip faults that cross cut the NE–SW trending thrusts.
5. The present day NW-wards movement of Nubia with respect to Iberia generates strain partitioning by means of dextral wrenching on WNW–ESE trending steep faults and thrusting on the NE–SW trending fault in the Gulf of Cadiz and Horseshoe Abyssal Plain. Further north, at the base of the continental slope of the southernmost part of the West Iberia Margin, NNE–SSW to N–S westerly dipping thrusts accommodate shortening in an area where wrenching has not been observed, which indicates that westward directed thrusting propagated from the Gibraltar Arc to the west (Horseshoe Fault) and to the north along the Portuguese margin (Marquês de Pombal Fault and Tagus Abyssal Plain Fault).

Acknowledgments

The work was sponsored by MATESPRO (PDCTM/P/MAR/15264/1999), EUROMARGINS SWIM (01-LEC-EMA09F), MVSEIS (01-LEC_EMA24F; PDCTM 72003/DIV/40018) and TOPOMED (TOPOEUROPE/0001/2007) projects and Instituto Scienze Marine (CNR) Bologna contribution 1630. JD and VV benefited from PhD grants from Fundação para a Ciência e a Tecnologia (SFRH/BD/31188/2006, SFRH/BD/17603/2004). We acknowledge the PARSIFAL Project MAR1998-1837-CE for the use of bathymetry data. We also wish to thank to the captain Cte. Paulo Marreiros and his crew of the *NRP D. Carlos I*. We acknowledge the financial support from the ESF EuroMargins Program, contract n. 01-LEC-EMA09F and from EU Specific Programme "Integrating and Strengthening the European Research Area", Sub-Priority 1.1.6.3, "Global Change and Ecosystems", contract n. 037110 (NEAREST). We acknowledge the support by Landmark Graphics Corporation via the Landmark University Grant Program.

References

Ambar, I., Serra, N., Brogueira, M.J., Cabecadas, G., Abrantes, F., Freitas, P., Gonçalves, C., Gonzalez, N., 2002. Physical, chemical and sedimentological aspects of the Mediterranean outflow off Iberia. Deep-Sea Research Part 2. Topical Studies in Oceanography 49, 4163–4177.

Argus, D.F., Gordon, R.G., DeMets, C., Stein, S., 1989. Closure of the Africa–Eurasia–North America plate motion circuit and tectonics of the Gloria fault. Journal of Geophysical Research 94 (B5), 5585–5602.

Arthaud, F., Matte, P., 1977. Late Paleozoic strike-slip faulting in Southern Europe and Northern Africa: result of a right-lateral shear zone between the Appalachians and the Urals. Geological Society of America Bulletin 88, 1305–1320.

Banda, E., Torné, M., IAM group, 1995. IAM group investigates deep structure of ocean margins: EOS (transaction of Am. Gephys. Union), 76, pp. 25–29.

Baptista, M.A., Miranda, P.M.A., Miranda, J.M., Victor, L.M., 1998. Constrains on the source of the 1755 Lisbon tsunami inferred from numerical modelling of historical data on the source of the 1755 Lisbon tsunami. Journal of Geodynamics 25 (1–2), 159–174.

Baptista, M.A., Miranda, J.M., Chierici, F., Zitellin, N., 2003. New study of the 1755 earthquake source based on multi-channel seismic survey data and tsunami modeling. Natural Hazards and Earth System Sciences 3, 333–340.

Bulat, J., Long, D., 2001. Images of the seabed in the Faroe–Shetland Channel from commercial 3D seismic data. Marine Geophysical Researches 22, 345–367.

Butler, R., Stewart, G.S., Kanamori, H., 1979. The July 27, 1976 Tangshan, China earthquake—a complex sequence of intraplate events. Bulletin of the Seismological Society of America 69 (1), 207–220.

Cabral, J., 1989. Na example of intraplate neotectonic activity, Vilariça Basin, Northeast Portugal. Tectonics 8 (2), 285–303.

Cabral, J., 1995. Neotectónica em Portugal Continental. Memórias do Instituto Geológico e Mineiro, Meméria 31, Lisboa, pp. 241.

Calais, E., Nocquet, J.-M., Jouanne, F., Tardy, M., 2002. Current strain regime in the Western Alps from continuous Global Positioning System measurements, 1996–2001. Geology 30 (7), 651–654.

Calais, E., DeMets, C., Nocquet, J.-M., 2003. Evidence for a post-3.16-Ma change in Nubia–Eurasia–North America plate motions? Earth and Planetary Science Letters 216, 81–92.

Camerlenghi, A., Pini, G.A., 2009. Mud volcanoes, olistostromes and Argille scagliose in the Mediterranean region. Sedimentology 56 (1), 319–365.

Carrilho, F., Teves-Costa, P., Morais, I., Pagarete, J., Dias, R., 2004. GEOALGAR Project: first results on seismicity and fault-plane solutions. Pure and Applied Geophysics 161 (3), 589–606.

Cunha, T., 2008. Gravity Anomalies, Flexure and the Thermo-Mechanical Evolution of the West Iberia Margin and its Conjugate of Newfoundland.; PhD Thesis, Department of Earth Sciences, University of Oxford.

DeMets, C., Gordon, R.G., Argus, D.F., Stein, S., 1994. Effect of recent revisions to the geomagnetic reversal time scale on estimates of current plate motions. Geophysical Research Letters 21 (20), 2191–2194.

Dewey, J.F., Helman, M.L., Turco, E., Hutton, D.H., Knott, S.D., 1989. Kinematics of the Western Mediterranean. In: Coward, M.P., Dietrich, D., Park, R.G. (Eds.), Alpine Tectonics: Geol. Soc. Spec. Publ., vol. No. 45, pp. 265–283.

Dias, R.P., 2001. Neotectónica da região do Algarve. Dissertação de doutoramento, Universidade de Lisboa, 369 pp.

Duarte, J.C., Rosas, F., Pinheiro, L.M., Matias, L.M., Carvalho, A.M., Terrinha, P., Ivanov, M., 2005. Interpretation of recent sedimentary and tectonic structures off SW Iberia from multibeam bathymetry, seismic reflection and experimental modeling. Geophysical Research Abstracts 7, 07867.

Duarte, J.C., Rosas, F., Terrinha, P., Valadares, V., Taborda, R., Matias, L., Roque, C., Magalhães, V., Henriet, J.P., Pinheiro, L., 2007. Deep Submarine Giant Scours in northern Gulf of Cadiz (offshore SW Iberia): a singular case of sedimentary and tectonic coupling. Geophysical Research Abstracts 9, 03940.

Dunn, A.M., Reynolds, P.H., Clarke, D.B., Ugidos, J.M., 1998. A comparison of the age and composition of the Shelburne dyke, Nova Scotia, and the Messejana Dyke, Spain. Canadian Journal of Earth Sciences 35 (10), 1110–1115.

Faccenna, C., Piromallo, C., Crespo-Blanc, A., Jolivet, L., Rossetti, F., 2004. Lateral slab deformation and the origin of the western Mediterranean arcs. Tectonics 23 (TC1012).

Faugères, J.C., Gonthier, È., Bobier, C., Griboulard, R., 1997. Tectonic control on sedimentary processes in the southern termination of the Barbados Prism. Marine Geology 140, 117–140.

Fernandes, R.M.S., Ambrosius, B.A.C., Noomen, R., Bastos, L., Wortel, M.J.R., Spakman, W., Govers, R., 2003. The relative motion between Africa and Eurasia as derived from ITRF2000 and GPS data. Geophysical Research Letters 30 (16).

Fildani, A., Normark, W.R., Kostic, S., Parker, G., 2006. Channel formation by flow stripping: large-scale scour features along the Monterey East Channel and their relation to sediment waves. Sedimentology 53, 1265–1287.

Fukao, Y., 1973. Thrust faulting at a lithospheric plate boundary, the Portugal earthquake of 1969. Earth and Planetary Science Letters 18, 205–216.

González, A., Córdoba, D., Vegas, R., Matias, L.M., 1998. Seismic crustal structure in the southwest of the Iberian Peninsula and the Gulf of Cadiz. Tectonophysics 296, 317–331.

Gràcia, E., Dañobeitia, J., Vergés, J., Bartolomé, R., 2003a. Crustal architecture and tectonic evolution of the Gulf of Cadiz (SW Iberian margin) at the convergence of the Eurasian and African plates. Tectonics 22 (4).

Gràcia, E., Danobeitia, J., Vergés, J., Cordoba, D., PARSIFAL Team, 2003b. Mapping active faults offshore Portugal (36°N–38°N): implications seismic hazard assessment along the southwest Iberian margin. Geology 31 (1), 83–86.

Gutscher, M.A., Malod, J., Rehault, J.-P., Contrucci, I., Klingelhoefer, F., Mendes-Victor, L., Spakman, W., 2002. Evidence for active subduction beneath Gibraltar. Geology 30 (12), 1071–1074.

Gutscher, M.-A., Dominguez, S., Westbrook, G.K., Gente, P., Babonneau, N., Mulder, T., Gonthier, E., Bartolome, R., Luis, J., Rosas, F., Terrinha, P., The Delila DelSis Scientific Teams, 2008. Tectonic shortening and gravitational spreading in the Gulf of Cadiz accretionary wedge: observations from multi-beam bathymetry and seismic profiling. Marine and Petroleum Geology 26, 647–659.

Hernandez-Molina, J., Llave, E., Somoza, L., Fernandez-Puga, M.C., Maestro, A., Leon, R., Medialdea, T., Barnolas, A., Garcia, M., del Rio, V.D., Fernandez-Salas, L.M., Vazquez, J.T., Lobo, F., Dias, J.M.A., Rodero, J., Gardner, J., 2003. Looking for clues to paleoceanographic imprints: a diagnosis of the Gulf of Cadiz contourite depositional systems. Geology 31 (1), 19–22.

Hernández-Molina, F.J., Llave, E., Stow, D.A.V., García, M., Somoza, L., Vázquez, J.T., Lobo, F.J., Maestro, A., Díaz del Río, V., León, R., Medialdea, T., Gardner, J., 2006. The contourite depositional system of the Gulf of Cádiz: a sedimentary model related to the bottom current activity of the Mediterranean outflow water and its interaction with the continental margin. Deep-Sea Research II 53, 1420–1463.

IOC, IHO and BODC, 2003. "Centenary edition of the GEBCO Digital Atlas", published on CDROM on behalf of the Intergovernmental Oceanographic Commission and the International Hydrographic Organization as part of the General Bathymetric Chart of the Oceans; British Oceanographic Data Centre, Liverpool.

Iribarren, L., Vergés, J., Camurri, F., Fullea, J., Fernàndez, M., 2007. The structure of the Atlantic–Mediterranean transition zone from the Alboran Sea to the Horseshoe Abyssal Plain (Iberia–Africa plate boundary). Marine Geology 243, 97–119.

Kenyon, N.H., Ivanov, M.K., Akhmetzanov, A., Akhmanov, G.G., 2000. Multidisciplinary study of geological processes on the North East Atlantic and Western Mediterranean Margins. IOC Technical Series, 56. UNESCO. 119 pp.

Kenyon, N.H., Ivanov, M., Akhmetzhanov, A., Koslova, E.V., 2006. Interdisciplinary geoscience studies of the Gulf of Cadiz and Western Mediterranean basins. : Intergovernmental Oceanographic Commission, Technical Series, 70. UNESCO. 115 pp.

Kreemer, C., Holt, W.E., 2001. A no-net-rotation model of present-day surface motions. Geophysical Research Letters 28 (23), 4407–4410.

Kurushin, R.A., Bayasgalan, A., Olziybat, M., Enhtuvshin, B., Molnar, P., Bayarsayhan, C., Hudnut, K.W., Lin, J., 1997. The surface rupture of the 1957 Gobi-Altay, Mongolia, Earthquake. Geological Society of America, Boulder.

Lopes, F.-C., Cunha, P.P., Le Gall, B., 2006. Cenozoic seismic stratigraphy and tectonic evolution of the Algarve Margin (offshore Portugal, southwestern Iberian Peninsula). Marine Geology 231, 1–36.

Maldonado, A., Somoza, L., Pallares, L., 1999. The Betic orogen and the Iberian–African boundary in the Gulf of Cadiz: geological evolution (central North Atlantic). Marine Geology 155 (1–2), 9–43.

Martinez-Solares, J.M., 2001. Los effectos en España del terremoto de Lisboa. Instituto Geografico Nacional, Madrid. 756 pp.

Medialdea, T., 2007. Estructura y evolucion tectonica del Golfo de Cadiz. Publicaciones del Instituto Geologico y Minero de España —Serie Tesis Doctorales N°8. ISBN 978-84-7840-728-2.

Medialdea, T., Vegas, R., Somoza, L., Vazquez, J.T., Maldonado, A., Diaz-del Rio, V., Maestro, A., Cordoba, D., Fernandes-Puga, M.C., 2004. Structure and evolution of the "Olistostrome" complex of the Gibraltar Arc in the Gulf of Cádiz (eastern Central Atlantic): evidence from two long seismic cross-sections. Marine Geology 209 (1 –4), 173–198.

Morel, J.L., Megrhraoui, M., 1996. Gorringe–Alboran–Tell tectonic zone: a transpression system along the Africa–Eurasia plate boundary. Geology 24 (8), 755–758.

Mulder, T., Voisset, M., Lecroart, P., Drezen, E.L., Gonthier, E., Hanquiez, V., Faugères, J.-C., Habgood, E., Hernandez -Molina, F.J., Estrada, F., Llave -Barranco, E., Poirier, D., Gorini, C., Fuchey, Y., Voelker, A., Freitas, P., Sanchez, F.L., Fernandez, L.M., Kenyon, N.H., Morel, J., 2003. The Gulf of Cadiz: an unstable giant contouritic levee. Geo -Marine Letters V23 (1), 7–18.

Neves, M.C., Terrinha, P., Afilhado, A., Moulin, M., Matias, L., Rosas, F., 2009. Response of a multi-domain continental margin to compression: study from seismic reflection–refraction and numerical modelling in the Tagus Abyssal Plain. Tectonophysics 468, 113–130.

Niemann, H., Duarte, J., Hensen, C., Omoregie, E., Magalhaes, V.H., Elvert, M., Pinheiro, L.M., Kopf, A., Boetius, A., 2006. Microbial methane turnover at mud volcanoes of the Gulf of Cadiz. Geochimica et Cosmochimica Acta 70 (21), 5336–5355.

Nocquet, J.M., Calais, E., 2004. Geodetic measurements of crustal deformation in the Western Mediterranean and Europe. Pure and Applied Geophysics 161, 661–681.

Pinheiro, L.M., Wilson, R., Pena dos Reis, R., Whitmarsh, R.B., Ribeiro, A., 1996. In: Whitmarsh, R.B., Sawyer, D.S., Klaus, A., Masson, D.G. (Eds.), The Western Iberia Margin: a Geophysical and Geological Overview. : Proceedings of the Ocean Drilling Program, Scientific Results, 149. Ocean Drilling Program, College Station, TX, pp. 3–23.

Pinheiro, L.M., Ivanov, M.K., Sautkin, A., Akhmanov, G., Magalhaes, V.H., Volkonskaya, A., Monteiro, J.H., Somoza, L., Gardner, J., Hamouni, N., Cunha, M.R., 2003. Mud volcanism in the Gulf of Cadiz: results from the TTR-10 cruise. Marine Geology 195, 131–151.

Pinheiro, L.M., Ivanov, M., Kenyon, N., Magalhães, V., Somoza, L., Gardner, J., Kopf, A., Van Rensbergen, P., Monteiro, J.H., Team, Euromargins MVSEIS, 2006. Structural control of mud volcanism and hydrocarbon-rich gas seepage: results from the TTR-15 and other previous cruises. Fluid seepages/mud volcanism in the Mediterranean and Adjacent Domains. CIESM Workshop Monographs 29, 53–58.

Ribeiro, A., 2002. Soft Plate and Impact Tectonics. Springer-Verlag. 324 pp.

Ribeiro, C., Terrinha, P., 2007. Formation, deformation and chertification of systematic clastic dykes in a differentially lithified carbonate multilayer. SW Iberia, Algarve Basin, Lower Jurassic. Sedimentary Geology 196 (1–4), 2001–2015.

Ribeiro, A., Antunes, M.T., Ferreira, M.P., Rocha, R., Soares, A., Zbyszewski, G., Moitinho de Almeida, F., 1979. Introduction à la géologie générale du Portugal. Serv. Geol. Portugal. 114 pp.

Ribeiro, A., Cabral, J., Baptista, R., Matias, L., 1996. Stress pattern in Portugal mainland and the adjacent Atlantic region, West Iberia. Tectonophysics 15 (2), 641–659.

Roque, C., 2007. Tectonostratigrafia do Cenozóico das margens continentais Sul e Sudoeste portuguesas: um modelo de correlação sismostratigráfica. Universidade de Lisboa, Departamento de Geologia.

Rosas, F.M., Duarte, J.C., Terrinha, P., Valadares, V., Matias, L., 2009. Morphotectonic characterization of major bathymetric lineaments in NW Gulf of Cadiz (Africa–Iberia plate boundary): insights from analogue modelling experiments. Marine Geology 261, 33–47.

Rosenbaum, G., Lister, G.S., Duboz, C., 2002. Reconstruction of the tectonic evolution of the western Mediterranean since the Oligocene. In: Rosenbaum, G., Lister, G.S. (Eds.), Reconstruction of the evolution of the Alpine-Himalayan Orogen. Journal of the Virtual Explorer, 8, 107–126.

Rovere, M., Ranero, C.R., Sartori, R., Torelli, L., Zitellini, N., 2004. Seismic images and magnetic signature of the Late Jurassic to Early Cretaceous Africa–Eurasia plate boundary off SW Iberia. Geophysical Journal International 158 (2), 554–568.

Sartori, R., Torelli, L., Zitellini, N., Peis, D., Lodolo, E., 1994. Eastern segment of the Azores–Gibraltar line (central–eastern Atlantic): an oceanic plate boundary with diffuse compressional deformation. Geology 22, 555–558.

Sella, G., Dixom, T., Mao, A., 2002. REVEL: a model for Recent plate velocities from space geodesy. Journal of Geophysical Research 107.

Sillard, P., Altamimi, Z., Boucher, C., 1998. The ITRF96 realization and its associated velocity field. Geophysical Research Letters 25 (17), 3223–3226.

Somoza, L., Díaz-del-Río, V., León, R., Ivanov, M.K., Fernández-Puga, M.C., Gardner, J.M., Hernández-Molina, F.J., Pinheiro, L.M., Rodero, J., Lobato, A., Maestro, A., Vázquez, J.T., Medialdea, T., Fernández-Salas, L.M., 2003. Seabed morphology and hydrocarbon seepage in the Gulf of Cádiz mud volcano area: acoustic imagery, multibeam and ultra-high resolution seismic data. Marine Geology 195, 153–156.

Srivastava, S.P., Roest, W.R., Kovacs, L.C., Oakey, G., Levesque, S., Verhoef, J., Macnab, R., 1990. Motion of Iberia since the Late Jurassic: results from detailed aeromagnetic measurements in the Newfoundland Basin. Tectonophysics 184 (3–4), 229–260.

Stich, D., Serpelloni, E., Mancilla, F.-L., Morales, J., 2006. Kinematics of the Iberia–Maghreb plate contact from seismic moment tensors and GPS observations. Tectonophysics 426, 295–317.

Stich, D., Mancilla, F.de L., Pondrelli, S., Morales, J., 2007. Source analysis of the February 12th 2007, M_w 6.0 Horseshoe earthquake: implications for the 1755 Lisbon earthquake. Geophysical Research Letters 34, 12.

Terrinha, P., 1998. Structural Geology and Tectonic Evolution of the Algarve Basin, South Portugal. Department of Geology, University of London, London.

Terrinha, P., Dias, R.P., Ribeiro, A., Cabral, J., 1999. The Portimão Fault, Algarve Basin, South Portugal. Comunicacões do Instituto Geológico e Mineiro 86, 107–120.

Terrinha, P., Ribeiro, C., Kullberg, J.C., Rocha, R., Ribeiro, A., 2002. Compression episodes during rifting and faunal isolation in the Algarve Basins, SW Iberia. Journal of Geology 110, 101.113.

Terrinha, P., Pinheiro, L.M., Henriet, J.-P., Matias, L., Ivanov, M.K., Monteiro, J.H., Akhmetzhanov, A., Volkonskaya, A., Cunha, T., Shaskin, P., Rovere, M., 2003. Tsunamigenic–seismogenic structures, neotectonics, sedimentary processes and slope instability on the southwest Portuguese Margin. Marine Geology 195 (1–4), 55–73.

Torelli, L., Sartori, R., Zitellini, N., 1997. The giant chaotic body in the Atlantic Ocean off Gibraltar: new results from a deep seismic reflection survey. Marine and Petroleum Geology 14 (2), 125–134.

Tortella, D., Torné, M., Pérez-Estáun, A., 1997. Geodynamic Evolution of the Eastern Segment of the Azores–Gibraltar Zone: the Gorringe Bank and the Gulf of Cadiz Region. Marine Geophysical Researches 19 (3), 211–230.

USGS, 2004. Shuttle Radar Topography Mission, 1 Arc Second scene SRTM_u03_n008e004, Unfilled Unfinished 2.0, Global Land Cover Facility. University of Maryland, College Park, Maryland. February 2000.

Van Rensbergen, P., Depreiter, D., Pannemans, B., Moerkerke, G., Van Rooij, D., Marsset, B., Akhmanov, G., Blinova, V., Ivanov, M., Rachidi, M., Magalhaes, V.H., Pinheiro, L.M., Cunha, M.R., Henriet, J.-P., 2005. The El Arraiche mud volcano field at the Moroccan Atlantic slope, Gulf of Cadiz. Marine Geology 219 (1), 1–17.

Verdicchio, G., Trincardi, F., 2006. Short-distance variability in slope bed-forms along the Southwestern Adriatic Margin (Central Mediterranean). Marine Geology 234, 271–292.

Vizcaino, A., Gracia, E., Pallas, R., Garcia-Orellana, J., Escutia, C., Casas, D., Willmott, V., Diez, S., Asioli, A., Danobeitia, J., 2006. Sedimentology, physical properties and age of mass transport deposits associated with the Marques de Pombal Fault, Southwest Portuguese Margin. Norwegian Journal of Geology 86 (3), 177–186.

Voelker, A., Lebreiro, S., Schonfeld, J., Cacho, I., Erlenkeuser, H., Abrantes, F., 2006. Mediterranean outflow strengthening during northern hemisphere coolings: a salt source for the glacial Atlantic? Earth and Planetary Science Letters 245, 39–55.

Zitellini, N., Chierici, F., Sartori, R., Torelli, L., 1999. The tectonic source of the 1755 Lisbon earthquake and tsunami. Annali di Geofisica 42 (1).

Zitellini, N., Mendes, L. A., Cordoba, D., Danobeitia, J., Nicolich, R., Pellis, G., Ribeiro, A., Sartori, R., Torelli, L., Bartolomé, R., Bortoluzzi, G., Calafato, A., Carrilho, F., Casoni, L., Chierici, F., Corela, C., Correggiari, A., Della Vedova, B., Gràcia, E., Jornet, P., Landuzzi, M., Ligi, M., Magagnoli, A., Marozzi, G., Matias, L., Penitenti, D., Rodriguez, P., Rovere, M., Terrinha, P., Vigliotti, L., Zahinos Ruiz, A., 2001. Source of 1755 Lisbon Earthquake and Tsunami Investigated. Eos Trans. AGU, 82, (26), 285, 290–291.

Zitellini, N., Ligi, M., Matias, L., Rovere, M., the Shipboard Scientific Parties, 2002. Voltaire 2002 Cruise Report. IGM-CNR Technical Report.

Zitellini, N., Rovere, M., Terrinha, P., Chierici, F., Matias, L., Team, B., 2004. Neogene through quaternary tectonic reactivation of SW iberian passive margin. Pure and Applied Geophysics 161, 565–587.

Zitellini, N., Gracia, E., Matias, L., Terrinha, P., Abreu, M.A., DeAlteriis, G., Henriet, J.P., Dañobeitia, J.J., Masson, D.G., Mulder, T., Ramella, R., Somoza, L., Diez, S., 2009. The quest for the Africa–Eurasia plate boundary west of the Strait of Gibraltar. Earth and Planetary Science Letters 280 (1–4), 13–50.

Marine Geology 261 (2009) 33–47

Contents lists available at ScienceDirect

Marine Geology

journal homepage: www.elsevier.com/locate/margeo

Morphotectonic characterization of major bathymetric lineaments in Gulf of Cadiz (Africa–Iberia plate boundary): Insights from analogue modelling experiments

F.M. Rosas [a,*], J.C. Duarte [a,b], P. Terrinha [b], V. Valadares [b], L. Matias [c]

[a] LATTEX, IDL, Universidade de Lisboa, Departamento de Geologia da Faculdade de Ciências, Edifício C6, Piso 4, 1749-016 Lisboa, Portugal
[b] LATTEX, IDL, INETI, Departamento de Geologia Marinha do INETI, Estrada da Portela Zambujal-Alfragide Apartado 7586, 2720-866 Amadora, Portugal
[c] CGUL, IDL, Universidade de Lisboa, Departamento de Física da Faculdade de Ciências, Edifício C8, Piso 6, 1749-016 Lisboa, Portugal

ARTICLE INFO

Article history:
Received 22 October 2007
Received in revised form 1 July 2008
Accepted 6 August 2008

Keywords:
Gulf of Cadiz
morphotectonic lineaments
seismotectonic interpretation
analogue modelling
dextral wrenching
low-angle transpression

ABSTRACT

New high-resolution multi-beam bathymetry data allowed the recognition of several bathymetric lineaments (ca. 100 km long, trending WNW–ESE) in seafloor sediments of the Gulf of Cadiz, offshore SW Iberia. The interpretation of multi-channel (MCS) profiles crosscutting these lineaments showed that they are controlled by underlying deep seated faults, which have endured a polyphase reactivation history. To get insights on the Recent tectonic evolution of these structures, we performed two sets of analogue modelling experiments, assuming: 1) right-lateral strike-slip basement faulting and coupled passive shearing affecting an overlying soft cover; and 2) low-angle transpressive deformation along a narrow shear band overlying the fault. Our results show a good correlation between the experimentally obtained structural patterns and the natural morphotectonic lineaments, allowing the use of some of the observed natural features as strain gauges. Based on this, we conclude that the study lineaments correspond to the bathymetric expression of ongoing dextral wrenching reactivation of WNW–ESE pre-existing faults, and we estimate the age of this tectonic reactivation as being ca. 1.8 Ma (i.e. form late Pliocene to Present day). These characteristics agree with the most recent kinematic models derived from geodetic observations, indicating that Present day convergence between Nubia and Iberia is subparallel to the newly identified lineaments and occurs at a 4 mm/yr rate.

© 2008 Elsevier B.V. All rights reserved.

1. Introduction

The Gulf of Cadiz area, located West of the Gibraltar Strait, offshore SW Iberia and NW Morocco (Fig. 1), has been increasingly recognized as a critical site for the understanding of the tectonics related with the Africa (Nubia)–Iberia plate boundary (e.g. Sartori et al., 1994; Zitellini et al., 1999; Maldonado et al., 1999; Gutscher et al., 2002; Gracia et al., 2003; Terrinha et al., 2003; Gutscher, 2004; Zitellini et al., 2001, 2004; Medialdea et al., 2004; Thiebot and Gutscher, 2006; Terrinha et al., under review). This boundary extends along the WNW–ESE Azores–Gibraltar line, comprising to the West the Azores triple junction and the Gloria fault, and to the East the Gulf of Cadiz domain (Fig. 1A). In this domain, the average direction of the Maximum Horizontal Compressive Stresses (S_{Hmax}), deduced from earthquake focal mechanisms, is ~N45W (Ribeiro et al., 1996; Borges et al., 2001), meanwhile recently reported geodetic models show the existence of WNW–ESE oblique convergence between Nubia and Iberia, at a Present day rate of approximately 4 mm/yr (e.g. Nocquet and Calais, 2004; Stich et al., 2006; Fernandes et al., 2007, inset of Fig. 1B). Recent mapping of the main tectonic structures in the area (Fig. 1B) suggests that compression is presently being dissipated in a complex manner, essentially through inter-plate brittle deformation, characterized by the development of different structures with different orientations and kinematics. Previously reported earthquake recurrence data, epicentre location data, and focal mechanisms (Buforn et al., 1995, 2004; Borges et al., 2001; Stich et al., 2005, 2006) point to a general scenario of moderate magnitude seismicity, mostly related to thrusting and strike-slip movement, along numerous faults at shallow to intermediate depths (above 60 km). This area is also prone to high magnitude earthquakes and destructive tsunami like the 1/11/1755 Great Lisbon Earthquake (estimated magnitude between 8.5 and 8.8, e.g. Abe, 1979; Johnston, 1996; Martínez-Solares and López Arroyo, 2004). Other large magnitude events, such as the 28/02/1969 earthquake (Ms = 7.9) occurring in the Gulf of Cadiz illustrate the practical need to improve our knowledge regarding the Present day tectonic evolution of this key region.

In this work we present new results concerning the study of several major bathymetric lineaments, recorded in recent seafloor sediments of the NW Gulf of Cadiz area. These features were firstly recognized using the high-resolution multi-beam bathymetry recently acquired during the MATESPRO campaign (MAjor TEctonic and Sedimentary PROcesses in the Portuguese Margins, Terrinha et al.,

* Corresponding author. Tel.: +351 21 7500375; fax: +351 21 7500064.
E-mail address: frosas@fc.ul.pt (F.M. Rosas).

0025-3227/$ – see front matter © 2008 Elsevier B.V. All rights reserved.
doi:10.1016/j.margeo.2008.08.002

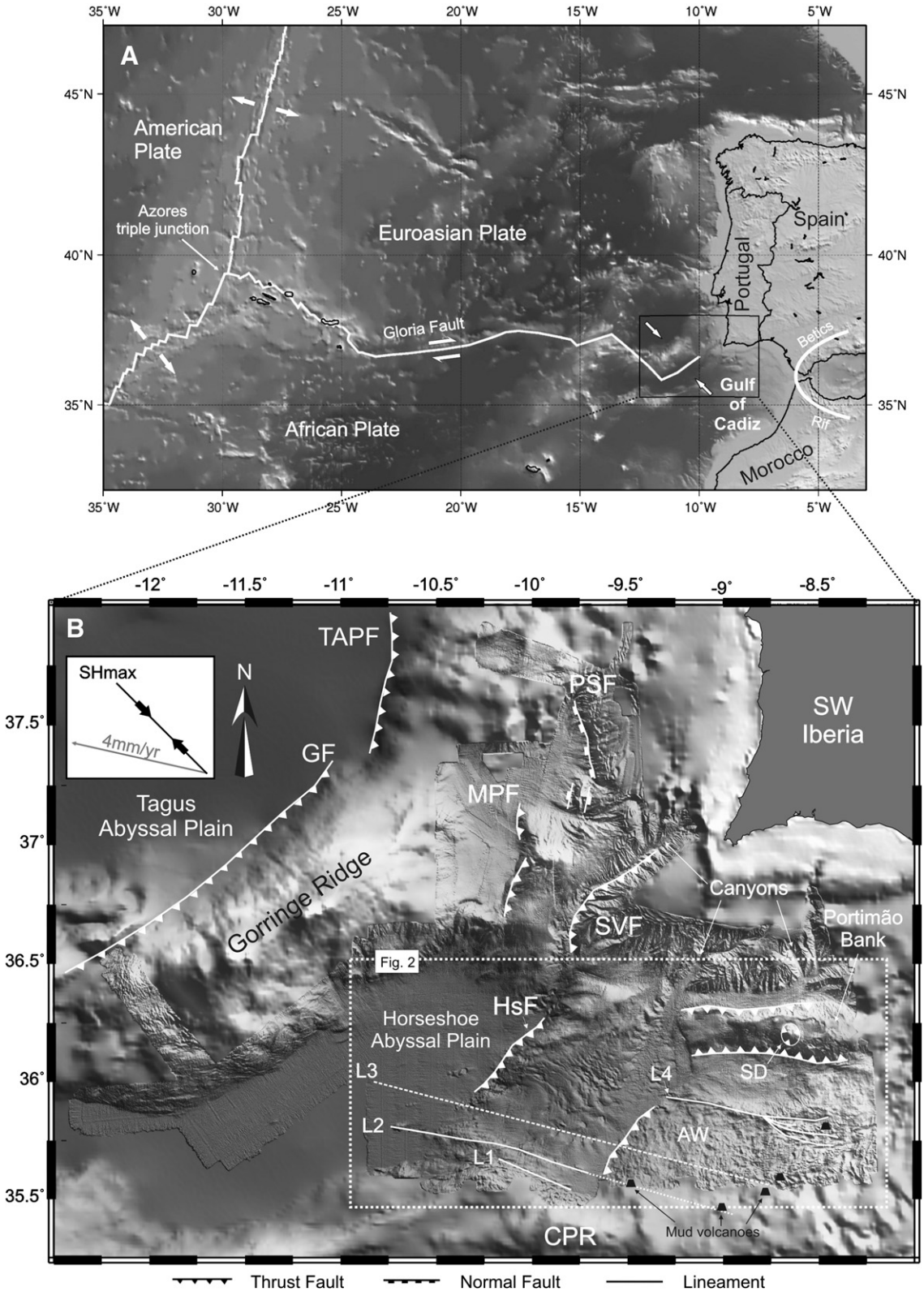


Fig. 1. (A) Location of the Gulf of Cadiz area in the general tectonic setting of the Euroasia (Iberia)–Africa (Nubia) plate boundary (Bathymetry GEBCO 2000; Plate boundaries according to model PB2002 of Bird, 2003); (B) Simplified tectonic map of the NW Gulf of Cadiz area (bathymetry corresponds to the PARSIFAL 2000, HITS 2001, and MATESPRO 2004 surveys, completed by GEBCO 2000). Inset in the upper left showing (in black) the average direction of the Maximum Horizontal Stresses—S_{Hmax}, and (in grey) the direction of the 4 mm/yr convergence rate between Nubia and Iberia (Nocquet and Calais, 2004; Stich et al., 2006; Fernandes et al., 2007). TAPF—Tagus Abyssal Plain Fault; GF—Gorringe Fault; PSF—Pereira de Sousa Fault; MPF—Marques de Pombal Fault; SVF—Sao Vicente Fault; HsF—Horseshoe Fault; SD—D. Carlos Salt Diapir; AW—Accretionary wedge; CPR—Coral Patch Ridge; L1–L4—Bathymetric lineaments.

under review), and were subsequently studied using several multi-channel seismic (MCS) profiles. In addition, several analogue modelling experiments were carried out to get new insight on their origin, kinematic evolution and tectonic meaning. This was done through comparison of the obtained experimental results with the correspondent natural examples, which showed that some morphotectonic patterns associated to the lineaments could be used in a quantitative manner, as natural strain gauges, allowing a better understanding of the main tectonic processes at stake.

2. Morphotectonic characterization of the study objects

2.1. Morphologic description

The new MATESPRO bathymetry dataset obtained in NW Gulf of Cadiz revealed a complex geomorphology, interpreted as the result of the combined action of different processes such as tectonics, sedimentation, gravity, and submarine erosion (Terrinha et al., under review). These data allowed, for the first time, the identification of several major bathymetric lineaments (L1 to L4 in Fig. 2). These linear features strike approximately WNW–ESE, exhibiting widths of a few kilometres (typically 1.5 km to 3 km), and maximum bathymetric lengths of ca. 100 km. L1 is best characterized by sets of discontinuous oblique (W–E) morphologic undulations, consisting in alternating crest and troughs up to 6 km long, displaying a general en-échelon geometrical disposition (Fig. 3A,B and C); L2 exhibits an overall more continuous morphology, characterized by two main wide elevated areas, elongated along strike, and located on opposite sides of a central linear trough (Fig. 3D).

Unlike the previous described lineaments, L3 is barely seen in the high-resolution bathymetry. The L4 lineament, although clearly observable in the bathymetry, does not show any consistently interpretable morphologic patterns, probably due to the incoherent rheology response to stress of the tectonic mélange of the Gulf of Cadiz accretionary wedge (see AW in Fig. 1B). For much of its length, L4 coincides with the northern border of this disturbed seafloor domain, suggesting that it may be controlled by a deep structure. Because of these features in the present work we will concentrate on L1 and L2 as the main targets for our analogue modelling.

2.2. Structural characterization

The MCS reflection profiles which crosscut the lineaments L1 to L3 show that these coincide with deep seated faults (Figs. 2 and 4). Taking into account the previously established seismostratigraphy in the area (e.g. Sartori et al., 1994; Torelli et al., 1997; Tortella et al., 1997), the interpretation of different segments of the IAM line (Fig. 4) shows that these faults cut through Mesozoic units (Jurassic to Cretaceous age), and through a late Miocene (Tortonian) body with a typical chaotic seismic signature. They also often seem to coincide with possible paths of abundant upwards fluid migration, seemingly originated at the base of the Mesozoic (Fig. 4A), and previously recognized by several authors in this area (e.g. Somoza et al., 2003; Pinheiro et al., 2003; Hensen et al., 2007).The upper units of the seismostratigraphic sequence correspond to hemipelagic sediments of Plio-Quaternary age, with thickness varying between 0.3 and 0.6 s TWT. In the IAM3 line, the fault corresponding to the L1 lineament, bordering the north-eastern flank of the Coral Patch Ridge (CPR, Fig. 4), is interpreted has having behaved as a reverse fault, since the Mesozoic reflectors in the hanging wall reveal a folding geometry congruent with shortening (Fig. 5). Based only on these profiles it was not possible to ascribe a definite kinematic evolution to the other (L2 and L3) faults. The Plio-Quaternary hemipelagic sediments, although some times locally folded, are generally not cut by the described faults (Fig. 4B). This suggests that the reverse fault kinematics mentioned above, does not correspond to the Present day active kinematics on these structures.

Both the morphological and structural description of the study objects points to the conclusion that these lineaments correspond to the bathymetric expression of major WNW–ESE trending faults. The examined MCS lines show the Plio-Quaternary hemipelagic sediments sealing the faults (Fig. 4), suggesting that the bulk movement along these structures does not correspond to active thrusting. Furthermore, the en-échelon crests and troughs associated to L1 seem compatible with a Present day dextral wrenching reactivation (Fig. 3A, B and C).

The same MCS lines also show that the fault associated to L2 extends along ca. 200 km, from the accretionary wedge in the East, coinciding with several previously described mud volcanoes (e.g. Pinheiro et al., 2003), to the Horseshoe abyssal plain in the West, where it looses its morphologic expression (Figs. 1B and 2). It should

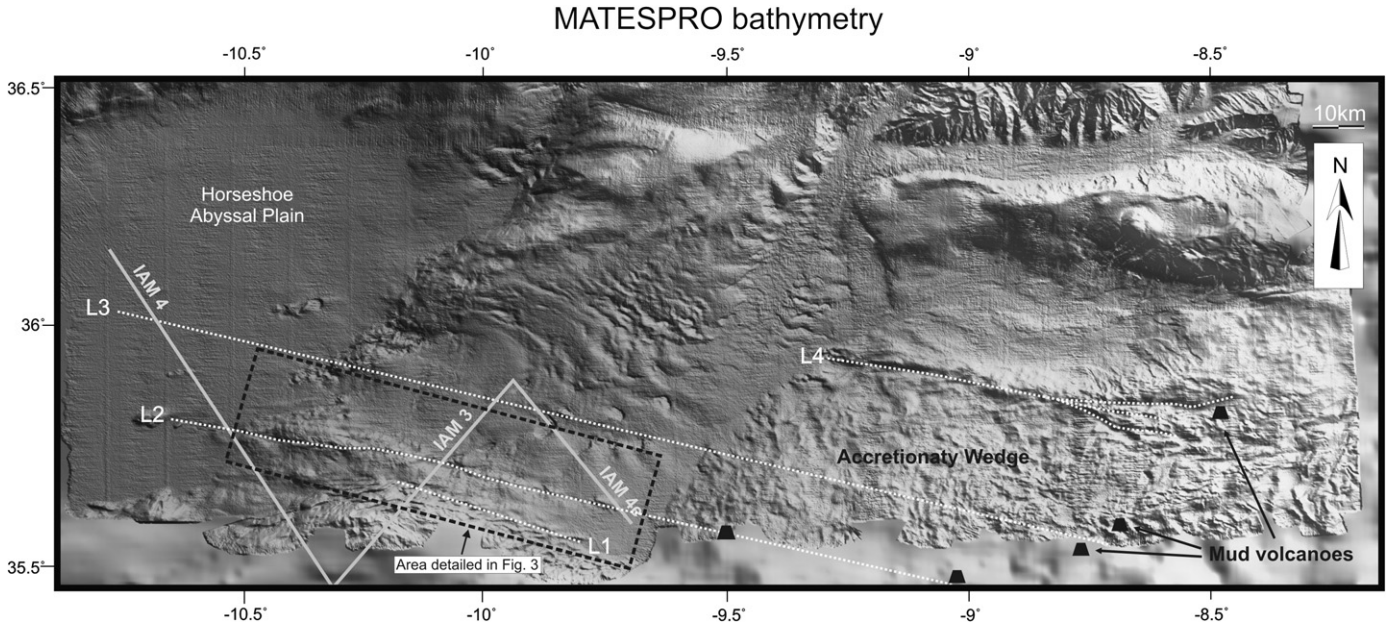
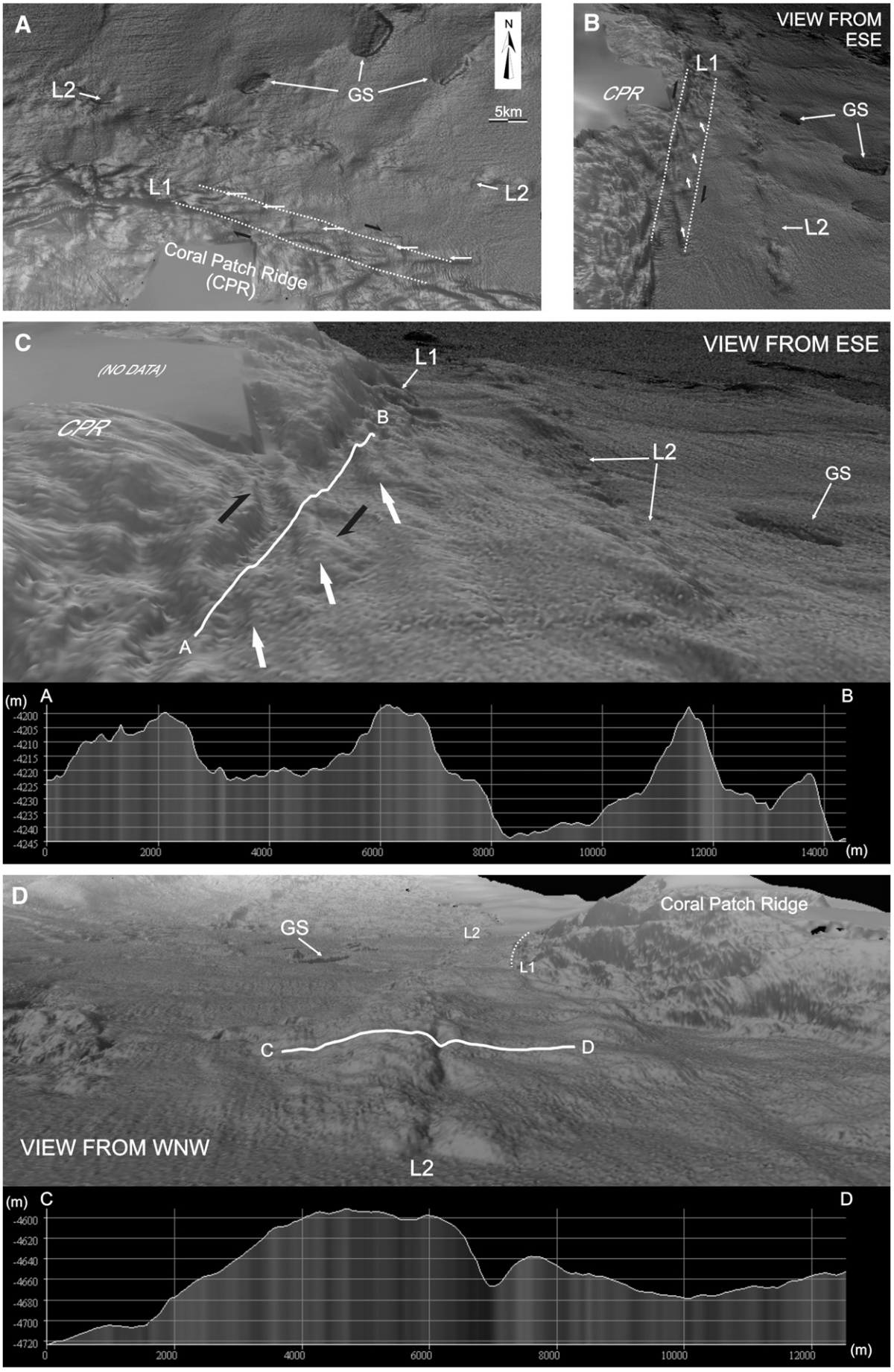


Fig. 2. Bathymetry of NW Gulf of Cadiz MATESPRO campaign, Terrinha et al. (under review). Location of the IAM multi-channel seismic reflection profiles intersecting the (L1 to L3) lineaments, interpreted in Fig. 4.


A
N
L2
GS
5km
L1
L2
Coral Patch Ridge
(CPR)
B
VIEW FROM
ESE
L1
CPR
GS
L2
C
VIEW FROM ESE
(NO DATA)
L1
CPR
B
L2
GS
A
(m)
A
B
-4200
-4205
-4210
-4215
-4220
-4225
-4230
-4235
-4240
-4245
0
2000
4000
6000
8000
10000
12000
14000
(m)
D
Coral Patch Ridge
GS
L2
L1
C
D
VIEW FROM WNW
L2
(m)
C
D
-4600
-4620
-4640
-4660
-4680
-4700
-4720
0
2000
4000
6000
8000
10000
12000
(m)

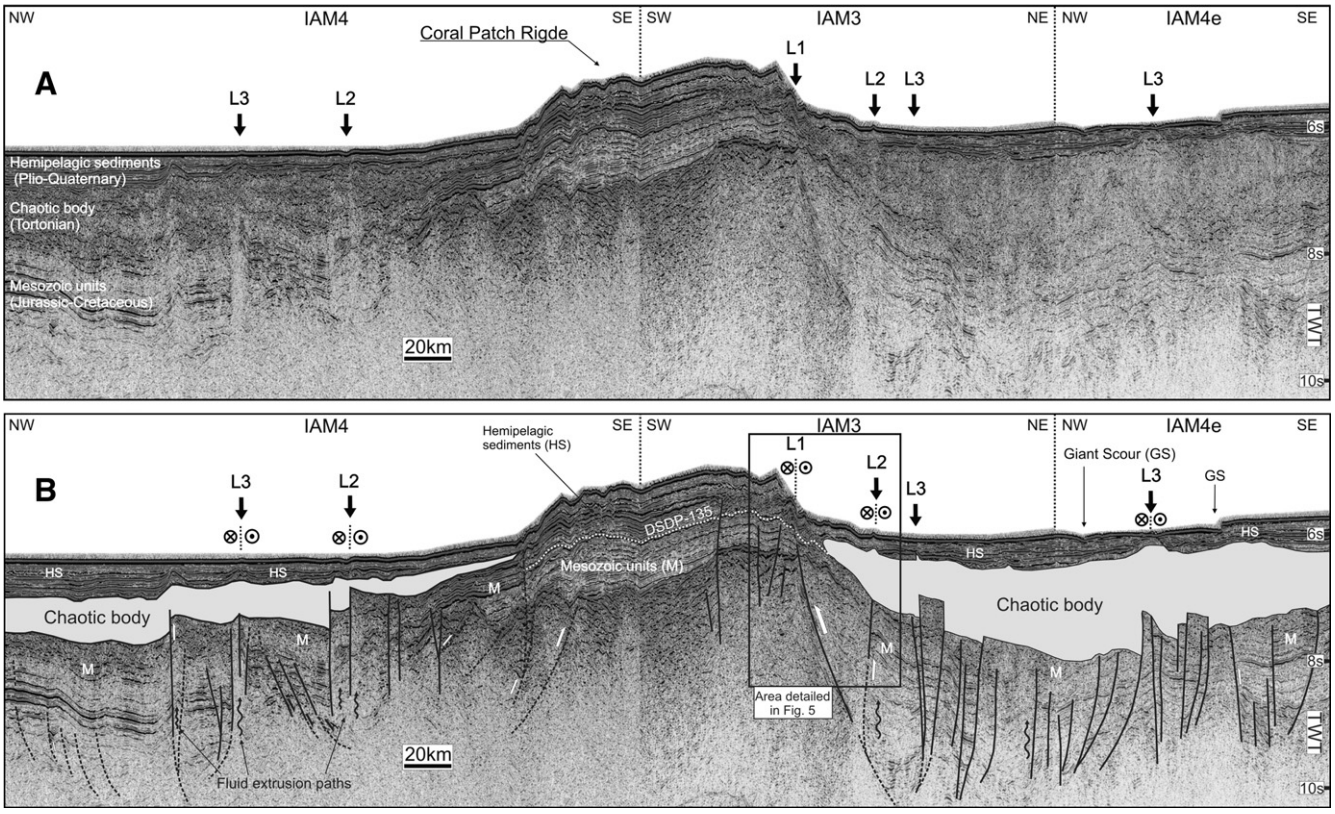


Fig. 4. (A) Uninterpreted multi-channel seismic profiles IAM4, IAM3 and IAM4e migrated with the water velocity (location in Fig. 2). (B) Simplified seismostratigraphic and tectonic interpretation of the same profiles. L1, L2 and L3 mark the intersection with the lineaments identified in the high-resolution bathymetry. Near the fault planes white arrows represent interpreted kinematics. HS—Hemipelagic sediments; M—Mesozoic units; GS—Giant Scours; (DSDP-135 marks the seismostratigraphic top of the Mesozoic units).

be noted that with the available MCS dataset the deep seated fault associated to L2 is perfectible traceable in the Horseshoe abyssal plain, and further to the West until the base of the Gorringe Ridge. The mentioned fact that its bathymetric expression is practically non-existent in this area is probably due to an average greater thickness of the post Mesozoic sediment pile, particularly in the area close to the footwall of the Horseshoe fault.

3. Analogue modelling

In the study area recently reported kinematic models derived from geodetic data (Nocquet and Calais, 2004; Stich et al., 2006; Fernandes et al., 2007) show a Present day 4 mm/yr convergence rate, along a direction subparallel to the trend of the study morphotectonic lineaments (see inset of Fig. 1B). This agrees with the general possibility of the prevailing compression being presently dissipated through bulk dextral wrenching along the major faults associated to these lineaments, which was the main focus of our analogue modelling.

In the NW Gulf of Cadiz area, the detailed vertical rheology profile of the lithosphere, and of the uppermost crust, is unknown. However, a non-negligible rheology contrast must exist between the lithified, harder, Mesozoic units, and the uppermost soft sedimentary cover, corresponding in part to the unconsolidated hemipelagic sediments of Plio-Quaternary age. If so, bulk dissipation of the compressive stress must preferably occur in the Mesozoic rigid basement, through dextral strike-slip faulting, deforming the overlying soft cover mostly in a passive manner. Therefore, our first set of experiments consisted on the simulation of basement, right-lateral, strike-slip faulting, and coupled passive shearing in an overlying soft cover.

Nonetheless, given the uncertainty of the upper crust rheology profile in the area, we also preformed a second set of experiments assuming that the study faults could nucleate low-angle transpressive shearing along an narrow band in the overlying sediments. This possibility implies the assumption of a different rheology structure for the upper crust, comprising a less abrupt rheology contrast between a somewhat less viscous basement and the softer sedimentary cover. Accordingly, the previously faulted Mesozoic basement must be able to deform, at least to some degree, in a ductile way to allow low-angle transpressive shearing in the soft cover sediments along a narrow band overlying the fault. It should be noted that in the case of this second set of experiments, our objective was simply to look at the kind of morphotectonic pattern that is expected to form in the soft cover alone, under the mentioned transpressional conditions. In all situations, we focused mainly on the ductile experimental output, comparing both results with the various natural examples. For the basement strike-slip deformation experiments, we further use this comparison to quantify the amount of shear strain (γ), the along strike displacement (Δx), and the age of the corresponding shearing deformation affecting the soft cover sediments.

The present simulation of wrench fault systems and associated passive shearing follows, with some modifications, the work

Fig. 3. (A and B) Different views of the L1 and L2 bathymetric lineaments and associated morphologic features. (C) View of L1 from ESE. AB bathymetric profile just north of L1. White arrows point the en-échelon morphologic crests and troughs; (D) View of L2 from WNW. CD bathymetric profile perpendicular to the L2 lineament. CPR—Coral Patch Ridge; GS—Giant scours. Black arrows always indicate the interpreted sense of shear.

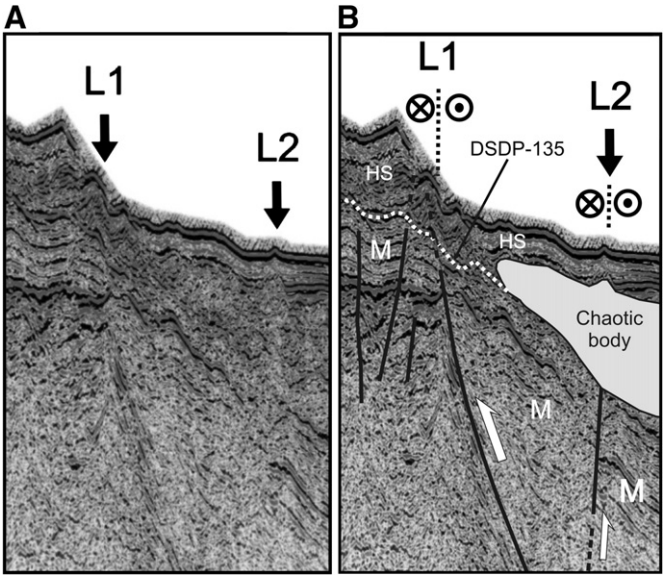


Fig. 5. (A) Zoomed segment of the IAM3 seismic profile of Fig. 4. (B) Illustration of the interpreted kinematics along L1 fault (white arrows); HS—hemipelagic sediments (Plio-Quaternary); M—Mesozoic units (DSDP-135 marks the seismostratigraphic top of the Mesozoic units).

previously put forward by other authors (e.g. Wilcox et al., 1973; Richard et al., 1991; Richard and Krantz, 1991; Casas et al., 2001). The main difference is that the prime motivation of our analogue modelling was not to theoretical address the study of the implicated deformation regimes (e.g. simple shear, transpression), but instead, to use the obtained experimental results instrumentally, i.e., to compare them with the natural structures to try to quantify the strain involved in their formation. Another important difference is that we focused in the formation of ductile structures, rather than brittle ones, to try to understand the way through which a soft sedimentary cover, comprising poorly or even unconsolidated sediments, endures deformation under the referred conditions.

3.1. First set of experiments: basement strike-slip faulting and coupled shear deformation

3.1.1. Experimental procedure

In the first set of experiments we used a Perspex strike-slip deformation rig (Fig. 6) with dimensions of $50 \times 25 \times 5$ cm, comprising two confining vertical walls and two basal, laterally juxtaposed, rigid plates, moving relatively to each other in opposite directions, driven at constant velocity (~0.028 mm s^{-1}) by an electric motor.

The materials used as analogues of the soft cover seafloor sediments include: (1) Dry quartz sand (grain size<0.25 mm) with negligible cohesion and a friction angle of about 30° to simulate brittle sedimentary layers (e.g. Hubbert, 1951; Horsfield, 1977); (2) Transparent silicone putty (PDMS, a polydimethyl-siloxane, manufactured by Dow Corning of Great Britain under the trade name SGM 36) as an analogue of weak layers within the upper crust (see Weijermars 1986a,b,c for PDMS properties), simulating the deformation behaviour of natural sedimentary rocks such as shales, clays or salt (e.g. Ballard et al., 1987; Vendeville et al., 1987; Richard et al., 1989, 1991; Marques and Coelho, 2001; Rosas et al., 2001, 2002). In some experiments a mixture of dry sand and a fraction of mortar (~40%) was also used to increase the cohesiveness of the material (measured internal friction angle around 35°), and thus improve the simulated reproduction of brittle structures in the model (e.g. Hampel et al., 2004).

To simulate passive deformation of a sedimentary cover above a basement strike-slip fault system, we constructed an initial model (see Fig. 6) in which the rigid basement is represented by the basal Perspex plates. These are overlain by a 1 cm thick silicone layer, corresponding to the approximately 1 km thickness of the Plio-Quaternary sedimentary cover (scale≈1/100.000). In most experiments a two-layered silicone-sand cake with the same total thickness was used instead, with the intention of monitoring the generation of brittle structures in the sand layers, as well as the ones expected to form in the silicone. The surface between the silicone layer and the basal rigid plates is non-lubricated, promoting total adherence between them. The relative opposite movement of the plates simulates dextral strike-slip along a pre-existent basement fault plane, transmitting this movement to the overlying silicone and sand layers. Square grids, straight lines and circles were drawn on top of the model surface to be used as passive strain markers. The dimensions of the deformation rig are sufficiently large to guarantee that the bulk of the model is not affected by boundary effects. The experiments were repeated several times to ensure the consistency of the obtained results, and top view photographs were taken at regular time intervals.

3.1.2. Experimental results

In the cover silicone-sand layers of our model, the strike-slip basement faulting was mostly accommodated through the development of different types of brittle and ductile structures (Figs. 7A, B and 8).

The obtained brittle structures are dominant in the sand (sand-mortar) layers and comprise mainly (inset of Fig. 8): a) Oblique synthetic Riedel shears (*R*), orientated at low angles to the bulk shear direction (15°–20° for the first increments of deformation); b) Synthetic *P* shears which originate at the tips of *R* shears also at low angles to the shear direction (10°–15°); c) Few antithetic Riedel shears (*R'*) at high angles (70°–75°) with the bulk shear direction; and d) Few tension gashes or extension fractures (*T*) at original 45° to the shear direction.

Ductile structures also developed in the sand layers, but were clearly dominant in the silicone cover layers of our models (lower right photos of Fig. 7A and B), consisting in sets of en-échelon folds, originally formed at 45° to the shear direction, and progressively rotating towards it as shear strain (γ) increased. In the sand layers, the en-échelon folds are also pervasively cut by an anastomosing grid of synthetic Riedels (*R*) and *P* shears (Figs. 7A and 8).

3.2. Second set of experiments: low-angle transpression

3.2.1. Experimental procedure

As mentioned above, we carried out this second set of experiments essentially to be able to monitor the type of morphotectonic patterns that are expected to form under dextral, low-angle, transpression, affecting soft cover sediments along a narrow shear band. To do so we used a transpressive deformation rig (Fig. 9) comprising two lateral (vertical) walls, moving relatively to each other in opposite directions on top of a fixed (horizontal) basal rigid plate. The walls are driven by a motor connected to a pair of long screws, pushing them along a direction making a horizontal angle of 15° with the shear direction, at the constant velocity of approximately 0.028 mm s^{-1}.

We employed the same materials with the same properties described for the first set of experiments: dry sand as an analogue of upper crust brittle behaviour, and transparent silicone putty (PDMS) to simulate week layers of the upper crust soft sedimentary cover. Similarly to what was described for the first set of experiments, a sand-mortar mixture was also some times used to favour the reproduction of brittle structures.

The constructed initial model consisted in a 1 cm-thick layered silicone-sand cake (Fig. 9) corresponding to the scaled estimated thickness of the Plio-Quaternary sedimentary cover (≈1:100,000). It should be noted that in this case the basal Perspex plate does not represent an analogue of the Mesozoic basement rocks, since we

focused exclusively on the low-angle transpressive shearing affecting the cover.

Total free slip was achieved along the contact surface of the basal Perspex plate with the silicone layer, by lubricating it with neutral soap. Conversely, the contact surface between the silicone layer and the vertical moving walls was non-lubricated, promoting a total adherence of the silicone to these walls. Straight lines and circles were drawn on top of the model surface to be used as passive strain markers. Experiments were repeated several times, and top view photographs were obtain at regular intervals.

3.2.2. Experimental results

In these experiments (Fig. 10A and B) synthetic Riedels (*R*) also formed at a low angle to the bulk shear direction, but neither in the silicone layer, nor in the sand-mortar one, did any set of en-échelon folds developed. Instead, in early stages (Fig. 10A), a central elongated bulge formed, consisting in two aligned asymmetric fold segments, trending parallel to the bulk shear direction, and bounded at both sides by incipient, opposite directed, early thrusts. For higher amounts of shortening and lateral displacement (Fig. 10B), synthetic *R* shears continued to form, and the folded bulged band narrowed as folds got tighter and thrusts developed.

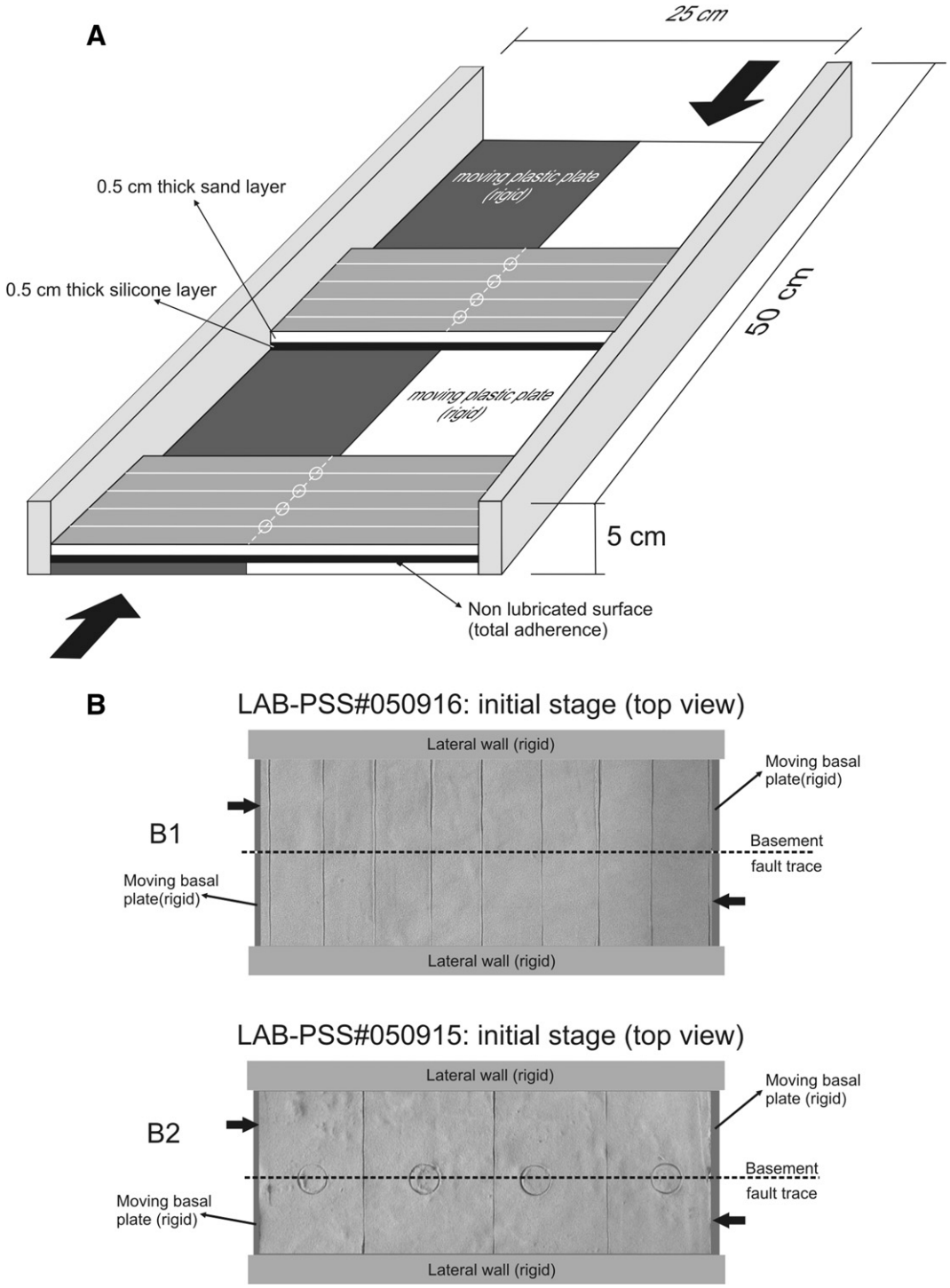


Fig. 6. (A) Experimental apparatus and model setting used in the first set of experiments to simulate basement strike-slip faulting and coupled shear deformation (modified after Casas et al., 2001); (B) Top views of the initial state for two of the preformed experiences (LAB-PSS#050915 and LAB-PSS#050916).

4. Comparison of the experimental results with the natural examples

For both sets of experiments the obtained brittle structural patterns recorded in the sand cover layers are similar, consisting essentially in the more or less pervasive development of synthetic *R* and *P* shears (see Figs. 7 and 10). Conversely, the ductile patterns, comprising the development of folds both in sand and silicone layers, are clearly different, depending on which set of experiments is considered: for strike-slip basement faulting and coupled passive shearing, an en-échelon fold pattern was obtained (see Fig. 7A and B), whereas for low-angle transpression a totally different pattern of folds formed (see Fig. 10).

In the first case, the experimentally obtained structural pattern correlates well with the en-échelon spatial distribution of bathymetric crests associated with L1 (Fig. 11A and B), which suggests that this corresponds to a morphotectonic pattern formed passively in the seafloor soft sediments, as the result of dominant right-lateral strike-slip reactivation of the underlying basement fault.

For the second set of experiments the obtained structural pattern resembles more the morphology characterizing L2 (Fig. 11C), suggesting an origin preferably related with low-angle dextral transpressive shearing along a narrow band nucleated by the reactivation of the underlying fault.

For both sets of experiments, the obtained structural patterns correlate with the natural examples, only when the ductile deformation output is considered. Both L1 and L2 lack any kind of associated brittle structures, such as the R or P shears that formed in the analogue models. This shows that the deformation which originated the natural morphotectonic patterns was essentially ductile, affecting poorly lithified soft sediments of Recent age.

Note that it was not possible to compare the obtained experimental results with L3 and L4 lineaments, because L3 is hardly recognizable in the bathymetry, and deformation associated with L4 is probably masked by the local wrinkled seafloor morphology (corresponding to the accretionary wedge domain, AW in Figs. 1B and 2).

4.1. Structural analysis

In our first set of experiments the en-échelon folds were observed to form and rotate closely to what is theoretically predicted for passive strain markers in simple shear progressive deformation. In this deformation regime, shear strain (γ) is defined as the ratio between the displacement parallel to the shear direction (Δx) and the width of

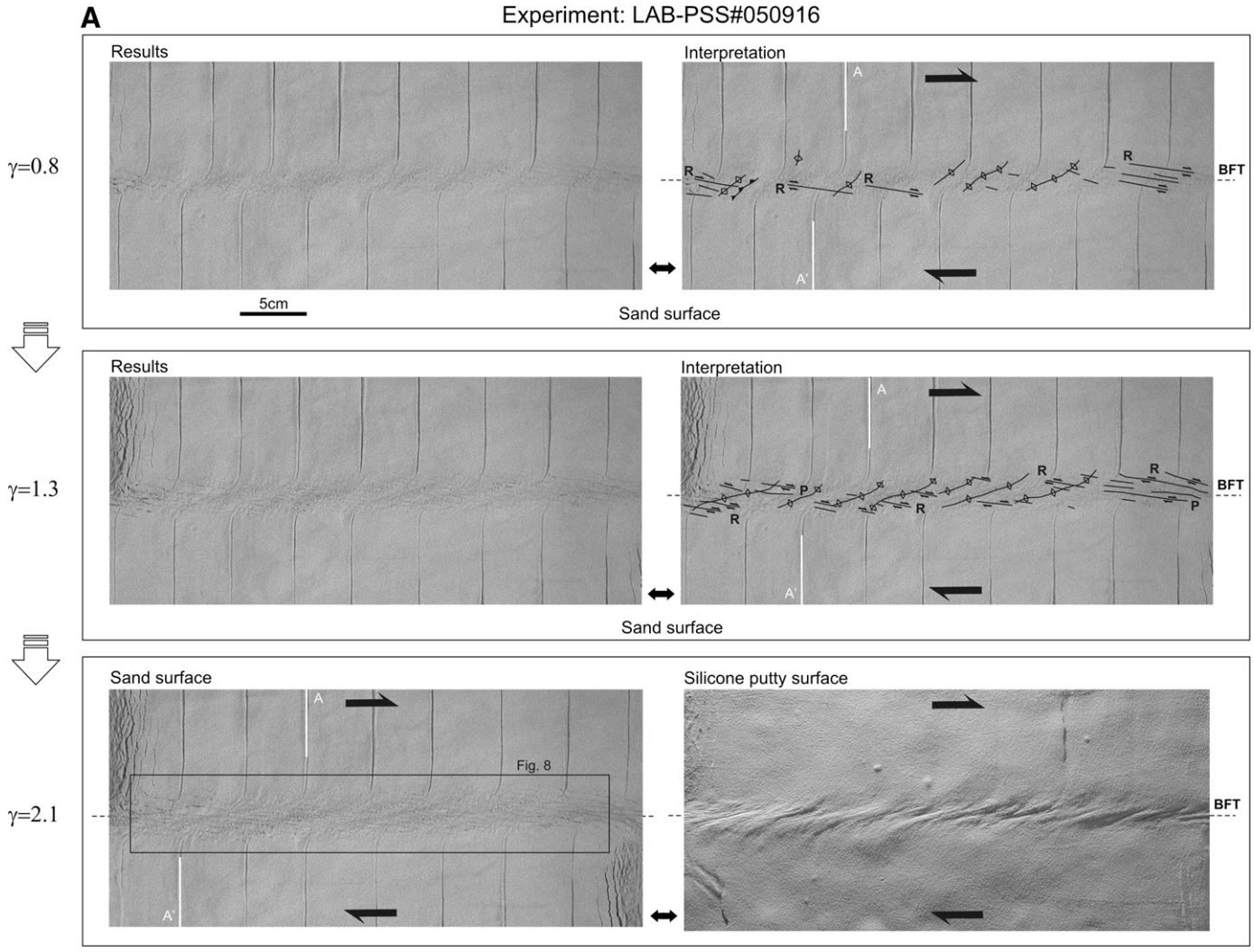


Fig. 7. Example of the results obtained in the first set of experiments to simulate basement strike-slip faulting and coupled shear deformation, (A) using a silicone-sand layered cake (experiment LAB-PSS#050916, see corresponding initial state in Fig. 6B1), and (B) using a top layer corresponding to a sand-mortar mixture (LAB-PSS#050915, initial state in Fig. 6B2). Top views of the sand/sand-mortar surface are shown for successive increments of γ shear strain. Lower right photos in A and B correspond to the silicone surface top view after removal of the previous overlying sand/sand-mortar layer. *R*—synthetic Riedel shears; *R'*—antithetic Riedel shears; *P*—synthetic *P* shears; *T*—tension gashes or extension fractures; BFT—Basement fault trace.

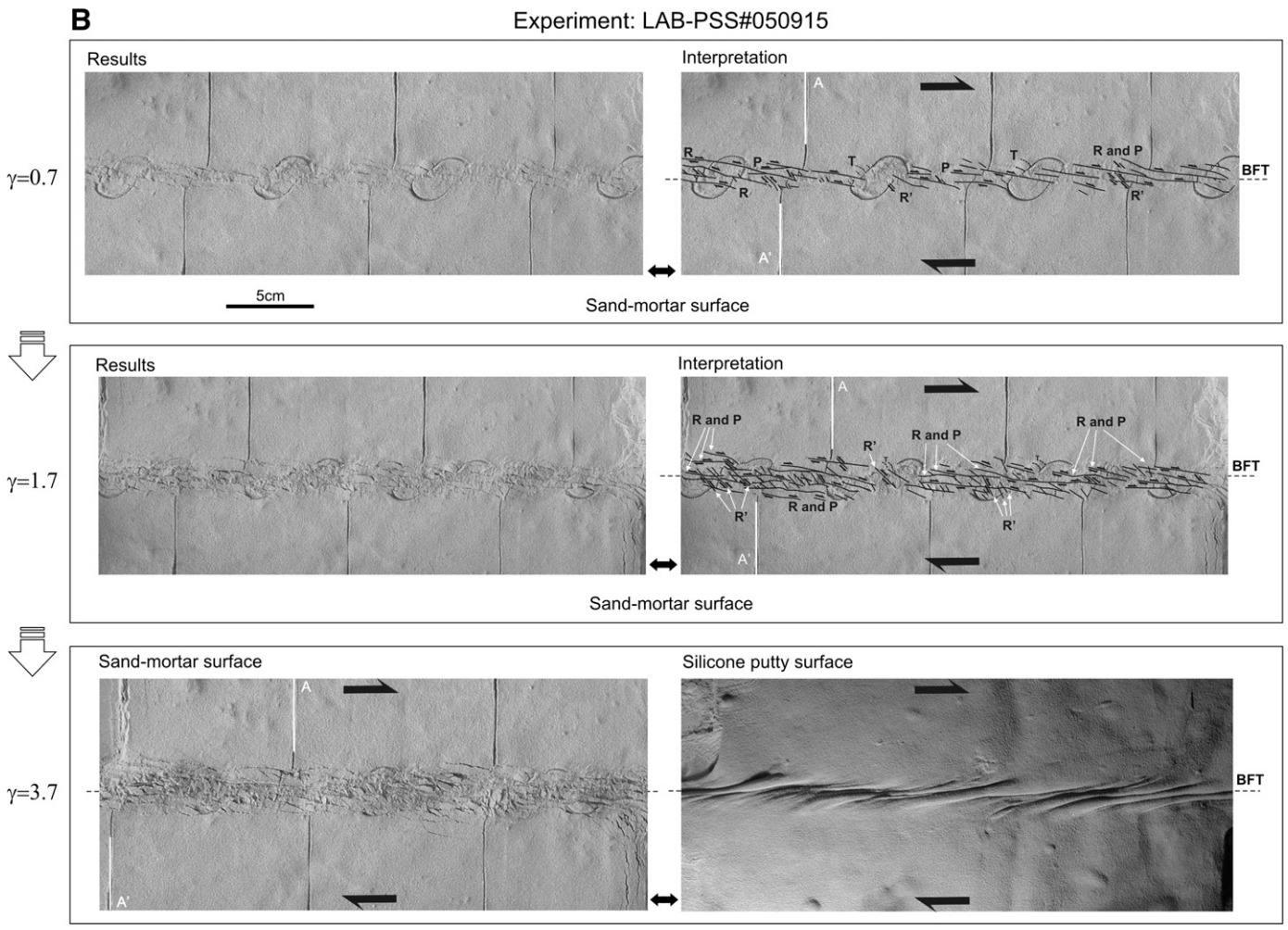


Fig. 7 (*continued*).

the shear zone (Y) (Fig. 12A). A classical strain maker corresponds to the strain ellipse of Ramsay and Huber (1983), which in simple shear forms instantaneously, for infinitesimal increments of shear strain, with its longest axis at an angle (θ) at 45° to the shear plane (Fig. 12B). As γ shear strain accumulates, the axial ratio of the strain ellipse increases and its longest axis rotates towards the shear plane, with consequent reduction of the angular θ value (Fig. 12B). This behaviour can be simply described in terms of the relation between γ and θ, as in the equation presented by Ramsay and Graham (1970) (see Eq. (1) below, and Fig. 12B). Accordingly, our experimental results show that, for infinitesimal deformation increments, the en-échelon folds formed with their hinges approximately parallel to the e_1 principal axis of the instantaneous strain ellipse, at an angle of $\theta \approx 45°$ to the shear plane (Fig. 12C), and rotated towards it during the progressive non-coaxial deformation, as γ shear strain increased. This similarity between the observed experimental behaviour of the en-échelon folds and the theoretical prediction for simple shear deformation, is shown by the good correlation that exists between the points corresponding to the measurements made for θ and γ in the succeeding progressive deformation stages of the several experiments done, and the equation curve of Ramsay and Graham (1970) (Fig. 12D). This correlation shows that the en-échelon folds obtained in our first set of experiments formed under deformation conditions similar to bulk simple shear, and hence, given the comparison with the natural examples presented above, that the same would also apply to the L1 bathymetric lineament and associated natural en-échelon folds.

Based on this deduction, measuring the mean value of θ (= 24.20°) in the natural en-échelon folds of L1 lineament (see Fig. 11B) made it possible to determine the approximate amount of shear strain (γ) that originated these structures in their present orientation. This was done using equation

$$\gamma = \frac{2}{\tan 2\theta}, \tag{1}$$

(Ramsay and Graham, 1970) in which $\theta = 24.20°$ gives $\gamma = 1.78$.

Furthermore, using this γ value and the mean width of the L1 shear zone Y (~4000 m), which was estimated based on the observed spatial distribution of the en-échelon folds (see Fig. 11B), it was also possible to determine the along strike displacement (Δx) implied in the shear deformation responsible for the present orientation of the en-échelon folds. This was done using equation

$$\gamma = tg(\Psi) = \frac{\Delta x}{Y}, \tag{2}$$

of Ramsay and Huber (1983), in which for $\gamma = 1.78$ and $Y = 4000$ m, we obtain $\Delta x \approx 7000$ m.

In our second set of experiments, concerning the L2 lineament and associated deformation pattern, the absence of natural structures useful as reliable (i.e. measurable) strain markers, did not allow a more quantitative insight, regarding strain quantification of the transpressive shearing, through comparison between the observations and the experimental results.

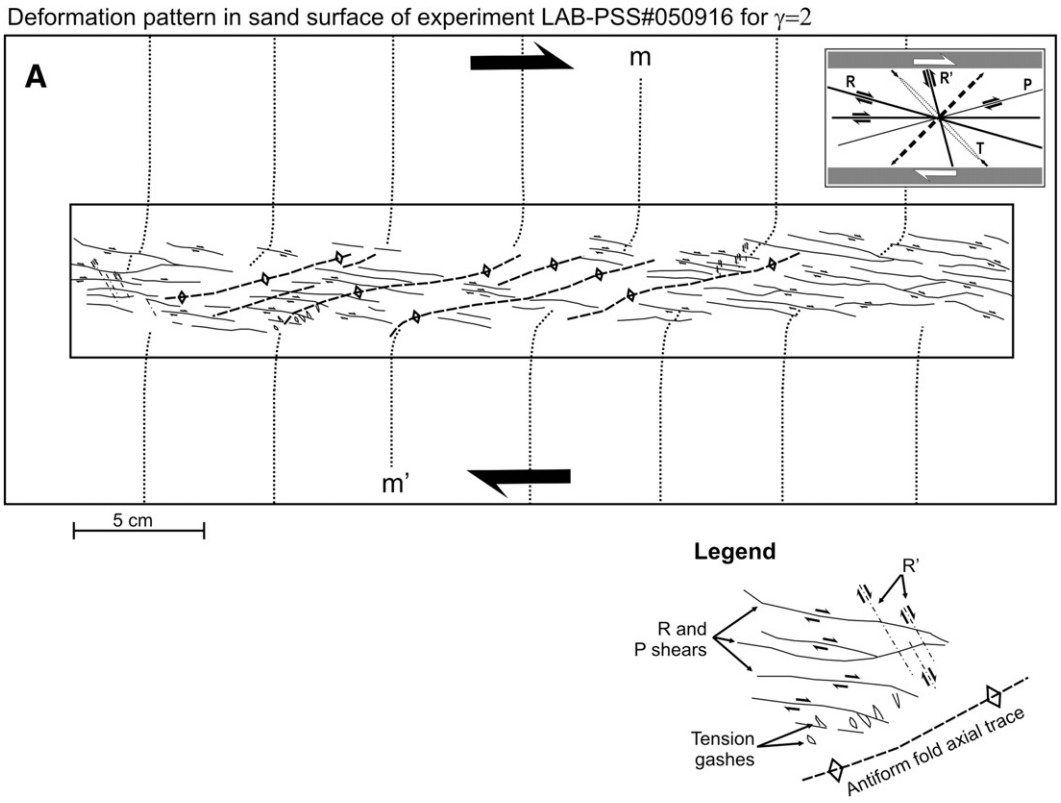


Fig. 8. Deformation pattern obtained in the sand layer of experiment LAB-PSS#050916 for $\gamma \approx 2$ (see Fig. 7A for location).

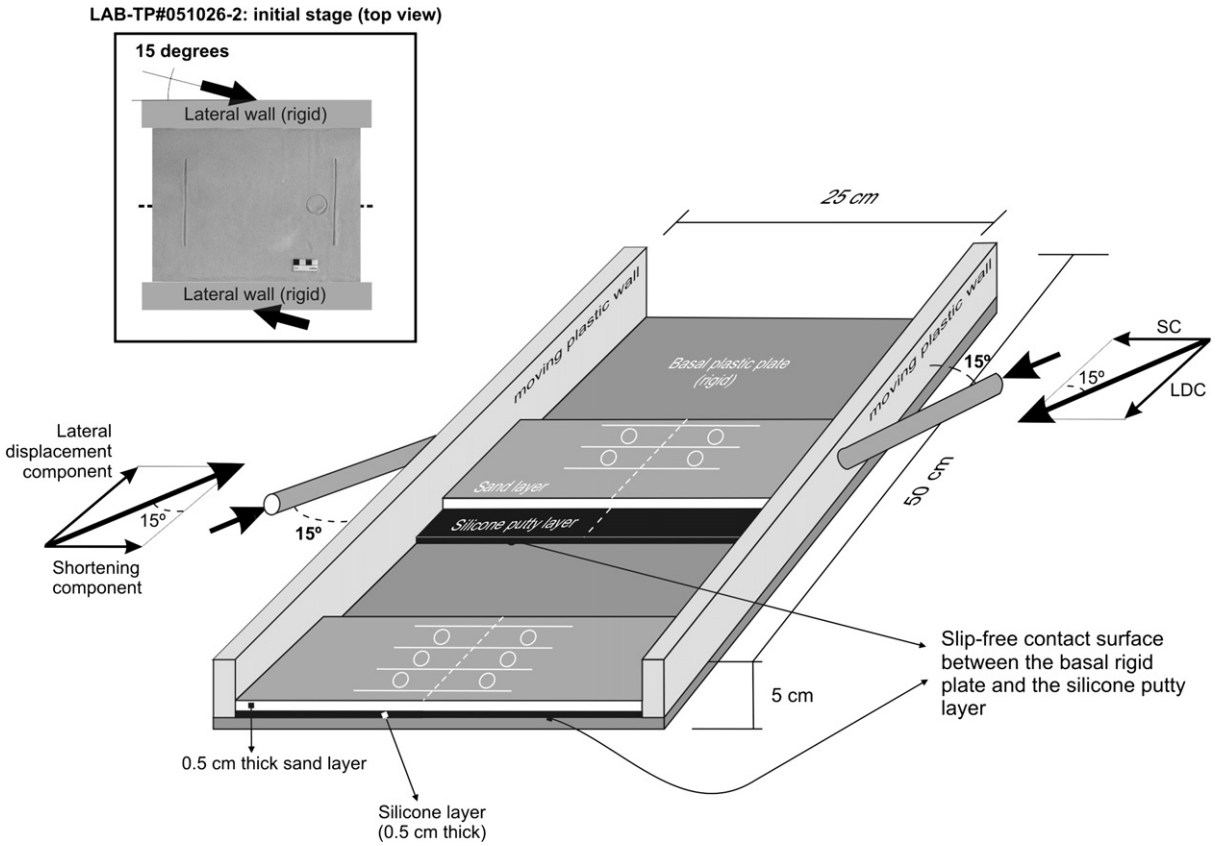


Fig. 9. Experimental apparatus and model setting used in the second set of experiments to simulate low-angle transpression (modified after Casas et al., 2001). Upper left inset showing top view initial state of one of the preformed experiences (LAB-TP#051026-2).

4.2. Age of the deformation associated to the L1 morphotectonic pattern

According to the recently reported kinematic models for the Gulf of Cadiz computed from geodetic data (e.g. Nocquet and Calais, 2004; Stich et al., 2006; Fernandes et al., 2007), the ongoing convergence between Nubia and Iberia occurs along a WNW–ESE direction, subparallel to the shear direction associated to L1, at a rate of approximately 4 mm/yr (see inset in Fig. 1B). Thus, by considering the value of the along strike

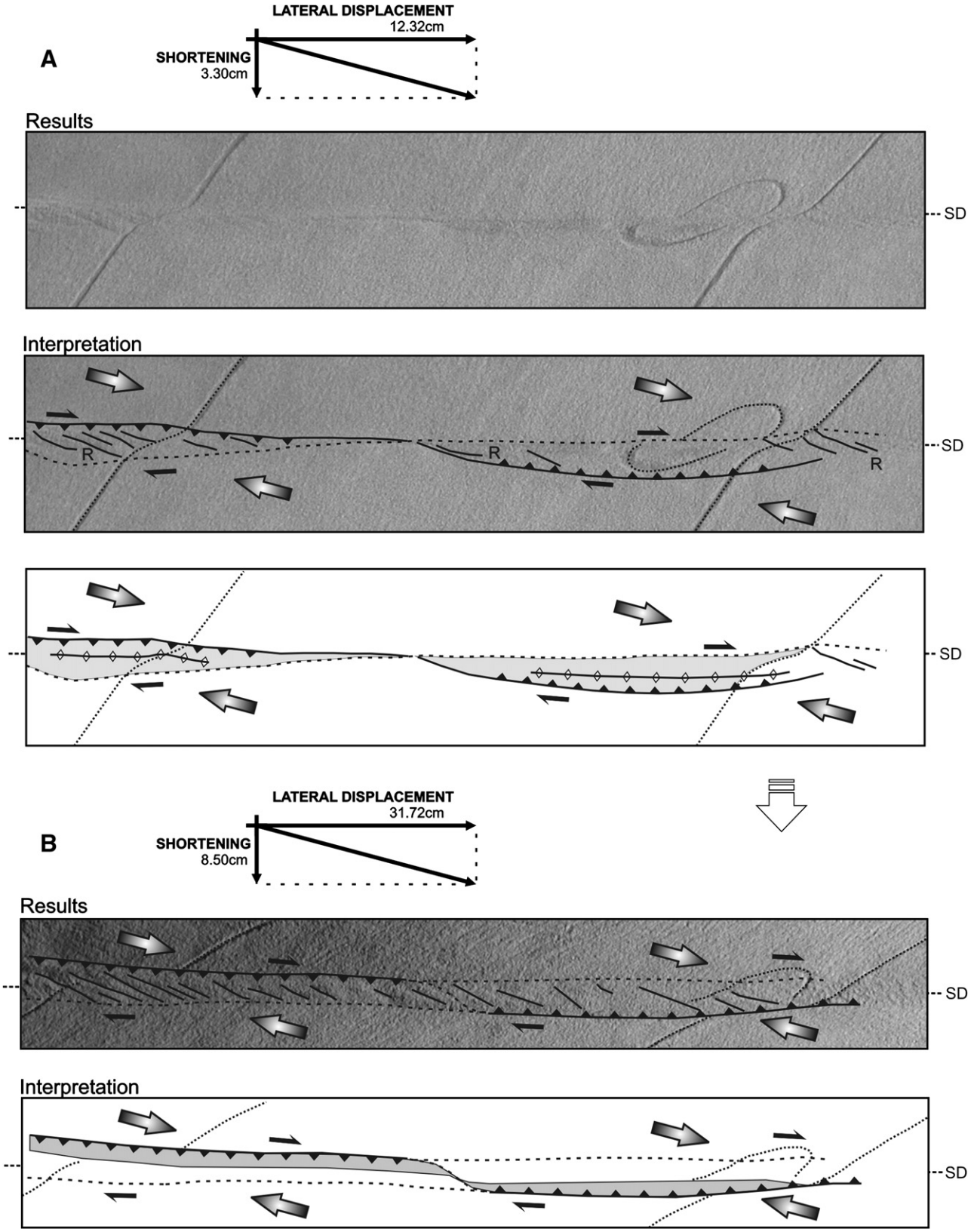


Fig. 10. Example of the results obtained in the second set of experiments to simulate low-angle transpression (exp: LAB-TP#051026-2, initial state in the inset of Fig. 9). *R*—synthetic Riedel shears. SD—Shear direction.

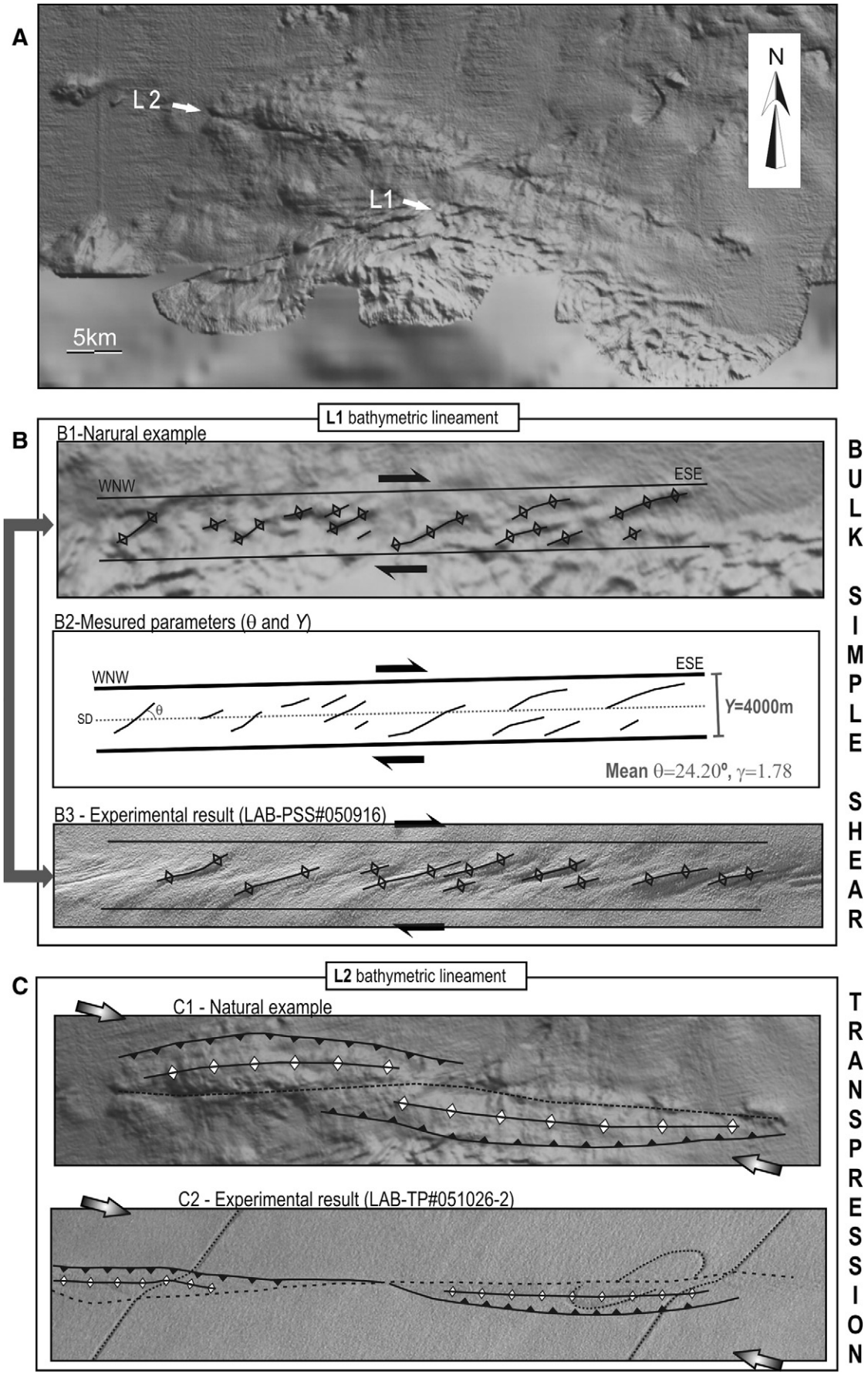


Fig. 11. Comparison of the natural examples (A—study bathymetric lineaments L1 and L2) with the obtained first (B) and second (C) set experiments. θ—angle between the en-échelon folds and the shear direction (SD); γ—corresponding shear strain; Y—shear zone width.

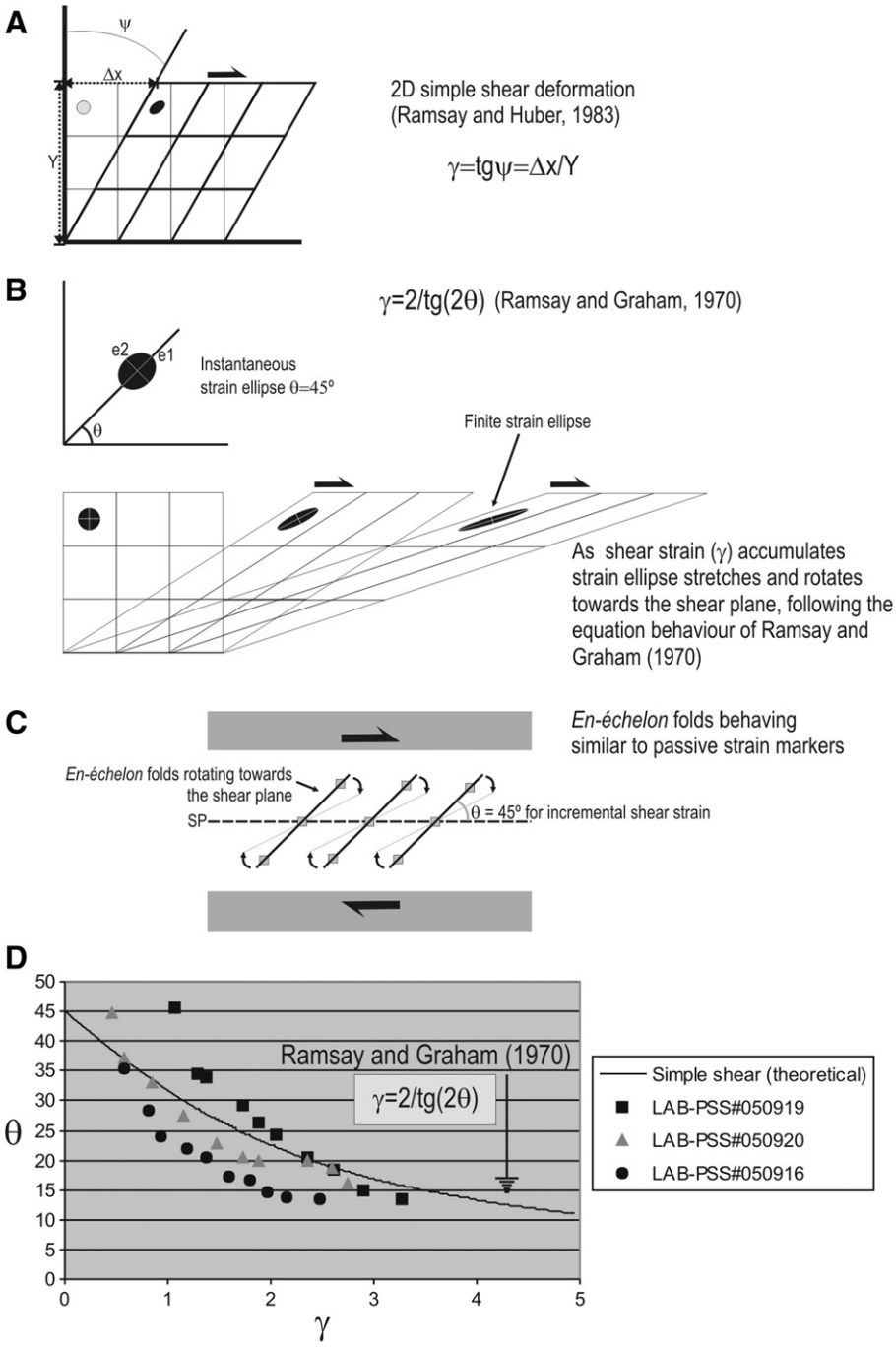


Fig. 12. (A and B) Schematic representation of the theoretical behaviour of passive strain markers under simple shear deformation (adapted from Ramsay and Huber, 1983). (C) Schematic representation of en-échelon folds behaving as passive strain markers under simple shear deformation. (D) Plot of θ and γ values, measured for succeeding deformation stages of several experiments, against the equation curve of Ramsay and Graham (1970).

displacement ($\Delta x \approx 7000$ m) obtained above, and the reported 4 mm/yr convergence rate, it was possible to estimate the maximum age of 1.8 Ma for the deformation responsible for the L1 morphotectonic pattern. This estimate is based on the assumption that the cover sediments recording this pattern are soft (poorly lithified), deforming mostly in a ductile manner, which suggests a simultaneous character of sedimentation and strain. In accordance, the syntectonic sedimentation rate would be of critical influence on the nucleation and development of the L1 structures, since relatively larger sedimentation rates would tend to attenuate the morphologic expression of the developing structures. Therefore, the well preserved L1 morphotectonic patterns seemingly suggest low syntectonic sedimentation rates, which agrees with the average 30 cm/Ky (0.3 mm/y) reported by Lebreiro et al. (1997) for the horseshoe abyssal plain.

5. Summary and conclusions

Based on our experimental results, and on the bathymetry and seismic reflection data presented above, we conclude that: (1) In the Gulf of Cadiz, the WNW-ESE lineaments correspond to the bathymetric expression of active deep seated faults; (2) These faults show a Present day kinematics consisting in bulk dextral wrenching; (3) The deformation which originated the study morphotectonic lineaments started at a maximum age of ca. 1.8 Ma. (4) These lineaments formed

in soft, most probably, poorly consolidated sediments, deposited at relatively low rates of syntectonic sedimentation.

Our results show that the morphotectonic pattern associated to L1 was formed as a consequence of dextral strike-slip reactivation of a basement fault, coupled with passive simple shear deformation of the overlying soft sedimentary cover. On other hand, the seafloor bathymetry pattern associated to L2 must have formed preferably as a consequence of low-angle dextral transpression. However, in this case, the uncertainty concerning the local upper crust vertical rheology profile, did not allow a better comprehension of the process governing the nucleation of a transpressive shear band in the soft sedimentary cover overlying the correspondent fault. Moreover, since no natural structural features useful as strain gauges were found in this case, a more quantitative insight was also impossible to achieve. It should be noted that L1 borders the northern–eastern flank of the CPR (Figs. 1B, 2 and 3), which could correspond to a rigid body resisting shortening and favouring lateral slip, instead of transpressive shearing, along this limit.

5.1. Tectonic implications

In the Gulf of Cadiz, the faults associated to the studied lineaments were previously reported to have endured a complex tectonic evolution from Early Mesozoic through Cenozoic (Terrinha et al., under review). Based on the inspected seismic profiles (see Figs. 4 and 5), it was in some cases possible to recognize a kinematic behaviour characterized by reverse faulting. These faults cut through the Mesozoic and the base of the Tortonian chaotic body, but do not affect the top of this unit, neither the overlying sediments which are generally sealing these structures (see Figs. 4 and 5). This shows that the reverse fault kinematics is not presently active.

Our conclusions fit the whole-scale strain partitioning scenario, recently proposed by Terrinha et al. (under review), according to which the Nubia–Iberia collision in the Gulf of Cadiz area is Presently being accommodated through oblique westwards thrusting along NNE–SSW faults, such as the Horseshoe fault and Marques de Pombal active faults (see Fig. 1B), and simultaneously through bulk dextral strike-slip reactivation of pre-existent WNW–ESE faults, corresponding to the studied bathymetric lineaments. According to our experimental results, the age of this deformation recorded by Recent bottom floor soft sediments in the Gulf of Cadiz is ca. 1.8 Ma (late Pliocene). Furthermore, given the WNW–ESE trend of the faults their interpreted kinematic behaviour is in good agreement with the kinematic models derived from geodetic data yielding a 4 mm/yr convergence rate, subparallel that same direction.

Acknowledgements

Experiments were performed in the Experimental Tectonics Laboratory of LATTEX-IDL, a research unit funded by PLURIANUAL (125/N/92). MATESPRO (PDCTM/P/MAR/15264/1999), EUROMARGINS SWIM (01-LEC-EMA09F). V. Valadares acknowledges a Ph.D. scholarship (SFRH/BD/17603/2004) of FCT. Dr. Rui Dias (Évora University) is acknowledged for constructive discussions, which helped to improve the present work. We also thank to two anonymous reviewers and the editor-in-chief of Marine Geology, Gert J. De Lange, for their constructive and thorough reviews of the manuscript.

References

Abe, K., 1979. Size of great earthquakes of 1837–1974 inferred from tsunami data. J. Geophys. Res. 84, 1561–1568.
Ballard, J.F., Brun, J.P., Van den Driessche, J., Allemand, P., 1987. Propagation des chevauchements au-dessus des zones de décollement: modèles experimentaux. Comptes Rendus de l'Académie des Sciences de Paris 305, 1249–1253.
Bird, P., 2003. An updated digital model of plate boundaries. Geochem. Geophys. Geosyst 4 (3), 1027. doi:10.1029/2001GC000252.
Borges, J.F., Fitas, A.J., Bezzeghoud, M., Costa, P.T., 2001. Seismotectonics of Portugal and its adjacent Atlantic Area. Tectonophysics 331, 373–387.
Buforn, E., Sanz de Galdenao, C., Udías, A., 1995. Seismotectonics of the Ibero–Maghrebian region. Tectonophysics 248, 247–261.
Buforn, E., Bezzeghoud, M., Udías, A., Pro, C., 2004. Seismic sources on the Iberia–African plate boundary and their tectonic implications. Pure Appl. Geophys. 161, 623–646.
Casas, A.M., Gapais, D., Nalpas, T., Besnard, K., Román-Berdiel, K., 2001. Analogue models of transpressive systems. J. Struct. Geol. 23, 733–743.
Fernandes, R.M.S., Miranda, J.M., Meijninger, B.M.L., Bos, M.S., Noomen, R., Bastos, L., Ambrosius, B.A.C., Riva, R.E.M., 2007. Surface velocity field of the Ibero-Maghrebian segment of the Eurasia–Nubia plate boundary. Geophys. J. Int. 169 (1), 315–324.
Gracia, E., Dañobeitia, J., Vergés, J., PARSIFAL Team, 2003. Mapping active faults offshore Portugal (36°N–38°N): implications seismic hazard assessment along the south-west Iberian margin. Geology 31 (1), 83–86.
Gutscher, M-A., 2004. What caused the Great Lisbon earthquake? Science 305, 1247–1248.
Gutscher, M.-A., Malod, J., Rehault, J.-P., Contrucci, I., Klingelhoefer, F., Spakman, W., Mendes-Victor, L., 2002. Evidence for active subduction beneath Gibraltar. Geology 30 (12), 1071–1074.
Hampel, A., Adam, J., Kukowski, N., 2004. Response of the tectonically erosive south Peruvian forearc to subduction of the Nazca Ridge: analysis of three-dimensional analogue experiments. Tectonics 23, TC5003. doi:10.1029/2003TC001585.
Hensen, C., Nuzzo, M., Hornibrook, E., Pinheiro, L.M., Bock, B., Magalhães, V.H., Bruckmann, W., 2007. Sources of mud volcano fluids in the Gulf of Cadiz—indications for hydrothermal imprint. Geochim Cosmochim Ac. 71, 1232–1248.
Horsfield, W.T., 1977. An experimental approach to basement-controlled faulting. Geol. Mijnbouw 56 (4), 363–370.
Hubbert, M.K., 1951. Mechanical basis for certain familiar geologic structures. Geol. Soc. Am. Bull. 62 (4), 355–372.
Johnston, A., 1996. Seismic moment assessment of earthquakes in stable continental regions—III. New Madrid, 1811–1812, Charleston 1886 and Lisbon 1755. Geophys. J. Int. 126, 314–344.
Lebreiro, S.M., McCave, N.I., Weaver, P.E., 1997. Late Quaternary turbidite emplacement on the Horseshoe abyssal plain (Iberian margin). J. Sediment. Res. 67 (5), 856–870.
Maldonado, A., Somoza, L., Pallarés, L., 1999. The Betic orogen and the Iberian–African boundary in the Gulf of Cadiz: geological evolution (central North Atlantic). Mar. Geol. 155, 9–43.
Marques, F.O., Coelho, S., 2001. Rotation of rigid elliptical cylinders in viscous simple shear flow: analogue experiments. J. Struct. Geol. 23, 609–617.
Martínez-Solares, J.M., López-Arroyo, A., 2004. The great historical 1755 earthquake. Effects and damage in Spain. J. Seismology 8, 275–294.
Medialdea, T., Vegas, R., Somoza, L., Vázquez, J.T., Maldonado, A., Díaz-del-Río, V., Maestro, A., Córdoba, D., Fernández-Puga, M.C., 2004. Structure and evolution of the "Olistostrome" complex of the Gibraltar Arc in the Gulf of Cádiz (eastern Central Atlantic): evidence from two long seismic cross-sections. Mar. Geol 209, 173–198.
Nocquet, J.-M., Calais, E., 2004. Geodetic measurements of crustal deformation in the Western Mediterranean and Europe. Pure Appl. Geophys. 161, 661–681.
Pinheiro, L., Ivanov, M.K., Sautkin, A., Akhmanov, G., Magalhães, V., Volkonskaya, A., Monteiro, J.H., Somoza, L., Gardner, J., Hamouni, N., Cunha, M.R., 2003. Mud volcanism in the Gulf of Cadiz: results from the TTR-10 cruise. Mar. Geol. 195, 131–151.
Ramsay, J.G., Graham, M.I., 1970. Strain variation in shear belts. Can. J. Earth Sci. 7, 786–813.
Ramsay, J.G., Huber, M.I., 1983. Modern Structural Geology: Volume 1: Strain Analysis. Academic Press, Londres. 307 pp.
Ribeiro, A., Cabral, J., Baptista, R., Matias, L., 1996. Stress pattern in Portugal mainland and the adjacent Atlantic region, West Iberia. Tectonophysics 15 (2), 641–659.
Richard, P., Ballard, J.F., Colletta, B., Cobbold, P., 1989. Naissance et evolution de failles audessus d'un décrochement de socle: modélisation analogique et tomographie. Cr. Acad. Sci. Paris 309, 2111–2118.
Richard, P., Krantz, R.W., 1991. Experiments on fault reactivation in strike-slip mode. Tectonophysics 188, 117–131.
Richard, P., Mocquet, B., Cobbold, P.R., 1991. Experiments on simultaneous faulting and folding above a basement wrench fault. Tectonophysics 188, 133–141.
Rosas, F.M., Marques, F.O., Coelho, S., Fonseca, P.E., 2001. Sheath fold development in bulk simple shear: analougue modeling of natural examples from the Southern Iberian Variscan Fold Belt. In: Koyi, H.A., Mancktelow, N.S. (Eds.), Tectonic Modeling: A Volume in Honor of Hans Ramberg. Geol. Soc. Am. Mem., 193, pp. 101–110.
Rosas, F.M., Marques, F.O., Luz, A., Coelho, S., 2002. Sheath folds formed by drag induced by rotation of rigid inclusions in viscous simple shear flow: nature and experiment. J. of Struct. Geol. 24, 45–55.
Sartori, R., Torelli, L., Zitellini, N., Peis, D., Lodolo, E., 1994. Eastern segment of the Azores–Gibraltar line (central-eastern Atlantic): an oceanic plate boundary with diffuse compressional deformation. Geology 22, 555–558.
Somoza, L., Díaz-del-Río, V., León, R., Ivanov, M., Fernandez-Puga, M.C., Gardner, J.M., Hernández-Molina, F.J., Pinheiro, L.M., Rodero, J., Lobato, A., Maestro, A., Vázquez, J.T., Medialdea, T., Fernández-Salas, L.M., 2003. Seabed morphology and hydrocarbon seepage in the Gulf of Cádiz mud volcano area: acoustic imagery, multibeam and ultra-high resolution seismic data. Mar. Geol. 195, 153–176.
Stich, D., Mancilla, F.-L., Morales, J., 2005. Crust–mantle coupling in the Gulf of Cadiz (SW-Iberia). Geophys. Res. Lett. 32, L13306. doi:10.1029/2005GL023098.
Stich, D., Serpelloni, E., Mancilla, F.-L., Morales, J., 2006. Kinematics of the Iberia–Maghreb plate contact from seismic moment tensors and GPS observations. Tectonophysics 426, 295–317.
Terrinha, P., Matias, L., Vicente, J.C., Duarte, J., Luís, J., Pinheiro, L., Lourenço, N., Diez, S., Rosas, F.M., Magalhães, V., Valadares, V., Zitellini, N., Mendes-Víctor, L., MATESPRO

Team, under review. Morphotectonics and Strain Partitioning at the Iberia–Africa plate boundary from multibeam and seismic reflection data. Marine Geology.
Terrinha, P., Pinheiro, L., Henriet, J.-P., Matias, L., Ivanov, M.K., Monteiro, J.H., Azhmetzhanov, A., Volkonskaya, A., Cunha, T., Shaskin, P., Rovere, M., 2003. Tsunamigenic–seismogenic structures, neotectonics, sedimentary process and slope instability on the southwest Portuguese margin. Mar. Geol. 195, 55–73.
Thiebot, E., Gutscher, M.-A., 2006. The Gibraltar Arc seismogenic zone (part 1): constraints on a shallow east dipping fault plane source for the 1755 Lisbon earthquake provided by seismic data, gravity and thermal modelling. Tectonophysics 426 (1–2), 135–152.
Torelli, L., Sartori, R., Zitellini, N., 1997. The giant chaotic body in the Atlantic Ocean off Gibraltar: new results from a deep seismic reflection survey. Mar. Petrol. Geol. 14 (2), 125–138.
Tortella, D., Torne, M., Pérez-Estaún, A., 1997. Geodynamic evolution of the eastern segment of the Azores–Gibraltar Zone: the Gorringe bank and the Gulf of Cadiz Region. Mar. Geophys. Res. 19, 211–230.
Vendeville, B., Cobbold, P.R., Davy, P., Brun, J.P., Choukroune, P., 1987. Physical models of extensional tectonics at various scales. In: Coward, M.P., Dewey, J.F., Hancock, P.L. (Eds.), Continental Extensional Tectonics. Special Publications, vol 28. Geological Society, London, pp. 95–107.
Weijermars, R., 1986a. Flow behaviour and physical chemistry of bouncing putties and related polymers in view of tectonic laboratory applications. Tectonophysics 124, 325–358.
Weijermars, R., 1986b. Polydimethyloxane flow defined for experiments in fluid dynamics. Appl. Phys. Lett. 48, 109–111.
Weijermars, R., 1986c. Finite strain of laminar flows can be visualized in SGM 36-polymer. Naturwissenschaften 73, 33.
Wilcox, R.E., Harding, T.P., Seely, D.R., 1973. Basic wrench tectonics. Am. Assoc. Petr. Geol. B. 57 (1), 74–96.
Zitellini, N., Chierici, F., Sartori, R., Torelli, L., 1999. The tectonic source of the 1755 Lisbon earthquake and tsunami. Ann. Geofis 42 (1), 49–55.
Zitellini, N., Mendes, L.A., Córdoba, D., Dañobeitia, J., Nicolich, R., Pellis, G., Ribeiro, A., Sartori, R., Torelli, L., Bartolomé, R., Bortoluzzi, G., Calafato, A., Carrilho, F., Casoni, L., Chierici, F., Corela, C., Correggiari, A., Della Vedova, B., Gràcia, E., Jornet, P., Landuzzi, M., Ligi, M., Magagnoli, A., Marozzi, G., Matias, L., Penitenti, D., Rodríguez, P., Rovere, M., Terrinha, L., Vigliotti, L., Zahinos-Ruiz, A., 2001. Source of the 1755 Lisbon earthquake and tsunami investigated. Eos Trans. AGU 82 (26), 290–291 285.
Zitellini, N., Rovere, M., Terrinha, P., Chierici, F., Matias, L., BIGSETS Team, 2004. Neogene through Quaternary tectonic reactivation of SW Iberian Passive Margin. Pure Appl. Geophys 161, 565–587.

Thrust-wrench interference between major active faults in the Gulf of Cadiz (Africa-Eurasia plate boundary, offshore SW Iberia): tectonic implications from analogue and numerical modeling

F.M. Rosas [a,b], J.C. Duarte [a,b,d], M.C. Neves [a,c], P. Terrinha [a,d], S. Silva [a,b,d], L. Matias [a,e]

[a] Instituto Dom Luiz, Campo Grande, Ed. C1, Piso 2, 1749-016 Lisboa, Portugal

[b] Universidade de Lisboa, Faculdade de Ciências, Departamento de Geologia, Campo Grande, Ed. C6, Piso 4, 1749-016 Lisboa, Portugal

[c] Universidade do Algarve, 8000 Faro, Portugal

[d] LNEG, Unidade de Geologia Marinha, Estrada da Portela Zambujal-Alfragide Apartado 7586, 2720-866 Amadora, Portugal

[e] Universidade de Lisboa, Faculdade de Ciências, Departamento de Engenharia Geográfica, Geofísica e Energia, Campo Grande, Ed. C8, piso 0, 1749-016 Lisboa, Portugal

[*]Corresponding author. Tel.: +351 21 7500375; fax: +351 21 7500064. E-mail address: frosas@fc.ul.pt (F.M. Rosas).

Abstract

Analogue and numerical modeling was carried out to test the existence of tectonic interference between major active strike-slip and thrust faults intersecting each other in the Gulf of Cadiz (Africa-Eurasia plate boundary, offshore SW Iberia). The obtained results show that newly mapped tectonic structures located in the fault intersection area (corner zone) consist mostly in oblique (dextral-reverse) faults that comply with a preferred stress-strain concentration in that location, caused by thrust-wrench tectonic interference. In view of these results, a multi-rupture scenario can be envisaged from comparison with the natural example, showing the need to carefully considered seismic-related hazards of low to moderate seismicity (up to M7) in the Gulf of Cadiz area. Moreover, the recognized depth discrepancy between the (upper crust) interference fault-pattern and the (lithospheric mantle) seismicity is interpreted as

suggestive of a decoupled manifestation of the same thrust-wrench tectonic interference at different lithospheric depths.

Keywords: Gulf of Cadiz; Thrust-wrench tectonics; Analogue Modeling; Numerical Modeling; Lithospheric depth-decoupled deformation.

1. Introduction

The Gulf of Cadiz (Fig. 1A) has long been considered a key domain to unravel the complex tectonics of the Eurasia-Africa plate boundary. It corresponds to a specific segment of this boundary characterized by the interplay between the Iberia and Nubia subplates, connecting the (Atlantic) transform Gloria Fault, in the West, with the dextral transpressive Rif-Tell shear zone (Morel and Meghraoui, 1996) to the East of Gibraltar Straits, and across the Betic-Rif orogenic arc. In the Gulf of Cadiz domain, the Iberia - Núbia plate boundary has been considered of a diffuse nature (Sartori et al., 1994; Medialdea et al., 2004), since a Present day WNW-ESE convergence between both plates at a ~ 4-5mm/yr rate, (e.g. Nocquet and Calais, 2004; Stich et al., 2006; Fernandes et al., 2007; Serpelloni et al., 2007, gray line in the inset of Fig. 1B) is here accommodated by a considerable number of widespread and differently orientated active tectonic structures, mostly exhibiting strike-slip and thrust fault kinematics (Fig. 1B). During the last decade, the systematic interpretation of acquired geophysical data (e.g. reflection/refraction seismics and multi-beam swath bathymetry) led to the progressive discover of several new tectonic features, resulting in the continuous upgrade of the Gulf of Cadiz tectonic map (see Fig. 1B, Gràcia et al., 2003a,b; Terrinha

et al., 2003; Zitellini et al., 2004; Rosas et al., 2009; Terrinha et al., 2009; Zitellini et al., 2009; Duarte et al., 2009, 2010).

The seismicity that has been recorded in the Gulf of Cadiz corresponds to a general scenario of moderate magnitude at shallow to intermediate depths (e.g. Fukao, 1973; Grimison and Chen, 1986; Buforn et al., 1995; Engdahl et al, 1998; Borges et al., 2001; Buforn et al., 2004; Stich et al., 2005), in which a direct correlation between earthquake location and known major tectonic structures is not straightforward. Large magnitude events also exist, such as the 28/02/1969 earthquake (Ms=7.9), and more noticeably the highly destructive 1755 Great Lisbon Earthquake (estimated magnitude between 8.5 and 8.8, e.g. Abe, 1979; Johnston, 1996; Solares and Arroyo, 2004), and associated tsunami (e.g. Baptista et al., 1998a,b; Zitellini et al., 2001; Terrinha et al., 2003; Baptista and Miranda, 2009). In addition, recent studies confirm higher depths for low-magnitude local earthquakes (40-60 km, Geissler et al., 2010), highlighting the relevance of seismogenic mantle rheology and deep lithospheric structures, complementary to the known (i.e. mapped) shallower crustal faults. The potential seismic hazard posed by the high magnitude earthquakes continuously triggers the interest, and the need, for determining their seismogenic (and tsunamigenic) sources, and hence to better understand the tectonic evolution of the region.

1.1. Tectonic setting

In the Gulf of Cadiz tectonic map of figure 1B three main sets of major structures can be recognized: 1) The frontal thrust that bounds the so called Gulf of Cadiz Accretionary Wedge (GCAW, in the eastern half of the study area, Fig. 1B); 2) a set of NE-SW striking thrust-faults, preferably located to the West of the Horseshoe

Valley (e.g. Horseshoe Thrust Fault, Marquês de Pombal Fault, Gorringe Fault); and 3) a set of WNW-ESE dextral strike-slip faults, corresponding to the SWIM wrench system, as defined by Zitellini et al. (2009). According to these authors, the later system corresponds to a broad deformation band extending across the whole of the Gulf of Cadiz domain (along 600 km), essentially characterized by sets of major deep seated, sub-vertical, dextral strike-slip faults: the SWIM faults (see Fig. 1B), which are thought to be active since at least ~1.8 My (Rosas et al., 2009). Noting the fact that these faults strike subparallel to the Present day convergence direction between Nubia and Iberia (WNW-ESE, see gray line in the inset of Fig. 1B), Zitellini et al. (2009) interpreted this SWIM Fault Zone as a precursor of a new (dextral) transcurrent plate boundary in the Gulf of Cadiz area. Apart from the GCAW, which Present day activeness and tectonic significance is still intensively debated (Gutscher et al., 2002; Gràcia et al., 2003a,b; Terrinha et al., 2003, 2009; Gutscher, 2004; Zitellini et al., 2004, 2009; Gutscher et al., 2009a,b), the other most important active structure intersected by one of the SWIM faults is the Horseshoe Thrust Fault (HTF - see Fig. 1B). Together with the Marquês de Pombal Fault (MPF) this Northwest directed thrust was previously proposed as a possible seismogenic source of the 1755 Lisbon Earthquake (Gràcia et al., 2003a,b; Terrinha et al., 2003), and corresponds to one of the most unequivocal active structures in this domain since Tortonian times (at least ~10My, e.g. Gràcia et al., 2003a,b; Zitellini et al., 2004; Terrinha et al., 2009).

1.2 Present work

If the SWIM 1 fault is part of a set of major active strike-slip structures delineating the onset of a new (dextral) transcurrent plate boundary, and if these same

structures intersect others such as the Horseshoe Thrust Fault also recognized as active, some kind of tectonic interference is expected to occur as a consequence. In the present work, analogue and 3D finite element numerical modeling experiments were carried out to understand the structural pattern that develops in a competent brittle medium (e.g. upper crust) as a result of the mechanical interference between a dominant right-lateral strike-slip fault, accounting for the Present day dextral transcurrent SWIM system (Zitellini et al., 2009), and a thrust fault complying with the also active, west-directed, Horseshoe thrust fault (see Fig. 1B). Model results were thoroughly compared with the natural example, and ensuing implications for its overall tectonic evolution explored and evaluated.

2. Morphotectonic characterization of the study fault-systems

The area studied in detail in the present work is limited by the dash-lined rectangle in figure 1B, which bathymetry and correspondent tectonic interpretation is depicted in figures 2 and 3, respectively. The newly proposed tectonic map of figure 3B corresponds mostly to the area of intersection between the Horseshoe thrust and the SWIM 1 faults, and it was investigated through the detailed combined analysis of the available multi-beam swath bathymetry (SWIM compilation, Zitellini et al., 2009), and a series of multi-channel seismic (MCS) reflection profiles, acquired during several different surveys (Fig. 3A; ARRIFANO – Arco Rifano, IAM - Iberian Atlantic Margin and SWIM – South West Iberian Margin, Sartori et al., 1994; Banda et al., 1995; Tortella et al., 1997; Martinez-Loriente et al., 2008). A detailed morphological characterization of the NW Gulf of Cadiz domain, and its several different sub-domains, was recently presented by Terrinha et al. (2009). Concurring with their proposal, the

main large-scale bathymetric features in the study area are here interpreted as being tectonically controlled by the activity of the recognized major fault-systems (described below, see Figs. 2 and 3).

Based on the seismic reflection dataset available, a general seismostratigraphy was also previously established for this domain (e.g. Sartori et al., 1994; Torelli et al., 1997; Tortella et al., 1997; Terrinha et al., 2009; Duarte et al., 2010) comprising (Figs. 4 and 5): a) A basal Mesozoic (Jurassic-Cretaceous) unit (~2 s twt) corresponding to carbonate sediments; b) A Late Miocene "chaotic body" unit (~1.5 s twt) with a semi-chaotic seismic signature, previously interpreted as an olistostrome body or as a tectonic mélange (Torelli et al., 1997; Tortella et al., 1997; Terrinha et al., 2009; Iribarren et al., 2007); and c) A top Late Miocene to Plio-Quaternary unit (~0.5 s twt), corresponding to a hemipelagic sedimentary cover.

2.1. Horseshoe Thrust Fault

The NE-SW trending HTF scarp is clearly observed in the bathymetry (Fig. 2A and B), displaying a maximum height of ca. 1000 m in its north-easternmost segment, gradually vanishing towards SW (Fig. 2 and 3). The SE half of the study area (mostly coinciding with the Horseshoe Valley at depths between -4200m and -4800m – see Fig. 2) is interpreted to correspond to the hanging wall of the NW directed Horseshoe Thrust Fault (e.g. Tortella et al., 1997; Zitellini et al., 2004;Terrinha et al., 2009), tectonically uplifted relatively to its footwall, which corresponds to the Horseshoe Abyssal Plain (HAP) in the NW half of the study area (at depths always greater than -4800 m). In the IAM4e profile (Figs. 4) the HTF (around shot point 1000 in Fig. 4) is clearly imaged as a SE dipping, deep seated fault. It roots well into the Mesozoic unit, prolonging

upwards across all the other overlying units, and breaching out at the sea-floor surface, where a resulting prominent deformation is marked by an offset of ca. 420 m (~0.6s twt in the IAM4e profile). The NW directed thrusting kinematics is clearly shown by the geometry of the folds affecting the Mesozoic reflectors near the fault plane, and by the unambiguous offset of the surface marking the top of the Mesozoic unit (see Fig. 4). To the SE of the HTF other relatively minor thrusts affecting the basal Mesozoic unit were previously described (e.g. Terrinha et al., 2009; Duarte et al., 2010), although these only affect the base of the overlying Late Miocene chaotic body (see Fig. 4). The same authors also report some degree of tectonic imbrication within the Miocene chaotic body further to SE, only mildly perturbing the sea-floor morphology.

2.2. SWIM 1 fault

The SWIM system was previously described by Zitellini et al. (2009) as corresponding to a set of WNW-ESE trending, vertical right-lateral strike-slip faults, characterized by a hundred-kilometer long linear bathymetric expression, ranging from the foots of the Gorringe Bank, in the West Gulf of Cadiz, across the HAP, the Horseshoe Valley and the GCAW, reaching its easternmost area near the Straits of Gibraltar (see Fig. 1B). The SWIM 1 fault (Figs. 1, 2 and 3) is crossed both by the IAM4 and the IAM3 seismic profiles (Fig. 5), where it can be observed to correspond to a deep-seated sub-vertical fault. It cuts across all the main seismostratigraphic units, occasionally breaching out, and it roots in the lower pre-Mesozoic (?) basement. Some segments of the fault exhibit an overall geometry resembling flower-like structures (Fig. 5B), agreeing with the previously proposed transcurrent kinematics (Duarte et al., 2009; Terrinha, et al., 2009; Zitellini, et al., 2009).

2.3. The new corner zone tectonic framework

The SWIM 1 fault intersects the Horseshoe thrust near its SW termination (Figs. 2 and 3). In the HAP, away from the HTF, the SWIM 1 lineament is not prominently recorded in the bathymetry, although the continuation of the correspondent basement strike-slip fault was thoroughly mapped further to the West, until the foothills of the Gorringe Bank, flanking its south-western termination (see Figs. 1B and 3B, Duarte et al., 2009; Terrinha et al., 2009). Interpretation of the available seismic dataset in this specific area (see Fig. 3A) led for the first time to the recognition of a new tectonic configuration (see map of Fig. 3B) comprising other faults – e.g. CF1 and CF2 - located near the intersection (corner zone) between the SWIM 1 strike-slip and the Horseshoe thrust, and also lacking any significant morphological expression in the HAP sea-floor (Fig. 3B and 5). In the IAM4 profile it is possible to observe that these corner faults correspond to steep (southwards) dipping faults, rooting in the basement underneath the Mesozoic unit and cutting across the overlying units, including the base of the Late Miocene to Plio-Quaternay top unit (see Fig. 5). In the case of CF1 the sea-floor surface is also perturbed (around sp 4840 in IAM4 profile, and black arrow in Figs. 2 and 3B), whereas CF2 lacks any kind of bathymetric expression. In the IAM4 profile a reverse-fault component of movement along both CF1 and CF2 faults is apparent, revealed namely by the offset of the upper limit of the Mesozoic unit across these faults that clearly denounces the upward movement of the respective SE fault blocks (see Fig. 5). Since the faults are highly steep, a pure dip-slip thrusting movement is mechanically implausible in this situation. In contrast, oblique-slip faults, characterized by a

fundamentally dextral transcurrent kinematics and a minor thrusting component, would mechanically adequate to the observed structural geometry.

Adding to this structural evidence, recently proposed relocation of low to moderate magnitude earthquakes in the study area (Geissler et al., 2010), showed the existence of two clusters, concentrating near the northern and southern terminations of the HTF (Fig. 6, Geissler et al., 2010). The southern cluster coincides with the SWIM 1-HTF corner zone area, and exhibits a WNW-ESE general trend parallel to the SWIM 1 fault. It should be noted that most of these hypocenters are located at relatively high depths (40-55 km), probably in the lithospheric mantle (Geissler et al., 2010; Sallarès et al., 2011), and thus cannot be directly linked to the faults imaged by the MCS profiles at upper crustal levels (maximum depths of ca.6km; see discussion below in section 5). Nevertheless, the reported corresponding focal mechanisms solutions in this corner zone domain show significant heterogeneity, possibly due to varied fault orientation, but generally accounting for dominant reverse and strike-slip faulting (Geissler et al., 2010).

These tectonic and seismic corner-zone manifestations are here hypothetically considered to have formed as the result of a particular type of thrust-wrench tectonic interference between the Horseshoe and the SWIM systems at different depths. The upper-crust fault interference between the SWIM1 dextral strike-slip and the HTF is expected to provide some insight on the causes for the recorded seismicity at higher (mantle) depths, and is thus investigated and tested through the analogue and numerical modeling experiments presented below.

3. Analogue modeling

Analogue modeling experiments of separated wrench systems (e.g. Mandl et al., 1977; Richard et al., 1991; Dooley and McClay, 1997; McClay and Bonora, 2001; Schopfer and Steyrer, 2001; Le Guerroue and Cobbold, 2006) and thrust systems (e.g. Malavieille, 1984; Mulugeta, 1988; Lallemand et al., 1994; Gutscher et al., 1998a,b; Agarwal and Agarwal 2002; Lohrmann et al., 2003; Ellis et al., 2004; McClay et al., 2004; Bonnet et al., 2007; Zhou et al., 2007; Malavieille, 2010) are common and well documented. Conversely, physical modeling dealing with the deformation caused by simultaneous thrusting and wrenching is less common, and generally focused on a variety of different specific aspects (e.g. Diraison et al., 2000; Di Bucci et al 2006, 2007). Hence the present work, in which sand-box analogue models were produced to better understand the deformation patterns resulting from thrust-wrench fault interference under the specific conditions of the study area.

3.1. Experimental method

3.1.1. Material properties and scaling

Experiments were done using dry quartz sand which properties are summarized in Table 1. Sand is considered a Coulomb material deforming in a brittle way according to the Coulomb fracture criterion (e.g. Hubbert, 1937, 1951; Davis et al., 1983, Appendix A), and it has been extensively used in scaled model experiments simulating brittle deformation in the upper crust or other lithospheric competent levels. Since brittle deformation is time independent while inertial acceleration is negligible, scaling was achieved through classically considering model-prototype ratios of fundamental units (Hubbert, 1937), only for mass (through density) and length ($\lambda=L_{mod}/L_{prot}=5x10^{-6}$

or 1/200.000). All the assumed model - prototype ratios are presented in Table 1, and the detailed procedure of scaling is specified in Appendix A.

3.1.2. Apparatus, initial stage and procedure

All the experiments were carried out in the 100 x 60 cm Perspex deformation box depicted in figure 7. The box consists in two horizontal 1cm thick basal plates (plates A and B in Fig. 7) that move relatively to each other along the X direction, simulating a right-lateral strike-slip (basement) fault. A thin metal sheet attached to the base of a backstop is moved by a stepping motor also along the X direction, sliding on top of both basal plates (Fig. 7A). The front of this metal sheet works as a velocity discontinuity (VD) at an angle of 60º/120º with the direction of the strike-slip fault (X direction). Two fixed lateral vertical walls confine the whole system. In the initial stage, a layered sand cake was mounted inside the box on top of the intersection between the basal strike-slip fault and the velocity discontinuity (Fig. 7B). This was achieved by pouring batches of differently colored sand from a moving elongated funnel (with a width matching the 60cm of the box), guarantying the leveling of its top surface. In most experiments the sand cake thickness was 3cm (corresponding to 6 km in nature), although in several experiments thickness of 4 and 5 cm (8 and 10 km) were also considered. Layering in the sand cake has no correspondence with any natural structures, and was used merely as a 3D strain marker, since in the end-stage of all the experiments the deformed sand cake was humidified, and several slices were serially cut along different chosen orientations. Likewise, parallel (or sometimes square) line grids were also imprinted on the top surface of the model to serve as (2D) passive strain markers. In the present modeling the driving kinematics was conceived to correspond to the basal right-lateral strike-slip faulting, concurring with the natural example where the

dextral SWIM faults are observed to strike subparallel to the Present day convergence between Iberia and Nubia as shown by the reported geodetic data (e.g. Nocquet and Calais, 2004; Stich et al., 2006; Fernandes et al., 2007; Serpelloni et al., 2007, see gray line in the inset of Fig. 1B). In accordance, all the experiments comprised the following two successive steps (see Fig. 7A):

1) A very brief preliminary one that consisted in moving the backstop (and the attached thin metal sheet) along the X direction to the left, only until few thrusts were observed to have formed breaching out at the top surface of the sand cake. This was done merely to produce an initial planar week anisotropy representing the original geometry of the HTF system, at an angle of 60/120º with the basal (SWIM) strike-slip direction.

2) A second one that consisted in moving the basal plates relatively to each other (also along X), by pushing the furthest plate (basal plate A) to the right (see Fig. 7A), producing a right-lateral strike-slip movement along the vertical contact surface between both basal plates, simulating the (SWIM 1) basement vertical strike-slip fault.

During step 2, the central ("corner zone") domain of basal plate A was limited by two main kinematically active boundaries: one corresponding to the trace of the basal strike-slip fault, and the other to the velocity discontinuity (see Fig. 7A). Since the dextral strike-slip along the contact with plate B was accomplished by moving plate A to the right, the boundary between this plate and the over-sliding thin metal sheet (velocity discontinuity) corresponded to a convergent limit between the sand above basal plate A,

and the sand sitting on top of the thin metal sheet (edged by the velocity discontinuity). Thus, the driving forces for deformation in the sand came from the relative movement between the sliding basal plates and the thin metal sheet, which were both in frictional contact with the overlying sand. As result, during the second experimental step, the sand cake on top of the boundary between both basal plates endured dextral wrenching deformation, whereas simultaneously shortening accommodated by thrusting occurred in the sand above the velocity discontinuity. Stepping motors were used to move both the backstop and the basal plates at a constant velocity (~20cm/hr). The dimensions of the deformation box were sufficiently large to guarantee that the bulk of the model was not affected by boundary effects, and experiments were repeated several times to ensure the consistency of the obtained results. Besides photos of serially cut sections of the (end-stage) deformed models, top view photographs were also taken at regular time intervals as the experiments unfolded.

3.2. Experimental results

The main obtained results are depicted in figures 8 and 9. During the first experimental step a pop-up structure always formed, bounded by a pair of opposite ~30º dipping (fore and back) thrusts, rooting in the velocity discontinuity (Fig. 8A1). During the second experimental step, different types of structures were simultaneously formed in the different areas of the model analyzed below.

3.2.1. Thrust-front and wrenching domains

In the area in front of the main thrust and relatively away from the corner zone (thrust-front domain depicted in Fig.8), the incremental accumulation of shortening

resulting from moving basal plate A to the right could no longer be exclusively accommodated by the original pair of thrusts (forethrust and backthrust) formed during experimental step1 (Fig. 8A1), and thus new forethrusts were successively formed (Fig. 8A2-A3 and B-C). As is classically the case in these type of experiments (e.g. Bonini et al., 2000; Persson and Sokoutis, 2002; Lohrmann et al., 2003; Maillot and Koyi, 2006; Koyi and Maillot, 2007) each new thrust rooted in the VD and accommodated a certain amount of shortening, before being transported along the backthrust fault plane when a newer forethrust was formed, leading to the end-term situation depicted in figure 9B (cross section 6).

Simultaneously, in the sand cake above the basal strike-slip fault (wrenching domain as defined in figure 8), the first formed structures were en-échelon Riedel faults (Riedel, 1929, R-faults in Fig. 8A2) orientated at low angles to the basement strike-slip direction (15° to 20° for the first increments of deformation). Between these, several P-faults also developed. Offset of parallel lines on model surface by R and P faults showed a synthetic (dextral) strike-slip component of movement along these structures. Further strike-slip increments (Fig. 8A3) originated Y-faults that formed parallel to the basement fault direction, cut the early R and P-faults, and also exhibited dextral strike-slip kinematics. As shear strain accumulated, the surface area between the R-faults rose significantly (compare the topography of Figs. 8A2 and A3) originating a deformation band parallel to the basement fault with a characteristic surface morphology, comprising several sub-parallel elongated bulges (see Fig. 8A3). Subsequent strike-slip increments mostly produced a continued reduction of the width of the previously formed deformation band, besides the amplification of its relief. In cross sections cut perpendicular to the deformation band (Fig. 9 – cross sections 1 and 2) the observed overall fault pattern corresponded to an upwards splaying from the basement fault,

typically defining a flower structure. Within this, R-faults exhibited in some degree a reverse component of movement, in line with an oblique (dextral-reverse) kinematics, although in the complete absence of any externally induced compression. These structures are typical of wrench fault systems, and confirm previous standard modeling results (e.g. Mandl et al., 1977; Richard et al., 1991; Dooley and McClay, 1997; McClay and Bonora, 2001; Schopfer and Steyrer, 2001; Le Guerroue and Cobbold, 2006). Specifically, the occurrence of oblique dextral-reverse kinematics along helicoidal R-faults in the absence of any externally induced compression, was previously explained as a result of 5-10% of dilatation in the sand, which is also thought to occur in similar degree in brittle natural rocks (e.g. Schopfer and Steyrer, 2001; Le Guerroue and Cobbold, 2006).

3.2.2. Corner zone

In the corner zone (as defined in Fig. 8), a lateral propagation of the thrust faults (F2,F3… Fn) to the wrenching domain was consistently observed, characterized by a rotation of these faults towards an orientation sub-parallel to the basal strike-slip direction (i.e. X axis, e.g. F2 in Fig.8A2 and B; F3 in Fig.8C). This parallelization occurred since relatively early strike-slip increments, and implied a clockwise rotation of about 60º around an inflexion point (IP in Figs. 8A2, B and C). Offset of parallel strain marker lines along these rotated fault segments agree with a dextral strike-slip component of movement. In sections cut across the same structures (Fig. 9 – cross section 3, 4 and 5), it was apparent that these also maintained a thrusting component, in accordance with general dextral-reverse oblique kinematics (e.g. F5 in cross section 3 and 4 of Fig.9). In some experiments, strain accommodation in the corner zone implied the formation of new forethrusts in front of previously rotated fault segments (e.g. F3

and F2 respectively in corner zone domain of Fig. 8A3), which as a result ceased to propagate and were passively thrusted in the hanging wall of the newer thrust-faults. Subsequently, these newer thrusts were themselves rotated also towards the basal strike-slip fault direction, mimicking the rotation of the previous ones. For further strike-slip increments, the early formed structures in the corner zone were masked by the later deformation and became eventually indistinguishable. As a result, only the younger outer (oblique) faults were possible to observe in this domain (compare F5 outer thrust with F3 and F4 in Fig. 9A). The earlier (inner) thrusts tended to become more parallel to the strike-slip direction (i.e. they rotated more, e.g. F2 in Figs. 8A2, B and F3 in Fig. 8C) than the later outer ones, which generally displayed a more oblique direction, subperpendicular to the one bisecting the angle made by basal strike-slip and the velocity discontinuity (e.g. F5 in Fig. 9A). In cross sections cutting both the wrenching deformation band and the thrust domain, obtained progressively closer to the zone of intersection between the basal strike-slip and the velocity discontinuity (Fig. 9A and B - cross sections 3, 4 and 5), it was possible to observe the along space variation of the interference between wrench-related and thrust-related structures:

In cross section 3 (Fig. 9B), wrench and thrust domains can still be individualized. In the wrench domain, the corresponding deformation band was observed to be bounded, on the left, by a rotated segment of an outer thrust (F5, in Figs. 9A and B), and on the right by a Riedel fault. Both these structures showed some degree of dip-slip reverse movement, corresponding to dextral-reverse oblique faults bounding a transpressive pop-up, cut by Y-faults in its middle. The thrust domain along this same direction also corresponded to a (slightly asymmetric) pop-up structure, although in this case bounded by faults lacking any kind of strike-slip component of movement, formed during the

first experimental step (faults in yellow in cross section 3 of Fig. 9B): on the left two forethrusts (F1 and F2), and on the right the original backthrust (BT).

Cross section 4 was cut closer to the intersection between the basal strike-slip fault and the velocity discontinuity (Fig. 9B – cross section 4). In this cross-section the right-bounding R-fault of the wrench domain was no longer observed, and instead the two original left-bounding faults of the thrust domain (F1 and F2) occurred immediately to the right of the Y-faults. It should be noted that to the left of these Y-faults, all the others (F3 – F5) also accommodated some amount of dextral wrenching, consisting in rotated segments of original thrusts exhibiting oblique (dextral-reverse) kinematics. Conversely, to the right of the Y-faults, the (F1 and F2) thrusts lacked any kind of wrenching component.

Cross section 5 was cut through a direction containing the intersection between the trace of the basal strike-slip fault and the velocity discontinuity (Fig. 9B – cross section 5). Along this direction the separation between thrust and wrench domains was no longer straightforward. Instead a single interference domain was observed, comprising both original pure thrusts, formed during the first experimental step (F1, F2 and BT faults in yellow in Fig. 9B – cross section 5), and dextral strike-slip Y-faults as well as oblique dextral-reverse faults, formed during experimental step 2 (Y and F3-F5 faults in black in Fig. 9B – cross section 5). F1 and F2 faults were positioned to the left of Y-faults along this same cross-section, with the first steepening at depth towards the second, together defining a tulip-like (positive) flower-structure geometry, complying with overall (dextral) transpressional kinematics.

4. Numerical modeling

Given the same general rheological, geometrical and kinematical constraints described above for the SWIM 1 - HTF tectonic system, wrench-thrust mechanical interference was simulated in a three-dimensional plate model using the ABAQUS/Standard software (ABAQUS, Inc. 2009). In this case the main objective was twofold:

a) Examine the patterns of stress and strain distribution in the corner zone area and at depth, which could not be achieved by analogue modeling alone;

b) Investigate the influence of an interbedded soft layer in the development of the corner zone deformation pattern, likewise benefiting from the numerical modeling approach that allows a simpler way of directly manipulating the rheological stratified structure of the model.

4.1. Model setup

A basic model was considered (MOD1) representing an upper crustal block covering an area of 480 x 180 km, with a thickness of 6 km (Fig. 10A and C). This thickness complies with the maximum depth imaged by the available reflection seismics (e.g. TWT-depth conversion of IAM-4 line across the HAP by Jiménez-Munt et al., 2010 and Gónzalez et al., 1998). Present model results were drawn from a central 240 x 180 km subarea, to avoid boundary effects. Two planes of weakness, i.e. idealized faults, account for the Horseshoe thrust and SWIM 1 dextral strike-slip, dipping 30° and

90° respectively, and intersecting each other with their surface traces making an angle of 120º/60º as in the natural example (see Figs. 2 and 3).

The interpretation of the available seismic reflection dataset also supports the assumption of a ~1.5 km thick layer, corresponding to the Late Miocene "Chaotic Body" unit (see Figs. 4 and 5), at approximately 1.5 km below the seafloor. This "chaotic" seismic signature has been previously interpreted as resulting from a mixture of olistostromes and tectonic mélanges (Torelli et al., 1997; Tortella et al., 1997; Terrinha et al., 2009; Iribarren et al., 2007), which could hypothetically determine a relatively less competent, or event somewhat soft, rheological behavior. Such a possibility is here simulated by including an interbedded soft layer in the second set of models (MOD2). Also in this case the strike-slip fault does not reach the seafloor surface, as it terminates at the top of the soft layer at 1.5 km depth (Fig. 10D). This mimics the natural example were the SWIM1 fault shows little bathymetric expression (see Figs. 2 and 3), only mildly perturbing the top Late Miocene to Plio-quaternary unit in a few situations, although always undoubtedly cutting across the underlying Miocene "Chaotic body" unit (see Fig. 5).

4.1.1. Rheologic and fault parameters

Although ABAQUS comes with many material behavior benchmarks we needed to conduct a large number of systematic tests to select the material properties. The most challenging were the material properties of the cohesive elements that constitute the faults, since they are commonly calibrated for small scale fractures found in engineering problems, and not for large scale geologic faults. Our approach was to iteratively change the parameters until we found displacement and stress solutions compatible with the natural estimates and observations. The Drucker-Prager plasticity model was chosen

to model the brittle crustal behavior, since it is intended for geological materials that exhibit pressure-dependent yield and was found to be more stable than the Mohr-Coulomb model. Since we were not interested in examining the details of the stress distribution within the soft layer a simple Von-Mises plasticity model was chosen to model the soft layer in MOD2. The Von-Mises material yields at a lower stress than the surrounding crustal material to simulate a decoupling layer.

The thrust and strike-slip faults are modeled as layers of cohesive elements. These are specifically designed for bonded interfaces where the interface thickness is negligibly small compared to other model dimensions. The constitutive response of the cohesive layer is defined in terms of an elastic traction versus separation law, i.e. there are three components of separation, one normal to the interface and two parallel to it. To prevent faults from opening or closing the normal component (E) is much stiffer than the in-plane components (G1 and G2). The thrust fault has greater G1 and G2 values than the strike-slip fault following the Coulomb-Navier's law of fracture strength. All the material parameters are listed in Table 2.

4.1.2 Boundary conditions and procedure

The boundary conditions try to match those of the analogue modeling experiments as closely as possible. Deformation is simulated by moving basal plate A to the right relatively to plate B (see Fig. 10A). Because there are some stiffness along the strike-slip fault, plate B is dragged by plate A towards the thrust fault. The maximum prescribed displacement along the X direction was 10 km, yielding a maximum shortening of 2%. Both basal plates are fixed in along the Y direction. Gravity (g=9.8m/s^2) is applied as a body force. To counterbalance the weight of the overlying crust a lithostatic pressure is applied at the bottom of the model. Isostasy is simulated by

applying spring forces at the bottom of the model with stiffness per unit area equal to $(\rho m - \rho w)g$ where ρm=3300 km/m^3 is the mantle density and ρw=1000 km/m^3 is the water density.

4.2. Model Results

4.2.1 Displacement pattern

Deformation of the basic model (MOD1) is illustrated by vertical displacement contours on a strained reference frame (i.e. grid, Fig. 10B), which shows that the rightwards push of basal plate A was accommodated by movement along both the thrust and strike-slip faults. Flexure of the plate also occurred in response to the topographical load caused by the fault offset, in agreement with the flexural theory of faulting. For 2% of shortening the maximum throw along the thrust fault was 1300 m (Fig. 10B), which is above the maximum observed throw along the Horseshoe Thrust Fault (~1000 m). It should be noted that in nature instead of a single thrust a system of thrusts accommodates the shortening (see, Fig. 4), implying that the maximum allowed shortening is underestimated in the simulation, whereas the fault's throw is overestimated.

4.2.2. Stress pattern

The stress field was analyzed in terms of maximum shear stress $\frac{1}{2}(\sigma_3 - \sigma_1)$ at the top and bottom of the plate (Fig. 11A). In both models (MOD1 and MOD2) it was observed that: a) The stresses were larger at the bottom than at the top of the plate, and largest stresses occurred at depth in the footwall of the thrust fault; b) At the top of the plate the largest stress contours occurred in the thrust hanging wall, elongated parallel to

the thrust direction; c) At the bottom of the plate the largest stress contours were also aligned parallel to the thrust, but were located in its footwall instead; and most important d) with the exception of MOD 2 surface, stress contours consistently show a stress concentration in the corner zone (MOD1 Z=0 and 6000m and MOD2 Z=6000m in Fig. 11A). These corner stress magnitudes were larger and their distribution was wider at depth, whereas at the surface of MOD2 stress concentration was practically absent in the corner zone area. In this case, where the strike-slip fault was not prescribed above a soft layer (see Fig. 10D), the level of stress affecting the model plate was generally lower relatively to MOD1. Additionally, shear stress was focused along the direction of the strike-slip fault at the model surface (MOD2, Z=0m in Fig. 11A), although not at its bottom (Z=6000m) where a corner stress concentration clearly persisted (MOD2, Z=6000m in Fig. 11A). Likewise, the plot of principal stresses at model surface shows that in MOD1 the stress directions clearly rotate near the corner zone, and the maximum compressive stress magnitude increases by a factor of 1/3 (Fig. 11B, MOD1). Conversely, in MOD2 the maximum compressive stress orientation showed a constant obliquity (of 45º-50º) relatively to the strike-slip direction, without significantly varying its magnitude (Fig. 11B, MOD2). This is consistent with the focusing of shear deformation along the direction of the SWIM fault, in accordance with the contoured stress distribution mentioned above (MOD2, Z=0m in Fig. 11A).

4.2.3. Initiation of brittle rupture (exceeded failure criterion)

The plot of the locations where the Drucker-Prager failure criterion was first exceeded in the plate model (Fig. 12) also showed the corner zone as one of the places where this occurred, both at the top (MOD1) and bottom of the plate. In both models, at 6 km depth, brittle failure was predicted to occur in the corner zone and parallel to the

Horseshoe Thrust Fault direction over a distance of 45 km. At the surface, both models showed rupture initiation in the hanging wall of the Horseshoe thrust, parallel to its direction, complying with the location of a backthrust. Also concurring with the stress distribution pattern described above, at the surface of the model plate, corner zone rupture initiation was only observed in MOD1 (Z=0m), and was absent at the surface of MOD 2 (Fig. 12, MOD2, Z=0m), where failure was preferably predicted to occur along the direction of the strike-slip fault.

4.2.4. Strain pattern

The strain pattern was analyzed in terms of the equivalent plastic strain, i.e. the total unrecoverable strain accumulated after the onset of yielding according to the Drucker-Prager criterion. The pattern of plastic strain for both models is shown at three levels (Fig. 13): the top of the plate (Z=0m), the level corresponding to base of the soft layer in MOD2 at 3000 m depth, and the bottom of the plate (Z=6000m). The results can be summarized as follows:

a) The largest strains were focused in the corner zone at all levels of MOD1, and strain concentration was larger in magnitude at depth than at the surface of the model (Fig. 13 compare in MOD1 Z=0m with Z=3000m and Z=6000m).

b) In MOD1 besides the corner zone, strain contours also occurred elongated parallel to the thrust direction, either in the footwall of the thrust at the base of the model (Fig. 13, Z=6000m), or more widely distributed in its hanging wall at the surface of the model (Z=0m).

c) At MOD2 surface (Fig. 13, Z=0m) strain concentration occurred in the footwall of the thrust, along a 20 km wide deformation band parallel to the direction of the underlying strike-slip fault. At the base of the soft layer, strain also concentrated in the same area, but was clearly more widely distributed within plate A (Fig. 13, Z=3000m).

d) In MOD2 at the base of the model (Fig. 13, Z=6000m) corner zone strain concentration persisted, but was clearly reduced relatively to MOD1 at the same depth.

5. Discussion

Both analogue and numerical modeling results clearly show the importance of a *corner effect* expressed by the deformation pattern that is expected to develop in a brittle medium due to the mechanical interference between a dextral strike-slip fault and a thrust, intersecting each other at an angle of 120º/60º. Analogue modeling provides a characterization of the resultant basic structural pattern, revealing its essential geometry and kinematics. Numerical modeling provides insight on the way stress and strain are fundamentally distributed under the same conditions, and considers the effects of simple rheological variation accounting for an interbedded soft layer within the same brittle medium.

5.1 Analogue modeling output

The experimentally obtained structural pattern is mostly characterized by a concentration in the corner zone of (see Figs. 8 and 9): a) oblique (dextral-reverse) faults, with different evolving geometries and associated kinematics; and b) vertical

(dextral) strike-slip Y-faults. While Y-faults remain geometrically and kinematically stationary as strain accumulates in this area, corner zone oblique faults do not, corresponding to segments of originally pure thrusts that progressively propagate and rotate from the thrust-front to the wrench domain (see Fig. 8). This propagation-rotation is matched by a corresponding change in kinematics; from pure (reverse dip-slip) thrusting, to oblique (transcurrent dominant) dextral-reverse faulting. Early formed faults undergo a greater amount of more abrupt rotation, with their planes being more promptly parallelized to the basal strike-slip direction (F2 in Figs. 8A2 and B, and F3 in Fig. 8C). As strain continues to accumulate in the corner zone these same planes also become steeper (from an original dip of ~30º), and eventually subparallel to the Y-faults, preferably accommodating dextral strike-slip movement (see for instance in F3 and F4 in cross section 4 of Fig.9B). Later (outer) faults in the corner zone endure relatively less displacement, and thus are less rotated and steepened, striking somewhat subperpendicularly to the bisector of the angle defined by the thrust-front and the wrenching domains (see for instance F5 in Fig. 9A and cross section 5).

These results show that in this particular structural setting faults genetically related either to the wrench or to the thrust system do not evolve independently. Active strike-slip faulting in the wrench domain simultaneously triggers reverse (dip-slip) faulting in the thrust domain, which subsequently evolve to oblique-slip faulting towards the corner zone.

5.2. Numerical modeling output

The numerical modeling results comply with the existence of a wrench-thrust interference corner effect, in accordance with the structural pattern obtained in the analogue modeling experiments.

5.2.1. MOD1

Stress and strain contours obtained for MOD1 reveal a consistent concentration in the corner zone, both at the bottom and at the surface of the model (see Figs. 11A and 13, MOD1). Likewise, plot of brittle rupture initiation (Fig. 12, MOD1) also shows that failure is prompt to initiate in the same interference area. This agrees with the corner zone concentration of faults that characterizes the structural pattern formed in the analogue models (see Figs. 8 and 9). Also, the rotation of the stress field and of the maximum compressive stress in the corner zone (see Fig. 11B – MOD1) agrees with the described geometry and kinematics of early formed (inner) faults in the analogue models, specifically with their steepness and dominant-transcurrent oblique kinematics (see F3 and F4 in Fig. 9A and cross section 4).

Besides the corner zone, the obtained stress and strain contours also show a preferable concentration parallel to the direction of the thrust-fault, both in its footwall at the bottom of the model (Figs. 11 and 13 MOD 1, Z=6000m), and in its hanging wall at model surface, corresponding to a wider distribution in this case (Figs. 11 and 13, MOD 1, Z=0m). In the footwall, this is compatible with the expected site of nucleation of a new forethrust at depth, which also complies with the obtained analogue results, whereas in the hanging wall the stress-strain wider distribution could result from the combined effect of backthrust nucleation and outer-arc extension, associated to some degree of fold-thrusting in the hanging wall. The plot of the locations where the brittle failure criterion was first exceeded in MOD1 also confirms these assumptions, showing

a narrow strip corresponding to the potential forethrust rupture zone in the footwall at depth (Fig. 12, MOD1, z=6000m), and a wider band that could correspond to the more distributed rupture area accommodating outer-arc extension in the hanging wall at model surface (see Fig. 12, MOD1, z=0m).

5.2.2. MOD2

The fact that the prescribed strike-slip fault in MOD2 does not breach out at the model surface, ending at the top of the interbedded soft later (at 1.5 km depth, Fig. 10D), explains the (almost complete) absence of a corner effect in this case, since it prevents the stress and strain from concentrating in the corner zone area above the strike-slip fault (see Figs. 11 and 13, MOD2 at Z=0m). Instead, stress and strain are preferably concentrated along a deformation (shear) band, coincident with the direction of the underlying strike-slip fault. The plot of the location where brittle rupture initiates also confirms the absence of corner zone rupture at the model surface, showing it is preferable expected to occur along the strike-slip fault direction (see Fig. 12, MOD2, Z=0m).

At the base of the soft layer, although strain concentration along the strike-slip direction is also apparent, a strain delocalization effect clearly occurs in the area corresponding to the footwall of plate A (Fig. 13, MOD2, Z=3000m). Such strain delocalization is determined by the (soft) rheological response of the interbedded layer that manifests by the hindering of fault nucleation and propagation.

At the base of MOD2 the corner effect, which is practically absent at model surface, persists (Figs. 11, 12 and 13, MOD2, Z= 6000m), since here the existent strike-slip fault favors stress concentration and strain accumulation the corner zone.

5.3. Comparison with the natural example and tectonic implications

The morphotectonic interpretation of the HAP corner zone area, based on the available bathymetry and MCS reflection dataset, revealed a natural structural pattern consistent with the one obtained in the analogue modeling experiments (Fig. 14). Similarities between the model and natural example are mostly represented by faults exhibiting matching particular geometries and kinematics. Such model-prototype congruence shows that the observed natural tectonic pattern was not formed randomly, but instead corresponds to what is to be expected for the described thrust-wrench interference between the SWM 1 and Horseshoe faults.

The modeled interdependency between both these fault systems, agrees with a possible multi-rupture scenario involving coeval strike-slip faulting in the wrenching domain (SWIM system), reverse-faulting in the thrust domain (Horseshoe system), and sequentially induced oblique, dextral-reverse faulting in corner zone (SWIM 1 – HTF intersection). Multi-rupture scenarios have been documented in other places involving dominant transcurrent continental fault-systems, in which main strike-slip earthquakes trigger thrust-related aftershocks, generally nucleating in restraining bends subsidiary of the main transcurrent system (e.g. Gobi-Altay fault and San Andreas fault, Bayarsayhan et al., 1996, Kurushin et al., 1997). Although also in continental domains, wrench-thrust interference faulting is likewise known to be associated to complex rupture, comprising triggering of thrust faulting only tens of seconds after strike-slip faulting (e.g. 1976 Tangshan earthquake, Butler et al., 1979). In the Gulf of Cadiz, multi-rupture associated to some kind of interference between different faults (e.g. the HTF, MPF and SWIM) has also been generically proposed by previous authors (e.g. Gràcia et al., 2003a,b; Terrinha et al., 2003, 2009). Specifically in the present case, and given the dimension of

the faults at stake, rupture areas associated to the corresponding earthquakes could hardly justify the energy release implied by high magnitude events (M>8.5), such as the 1755 Great Lisbon Earthquake (Gutscher et al., 2009b). Nonetheless, the potential multi-rupture associated to the study thrust-wrench tectonic interference should be taken into consideration while addressing seismic hazards for low to moderate magnitude events (up to M7).

In the study area, recent reports on the local seismicity corresponding to these low to moderate magnitude events (Geissler et al., 2010; Silva et al., 2010) showed a strong concentration in the SWIM1-HTF corner zone (see Fig. 6). However, it should be noted that these earthquakes are located at depths mostly comprised between 40 and 55 km, corresponding to the base of the seismogenic layer (within lithospheric mantle), whilst in the available MCS profiles corner faults are imaged at maximum depths of approximately 6km: one order of magnitude below (e.g. CF1 and CF2 in Fig. 5). It is thus difficult to envisage a direct connection between these faults, imaged at upper crustal depths, and the reported seismicity originated at lithospheric mantle depths. Nonetheless, it should be noted that the great majority of these earthquakes is concentrated ~14 and ~25km to the SE of CF1 and CF2 corner faults, respectively (see Fig. 6) in an area closer to the intersection between the SWIM1 and Horseshoe faults. Such earthquake location would comply with a southeastwards dip of CF1 and CF2 faults of about 74º and 62º respectively, admitting the unlikely possibility that they could prolong 40-50km downwards to the lithospheric mantle without being significantly deflected. Even so, the mentioned fault steepness qualitatively agrees with the interpretation proposed for these structures in the MCS profiles (see Fig. 5), and is also compatible with their interpreted dominant transcurrent oblique kinematics. In spite of the seemingly congruence regarding these aspects, no direct evidence exists at this

point to support that these corner structures correspond to translithospheric, or even deep seated faults, as is the case of the SWIM 1 and the HTF. As a result, it is more likely that the studied thrust-wrench interference corner effect recognized in the upper-crust could also exist at deeper lithospheric levels. Accordingly, a replication of the same tectonic interference pattern would occur at different depths, in different lithospheric layers with similar bulk rheology, under the same regional (tectonic) stress constraints. This is seemingly supported by the congruency between the variable orientation of the seismically imaged faults (at upper crustal depths), and the variation of planes deduced from focal mechanisms (at mantle lithospheric depths). These same focal mechanisms were also reported as somewhat heterogeneous by Geissler et al. (2010), although mostly compatible with reverse and strike-slip faulting. Such heterogeneity agrees with the modeled thrust-wrench tectonic scenario as shown by the obtained interference structural pattern in the analogue models, where corner zone faults assume evolving different geometries and kinematics (see Figs. 8 and 9). Geissler et al. (2010) also report the direction of the principal stress components, based on the estimated average stress tensors consistent with observed fault slip orientations. According to this, the maximum compressive stress rotates from an approximately E-W direction, near the northern termination of the HTF ($\sigma 1$ at N103ºE/26º strike/plunge), to a more N-S direction in the corner zone ($\sigma 1$ at N351º/12º), roughly bisecting the angle between the SWIM 1 and the Horseshoe Thrust Fault (see $\sigma 1$ in Fig. 6). This rotation complies, not only with the corner zone rotation of the maximum compressive stress obtained for MOD1 numerical results (see Fig. 11B, MOD1), but also with the orientation of the characteristic oblique corner faults, observed both in the analogue model and natural structural patterns (see Figs. 8, 9 and 14).

The idea that the same thrust-wrench tectonic interference can manifest in a decoupled manner at different (crustal and mantle) lithospheric depths, could explain the recurrently recognized spatial discrepancy in the Gulf of Cadiz between: (a) the mapped main tectonic structures, possible associated to high magnitude earthquakes, and (b) the dominant low to intermediate "background" seismicity (up to M7), to which specific faults are generally difficult to ascribe.

Such a decoupling is also illustrated at a different scale, in the upper crust, by MOD2 numerical modeling results (see Figs. 11, 12 and 13), which show that an interbedded soft layer can be responsible for some degree of strain delocalization, hindering the propagation of faults, and thus inhibiting the morphological expression of the fault interference pattern in the corner zone area. This could explain the poor bathymetric expression of the corner zone structural pattern in the HAP seafloor, caused by a soft-like rheological behavior of the Late Miocene "Chaotic Body" unit determined by its postulated olistostromic nature.

6. Conclusions

The following main conclusions are drawn:

a) The detailed newly mapped tectonic pattern, observed in the intersection area (corner zone) between the SWIM 1 fault and the Horseshoe thrust, formed as the result of the tectonic interference between correspondent active strike-slip and thrust faulting, respectively.

b) Modeling results show that dextral strike-faulting in the SWIM wrenching domain promotes reverse faulting in the Horseshoe frontal-thrust domain, and sequentially (dextral-reverse) oblique faulting in the (corner) zone of intersection between both main faults. Results show that in the corner zone domain a preferred concentration of stress and strain occurs (corner effect), and is mainly accommodated by oblique faulting, although faults exhibit different evolving geometries and matching kinematics as they endure some degree of rotation.

c) In view of the present results, a multi-rupture scenario, within the active tectonic framework of the connected SWIM 1 and the HTF systems can be envisaged, and should be carefully considered in assessing the seismic-related hazards of low to moderate seismicity (up to M7) in the Gulf of Cadiz region.

d) In the SWIM 1- HTF corner zone the tectonic pattern is seismically imaged at upper crustal depths, whereas the local seismicity is reported to preferentially occur in the lithospheric mantle (Geissler et al., 2010). Nonetheless, faults and seismicity data are congruent in a number of aspects (orientation of fault planes and planes deduced from focal mechanisms, fault kinematics and focal mechanisms, compatibility with similar stress filed orientation). This suggests the possibility of a decoupled manifestation of the same thrust-wrench tectonic interference at different lithospheric depths, which would explain the recurrently observed discrepancy between the mapped main tectonic structures in the Gulf of Cadiz, that could originate high magnitude earthquakes, and the existent low to intermediate seismicity (up to M7).

e) Numerical modeling results also illustrate the influence that rheological stratigraphy might exert on the nucleation and propagation of the corner zone fault pattern in the upper crust. Specifically, an interbedded soft layer is shown to inhibit the stress-strain corner zone concentration in the overlying competent layer. In accordance, the mild morphological (bathymetric) expression of the corner zone interference tectonic pattern in the HAP seafloor, can be explain by strain delocalization, and consequent hinder of fault propagation, induced by a soft rheological response of the Late Miocene "Chaotic" unit.

Acknowledgments

Experiments were performed in the Analogue Modeling Lab of Instituto Dom Luiz (IDL), a research Associate Laboratory funded by FCT. ALMOND - Multiscale modelling of deformation in the Gulf of Cadiz (PTDC/CTE-GIN/71862/2006). TOPOEUROPE/0001/2007-TOPOMED (Plate re-organization in the western Mediterranean: lithospheric causes and topographic consequences). J.C. Duarte acknowledges a Ph.D. grant (SFRH/BD/31188/2006) to FCT.

Appendix A

Dry quartz sand is classically used to simulate the mechanical behavior of upper crustal rocks, since it deforms in a brittle way according to the Coulomb fracture criterion (e.g. Hubbert, 1937, 1951; Davis et al., 1983):

$$\tau_{ss} = \mu_c \sigma_n + c_0 \quad (1)$$

where τ_{ss} is the shear stress, μ_c is the coefficient of internal friction ($\mu_c = \tan\phi$, and $\phi =$ internal friction angle), σ_n is the normal stress, and c_0 is the cohesion of the material. According to the scale model theory (Hubbert, 1937), proper scaling is achieved when the ratios λ, τ and μ between model and natural prototype are independently established for the three fundamental units of length (L), time (T) and mass (M), respectively:

$$\lambda = \frac{L_{(m)}}{L_{(p)}};\ \tau = \frac{T_{(m)}}{T_{(p)}};\ \mu = \frac{M_{(m)}}{M_{(p)}} \quad (2)$$

where (m) stands for model and (p) for natural prototype. The Coulomb fracture criterion governs time independent deformation of brittle materials, since yield stress is insensitive to the rate of deformation provided that the inertial forces are negligible, as in the present case. Thus, τ ratio is redundant for the present scaling. Length ratio (λ) was chosen given the dimensions of the employed deformation apparatus (see section 3.1.2 and Fig. 7) as $\lambda = 5 \times 10^{-6}$. Of the two relevant material properties, coefficient of internal friction (μ_c) and cohesion (c_0), the first is dimensionless, and approximately the same in both model and prototype (see Table 1), whereas the second has dimension of stress and thus must be scaled accordingly (Hubbert, 1937):

$$\Sigma = \frac{c_{0(m)}}{c_{0(p)}} = \frac{\mu\gamma}{\lambda^2} \quad (3)$$

where Σ and γ are the model/prototype ratio for stress and for acceleration respectively. Since inertial forces are negligible when compared with gravity,

$$\gamma = \gamma_g = \frac{g_{(m)}}{g_{(p)}} = \frac{\lambda}{\tau^2} = 1 \quad (4)$$

where γ_g is the model/prototype gravity acceleration ratio. Thus, substituting $\gamma = 1$ in equation (3) allows the following simplification:

$$\Sigma = \frac{c_{0(m)}}{c_{0(p)}} = \frac{\mu}{\lambda^2} = \frac{\mu\lambda}{\lambda^3} = \delta\lambda \quad (5)$$

where δ corresponds to the model/prototype density ratio. Substituting δ and λ in equation (5) by the respective values of Table 1, immediately allows the determination of the implied mass ratio $\mu = 6.25 \times 10^{-17}$. It should also be noted that since δ is generally close to one (between 0.5 and 0.7, e.g. Withjack et al., 2007) the strength of the materials expressed by Σ is scaled with the lengh (λ). Given the fact that in the present case $\lambda = 5 \times 10^{-6}$ and since cohesion for upper crustal rocks is clearly typically less than 50 MPa, it becomes immediately evident the utility of model materials with very low cohesion (<100Pa), such as dry quartz sand, as analogues of upper crustal rocks.

References

Abe, K., 1979. Size of great earthquakes of 1837-1974 inferred from tsunami data. Journal of Geophysical Research, 84(NB4): 1561-1568.

Agarwal, K.K. and Agrawal, G.K., 2002. Analogue Sandbox Models of Thrust Wedges with Variable Basal Frictions. Gondwana Research, 5(3): 641-647.

Banda, E., M. Torné and I. A. M. Group, 1995. Iberia Atlantic Margin Group investigates deep structure of ocean margins. Eos Trans. AGU, 76, 25-29.

Baptista, M.A., Heitor, S., Miranda, J.M., Miranda, P. and Victor, L.M., 1998a. The 1755 Lisbon tsunami; Evaluation of the tsunami parameters. Journal of Geodynamics, 25(1-2): 143-157.

Baptista, M.A., Miranda, P.M.A., Miranda, J.M. and Victor, L.M., 1998b. Constrains on the source of the 1755 Lisbon tsunami inferred from numerical modelling of historical data on the source of the 1755 Lisbon tsunami. Journal of Geodynamics, 25(1-2): 159-174.

Baptista, M.A., and Miranda, J.M., 2009. Revision of the Portuguese catalog of tsunamis. Natural Hazards and Earth System Sciences, 9(1): 25-42.

Bayarsayhan, C. et al., 1996. 1957 Gobi-Altay, Mongolia, earthquake as a prototype for southern California's most devastating earthquake. Geology, 24(7): 579-582.

Blanco, M.J. and Spakman, W., 1993. The p-wave velocity structure of the mantle below the iberian peninsula - evidence for subducted lithosphere below southern spain. Tectonophysics, 221(1): 13-34.

Bonini, M., Sokoutis, D., Mulugeta, G., Katrivanos, E., 2000. Modelling hanging wall accommodation above rigid thrust ramps. Journal of Structural Geology, 22: 1165-1179.

Bonnet, C., Malavieille, J., and Mosar, J., 2007, Interactions between tectonics, erosion, and sedimentation during the recent evolution of the Alpine orogen: Analogue modeling insights. Tectonics, 26, TC6016, doi: 10.1029/2006TC002048.

Borges, J.F., Fitas, A.J.S., Bezzeghoud, M. and Teves-Costa, P., 2001. Seismotectonics of Portugal and its adjacent Atlantic area. Tectonophysics, 331(4): 373-387.

Bose, S., Mandal, N., Mukhopadhyaly, D.K. and Mishra, P., 2009. An unstable kinematic state of the Himalayan tectonic wedge: Evidence from experimental thrust-spacing patterns. Journal of Structural Geology, 31(1): 83-91.

Buforn, E., Degaldeano, C.S. and Udias, A., 1995. Seismotectonics of the Ibero-Maghrebian region. Tectonophysics, 248(3-4): 247-261.

Buforn, E., Bezzeghoud, M., Udias, A. and Pro, C., 2004. Seismic sources on the Iberia-African plate boundary and their tectonic implications. Pure and Applied Geophysics, 161(3): 623-646.

Butler, R., Stewart, G.S. and Kanamori, H., 1979. July 27, 1976 Tangshan, China earthquake - complex sequence of intraplate events. Bulletin of the Seismological Society of America, 69(1): 207-220.

Davis, D., Suppe, J., Dahlen, F.A., 1983. Mechanics of fold and thrust belts and accretionary wedges. Journal of Geophysical Research 88: 1153–1172.

Di Bucci, D., Ravaglia, A., Seno, S., Toscani, G., Fracassi, U., and Valensise, G., 2006. Seismotectonics of the southern Apennines and Adriatic foreland: Insights on active regional E-W shear zones from analogue modeling. Tectonics, 25(4).

Di Bucci, D., Ravaglia, A., Seno, S., Toscani, G., Fracassi, U., and Valensise, G., 2007. Modes of fault reactivation from analogue modeling experiments: Implications for the seismotectonics of the Southern Adriatic foreland (Italy). Quaternary International, 171-72: 2-13.

Diraison, M., Cobbold, P.R., Gapais, D., Rossello, E.A. and Le Corre, C., 2000. Cenozoic crustal thickening, wrenching and rifting in the foothills of the southernmost Andes. Tectonophysics, 316(1-2): 91-119.

Dooley, T. and McClay, K., 1997. Analog modelling of pull-apart basins. AAPG Bulletin-American Association of Petroleum Geologists, 81(11): 1804-1826.

Duarte, J.C., Valadares, V., Terrinha, P., Rosas, F., Zitellini, N. and Gràcia, E., 2009. Anatomy and tectonic significance of WNW-ESE and NE-SW lineaments at a transpressive plate boundary (Nubia-Iberia). Trabajos de Geología, 29: 237-241.

Duarte, J.C., Terrinha, P., Rosas, F.M., Valadares, V., Pinheiro, L.M., Matias, L., Magalhães, V. and Roque, C., 2010. Crescent-shaped morphotectonic features in the Gulf of Cadiz (offshore SW Iberia). Marine Geology, 271: 236-249.

Ellis, S., Schreurs, G. and Panien, M., 2004. Comparisons between analogue and numerical models of thrust wedge development. Journal of Structural Geology, 26(9): 1659-1675.

Engdahl, R., R. van der Hilst, and Buland, R., 1998. Global teleseismic earthquake relocation with improved traveltimes and procedures for depth determination. Bulletin of the Seismological Society of America, 88: 722‑743.

Fernandes, R.M.S., Miranda, J.M., Meijninger, B.M.L., Bos, M.S., Bastos, L., Ambrosius, B.A.C. and Riva, R.E.M., 2007. Surface velocity field of the Ibero-Maghrebian segment of the Eurasia-Nubia plate boundary. Geophysical Journal International, 169(1): 315-324.

Fukao, Y., 1973. Thrust faulting at a lithospheric plate boundary Portugal earthquake of 1969. Earth and Planetary Science Letters, 18(2): 205-216.

Gebco, 2003. British Oceanographic Data Centre on behalf of IOC and IHO. GEBCO Digital Atlas.

Geissler, W.H., Matias, L., Stich, F., Carrilho, F., Jokat, W., Monna, S., IbenBrahim, A., Mancilla, F., Gutscher, M.-A., Sallarès, V. and Zitellini, N., 2010. Focal mechanisms for sub-crustal earthquakes in the Gulf of Cadiz from a dense OBS deployment. Geophysical Research Letters, 37: L18309.

Gill, R.C.O., Aparicio, A., El Azzouzi, M., Hernandez, J., Thirlwall, M.F., Bourgois, J. and Marriner, G.F., 2004. Depleted arc volcanism in the Alboran Sea and shoshonitic volcanism in Morocco: geochemical and isotopic constraints on Neogene tectonic processes. Lithos, 78(4): 363-388.

González, A., Córdoba, D., Vegas, R. and Matias, L.M., 1998. Seismic crustal structure in the southwest of the Iberian Peninsula and the Gulf of Cadiz. Tectonophysics, 296: 317‑331.

Gràcia, E., Dañobeitia, J., Vergés, J., and Bartolomé, R., 2003a. Crustal architecture and tectonic evolution of the Gulf of Cadiz (SW Iberian margin) at the convergence of the Eurasian and African plates. Tectonics, 22(4): 1033-1052.

Gràcia, E., Dañobeitia, J., Vergés, J. and Team, P., 2003b. Mapping active faults offshore Portugal (36 degrees N-38 degrees N): Implications for seismic hazard assessment along the southwest Iberian margin. Geology, 31(1): 83-86.

Grimison, N. L., and W. ‑ P. Chen., 1986. The Azores ‑ Gibraltar plate boundary: Focal mechanisms, depths of earthquakes, and their tectonic implications, Journal of Geophysical Research, 91: 2029‑2047.

Gutscher, M.A., Kukowski, N., Malavieille, J., Lallemand, S., 1998a. Episodic imbricate thrusting and underthrusting: analog experiments and mechanical analysis applied to the Alaskan accretionary wedge. Journal of Geophysical Research 103, 10161–10176.

Gutscher, M.A., Kukowski, N., Malavieille, J., Lallemand, S., 1998b. Material transfer in accretionary wedges from analysis of a systematic series of analog experiments. Journal of Structural Geology 20, 407–416.

Gutscher, M.A., Malod, J., Rehault, J.P., Contrucci, I., Klingelhoefer, F., Mendes-Victor, L. and Spakman, W., 2002. Evidence for active subduction beneath Gibraltar. Geology, 30(12): 1071-1074.

Gutscher, M.A., 2004. What caused the Great Lisbon earthquake? Science, 305(5688): 1247-1248.

Gutscher, M.A., Dominguez, S., Westbrook, G.K., Gente, P., Babonneau, N., Mulder, T., Gonthier, E., Bartolome, R., Luis, J., Rosas, F., Terrinha, P., DELILA and DELSIS scientific Teams., 2009a. Tectonic shortening and gravitational spreading in the Gulf of Cadiz accretionary wedge: Observations from multi-beam bathymetry and seismic profiling. Marine and Petroleum Geology, 26(5): 647-659.

Gutscher, M.A., Dominguez, S., Westbrook, G.K. and Leroy, P., 2009b. Deep structure, recent deformation and analog modelling of the Gulf of Cadiz accretionary wedge: Implications for the 1755 Lisbon earthquake. Tectonophysics, 475(1): 85-97.

Hensen, C., Nuzzo, M., Hornibrook, E., Pinheiro, L.M., Bock, B.,Magalhaes, V.H., Bruckmann, W., 2007. Sources of mud volcano fluids in the Gulf of Cadiz — indications for hydrothermally alteres fluids. Geochim. Cosmochim. Acta 71: 1232–1248.

Hoshino, K., Koide, H., Inami, K., Iwamura, S., Mitsui, S., 1972. Mechanical properties of Japanese Tertiary sedimentary rocks under high confining pressure. Geological Survey of Japan Report 244.

Hubbert, M.K., 1937. Theory of scale models as applied to the study of geologic structures. Geological Society of America Bulletin, 48: 1459-1520.

Hubbert, M.K., 1951. Mechanical basis for certain familiar geologic structures. Geological Society of America Bulletin 62: 355– 372.

Iribarren, L., Vergés, J., Camurri, F., Fullea, J., Fernàndez, M., 2007. The structure of the Atlantic-Mediterranean transition zone from the Alboran Sea to the Horseshoe Abyssal Plain (Iberia–Africa plate boundary). Marine Geology 243, 97-119

Jimenez-Munt, I., M. Fernandez, J. Verges, J.C. Afonso, D. Garcia-Castellanos, Fullea, J., 2010. Lithospheric structure of the Gorringe Bank: Insights into its origin and tectonic evolution. Tectonics, 29.

Johnston, A.C., 1996. Seismic moment assessment of earthquakes in stable continental regions .3. New Madrid 1811-1812, Charleston 1886 and Lisbon 1755. Geophysical Journal International, 126(2): 314-344.

Kim, Y.-S., Peacock, D.C.P., Sanderson, D.J., 2004. Fault damage zones. Journal of Structural Geology, 26: 503–517.

Koyi, H., Maillot, B., 2007. Tectonic thickening of hanging-wall units over a ramp. Journal of Structural Geology, 29: 924-932.

Lallemand, S., Schnürle, P., Malavieille, J., 1994. Coulomb theory applied to accretionary and nonaccretionary wedges: possible causes for tectonic erosion and/or frontal accretion. Journal of Geophysical Research, 99: 12033–12055.

Le Guerroue, E. and Cobbold, P.R., 2006. Influence of erosion and sedimentation on strike-slip fault systems: insights from analogue models. Journal of Structural Geology, 28(3): 421-430.

Lohrmann, J., Kukowski, N., Adam, J. and Oncken, O., 2003. The impact of analogue material properties on the geometry, kinematics, and dynamics of convergent sand wedges. Journal of Structural Geology, 25(10): 1691-1711.

Lonergan, L. and White, N., 1997. Origin of the Betic-Rif mountain belt. Tectonics, 16(3): 504-522.

Lopes Cardozo, G., Bada, G., Lankreijer, A., Nieuwland, D., 2002. Analogue modeling of a prograding strike-slip fault: case study of the Balatonfo fault, western Hungary. EGU Stephan Mueller Special Publication Series 3: 217–226.

Maillot, B. and Koyi, H., 2006. Thrust dip and refraction in fault-bend folds: analogue models and theoretical predictions. Journal of Structural Geology, 28: 36-49.

Malavieille, J., 1984, Modélisation expérimentale des chevauchements imbriqués: application aux chaînes de montagnes. Bulletin de la Société Géologique de France, 26: 129-138.

Malavieille, J., 2010. Impact of erosion, sedimentation and structural heritage on the structure and kinematics of orogenic wedges : analog models and case studies. Geological Society of America, account GSA Today, 20(1), doi: 10.1130/GSATG48A.1

Mandl, G., L.N.J. de Jong, and A. Maltha, 1977. Shear zones in granular material; an experimental study of their structure and mechanical genesis, Rock Mechanics, 9: 95-144.

Mandl, G., 2000. Faulting in Brittle Rocks. Springer, Berlin, 434 pp.

Martinez-Loriente, S., Gràcia, E., Bartolomé, R., Sallarès, V., Dañobeitia, J.J., And Swim-06 Cruise Party, 2008. Pre-stack depth migration seismic imaging of the Coral Patch Ridge and adjacent Horseshoe and Seine Abyssal Plains (Gulf of Cadiz): Tectonic implications. Trabajos de Geología, 30: 49-54

Martinez-Solares, J.M., 2001. Los effectos en España del terremoto de Lisboa. Instituto Geografico Nacional, Madrid. 756 pp.

McClay, K. and Bonora, M., 2001. Analog models of restraining stepovers in strike-slip fault systems. AAPG Bulletin, 85(2): 233-260.

McClay, K.R., Whitehouse, P.S., Dooley, T. and Richards M., 2004. 3D evolution of fold and thrust belts formed by oblique convergence. Marine and Petroleum Geology, 21: 857–877

Medialdea, T., Vegas, R., Somoza, L., Vázquez, J.T., Maldonado, A., Díaz-del-Río, V., Maestro, A., Córdoba, D. and Fernández-Puga, M.C., 2004. Structure and evolution of the "Olistostrome" complex of the Gibraltar Arc in the Gulf of Cadiz (eastern Central Atlantic): evidence from two long seismic cross-sections. Marine Geology, 209(1-4): 173-198.

Morel, J.L. and Meghraoui, M., 1996. Goringe-Alboran-Tell tectonic zone: A transpression system along the Africa-Eurasia plate boundary. Geology, 24(8): 755-758.

Mueller, S. and Phillips, R.J., 1991. On the initiation of subduction. Journal of Geophysical Research-Solid Earth and Planets, 96(B1): 651-665.

Mulugeta, G., 1988. Modelling the geometry of Coulomb thrust wedges. Journal of Structural Geology 10, 847–859

Nocquet, J.M. and Calais, E., 2004. Geodetic measurements of crustal deformation in the Western Mediterranean and Europe. Pure and Applied Geophysics, 161(3): 661-681.

Persson, K., Sokoutis, D., 2002. Analogue models of orogenic wedges controlled by erosion. Tectonophysics, 356: 323-336.

Richard, P., Mocquet, B. and Cobbold, P.R., 1991. Experiments on simultaneous faulting and folding above a basement wrench fault. Tectonophysics, 188(1-2): 133-141.

Riedel, W., 1929. Zur Mechanik geologischer Brucherscheinungen. Zentralblatt fur Mineralogie, Geologie und Palaontologie 1929B, 354–368.

Rosas, F.M., Duarte, J.C., Terrinha, P., Valadares, V. and Matias, L., 2009. Morphotectonic characterization of major bathymetric lineaments in Gulf of Cadiz (Africa-Iberia plate boundary): Insights from analogue modelling experiments. Marine Geology, 261(1-4): 33-47.

Royden, L.H., 1993. Evolution of retreating subduction boundaries formed during continental collision. Tectonics, 12(3): 629-638.

Sallarès, V., Gailler, A., Gutscher, M-A., Bartolomé, R., Díaz, J., Gràcia, E., Graindorge, D., 2011. Seismic evidence for the presence of Jurassic oceanic crust in the Gulf of Cádiz (SW Iberia). Geophysical Research Abstracts, 13 (EGU2011): 3274-1.

Sartori, R., Torelli, L., Zitellini, N., Peis, D. and Lodolo, E., 1994. Eastern segment of The Azores-Gibraltar Line (Central-Eastern Atlantic) - An oceanic plate boundary with diffuse compressional deformation. Geology, 22(6): 555-558.

Serpelloni, E., G. Vannucci, S. Pondrelli, A. Argnani, G. Casula, M. Anzidei, P. Baldi, and Gasperini, P., 2007. Kinematics of the Western Africa-Eurasia plate boundary from focal mechanisms and GPS data. Geophysical Journal International, 169(3): 1180-1200.

Schopfer, M.P.J., Steyrer, H.P., 2001. Experimental modeling of strike-slip faults and the self-similar behavior. In: Koyi, H.A., Mancktelow, N.S. (Eds.), Tectonic Modelling: A Volume in Honor of Hans Ramberg Geological Society of America Memoir 193, pp. 21–27.

Silva, S., Romsdorf, M., Matias, L., Geissler, W. H., Terrinha, P. and Carrilho, F., 2010. Characterization of the seismicity in the Gulf of Cadiz based on eleven month monitoring by the NEAREST OBS network. Geophysical Research Abstracts (EGU General Assembly), 12: 11554.

Solares, J.M.M. and Arroyo, A.L., 2004. The great historical 1755 earthquake. Effects and damage in Spain. Journal of Seismology, 8(2): 275-294.

Stich, D., Mancilla, F.D. and Morales, J., 2005. Crust-mantle coupling in the Gulf of Cadiz (SW-Iberia). Geophysical Research Letters, 32(13).

Stich, D., Serpelloni, E., Mancilla, F.D. and Morales, J., 2006. Kinematics of the Iberia-Maghreb plate contact from seismic moment tensors and GPS observations. Tectonophysics, 426(3-4): 295-317.

Terrinha, P., Pinheiro, L.M., Henriet, J.P., Matias, L., Ivanov, M.K., Monteiro, J.H., Akhmetzhanov, A., Volkonskaya, A., Cunha, T., Shaskin, P. and Rovere, M., 2003. Tsunamigenic-seismogenic structures, neotectonics, sedimentary processes and slope instability on the southwest Portuguese Margin. Marine Geology, 195(1-4): 55-73.

Terrinha, P., Matias, L., Vicente, J., Duarte, J., Luis, J., Pinheiro, L., Lourenço, N., Diez, S., Rosas, F., Magalhães, V., Valadares, V., Zitellini, N., Roque, C., Victor, L.M. and MATESPRO Team., 2009. Morphotectonics and strain partitioning at the Iberia-Africa plate boundary from multibeam and seismic reflection data. Marine Geology, 267(3-4): 156-174.

Torelli, L., Sartori, R. and Zitellini, N., 1997. The giant chaotic body in the Atlantic Ocean off Gibraltar: New results from a deep seismic reflection survey. Marine and Petroleum Geology, 14(2): 125-138.

Tortella, D., Torné, M., Pérez-Estáun, A., 1997. Geodynamic Evolution of the Eastern Segment of the Azores-Gibraltar Zone: The Gorringe Bank and the Gulf of Cadiz Region. Marine Geophysical Researches, 19: 211-230.

Weijermars, R., Jackson, M.P.A., Vendeville, B., 1993. Rheological and tectonic modeling of salt provinces. Tectonophysics, 217: 143-174.

Wells, D., Coppersmith, K., 1994. New empirical relationships among magnitude, rupture length, rupture width, rupture area and surface displacement. Bulletin of the Seismological Society of America 84: 974–1002.

Withjack, M.O., Schlische, R.W., Henza, A.A., 2007. Scaled Experimental Models of Extension: Dry Sand vs.Wet Clay. Houston Geological Society Bulletin, 49 (8): 31-49.

Zitellini, N., Mendes, L. A., Cordoba, D., Danobeitia, J., Nicolich, R., Pellis, G., Ribeiro, A., Sartori, R., Torelli, L., Bartolomé, R., Bortoluzzi, G., Calafato, A., Carrilho, F., Casoni, L., Chierici, F., Corela, C., Correggiari, A., Della Vedova, B., Gràcia, E., Jornet, P., Landuzzi, M., Ligi, M., Magagnoli, A., Marozzi, G., Matias, L., Penitenti, D., Rodriguez, P., Rovere, M., Terrinha, P., Vigliotti, L., Zahinos Ruiz, A., 2001. Source of 1755 Lisbon Earthquake and Tsunami Investigated. EOS Transactions, American Geophysical Union, 82(26): 290–291.

Zitellini, N., Rovere, M., Terrinha, P., Chierici, F., Matias, L. and Bigsets Team., 2004. Neogene through quaternary tectonic reactivation of SW Iberian passive margin. Pure and Applied Geophysics, 161(3): 565-587.

Zitellini, N., Gràcia, E., Matias, L., Terrinha, P., Abreu, M.A., DeAlteriis, G., Henriet, J.P., Dañobeitia, J.J., Masson, D.G., Mulder, T., Ramella, R., Somoza, L. and Diez, S., 2009. The quest for the Africa-Eurasia plate boundary west of the Strait of Gibraltar. Earth and Planetary Science Letters, 280(1-4): 13-50.

Zhou, J., Xu, F., Wei, C., Li, G., Yu, F. and Tong, H., 2007. Shortening of analogue models with contractive substrata: Insights into the origin of purely landward-vergent thrusting wedge along the Cascadia subduction zone and the deformation evolution of Himalayan–Tibetan orogen. Earth and Planetary Science Letters, 260: 313–327.

Figure captions

Fig. 1 - (A) Location of the Gulf of Cadiz area in the general tectonic setting of the Euroasia (Iberia) - Africa (Nubia) plate boundary. TR: Terceira Ridge; GF: Gloria Fault. (B) Simplified tectonic map of the Gulf of Cadiz area (tectonic interpretation from Zitellini et al., 2009); Bathymetry from SWIM compilation of Zitellini et al. (2009) completed with GEBCO (2003). GCAW - Gulf of Cadiz Accretionary Wedge; Black dots correspond to the location of known mud volcanoes (e.g. Hensen et al., 2007). Inset in the upper left showing (in black) the average direction of the Maximum Horizontal Stresses—SHmax, and (in grey) the average direction of the ~4 mm/yr convergence rate between Nubia and Iberia (Nocquet and Calais, 2004; Stich et al., 2006; Fernandes et al., 2007).

Fig. 2 - (A) Detailed bathymetry and main morphological features in the study area (dashed-lined rectangle in figure 1B). (B) Perspective view (from WNW). HTF: Horseshoe Thrust Fault; GCAW: Gulf of Cadiz Accretionary Wedge; CS: Crescentic scours (Duarte et al., 2010b); CPR: Coral Patch Ridge. Black arrow signals the location of the mild bathymetric perturbation associated to Corner Fault 1 (CF1 in Figs. 3 and 5). Digital 3D bathymetry model (vertical exaggeration factor of 8) from SWIM dataset (Zitellini et al., 2009).

Fig. 3 – (A) General seismic reflection dataset used as a basis for the new tectonic interpretation proposed for the corner zone study area (dashed-lined rectangle in figure 1B, ARRIFANO – Arco Rifano, IAM - Iberian Atlantic Margin, and SWIM – South

West Iberian Margin surveys, Sartori et al., 1994; Banda et al., 1995; Tortella et al., 1997; Martinez-Loriente et al., 2008). Thick green lines correspond to the IAM4e and IAM4-IAM3 multi-channel seismic profiles shown in B and figures 4 and 5; (B) Newly proposed tectonic map of the study area, mostly corresponding to the (corner) zone of intersection between the SWIM 1 dextral strike-slip fault, and the Horseshoe Thrust Fault (HTF). CF1 and CF2: Corner Faults (CS, GCAW and black arrow as in Fig. 2B).

Fig. 4 - (A) Multi-channel seismic profile IAM-4e (see Fig. 3 for location); and (B) correspondent seismostratigraphic and tectonic interpretation (adapted from Duarte et al. 2010). Thin black lines: seismic reflectors interpreted as stratigraphic horizons; Double-dashed black and white lines: intra-chaotic body reflections interpreted as decollement horizons and folded layered sediments.

Fig. 5 - (A) Multi-channel seismic profiles IAM4 and IAM3 (see Fig. 3 for location); and (B) correspondent seismostratigraphic and tectonic interpretation (modified after Rosas et al., 2009). DSDP-135 marks the seismostratigraphic top of the Mesozoic units.

Fig. 6 – Map of the newly proposed tectonic interpretation for the study area (as in figure 3B), showing the (dashed) elliptic outlines of low magnitude earthquake clusters and associated focal mechanisms reported by Geissler et al. (2010). Note the marked coincidence of the southern cluster with the intersection between the SWIM 1 and Horseshoe faults.CF1 and CF2: Corner Faults. $\sigma 1$: orientation of the main compressive stress components deduce from the focal mechanisms of each of the depicted clusters (adapted from Geissler et al., 2010).

Fig. 7 - Analogue modeling experimental apparatus and setup. (A) Perspex deformation box. Arrows (1st and 2nd) indicate movement induced by stepping motors during the first and second experimental steps respectively (see detail explanation in the text). (B) Experimental initial stage depicting the sand cake mounted inside the Perspex box before the onset of deformation. Notice Cartesian coordinate system (upper left).

Fig. 8 - Analogue modeling results: top view photos and interpretation. All models are dynamically scaled relatively to the natural prototype (see Appendix A for details), length scale λ=1/200.000. (A) Results for a considered sand-cake thickness of 5 cm (10 km). (A1-A1') Experimental step 1 corresponding to initial bulk shortening (Inset A'': schematic cross-section). (A2, A3) Successive stages of experimental step 2, after basal-plate strike-slip displacement of 3.5cm and 7cm, respectively (horizontal displacement given by labeled a-a' to e-e' strain-marker lines). (B, C): Experimental results for sand-cake thickness of 4 and 3 cm (8 and 6 km, respectively), showing consistent corner zone deformation patterns (see text for further detailed explanation). VD: Trace of velocity discontinuity; D: Strike-slip displacement; F1- F3: Thrust faults (orange and yellow indicate faults originated during experimental step 1); R: Riedel-faults; Y: Y-faults (strike-slips); P: P-shears. Notice Cartesian coordinate system.

Fig. 9 - (A) Analogue modeling results: top view photo and interpretation of experimental step 2 (final stage): along strike displacement of ~7.5cm (15km). (B) Cross sections of sand model depicted in A. Cross sections1and 2: flower-structures orthogonal to the wrenching domain; Cross sections 3 to 5: structure along sectioned planes successively closer to the intersection between the trace of the basal strike-slip

and the velocity discontinuity; Cross section 6: structure across the thrusting domain. F1, F2 and Backthrust (BT) originated during experimental step 1 (structures in yellow and orange); F3 to F5, Riedel-faults (R) and Y-faults (Y) originated during experimental step 2 (structures in black). See text for further detailed explanation.

Fig. 10 - (A) Geometry and boundary conditions of numerical model. Plate A moves to the right along the X direction. All other boundaries are fixed in the normal Y and Z directions. Gravity is balanced by an applied lithostatic pressure at the base of the model. Spring forces are also applied at the base to simulate isostasy. (B) Deformation of finite element grid and vertical displacement (U3) obtained for 10 km of applied shortening (MOD1). The results are displayed in the central 240 km region of the model. (C and D) Conceptual YZ sections illustrating model setup for MOD1 and MOD 2, respectively. In MOD2 a 1.5 km thick soft layer is placed at 1.5 km beneath the surface, with the strike-slip (SWIM) fault not defined above it.

Fig. 11 - (A) Maximum shear stress contours on a non-deformed frame (view from above of the central 240x180 km of the model). Surface (z=0m) and depth (z=6000m) results for MOD1 (left column) and MOD2 (right column). (B) Top view of principal stress components at the thrust/strike-slip intersection (area in MOD1 and MOD2 given by the parallelogram in A). Element dimensions ~4x4x1.5 km.

Fig. 12 - Model regions where failure (Drucker-Prager) criterion is first exceeded (view from above of the central 240x180 km of the model). Surface (z=0m) and depth (z=6000m) results for MOD1 (left column) and MOD2 (right column).

Fig. 13 - Accumulated plastic strain contours on a non-deformed frame (view from above of the central 240x180 km of the model). Results for MOD1 (left column) and MOD2 (right column) are shown for different depths: surface (z=0m), base of soft layer (z=3000m) and base of the model (z=6000m).

Fig. 14 – Comparison of the natural morphotectonic pattern and the obtained analogue modeling structural pattern.

Figure 1

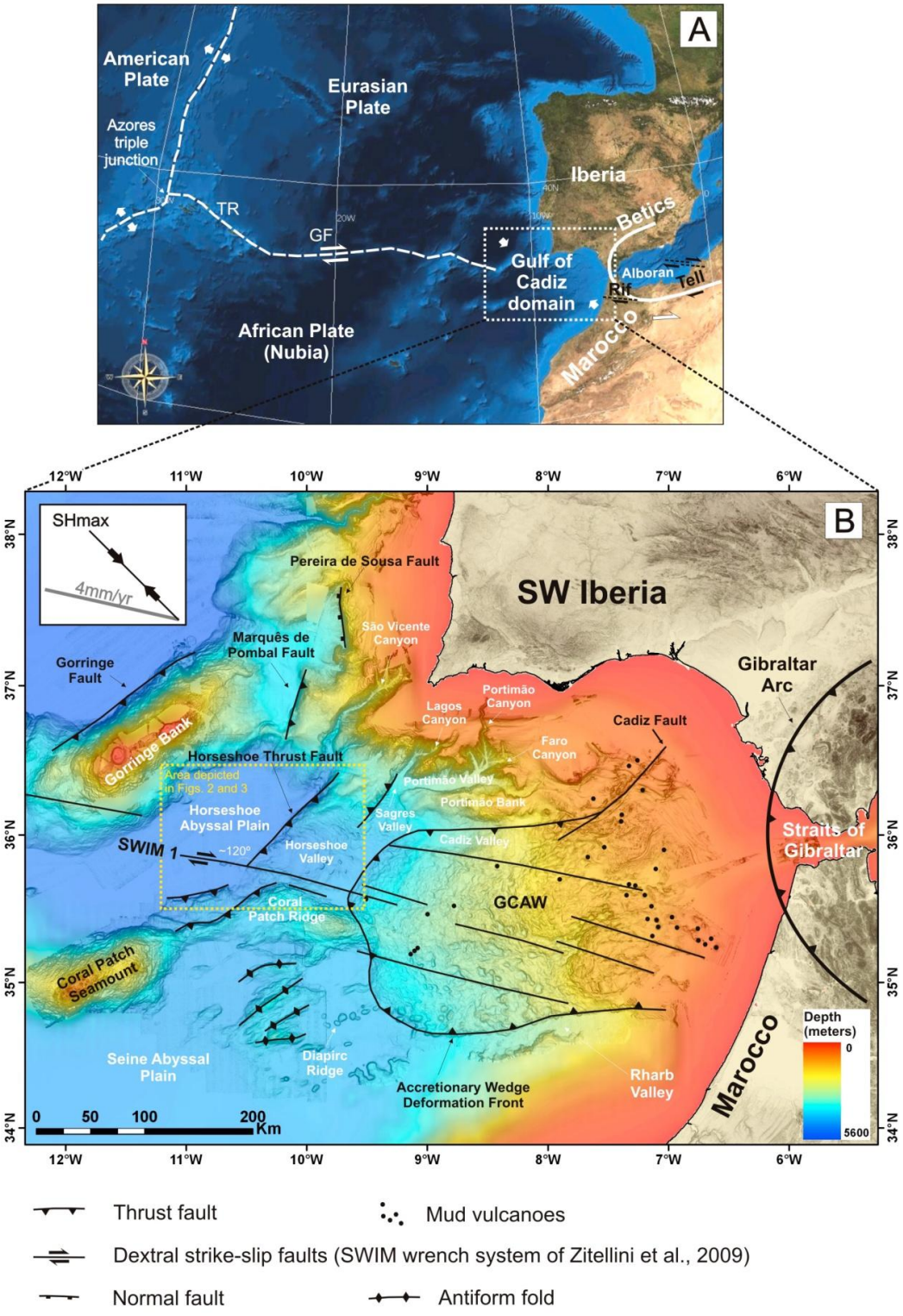
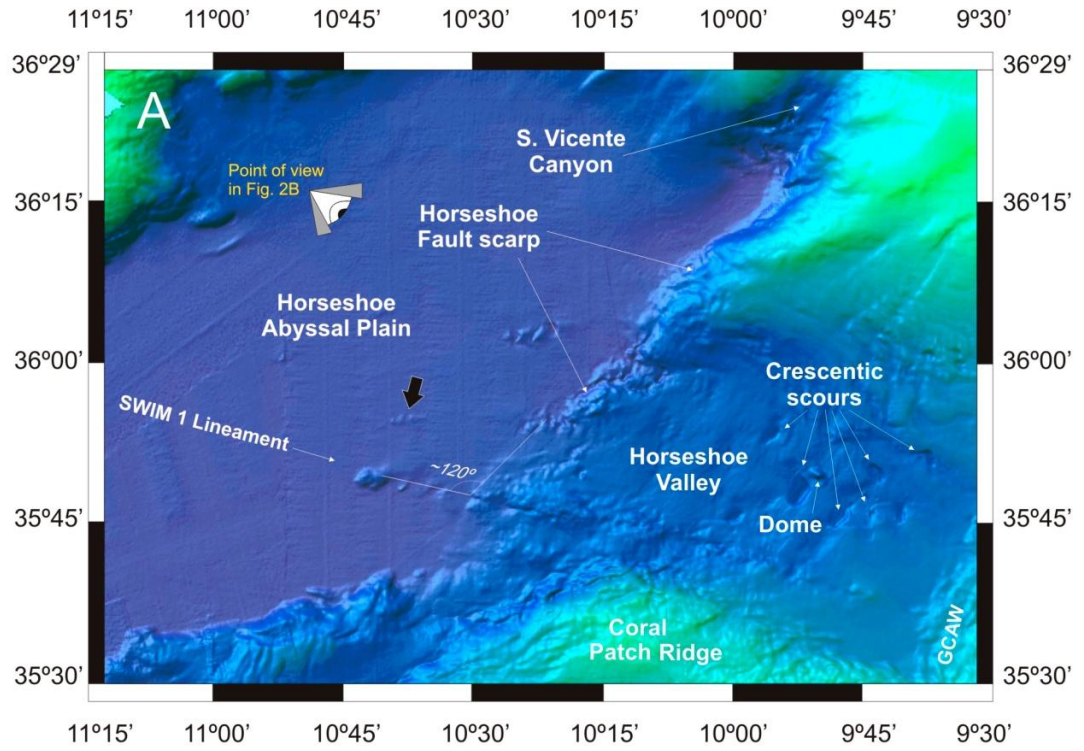
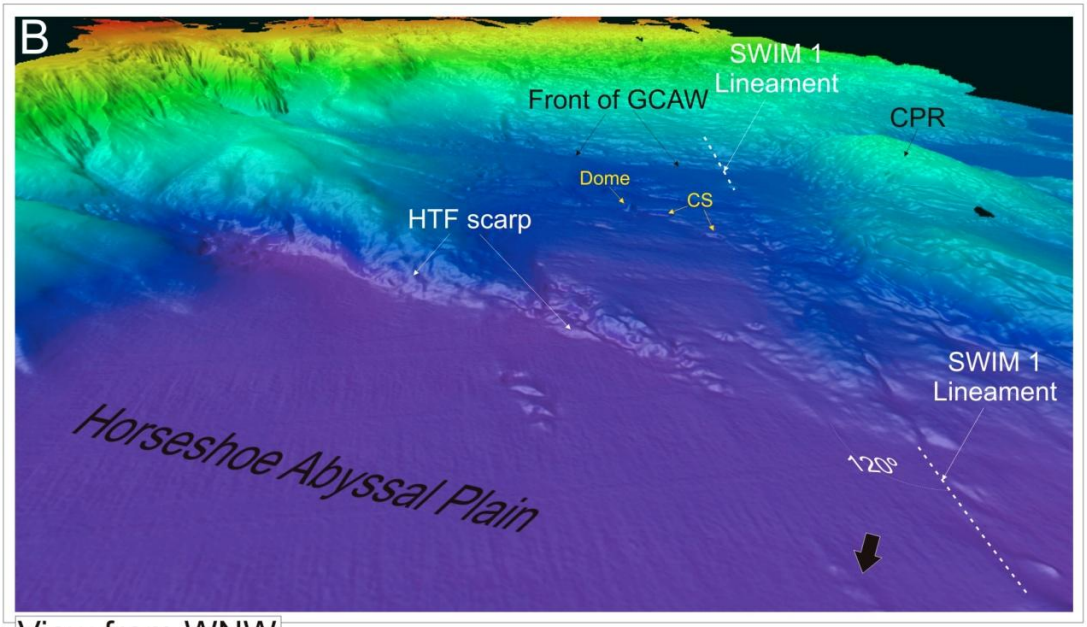

A
American Plate
Eurasian Plate
Azores triple junction
TR
GF
Iberia
Betics
Gulf of Cadiz domain
Alboran
Rif
Tell
Marocco
African Plate (Nubia)
B
SHmax
4mm/yr
Pereira de Sousa Fault
SW Iberia
São Vicente Canyon
Marquês de Pombal Fault
Gorringe Fault
Gibraltar Arc
Portimão Canyon
Lagos Canyon
Cadiz Fault
Gorringe Bank
Faro Canyon
Horseshoe Thrust Fault
Area depicted in Figs. 2 and 3
Portimão Valley
Portimão Bank
Horseshoe Abyssal Plain
Sagres Valley
Straits of Gibraltar
SWIM 1
~120°
Horseshoe Valley
Cadiz Valley
Coral Patch Ridge
GCAW
Coral Patch Seamount
Depth (meters)
0
5600
Seine Abyssal Plain
Diapirc Ridge
Accretionary Wedge Deformation Front
Rharb Valley
Marocco
0 50 100 200 Km
12°W
11°W
10°W
9°W
8°W
7°W
6°W
38°N
37°N
36°N
35°N
34°N
Thrust fault
Mud vulcanoes
Dextral strike-slip faults (SWIM wrench system of Zitellini et al., 2009)
Normal fault
Antiform fold

Figure 2





View from WNW

Figure 3

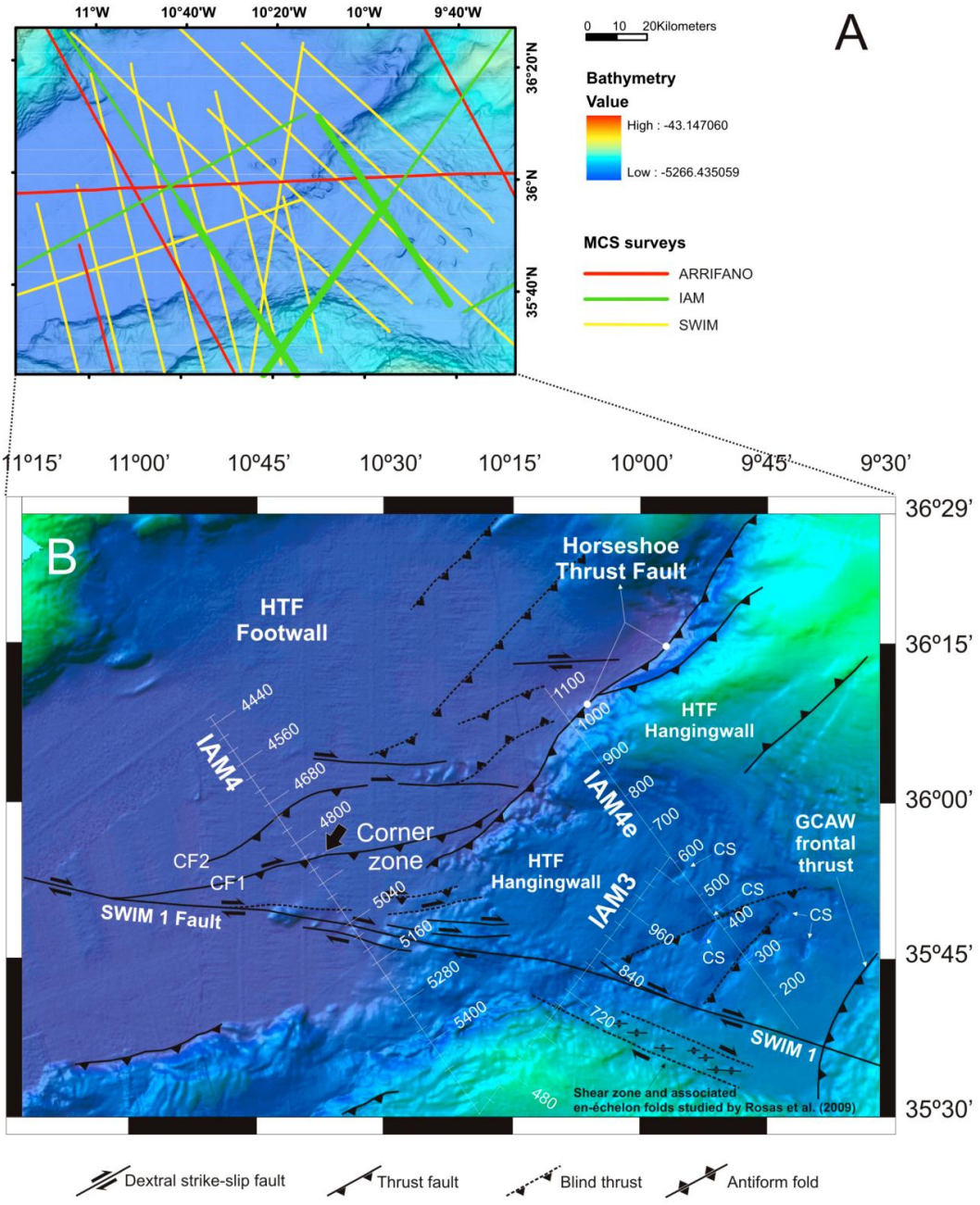

A
11°W
10°40'W
10°20'W
10°W
9°40'W
36°20'N
36°N
35°40'N
0 10 20Kilometers
Bathymetry
Value
High : -43.147060
Low : -5266.435059
MCS surveys
ARRIFANO
IAM
SWIM
11°15'
11°00'
10°45'
10°30'
10°15'
10°00'
9°45'
9°30'
36°29'
36°15'
36°00'
35°45'
35°30'
B
Horseshoe
Thrust Fault
HTF
Footwall
HTF
Hangingwall
IAM4
IAM4e
IAM3
Corner
zone
CF2
CF1
SWIM 1 Fault
SWIM 1
GCAW
frontal
thrust
CS
4440
4560
4680
4800
5040
5160
5280
5400
1100
1000
900
800
700
600
500
400
960
840
720
480
300
200
Shear zone and associated
en-échelon folds studied by Rosas et al. (2009)
Dextral strike-slip fault
Thrust fault
Blind thrust
Antiform fold

Figure 4

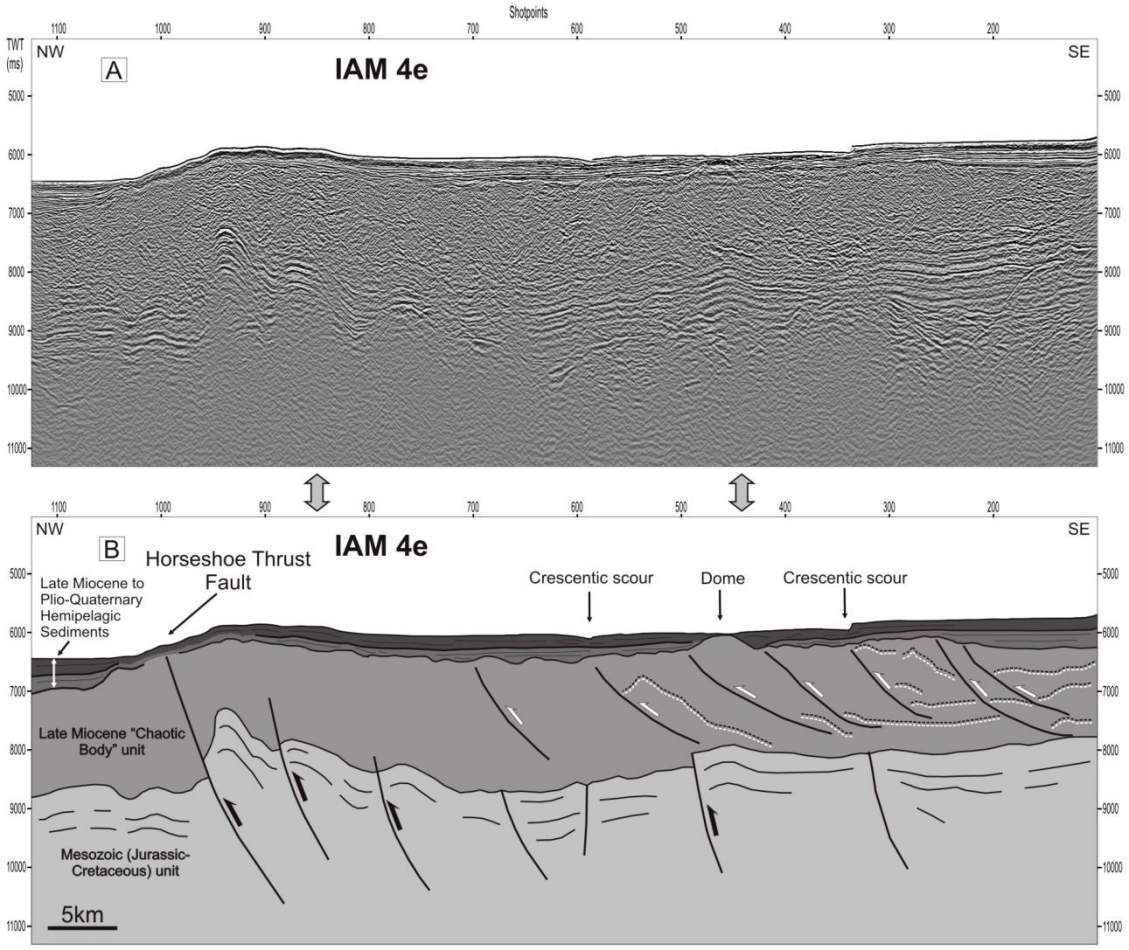

Shotpoints
1100
1000
900
800
700
600
500
400
300
200
TWT (ms)
NW
SE
A
IAM 4e
5000
6000
7000
8000
9000
10000
11000
B
IAM 4e
Horseshoe Thrust Fault
Late Miocene to Plio-Quaternary Hemipelagic Sediments
Crescentic scour
Dome
Crescentic scour
Late Miocene "Chaotic Body" unit
Mesozoic (Jurassic-Cretaceous) unit
5km

Figure 5

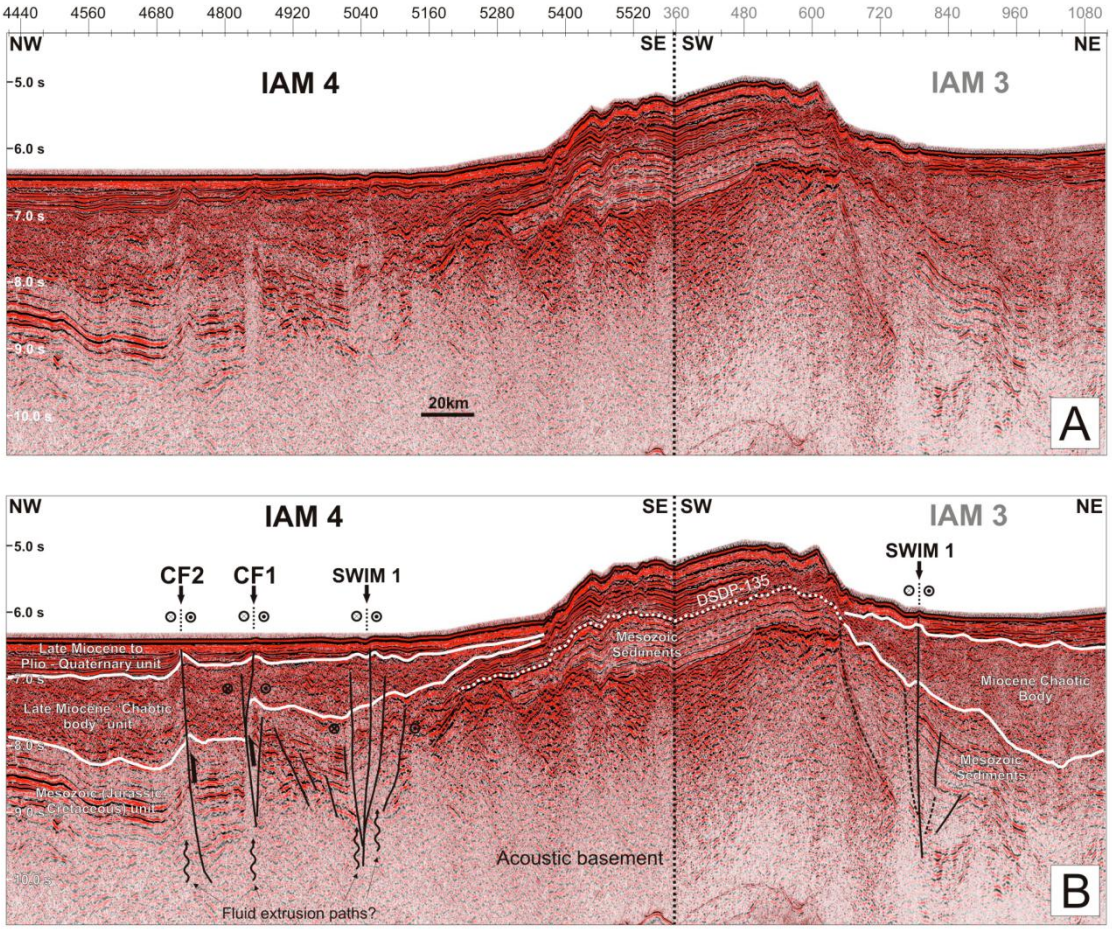

4440
4560
4680
4800
4920
5040
5160
5280
5400
5520
360
480
600
720
840
960
1080
NW
SE
SW
NE
IAM 4
IAM 3
5.0 s
6.0 s
7.0 s
8.0 s
9.0 s
10.0 s
20km
A
IAM 4
IAM 3
CF2
CF1
SWIM 1
SWIM 1
DSDP-135
Mesozoic Sediments
Late Miocene to Plio. - Quaternary unit
Late Miocene "Chaotic body" unit
Miocene Chaotic Body
Mesozoic Sediments
Mesozoic (Jurassic - Cretaceous) unit
Acoustic basement
Fluid extrusion paths?
B

Figure 6

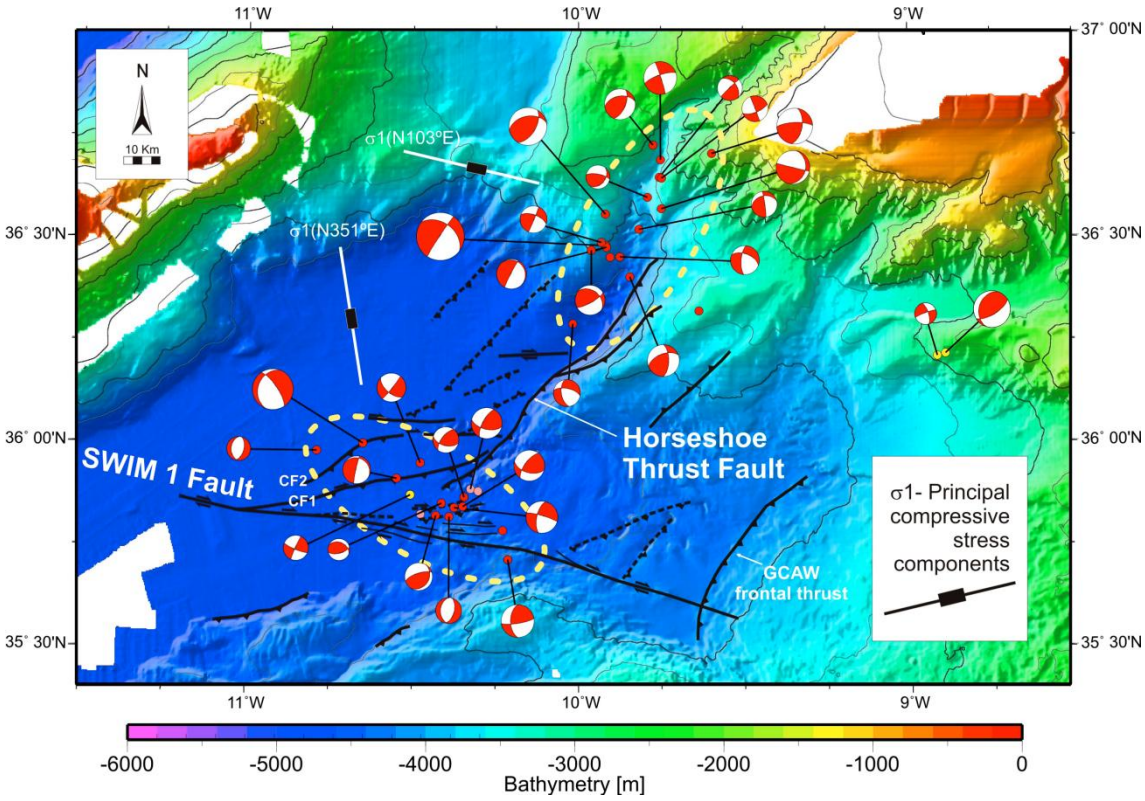

11°W
10°W
9°W
37° 00'N
36° 30'N
36° 00'N
35° 30'N
N
10 Km
σ1(N103°E)
σ1(N351°E)
SWIM 1 Fault
CF2
CF1
Horseshoe
Thrust Fault
GCAW
frontal thrust
σ1- Principal
compressive
stress
components
-6000
-5000
-4000
-3000
-2000
-1000
0
Bathymetry [m]

Figure 7

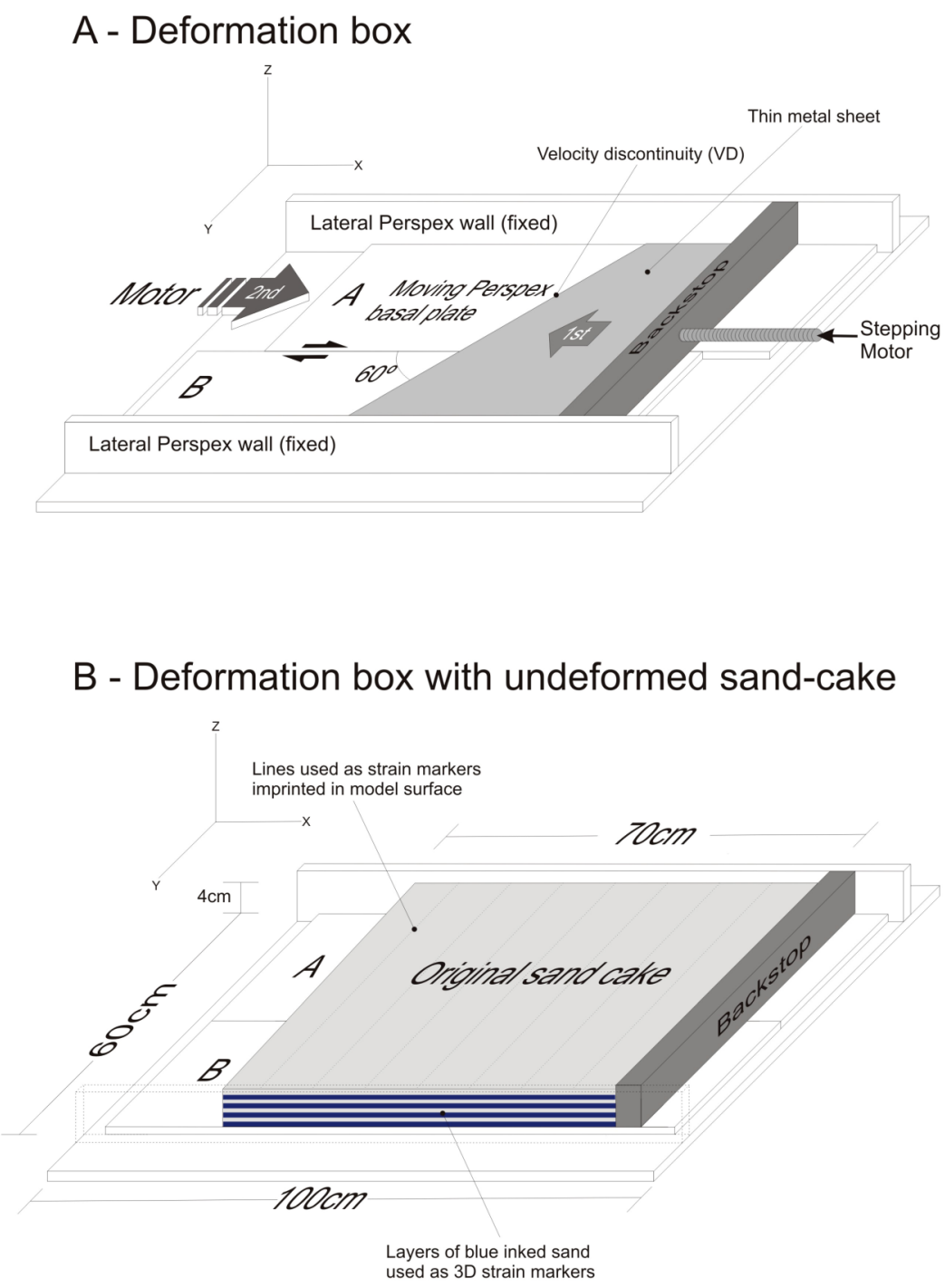

A - Deformation box
Z
X
Y
Thin metal sheet
Velocity discontinuity (VD)
Lateral Perspex wall (fixed)
Motor
2nd
A
Moving Perspex basal plate
1st
Backstop
Stepping Motor
60°
B
Lateral Perspex wall (fixed)
B - Deformation box with undeformed sand-cake
Z
X
Y
Lines used as strain markers imprinted in model surface
70cm
4cm
A
Original sand cake
Backstop
60cm
B
100cm
Layers of blue inked sand used as 3D strain markers

Figure 8

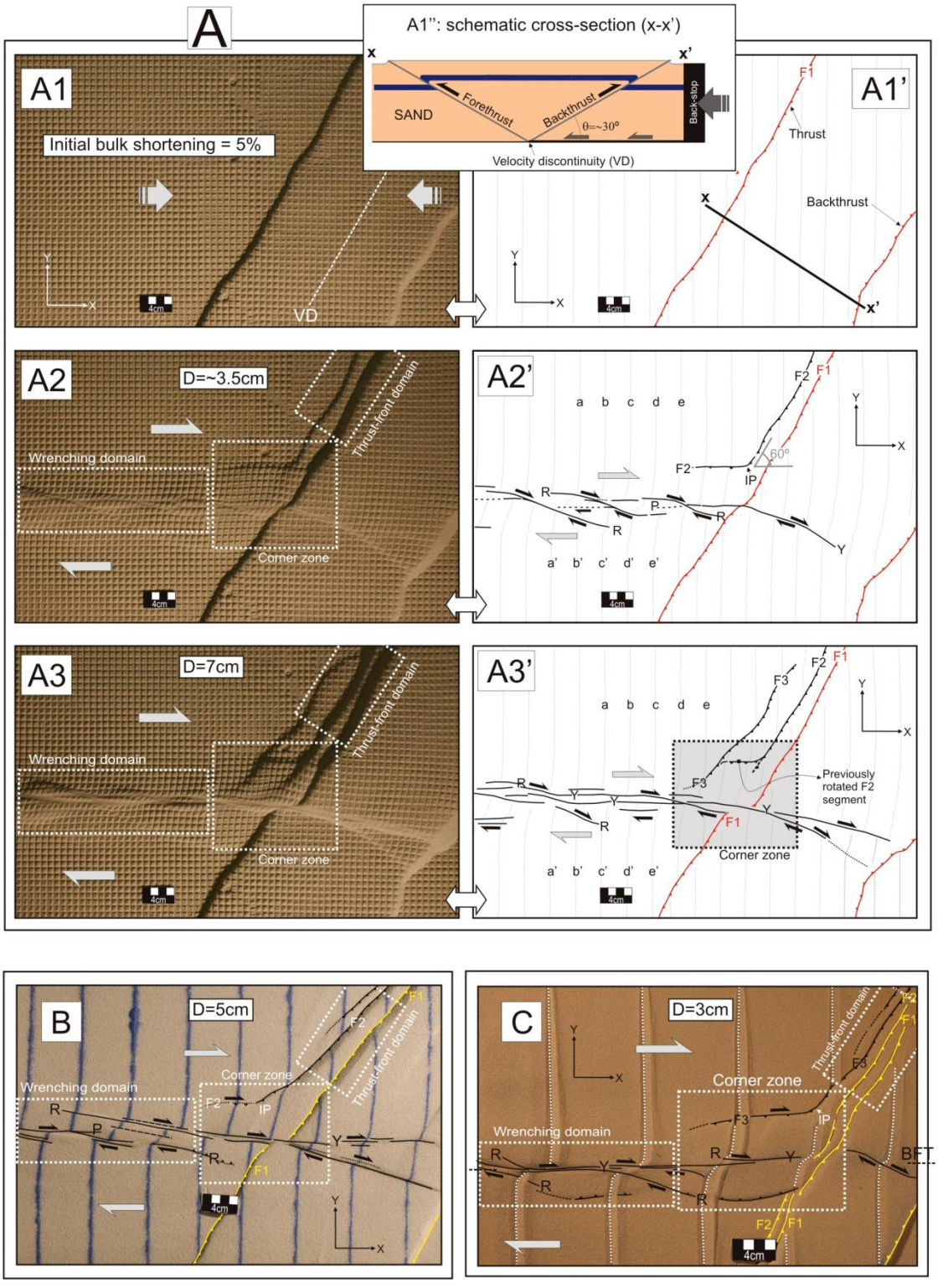

A
A1
Initial bulk shortening = 5%
VD
A1": schematic cross-section (x-x')
SAND
Forethrust
Backthrust
θ=~30°
Back-stop
Velocity discontinuity (VD)
A1'
Thrust
Backthrust
A2
D=~3.5cm
Wrenching domain
Thrust-front domain
Corner zone
A2'
a b c d e
F2 F1
IP
60°
R
Y
a' b' c' d' e'
A3
D=7cm
A3'
F3
Previously rotated F2 segment
B
D=5cm
C
D=3cm
BFT
4cm

Figure 9

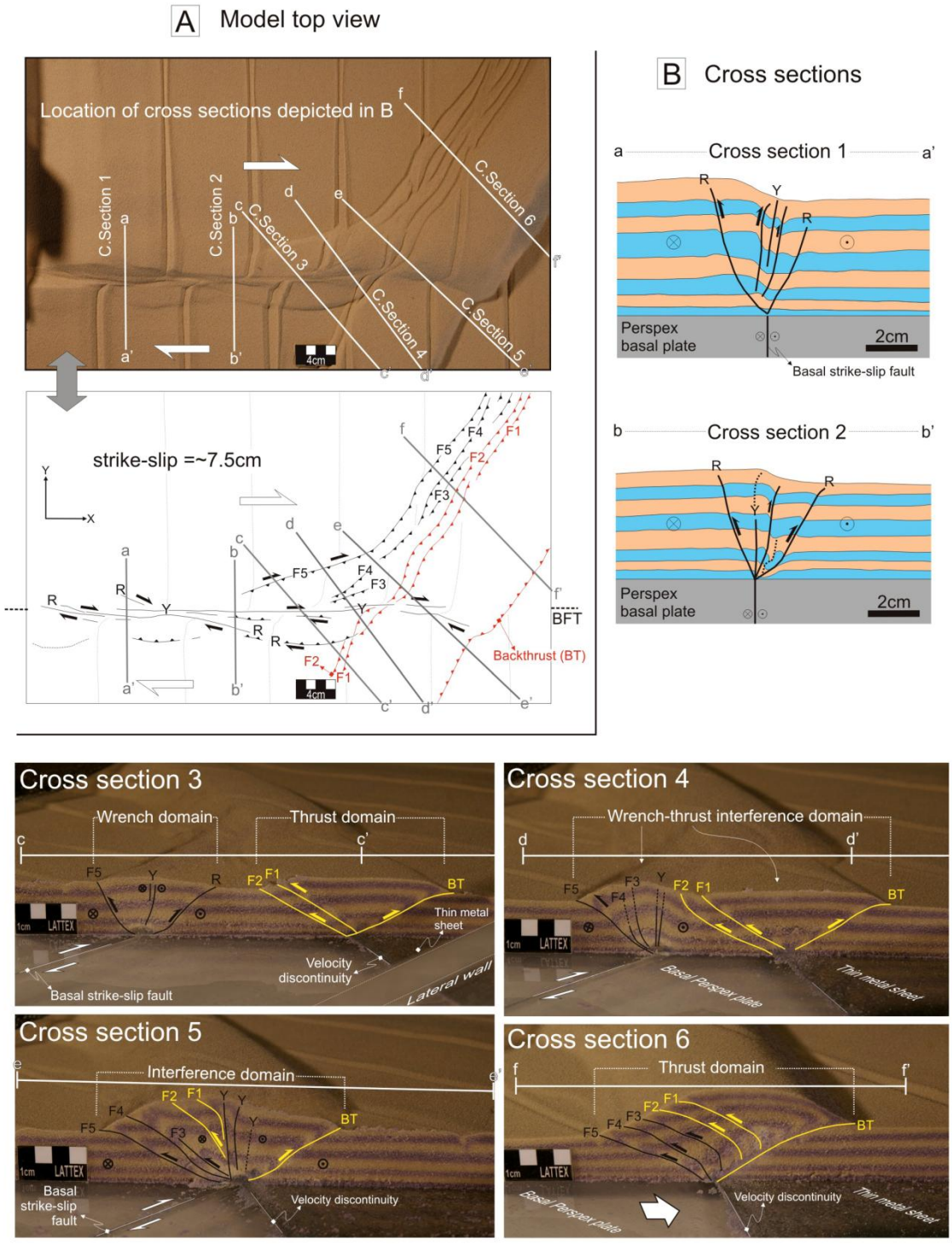

A Model top view
Location of cross sections depicted in B
C.Section 1
C.Section 2
C.Section 3
C.Section 4
C.Section 5
C.Section 6
4cm
strike-slip =~7.5cm
BFT
Backthrust (BT)
B Cross sections
Cross section 1
Perspex basal plate
2cm
Basal strike-slip fault
Cross section 2
Perspex basal plate
2cm
Cross section 3
Wrench domain
Thrust domain
Thin metal sheet
Velocity discontinuity
Basal strike-slip fault
Lateral wall
Cross section 4
Wrench-thrust interference domain
Basal Pergamet plate
Thin metal sheet
Cross section 5
Interference domain
Basal strike-slip fault
Velocity discontinuity
Cross section 6
Thrust domain
Basal Pergamet plate
Velocity discontinuity
Thin metal sheet

Figure 10

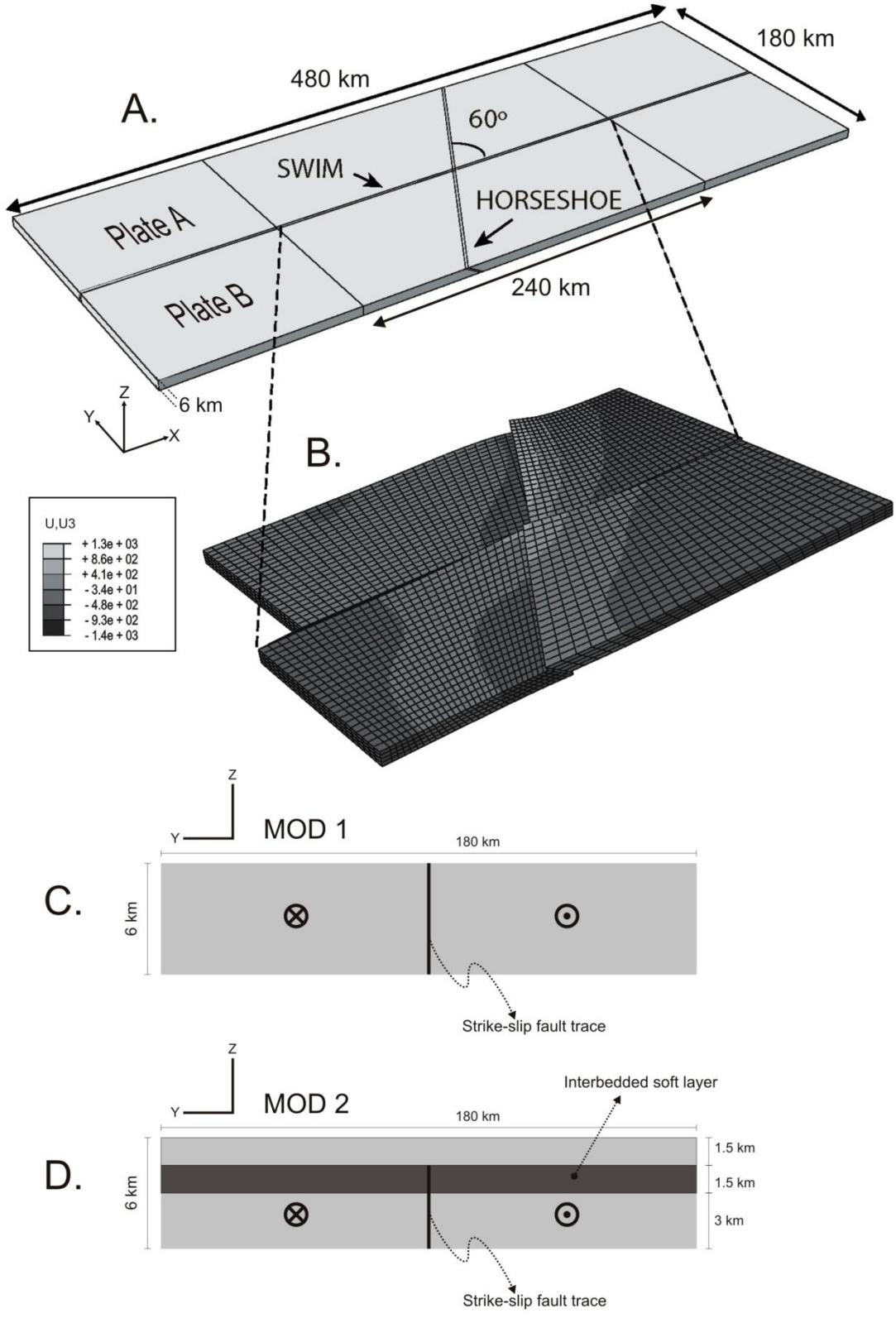

A.
480 km
180 km
60°
SWIM
HORSESHOE
Plate A
Plate B
240 km
6 km
Z
Y
X
B.
U,U3
+ 1.3e + 03
+ 8.6e + 02
+ 4.1e + 02
- 3.4e + 01
- 4.8e + 02
- 9.3e + 02
- 1.4e + 03
C.
MOD 1
180 km
6 km
Strike-slip fault trace
D.
MOD 2
Interbedded soft layer
180 km
6 km
1.5 km
1.5 km
3 km
Strike-slip fault trace

Figure 11

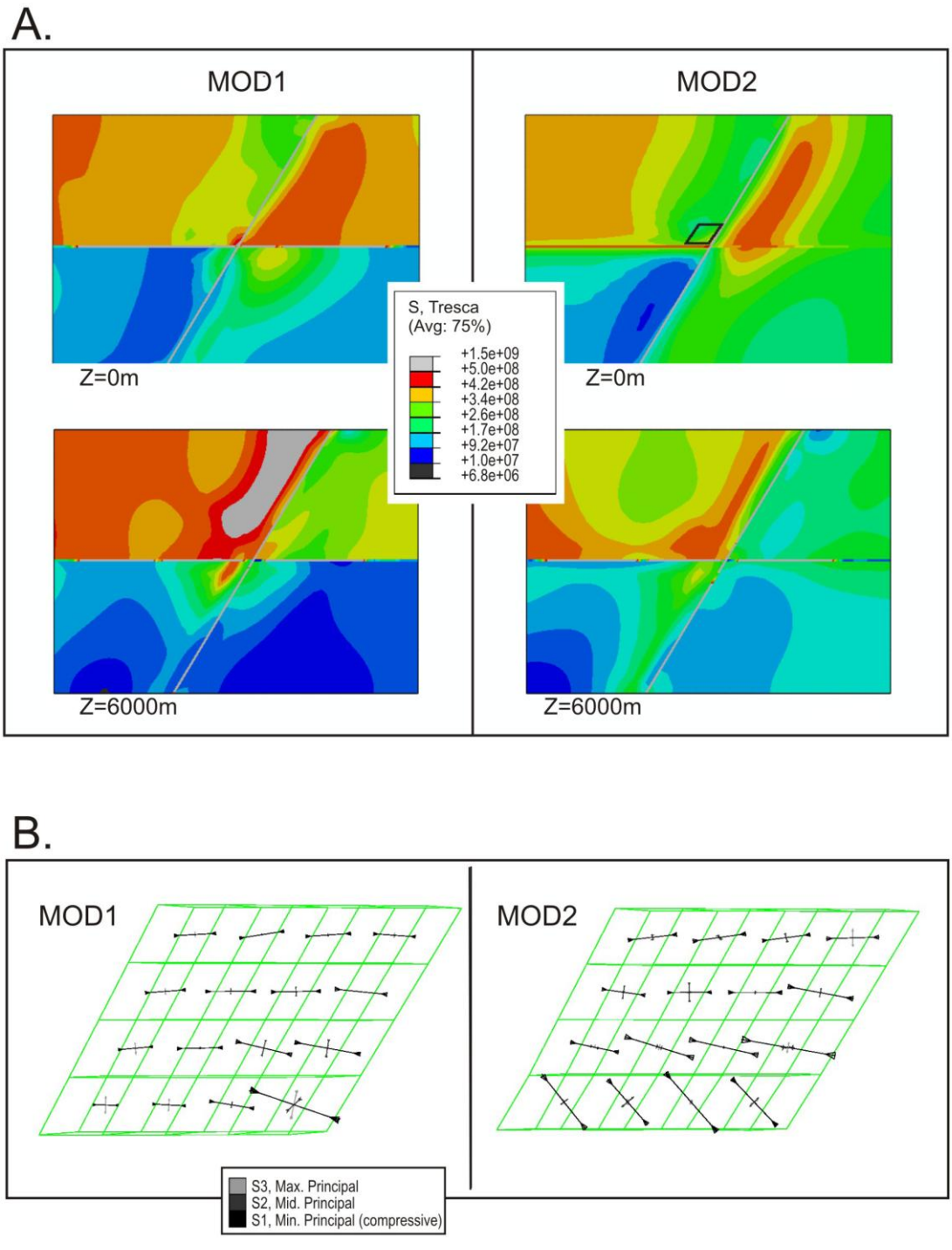

A.
MOD1
MOD2
S, Tresca
(Avg: 75%)
+1.5e+09
+5.0e+08
+4.2e+08
+3.4e+08
+2.6e+08
+1.7e+08
+9.2e+07
+1.0e+07
+6.8e+06
Z=0m
Z=0m
Z=6000m
Z=6000m
B.
MOD1
MOD2
S3, Max. Principal
S2, Mid. Principal
S1, Min. Principal (compressive)

Figure 12

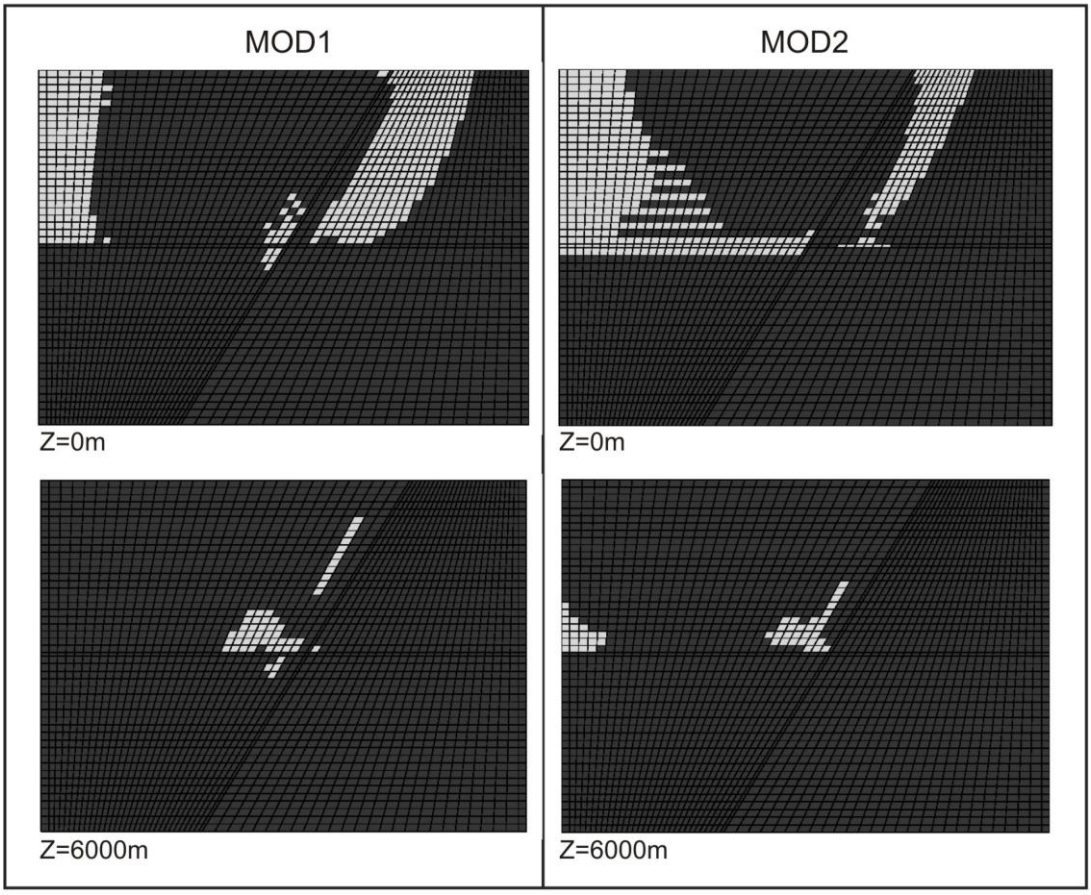


Figure 13

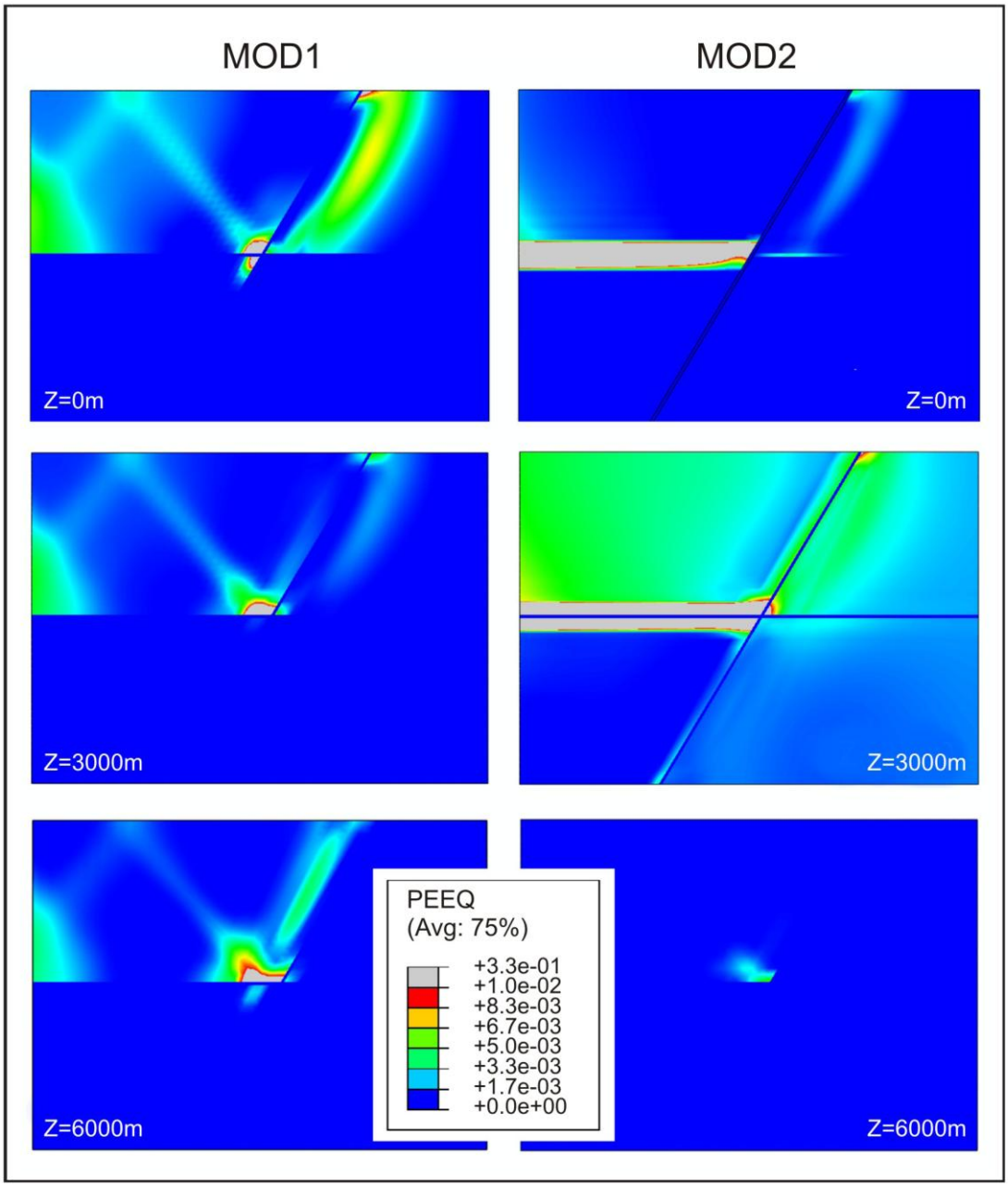

MOD1
MOD2
Z=0m
Z=0m
Z=3000m
Z=3000m
Z=6000m
Z=6000m
PEEQ
(Avg: 75%)
+3.3e-01
+1.0e-02
+8.3e-03
+6.7e-03
+5.0e-03
+3.3e-03
+1.7e-03
+0.0e+00

Figure 14

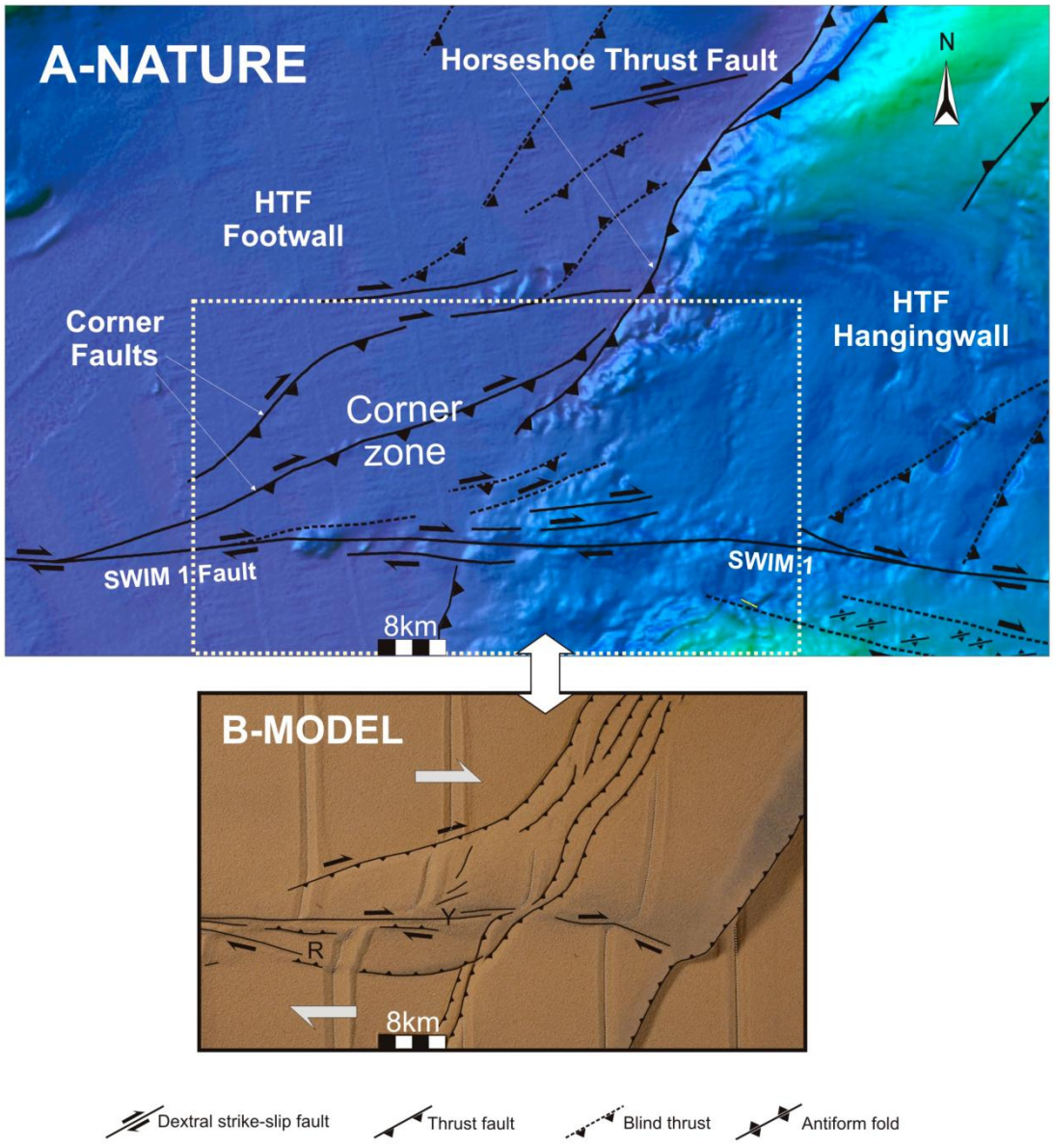

A-NATURE
Horseshoe Thrust Fault
N
HTF
Footwall
Corner
Faults
Corner
zone
HTF
Hangingwall
SWIM 1 Fault
SWIM 1
8km
B-MODEL
Y
R
8km
Dextral strike-slip fault
Thrust fault
Blind thrust
Antiform fold

Table 1 – Analogue modeling parameters and material properties

Parameters and material properties	**Quartz sand (model)**	**Natural prototype (upper crust)**	**Ratio: Model/Nature**
Composition (%)	99.7 % quartz	-	-
Grain shape	well-rounded	-	-
Grain size (mm)	< 0.30	-	-
Density (kgm^{-3})	1300	2600	$\delta = 0.5$
Internal friction angle, ϕ (°)	~30	-	-
Coefficient of internal friction, μ_c	~0.6	0.6-0.85	-
Cohesion, c_0 (Pa)	negligible	$40x10^6$	-
Gravity acceleration, g (ms^{-2})	9.81	9.81	$\gamma_g = 1$
Length, L (m)	0.01	2000	$\boldsymbol{\lambda = 5\times10^{-6}}$
Mass, M (Kg)	-	-	$\boldsymbol{\mu = 6.25x10^{-17}}$

- Scaled fundamental units are in **bold**
- A mean cohesion of $\mathbf{C_o}$**=40 MPa** was assumed from the natural prototype (e.g. Hoshino et al., 1972; Weijermars et al., 1993)

Table 2 - Rheological properties of the finite element models

	General properties			Specific material properties		
	ρ(kg/m^3)	**E (GPa)**	**ν**	**ϕ**	**ψ**	**σ_y (MPa)**
Crust (Drucker-Prager)	2900	70	0.25	27°	25°	350
Soft layer (Von-Mises)	2900	70	0.25	-	-	100
Thrust fault (cohesive material)	2900	70	0.25	G1=30000	G2=30000	-
Strike-slip fault (cohesive material)	2900	70	0.25	G1=10000	G2=10000	-

ρ=density, E=Young's Modulus, ν=Poisson's ratio, ϕ=friction angle, ψ=dilation angle, σy=Yield Stress , G1=G2=cohesive stiffness